Nucleobase Deamination as a Biomarker of Inflammatory Processes

by

Min Dong

B.S. in Pharmaceutical Science (1994)
Beijing Medical University, Beijing, PR China
M.S. in Biophysics (1999)
Tsinghua University, Beijing, PR China

SUBMITTED TO BIOLOGICAL ENGINEERING DIVISION
IN PARTIAL FULFILLMENT OF THE REQUIREMENTS
FOR THE DEGREE OF

DOCTOR OF PHILOSOPHY

at the

MASSCHUSETTS INSTITUTE OF TECHNOLOGY
[February 2005]
January 2005

Signature of Author_____
Biological Engineering Division
January 25, 2005

Certified by_____
Dr. Peter C. Dedon
Professor of Toxicology and Biological Engineering
January 25, 2005

Accepted by_____
Dr. Alan J. Grodzinsky
Chairman, Committee on Graduate Students,
Biological Engineering Division

This doctoral thesis has been examined by a committee as follows:

Professor Steven R. Tannenbaum
Chairman

Professor Gerald N. Wogan

Professor William G. Thilly

Professor Bruce Demple

Dr. John S. Wishnok

Professor Peter C. Dedon
.....Thesis Advisor

Nucleobase Deamination as a Biomarker of Inflammatory Processes

by

Min Dong

SUBMITTED TO THE BIOLOGICAL ENGINEERING DIVISION IN PARTIAL FULFILLMENT OF THE REQUIREMENTS FOR THE DEGREE OF DOCTOR OF PHILOSOPHY IN MOLECULAR TOXICOLOGY

ABSTRACT

The objective of this thesis project was to develop nucleobase deamination products as biomarkers of inflammation and to study the role of these DNA lesions in the pathophysiology of inflammation-induced carcinogenesis. The basis of this research is the epidemiological evidence that chronic inflammation is associated with an increased risk of cancer, yet the link between the inflammatory process and the development of cancer has eluded definition.

Biomarker development began with the establishment of a sensitive liquid chromatography-mass spectrometry (LC-MS) method to quantify four of the nucleobase deamination products: 2'-deoxyxanthosine (dX) and 2'-deoxyoxanosine (dO) from the deamination of dG; 2'-deoxyuridine (dU) from dC; and 2'-deoxyinosine (dI) from dA. The analytical method was then validated and tested with both *in vitro* and *in vivo* studies involving quantification of nucleobase deamination products in isolated plasmid DNA and human lymphoblastoid cells exposed to nitric oxide ($NO^{\bullet}$) at controlled physiological concentrations. Finally, the formation of nucleobase deamination products was analyzed in SJL/RcsX mice, an established mouse model of $NO^{\bullet}$ over production.

This set of studies revealed several important features of the nitrosative chemistry of $NO^{\bullet}$ derivatives. The *in vitro* formation of dX, dI and dU was found to occur at nearly identical rates ($k = 1.2 \times 10^5\ M^{-1}s^{-1}$). Low levels of nucleobase deamination products were formed in cells exposed to $NO^{\bullet}$, which suggests that cellular factors significantly influence the nitrosative chemistry. However, cellular glutathione (GSH) was found to play a smaller role than expected, considering the effects of GSH on steady-state concentrations of N_2O_3 in *in vitro* kinetic studies. Moderate increases (~30%) in nucleobase deamination products were observed in the SJL mice bearing the RcsX tumor, but the biological meaning of these increases awaits studies of DNA repair kinetics. dO was not detected in any study at levels above 5 per 10^8 nt, leading to the prediction that it will not be present at significant levels in inflamed tissues in humans.

As a complement to the LC-MS method for the quantification of nucleobase deamination products, enzymatic probes were also developed for oxidative and nitrosative DNA lesions. These probes would not only allow differential quantification of the two types of DNA damage, but would also allow the lesions to be mapped in any DNA sequence by coupling their activity with the technique of ligation-mediated PCR.

As an extension of the biomarker study, the effects of $ONOO^-$ dose and dose-rate on the DNA damage and mutations induced in the *supF* gene were investigated. The observations suggest that both the dose and dose-rate at which a genetic target is exposed to $ONOO^-$ substantially influence the damage and mutational response and these parameters will need to be considered in assessing the potential effects of $ONOO^-$ *in vivo*.

Finally, an extended study using the analytical method developed in this thesis yielded results in *E. coli* consistent with a new paradigm: perturbations of nucleobase metabolism may lead to incorporation of the purine precursors hypoxanthine (I) and xanthine (X) into DNA. This can be regarded as another endogenous process causing DNA damage that may lead to human diseases such as cancer.

In summary, this thesis work established an analytical method for the quantification of a collection of representative nucleobase deamination products. The analytical method has been applied to address a series of biologically important questions. Results obtained in this thesis contribute to the development of nucleobase deamination products as biomarkers of the inflammatory process.

ACKNOWLEDGMENTS

No research endeavor is ever carried out in solitude. This thesis would not have been possible without the assistance and encouragement of many individuals to whom my deep gratitude is owed.

First and foremost, I would like to thank my thesis advisor, Prof. Peter C. Dedon, for giving me an opportunity to work in his laboratory. My warmest and deepest gratitude is expressed for his scientific guidance, for his continuous support and encouragement, and for the enthusiasm and inspiration, which was always there when I needed it. His careful reviewing of draft papers and the thesis manuscript was very much appreciated.

I have also been fortunate to benefit from interactions with each member of my thesis committee: Profs. Steven R. Tannenbaum, Gerald N. Wogan, Bruce Demple, William G. Thilly and Dr. John S. Wishnok. I would like to thank them for providing much appreciated insight, interest, and encouragement in this research, as well as invaluable guidance and advice on certain questions and dilemmas, which really helped shape this work into what it is now. I would also like to acknowledge the generosity of my committee members in making resources in their groups available to me.

I am deeply indebted to a group of scientists for valuable contributions to this work. Dr. Chen Wang from the research group of Prof. William M. Deen contributed to the work described in Chapter 3. She was the person who developed the novel nitric oxide delivery system and performed the kinetic modeling of the *in vitro* formation of nucleobase deamination products. Drs. Chunqi Li, Min Young Kim and Ms. Laura J. Trudel from the research group of Prof. Gerald N. Wogan contributed the work in Chapters 4, 5 and 7. Dr. Li and Ms. Trudel provided generous assistant and valuable inputs in designing and implementing the cell experiments. Mutation study by Dr. Kim highlighted the biological significance of the DNA damage caused by peroxynitrite described in Chapter 7. Dr. Hongbin Yu from the research group of Prof. Steven R Tannenbaum kindly provided his data regarding the formation of nucleobase oxidation products for an insightful discussion of the SJL/RcsX mice study that is described in Chapter 5. For the studies described in the Appendix, Dr. Nicholas E. Burgis from the research group of Prof. Richard P. Cunningham provided the bacteria strains. Dr. Lisiane B. Meira from the research of Prof. Leona D. Samson provided the tissue sample of the Aag mice.

I am also very grateful to Dr. Koli Taghizadeh and Ms. Elaine Plummer Turano from the Bioanalytical Facilities Core of the Center for Environmental Health Sciences (CEHS) at MIT. Without their expertise and generous help in using the mass spectrometry and other equipments, this thesis work could not have been carried out this smoothly.

In my daily work I have been blessed with a friendly and cheerful group of fellows who have given me wonderful help during the past five years. Very special thanks go to Dr. Michael DeMott for a lot of stimulating discussions and for his tremendous amounts of time and effort devoted to reviewing and correcting a substantial portion of this thesis. Very special thanks also go to Ms. Marita Barth for her proof reading of my thesis and for other helps in various aspects.

Very special thanks are due to Mr. Xinfeng Zhou and Drs. Bingzi Chen, Tao Jiang and Bo Pang for sharing their ideas and expeience, and for the terridic assistance on many occasions that really expedited my progress in research. Their caring friendship throughout my graduate study will always be cherished. Special thanks go to Miss Yelena Margolin and Dr. Christiane Collins for the pleasure of being classmates and labmates with them. My specila tanks also go to Ms. Olga V. Parkin who acts as a stand-in mother figure, but of course mainly for helping out with all the things a student in our lab needs helping out with. As well as keeping me stocked with general supplies, Ms. Jacklene Goodluck Griffith has also inadvertently, and without fail, provided something much greater in all the years I've known her: a friendly smile and a hug every time we met.

Ms. Debra Luchanin and Ms. Dalia Gabour, the former and current academic administrator, and Ms. Rolanda Dudley-Cowans, the administrative officer, deserved a separate acknowledgement. Their assistant and support made my life a lot easier at MIT.

I would also like to thank my parents for their love and support, for instilling my love of science when I was young, and for creating an environment in which following this path seemed so natural.

And last but not least Donghao, for the very special person he is, for the incredible amount of support and patience he had with me, and for being a marvelous friend whom I can always count on.

This work was supported mainly by a grant from the National Cancer Institute (CA26735) and partly by the David Koch graduate fellowship in cancer research from Center of Cancer Research at MIT. LC-MS analyses were performed in the Bioanalytical Facilities Core of the Center for Environmental Health Sciences at MIT, which is supported by a Center grant from the NIEHS (ES02109). I am also grateful for the generous financial support from the Marian Marcelle Znaty Award, which, together with the NCI grant, provided invaluable opportunities for me to attend various conferences to present my work and learn from the wider international community. My special thanks go to the Biogen Idec-MIT Fellowship, which provided me a unique opportunity to experience pharmaceutical and biotech industry and influenced tremendously on my own career decision.

This document is dedicated to my parents and in loving memory of my grand parents

TABLE OF CONTENTS

Chapter 1 Background and Literature Review

Chapter 2 Development of a Novel LC-MS Method for the Quantification of Nucleobase Deamination Products

Chapter 3 Absence of 2'-Deoxyoxanosine and Presence of Abasic Sites in DNA Exposed to Nitric Oxide at Controlled Physiological Concentrations

Chapter 4 Formation of Nucleobase Deamination Products in Human Lymphoblastoid Cells Exposed to Nitric Oxide at Controlled Physiological Concentrations

Chapter 5 Formation of Nucleobase Deamination Products in Spleen and Liver of SJL Mice Bearing the RcsX Tumor

Chapter 6 Development of Enzymatic Probes to Analyze DNA Damage Caused by Reactive Nitrogen Species

Chapter 7 Effect of Peroxynitrite Dose and Dose-rate on DNA Damage in the *supF* Shuttle Vector

ABBREVIATIONS

AlkA	*E. coli* 3-methyladenine-DNA glycosylase
AlkB	*E. coli* 1-methyladenine-DNA dioxygenase
APC	adenomatous polyposis coli
BER	base excision repair
8-Br-dG	8-bromo-2'-deoxyguanosine
8-Cl-dG	8-chloro-2'-deoxyguanosine
CO_2	carbon dioxide
dA	2'-deoxyadenosine
dC	2'-deoxycytidine
DHR123	dihydrorhodamine123
DTH	delayed-type hypersensitivity
DTNB	5,5'-dithiobisthio-2-nitrobenzoic acid
EndoIII	endonuclease III
EndoV	endonuclease V
Fpg	formamidopyrimidine-DNA glycosylase
dG	2'-deoxyguanosine
dI	2'-deoxyinosine
dO	2'-deoxyoxanosine
dU	2'-deoxyuridine
dX	2'-deoxyxanthosine
Gh	guanidinohydantoin

GSH	glutathione
GSSG	oxidized glutathione
HCC	hepatocellular carcinoma
HPLC	high performance liquid chromatography
IFN-γ	interferon-gamma
iNOS	inducible nitric oxide synthase
LC-MS	liquid chromatography-mass spectrometry
LPS	lipopolysaccharide
MF	mutation frequency
$NaHCO_3$	sodium bicarbonate
NI	nitroimidazole
8-Nitro-G	8-nitroguanosine
NER	nucleotide excision repair
NMA	N-methyl-L-arginine acetate
$NO^{\bullet}$	nitric oxide
ODS	octadecylsiloxane
$ONOO^-$	peroxynitrite
ONOOH	peroxynitrous acid
$ONOOCO_2^-$	nitrosoperoxycarbonate
Ox	oxazolone
8-Oxo-dG	8-oxo-2'-deoxyguanosine
PUFA	polyunsaturated fatty acids
ROS	reactive oxygen species

RNS	reactive nitrogen species
sccm	standard cubic millimeter per minute
SIN-1	3-morpholinosydnonimine
Sp	spiroiminodihydantoin
TNB	5-thio-2-nitrobenzoic acid
UDG	uracil DNA glycosylase

Chapter 1

Background and Literature Review

1.1 Introduction

The goal of the research presented in this thesis was to develop nucleobase deamination products as biomarkers of inflammation and to study the role of these DNA lesions in the pathophysiology of inflammation-induced carcinogenesis. The basis for these studies is the epidemiological evidence that a significant fraction of the global cancer burden is attributable to chronic infection and inflammation (Graham et al., 1995; IARC, 1994; IARC, 1996; Ohshima and Bartsch, 1994; Thun et al., 2004). Central to the notion that inflammation plays a role in the carcinogenic process is the finding that chronic irritation of parenchymal tissues results in migration of inflammatory cells to the injured site where they secret chemically reactive oxygen (ROS) and nitrogen (RNS) species aimed eliminating the infectious agent. However, diffusion of the chemical mediators of inflammation into surrounding healthy tissue could lead to reactions that damage cellular proteins, lipids, carbohydrates and nucleic acids and, as a result, cause the cell death or mutations that facilitate malignant transformation.

While the causative association between inflammation and cancer has eluded definition, there is a growing body of evidence supporting various mechanisms that link the chemical stresses of inflammation with the carcinogenic process (Klaunig and Kamendulis, 2004). For example, genotoxicity associated with DNA damage by chemical mediators of inflammation may lead to the inactivation of tumor suppressor genes and the activation of oncogenes that comprise multi-step carcinogenesis (Feig et al., 1994; Grisham et al., 2000). This process is complicated by mechanisms that are independent of genotoxicity, such as resistance to apoptosis (Li et al., 1997; Park et al., 2001), cytotoxicity and compensatory hyperproliferation that force polymerase errors (Rosin et al., 1994a; Rosin et al., 1994b), adaptive survival responses that may pass abnormal

genome into following generation cells, resulting in carcinogenesis (Ambs et al., 1998), and enhanced angiogenesis, the creation of blood vessels that nourish new, secondary tumors (Jenkins et al., 1995).

A critical step in sorting out the complex role of the chemical stress of inflammation in the process of carcinogenesis is resolving the underlying chemistry. However, a basic fact in studying the chemistry of inflammation is that the concentrations of most of the reactive oxygen (ROS) and nitrogen species (RNS) are too low and their half-lives are too short to study them directly under biologically relevant conditions. The difficulty in making direct measurements motivates the complementary development of biomarkers as surrogates for the RNS and ROS. True biomarkers will serve to establish the chemistry leading to molecular changes, such as mutation and cell signaling, which in turn lead to cellular responses on the pathway to cancer. In the development of any biomarker, there are three steps (Halliwell, 2002), the first of which is to identify DNA and protein lesions that are specific to the disease in question. As discussed shortly, the specific lesions dealt with in this thesis are the four nucleobase lesions arising from nitrosative deamination of DNA caused by chemical mediators of inflammation. The second step in biomarker development is to create and validate analytical methods. This is addressed in Chapter 2 with the development of an LC-MS method to quantify the nucleobase deamination products, with validation *in vitro* and *in vivo* in Chapters 3-4. The final step is to demonstrate that changes in the levels of the markers correlate with the pathophysiology of inflammation and subsequent carcinogenesis. If DNA lesions represent a critical link in the pathway to cancer (Feig et al., 1994; Grisham et al., 2000), then their formation in inflamed tissues must be proven and a relationship between the quantities of the various lesions and disease progression must be established. This facet of biomarker development is addressed in Chapter 5.

In this literature review, evidence in support of chronic inflammation as a cancer risk factor is first introduced, followed by a brief review of the aspects of neutrophil and macrophage biology pertinent to the production of RNS and ROS. The majority of the review is devoted to a discussion of the chemical biology of inflammation, with a primary focus on the RNS-mediated genotoxicity. The concepts of biomarker development and application in cancer studies are then reviewed and the advantages of DNA damage products as biomarkers of a pathphysiological process are discussed. Finally, current bioanalytical methods for the detection of DNA damage products are reviewed and their relative merits are evaluated.

1.2 Chronic Inflammation and Cancer

It is well established that cancer arises in chronically inflamed tissues, as demonstrated by hepatitis virus-associated hepatocellular carcinoma (HCC) (Chisari et al., 1989; Nair et al., 1996; Sezaki et al., 2004), *Helicobacter pylori*-induced gastric cancer (Ebert et al., 2000; Graham et al., 1995), and inflammatory bowel disease leading to colorectal cancer (Kumamoto and Takenoshita, 2003). Chronic inflammation is caused by a variety of factors, including viral, bacterial, and parasitic infections, chemical irritants, and particulate matter (Shacter and Weitzman, 2002). The longer the inflammation persists, the higher the risk of cancer (Shacter and Weitzman, 2002). A growing body of evidence suggests that the association between chronic inflammation and increased risk of cancer is not coincidental and may indeed be causal.

A. Evidence from Epidemiological Studies

The link between inflammation and cancer was first suggested by Rudolph Virchow in 1863 when he demonstrated the presence of leukocytes in neoplastic tissues. Since then, a wide variety of inflammatory conditions have been hypothesized to predispose susceptible cells to neoplastic transformation. Based on a recent IARC statistical evaluation, about 1.8 million cancer cases in 2000, or ~18 % of the total, were attributable to infectious agents (Franceschi, 2000; Newton, 2000). Among these, ~13% were related to infections with viruses, such as human papillomavirus, hepatitis virus, and human immunodeficiency virus, while ~5 % were elated to the bacterium *Helicobacter pylori* and a small portion to parasitic infection (Parkin, 2001; Parkin et al., 2001). Infections can cause cancer by different mechanisms including direct transformation of cells (De Luca et al., 2004), induction of immunosuppression with consequent

reduced cancer immunosurveillance (Shah et al., 2003), or by causing chronic inflammation (Ohshima et al., 2003). The latter is becoming increasingly recognized as an essential component of many epithelial cancers by virtue of the combined effects of generating genotoxic by-products and increased cellular proliferation, thus maximizing the potential for DNA damage.

Table 1 summarizes our current understanding of infectious agents that have been associated with malignancies. Two examples of well-established preneoplastic conditions associated with infection/inflammation are reviewed below: human hepatitis virus infection and hepatocellular carcinoma (HCC), and *Helicobacter pylori* (*H. pylori*) infection and gastric carcinoma.

Table 1. Infectious agents associated with malignancies (adapted from Parkin, 2001)

Infectious agents	Neoplasia
Virus	
Hepatitis B and C viruses	Hepatitis, chronic active hepatitis, and hepatocellular carcinoma
Epstein-Barr virus	Burkitt lymphoma, nasopharyngeal carcinoma, and reversible lymphoproliferative diseases in immunodeficient patients
Human T-lymphotropic virus types 1 and 2	Adult T-cell leukemia, T-cell lymphoma
Human papillomavirus	Cutaneous and mucosal papillomas and carcinomas
Human herpesvirus-8 (KSHV)	Kaposi sarcoma, body cavity lymphoma
Human immunodeficiency virus	Kaposi sarcoma, non-Hodgkin lymphoma, and cutaneous and mucosal papilloma, and carcinoma
SV-40	Possible associations with mesothelioma and ependymoma
Bacteria	
Helicobacter pylori	Gastric adenocarcinoma, intestinal type, mucosa-associated lymphoid tissue lymphoma, non-Hodgkin lymphoma
Fusobacterium fusitome and *Borrelia vincentill*	Squamous cell carcinoma arising from tropical phagedenic ulcer
Possible association, *Vibrio cholerae*	Immunoproliferative small intestinal disease, non-Hodgkin lymphoma
Protozoa	
Strongyloides sterocoralis	T-cell leukemia (with human T-lymphotropic virus)
*Plasmodium falciparum**	Burkitt lymphoma
Schistosoma haematobium	Squamous cell carcinoma of the urinary bladder
Schistosoma mansoni, Schistosoma japonicum	Colonic carcinomas
Clonorchis sinensis	Cholangiocarcinoma
Opisthorchis viverrini	Cholandiocarcinoma

* Cofactor for development of Burkitt lymphoma in endemic regions

Viral Infection and Cancer. Malignancies associated with viral infection have been studied in animal models for decades (Hayashi et al., 2002). However, only recently has there been evidence that clearly demonstrates an association between viral infection and human malignancies. A classic example is the link between hepatitis virus infection and the increased risk of HCC (Liu and Hotchkiss, 1995; zur Hausen, 1991). Among seven human hepatitis viruses, hepatitis B (HBV) and C (HCV) viruses are able to persist in the host for years and principally contribute to the establishment of chronic hepatitis (Nordenfelt, 1990; Petrelli et al., 1994). During the course of persistent infection, continuous intrahepatic inflammation maintains a cycle of liver cell destruction and regeneration that often terminates in HCC. The role of $NO^{\bullet}$ has been suggested on the basis of the observation of enhanced iNOS expression in the liver of HCV-infected patients (Majano et al., 1998; Mihm et al., 1997). Majano *et al.* recently proposed a model of $NO^{\bullet}$-mediated HCV infection in which $NO^{\bullet}$ plays several roles. On the one hand, $NO^{\bullet}$ may induce viral mutations and a selective suppressive effect on Th1 cells, thus allowing HCV to escape the host immune system. Additionally, the anti-apoptotic effect of $NO^{\bullet}$ in hepatocytes could facilitate HCV replication in a long-lived cellular compartment. On the other hand, $NO^{\bullet}$ can also promote apoptosis and mitochondrial dysfunction, and cause DNA damage, which leads to mutagenesis and the subsequent development of HCC (Majano and Garcia-Monzon, 2003).

Bacterial Infection and Cancer. The pathogenic role of bacteria in carcinogenesis has been largely overlooked until the recent demonstration of a link between *H. pylori* and gastric adenocarcinaoma, the second most common malignancy worldwide (reviewed in Nardone and Morgner, 2003; and IARC, 1994). *H. pylori* has been shown to chronically infect over half of

the world's population (IARC, 1994). The key pathophysiological event in *H. pylori* infection is the initiation of an inflammatory response, most likely triggered by the bacterium's lipopolysaccharide, urease, and/or cytotoxins (Israel and Peek, 2001), leading to the over-production of $NO^{\bullet}$ and the generation of RNS (Li et al., 2001; Moss, 1998; Sepulveda, 2001). An increase in the level of 8-oxo-dG as well as enhanced anti-apoptotic signal transduction was also observed (Chang et al., 2004; Farinati et al., 1998). Park *et al.* recently reviewed the evidence that anti-inflammatory regimens can decrease the development of tumors, which suggests that chemopreventative strategies might ameliorate gastric inflammation by the attenuation of oxidative stress (Park et al., 2004).

In summary, there is abundant epidemiological evidence supporting a link between chronic inflammation and carcinogenesis, along with a growing body of research revealing the basic molecular pathways of this association. Inflammatory cells produce a wide range of chemical mediators of inflammation, including pro-inflammatory cytokines, chemokines, RNS, ROS, growth factors, and eicosanoids, any or all of which may be responsible for cellular changes that lead to transformation.

B. Evidence from *In Vitro* Studies and Animal Models

A substantial body of experimental evidence, derived from *in vitro* studies and animal models, also supports the association between chronic inflammation and increased cancer risk. A complete review is beyond the scope of this dissertation, so only a few representative studies aimed at elucidating the chemical basis of inflammation-induced carcinogenesis are discussed here.

In Vitro and Cell Culture Studies. In early 1980's, Tannenbaum and coworkers reported their discovery of increased levels of nitrite/nitrates in urine from individuals who suffered from infections (Green et al., 1981). Marletta and coworkers demonstrated that the nitrite/nitrates were produced from macrophages and nitrosation of amines could occur from activated macrophages (Marletta et al., 1988). At the same time, Hibbs and coworkers showed that nitrite formation from arginine was critical in host defense against pathogens and tumors (Hibbs et al., 1988). Collectively, these observations, on the one hand, raised concerns about a new potential endogenous mechanism of chemical carcinogenesis, while on the other hand, the results suggested that NO$^{\bullet}$ was required for the tumoricidal activity of the immune system.

In addition to the formation of nitrosamines, Wink et al. proposed that NO$^{\bullet}$ and the derivative RNS could be directly genotoxic based on their observation that, under aerobic conditions, NO$^{\bullet}$ exposure could cause deamination of DNA through a nitrosative mechanism (Wink et al., 1991). Prolonged exposure of nucleic acids to NO$^{\bullet}$/RNS resulted in conversion of 2'-deoxycytidine (dC) to 2'-deoxyuridine (dU), of 2'-deoxyguanosine (dG) to 2'-deoxyxanthine (dX), and 5-methyl-2'-deoxycytidine (MedC) to 2'-deoxythymidine (dT) (Wink et al., 1991). Tannenbaum and coworkers confirmed this hypothesis by showing that DNA deamination products formed in human cells exposed to NO$^{\bullet}$ (Nguyen et al., 1992) and in activated macrophages producing large quantities of NO$^{\bullet}$ (deRojas-Walker et al., 1995). Similar arguments can be made for peroxynitrite ($ONOO^-$), the reaction product of superoxide ($O_2^{\bullet-}$) and NO$^{\bullet}$, which has been shown to cause strand breaks and base oxidation and nitration in DNA (Beckman, 1991; deRojas-Walker et al., 1995; Salgo et al., 1995a; Salgo et al., 1995b; Tamir et al., 1996). Collectively, these studies established a new mechanism for genotoxicity mediated by NO$^{\bullet}$ and its reactive species.

In addition to direct DNA damage, NO• contributes to genotoxicity through alternative mechanisms. Wink and Laval found that DNA repair proteins, including formamidopyrimidine-DNA glycosylase (Fpg) and 3-methyladenine-DNA glycosylase (AlkA), could be inhibited by RNS through nitrosation at amounts 100-fold less than those required to deaminate DNA (Laval et al., 1997; Wink and Laval, 1994a). Furthermore, metallothionein, a metal-chelating protein, was found to lose its structural integrity upon exposure to NO• (St Croix et al., 2004). Hence, through degradation of specific repair and protective proteins, NO• could leave cells susceptible to other toxins and genotoxic agents.

Animal Models of Inflammation. Animal models of a variety of diseases have been developed to provide a better understanding of the mechanisms by which inflammation leads to cancer. Berenblum and Friedwardl first reported the increased cancer incidence in animals specifically in areas of the body subjected to chemical or physical irritation for prolonged periods (Berenblum, 1941; Friedwardl and Rous, 1944). There is early tumor onset in animals carrying a germline mutation that either inactivates a tumor suppressor gene or activates an oncogene (Knudson, 2001). One such model is the multiple intestinal neoplasia (Min) mice, which like humans with familial adenomatous polyposis (FAP), express an abnormal genotype for the adenomatous polyposis coli (APC) tumor suppressor gene. Feeding dextran sodium sulphate (DSS) to the Min mice led to the onset of inflammatory bowel disease and, subsequently, colon cancer (Cooper et al., 2001; Hokari et al., 2001).

Given the strong correlation between infection and cancer in humans, a number of animal models have been developed to define the mechanistic basis for this link. Examples include the development of liver cancer in mice infected with hepatitis B virus (Chisari et al., 1989) and the

growth of gastric adenocarcinoma in mice infected with *H. pylori* (Lee, 1999). In addition to the SJL/RcsX mouse model of inflammation-mediated NO• overproduction, which will be discussed in detail in Chapter 5, there are several widely used animal models of inflammation-induced cancer, including the iNOS knockout (KO) mice (*iNOS*$^{-/-}$ mice), the recombinase-activating gene 2 KO mice (*Rag-2*$^{-/-}$ mice), the T cell receptor αβ (TCR αβ) KO mice (*TCR αβ*$^{-/-}$ mice), the IL-10 KO mice (*IL-10*$^{-/-}$ mice), and the Cox-1 and Cox-2 KO mice (*Cox-1*$^{-/-}$ mice and *Cox-2*$^{-/-}$ mice). These are discussed in detail in the following sections.

iNOS-Knockout Mice

As discussed in next section, the generation of NO• by nitric oxide synthase (NOS) is a key feature of chronic inflammation. The *iNOS*$^{-/-}$ (inducible NOS knockout) mouse was first generated by MacMicking et al. to study the role of iNOS in host defenses against infectious agents and tumor cells (MacMicking et al., 1995). Since then, these mice have been used to investigate the role of iNOS in many pathological processes including inflammation, liver regeneration, tumorigenesis and sepsis-induced hypotension (Mashimo and Goyal, 1999). An interesting example is the generation of iNOS knockout Min mice (Scott et al., 2001). No significant difference in the number of adenomas in the large intestine or in the proximal two-thirds of the small intestine of *iNOS*$^{-/-}$ and *iNOS*$^{+/+}$ Min mice was observed. However, a small, but significant increase in the number of adenomas in the distal third of the small intestine in *iNOS*$^{-/-}$ Min mice was found, suggesting that iNOS played an antineoplastic role in the APC (Min) mouse model of familial adenomatous polyposis (Scott et al., 2001). In contrast, studies by Ahn and Ohshima showed a significant reduction in the number of adenomas in *iNOS*$^{-/-}$ Min mice compared with the *iNOS*$^{+/+}$ Min mice, indicating that NO• and its derivatives played an important role in promoting colon carcinogenesis in a background of APC mutations (Ahn et al.,

1999). These seemingly contradictory observations imply the complicated nature of $NO^{\bullet}$ biological functions, with environmental factors possibly enhancing the adenoma development in the latter studies.

Rag-2-Knockout Mice.

The *Rag2*$^{-/-}$ mice, deficient in the recombinase activating 2 gene, are unable to initiate V(D)J rearrangement, resulting in the failure to generate mature T or B lymphocytes (Shinkai et al., 1992). 129/SvEv *Rag-2*$^{-/-}$ mice infected with the encephalomyocarditis virus (EMCV) developed sever myocardial necrosis (Kanda et al., 1999). However, when the same mouse model was inoculated with *Helicobacter hepaticus*, an enteric bacterial pathogen of mice, they developed a severe inflammatory bowel disease (IBD). The incidence of IBD was reduced with adoptive transfer of IL-10 positive CD4 (+) CD45RB (lo) CD25 (+)-regulatory cells, which suggests that IL-10-mediated suppression of the host innate inflammatory response was pivotal in interrupting the carcinogenic process (Erdman et al., 2003a; Erdman et al., 2003b).

TCR αβ-Knockout Mice.

Mice in which the T cell receptor α and β genes are knocked out (*TCR* $\alpha^{-/-}$ *or TCR* $\beta^{-/-}$ *mice*) provide useful models to study the development of mucosal inflammation and IBD (e.g., Crohn's disease and ulcerative colitis). As reviewed by Bhan *et al.*, genetic and environmental factors along with the spectrum of enteric flora are important factors in the development of mucosal inflammation (Bhan et al., 1999). The normal mucosal homeostasis is disrupted when there is either cytokine imbalance or loss of immunoregulatory cells. CD4+ T cells have been identified as the pathogenic T cells in colitis and they mediate inflammation by either the Th1 or the Th2 pathway (Salem, 2004). Th1 cells drive the type-1 pathway ("cellular immunity") to fight viruses and other intracellular pathogens, eliminate cancerous cells, and stimulate delayed-type

hypersensitivity (DTH) skin reactions. Th2 cells drive the type-2 pathway ("humoral immunity") and up-regulate antibody production to fight extracellular organisms; type 2 dominance is credited with tolerance of xenografts and of the fetus during pregnancy. Over-reactivation of either pattern can cause diseases, and either pathway can down-regulate the other. The Th1 pathway dominates most colitis and Crohn's disease models, as observed in the *TCR* $\beta^{-/-}$ mice (Bamias et al., 2003). In contrast, the colitis in *TCR* $\alpha^{-/-}$ mice shares many features of ulcerative colitis including the dominance of Th2 pathway in colonic inflammation (Bhan et al., 2000).

Interleukin 10-Knockout Mice.

Interleukin-10 (IL-10) is an anti-inflammatory cytokine and a molecule with pleiotropic effects, including regulation of T-cell response, acute inflammatory response, and free-radical release (Kumar and Creery, 2000). Knockout IL-10 gene in mice leads to enterocolitis, which is similar to human inflammatory bowel disease and thus represents another useful model to study the association of ulcerative colitis and Crohn's disease with carcinogenesis (Kuhn et al., 1993). Berg *et al.* demonstrated that specific pathogen-free (SPF) *IL-10*$^{-/-}$ mice develop spontaneously progressive chronic intestinal inflammation and colorectal adenocarcinomas, but the enterocolitis pathology can be improved by exogenous IL-10 administration to the mice (Berg et al., 1996). Rennick and Fort intensively reviewed the studies of *IL-10*$^{-/-}$ mice in elaborating the role of enteric organisms in triggering intestinal disease, suggesting that insufficient counter regulation of a Th1 inflammation response due to the lack of IL-10 underlies the pathology (Rennick and Fort, 2000).

COX1- and COX2-Knockout Mice.

Cyclooxygenase (COX) is the rate-limiting enzyme in the conversion of arachidonic acid to prostanoids (Gerstenfeld, 2004). Two COX isoforms have been cloned, of which COX-1 is

constitutively expressed, while the expression of COX-2 is low or non-detectable in most tissues, but can be readily induced in response to cell activation by cytokines, growth factors and tumor promoters. Thus, COX-2 has been related to inflammation, reproduction and carcinogenesis (Hinz and Brune, 2002).

Several recent studies using *Cox1*$^{-/-}$, *Cox2*$^{-/-}$ or double knockout mice clearly indicate that both of these enzymes are important in cancer development. Loss of COX2 led to a reduction in the number and size of intestinal polyps in a mouse model of human familial adenomatous polyposis (Oshima et al., 1996). Homologous disruption of either Ptgs-1 or Ptgs-2, genes encoding COX-1 and COX-2 respectively, dramatically reduced polyp formation in Min mice (Chulada et al., 2000) and skin tumorigenesis in a multistage mouse skin model (Tiano et al., 2002).

1.3 Chemical Biology of Inflammation

Inflammation begins with a reaction to an irritant or infection and is characterized by the movement of fluid and white blood cells into extravascular space. This is followed by tissue repair and regeneration that involve cell proliferation. There is no sharp line of division between acute and chronic, since chronic inflammation may progress from acute inflammation if the injurious agent persists. In contrast to the largely vascular changes of acute inflammation, such as increased permeability and changes in blood flow rate and lymphatic flow, chronic inflammation is characterized by infiltration of damaged tissue by mononuclear cells such as macrophages, lymphocytes, and plasma cells, together with tissue destruction and attempts at repair (Stvrtionva et al., 1995).

The inflammatory response draws on both innate and acquired immunity, with the former being more relevant to the work presented in this thesis. A hallmark of non-specific innate immunity is phagocytosis accomplished by neutrophils (polymorphonuclear leukocytes, PMN), circulating phagocytic monocytes or macrophages, eosinophils, and fixed macrophages of the reticuloendothelial system (Bainton, 1992).

Neutrophils are typically the first cells responding to an inflammatory stimulus, with macrophages infiltrating the inflamed area as the insult persists. Upon stimulation by cytokines and other factors generated at sites of inflammation, both cell types produce an abundance of ROS and RNS, as shown in Figure 1. The hypothesis driving this proposal is that both RNS and ROS generated at sites of inflammation diffuse into normal tissues and cause cytotoxic and mutagenic damage that plays a causative role in the link between inflammation and cancer (reviewed in Dedon and Tannenbaum, 2004). This section reviews the cell types and the

spectrum of chemical mediators of inflammation that serve as the focus of the research presented in this thesis.

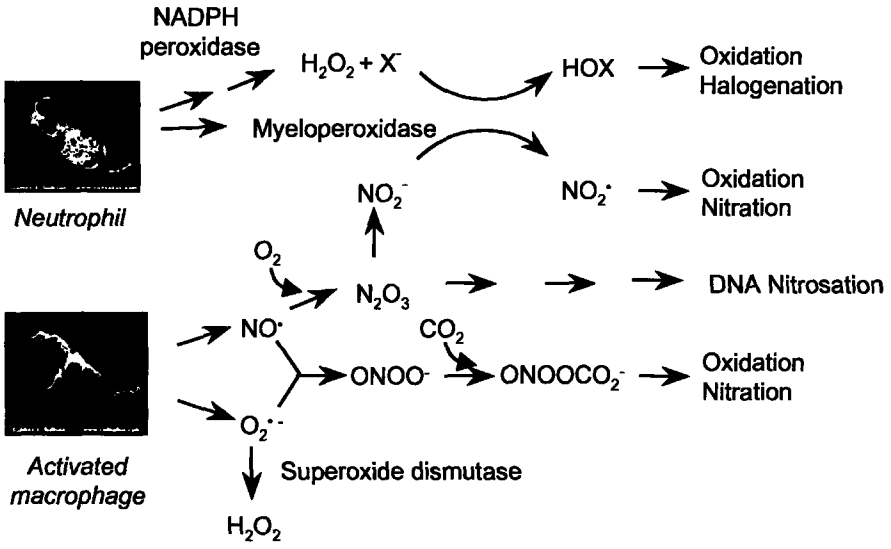

Figure 1. Cells and reactive species implicated in the process of inflammation

A. Major Phagocytic Cells Involved in Inflammation

Neutrophils

Neutrophils represent 50 to 60% of the total circulating leukocytes and constitute the "first line of defense" against infectious agents or nonself substances that penetrate the body's physical barriers. Derived from bone marrow, neutrophils are released into tissue pools at a rate of 10^{11} per day in a normal healthy adult and at 10^{12} per day in settings of acute inflammation (Bainton, 1992).

The major role of neutrophils is to phagocytose and destroy infectious agents by opsonization. They also limit the growth of some microbes, thereby benefiting adaptive (specific) immunological responses (Elsbach and Weiss, 1992). In addition to a variety of enzymes and biologically active substances that are stored in granules to control inflammatory and cytotoxic reactions (Table 2), a respiratory burst is triggered to generate $O_2^{\cdot}$ and other oxygen radicals that, together with lysosomes, are responsible for the killing of the engulfed microorganisms.

The importance of neutrophils in fighting bacterial and fungal infections is well recognized. It has also been shown that neutrophils are involved in viral infections (Fujisawa et al., 1987; Tsuru et al., 1987), though the response of neutrophils is not triggered by endotoxins that are generally secreted by bacteria. Viruses such as influenza can be inactivated by neutrophils through damage to viral proteins (e.g., hemagglutinin and neuraminidase) mediated by myeloperoxidase during the acute phase of infection (Hartshorn et al., 1990). While, in contrast, chronic virus infections can diminish or exhaust the microbicidal potency of neutrophils (Colamussi et al., 1999).

Despite their essential role in host defense, neutrophils have also been implicated in the pathology of many chronic inflammatory conditions and ischemia-reperfusion injury (Liu and Pope, 2004). In addition to hydrolytic enzymes, the host tissue damage is largely attributable to free radicals released by neutrophils, which will be reviewed later.

Table 2. Important enzymes and other constituents in human neutrophil granules (adapted from Stvrtionva et al., 1995)

Constituents	**Granules**		
	Azurophil	**Specific**	**Small storage**
Antimicrobial	Myeloperoxidase Lysozyme Defensins BPI	Lysozyme Lactoferrin	
Neutral Proteinases	Elastase Cathepsin G Proteinas 3	Collagenase Complement activator	Gelatinase Plasminogen activator
Acid hydrolases	Cathepsin B Cathepsin D β-D-Glucuronidase α-Mennosidase Phospholipase A_2	 Phospholipase A_2	Cathepsin B Cathepsin D β-D-Glucuronidase α-Mennosidase
Cytoplasmic membrane receptors		CR3, CR4 FMLP receptors Laminin receptors	
Others	Chondroitin-4-sulphate	Cytochrome b558 Monocytoe-chemo-tactic factor Histaminase Vitamin B12 binding protein	Cytochrome b558

Mononuclear Phagocytes (Monocytes and Macrophages)

Macrophages are generally a population of ubiquitously distributed mononuclear phagocytes responsible for numerous homeostatic, immunological, and inflammatory processes. Developed from bone marrow precursors, pre-mature macrophages enter the bloodstream as monocytes. Approximately 60% of monocytes are recruited into different tissues where they differentiate into tissue resident macrophages, while the rest presumably stay in the circulation and can further mature to inflammatory macrophages that are present in various exudates (van Furth, 1992).

Macrophages are heterogeneous, differing in their site of location, morphology and function (reviewed in Takahashi et al., 1996). The presence of functionally distinct macrophage populations gives the nonspecific immune system added flexibility in responding to various immunological or inflammatory stimuli. It is hypothesized that the nature of an immune response is dictated in large part by the functional phenotype(s) of the macrophages present within the lesion (Naito et al., 1996). Evidence supporting this hypothesis includes the existence of distinct subsets of helper T lymphocytes, suggesting that the predominance of Th1 (IFN-γ and IL-2 producing) or Th2 (IL-4 and IL-10 producing) cells may, in turn, favor the production or activation of a particular macrophage subset (Ma et al., 2003). For example, IFN-γ rapidly primes macrophages via JAK1/2-STAT1 pathway so that it can subsequently undergo a slower classical type 1 activation upon exposure to T helper (Th) 1 cytokines such as IFN-γ or other activators, including tumor necrosis factor and lipopolysaccharide (Ma et al., 2003).

Macrophage activation is a physiological process of phenotypic change in response to a variety of stimuli. Two stages delineate the activation of macrophages: a primed stage and a

fully activated stage. IFN-γ is a product of stimulated Th1 and Th0 cells and acts as priming agent. Many agents can provide the full activation signal, including LPS, heat-killed gram-positive bacteria, yeast glucans, and other molecules (Nacy and Meltzer, 1991). Activated macrophages distinguish themselves by their high oxygen consumption (through NADPH oxidase), killing of facultative and intracellular parasites, and maximal secretion of mediators of inflammation such as TNF-α, PGE_2, IL-1, IL-6, ROS, and $NO^{\bullet}$, as summarized in Table 3 (Goerdt et al., 1999). Interestingly, activated macrophages can also be deactivated by some cytokines, such as TGF-β and IL-4 (Bogdan and Nathan, 1993), which adds another dimension to the complexity of macrophage-mediated inflammatory process.

Table 3. Effecter and regulatory products of macrophages (adapted from Stvrtionva et al., 1995)

Group of substances	Individual products
Microbicidal and cytotoxic	
Reactive oxygen species (ROS)	Superoxide ($O_2^{\bullet}$), hydrogen peroxide (H_2O_2), hydroxyl radical ($OH^{\bullet}$), hypohalite, chloramines
Reactive nitrogen species (RNS)	Nitric oxide ($NO^{\bullet}$), nitrites, nitrates
Oxygen independent	Neutral proteases, acid hydrolases, lysozyme, defensins
Tumoricidal	H_2O_2, $NO^{\bullet}$, TNF-α, C3a, proteases, arginase, thymidine
Tissue damaging	H_2O_2, $NO^{\bullet}$, TNF-α, C3a, neutral proteases
Fever inducing	
Pyrogenic cytokines	IL-1, TNF-α, IL-6
Inflammation regulators	
Bioactive lipids	Prostaglandins (PGE_2, PGF_2a), prostacyclin (PGI_2), tromboxans, leukotrienes (LTB_4, LTC_4, LTD_4, LTE_4)
Bioactive oligopeptides	Glutathione
Complement components	C1, C4, C2, C3, C5, factors B, D, P, I, H
Clothing factors	V, VII, IX, X, prothrombin, plasminogen activator, plasminogen activator inhibitors
Cytokines	IL-1, IL-6, IL-8, TNF-α, INF-γ Macrophage inflammatory proteins (MIP-1, 2, 3) Regulatory growth factors (M-CSF, GM-CSF, g-csf, PDGF)
Neural proteinases	Elastase, collagenase, angiotensin covertase, stromelysin
Protease inhibitors	α_2-Macroglobulin, α-1-proteinase inhibitor, plasmin and collagenase inhibitors, plasminogen activator inhibitors
Acid hydrolases	Acid proteases (cathepsin D and L), peptidases, lipases, lysozyme and other glycosidases, ribonucleases, phosphatases, sulphatases
Stress proteins	Heat shock proteins (HSP)
Participating in tissue reorganization	Elastase, collagenase, hyaluronidase, regulatory growth factors, fibroblast growth factor (FGF), transforming growth factors (TGF-α, TGF-β), angiogenesis factors
Others:	Apolipoprotein E, IL-1 inhibitors, purine and pyrimidine derivates (thymidine, uracil, neopterin)

B. Reactive Chemical Species Produced at Sites of Inflammation

Inflammation induces and activates various oxidant-generating enzymes to produce a constellation of reactive intermediates that can be broadly classified into three categories: reactive oxygen species (ROS), reactive halogen species (RHS), and reactive nitrogen species (RNS). In some publications, the first two have been collectively called ROS.

Many factors influence the formation of reactive species. Generally, the level of a particular species produced *in vivo* is best viewed in terms of the steady-state concentration that reflects a balance of its production, diffusion and consumption. Those species are important components of the host defense system, but their sustained production and presence during chronic inflammation induce collateral damage in adjacent normal tissue, which contributes to a range of diseases. In many cases, the initially generated reactive intermediates convert cellular constituents into second-generation reactive intermediates capable of inducing further damage.

Reactive Oxygen Species (ROS)

Reactive oxygen species (ROS) are formed in neutrophils and macrophages through a process known as the respiratory burst, during which, oxygen is univalently reduced by NADPH oxidase to superoxide anion ($O_2^{\bullet-}$) or its protonated form, perhydroxyl radical ($HO_2^{\bullet}$). The resulting $O_2^{\bullet-}$ is then catalytically converted by superoxide dismutase (SOD) to hydrogen peroxide (H_2O_2) that is further decomposed by catalase to H_2O and O_2 or by divalent metals (e.g., Fe^{2+}) to HO^- and $HO^{\bullet}$ (Figure 1) (reviewed in Dedon and Tannenbaum, 2004). $O_2^{\bullet-}$ is both a one-electron reductant and a one-electron oxidant that can pass through cell membrane *via* anion channels (Auchere and Rusnak, 2002). The redox potentials of $O_2^{\bullet-}$, H_2O_2, and $HO^{\bullet}$ dictate that,

in thermodynamic terms, they are all much stronger univalent oxidants than dioxygen (Figure 2). However, the anionic charge of $O_2^{\bullet}$ inhibits its effectiveness as an oxidant of electron-rich molecules, while the reactivity of H_2O_2 is diminished by the stability of its oxygen-oxygen bond. Neither of these features applies to the $HO^{\bullet}$, and indeed $HO^{\bullet}$ reacts at virtually diffusion-limited rates with most biomolecules (Imlay, 2003).

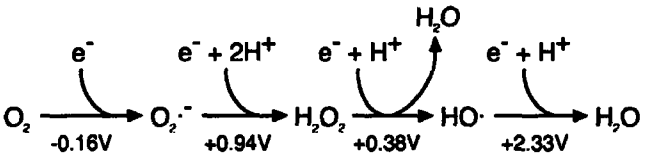

Figure 2. Redox potentials of oxygen species. 1 M dioxygen is used as the standard state for the first step (adapted from Imlay, 2003).

Singlet oxygen ($^1O_2$) is an excited form of dioxygen in which the *pi* antibonding electrons are spin-paired. It can be formed by energy transfer to oxygen by excited chromophores in stimulated phagocytes during respiratory burst. As reviewed by Klotz *et al.*, $^1O_2$ has damaging effects on biomolecules and exerts genotoxic, virucidal and cytotoxic effects (Klotz et al., 1997).

Reactive Halogen Species (RHS)

Myeloperoxidase (MPO) is an enzyme found in high abundance in the azurophil granules of neutrophils and it catalyzes the H_2O_2-mediated oxidation of halides to form the so-called reactive halogen species (RHS) including hypochlorus acid, hypobromous acid, and hypoiodous acid (Klebanoff and Rosen, 1978) (equations 1-3). Monocytes lose their MPO activity during the course of maturation. However, macrophages may acquire MPO from environment by pinocytosis or from ingested neutrophils, especially when macrophages are at sites of inflammation (Klebanoff, 1970; Sugiyama et al., 2004), a situation that complicates our understanding of the chemistry of inflammation.

$$Cl^- + H_2O_2 + H^+ \rightarrow HOCl + H_2O \quad (1)$$

$$Br^- + H_2O_2 + H^+ \rightarrow HOBr + H_2O \quad (2)$$

$$I^- + H_2O_2 + H^+ \rightarrow HOI + H_2O \quad (3)$$

RHS are strong oxidizing and halogenating species. For example, HOCl has been shown to mediate lipid peroxidation leading to the formation of genotoxic product 4-hydroxynonenal (HNE) (Spickett et al., 2000). Interestingly, several lines of evidence show that activated human neutrophils convert NO_2^- into the inflammatory oxidant NO_2Cl through MPO-dependent pathways (equation 4), which suggests that NO_2^- may play a role in phagocyte-mediated oxidative reactions at sites of inflammation and infection (Eiserich et al., 1996; Spickett et al., 2000). Further, at physiological or pathological levels, NO_2^- can act as a substrate for MPO and lactoperoxidase (LPO), even in the presence of chloride (Cl^-) and thiocyanate (SCN^-), the proposed major physiological substrates for these peroxidases. Hence, formation of reactive

nitrogen intermediates *via* peroxidase-catalyzed oxidation of NO_2^- could represent an important contributing mechanism to NO•-mediated toxicity (van der Vliet et al., 1997).

$$HOCl + NO_2^- \rightarrow NO_2Cl + HO^- \quad (4)$$

Reactive Nitrogen Species (RNS)

The biosynthesis of NO• is catalyzed by a family of enzymes called nitric oxide synthases (NOS) using L-arginine and O_2 as substrates, with NADPH as an electron donor and using heme, FMN, FAD and tetrahydrobiopterin (H_4B) as cofactors (reviewed in Alderton et al., 2001) (Figure 3). Currently, at least three distinct isoforms of NOS have been identified: endothelial NOS (eNOS, NOS I), inducible NOS (iNOS, NOS II) and neuronal NOS (nNOS, NOS III). nNOS and iNOS are soluble whereas eNOS is membrane bound with a myristoylated N-terminus (Liu et al., 1995). Both eNOS and nNOS are constitutively expressed in resting cells and are activated by calcium and calmodulin (CaM), while iNOS is induced by immunostimulatory cytokines, bacterial products or microbial infection in a number of cell types, including endothelium, hepatocytes, monocytes, mast cells, macrophages and smooth muscle cells (Alderton et al., 2001) (Table 4).

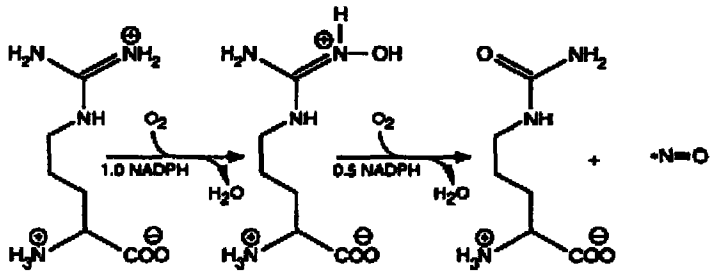

Figure 3. Nitric oxide synthesis catalyzed by nitric oxide synthase (NOS)

NO• can also be produced nonenzymatically from nitrite at low pH under reducing conditions (Samouilov et al., 1998). Nonenzymatic NO• production has been demonstrated in a variety of tissues, including the stomach, skin, ischemic heart, and in infected nitrite-containing urine (Weitzberg and Lundberg, 1998).

Table 4. Isoforms of human NO• synthase and their characteristics

Characteristic	Endothelial NOS (eNOS)	Neuronal NOS (nNOS)	Inducible NOS (iNOS)
MW ($X10^3$)	150-160	150-160	132
Chromosomal location	7q35-36	12q24.2	17q11-12
Ca^{+2} Dependency	Ca^{2+}, calmodulin	Ca^{2+}, calmodulin	Independent
Producing cells	Endothelial	Neurons	Macrophages, monocytes, Kupffer cells, neutrophils, hepatocytes, myocytes, chondrocytes, smooth muscle cells
Inducers	No	No	LPS, TNF-α, IL-1, IFN-γ, GM-CSF
Inhibition by L-arginine analogs	Yes	Yes	Yes
Inhibition by glucocorticoids	No	No	Yes

Reactions of NO•. NO• is a free radical having dramatic reactivity. Stamler *et al.* proposed that important categories of NO• chemistry relative to biological actions are the following three redox–related forms: NO•, nitrosonium ion (NO^+), and nitroxyl anion (NO^-), with the latter two species representing one-electron oxidation and reduction products, respectively (Stamler et al., 1992b). NO• can donate its unpaired electron to some transition metal cations to form complexes, an example of which is the binding to the ferrous ion (Fe_2^+) in deoxyhemoglobin. This direct binding only requires low concentrations of NO• (nanomolar) and is involved in the regulation of vascular tone, neuronal function and biosynthesis of iron-binding-protein (Moncada et al., 1991).

Interaction of NO• with O_2, or $O_2^{\bullet-}$ generates a variety of reactive species, including NO_2, N_2O_3, N_2O_4, and $ONOO^-$, which are collectively referred to as reactive nitrogen species (RNS) and are capable of reacting with a wider range of biomolecules than NO• itself. It is commonly believed that formation of RNS becomes significant only at higher (micromolar) concentrations of NO• (Wink and Mitchell, 1998).

Oxidation of NO• forms higher nitrogen oxides such as NO_2, N_2O_3 (equations 5-6; k_1 and k_2 are $2.1 \times 10^6\ M^{-2}s^{-1}$ and $1.1 \times 10^9 M^{-1}s^{-1}$, respectively). Current evidence suggests that N_2O_3 is the predominant species in aqueous media (Ford et al., 1993; Espey et al., 2001). In the absence of other reactive species, N_2O_3 is hydrolyzed to form nitrite (equation 7) (Lewis et al., 1995b). Based on these equations, the half-life of NO• in an oxygenated solution is dependent on the initial NO• concentration and inversely proportional to its concentration. The NO• and O_2 concentration-dependent kinetics of N_2O_3 formation suggest that the rate of NO• oxidation will vary as a function of the hydrophobicity of the solvent, since NO• and O_2 will partition such that their levels in lipid membranes and hydrophobic cellular regions will be ~10-fold greater than

those in the aqueous cytosol. This prediction is consistent with the observation of Liu *et al.* that a 300-fold increases in NO$^{\bullet}$ autoxidation was found in the presence of detergent micelles (Liu et al., 1998).

$$2NO + O_2 \xrightarrow{k1} 2NO_2 \quad (5)$$

$$NO + NO_2 \underset{k-2}{\overset{k2}{\rightleftharpoons}} N_2O_3 \quad (6)$$

$$N_2O_3 + H_2O \xrightarrow{k3} 2NO_2^- + 2H^+ \quad (7)$$

In contrast, simultaneous generation of NO$^{\bullet}$ and $O_2^{\bullet-}$ leads to the formation of $ONOO^-$ at nearly diffusion controlled rates (equation 8; k_4 is 6.6-19 x 10^9 $M^{-1}s^{-1}$) (Huie and Padmaja, 1993; Kissner et al., 1997). Maximal $ONOO^-$ formation was found when the rates NO$^{\bullet}$ and $O_2^{\bullet-}$ generation are approximately the same (Miles et al., 1996). With widely differing NO$^{\bullet}$ and $O_2^{\bullet-}$ concentrations, $ONOO^-$ preferentially reacts with either substrate to form NO_2, thereby reducing the overall extent of $ONOO^-$ formation (equations 9 and 10). As discussed previously, NO_2 can be further oxidized to form N_2O_3, which can also react with $ONOO^-$ to form $NO_2^{\bullet}$ (Goldstein et al., 1999) (equation 11).

$$NO + O_2^- \xrightarrow{k4} ONOO^- \quad (8)$$

$$ONOO + NO \longrightarrow NO_2 + NO_2^- \quad (9)$$

$$ONOO + O_2^- + H^+ \longrightarrow NO_2 + O_2 + H_2O \quad (10)$$

$$N_2O_3 + ONOO^- \longrightarrow ONOONO + NO_2^- \quad (11)$$

In the absence of NO$^{\bullet}$, or $O_2^{\bullet-}$, the decomposition of $ONOO^-$ can be catalyzed by either a proton or CO_2. Several lines of evidence suggest that in the absence of CO_2, a proton-catalyzed

pathway yields $^{\bullet}OH$ and $^{\bullet}NO_2$, whereas in the presence of CO_2, $CO_3^{\bullet-}$ and $^{\bullet}NO_2$ results via the formation and decomposition of nitrosoperoxycarbonate ($ONOOCO_2$) (Figure 4) (Denicola et al., 1996; Goldstein et al., 1998; Lymar and Hurst, 1998; Merenyi et al., 1998).

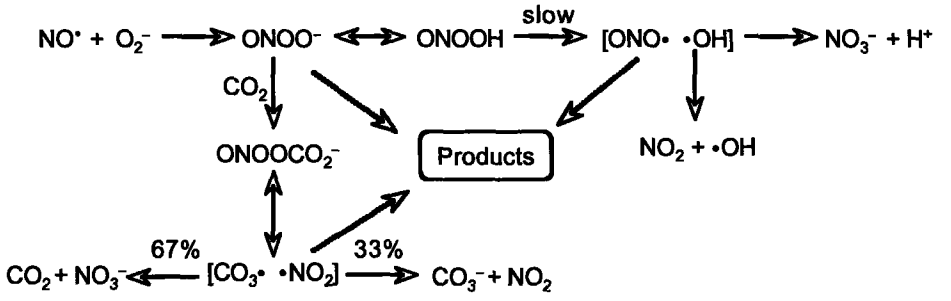

Figure 4. Reactive species produced during peroxynitrite decomposition

Nitrosonium Cation (NO^+). NO^+ can exist in aqueous media, but a major manifestation of an NO^+ equivalent in biological environments is in the forms of nitroso compounds (Stamler et al., 1992b). Nitroso compounds can be made chemically through the reaction of sodium nitrite and a nucleophile in the presence of acid. However, biological production of nitroso compounds mainly occurs in the direct reactions of NO_2 or N_2O_3, two species derived from $NO^{\bullet}$, with nucleophiles (equations 12 and 13) (Stamler et al., 1992b). S-Nitrosothiols are nitroso compounds that are regarded as $NO^{\bullet}$ carriers due to the spontaneous $NO^{\bullet}$ release through homolytic cleavage (Ng et al., 2004).

$$NO_2 + RSH \longrightarrow RSNO + H_2O \quad (12)$$

$$N_2O_3 + RSH \longrightarrow RSNO + HNO_2 \quad (13)$$

Nitroxyl Anion (NO^-). NO^- is a much stable form of $NO^\bullet$ and formed biologically either through a 4-electron oxidation of the guanidino nitrogen in arginine by NOS (Fukuto et al., 1992) or in reactions of thiols with nitrosotiols (Wong et al., 1998). The physiological significance of NO^- is largely undefined. However recent studies suggest that NO^- and its protonated form, HNO, may play an important role in biology and pharmacology. Unlike $NO^\bullet$, HNO appears to increase levels of cyclic adenosine monophosphate (cAMP) (Miranda et al., 2003b). HNO can be generated from Angeli's salt (NaN_2O_3) (equation 14) and prefers to react with ferric heme, as opposed to the favored reaction of $NO^\bullet$ with ferrous heme (Miranda et al., 2003a). Strong cytotoxicity was observed for HNO released from Angeli's salt (Wink et al., 1998), possibly due to the production of $HO^\bullet$ (Ohshima et al., 1999) or $ONOO^-$ (Kirsch and de Groot, 2002).

$$HN_2O_3 \longleftrightarrow HNO + NO_2^- \qquad (14)$$

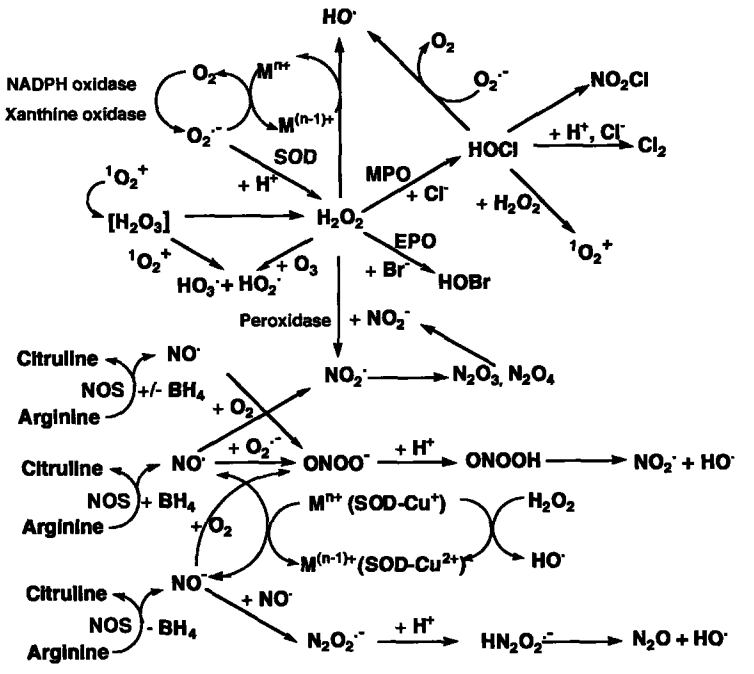

Figure 5. Production of ROS and RNS by various oxidant-generating enzymes. New potent oxidants are also formed by interactions of $NO^{\bullet}$, $O_2^{\bullet-}$, H_2O_2, and HOCl. SOD, superoxide dismutase; MPO, myeloperoxidase; and EPO, eosinophil peroxidase (adapted from Ohshima et al., 2003).

Electrophiles Derived from Reactions of RNS with Biomolecules.

The activation of inflammatory cells leads to the formation of a variety of RNS and ROS. While these reactive species can alter cell function by directly damaging cellular molecules, these reactions also lead to the generation of electrophilic species capable of causing damage themselves as shown in Figure 5) (revised in Dedon and Tannenbaum, 2004; Ridnour, *et al.*, 2004, Ohshima, *et al.*, 2003).

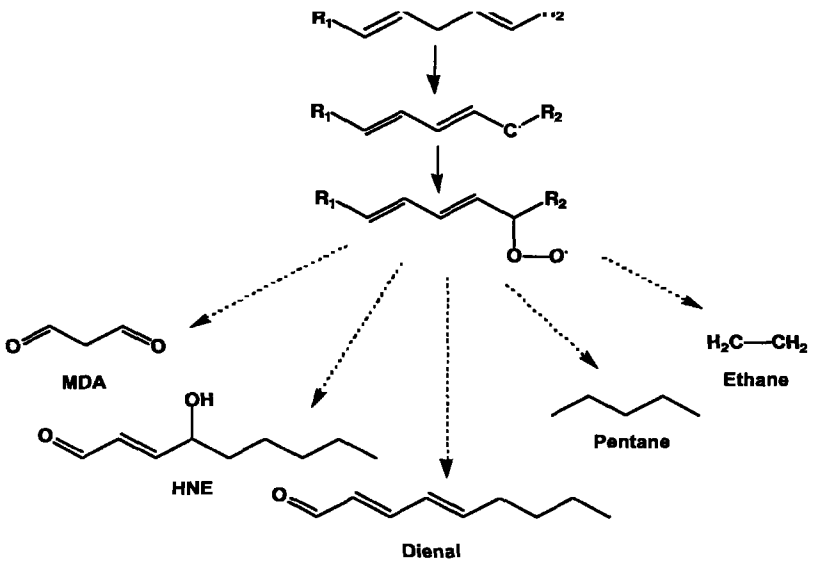

Figure 6. Chemistry of lipid peroxidation. MDA represents malondialdehyde; HNE represents 4-hydroxy-2-nonenal

A well-established example is lipid peroxidation (Figure 6). Polyunsaturated fatty acids (PUFA) in phospholipids, cholesterol esters, and triglycerides are very sensitive to oxidation by $OH^{\bullet}$ and $ONOO^{-}$, leading to a complex series of reactions that ultimately generate a range of electrophilic derivatives. The major products are α,β-unsaturated aldehydes that are capable of reacting with proteins and nucleic acids (Marnett et al., 2003). Among the various 4-hydroxy-2-alkenals that represent the most prominent aldehyde substances generated during lipid peroxidation, 4-hydroxy-2-nonenal (HNE) is the major product and can accumulate in membranes to concentrations of 10 to 50 μM in response to oxidative insults (Esterbauer et al., 1991). Other important reactive aldehydes are ketoaldehydes, including malondialdehyde (MDA). MDA is in many instances the most abundant individual aldehyde resulting from lipid peroxidation and has been shown to disturb the organization erythrocyte membranes (Jain, 1984).

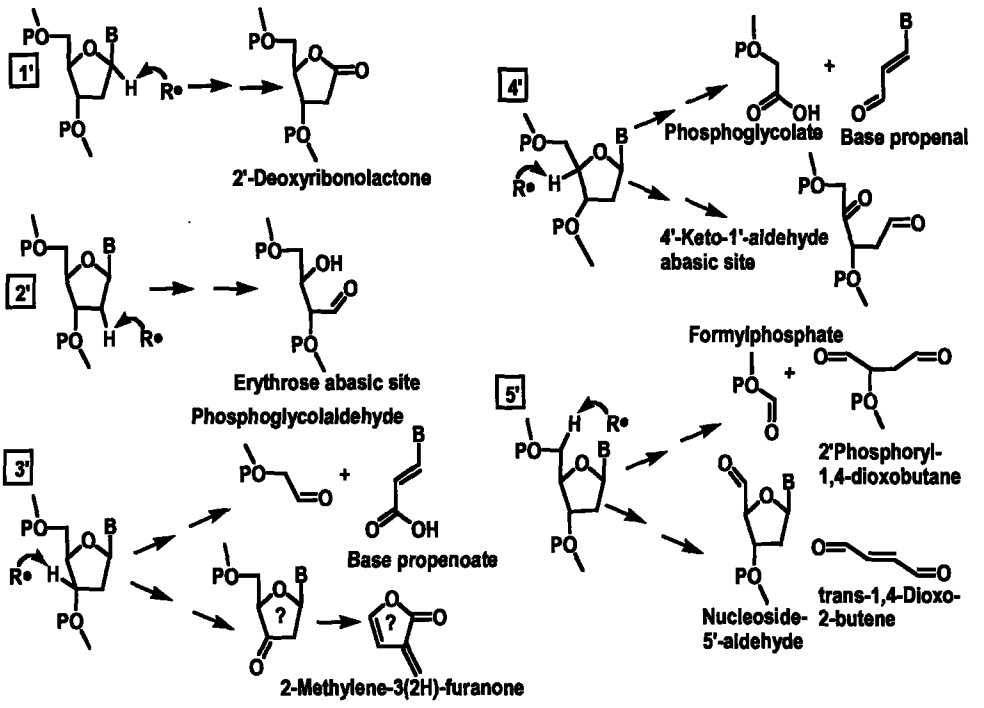

Figure 7. Reactive electrophiles produced by oxidation of deoxyribose

Oxidation of deoxyribose in DNA results in the formation of a variety of electrophilic products (reviewed in Pogozelski and Tullius, 1998) (Figure 7), many of which have the potential to react with nucleobases to form adducts. For instance, base propenals are produced by oxidation of the 4'-position in deoxyribose by reagents such as bleomycin, peroxynitrite, and chromium (V) (Giloni et al., 1981; Sugden and Wetterhahn, 1997; Yermilov et al., 1996). These structural analogues of MDA react with dG to form the pyriminopuranone adduct, M_1G, which is present as an endogenous DNA adduct in human tissues (Chaudhary et al., 1994a). Another example is the formation of the diastereomeric 1,N2-glyoxal adducts of dG by glyoxal derived from 3'-phosphoglycolaldehyde residues that arise by 3'-oxidation of deoxyribose in DNA (Awada and Dedon, 2001). Finally, novel diastereomeric oxadiazabicyclo (3.3.0) octaimine

adducts of dC, dG and dA arise in reactions of DNA with *trans*-1,4-dioxo-2-butene, a product of 5'-oxidation of deoxyribose in DNA (Bohnert et al., 2004; Chen and Chung, 1996).

Amino acid oxidation is another source of forming reactive aldehydes. It has been shown that *in vitro* oxidation of free hydroxy-amino acids with myeloperoxidase in the presence of H_2O_2 and chloride ions generates reactive aldehydes, such as acrolein, via the formation of 2-hydroxypropanal (Anderson et al., 1997). The myeloperoxidase-dependent amino acid oxidation as a source of reactive aldehydes has been reviewed by Anderson *et al.* (Anderson et al., 1997) (Figure 8).

In summary, various secondary reactive intermediates are generated from oxidation of lipids, deoxyriboses, and amino acids. Compared to free radicals, these secondary reactive species are relatively stable and can diffuse within cells or even escape from cells to attack targets far from the site of the original event. Therefore, they are not only end products, but also act as "second cytotoxic messengers" for the primary reactions.

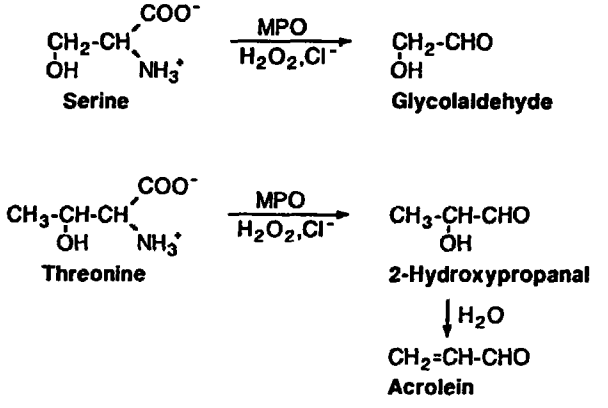

Figure 8. Reaction pathway for the generation of α-hydroxy and α,β-unsaturated aldehydes from hydroxy-amino acids by myeloperoxidase (MPO) (adapted from Anderson et al., 1997; Cadet et al., 2003).

1.4 Genotoxicity of Reactive Nitrogen Species

Chronic inflammation has been shown to predispose individuals to cancer (Ohshima and Bartsch, 1994). The process of chemical carcinogenesis is currently viewed as a series of steps involving both mutation and increased cell proliferation. Important to carcinogenesis *via* the inflammatory process is the unregulated or prolonged production of cellular toxins. Over the past decade, there has been significant progress in defining the products arising in the reactions of DNA and other cellular molecules with agents generated by inflammatory cells (Dedon and Tannenbaum, 2004). In this section of the thesis, the genotoxicity of RNS with regard to the direct genotoxicity by N_2O_3, $ONOO^-$ and NO^-, and the indirect genotoxicity due to activation of nitrosamines, lipidoxidation-induced DNA damage, inhibition of DNA repair enzymes, will be reviewed. Epigenetic modification by RNS will also be addressed.

A. DNA Damage by Reactive Nitrogen Species

Direct DNA Damage

Direct damage to DNA by RNS is governed by essentially three chemical processes: deamination, oxidation and nitration (Burney et al., 1999; Dedon and Tannenbaum, 2004; Tamir et al., 1996). One of the key questions in the *in vivo* chemical biology of inflammation is which chemical process, if any, predominates.

Nucleobase Deamination. Deamination of primary amines *in vivo* is mediated primarily by the nitrosative chemistry of N_2O_3, a derivative of $NO^{\bullet}$ and O_2 (Lewis et al., 1995a; Wink et al., 1996). Nitrosative chemistry also occurs through oxidative nitrosylation, which involves oxidation of amines to their corresponding radicals by oxidants such as $ONOO^-$, followed by rapid coupling with $NO^{\bullet}$ (Espey et al., 2002). *N*-Nitrosation of a primary amine initially produces a nitrosamine, which is quickly followed by the replacement of NH_2 group with HO^- group. In this way, nitrosation of exocyclic amines in DNA nucleobases results in the conversion of cytosine to uracil (dU in nucleoside form), guanine to xanthine (dX in nucleoside form) and oxanine (dO in nucleoside form), methylcytosine to thymine (dT in nucleoside form), and adenine to hypoxanthine (dI in nucleoside form), and abasic sites, as well as inter- or intra strand cross-links (Figure 9).

Several lines of evidence have demonstrated the formation of base deamination products following $NO^{\bullet}$ exposure. As discussed earlier, prolonged exposure of nucleic acids to $NO^{\bullet}$ gas resulted in nucleobase deamination (Caulfield et al., 1998; Merchant et al., 1996; Nguyen et al., 1992; Wink et al., 1991), while exposure of whole cells to $NO^{\bullet}$ gas or $NO^{\bullet}$-releasing drugs also

led to significant increases in base deamination products (Grishko et al., 1999; Nguyen et al., 1992). Similar results were found in activated macrophages (deRojas-Walker et al., 1995). The observation of single strand breaks in cellular DNA following NO$^{\bullet}$ exposure was originally attributed to the depurination of dX (deRojas-Walker et al., 1995; Nguyen et al., 1992), but later studies demonstrated that dX was a relatively stable lesion (Vongchampa et al., 2003). Other factors, such as DNA repair and the presence of $ONOO^-$ chemistry *in vivo* were likely the real causes of the DNA strand breaks (Spek et al., 2002; Spek et al., 2001). Furthermore, adjacent guanines can cross-link by an N_2O_3-mediated conversion of the amine on one guanine to a diazonium ion, followed by the attack of the exocyclic amine of the neighboring dG (Caulfield et al., 2003).

Nucleobase Oxidation. The oxidative chemistry associated with RNS is mediated primarily by $ONOO^-$ with additional contributions from $NO_2^{\bullet}$ (Burney et al., 1999; Dedon and Tannenbaum, 2004; Szabo and Ohshima, 1997). In addition to DNA strand breaks, $ONOO^-$ and its CO_2 adduct, $ONO_2CO_2^-$, react preferentially with dG due to its low oxidation potential relative to the other bases (Figure 10). The reaction with dG produces several primary oxidation products including 8-oxo-dG, 5-guanidino-4-nitroimidazole (NitroIm), 2,2–diamino–4–{(2-deoxypentofuranosyl) amino}-5(2H)–oxazolone (oxazolone; OZ), and 8-nitro-dG as shown in Figure 11.

There are several important features of $ONOO^-$-mediated DNA damage. The first is the ability of $ONOO^-$ to oxidize 8-oxo-dG due to its low redox potential. As shown in Figure 12, the resulting collection of secondary oxidation products has been well characterized by several groups (Niles et al., 1999; Niles et al., 2000). The second issue involves the roles of $ONOO^-$

concentration and delivery rate on the chemistry of 8-oxo-dG oxidation, which changes in the spectrum of lesions with changes in the $ONOO^-$ flux. As the $ONOO^-$ flux is lowered, for instance when switching from bolus addition to infusion, or to SIN-1-mediated *in situ* $ONOO^-$ production, spiroiminodihydantoin (Sp) formation increases largely at the expense of {3-(2-deoxy-b-D-erythro-pentofuranosyl)-2,5-dioxo-4-imidazolidinylidene}-guanidine (DGh) (Dedon and Tannenbaum, 2004) (Figure 12). The final issue relates to the effect of CO_2 on the chemistry of $ONOO^-$-induced DNA damage. The presence of CO_2 caused a shift from deoxyribose oxidation to base oxidation and nitration with little change in the total number of lesions (Kennedy et al., 1997).

Nucleobase Nitration. $ONOO^-$ and $ONO_2CO_2^-$ have been shown to react with DNA to form nitrated nucleosides, the most abundant of which involves nitration of dG to 8-nitro-dG (Burney et al., 1999; Tretyakova et al., 1999; Yermilov et al., 1995a). 8-Nitro-dG is unstable and undergoes depurination with a half-life of a few hours to form an abasic site. In the presence of bicarbonate, a significant portion of base damage consists of 8-nitro-dG (Yermilov et al., 1995a; Yermilov et al., 1995b). Alternatively, 8-nitro-dG may decompose by reaction with another equivalent of ONOOH to form 8-oxo-dG (Lee, J.M, 2002). 8-Nitro-dG has been proposed as a biomarker for $ONOO^-$-mediated DNA damage since it was assumed to form only by $ONOO^-$, but not nitrous acid, tetranitromethane or $NO^{\bullet}$-releasing compounds (Yermilov et al., 1995a; Yermilov et al., 1995b). However, new sources of 8-nitro-dG formation have been identified. For example, Byun *et al.* reported its formation from the reaction of dG with nitryl chloride (NO_2Cl) and/or nitrogen dioxide radical ($NO_2^{\bullet}$) that are produced in activated phagocytes at sites of inflammation (Figure 13) (Byun et al., 1999). Nitryl chloride is capable of nitrating guanine,

tyrosine, and lipids as well as chlorinating and oxidizing tyrosine (Byun et al., 1999; Eiserich et al., 1996; Schmitt et al., 1999). Suzuki and co-workers reported formation of 8-nitro-dG in reactions of dG with an $NO^{\bullet}/O_2$ gas mixture under physiological conditions (Suzuki et al., 1999). Under the same condition, Yamada and co-workers identified a new guanine nitration product, N_2-nitro-2'-deoxyguanosine (Figure 14) (Yamada et al., 2003).

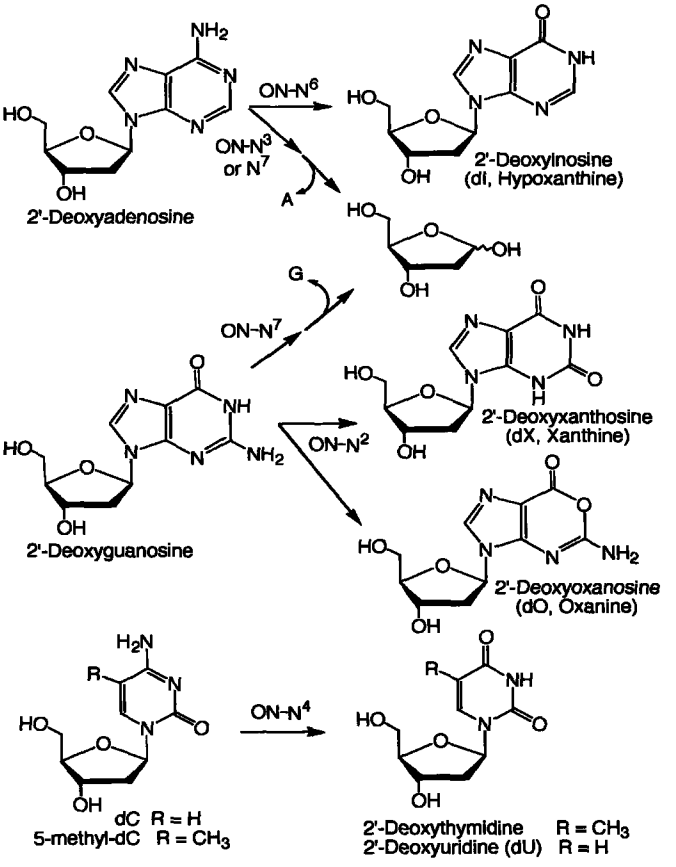

Figure 9. Products of N-nitrosative nucleobase deamination

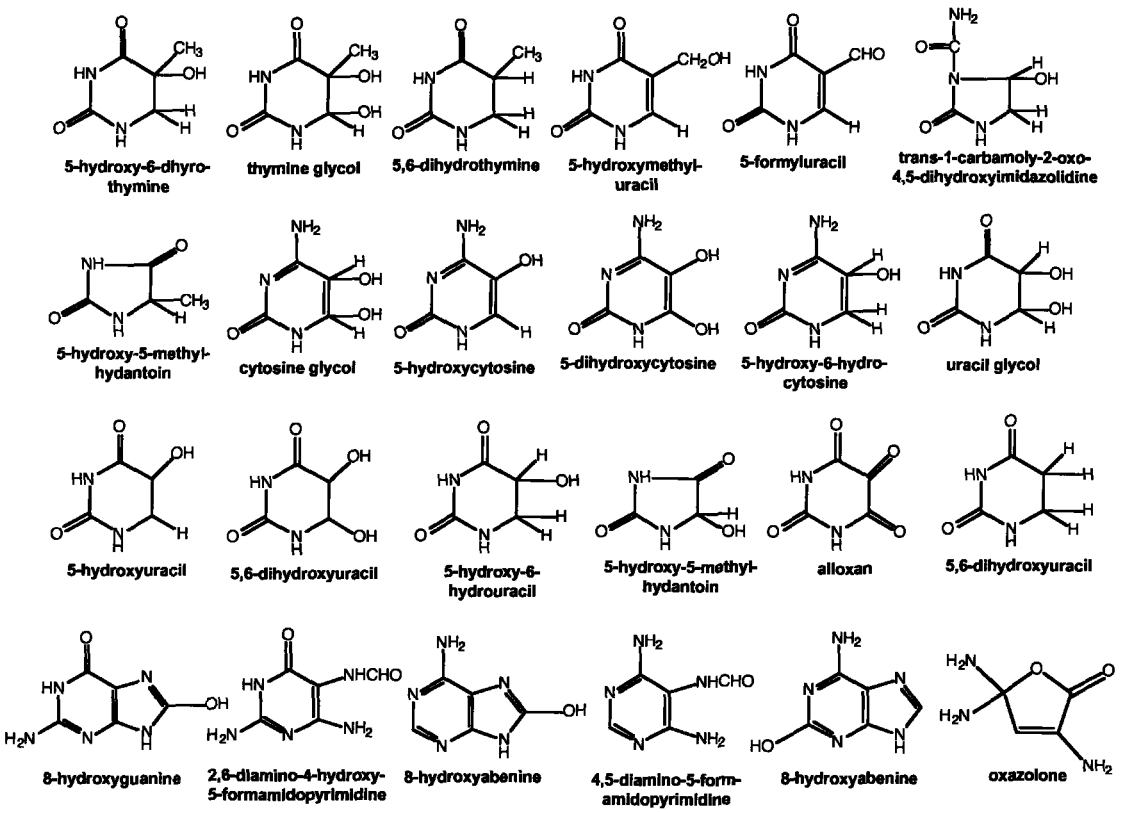

Figure 10. Structures of typical DNA base modifications caused by ROS and RNS (adapted from Ohshima et al., 2003; and Cadet et al., 2003)

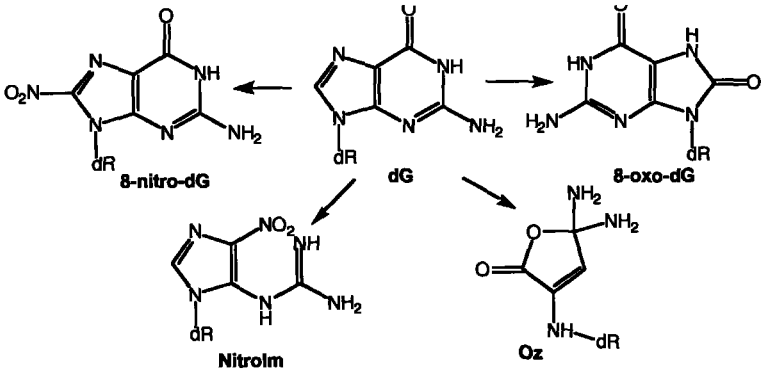

Figure 11. Oxidation products from the reaction of dG with $ONOO^-$ (Primary oxidation products; adapted from Dedon and Tannenbaum, 2004)

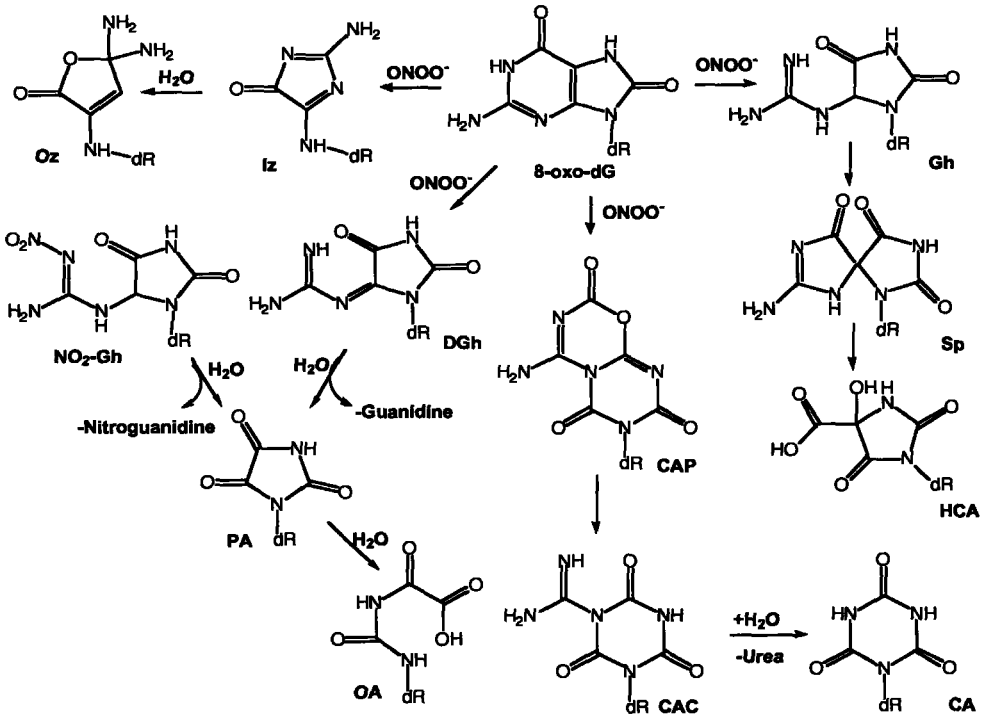

Figure 12. Oxidation products of dG reaction with $ONOO^-$ (Secondary oxidation products; adapted from Dedon and Tannenbaum, 2004)

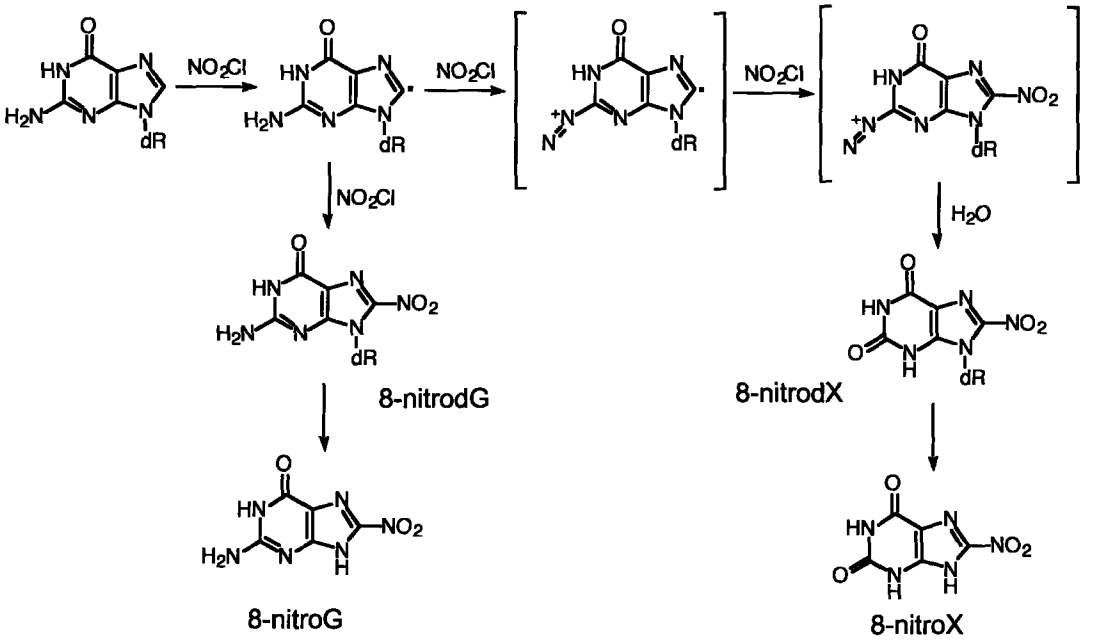

Figure 13. Formation of 8-nitro-dG and 8-nitro-dX from the reaction of dG and nitryl chloride (NO_2Cl) (adapted from Byun et al., 1999; and Cadet et al., 2003).

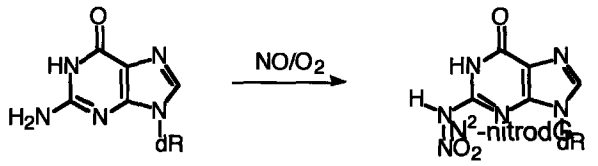

Figure 14. Formation of N^2-nitro-2'-deoxyguanosine (N^2-nitrodG) from the reaction of dG with $NO^{\bullet}/O_2$ (adapted from Yamada et al., 2003)

Indirect DNA Damage

Indirect DNA damage is mediated by electrophiles arising from reactions of RNS and ROS with proteins, carbohydrates, lipids and, in some cases, nucleic acids themselves. Perhaps the best-characterized examples of indirect DNA damage come from studies of lipid peroxidation and deoxyribose oxidation. As discussed earlier, lipid peroxidation gives rise to a variety of α,β-unsaturated aldehydes and diketo compounds (Figure 6) that can react with the heterocyclic and exocyclic nitrogens of DNA nucleobases to form mono- and bis-adducts. For example, hydroxyalkenals can react directly with DNA nucleobases to form propano and ethano adducts as shown in Figure 15. Those hydroxyalkenals can be further oxidized to form epoxides of the hydroxyalkenals and subsequently react with DNA nucleobases to form the unsaturated etheno adducts as shown in Figure 16 (Chen and Chung, 1996; Chung et al., 1996). Etheno adducts have been detected in a variety of human tissues and animal models. Formation of ε-dA and ε-dC occurred in the SJL-mouse model as a consequence of $NO^{\bullet}$ overproduction after injection of RcsX (pre-B lymphoma) cells (Nair et al., 1998b). Compared to the controls, the SJL/RcsX mice showed ~6-fold increases in the levels of etheno-adducts of dA and dC in the spleen DNA. Etheno adducts of DNA nucleobases were also found to be elevated in tissues of cancer-prone patients and rodents (liver, pancreas, colon) as a consequence of persistent oxidative stress, which suggests that promutagenic etheno-adducts, among other oxidative damage, could drive cells to malignancy (Nair et al., 1997; Schmid et al., 2000b). In the cases of patients, the products generated are mainly the known cyclic pyrimidopurinone (M_1G) and acyclic adducts formed with deoxyadenosine (M_1A) and deoxycytidine (M_1C) for the MDA reactions (Stone et al., 1990; Winter et al., 1986; Yi et al., 1997) (Figure 15).

Another example involves adduct formation of MDA, a product of lipid peroxidation, and its structural analogs, the base propenals, which are derived from the oxidation of deoxyribose in DNA. Both MDA and base propenals can react with dG to form the exocyclic pyrimidopurinone adduct, M_1G (Dedon et al., 1998; Marnett, 2002a). This adduct has been detected in the livers of 6-week-old rats at the level of ~ 6 lesions per 10^7 nt and in comparable levels in human (Chaudhary et al., 1994b), but the level of M_1G in 2-year-old rats is nearly double (Chaudhary et al., 1994b). The central question now is which species, MDA or base propenals, is responsible for the formation of M_1G *in vivo*. Base propenals have been shown to be more reactive and mutagenic than MDA (Plastaras et al., 2000). Recent studies by Zhou and Dedon showed increased level of M_1G even in cells that lack polyunsaturated fatty acids (PUFA) in cell membrane following exposure to $ONOO^-$, which suggests that base propenals may be critical for the formation of M_1G in DNA (manuscript submitted). This observation implies that products derived from direct DNA oxidation may be an important source for DNA damage.

This review of direct and indirect DNA damage produced by ROS and RNS highlights the complexity of inflammation-induced damage that could be encountered in animal models and human tissues. One of the goals of the research undertaken in this thesis is to resolve this complexity by developing sensitive analytical methods to quantify DNA lesions hypothesized to arise at sites of inflammation. Application of this method to studies in cell and animal models should provide important insights into understanding the relationship between DNA damage and mutations associated with cancer formation at sites of inflammation. The issue of mutations is addressed next.

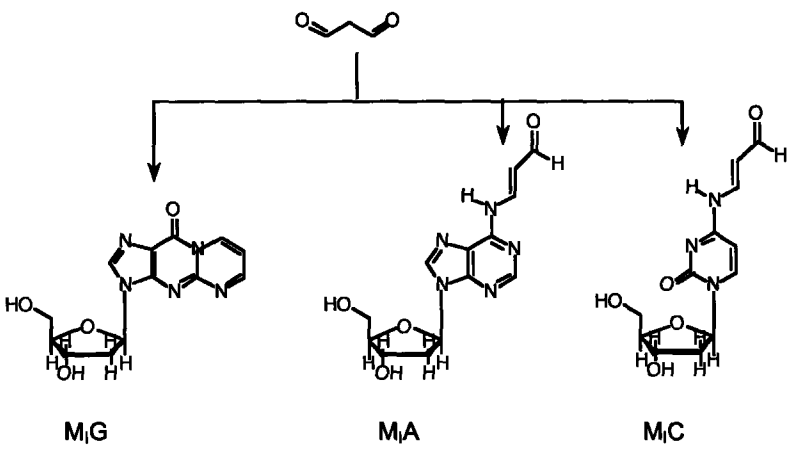

Figure 15. Structures of MDA adducts of dG, dA and dC

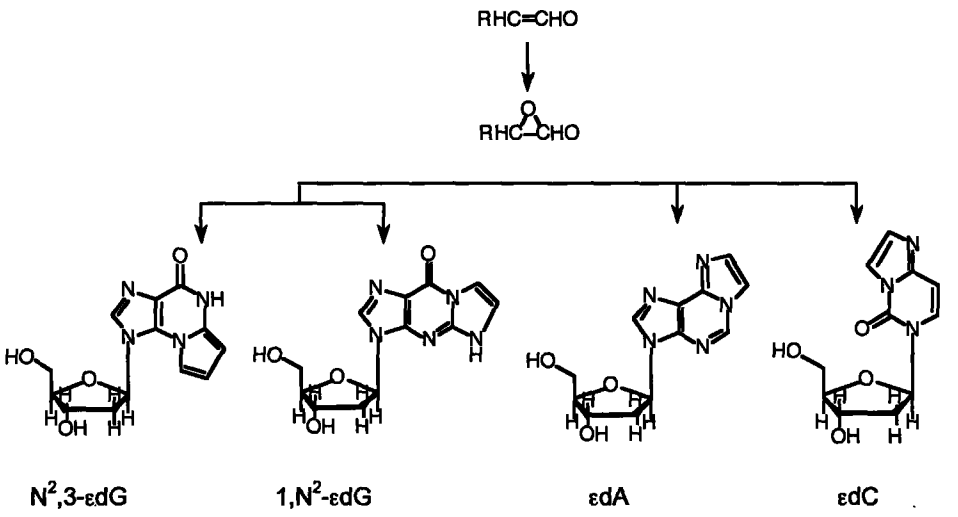

Figure 16. Structures of etheno adducts of dG, dA and dC formed upon reaction of oxidized α,β-unsaturated aldehydes with DNA bases

B. Mutations and Mechanisms of Mutagenesis Associated with Reactive Nitrogen Species

DNA lesions formed by RNS have the potential to cause mutations, with numerous studies have demonstrating the mutagenicity of exposure to both exogenous and endogenous NO•. Mutations in the *supF* gene in plasmid pSP189 by *in vitro* treatment with NO• gas, NO• donor drugs, or peroxynitrite were characterized at the molecular level (Juedes and Wogan, 1996; Routledge et al., 1994). NO• gas is mutagenic in *Salmonella typhimurium* and human lymphoblastoid cells (Zhuang et al., 2000), with a mutation spectrum that is characterized mainly by G:C → A:T and A:T → G:C transitions (Zhuang et al., 2000). This is different from that observed with peroxynitrite, which consists primarily of point mutations consisting of G:C → T:A or G:C→ C:G transversions (Juedes and Wogan, 1996; Routledge et al., 1994). The fact that the majority of base substitutions caused by $ONOO^-$ are located at GC base pairs, including G:C→T:A transversions, G:C→C:G transversions (Juedes and Wogan, 1996) is consistent with involvement of 8-oxo-dG, 8-nitro-dG (depurination to form an apurinic site) and secondary products of 8-oxo-dG oxidation, including spiroiminodihydantoin, guanidinohydantoin, and iminoallantoin, which are further oxidized products of 8-oxo-dG(Niles et al., 1999; Niles et al., 2000; Burrows et al., 2002).

Mutagenic effects of ROS and RNS produced by activated neutrophils and macrophages have also been clearly demonstrated in several *in vivo* systems. TPA-activated human neutrophils caused malignant transformation in C3H 10T1/2 mouse fibroblasts (Weitzman et al., 1985). iNOS of neutrophils that infiltrated into tumors has been shown to induce mutations in the *hprt* locus of Mutatec tumor cells (Sandhu et al., 2000), while an increased mutation frequency in the *hprt* locus was observed in mouse macrophage cells that were stimulated for

sustained NO• production (Zhuang et al., 1998). Interestingly, the types and proportion of *hprt* mutations were strikingly similar to those associated with long-term NO• exposure, suggesting that NO• exposure results in gene mutations through mechanisms that may also contribute to spontaneous mutagenesis (Zhuang et al., 1998). RNS formed by activated macrophages in the spleen of *lac Z*-transgenic SJL mice were responsible for an increased mutation frequency, which was prevented by administration of N-methylarginine, an inhibitor of NOS (Gal and Wogan, 1996). High levels of NO• and RNS produced in the lung of wild-type mice infected with Sendai virus, but not in iNOS-deficient mice, were shown to cause elevated viral RNA mutations (indicated gene) (Akaike et al., 2000).

NO• has also been shown to induce mutations in chronic inflammatory diseases, as illustrated by ulcerative colitis (UC). UC is an inflammatory bowel disease (IBDs) of unknown etiology and is characterized by uniform and continuous inflammation and genomic instability (Loeb and Loeb, 1999; Riddell et al., 1983). Increased iNOS staining has been observed in UC lesions, suggesting NO• production (Singer et al., 1996). Harris and coworkers have examined p53 mutations in colon tissue from UC patients and normal controls to investigate whether UC lesions contained a high p53 mutation load compared with normal colon. Higher p53 mutant frequencies for both C:G→A:T transitions at the CpG site of codon 248 and C:G→T:A transitions at codon 247 were observed in colonic lesions from the 18 UC cases when compared with 10 normal adult controls (Hussain et al., 2000). Additionally, iNOS activity was shown higher in colonic lesions from the 18 UC cases than that in the then non-UC adult controls (Hussain et al., 2000), which further confirmed the association between NO• production and p53 mutations.

Another mechanism of RNS-induced mutagenesis may involve cytosine methylation, a key element in the control of gene expression (Yu and Kone, 2004). Altered methylation does not

involve mutations per se, but rather leads to aberrant gene expression, in part, by affecting the ability of methylation-sensitive DNA-binding proteins to interact with their regulation sites (Samiec and Goodman, 1999). ROS and RNS can modify DNA methylation patterns by several mechanisms. For example, replacement of guanine with 8-oxo-dG greatly decreases methylation of adjacent cytosines, suggesting a role for oxidative injury in the formation of aberrant DNA methylation patterns during carcinogenesis (Weitzman et al., 1994). Additionally, oxidative DNA damage can interfere with the ability of methyltransferases to interact with DNA, thus resulting in a generalized hypomethylation of cytosine residues at CpG sites (Turk et al., 1995).

Accumulation of DNA damage during inflammation represents the net result of both direct damage and ineffective repair. $NO^{\bullet}$ and its derivative reactive species can directly damage DNA, but, mammalian cells have rich and complex mechanisms to repair the genome (Table 5). DNA damage in inflammation can be excised from DNA by multiple pathways and BER is quantitatively the most important (Jaiswal et al., 1998). Unfortunately, several key DNA repair enzymes are inhibited by $NO^{\bullet}$-mediated nitrosylation of cysteines at the active sites, including 6-O-alkyl DNA transferase (Laval and Wink, 1994), foramidopyrimidine glycosylase (Wink and Laval, 1994b), xeroderma pigmentosum A protein (Morita et al., 1996), and DNA ligases with active site lysine residues (Lindahl and Barnes, 1992). Further, cytokine-mediated induction of iNOS with $NO^{\bullet}$ production is associated with diminished global DNA repair capacity in cholangiocarcinoma cell lines (Jaiswal et al., 2000). Thus, $NO^{\bullet}$ may give the cell a double hit by both damaging the DNA and inhibiting its repair processes. This effect of $NO^{\bullet}$ and its reactive species may further make $NO^{\bullet}$ one of the pivotal mediators linking inflammation and carcinogenesis.

Table 5. DNA repair pathways in mammalian cells

Repair mechanism	Description and examples
Direct repair	• Photoreversal of UV-induced pyrimidine dimmers by DNA photolyase • Removal of methyl group from O^6-methylgauanine by methyltransfrase • Oxidative dealkylation of 1-methyladenine and 3-methylcytidine in DNA by AlkB (Anantharaman et al., 2001; Daniels and Tainer, 2000; Koivisto et al., 2003; Sancar, 1994; Todo et al., 1993; Welford et al., 2003)
Base excision repair (BER)	• Executed by substrate-specific DNA glycosylases. • Recognize oxidized/reduced bases, alkylated (usually methylated) bases, deaminated bases (e.g., uracil, xanthine), or base mismatches. • Examples, UDG, Fpg (Frosina et al., 1996; Matsumoto and Kim, 1995; McCullough et al., 1999)
Nucleotide excision repair (NER)	• Major repair system for bulky DNA lesions • Executed by a complex multisubunit enzyme system that makes dual incisions bracketing the lesion in the damaged strand • Factors of the human excision nuclease: XPA, RPA, XPC, TFIIH, XPG, XPF-ERCC1 (Branum et al., 2001; Petit and Sancar, 1999)
Double-strand break repair	• Executed either by homologous recombination (HR) or nonhomologous end-joining (NHEJ) • HR depends mainly on Rad51-family proteins • NHEJ depends mainly on DNA-PK complex (Ferguson and Alt, 2001; Gottlieb and Jackson, 1993; Petrini, 1999; Rouse and Jackson, 2002; Sung, 1994)
Repair of cross-link (X-link)	• Executed by either error-free mechanism or error-prone pathway • In the error-free pathway, a replication fork induces a double-strand break upon encountering a X-link, followed by HR repair pathway • In the error-prone pathway, NER pathway makes the dual incision, followed by an error-prone polymerase (such as Polη) fills in the gap (Jachymczyk et al., 1981; McHugh et al., 2000; Van Houten et al., 1986)

1.5 Biomarkers of Inflammation

A biomarker is defined as a biological parameter (gene, metabolite or protein) or laboratory measurement that occurs in association with a physiological or pathological process and that has putative diagnostic or prognostic utility (Lesko and Atkinson, 2001; Rolan et al., 2003). In the free radical studies performed here, the working definition can be more narrowly defined as a chemical change in a biological molecule caused by reactions with RNS, RHS and ROS (Griffiths et al., 2002). The rationale for this definition is that true biomarkers serve to establish the chemistry leading to molecular changes, such as mutation and cell signaling, which in turn lead to cellular responses on the pathway to cancer.

A. Criteria for Biomarkers

In the development of any biomarker, there are three basic steps (Halliwell, 2002), the first of which is to identify DNA and protein lesions that are specific to the disease in question. As discussed earlier, the specific lesions dealt with in this thesis are the four nucleobase lesions arising from nitrosative deamination of DNA caused by chemical mediators of inflammation. The second step in biomarker development is to create and validate analytical methods. This is addressed in Chapter 2 with the development of an LC/MS method to quantify the nucleobase deamination products, with validation *in vitro* and *in vivo* in Chapters 3-4. The final step is to demonstrate that changes in the levels of the markers correlate with the pathophysiology of inflammation and subsequent carcinogenesis. If DNA lesions represent a critical link in the pathway to cancer (Feig et al., 1994; Grisham et al., 2000), then their formation in inflamed tissues must be proven and a relationship between the quantities of the various lesions and

disease progression must be established. This facet of biomarker development is addressed in Chapter 5.

There are different expectations regarding the information that biomarkers can yield. Broadly, biomarkers may yield information on three levels of disease outcome: (i) as measurable endpoints of damage to proteins/amino acids, DNA molecules, lipids, and carbohydrates; (ii) as functional markers of, for example, blood flow, platelet aggregation, or cognitive function; and (iii) as endpoints related to specific disease. Biomarkers in the first category may ultimately be proven to relate directly to functional changes and disease. In the meantime, they can yield important information on the nature of pathological processes like inflammation, particularly regarding the nature of the radical-induced damage, compartmentalization and bioavailability, as well as antioxidant action.

As reviewed by Griffiths *et al.* (Griffiths et al., 2002), a valid biomarker should, to a large extent, meet the criteria of a major, stable, representative chemical modification that is implicated directly in the development of disease and can be determined by a specific, sensitive, reproducible and robust assay free of confounding factors. Further, the biomarker should be accessible in a target tissues or a valid surrogate tissue such as a leukocyte (Griffiths et al., 2002).

The current status of biomarkers in the context of the desirable properties listed above has recently been reviewed by several elegant articles, including Leasko and Atkinson, 2001, Grifiths *et al.*, 2002, and Rolan *et al.*, 2003. The review that follows will only focus on biochemical markers of the inflammatory process. The chemistry of formation of each biomarker will be considered along with an overview of the current analytical procedures,

highlighting the limitations and validity of each biomarker where possible. Finally, their application as endpoint analytes in supplementation studies will be discussed.

B. Protein Biomarkers

Protein nitration and nitrosation are becoming increasingly recognized as prevalent, functionally significant post-translational protein modifications that serve as indicators of $NO^{\bullet}$-mediated oxidative inflammatory reactions. The processes of protein nitration and nitrosation introduce new functional groups that contribute to altered protein function and turnover. Improved characterization of the impact of these protein modifications has revealed a spectrum of secondary effects including fragmentation, cross-linking and unfolding, which may accelerate or hinder proteolytic and proteosome-mediated turnover that ultimately leads to changes in the catalytic activity of enzymes, cytoskeletal organization and cell signal transduction (Dean et al., 1997).

Tyrosine Nitration

$NO^{\bullet}$-dependent nitration of protein tyrosine (Tyr) to 3-nitrotyrosine (NO_2Tyr) was found to occur under inflammatory conditions (Greenacre and Ischiropoulos, 2001), resulting in a post-translational modification that reflects the extent of oxidant production during both physiological and pathological conditions. NO_2Tyr and its deaminated and decarboxylated metabolite, 3-nitro-4-hydroxyphenylacetic acid, were first observed in the urine of humans with sepsis, a pathologic process that involves a widespread release of inflammatory mediators leading to organ injuries (Ohshima et al., 1990) (Figure 17).

There is an abundance of literature referring to the studies of cell and tissue protein nitration. In most of these reports, detection of nitrated Tyr residues derives from the use of anti-NO_2Tyr antibodies for analysis by immunohistochemistry (Gal et al., 1997), western blot, enzyme-linked immunoabsorbent assays and, in some cases, immunoaffinity purification prior to analysis of hydrolyzed protein and tissue homogenates by HPLC (Lorch et al., 2002). While the anti-NO_2Tyr has been proven useful in a variety of applications, there are limitations with respect to quantitation and the antigenic specificity of the anti-NO_2Tyr immunoreagents. More recently, the concomitant application of proteomics-based strategies for the analysis of nitrated proteins *in vitro* and *in vivo* has yielded important information about the extent of nitration of specific amino acids and the functional significance of the lesions (Nikov et al., 2003). An illustrative example comes from the study of the nitration of serum albumin, a clinically relevant dosimeter that may reflect the extent and nature of vascular oxidation and nitration reactions. Albumin is the most abundant protein in the vascular compartment and it contains 18 Tyr residues. Recently, three novel nitration sites were identified at Tyr^{84}, Tyr^{341}, and Tyr^{332} or Tyr^{334} bovine serum albumin treated with $ONOO^-$ *in vitro* (Nikov et al., 2003).

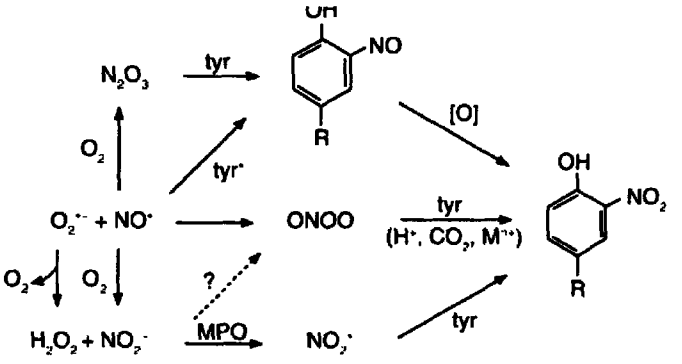

Figure 17. Representative pathways for biological formation of 3-nitrotyrosine. This product has been widely assumed to arise from the interaction of $ONOO^-$, and secondary oxidants derived from $ONOO^-$, with tyrosine-containing proteins. However, several alternative pathways exist, including one mediated by the enzyme myeloperoxidase (MPO), which may be important in respiring tissues. tyr, tyrosine; tyr•, tyrosyl radical.

Nitrosothiols

$NO^{\bullet}$ derivatives are able to nitrosate a number of nucleophilic sites on proteins, including amines, aromatic rings, alcohols, and reduced sulfur (thiol), among which the thiol group is most active (Zhang and Hogg, 2004). The modification of thiol residues by $NO^{\bullet}$ derivatives to produce a S-nitrosothiol (SNO) was originally proposed to have a role in physiology (Stamler et al., 1992a). Since then, about 115 different proteins, including kinases, channels, transcription factors, structural proteins, proteases, and respiratory enzymes, have so far been identified as targets for the SNO formation, suggesting that S-nitrosylation may represent a physiological modification in the signaling pathway of $NO^{\bullet}$ (Stamler et al., 2001).

The formation of SNO has been considered to occur mainly *via* N_2O_3, following the autoxidation of NO$^{\bullet}$ (Kharitonov et al., 1995). It should occur more readily under inflammatory conditions where the flux of NO$^{\bullet}$ is greatly increased and in lipid-rich environments where the hydrophobicity of NO$^{\bullet}$ should cause it to accumulate (Figure 18).

The detection of SNO has often employed chemiluminescent or colorimetric methods to measure the nitrite or NO$^{\bullet}$ generated from the spontaneous decomposition of NO^{+} that is released from SNO by mercury salts (Ewing and Janero, 1998). These methods involve equipment and expertise not always found in most laboratories and large amounts of nitrite can interfere with these methods under acidic conditions. To overcome these problems, two methods have been devised to detect SNO-derived nitrosating species at neutral pH (Wink et al., 1999). One is a colorimetric assay that has a detection range of 0.5-100 μM, while the other is a fluorometric assay that is claimed to be effective in the range of 50-1,000 nM (Wink et al., 1999). However, all of these methods are still subjected to adventitious generation of SNO from nitrite and thiols when samples are subjected to acidification, which suggests that there is further room for the development of analytical methods to quantify this important NO$^{\bullet}$ derivative.

In summary, protein nitration and nitrosation represent potentially useful biomarkers of chronic inflammation due to their functional importance in diverse physiological and pathological responses.

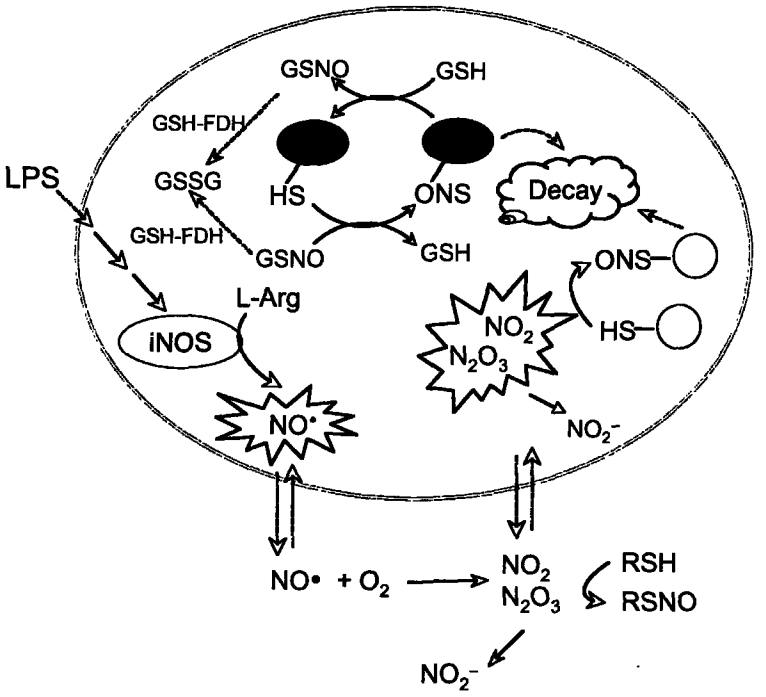

Figure18. A model of *S*-nitrosothiol formation and metabolism in mammalian cells. GSSG, glutathione disulfide; GSH-FDH, GSH-dependent formaldehyde hehydrogenase; iNOS, inducible nitric oxide synthase; NO, nitric oxide (adapted from Cadet et al., 2003; and Zhang and Hogg, 2004).

C. Biomarkers of Lipid Peroxidation

Lipid peroxidation such as that caused by $ONOO^-$ (Darley-Usmar et al., 1992; Radi et al., 1991; van der Veen and Roberts, 1999), involves H-atom abstraction from the methylene groups conjugated to pairs of carbon-carbon double bonds that define polyunsaturated fatty acids, subsequent peroxyl radical formation and degradation, produces a range of products, among which malondialdehyde (MDA) and 4-hydroxynonenal (4-HNE) are prominent (Darley-Usmar et al., 1992; Marnett, 2002a; Radi et al., 1991). The biological activities of MDA and 4-HNE

include the formation of DNA-protein cross-linking and DNA adducts, which alter the function or activity of these molecules. MDA and 4-HNE have been shown to be toxic to tissues (Mukai and Goldstein, 1976).

Direct lipid peroxidation products have been regarded as inappropriate biomarkers of inflammation owing to the difficulty of detecting and identifying the products. One of the most frequently used methods for MDA detection is thiobarbituric acid (TBA) derivatives (Yu and Sinnhuber, 1957) (Figure 18). Despite its simplicity, the TBS assay is fraught with errors that reduce its reliability (Janero, 1990). One reason for this is the instability of MDA. The other is that TBA also reacts with various other dialdehyiec or α,β-unsaturated aldehydes, which make the separation of MDA adduct and the interfering products using HPLC a required step. Further, the HPLC assay accurately measures MDA–TBA, but there is no guarantee that the MDA present has arisen from oxidative processes. Finally, the exact intensity of color that is formed during the TBA reaction depends on the type and strength of the acid that is used. Since different laboratories use different TBA assays, it is difficult to compare results from the literature.

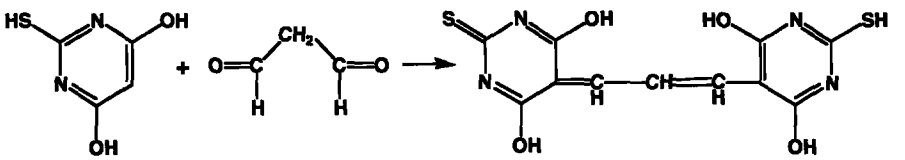

(1) (2) (3)

Figure 18. Reaction of TBA (1) and MDA (2) leading to the TBA–MDA

The direct Schiff's reaction has also long been employed for the histochemical identification of aldehydes in tissues, and was used for the visualization of lipid peroxidation in organs,

particularly liver (Benedetti et al., 1984; Pompella et al., 1987). However, the use of the Schiff's reaction is limited by poor reproducibility and false-positive results induced by the strong acidity of the reagent in tissues rich in plasmalogens (Toyokuni et al., 1994). Subsequent improvements include the use of mild 3-hydroxy-2-naphthoic acid hydrazide (NAH) and the use of fluorescent reagents (Hedley and Chow, 1992).

A significant improvement in the measurement of direct lipid peroxidation products has been recently obtained with the availability of the advanced mass spectrometry techniques. Andreoli *et al.* established a method for simultaneous determination of several classes of aldehydes in exhaled breath condensate using liquid chromatography/atmospheric pressure chemical ionization tandem mass spectrometry (Andreoli et al., 2003). Nagy et al. successfully detected several aldehydes in complex biological matrices such as milk and blood (Nagy et al., 2004). With improvement of the detection methods, direct lipid peroxidation products, like HNE, are becoming attractive biomarkers of oxidative stress (reviewed in Zarkovic, 2003).

D. DNA Biomarkers

DNA is an important target for attack by endogenous oxidants and it is widely thought that continuous oxidative damage to DNA is a significant contributor to the age-related development of major cancers, such as those of the colon, breast, rectum, and prostate (Ames et al., 1993; Halliwell, 1999). As reviewed earlier, a constellation of DNA damage products arising from inflammation has been identified, among which 8-oxo-dG and etheno adducts of dA and dC have drawn a great deal of attention in the efforts aimed at developing biomarkers of oxidative stress (Bartsch et al., 2002).

8-Oxo-2'-deoxyguanosine (8-oxo-dG)

8-Oxo-dG is one of the most thoroughly studied DNA oxidative lesions. The presence of 8-oxo-dG residues in DNA can lead to G:C to T:A transversion mutation (Cheng et al., 1992). Furthermore, a direct correlation between 8-oxo-dG formation and carcinogenesis *in vivo* has been claimed in several studies (Feig et al., 1994; Floyd et al., 1986). Major efforts have been devoted to the development of accurate assays for its measurement (reviewed in Cadet et al., 2002b). These assays can be grouped into "indirect" approaches that include alkaline elution, alkaline unwinding and the comet assay, and "direct" approaches that consist of post-labeling, HPLC, GC-MS, LC-MS and LC-MS/MS. In order to understand the biological consequences of DNA damage, it is imperative to know the chemical structure of a DNA modification observed in a spectrum of lesions. Methods like the comet assay involve enzymatic derivatization, although very sensitive, detect only the oxidative lesions recognized by the enzyme, which generally means more than one lesion. Thus, for the sake of brevity, the review that follows is focused on "direct approaches".

The post-labeling assay for the analysis of oxidative DNA adducts relies on enzymatic incorporation of ^{32}P into deoxynucleoside-forms of adducts and is very sensitive (~1 lesion per 10^9 nt) and reproducible (Cui et al., 1995; Moller et al., 1996; Zeisig and Moller, 1995). However, post-labeling method is not applicable to the detection of 8-oxo-dG because of the autoxidation of dG by ^{32}P and the post-labeling process (Moller and Hofer, 1997). A pre-purification of 8-oxo-dG prior to ^{32}P labeling dramatically reduced the level of further dG oxidization (Zeisig et al., 1999). Coupling the post-labeling method to HPLC separation also enabled the analysis of complex mixtures (i.e., human tissues) (Zeisig and Moller, 1997).

HPLC methods are widely used for the measurement of 8-oxo-dG in biological DNA samples such as animal tissue or white blood cells. However, the small extent of base oxidation requires the use of a detector more sensitive than UV absorbance, such as electrochemical detection (ECD) (Escodd, 2000).

GC-MS and LC–MS/MS, two current techniques used to analyze the DNA damage products, can unequivocally identify a wide spectrum of lesions. These two techniques can also provide rigorous quantification of lesions when used with appropriate stable isotope-labeled internal standards (reviewed in Cadet et al., 2002b). While GC-MS methods have been criticized for oxidation artefacts during sample preparation (reviewed.in Cadet et al., 2002a), precautions such as HPCL purification and the use of repair endonucleases (FPG and endonuclease III) instead of acid hydrolysis to liberate the base lesions, greatly reduces artifacts (Jaruga et al., 2000).

HPLC-MS/MS methods have significantly improved the detection of oxidative DNA damage. The assay combines the efficiency of HPLC separation with the accuracy, versatility and sensitivity afforded by tandem mass spectrometry. In contrast to GC-MS methods, the LC-MS/MS methods measure DNA base damage products in form of nucleosides that exhibit suitable chromatographic properties on octadecylsilyl silica gel (ODS) columns and are easily fragmentated to unique daughter ions that enable highly specific and sensitive detection (reviewed in Cadet et al., 2002a).

LC-MS/MS was first applied to the measurement of 8-oxo-dG by Serrano *et al* (Serrano et al., 1996). Subsequent improvement and the method by use of isotope-labeled internal standards allowed the determination of the level of 8-oxo-dG in cellular liver DNA and in urine samples (Ravanat et al., 1998). The power of the technique is illustrated by a recent study in which six

DNA modifications (including 8-oxo-dG) were quantified in cells exposed to ionizing radiation (Frelon et al., 2000).

In summary, while 8-oxo-dG has been widely studied in human tissues, the ease of its formation as an artifact and the ease of its oxidation suggest that it is not appropriate for use as a biomarker of inflammation and oxidative stress. Also, 8-oxo-dG is not a unique marker for inflammation, since other pathophysiological processes lead to its formation. Another potential problem exists for the use of 8-oxo-dG as a marker of oxidative stress in chronic inflammation/infection due to its further reaction with $ONOO^-$ to form secondary oxidative products (reviewed in Dedon and Tannenbaum, 2004).

DNA Etheno Adducts

Lipid peroxidation leads to the formation of reactive species such as 4-hydroxynonenal (HNE) and malondialdehyde (MDA). These reactive electrophiles can alkylate DNA bases to yield the promutagenic lesions shown in Figures 15 and 16. Exocyclic DNA adducts of endogenous origin are recognized as potential biomarkers of oxidative stress and cancer etiology, and also in the assessment of the efficacy of chemopreventive agents (Bartsch and Nair, 2000a; Bartsch and Nair, 2000b; Guengerich, 2001; Marnett and Plastaras, 2001)

MDA reacts with nucleic acid bases at physiological pH to form adducts to dG, dA, and dC (Figure 15), but comparison of the yields of the various adducts produced in the reaction of MDA with DNA *in vitro* indicates that M_1G is produced in at levels ~5-fold higher than M_1A, with M_1C formed in trace amounts (reviewed in Marnett, 2002b). M_1G has indeed been detected in human liver (Chaudhary et al., 1994a) and leukocytes (Rouzer et al., 1997).

Etheno adducts, mainly 1,N^6-etheno-2'-deoxyadenosine (ε-dA) and 3,N^4-etheno-2'-deoxycytidine (ε-dC), have been detected in unstressed rodent and human tissues (Chen et al., 1999; Chung et al., 1996; Doerge et al., 2000; Nair et al., 1995; Nair et al., 1999; Roberts et al., 2001). However, the occurrence of N^2,3-etheno-2'-deoxyguanosine (N^2,3-dG) was only found in a few studies (Fedtke et al., 1990; Ham et al., 1999; Yen et al., 1996). Interestingly, the levels of both ε-dA and ε-dC were elevated in clinical situations associated with oxidative stress, such as metal storage diseases (Nair et al., 1998a; Nair et al., 1996) and chronic infections and inflammation (Nair et al., 1998b). These lesions were also shown to be increased in colon polyps of patients with familial adenomatous polyposis, who later developed carcinomas of the colon (Schmid et al., 2000a) and in white blood cell DNA from women consuming diets rich in polyunsaturated fatty acids (Nair et al., 1997).

Analysis of endogenous DNA adducts, especially low-level etheno adducts, is a challenging task that demands high specificity and sensitivity for unequivocal identification and quantification. Significant efforts have been put into the development of analytical techniques to detect basal levels of certain exocyclic DNA adducts in unexposed human and rodent tissues. Gas chromatography/electron capture negative-ion chemical ionization mass spectrometry (GC-ECNCI/MS) (Chaudhary et al., 1994a) and liquid chromatography in combination with electrospray and tandem mass spectrometry (LC-ESI/MS/MS) have been developed for the detection of M_1G in DNA of human liver and leukocytes respectively (Rouzer et al., 1997). ^{32}P-post-labelling was first employed for the detection of etheno adducts of dA and dC (Nair et al., 1995). Improvement of the ^{32}P-post-labelling method by combining it with immunoaffinity purification to achieve the high sensitivity and specificity has been the principal approach to detect etheno adducts of dA and dC in untreated tissue (Bartsch and Nair, 2000a). On-line

immunoaffinity chromatography coupled with HPLC-ESI/MS/MS has recently been applied to the detection and automated quantification of trace levels of ε-dC in crude DNA hydrolysates (Roberts et al., 2001)

In summary, lipid peroxidation appears to be one of the major sources of endogenous DNA damage in humans that may contribute significantly to cancer and other genetic diseases linked to pathological process of inflammation. Furthermore, DNA adducts have the potential to be biomarkers of cancer and other diseases.

1.6 Summary

A growing body of evidence from human and animal studies supports a causative role for inflammation in carcinogenesis (Graham et al., 1995; IARC, 1994; IARC, 1996; Ohshima and Bartsch, 1994; Thun et al., 2004). Mechanisms by which persistent infection or inflammation increase the risk of cancer have remain unsolved. Inflammatory mediators linking chronic inflammation to carcinogenesis are numerous, but current information strongly suggests that $NO^{\bullet}$ contributes to this process (Dedon and Tannenbaum, 2004; Ohshima et al., 2003). Unregulated production of this ubiquitous and physiologically important molecule leads to high levels of derivative RNS that cause oxidation, nitrosation and nitration of biomolecules. The difficulty in direct measuring these species has stimulated the complementary development of biomarkers; of particular interests here is DNA damage. DNA adducts has the potential to be excellent biomarkers in dissecting mechanism of carcinogenesis and the assessment of cancer risk imposed by a particular chemical exposure. RNS has been shown to cause three major types of DNA

modifications: deamination, oxidation and nitration. Despite huge efforts in developing oxidative DNA adducts (e.g. 8-oxo-dG) as biomarkers of inflammation, there is little known about the relative quantities of different DNA damage products arising under biologically relevant conditions. Systematic studies to define the predominant DNA damage produced by RNS will assist the evaluation of their contributions to the pathophysiological changes during inflammatory processes.

The goal of the research presented in this thesis was to develop nucleobase deamination products as biomarkers of inflammation and to study the role of these DNA lesions in the pathophysiology of inflammation-induced carcinogenesis. Three critical steps govern the development of any biomarker (Halliwell, 2002), the first of which is to identify DNA and protein lesions that are specific to the disease in question. The specific lesions dealt with in this thesis are the four nucleobase lesions, dX, dO, dI and dU, which arise from nitrosative deamination of DNA caused by chemical mediators of inflammation. The second step in biomarker development is to create and validate analytical methods. This is addressed in Chapter 2 with the development of an LC-MS method to quantify the four nucleobase deamination products, with validation *in vitro* and *in vivo* in Chapters 3 and 4 respectively in quantification of nucleobase deamination products in isolated plasmid DNA and human lymphoblastoid cells exposed to $NO^{\bullet}$ at controlled physiological concentrations using a novel $NO^{\bullet}$ delivery system. The final step is to demonstrate that changes in the level of the biomarkers correlate with the pathophysiology of inflammation and subsequent carcinogenesis. If DNA lesions represent a critical link in the pathway to cancer (Feig et al., 1994; Grisham et al., 2000), then their formation in inflamed tissues must be proven and a relationship between the quantities of the various lesions and disease progression must be established. This facet of biomarker

development is addressed in Chapter 5 in study the formation of nucleobase deamination products in spleen and liver of SJL mice bearing the RcsX tumor.

As a complement to the LC-MS method for the quantification of nucleobase deamination products, we developed enzymatic probes for oxidative and nitrosative DNA lesions, which is addressed in Chapter 6. These probes would not only allow differential quantification of the two types of DNA damage, but would also allow the lesions to be mapped in any DNA sequence by coupling their activity with the technique of ligation-mediated PCR.

As an extension of the biomarker study, the effects of $ONOO^-$ dose and dose-rate on the DNA damage and mutations induced in the *supF* gene were investigated and reported in Chapter 7. The observations suggest that both dose and dose-rate at which a genetic target is exposed to $ONOO^-$ substantially influence the damage and mutational response and these parameters will need to be taken into account in assessing the potential effects of $ONOO^-$ *in vivo*.

Summarized in the Appendix I is the data consistent with a new paradigm we proposed: perturbations of nucleobase metabolism may lead to incorporation of the purine precursors hypoxanthine (I) and xanthine (X) into DNA, which can be regarded as another endogenous processes causing DNA damage that leads to human diseases such as cancer.

1.6 References

Ahn, B., Han, B. S., Kim, D. J., and Ohshima, H.: Immunohistochemical localization of inducible nitric oxide synthase and 3-nitrotyrosine in rat liver tumors induced by N-nitrosodiethylamine. Carcinogenesis **20** (7): 1337-44, 1999.

Akaike, T., Fujii, S., Kato, A., Yoshitake, J., Miyamoto, Y., Sawa, T., Okamoto, S., Suga, M., Asakawa, M., Nagai, Y., and Maeda, H.: Viral mutation accelerated by nitric oxide production during infection *in vivo*. Faseb J **14** (10): 1447-54, 2000.

Alderton, W. K., Cooper, C. E., and Knowles, R. G.: Nitric oxide synthases: structure, function and inhibition. Biochem J **357** (Pt 3): 593-615, 2001.

Ambs, S., Ogunfusika, M. O., Merriam, W. G., Bennett, W. P., Billiar, T. R., and Harris, C. C.: Up-regulation of inducible nitric oxide synthase expression in cancer-prone p53 knockout mice. Proc Natl Acad Sci U S A **95** (15): 8823-8, 1998.

Ames, B. N., Shigenaga, M. K., and Hagen, T. M.: Oxidants, antioxidants, and the degenerative diseases of aging. Proc Natl Acad Sci U S A **90** (17): 7915-22, 1993.

Anantharaman, V., Koonin, E. V., and Aravind, L.: Regulatory potential, phyletic distribution and evolution of ancient, intracellular small-molecule-binding domains. J Mol Biol **307** (5): 1271-92, 2001.

Anderson, M. M., Hazen, S. L., Hsu, F. F., and Heinecke, J. W.: Human neutrophils employ the myeloperoxidase-hydrogen peroxide-chloride system to convert hydroxy-amino acids into glycolaldehyde, 2-hydroxypropanal, and acrolein. A mechanism for the generation of highly reactive alpha-hydroxy and alpha,beta-unsaturated aldehydes by phagocytes at sites of inflammation. J Clin Invest **99** (3): 424-32, 1997.

Andreoli, R., Manini, P., Corradi, M., Mutti, A., and Niessen, W. M.: Determination of patterns of biologically relevant aldehydes in exhaled breath condensate of healthy subjects by liquid chromatography/atmospheric chemical ionization tandem mass spectrometry. Rapid Commun Mass Spectrom **17** (7): 637-45, 2003.

Auchere, F., and Rusnak, F.: What is the ultimate fate of superoxide anion *in vivo*? J Biol Inorg Chem **7** (6): 664-7, 2002.

Awada, M., and Dedon, P. C.: Formation of the 1,N2-glyoxal adduct of deoxyguanosine by phosphoglycolaldehyde, a product of 3'-deoxyribose oxidation in DNA. Chem Res Toxicol **14** (9): 1247-53, 2001.

Bainton, D.: Phagocytic cells: developmental biology of neutrophils and eosinophils. *In* Inflammation: basic principles and clinical correlates, ed. by J. Gallin, I. Goldstein, and R. Snyderman, pp. Chapter 16, Raven Press, New York, 1992.

Bamias, G., Sugawara, K., Pagnini, C., and Cominelli, F.: The Th1 immune pathway as a therapeutic target in Crohn's disease. Curr Opin Investig Drugs **4** (11): 1279-86, 2003.

Bartsch, H., and Nair, J.: New DNA-based biomarkers for oxidative stress and cancer chemoprevention studies. Eur J Cancer **36** (10): 1229-34, 2000a.

Bartsch, H., and Nair, J.: Ultrasensitive and specific detection methods for exocylic DNA adducts: markers for lipid peroxidation and oxidative stress. Toxicology **153** (1-3): 105-14, 2000b.

Bartsch, H., Nair, J., and Owen, R. W.: Exocyclic DNA adducts as oxidative stress markers in colon carcinogenesis: potential role of lipid peroxidation, dietary fat and antioxidants. Biol Chem **383** (6): 915-21, 2002.

Beckman, J. S.: The double-edged role of nitric oxide in brain function and superoxide-mediated injury. J Dev Physiol **15** (1): 53-9, 1991.

Benedetti, A., Malvaldi, G., Fulceri, R., and Comporti, M.: Loss of lipid peroxidation as a histochemical marker for preneoplastic hepatocellular foci of rats. Cancer Res **44** (12 Pt 1): 5712-7, 1984.

Berenblum, I.: Teh cocarcinogenic action of croton resin. Cancer Res **1**: 44-48, 1941.

Berg, D. J., Davidson, N., Kuhn, R., Muller, W., Menon, S., Holland, G., Thompson-Snipes, L., Leach, M. W., and Rennick, D.: Enterocolitis and colon cancer in interleukin-10-deficient mice are associated with aberrant cytokine production and CD4(+) TH1-like responses. J Clin Invest **98** (4): 1010-20, 1996.

Bhan, A. K., Mizoguchi, E., Smith, R. N., and Mizoguchi, A.: Colitis in transgenic and knockout animals as models of human inflammatory bowel disease. Immunol Rev **169**: 195-207, 1999.

Bhan, A. K., Mizoguchi, E., Smith, R. N., and Mizoguchi, A.: Spontaneous chronic colitis in TCR alpha-mutant mice; an experimental model of human ulcerative colitis. Int Rev Immunol **19** (1): 123-38, 2000.

Bogdan, C., and Nathan, C.: Modulation of macrophage function by transforming growth factor beta, interleukin-4, and interleukin-10. Ann N Y Acad Sci **685:** 713-39, 1993.

Bohnert, T., Gingipalli, L., and Dedon, P. C.: Reaction of 2'-deoxyribonucleosides with cis- and trans-1,4-dioxo-2-butene. Biochem Biophys Res Commun **323** (3): 838-44, 2004.

Branum, M. E., Reardon, J. T., and Sancar, A.: DNA repair excision nuclease attacks undamaged DNA. A potential source of spontaneous mutations. J Biol Chem **276** (27): 25421-6, 2001.

Burney, S., Niles, J. C., Dedon, P. C., and Tannenbaum, S. R.: DNA damage in deoxynucleosides and oligonucleotides treated with peroxynitrite. Chem Res Toxicol **12** (6): 513-20, 1999.

Burrows, C. J., Muller, J. G., Kornyushyna, O., Luo, W., Duarte, V., Leipold, M. D., and David, S. S.: Structure and potential mutagenicity of new hydantoin products from guanosine and 8-oxo-7,8-dihydroguanine oxidation by transition metals. Environ Health Perspect **110 Suppl 5:** 713-7, 2002.

Byun, J., Henderson, J. P., Mueller, D. M., and Heinecke, J. W.: 8-Nitro-2'-deoxyguanosine, a specific marker of oxidation by reactive nitrogen species, is generated by the myeloperoxidase-hydrogen peroxide-nitrite system of activated human phagocytes. Biochemistry **38** (8): 2590-600, 1999.

Cadet, J., Bellon, S., Berger, M., Bourdat, A. G., Douki, T., Duarte, V., Frelon, S., Gasparutto, D., Muller, E., Ravanat, J. L., and Sauvaigo, S.: Recent aspects of oxidative DNA damage: guanine lesions, measurement and substrate specificity of DNA repair glycosylases. Biol Chem **383** (6): 933-43, 2002a.

Cadet, J., Douki, T., Frelon, S., Sauvaigo, S., Pouget, J. P., and Ravanat, J. L.: Assessment of oxidative base damage to isolated and cellular DNA by HPLC-MS/MS measurement. Free Radic Biol Med **33** (4): 441-9, 2002b.

Cadet, J., Douki, T., Gasparutto, D., and Ravanat, J. L.: Oxidative damage to DNA: formation, measurement and biochemical features. Mutat Res **531** (1-2): 5-23, 2003.

Caulfield, J. L., Wishnok, J. S., and Tannenbaum, S. R.: Nitric oxide-induced deamination of cytosine and guanine in deoxynucleosides and oligonucleotides. J Biol Chem **273** (21): 12689-95, 1998.

Caulfield, J. L., Wishnok, J. S., and Tannenbaum, S. R.: Nitric oxide-induced interstrand cross-links in DNA. Chem Res Toxicol **16** (5): 571-4, 2003.

Chang, C. S., Chen, W. N., Lin, H. H., Wu, C. C., and Wang, C. J.: Increased oxidative DNA damage, inducible nitric oxide synthase, nuclear factor kappaB expression and enhanced antiapoptosis-related proteins in Helicobacter pylori-infected non-cardiac gastric adenocarcinoma. World J Gastroenterol **10** (15): 2232-40, 2004.

Chaudhary, A. K., Nokubo, M., Reddy, G. R., Yeola, S. N., Morrow, J. D., Blair, I. A., and Marnett, L. J.: Detection of endogenous malondialdehyde-deoxyguanosine adducts in human liver. Science **265** (5178): 1580-2, 1994a.

Chaudhary, A. K., Nokubo, M., Reddy, G. R., Yeola, S. N., Morrow, J. D., Blair, I. A., and Marnett, L. J.: Detection of endogenous malondialdehyde-deoxyguanosine adducts in human liver. *In* Science, vol. 265, pp. 1580-2, 1994b.

Chen, H. J., Chiang, L. C., Tseng, M. C., Zhang, L. L., Ni, J., and Chung, F. L.: Detection and quantification of 1,N(6)-ethenoadenine in human placental DNA by mass spectrometry. Chem Res Toxicol **12** (12): 1119-26, 1999.

Chen, H. J., and Chung, F. L.: Epoxidation of trans-4-hydroxy-2-nonenal by fatty acid hydroperoxides and hydrogen peroxide. Chem Res Toxicol **9** (1): 306-12, 1996.

Cheng, K. C., Cahill, D. S., Kasai, H., Nishimura, S., and Loeb, L. A.: 8-Hydroxyguanine, an abundant form of oxidative DNA damage, causes G----T and A----C substitutions. J Biol Chem **267** (1): 166-72, 1992.

Chisari, F. V., Klopchin, K., Moriyama, T., Pasquinelli, C., Dunsford, H. A., Sell, S., Pinkert, C. A., Brinster, R. L., and Palmiter, R. D.: Molecular pathogenesis of hepatocellular carcinoma in hepatitis B virus transgenic mice. Cell **59** (6): 1145-56, 1989.

Chulada, P. C., Thompson, M. B., Mahler, J. F., Doyle, C. M., Gaul, B. W., Lee, C., Tiano, H. F., Morham, S. G., Smithies, O., and Langenbach, R.: Genetic disruption of Ptgs-1, as well as Ptgs-2, reduces intestinal tumorigenesis in Min mice. Cancer Res **60** (17): 4705-8, 2000.

Chung, F. L., Chen, H. J., and Nath, R. G.: Lipid peroxidation as a potential endogenous source for the formation of exocyclic DNA adducts. Carcinogenesis **17** (10): 2105-11, 1996.

Colamussi, M. L., White, M. R., Crouch, E., and Hartshorn, K. L.: Influenza A virus accelerates neutrophil apoptosis and markedly potentiates apoptotic effects of bacteria. Blood **93** (7): 2395-403, 1999.

Cooper, H. S., Everley, L., Chang, W. C., Pfeiffer, G., Lee, B., Murthy, S., and Clapper, M. L.: The role of mutant Apc in the development of dysplasia and cancer in the mouse model of dextran sulfate sodium-induced colitis. Gastroenterology **121** (6): 1407-16, 2001.

Cui, X. S., Torndal, U. B., Eriksson, L. C., and Moller, L.: Early formation of DNA adducts compared with tumor formation in a long-term tumor study in rats after administration of 2-nitrofluorene. Carcinogenesis **16** (9): 2135-41, 1995.

Daniels, D. S., and Tainer, J. A.: Conserved structural motifs governing the stoichiometric repair of alkylated DNA by O(6)-alkylguanine-DNA alkyltransferase. Mutat Res **460** (3-4): 151-63, 2000.

Darley-Usmar, V. M., Hogg, N., O'Leary, V. J., Wilson, M. T., and Moncada, S.: The simultaneous generation of superoxide and nitric oxide can initiate lipid peroxidation in human low density lipoprotein. Free Radic Res Commun **17** (1): 9-20, 1992.

De Luca, A., De Falco, M., Iaquinto, S., and Iaquinto, G.: Effects of Helicobacter pylori infection on cell cycle progression and the expression of cell cycle regulatory proteins. J Cell Physiol **200** (3): 334-42, 2004.

Dean, R. T., Fu, S., Stocker, R., and Davies, M. J.: Biochemistry and pathology of radical-mediated protein oxidation. Biochem J **324 (Pt 1)**: 1-18, 1997.

Dedon, P. C., Plastaras, J. P., Rouzer, C. A., and Marnett, L. J.: Indirect mutagenesis by oxidative DNA damage: formation of the pyrimidopurinone adduct of deoxyguanosine by base propenal. Proc Natl Acad Sci U S A **95** (19): 11113-6, 1998.

Dedon, P. C., and Tannenbaum, S. R.: Reactive nitrogen species in the chemical biology of inflammation. Arch Biochem Biophys **423** (1): 12-22, 2004.

Denicola, A., Freeman, B. A., Trujillo, M., and Radi, R.: Peroxynitrite reaction with carbon dioxide/bicarbonate: kinetics and influence on peroxynitrite-mediated oxidations. Arch Biochem Biophys **333** (1): 49-58, 1996.

deRojas-Walker, T., Tamir, S., Ji, H., Wishnok, J. S., and Tannenbaum, S. R.: Nitric oxide induces oxidative damage in addition to deamination in macrophage DNA. Chem Res Toxicol **8** (3): 473-7, 1995.

Doerge, D. R., Churchwell, M. I., Fang, J. L., and Beland, F. A.: Quantification of etheno-DNA adducts using liquid chromatography, on-line sample processing, and electrospray tandem mass spectrometry. Chem Res Toxicol **13** (12): 1259-64, 2000.

Ebert, M. P., Yu, J., Sung, J. J., and Malfertheiner, P.: Molecular alterations in gastric cancer: the role of Helicobacter pylori. Eur J Gastroenterol Hepatol **12** (7): 795-8, 2000.

Eiserich, J. P., Cross, C. E., Jones, A. D., Halliwell, B., and van der Vliet, A.: Formation of nitrating and chlorinating species by reaction of nitrite with hypochlorous acid. A novel mechanism for nitric oxide-mediated protein modification. J Biol Chem **271** (32): 19199-208, 1996.

Elsbach, P., and Weiss, J.: Phagocytic cells: oygen-independent antimicrobial systems. *In* Inflammation: basic principles and clinical correlates, ed. by J. Gallin, I. Goldstein, and R. Snyderman, pp. Chapter 24, Raven Press, New York, 1992.

Erdman, S. E., Poutahidis, T., Tomczak, M., Rogers, A. B., Cormier, K., Plank, B., Horwitz, B. H., and Fox, J. G.: CD4+ CD25+ regulatory T lymphocytes inhibit microbially induced colon cancer in Rag2-deficient mice. Am J Pathol **162** (2): 691-702, 2003a.

Erdman, S. E., Rao, V. P., Poutahidis, T., Ihrig, M. M., Ge, Z., Feng, Y., Tomczak, M., Rogers, A. B., Horwitz, B. H., and Fox, J. G.: CD4(+)CD25(+) regulatory lymphocytes require interleukin 10 to interrupt colon carcinogenesis in mice. Cancer Res **63** (18): 6042-50, 2003b.

Escodd: Comparison of different methods of measuring 8-oxoguanine as a marker of oxidative DNA damage. ESCODD (European Standards Committee on Oxidative DNA Damage). Free Radic Res **32** (4): 333-41, 2000.

Espey, M. G., Miranda, K. M., Thomas, D. D., and Wink, D. A.: Distinction between nitrosating mechanisms within human cells and aqueous solution. J Biol Chem **276** (32): 30085-91, 2001.

Espey, M. G., Thomas, D. D., Miranda, K. M., and Wink, D. A.: Focusing of nitric oxide mediated nitrosation and oxidative nitrosylation as a consequence of reaction with superoxide. Proc Natl Acad Sci U S A **99** (17): 11127-32, 2002.

Esterbauer, H., Schaur, R. J., and Zollner, H.: Chemistry and biochemistry of 4-hydroxynonenal, malonaldehyde and related aldehydes. Free Radic Biol Med **11** (1): 81-128, 1991.

Ewing, J. F., and Janero, D. R.: Specific S-nitrosothiol (thionitrite) quantification as solution nitrite after vanadium(III) reduction and ozone-chemiluminescent detection. Free Radic Biol Med **25** (4-5): 621-8, 1998.

Farinati, F., Cardin, R., Degan, P., Rugge, M., Mario, F. D., Bonvicini, P., and Naccarato, R.: Oxidative DNA damage accumulation in gastric carcinogenesis. Gut **42** (3): 351-6, 1998.

Fedtke, N., Boucheron, J. A., Walker, V. E., and Swenberg, J. A.: Vinyl chloride-induced DNA adducts. II: Formation and persistence of 7-(2'-oxoethyl)guanine and N2,3-ethenoguanine in rat tissue DNA. Carcinogenesis **11** (8): 1287-92, 1990.

Feig, D. I., Reid, T. M., and Loeb, L. A.: Reactive oxygen species in tumorigenesis. Cancer Res **54** (7 Suppl): 1890s-1894s, 1994.

Ferguson, D. O., and Alt, F. W.: DNA double strand break repair and chromosomal translocation: lessons from animal models. Oncogene **20** (40): 5572-9, 2001.

Floyd, R. A., Watson, J. J., Wong, P. K., Altmiller, D. H., and Rickard, R. C.: Hydroxyl free radical adduct of deoxyguanosine: sensitive detection and mechanisms of formation. Free Radic Res Commun **1** (3): 163-72, 1986.

Ford, P. C., Wink, D. A., and Stanbury, D. M.: Autoxidation kinetics of aqueous nitric oxide. FEBS Lett **326** (1-3): 1-3, 1993.

Franceschi, S.: Strategies to reduce the risk of virus-related cancers. Ann Oncol **11** (9): 1091-6, 2000.

Frelon, S., Douki, T., Ravanat, J. L., Pouget, J. P., Tornabene, C., and Cadet, J.: High-performance liquid chromatography--tandem mass spectrometry measurement of radiation-induced base damage to isolated and cellular DNA. Chem Res Toxicol **13** (10): 1002-10, 2000.

Friedwardl, W., and Rous, P.: The initiating and promoting elements in tumor production: an analysis of the effects of tar, benzpyren, and methylcholanthrene on rabbit skin. J Exp Med **80**: 101=126, 1944.

Frosina, G., Fortini, P., Rossi, O., Carrozzino, F., Raspaglio, G., Cox, L. S., Lane, D. P., Abbondandolo, A., and Dogliotti, E.: Two pathways for base excision repair in mammalian cells. J Biol Chem **271** (16): 9573-8, 1996.

Fujisawa, H., Tsuru, S., Taniguchi, M., Zinnaka, Y., and Nomoto, K.: Protective mechanisms against pulmonary infection with influenza virus. I. Relative contribution of

polymorphonuclear leukocytes and of alveolar macrophages to protection during the early phase of intranasal infection. J Gen Virol **68 (Pt 2)**: 425-32, 1987.

Fukuto, J. M., Wallace, G. C., Hszieh, R., and Chaudhuri, G.: Chemical oxidation of N-hydroxyguanidine compounds. Release of nitric oxide, nitroxyl and possible relationship to the mechanism of biological nitric oxide generation. Biochem Pharmacol **43** (3): 607-13, 1992.

Gal, A., Tamir, S., Kennedy, L. J., Tannenbaum, S. R., and Wogan, G. N.: Nitrotyrosine formation, apoptosis, and oxidative damage: relationships to nitric oxide production in SJL mice bearing the RcsX tumor. Cancer Res **57** (10): 1823-8, 1997.

Gal, A., and Wogan, G. N.: Mutagenesis associated with nitric oxide production in transgenic SJL mice. Proc Natl Acad Sci U S A **93** (26): 15102-7, 1996.

Giloni, L., Takeshita, M., Johnson, F., Iden, C., and Grollman, A. P.: Bleomycin-induced strand-scission of DNA. Mechanism of deoxyribose cleavage. J Biol Chem **256** (16): 8608-15, 1981.

Goerdt, S., Politz, O., Schledzewski, K., Birk, R., Gratchev, A., Guillot, P., Hakiy, N., Klemke, C. D., Dippel, E., Kodelja, V., and Orfanos, C. E.: Alternative versus classical activation of macrophages. Pathobiology **67** (5-6): 222-6, 1999.

Goldstein, S., Czapski, G., Lind, J., and Merenyi, G.: Mechanism of Decomposition of Peroxynitric Ion (O(2)NOO(-)): Evidence for the Formation of O(2)(*-) and (*)NO(2) Radicals. Inorg Chem **37** (16): 3943-3947, 1998.

Goldstein, S., Czapski, G., Lind, J., and Merenyi, G.: Effect of *NO on the decomposition of peroxynitrite: reaction of N2O3 with ONOO. Chem Res Toxicol **12** (2): 132-6, 1999.

Gottlieb, T. M., and Jackson, S. P.: The DNA-dependent protein kinase: requirement for DNA ends and association with Ku antigen. Cell **72** (1): 131-42, 1993.

Graham, D. Y., Go, M. F., and Genta, R. M.: Helicobacter pylori, duodenal ulcer, gastric cancer: tunnel vision or blinders? Ann Med **27** (5): 589-94, 1995.

Green, L. C., Ruiz de Luzuriaga, K., Wagner, D. A., Rand, W., Istfan, N., Young, V. R., and Tannenbaum, S. R.: Nitrate biosynthesis in man. Proc Natl Acad Sci U S A **78** (12): 7764-8, 1981.

Greenacre, S. A., and Ischiropoulos, H.: Tyrosine nitration: localisation, quantification, consequences for protein function and signal transduction. Free Radic Res **34** (6): 541-81, 2001.

Griffiths, H. R., Moller, L., Bartosz, G., Bast, A., Bertoni-Freddari, C., Collins, A., Cooke, M., Coolen, S., Haenen, G., Hoberg, A. M., Loft, S., Lunec, J., Olinski, R., Parry, J., Pompella, A., Poulsen, H., Verhagen, H., and Astley, S. B.: Biomarkers. Mol Aspects Med **23** (1-3): 101-208, 2002.

Grisham, M. B., Jourd'heuil, D., and Wink, D. A.: Review article: chronic inflammation and reactive oxygen and nitrogen metabolism--implications in DNA damage and mutagenesis. Aliment Pharmacol Ther **14 Suppl 1**: 3-9, 2000.

Grishko, V. I., Druzhyna, N., LeDoux, S. P., and Wilson, G. L.: Nitric oxide-induced damage to mtDNA and its subsequent repair. Nucleic Acids Res **27** (22): 4510-6, 1999.

Guengerich, F. P.: Forging the links between metabolism and carcinogenesis. Mutat Res **488** (3): 195-209, 2001.

Halliwell, B.: Oxygen and nitrogen are pro-carcinogens. Damage to DNA by reactive oxygen, chlorine and nitrogen species: measurement, mechanism and the effects of nutrition. Mutat Res **443** (1-2): 37-52, 1999.

Halliwell, B.: Effect of diet on cancer development: is oxidative DNA damage a biomarker? Free Radic Biol Med **32** (10): 968-74, 2002.

Ham, A. J., Ranasinghe, A., Morinello, E. J., Nakamura, J., Upton, P. B., Johnson, F., and Swenberg, J. A.: Immunoaffinity/gas chromatography/high-resolution mass spectrometry method for the detection of N(2),3-ethenoguanine. Chem Res Toxicol **12** (12): 1240-6, 1999.

Hartshorn, K. L., Karnad, A. B., and Tauber, A. I.: Influenza A virus and the neutrophil: a model of natural immunity. J Leukoc Biol **47** (2): 176-86, 1990.

Hayashi, K., Teramoto, N., and Akagi, T.: Animal *in vivo* models of EBV-associated lymphoproliferative diseases: special references to rabbit models. Histol Histopathol **17** (4): 1293-310, 2002.

Hedley, D., and Chow, S.: Flow cytometric measurement of lipid peroxidation in vital cells using parinaric acid. Cytometry **13** (7): 686-92, 1992.

Hibbs, J. B., Jr., Taintor, R. R., Vavrin, Z., and Rachlin, E. M.: Nitric oxide: a cytotoxic activated macrophage effector molecule. Biochem Biophys Res Commun **157** (1): 87-94, 1988.

Hinz, B., and Brune, K.: Cyclooxygenase-2--10 years later. J Pharmacol Exp Ther **300** (2): 367-75, 2002.

Hokari, R., Kato, S., Matsuzaki, K., Kuroki, M., Iwai, A., Kawaguchi, A., Nagao, S., Miyahara, T., Itoh, K., Sekizuka, E., Nagata, H., Ishii, H., and Miura, S.: Reduced sensitivity of inducible nitric oxide synthase-deficient mice to chronic colitis. Free Radic Biol Med **31** (2): 153-63, 2001.

Huie, R. E., and Padmaja, S.: The reaction of no with superoxide. Free Radic Res Commun **18** (4): 195-9, 1993.

Hussain, S. P., Amstad, P., Raja, K., Ambs, S., Nagashima, M., Bennett, W. P., Shields, P. G., Ham, A. J., Swenberg, J. A., Marrogi, A. J., and Harris, C. C.: Increased p53 mutation load in noncancerous colon tissue from ulcerative colitis: a cancer-prone chronic inflammatory disease. Cancer Res **60** (13): 3333-7, 2000.

IARC: Schistosomes, liver flukes and Helicobacter pylori. IARC Working Group on the Evaluation of Carcinogenic Risks to Humans. Lyon, 7-14 June 1994. IARC Monogr Eval Carcinog Risks Hum **61**: 1-241, 1994.

IARC: IARC Working Group on the Evaluation of Carcinogenic Risks to Humans: Human Immunodeficiency Viruses and Human T-Cell Lymphotropic Viruses. Lyon, France, 1-18 June 1996. IARC Monogr Eval Carcinog Risks Hum **67**: 1-424, 1996.

Imlay, J. A.: Pathways of oxidative damage. Annu Rev Microbiol **57**: 395-418, 2003.

Israel, D. A., and Peek, R. M.: pathogenesis of Helicobacter pylori-induced gastric inflammation. Aliment Pharmacol Ther **15** (9): 1271-90, 2001.

Jachymczyk, W. J., von Borstel, R. C., Mowat, M. R., and Hastings, P. J.: Repair of interstrand cross-links in DNA of Saccharomyces cerevisiae requires two systems for DNA repair: the RAD3 system and the RAD51 system. Mol Gen Genet **182** (2): 196-205, 1981.

Jain, S. K.: The accumulation of malonyldialdehyde, a product of fatty acid peroxidation, can disturb aminophospholipid organization in the membrane bilayer of human erythrocytes. J Biol Chem **259** (6): 3391-4, 1984.

Jaiswal, M., LaRusso, N. F., Burgart, L. J., and Gores, G. J.: Inflammatory cytokines induce DNA damage and inhibit DNA repair in cholangiocarcinoma cells by a nitric oxide-dependent mechanism. *In* Cancer Res, vol. 60, pp. 184-90, 2000.

Jaiswal, M., Lipinski, L. J., Bohr, V. A., and Mazur, S. J.: Efficient *in vitro* repair of 7-hydro-8-oxodeoxyguanosine by human cell extracts: involvement of multiple pathways. Nucleic Acids Res **26** (9): 2184-91, 1998.

Janero, D. R.: Malondialdehyde and thiobarbituric acid-reactivity as diagnostic indices of lipid peroxidation and peroxidative tissue injury. Free Radic Biol Med **9** (6): 515-40, 1990.

Jaruga, P., Speina, E., Gackowski, D., Tudek, B., and Olinski, R.: Endogenous oxidative DNA base modifications analysed with repair enzymes and GC/MS technique. Nucleic Acids Res **28** (6): E16, 2000.

Jenkins, D. C., Charles, I. G., Thomsen, L. L., Moss, D. W., Holmes, L. S., Baylis, S. A., Rhodes, P., Westmore, K., Emson, P. C., and Moncada, S.: Roles of nitric oxide in tumor growth. Proc Natl Acad Sci U S A **92** (10): 4392-6, 1995.

Juedes, M. J., and Wogan, G. N.: Peroxynitrite-induced mutation spectra of pSP189 following replication in bacteria and in human cells. Mutat Res **349** (1): 51-61, 1996.

Kanda, T., Koike, H., Arai, M., Wilson, J. E., Carthy, C. M., Yang, D., McManus, B. M., Nagai, R., and Kobayashi, I.: Increased severity of viral myocarditis in mice lacking lymphocyte maturation. Int J Cardiol **68** (1): 13-22, 1999.

Kennedy, L. J., Moore, K., Jr., Caulfield, J. L., Tannenbaum, S. R., and Dedon, P. C.: Quantitation of 8-oxoguanine and strand breaks produced by four oxidizing agents. Chem Res Toxicol **10** (4): 386-92, 1997.

Kharitonov, V. G., Sundquist, A. R., and Sharma, V. S.: Kinetics of nitrosation of thiols by nitric oxide in the presence of oxygen. J Biol Chem **270** (47): 28158-64, 1995.

Kirsch, M., and de Groot, H.: Formation of peroxynitrite from reaction of nitroxyl anion with molecular oxygen. *In* J Biol Chem, vol. 277, pp. 13379-88, 2002.

Kissner, R., Nauser, T., Bugnon, P., Lye, P. G., and Koppenol, W. H.: Formation and properties of peroxynitrite as studied by laser flash photolysis, high-pressure stopped-flow technique, and pulse radiolysis. Chem Res Toxicol **10** (11): 1285-92, 1997.

Klaunig, J. E., and Kamendulis, L. M.: The role of oxidative stress in carcinogenesis. Annu Rev Pharmacol Toxicol **44**: 239-67, 2004.

Klebanoff, S. J.: Myeloperoxidase: contribution to the microbicidal activity of intact leukocytes. Science **169** (950): 1095-7, 1970.

Klebanoff, S. J., and Rosen, H.: The role of myeloperoxidase in the microbicidal activity of polymorphonuclear leukocytes. Ciba Found Symp (65): 263-84, 1978.

Klotz, L. O., Briviba, K., and Sies, H.: Singlet oxygen mediates the activation of JNK by UVA radiation in human skin fibroblasts. FEBS Lett **408** (3): 289-91, 1997.

Knudson, A. G.: Two genetic hits (more or less) to cancer. Nat Rev Cancer **1** (2): 157-62, 2001.

Koivisto, P., Duncan, T., Lindahl, T., and Sedgwick, B.: Minimal methylated substrate and extended substrate range of Escherichia coli AlkB protein, a 1-methyladenine-DNA dioxygenase. J Biol Chem **278** (45): 44348-54, 2003.

Kowalczuk, K., and Stryjecka-Zimmer, M.: The influence of oxidative stress on the level of malondialdehyde (MDA) in different areas of the rabbit brain. Ann Univ Mariae Curie Sklodowska [Med] **57** (2): 160-4, 2002.

Kuhn, R., Lohler, J., Rennick, D., Rajewsky, K., and Muller, W.: Interleukin-10-deficient mice develop chronic enterocolitis. Cell **75** (2): 263-74, 1993.

Kumamoto, K., and Takenoshita, S.: [Mechanism of carcinogenesis in colorectal cancer]. Nippon Rinsho **61 Suppl 7:** 55-60, 2003.

Kumar, A., and Creery, W. D.: The therapeutic potential of interleukin 10 in infection and inflammation. Arch Immunol Ther Exp (Warsz) **48** (6): 529-38, 2000.

Laval, F., and Wink, D. A.: Inhibition by nitric oxide of the repair protein, O6-methylguanine-DNA-methyltransferase. Carcinogenesis **15** (3): 443-7, 1994.

Laval, F., Wink, D. A., and Laval, J.: A discussion of mechanisms of NO genotoxicity: implication of inhibition of DNA repair proteins. Rev Physiol Biochem Pharmacol **131:** 175-91, 1997.

Lee, A.: Animal models of Helicobacter infection. Mol Med Today **5** (11): 500-1, 1999.

Lesko, L. J., and Atkinson, A. J., Jr.: Use of biomarkers and surrogate endpoints in drug development and regulatory decision making: criteria, validation, strategies. Annu Rev Pharmacol Toxicol **41:** 347-66, 2001.

Lewis, R. S., Tamir, S., Tannenbaum, S. R., and Deen, W. M.: Kinetic analysis of the fate of nitric oxide synthesized by macrophages *in vitro*. J Biol Chem **270** (49): 29350-5, 1995a.

Lewis, R. S., Tamir, S., Tannenbaum, S. R., and Deen, W. M.: Kinetic analysis of the fate of nitric oxide synthesized by macrophages *in vitro*. *In* J Biol Chem, vol. 270, pp. 29350-5, 1995b.

Li, C. Q., Pignatelli, B., and Ohshima, H.: Increased oxidative and nitrative stress in human stomach associated with cagA+ Helicobacter pylori infection and inflammation. Dig Dis Sci **46** (4): 836-44, 2001.

Li, J., Billiar, T. R., Talanian, R. V., and Kim, Y. M.: Nitric oxide reversibly inhibits seven members of the caspase family via S-nitrosylation. Biochem Biophys Res Commun **240** (2): 419-24, 1997.

Lindahl, T., and Barnes, D. E.: Mammalian DNA ligases. Annu Rev Biochem **61:** 251-81, 1992.

Liu, H., and Pope, R. M.: Phagocytes: mechanisms of inflammation and tissue destruction. Rheum Dis Clin North Am **30** (1): 19-39, v, 2004.

Liu, J., Garcia-Cardena, G., and Sessa, W. C.: Biosynthesis and palmitoylation of endothelial nitric oxide synthase: mutagenesis of palmitoylation sites, cysteines-15 and/or -26, argues against depalmitoylation-induced translocation of the enzyme. Biochemistry **34** (38): 12333-40, 1995.

Liu, R. H., and Hotchkiss, J. H.: Potential genotoxicity of chronically elevated nitric oxide: a review. Mutat Res **339** (2): 73-89, 1995.

Liu, X., Miller, M. J., Joshi, M. S., Thomas, D. D., and Lancaster, J. R., Jr.: Accelerated reaction of nitric oxide with O2 within the hydrophobic interior of biological membranes. Proc Natl Acad Sci U S A **95** (5): 2175-9, 1998.

Loeb, K. R., and Loeb, L. A.: Genetic instability and the mutator phenotype. Studies in ulcerative colitis. Am J Pathol **154** (6): 1621-6, 1999.

Lorch, S., Lightfoot, R., Ohshima, H., Virag, L., Chen, Q., Hertkorn, C., Weiss, M., Souza, J., Ischiropoulos, H., Yermilov, V., Pignatelli, B., Masuda, M., and Szabo, C.: Detection of peroxynitrite-induced protein and DNA modifications. Methods Mol Biol **196:** 247-75, 2002.

Lymar, S. V., and Hurst, J. K.: Radical nature of peroxynitrite reactivity. Chem Res Toxicol **11** (7): 714-5, 1998.

Ma, J., Chen, T., Mandelin, J., Ceponis, A., Miller, N. E., Hukkanen, M., Ma, G. F., and Konttinen, Y. T.: Regulation of macrophage activation. Cell Mol Life Sci **60** (11): 2334-46, 2003.

MacMicking, J. D., Nathan, C., Hom, G., Chartrain, N., Fletcher, D. S., Trumbauer, M., Stevens, K., Xie, Q. W., Sokol, K., Hutchinson, N., and et al.: Altered responses to bacterial infection and endotoxic shock in mice lacking inducible nitric oxide synthase. Cell **81** (4): 641-50, 1995.

Majano, P. L., and Garcia-Monzon, C.: Does nitric oxide play a pathogenic role in hepatitis C virus infection? Cell Death Differ **10 Suppl 1**: S13-5, 2003.

Majano, P. L., Garcia-Monzon, C., Lopez-Cabrera, M., Lara-Pezzi, E., Fernandez-Ruiz, E., Garcia-Iglesias, C., Borque, M. J., and Moreno-Otero, R.: Inducible nitric oxide synthase expression in chronic viral hepatitis. Evidence for a virus-induced gene upregulation. J Clin Invest **101** (7): 1343-52, 1998.

Marletta, M. A., Yoon, P. S., Iyengar, R., Leaf, C. D., and Wishnok, J. S.: Macrophage oxidation of L-arginine to nitrite and nitrate: nitric oxide is an intermediate. Biochemistry **27** (24): 8706-11, 1988.

Marnett, L. J.: Oxy radicals, lipid peroxidation and DNA damage. Toxicology **181-182:** 219-22, 2002a.

Marnett, L. J.: Oxy radicals, lipid peroxidation and DNA damage. *In* Toxicology, vol. 181-182, pp. 219-22, 2002b.

Marnett, L. J., and Plastaras, J. P.: Endogenous DNA damage and mutation. Trends Genet **17** (4): 214-21, 2001.

Marnett, L. J., Riggins, J. N., and West, J. D.: Endogenous generation of reactive oxidants and electrophiles and their reactions with DNA and protein. J Clin Invest **111** (5): 583-93, 2003.

Mashimo, H., and Goyal, R. K.: Lessons from genetically engineered animal models. IV. Nitric oxide synthase gene knockout mice. Am J Physiol **277** (4 Pt 1): G745-50, 1999.

Matsumoto, Y., and Kim, K.: Excision of deoxyribose phosphate residues by DNA polymerase beta during DNA repair. Science **269** (5224): 699-702, 1995.

McCullough, A. K., Dodson, M. L., and Lloyd, R. S.: Initiation of base excision repair: glycosylase mechanisms and structures. Annu Rev Biochem **68:** 255-85, 1999.

McHugh, P. J., Sones, W. R., and Hartley, J. A.: Repair of intermediate structures produced at DNA interstrand cross-links in Saccharomyces cerevisiae. Mol Cell Biol **20** (10): 3425-33, 2000.

Merchant, K., Chen, H., Gonzalez, T. C., Keefer, L. K., and Shaw, B. R.: Deamination of single-stranded DNA cytosine residues in aerobic nitric oxide solution at micromolar total NO exposures. Chem Res Toxicol **9** (5): 891-6, 1996.

Merenyi, G., Lind, J., Goldstein, S., and Czapski, G.: Peroxynitrous acid homolyzes into *OH and *NO2 radicals. Chem Res Toxicol **11** (7): 712-3, 1998.

Mihm, S., Fayyazi, A., and Ramadori, G.: Hepatic expression of inducible nitric oxide synthase transcripts in chronic hepatitis C virus infection: relation to hepatic viral load and liver injury. Hepatology **26** (2): 451-8, 1997.

Miles, A. M., Bohle, D. S., Glassbrenner, P. A., Hansert, B., Wink, D. A., and Grisham, M. B.: Modulation of superoxide-dependent oxidation and hydroxylation reactions by nitric oxide. J Biol Chem **271** (1): 40-7, 1996.

Miranda, K. M., Nims, R. W., Thomas, D. D., Espey, M. G., Citrin, D., Bartberger, M. D., Paolocci, N., Fukuto, J. M., Feelisch, M., and Wink, D. A.: Comparison of the reactivity of nitric oxide and nitroxyl with heme proteins. A chemical discussion of the differential biological effects of these redox related products of NOS. J Inorg Biochem **93** (1-2): 52-60, 2003a.

Miranda, K. M., Paolocci, N., Katori, T., Thomas, D. D., Ford, E., Bartberger, M. D., Espey, M. G., Kass, D. A., Feelisch, M., Fukuto, J. M., and Wink, D. A.: A biochemical rationale for the discrete behavior of nitroxyl and nitric oxide in the cardiovascular system. Proc Natl Acad Sci U S A **100** (16): 9196-201, 2003b.

Moller, L., Grzybowska, E., Zeisig, M., Cimander, B., Hemminki, K., and Chorazy, M.: Seasonal variation of DNA adduct pattern in human lymphocytes analyzed by 32P-HPLC. Carcinogenesis **17** (1): 61-6, 1996.

Moller, L., and Hofer, T.: [32P]ATP mediates formation of 8-hydroxy-2'-deoxyguanosine from 2'-deoxyguanosine, a possible problem in the 32P-postlabeling assay. Carcinogenesis **18** (12): 2415-9, 1997.

Moncada, S., Palmer, R. M., and Higgs, E. A.: Nitric oxide: physiology, pathophysiology, and pharmacology. Pharmacol Rev **43** (2): 109-42, 1991.

Morita, E. H., Ohkubo, T., Kuraoka, I., Shirakawa, M., Tanaka, K., and Morikawa, K.: Implications of the zinc-finger motif found in the DNA-binding domain of the human XPA protein. Genes Cells **1** (5): 437-42, 1996.

Moss, S. F.: Review article: Cellular markers in the gastric precancerous process. Aliment Pharmacol Ther **12 Suppl 1:** 91-109, 1998.

Mukai, F. H., and Goldstein, B. D.: Mutagenicity of malonaldehyde, a decomposition product of peroxidized polyunsaturated fatty acids. Science **191** (4229): 868-9, 1976.

Nacy, C. A., and Meltzer, M. S.: T-cell-mediated activation of macrophages. Curr Opin Immunol **3** (3): 330-5, 1991.

Nagy, K., Pollreisz, F., Takats, Z., and Vekey, K.: Atmospheric pressure chemical ionization mass spectrometry of aldehydes in biological matrices. Rapid Commun Mass Spectrom **18** (20): 2473-8, 2004.

Nair, J., Barbin, A., Guichard, Y., and Bartsch, H.: 1,N6-ethenodeoxyadenosine and 3,N4-ethenodeoxycytine in liver DNA from humans and untreated rodents detected by immunoaffinity/32P-postlabeling. Carcinogenesis **16** (3): 613-7, 1995.

Nair, J., Barbin, A., Velic, I., and Bartsch, H.: Etheno DNA-base adducts from endogenous reactive species. Mutat Res **424** (1-2): 59-69, 1999.

Nair, J., Carmichael, P. L., Fernando, R. C., Phillips, D. H., Strain, A. J., and Bartsch, H.: Lipid peroxidation-induced etheno-DNA adducts in the liver of patients with the genetic metal storage disorders Wilson's disease and primary hemochromatosis. Cancer Epidemiol Biomarkers Prev **7** (5): 435-40, 1998a.

Nair, J., Gal, A., Tamir, S., Tannenbaum, S. R., Wogan, G. N., and Bartsch, H.: Etheno adducts in spleen DNA of SJL mice stimulated to overproduce nitric oxide. Carcinogenesis **19** (12): 2081-4, 1998b.

Nair, J., Sone, H., Nagao, M., Barbin, A., and Bartsch, H.: Copper-dependent formation of miscoding etheno-DNA adducts in the liver of Long Evans cinnamon (LEC) rats developing hereditary hepatitis and hepatocellular carcinoma. *In* Cancer Res, vol. 56, pp. 1267-71, 1996.

Nair, J., Vaca, C. E., Velic, I., Mutanen, M., Valsta, L. M., and Bartsch, H.: High dietary omega-6 polyunsaturated fatty acids drastically increase the formation of etheno-DNA base

adducts in white blood cells of female subjects. Cancer Epidemiol Biomarkers Prev **6** (8): 597-601, 1997.

Naito, M., Umeda, S., Yamamoto, T., Moriyama, H., Umezu, H., Hasegawa, G., Usuda, H., Shultz, L. D., and Takahashi, K.: Development, differentiation, and phenotypic heterogeneity of murine tissue macrophages. J Leukoc Biol **59** (2): 133-8, 1996.

Nardone, G., and Morgner, A.: Helicobacter pylori and gastric malignancies. Helicobacter **8 Suppl 1:** 44-52, 2003.

Newton, R.: Infections and human cancer. Ann Oncol **11** (9): 1081-2, 2000.

Ng, E. S., Jourd'heuil, D., McCord, J. M., Hernandez, D., Yasui, M., Knight, D., and Kubes, P.: Enhanced S-nitroso-albumin formation from inhaled NO during ischemia/reperfusion. Circ Res **94** (4): 559-65, 2004.

Nguyen, T., Brunson, D., Crespi, C. L., Penman, B. W., Wishnok, J. S., and Tannenbaum, S. R.: DNA damage and mutation in human cells exposed to nitric oxide *in vitro*. Proc Natl Acad Sci U S A **89** (7): 3030-4, 1992.

Nikov, G., Bhat, V., Wishnok, J. S., and Tannenbaum, S. R.: Analysis of nitrated proteins by nitrotyrosine-specific affinity probes and mass spectrometry. Anal Biochem **320** (2): 214-22, 2003.

Niles, J. C., Burney, S., Singh, S. P., Wishnok, J. S., and Tannenbaum, S. R.: Peroxynitrite reaction products of 3',5'-di-O-acetyl-8-oxo-7, 8-dihydro-2'-deoxyguanosine. Proc Natl Acad Sci U S A **96** (21): 11729-34, 1999.

Niles, J. C., Wishnok, J. S., and Tannenbaum, S. R.: A novel nitration product formed during the reaction of peroxynitrite with 2',3',5'-tri-O-acetyl-7,8-dihydro-8-oxoguanosine: N-nitro-N'-[1-(2,3,5-tri-O-acetyl-beta-D-erythro-pentofuranosyl)- 2, 4-dioxoimidazolidin-5-ylidene]guanidine. Chem Res Toxicol **13** (5): 390-6, 2000.

Nordenfelt, E.: Persistence of hepatitis B virus and establishment of delta virus infection. Scand J Infect Dis Suppl **69:** 121-4, 1990.

Ohshima, H., and Bartsch, H.: Chronic infections and inflammatory processes as cancer risk factors: possible role of nitric oxide in carcinogenesis. Mutat Res **305** (2): 253-64, 1994.

Ohshima, H., Friesen, M., Brouet, I., and Bartsch, H.: Nitrotyrosine as a new marker for endogenous nitrosation and nitration of proteins. Food Chem Toxicol **28** (9): 647-52, 1990.

Ohshima, H., Gilibert, I., and Bianchini, F.: Induction of DNA strand breakage and base oxidation by nitroxyl anion through hydroxyl radical production. Free Radic Biol Med **26** (9-10): 1305-13, 1999.

Ohshima, H., Tatemichi, M., and Sawa, T.: Chemical basis of inflammation-induced carcinogenesis. Arch Biochem Biophys **417** (1): 3-11, 2003.

Oshima, M., Dinchuk, J. E., Kargman, S. L., Oshima, H., Hancock, B., Kwong, E., Trzaskos, J. M., Evans, J. F., and Taketo, M. M.: Suppression of intestinal polyposis in Apc delta716 knockout mice by inhibition of cyclooxygenase 2 (COX-2). Cell **87** (5): 803-9, 1996.

Park, S., Kim, W. S., Choi, U. J., Han, S. U., Kim, Y. S., Kim, Y. B., Chung, M. H., Nam, K. T., Kim, D. Y., Cho, S. W., and Hahm, K. B.: amelioration of oxidative stress with ensuing inflammation contributes to chemoprevention of H. pylori-associated gastric carcinogenesis. Antioxid Redox Signal **6** (3): 549-60, 2004.

Park, W. S., Oh, R. R., Kim, Y. S., Park, J. Y., Lee, S. H., Shin, M. S., Kim, S. Y., Kim, P. J., Lee, H. K., Yoo, N. Y., and Lee, J. Y.: Somatic mutations in the death domain of the Fas (Apo-1/CD95) gene in gastric cancer. J Pathol **193** (2): 162-8, 2001.

Parkin, D. M.: Global cancer statistics in the year 2000. Lancet Oncol **2** (9): 533-43, 2001.

Parkin, D. M., Bray, F., Ferlay, J., and Pisani, P.: Estimating the world cancer burden: Globocan 2000. Int J Cancer **94** (2): 153-6, 2001.

Petit, C., and Sancar, A.: Nucleotide excision repair: from E. coli to man. Biochimie **81** (1-2): 15-25, 1999.

Petrelli, E., Manzin, A., Paolucci, S., Cioppi, A., Brugia, M., Muretto, P., and Clementi, M.: Chronic liver disease and active hepatitis C virus infection in patients with antibodies to this virus. J Clin Pathol **47** (2): 148-51, 1994.

Petrini, J. H.: The mammalian Mre11-Rad50-nbs1 protein complex: integration of functions in the cellular DNA-damage response. Am J Hum Genet **64** (5): 1264-9, 1999.

Plastaras, J. P., Riggins, J. N., Otteneder, M., and Marnett, L. J.: Reactivity and mutagenicity of endogenous DNA oxopropenylating agents: base propenals, malondialdehyde, and N(epsilon)-oxopropenyllysine. Chem Res Toxicol **13** (12): 1235-42, 2000.

Pogozelski, W. K., and Tullius, T. D.: Oxidative Strand Scission of Nucleic Acids: Routes Initiated by Hydrogen Abstraction from the Sugar Moiety. Chem Rev **98** (3): 1089-1108, 1998.

Pompella, A., Maellaro, E., Casini, A. F., and Comporti, M.: Histochemical detection of lipid peroxidation in the liver of bromobenzene-poisoned mice. Am J Pathol **129** (2): 295-301, 1987.

Radi, R., Beckman, J. S., Bush, K. M., and Freeman, B. A.: Peroxynitrite oxidation of sulfhydryls. The cytotoxic potential of superoxide and nitric oxide. *In* J Biol Chem, vol. 266, pp. 4244-50, 1991.

Ravanat, J. L., Duretz, B., Guiller, A., Douki, T., and Cadet, J.: Isotope dilution high-performance liquid chromatography-electrospray tandem mass spectrometry assay for the measurement of 8-oxo-7,8-dihydro-2'-deoxyguanosine in biological samples. *In* J Chromatogr B Biomed Sci Appl, vol. 715, pp. 349-56, 1998.

Rennick, D. M., and Fort, M. M.: Lessons from genetically engineered animal models. XII. IL-10-deficient (IL-10(-/-) mice and intestinal inflammation. Am J Physiol Gastrointest Liver Physiol **278** (6): G829-33, 2000.

Riddell, R. H., Goldman, H., Ransohoff, D. F., Appelman, H. D., Fenoglio, C. M., Haggitt, R. C., Ahren, C., Correa, P., Hamilton, S. R., Morson, B. C., and et al.: Dysplasia in inflammatory bowel disease: standardized classification with provisional clinical applications. Hum Pathol **14** (11): 931-68, 1983.

Roberts, D. W., Churchwell, M. I., Beland, F. A., Fang, J. L., and Doerge, D. R.: Quantitative analysis of etheno-2'-deoxycytidine DNA adducts using on-line immunoaffinity chromatography coupled with LC/ES-MS/MS detection. Anal Chem **73** (2): 303-9, 2001.

Rolan, P., Atkinson, A. J., Jr., and Lesko, L. J.: Use of biomarkers from drug discovery through clinical practice: report of the Ninth European Federation of Pharmaceutical Sciences Conference on Optimizing Drug Development. Clin Pharmacol Ther **73** (4): 284-91, 2003.

Rosin, M. P., Anwar, W. A., and Ward, A. J.: Inflammation, chromosomal instability, and cancer: the schistosomiasis model. Cancer Res **54** (7 Suppl): 1929s-1933s, 1994a.

Rosin, M. P., Saad el Din Zaki, S., Ward, A. J., and Anwar, W. A.: Involvement of inflammatory reactions and elevated cell proliferation in the development of bladder cancer in schistosomiasis patients. Mutat Res **305** (2): 283-92, 1994b.

Rouse, J., and Jackson, S. P.: Interfaces between the detection, signaling, and repair of DNA damage. Science **297** (5581): 547-51, 2002.

Routledge, M. N., Wink, D. A., Keefer, L. K., and Dipple, A.: DNA sequence changes induced by two nitric oxide donor drugs in the supF assay. Chem Res Toxicol **7** (5): 628-32, 1994.

Rouzer, C. A., Chaudhary, A. K., Nokubo, M., Ferguson, D. M., Reddy, G. R., Blair, I. A., and Marnett, L. J.: Analysis of the malondialdehyde-2'-deoxyguanosine adduct pyrimidopurinone in human leukocyte DNA by gas chromatography/electron capture/negative chemical ionization/mass spectrometry. Chem Res Toxicol **10** (2): 181-8, 1997.

Salem, M. L.: Estrogen, a double-edged sword: modulation of TH1- and TH2-mediated inflammations by differential regulation of TH1/TH2 cytokine production. Curr Drug Targets Inflamm Allergy **3** (1): 97-104, 2004.

Salgo, M. G., Bermudez, E., Squadrito, G. L., and Pryor, W. A.: Peroxynitrite causes DNA damage and oxidation of thiols in rat thymocytes [corrected]. Arch Biochem Biophys **322** (2): 500-5, 1995a.

Salgo, M. G., Stone, K., Squadrito, G. L., Battista, J. R., and Pryor, W. A.: Peroxynitrite causes DNA nicks in plasmid pBR322. *In* Biochem Biophys Res Commun, vol. 210, pp. 1025-30, 1995b.

Samiec, P. S., and Goodman, J. I.: Evaluation of methylated DNA binding protein-1 in mouse liver. Toxicol Sci **49** (2): 255-62, 1999.

Samouilov, A., Kuppusamy, P., and Zweier, J. L.: Evaluation of the magnitude and rate of nitric oxide production from nitrite in biological systems. Arch Biochem Biophys **357** (1): 1-7, 1998.

Sancar, A.: Structure and function of DNA photolyase. Biochemistry **33** (1): 2-9, 1994.

Sandhu, J. K., Privora, H. F., Wenckebach, G., and Birnboim, H. C.: Neutrophils, nitric oxide synthase, and mutations in the mutatect murine tumor model. Am J Pathol **156** (2): 509-18, 2000.

Schmid, K., Nair, J., Winde, G., Velic, I., and Bartsch, H.: Increased levels of promutagenic etheno-DNA adducts in colonic polyps of FAP patients. *In* Int J Cancer, vol. 87, pp. 1-4, 2000a.

Schmid, K., Nair, J., Winde, G., Velic, I., and Bartsch, H.: Increased levels of promutagenic etheno-DNA adducts in colonic polyps of FAP patients. Int J Cancer **87** (1): 1-4, 2000b.

Schmitt, D., Shen, Z., Zhang, R., Colles, S. M., Wu, W., Salomon, R. G., Chen, Y., Chisolm, G. M., and Hazen, S. L.: Leukocytes utilize myeloperoxidase-generated nitrating intermediates as physiological catalysts for the generation of biologically active oxidized lipids and sterols in serum. Biochemistry **38** (51): 16904-15, 1999.

Scott, D. J., Hull, M. A., Cartwright, E. J., Lam, W. K., Tisbury, A., Poulsom, R., Markham, A. F., Bonifer, C., and Coletta, P. L.: Lack of inducible nitric oxide synthase promotes intestinal tumorigenesis in the Apc(Min/+) mouse. Gastroenterology **121** (4): 889-99, 2001.

Sepulveda, A. R.: Molecular testing of Helicobacter pylori-associated chronic gastritis and premalignant gastric lesions: clinical implications. J Clin Gastroenterol **32** (5): 377-82, 2001.

Serrano, J., Palmeira, C. M., Wallace, K. B., and Kuehl, D. W.: Determination of 8-hydroxydeoxyguanosine in biological tissue by liquid chromatography/electrospray ionization-mass spectrometry/mass spectrometry. Rapid Commun Mass Spectrom **10** (14): 1789-91, 1996.

Sezaki, H., Kobayashi, M., Hosaka, T., Someya, T., Akuta, N., Suzuki, F., Tsubota, A., Suzuki, Y., Saitoh, S., Arase, Y., Ikeda, K., Matsuda, M., Takagi, K., Sato, J., and Kumada, H.: Hepatocellular carcinoma in noncirrhotic young adult patients with chronic hepatitis B viral infection. J Gastroenterol **39** (6): 550-6, 2004.

Shacter, E., and Weitzman, S. A.: Chronic inflammation and cancer. Oncology (Huntingt) **16** (2): 217-26, 229; discussion 230-2, 2002.

Shah, M. H., Porcu, P., Mallery, S. R., and Caligiuri, M. A.: AIDS-associated malignancies. Cancer Chemother Biol Response Modif **21**: 717-46, 2003.

Shinkai, Y., Rathbun, G., Lam, K. P., Oltz, E. M., Stewart, V., Mendelsohn, M., Charron, J., Datta, M., Young, F., Stall, A. M., and et al.: RAG-2-deficient mice lack mature lymphocytes owing to inability to initiate V(D)J rearrangement. Cell **68** (5): 855-67, 1992.

Singer, II, Kawka, D. W., Scott, S., Weidner, J. R., Mumford, R. A., Riehl, T. E., and Stenson, W. F.: Expression of inducible nitric oxide synthase and nitrotyrosine in colonic epithelium in inflammatory bowel disease. Gastroenterology **111** (4): 871-85, 1996.

Spek, E. J., Vuong, L. N., Matsuguchi, T., Marinus, M. G., and Engelward, B. P.: Nitric oxide-induced homologous recombination in Escherichia coli is promoted by DNA glycosylases. J Bacteriol **184** (13): 3501-7, 2002.

Spek, E. J., Wright, T. L., Stitt, M. S., Taghizadeh, N. R., Tannenbaum, S. R., Marinus, M. G., and Engelward, B. P.: Recombinational repair is critical for survival of Escherichia coli exposed to nitric oxide. J Bacteriol **183** (1): 131-8, 2001.

Spickett, C. M., Jerlich, A., Panasenko, O. M., Arnhold, J., Pitt, A. R., Stelmaszynska, T., and Schaur, R. J.: The reactions of hypochlorous acid, the reactive oxygen species produced by myeloperoxidase, with lipids. Acta Biochim Pol **47** (4): 889-99, 2000.

St Croix, C. M., Stitt, M. S., Leelavanichkul, K., Wasserloos, K. J., Pitt, B. R., and Watkins, S. C.: Nitric oxide-induced modification of protein thiolate clusters as determined by spectral fluorescence resonance energy transfer in live endothelial cells. Free Radic Biol Med **37** (6): 785-92, 2004.

Stamler, J. S., Jaraki, O., Osborne, J., Simon, D. I., Keaney, J., Vita, J., Singel, D., Valeri, C. R., and Loscalzo, J.: Nitric oxide circulates in mammalian plasma primarily as an S-nitroso adduct of serum albumin. Proc Natl Acad Sci U S A **89** (16): 7674-7, 1992a.

Stamler, J. S., Lamas, S., and Fang, F. C.: Nitrosylation. the prototypic redox-based signaling mechanism. Cell **106** (6): 675-83, 2001.

Stamler, J. S., Singel, D. J., and Loscalzo, J.: Biochemistry of nitric oxide and its redox-activated forms. Science **258** (5090): 1898-902, 1992b.

Stone, K., Ksebati, M. B., and Marnett, L. J.: Investigation of the adducts formed by reaction of malondialdehyde with adenosine. Chem Res Toxicol **3** (1): 33-8, 1990.

Stvrtionva, V., Jakubovsky, J., and Hulin, I.: Inflammation and fever. *In* Pathophysiology principles of diseases, Academic Electronic Press, 1995.

Sugden, K. D., and Wetterhahn, K. E.: Direct and hydrogen peroxide-induced chromium(V) oxidation of deoxyribose in single-stranded and double-stranded calf thymus DNA. Chem Res Toxicol **10** (12): 1397-406, 1997.

Sugiyama, S., Kugiyama, K., Aikawa, M., Nakamura, S., Ogawa, H., and Libby, P.: Hypochlorous acid, a macrophage product, induces endothelial apoptosis and tissue factor expression: involvement of myeloperoxidase-mediated oxidant in plaque erosion and thrombogenesis. Arterioscler Thromb Vasc Biol **24** (7): 1309-14, 2004.

Sung, P.: Catalysis of ATP-dependent homologous DNA pairing and strand exchange by yeast RAD51 protein. Science **265** (5176): 1241-3, 1994.

Suzuki, T., Yamada, M., Kanaori, K., Tajima, K., Morii, T., and Makino, K.: Formation of 8-nitroguanine from 2'-deoxyguanosine by NO/O2 system. Nucleic Acids Symp Ser (42): 155-6, 1999.

Szabo, C., and Ohshima, H.: DNA damage induced by peroxynitrite: subsequent biological effects. Nitric Oxide **1** (5): 373-85, 1997.

Takahashi, K., Naito, M., and Takeya, M.: Development and heterogeneity of macrophages and their related cells through their differentiation pathways. Pathol Int **46** (7): 473-85, 1996.

Tamir, S., deRojas-Walker, T., Wishnok, J. S., and Tannenbaum, S. R.: DNA damage and genotoxicity by nitric oxide. Methods Enzymol **269**: 230-43, 1996.

Thun, M. J., Henley, S. J., and Gansler, T.: Inflammation and cancer: an epidemiological perspective. Novartis Found Symp **256**: 6-21; discussion 22-8, 49-52, 266-9, 2004.

Tiano, H. F., Loftin, C. D., Akunda, J., Lee, C. A., Spalding, J., Sessoms, A., Dunson, D. B., Rogan, E. G., Morham, S. G., Smart, R. C., and Langenbach, R.: Deficiency of either cyclooxygenase (COX)-1 or COX-2 alters epidermal differentiation and reduces mouse skin tumorigenesis. Cancer Res **62** (12): 3395-401, 2002.

Todo, T., Takemori, H., Ryo, H., Ihara, M., Matsunaga, T., Nikaido, O., Sato, K., and Nomura, T.: A new photoreactivating enzyme that specifically repairs ultraviolet light-induced (6-4)photoproducts. Nature **361** (6410): 371-4, 1993.

Toyokuni, S., Uchida, K., Okamoto, K., Hattori-Nakakuki, Y., Hiai, H., and Stadtman, E. R.: Formation of 4-hydroxy-2-nonenal-modified proteins in the renal proximal tubules of rats treated with a renal carcinogen, ferric nitrilotriacetate. Proc Natl Acad Sci U S A **91** (7): 2616-20, 1994.

Tretyakova, N. Y., Niles, J. C., Burney, S., Wishnok, J. S., and Tannenbaum, S. R.: Peroxynitrite-induced reactions of synthetic oligonucleotides containing 8-oxoguanine. Chem Res Toxicol **12** (5): 459-66, 1999.

Tsuru, S., Fujisawa, H., Taniguchi, M., Zinnaka, Y., and Nomoto, K.: Mechanism of protection during the early phase of a generalized viral infection. II. Contribution of polymorphonuclear leukocytes to protection against intravenous infection with influenza virus. J Gen Virol **68 (Pt 2)**: 419-24, 1987.

Turk, P. W., Laayoun, A., Smith, S. S., and Weitzman, S. A.: DNA adduct 8-hydroxyl-2'-deoxyguanosine (8-hydroxyguanine) affects function of human DNA methyltransferase. Carcinogenesis **16** (5): 1253-5, 1995.

Van der Veen, R. C., and Roberts, L. J.: Contrasting roles for nitric oxide and peroxynitrite in the peroxidation of myelin lipids. J Neuroimmunol **95** (1-2): 1-7, 1999.

Van der Vliet, A., Eiserich, J. P., Halliwell, B., and Cross, C. E.: Formation of reactive nitrogen species during peroxidase-catalyzed oxidation of nitrite. A potential additional mechanism of nitric oxide-dependent toxicity. J Biol Chem **272** (12): 7617-25, 1997.

Van Furth, R.: Phagocytic cells: development and distribution of mononuclear phagocytes in normal steady state and inflammation. *In* Inflammation: basic principles and clinical correlates, ed. by J. Gallin, I. Goldstein, and R. Snyderman, pp. Chapter 17, Raven Press, New York, 1992.

Van Houten, B., Gamper, H., Holbrook, S. R., Hearst, J. E., and Sancar, A.: Action mechanism of ABC excision nuclease on a DNA substrate containing a psoralen crosslink at a defined position. Proc Natl Acad Sci U S A **83** (21): 8077-81, 1986.

Vongchampa, V., Dong, M., Gingipalli, L., and Dedon, P.: Stability of 2'-deoxyxanthosine in DNA. Nucleic Acids Res **31** (3): 1045-51, 2003.

Weitzberg, E., and Lundberg, J. O.: Nonenzymatic nitric oxide production in humans. Nitric Oxide **2** (1): 1-7, 1998.

Weitzman, S. A., Turk, P. W., Milkowski, D. H., and Kozlowski, K.: Free radical adducts induce alterations in DNA cytosine methylation. Proc Natl Acad Sci U S A **91** (4): 1261-4, 1994.

Weitzman, S. A., Weitberg, A. B., Clark, E. P., and Stossel, T. P.: Phagocytes as carcinogens: malignant transformation produced by human neutrophils. Science **227** (4691): 1231-3, 1985.

Welford, R. W., Schlemminger, I., McNeill, L. A., Hewitson, K. S., and Schofield, C. J.: The selectivity and inhibition of AlkB. J Biol Chem **278** (12): 10157-61, 2003.

Wink, D. A., Cook, J. A., Pacelli, R., DeGraff, W., Gamson, J., Liebmann, J., Krishna, M. C., and Mitchell, J. B.: The effect of various nitric oxide-donor agents on hydrogen peroxide-mediated toxicity: a direct correlation between nitric oxide formation and protection. Arch Biochem Biophys **331** (2): 241-8, 1996.

Wink, D. A., Feelisch, M., Fukuto, J., Chistodoulou, D., Jourd'heuil, D., Grisham, M. B., Vodovotz, Y., Cook, J. A., Krishna, M., DeGraff, W. G., Kim, S., Gamson, J., and Mitchell, J. B.: The cytotoxicity of nitroxyl: possible implications for the pathophysiological role of NO. Arch Biochem Biophys **351** (1): 66-74, 1998.

Wink, D. A., Kasprzak, K. S., Maragos, C. M., Elespuru, R. K., Misra, M., Dunams, T. M., Cebula, T. A., Koch, W. H., Andrews, A. W., Allen, J. S., and et al.: DNA deaminating ability and genotoxicity of nitric oxide and its progenitors. Science **254** (5034): 1001-3, 1991.

Wink, D. A., Kim, S., Coffin, D., Cook, J. C., Vodovotz, Y., Chistodoulou, D., Jourd'heuil, D., and Grisham, M. B.: Detection of S-nitrosothiols by fluorometric and colorimetric methods. Methods Enzymol **301**: 201-11, 1999.

Wink, D. A., and Laval, J.: The Fpg protein, a DNA repair enzyme, is inhibited by the biomediator nitric oxide *in vitro* and *in vivo*. Carcinogenesis **15** (10): 2125-9, 1994a.

Wink, D. A., and Laval, J.: The Fpg protein, a DNA repair enzyme, is inhibited by the biomediator nitric oxide *in vitro* and *in vivo*. *In* Carcinogenesis, vol. 15, pp. 2125-9, 1994b.

Wink, D. A., and Mitchell, J. B.: Chemical biology of nitric oxide: Insights into regulatory, cytotoxic, and cytoprotective mechanisms of nitric oxide. Free Radic Biol Med **25** (4-5): 434-56, 1998.

Winter, C. K., Segall, H. J., and Haddon, W. F.: Formation of cyclic adducts of deoxyguanosine with the aldehydes trans-4-hydroxy-2-hexenal and trans-4-hydroxy-2-nonenal *in vitro*. Cancer Res **46** (11): 5682-6, 1986.

Wong, P. S., Hyun, J., Fukuto, J. M., Shirota, F. N., DeMaster, E. G., Shoeman, D. W., and Nagasawa, H. T.: Reaction between S-nitrosothiols and thiols: generation of nitroxyl (HNO) and subsequent chemistry. Biochemistry **37** (16): 5362-71, 1998.

Yamada, M., Suzuki, T., Kanaori, K., Tajima, K., Sakamoto, S., Kodaki, T., and Makino, K.: Nitration of 2'-deoxyguanosine by a NO/O2 gas mixture: identification and characterization of N2-nitro-2'-deoxyguanosine. Org Lett **5** (18): 3173-6, 2003.

Yen, T. Y., Christova-Gueoguieva, N. I., Scheller, N., Holt, S., Swenberg, J. A., and Charles, M. J.: Quantitative analysis of the DNA adduct N2,3-ethenoguanine using liquid chromatography/electrospray ionization mass spectrometry. J Mass Spectrom **31** (11): 1271-6, 1996.

Yermilov, V., Rubio, J., Becchi, M., Friesen, M. D., Pignatelli, B., and Ohshima, H.: Formation of 8-nitroguanine by the reaction of guanine with peroxynitrite *in vitro*. Carcinogenesis **16** (9): 2045-50, 1995a.

Yermilov, V., Rubio, J., and Ohshima, H.: Formation of 8-nitroguanine in DNA treated with peroxynitrite *in vitro* and its rapid removal from DNA by depurination. FEBS Lett **376** (3): 207-10, 1995b.

Yermilov, V., Yoshie, Y., Rubio, J., and Ohshima, H.: Effects of carbon dioxide/bicarbonate on induction of DNA single-strand breaks and formation of 8-nitroguanine, 8-oxoguanine and base-propenal mediated by peroxynitrite. FEBS Lett **399** (1-2): 67-70, 1996.

Yi, P., Zhan, D., Samokyszyn, V. M., Doerge, D. R., and Fu, P. P.: Synthesis and 32P-postlabeling/high-performance liquid chromatography separation of diastereomeric 1,N2-(1,3-propano)-2'-deoxyguanosine 3'-phosphate adducts formed from 4-hydroxy-2-nonenal. Chem Res Toxicol **10** (11): 1259-65, 1997.

Yu, T., and Sinnhuber, R.: 2'-Thiobarbituric acid method for the measurement of rancidity in fishery products. Food Tcehnology **11** (6): 104-108, 1957.

Yu, Z., and Kone, B. C.: Hypermethylation of the Inducible Nitric-oxide Synthase Gene Promoter Inhibits Its Transcription. J Biol Chem **279** (45): 46954-61, 2004.

Zarkovic, N.: 4-hydroxynonenal as a bioactive marker of pathophysiological processes. Mol Aspects Med **24** (4-5): 281-91, 2003.

Zeisig, M., Hofer, T., Cadet, J., and Moller, L.: 32P-postlabeling high-performance liquid chromatography (32P-HPLC) adapted for analysis of 8-hydroxy-2'-deoxyguanosine. Carcinogenesis **20** (7): 1241-5, 1999.

Zeisig, M., and Moller, L.: 32P-HPLC suitable for characterization of DNA adducts formed *in vitro* by polycyclic aromatic hydrocarbons and derivatives. Carcinogenesis **16** (1): 1-9, 1995.

Zeisig, M., and Moller, L.: 32P-Postlabeling high-performance liquid chromatographic improvements to characterize DNA adduct stereoisomers from benzo[a]pyrene and benzo[c]phenanthrene, and to separate DNA adducts from 7,12-dimethylbenz[a]anthracene. J Chromatogr B Biomed Sci Appl **691** (2): 341-50, 1997.

Zhang, Y., and Hogg, N.: Formation and stability of S-nitrosothiols in RAW 264.7 cells. Am J Physiol Lung Cell Mol Physiol **287** (3): L467-74, 2004.

Zhuang, J. C., Lin, C., Lin, D., and Wogan, G. N.: Mutagenesis associated with nitric oxide production in macrophages. *In* Proc Natl Acad Sci U S A, vol. 95, pp. 8286-91, 1998.

Zhuang, J. C., Wright, T. L., deRojas-Walker, T., Tannenbaum, S. R., and Wogan, G. N.: Nitric oxide-induced mutations in the HPRT gene of human lymphoblastoid TK6 cells and in Salmonella typhimurium. Environ Mol Mutagen **35** (1): 39-47, 2000.

zur Hausen, H.: Viruses in human cancers. Science **254** (5035): 1167-73, 1991.

Chapter 2

Development of a Novel LC-MS Method for the Quantification of Nucleobase Deamination Products

[The work in this chapter has been published in "Dong, M., Wang, C., Deen, W. M. and Dedon, P. C. (2003). "Absence of 2'-deoxyoxanosine and presence of abasic sites in DNA exposed to nitric oxide at controlled physiological concentrations." Chem Res Toxicol **16**(9): 1044-55". A reprint of the paper is included in Appendix II]

2.1 Abstract

Nitric oxide ($NO^{\bullet}$) is physiologically important at low concentrations, but at high levels this molecule has been implicated in the pathophysiology of many diseases associated with chronic inflammation, including several cancers. One challenge facing the study of $NO^{\bullet}$ genotoxicty in biological systems is to define the spectrum of DNA lesions that arise in cells exposed to activated macrophages. A central question is which DNA lesions play a predominate role in the genotoxic effects of reactive nitrogen species (RNS): N_2O_3-induced base deamination products or $ONOO^-$-induced base oxidation products. To this end, we, in collaboration with the research group of Prof. Steven Tannenbaum, have developed sensitive liquid chromatography-mass spectrometry (LC-MS) methods to quantify a collection of modified nucleobase products derived from RNS with an emphasis here on the following deamination products: 2'-deoxyxanthosine (dX) and 2'-deoxyoxanosine (dO) from dG; 2'-dexyuridine (dU) from dC; and 2'-deoxyinosine (dI) from dA.

Method development began with the establishment of chromatographic conditions that provided base-line separation of all normal deoxynucleosides and deamination products. Isotopically labeled internal standards were synthesized and characterized from uniform [^{15}N]-labeled deoxynucleosides, chemically characterized and used to prepare calibration curves with DNA digested by a nuclease P1, phosphodiesterase, and alkaline phosphatase cocktail in the presence of coformycin, a specific inhibitor of deoxyadenosine deaminase. Conditions were optimized to achieve a detection limit of 100 fmol for each deamination product.

As an integrated part of the method development, the stability of dX in DNA was studied. Contrary to a common assumption that it is unstable and undergoes rapid depurination, we found

that the half-life of dX in double-stranded oligodeoxynucleotide to be 2.4 yr at pH 7, showing that it is a relatively stable lesion.

The analytical method was first validated by the accurate quantification of dI in oligoucleotides containing defined quantities of this nucleobase lesion. The amount of dI detected by the LC-MS method was 100 ± 5% of the calculated value. A second validation was using an independent analytical method, the plasmid nicking assay, to quantify strand breaks in NO•-treated supercoiled plasmid DNA revealed by DNA glycosylases (uracil DNA glycosylase for dU and *E. coli* alkyladenine DNA glycosylase for dX and dI). The amount of dU and dX plus dI determined by the plasmid nicking assay was ~90 ± 5% of that quantified by the LC-MS method.

Finally, strategies for the improvement of the analytical method are discussed in the context of managing samples from complicated biological systems.

2.2 Introduction

Nucleobase deamination by any mechanism results in the formation of xanthine (dX as a 2'-deoxynucleoside) from guanine, hypoxanthine (2'-deoxyinosine, dI) from adenine, uracil (2'-deoxyuridine, dU) from cytosine, and thymine (2'-deoxythymidine) from 5-methylcytosine, as shown in Scheme 1. Of particular interest is the observation of Suzuki *et al.* that deamination of guanine by nitrous acid *in vitro* partitions to form both xanthine and oxanine (2'-deoxyoxanosine, dO) (Suzuki et al., 1997b).

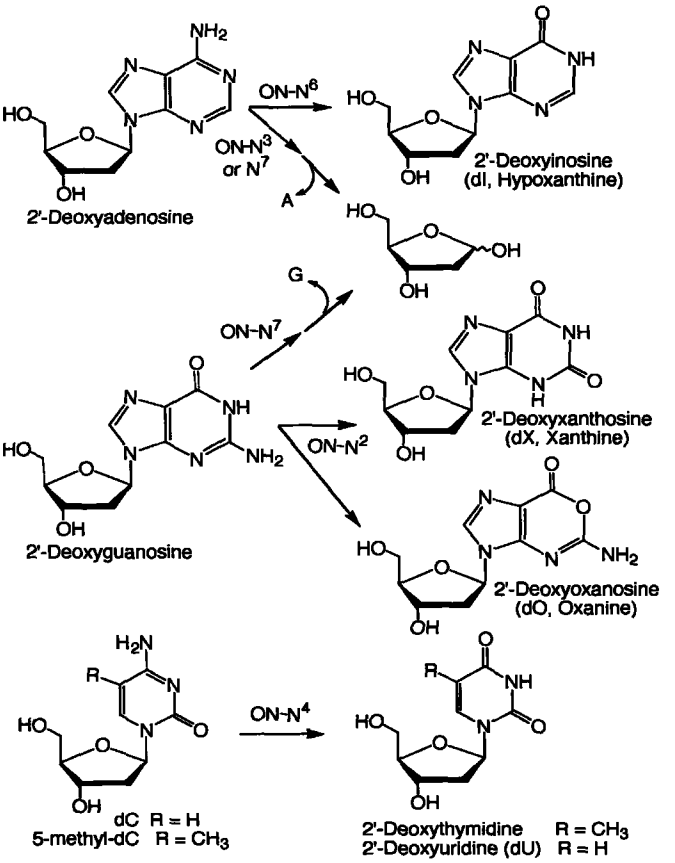

Scheme 1: Products of N-nitrosative nucleobase deamination

A. Sources and Mechanisms of Nucleobase Deamination

Several endogenous and exogenous sources can lead to nucleobase deamination. In addition to enzymatic deamination of 2'-deoxynucleosides (Bass, 2002; Chan et al., 1975) and bisulfite-induced deamination of dC (Shapiro et al., 1974), the two major mechanisms for deamination of nucleobases in DNA are hydrolysis and nitrosation. The propensity of the hydrolytic deamination of nucleobases in DNA occurs in the order of 5-methylcytosine > cytosine > adenine > guanine (Lindahl and Nyberg, 1974; Shapiro and Klein, 1966), with a half-life of cytosine in the range of 10^2-10^3 years in single-stranded DNA and 10^4-10^5 years in double-stranded DNA (Frederico et al., 1990a; Shen et al., 1994a; Zhang and Mathews, 1994). C5-methylation of cytosine increases the rate of deamination by 2- to 20-fold (Shen et al., 1994a; Zhang and Mathews, 1994). The hydrolytic deamination of purines, however, occurs at a rate that is at least an order of magnitude slower (Karran and Lindahl, 1980), and thus, consideration of only the hydrolysis rates would suggest that the occurrence of nucleobase deamination products in DNA would be extremely limited.

Nitrosative deamination of nucleobases has been shown to occur in acidified solutions of nitrite and in oxygenated solutions in the presence of NO$^{\bullet}$ (Dubelman and Shapiro, 1977; Kirchner et al., 1992; Nguyen et al., 1992; Shapiro and Pohl, 1968; Shapiro and Yamaguchi, 1972; Suzuki et al., 1997a; Wink et al., 1991). The reactive species in both cases appears to be nitrous anhydride (N_2O_3) (Lewis and Deen, 1994), a potent nitrosating agent that causes deamination of primary aromatic amines. The reactivity of N_2O_3 with nucleobases is reversed relative to the hydrolytic deamination, with xanthine formation proposed to occur at twice the rate of uracil (Caulfield et al., 1998).

Current theory, based on the chemistry of primary amines, suggests that nitrosative deamination of a nucleobase proceeds through the nitrosation of the exocyclic primary amino groups, which then leads to the formation of diazonium ions of the nucleobase as a crucial reactive intermediate (Figure 1). However, no diazonium ion of any nucleobase has ever been isolated or observed experimentally, which can be partially explained by the theoretical studies (*ab* initio studies) done in the Glaser group suggesting that DNA base diazonium ions are more prone to lose dinitrogen than the prototypical benzenediazium ion (Hodgen et al., 2003). Therefore, the exact mechanism of nitrosative deamination of nucleobase still eludes definition.

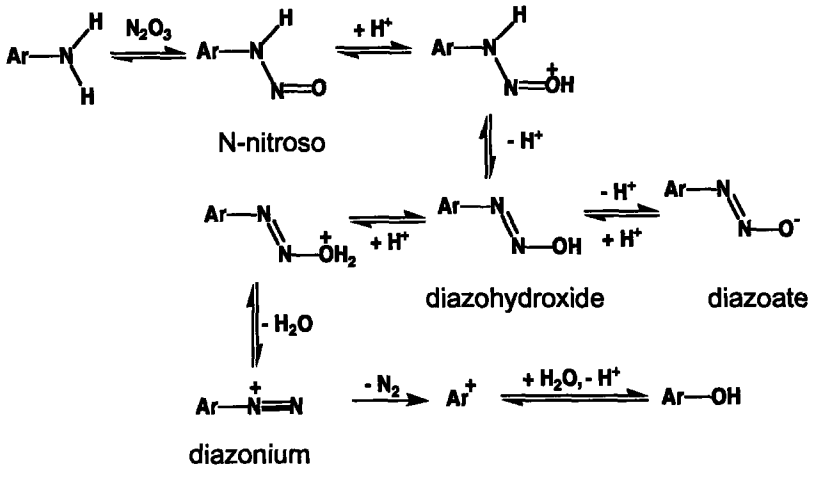

Figure 1. Proposed reaction pathways for the nitrosative deamination of aromatic amines by nitrous acid (adapted from Suzuki et al., 1999)

In addition to deamination of the exocyclic amines, nitrosation of the heterocyclic amines of dA and dG leads to depurination (Lucas et al., 2001; Lucas et al., 1999), as shown in Scheme 1. The mechanistic basis for depurination apparently involves nitrosation of the N^7 of dG and N^7 or

N^3 of dA, with the resulting destabilization of the glycosidic bond in the cationic bases (Lucas et al., 2001; Lucas et al., 1999).

B. Current Technologies for Quantification of Nucleobase Deamination Products

Nucleobase deamination can be measured by a variety of analytical techniques, each of which has its own advantages and drawbacks as well. Broadly, those techniques can be divided into two categories: the "indirect" approach and the "direct" approach. The first category includes those assays in which a DNA lesion is quantified by a biochemical or biological response thought to arise as a result of the specific DNA lesion. These assays include genetic assays and the combined use of a specific DNA repair enzyme and a technique to measure DNA strand breaks. The second category consists of those assays in which a DNA lesion is quantified by specific analytical means such as chromatography, spectroscopy or mass spectrometry. Commonly, DNA molecules are first extracted (or recovered) and then subjected to either enzymatic or chemical hydrolysis. The resulting mixture of DNA constituents is fractionated by high-resolution liquid chromatography and each particular lesion is detected at the output of the chromatographic column using sensitive analytical techniques.

"Indirect" Approaches

The first of the "indirect" approaches involves genetic methods. These are represented by Frederico's reversion of a mutant in the *lacZ* alpha gene coding sequence of bacteriophage M13mp2 and Shen's reversion to neomycin resistance of a mutant pSV2-*neo* plasmid (Frederico et al., 1990b; Shen et al., 1994b). Though sensitive to ~1 modification per 10^7 normal

nucleosides, these genetic methods apply only to the measurement of the deamination rates of cytosine and 5'-methylcytosine (Frederico et al., 1990b; Shen et al., 1994b).

Another set of "indirect" DNA damage assay involves the comet assay and the alkaline elution technique. These are sensitive methods for measuring both direct DNA strand breaks and alkali-labile sites (Olive et al., 1990; Swenberg et al., 1976). In the former assay, cells are embedded in an agarose gel on a microscope slide. Then, the cells are lysed under alkaline conditions and subsequently an electrophoresis is performed. Broken DNA loops migrate more rapidly than the nonfragmented part of the nucleus towards the anode, which results in a DNA migration pattern that resembles a comet. The percentage of DNA in the tail is related to the strand break frequency. In the latter assay, cells are lysed on the top of a filter and DNA is eluted through the filter using an alkaline solution. The rapidity of DNA elution through the filter is correlated with the number of strand breaks. These two methods have been modified in association with specific DNA repair enzymes in order to monitor altered DNA bases in addition to strand breaks. For instance, combined with uracil DNA glycosylase (UDG) isolated from *E. coli*, the comet assay allows an estimation of the number of uridine residues in genomic DNA (Duthie and Hawdon, 1998; Duthie and McMillan, 1997). These techniques have the advantage of dealing with reduced numbers of cells and the elimination of a multi-step DNA purification process (Pouget et al., 2000; Pouget et al., 1999). However, the assays rely on non-chemical mechanisms for quantifying specific chemical products of DNA damage and, in most cases, have not been rigorously calibrated.

"Direct" Approaches

^{32}P-postlabeling, one of the most commonly used methods to quantify DNA adducts, is based on the following simple steps: DNA digestion to 3′-phosphates by a DNA exonuclease; 5′-radiolabeling of adducts using T4 polynucleotide kinase; and separation of the bis-phosphates on thin layer chromatography (TLC). Highly sensitive, the ^{32}P-postlabeling technique is able to reliably detect DNA modifications in a level that is as low as ~1 per 10^9 nucleotides (Nair et al., 1998). Such methods, however, do not have the specificity desired for accurate and reliable quantitation, and are prone to produce false positives and artifacts. This technology has been rarely used to detect nucleobase deamination products, however, because of the poor separation of deaminated nucleobases from the normal ones on TLC (Green and Deutsch, 1984).

In the last decade, there has been a tremendous increase in the use of mass spectrometry (MS) for the analysis of DNA adducts. This increase can largely be attributed to two unique features of MS. Unlike other techniques, MS provides direct structural evidence for any given analyte, allowing for greater specificity. Furthermore, isotope-dilution MS (IDMS), which involves the use of stable isotope-labeled internal standards, allows for greater accuracy during quantification of the analytes. Among the various mass spectrometric methods, gas chromatography with negative ion chemical ionization mass spectrometry (GC–EC/MS) and liquid chromatography with electrospray mass spectrometry (LC–ESI/MS) are rapidly becoming the methods of choice in quantification of DNA adducts (Cadet et al., 2003; Koc and Swenberg, 2002; Phillips et al., 2000).

For the quantification of deamination products, most published studies have employed GC-MS techniques. In early 90's, Tannenbaum and colleagues detected increases of both xanthine and hypoxanthine in cells following NO$^{\bullet}$ exposure using an electron ionization (EI) GC-MS

method (Nguyen et al., 1992). Around the same time, Blout and Ames reported a GC-EC/MS method for the quantitative detection of dU as low as 1 pg in 100 μg DNA (Blount and Ames, 1994). Successive studies have provided improvements for various individual analytes so that, even today, GC-MS is still an applied method for analysis of deamination products (Caulfield et al., 1998; Mashiyama et al., 2004; Nguyen et al., 1992).

Nonetheless, some intrinsic drawbacks continue to hinder the application of GC-MS to detect DNA damage products. DNA molecules must first be hydrolyzed by acid to nucleobases and then derivatized by silylating agents to increase the volatility of the modified bases, which is followed by gas chromatographic separation. A plethora of evidence indicates that the derivatization procedure can cause artifacts, especially for the analysis of oxidative products like 8-oxo-dG, because of the presence of large quantities of normal DNA bases that are subjected to adventitious oxidation during derivatization (Cadet et al., 2002). The acidic conditions used for depurination of DNA in GC-MS analysis are generally believed to be mild enough to release both normal and altered bases. However, we found the decomposition of dO during acidic hydrolysis (Dong et al., unpublished observations). In addition, Schein reported the adventitious formation of uracil in formic acid hydrolysates of deoxyribonucleic acids (Schein, 1966). Therefore, to reach the goal of quantifying a spectrum of deamination lesions (including dX, dO, dI and dU) simultaneously, we chose to avoid the inherent difficulties associated with GC-MS and were thus compelled to develop alternative analytical methods.

LC-MS technology integrates the efficiency of HPLC separation together with the accuracy, versatility, and sensitivity afforded by mass spectrometry, and has brought significant improvements to the measurement of DNA damage products. A good example is the successful application of LC-MS to analyze oxidized DNA bases and nucleosides, including 8-oxo-dG

(Ravanat et al., 1998; Serrano et al., 1996), 8-oxo-dA (Podmore et al., 2000; Weimann et al., 2001), FapyGua, 5-(hydroxymethyl)-2'-deoxyuridine (5-HmdUrd), 5-formyl-2'-deoxyuridine (5-FordUrd), 5-hydroxy-2'-deoxyuridine (5-OHdUrd), and the *cis* and *trans* diastereomers of 5,6-dihydroxy-5,6-dihydrothymidine (dThdGly) (Frelon et al., 2000). In contrast, less has been done in using LC-MS to quantify base deamination products except for a few published studies about the detection of uracil or uridine (Jiang et al., 2002; Williams et al., 2003).

Given the fact that nucleobase deamination represents an important type of DNA damage and possesses a great potential to cause genomic instability and various diseases *via* mutagenesis and cytotoxicity, it is imperative to develop novel analytical methods to systematically and quantitatively evaluate the contribution of nucleobase deamination to a variety of biological and pathophysiological processes. The analytical method we chose to develop is an LC-MS method.

2.3 Materials and Methods

Materials. All chemicals and reagents were of highest purity available and were used without further purification unless noted otherwise. dG, dA, dU, and dI were purchased from Sigma Chemical Co. (St. Louis, MO). Nuclease P1 and acid phosphatase were obtained from Roche Diagnostic Corporation (Indianapolis, IN) and phosphodiesterase I from USB (Cleveland, Ohio). Alkaline phosphatases were obtained from a variety of sources, including Sigma, Roche, USB and New England Biolabs (Beverly, MA). Coformycin was obtained from Calibochem (San Diego, CA). Plasmid pUC19 was obtained from DNA Technologies, Inc. (Gaithersburg, MD). Uniformly ^{15}N-labeled 5'-triphosphate-2'-deoxyguanosine, 5'-triphosphate-2'-deoxyadenosine, and 5'-triphosphate-2'-deoxycytidine were obtained from Silantes (Munich, Germany). Acetonitrile and HPLC-grade water were purchased from Mallinckrodt Baker (Phillipsburg, NJ). Water purified through a Milli-Q system (Millipore Corporation, Bedford, MA) was used for all other applications.

Instrumental Analyses. All HPLC analyses were performed on an Agilent Model 1100, equipped with a 1040A diode array detector. Mass spectra were recorded with an Agilent Model 1100 electrospray mass spectrometer coupled to an Agilent Model 1100 HPLC with diode array detector. UV spectra were obtained using a Beckman DU640 UV-visible spectrophotometer.

HPLC Separation Methods. Five different HPLC conditions were employed during method development. System 1 consisted of a Phenomenex LUNA C18 reversed phase column (250 x 3 mm, 5 μm particle size, 100 Å pore size, Phenomenex, Torrance, CA) with elution performed at

a flow rate of 0.4 mL/min with 1% acetonitrile in 50 mM ammonium acetate (pH 7.4) for the first 5 min, followed by a linear gradient of 1→25% acetonitrile for 5 min; holding at 25% for 10 min; then a reversal of the gradient to 1% for 5 min, and finally eluting at 1% acetonitrile over the last 5 min. System 2 consisted of a HAISIL HL C18 reversed phase column (250 x 4.6 mm, 5 μm particle size, 100 Å pore size, Higgins Analytic Inc, Mountain View, CA) with isocratic conditions of acetonitrile/H_2O (5/95 v/v) at a flow rate of 0.4 mL/min. System 3 consisted of a HAISIL HL C18 reversed phase semi-preparation column (250 x 10 mm, 5 μm particle size, 100 Å pore size) eluted with acetonitrile/H_2O (5/95 v/v) at a flow rate of 4.0 mL/min. System 4 consisted of a Varian C18 reversed phase column (250 x 4.6 mm, 5 μm particle size, 100 Å pore size, Varian Analytical Supplies, Harbor, CA) with elution performed at a flow rate of 0.4 mL/min with a linear gradient of 1→10% acetonitrile in H_20 containing 0.03% of acetic acid for 50 min, followed by a reversal of the gradient to 1% for 5 min, and eluting at 1% acetonitrile over the last 5 min. System 5 consisted of a Vydac C 18 reversed phase column (250 x 2.1 mm, 5 μm particle size, 100 Å pore size, Grace Vydac, Hesperia, CA) with elution performed at a flow rate of 0.4 mL/min with a linear gradient of 1→5% acetonitrile in H_20 containing 0.1% acetic acid for 10 min, followed by eluting at 1% acetonitrile for 5 min.

Synthesis of dX and dO. dX and dO were synthesized by the method of Suzuki *et al.* (Suzuki et al., 1997a) with modifications. Briefly, 10 mM dG was incubated with 100 mM $NaNO_2$ in 3.0 M sodium acetate buffer (pH 3.7) at 37 °C for 6 hr. dX and dO were purified by HPLC using system 1, with retention times similar to literature values (Suzuki et al., 1997a), followed by desalting with HPLC system 2 and drying under vacuum. Products were characterized by mass spectrometry and UV spectroscopy relative to published data (Suzuki et al., 1996).

Synthesis of ^{15}N-labeled dX, dO, dI and dU. $^{15}N_5$-5'-triphosphate-2'-deoxyguanosine was dephosphorylated by incubation with alkaline phosphatase (0.5 U/μg nt) at 37 °C for 1 hr, followed by purification of $^{15}N_5$-dG by sequential filtration on a Microcon YM-30 column (Millipore Corporation, Bedford, MA), and then by HPLC system 2. $^{15}N_4$-dX and -dO were prepared as described earlier and quantified using the following extinction coefficients: $^{15}N_4$-dX, 7800 $M^{-1}cm^{-1}$ at 260 nm; $^{15}N_4$-dO, 5100 $M^{-1}cm^{-1}$ at 260 nm (Suzuki et al., 1996).

$^{15}N_4$-dI and $^{15}N_2$-dU were prepared by taking advantage of the presence of adenosine deaminase and cytidine deaminase, respectively, in commercial sources of alkaline phosphatase (Roche) and acid phosphatase (Roche), respectively. $^{15}N_5$-5'-triphosphate-2'-deoxyadenosine and dC were incubated with alkaline phosphatase and acid phosphatase (0.5 U/μg nt), respectively, at 37 °C for 3 hr. The resulting $^{15}N_4$-dI and $^{15}N_2$-dU were purified using HPLC system 3 and characterized by HPLC co-elution, mass spectrometry and UV spectroscopy relative to commercial standards. The products were quantified using the following extinction coefficients: $^{15}N_4$-dI, 12800 $M^{-1}cm^{-1}$ at 249 nm; $^{15}N_2$-dU, 10100 $M^{-1}cm^{-1}$ at 262 nm (Stimson, 1943).

Mass Spectral Instrumentation and Optimization. The quantification of the analytes was performed by electrospray LC-MS in the selected ion monitoring (SIM) mode on an Agilent mass spectrometer (Model 1100) coupled to an Agilent HPLC (Model 1100) with diode array detector, operated in the positive (for dX, dI and dO) or negative (for dU) ionization mode, with the Agilent MSD security ChemStation controlling software. MS parameters were as follows: drying gas (N_2) flow, 12 L/min at 330 °C for dU and 350 °C for dX, dI and dO; nebulizing gas

pressure, 35 kPa; capillary potential, 3300 V; fragmentor potential, 50-125 V (optimized for each lesion); electron multiplier potential, 2500 V; quadruple temperature, 99 °C.

Calibration Curves for LC-MS Quantification. To account for matrix effects, calibration curves for the analysis of dX, dI, dO, and dU were obtained under conditions identical to the analysis of unknown samples. Briefly, known quantities of unlabeled 2'-deoxynucleosides (0 to 10 pmol, forming the 7-point calibration curve) and a fixed amount of N^{15}-labeled internal standard (3 pmol) underwent enzymatic digestion in the present of 50 μg of plasmid DNA. The samples were dissolved in 13 μL of sodium acetate buffer (30 mM, pH 5.8) and 10 μL of zinc chloride (10 mM) and digested to 2'-deoxynucleoside monophosphates by addition of nuclease P1 (4 U, 2 μL, Roche) and incubation at 37 °C for 3 hr. Following addition of 30 μL of sodium acetate buffer (30 mM, pH 7.4), phosphate groups were removed with alkaline phosphatase (1 μL, 12.5 U, Sigma) and phosphodiesterase I (4 μL, 0.1 U, USB) by incubation at 37 °C for 6 hr. The enzymes were subsequently removed by passing the reaction mixture over a Microcon YM-30 column and deaminated 2'-deoxynucleosides were isolated by collection of HPLC (system 4) fractions bracketing empirically determined elution times for each product. Individual fraction containing each product was dried under vacuum and dissolved in 40 μL water containing 1% acetonitrile and 0.1% acetic acid for the succeeding LC-MS analysis.

Assay Method. A typical quantitative assay for each nucleobase deamination product consists of a single 7-point calibration curve, study samples and quality controls (QCs). QCs consisted of a series of solutions with known concentrations of unlabeled deamination products ranging from 0.01 to 1 μM and a fixed amount of N^{15}-labeled internal standards (0.3 μM) in water containing

0.1% acetic acid and 1% acetonitrile. Samples, standards, and QCs can be interspersed throughout the assay sequence, but an assay run normally began with the QCs to ensure that the mass spectrometer was in good condition.

2.4 Results

Synthesis and Characterization of Standards. dX and dO were synthesized by reaction of dG with nitrous acid followed by HPLC purification, as illustrated in Figure 3. The first peak (retention time t_R = 10.1 min) was identified as xanthine (X) by agreement with the retention time and the on-line UV spectrum of the authentic X. The second (t_R = 14.1 min) and fourth peaks (t_R = 27.9 min) were identified as dX and dO respectively by coincidence with the reported UV spectra (Suzuki et al., 1997a). The third peak was unreacted dG. $^{15}N_4$-dX and -dO were prepared from $^{15}N_5$-dG in a similar manner. Both unlabeled and labeled dX and dO were further characterized by electrospray mass spectrometry (Figures 4 and 5). Instead of using chemical deamination, $^{15}N_4$-dI and $^{15}N_2$-dU were prepared by enzymatic deamination of $^{15}N_4$-dA and $^{15}N_2$-dC using adenosine and cytidine deaminases, respectively. The resulting labeled deamination products were identified by agreement with the retention times and the on-line UV spectra of the authentic samples and further characterized by electrospray mass spectrometry (Figures 6 and 7).

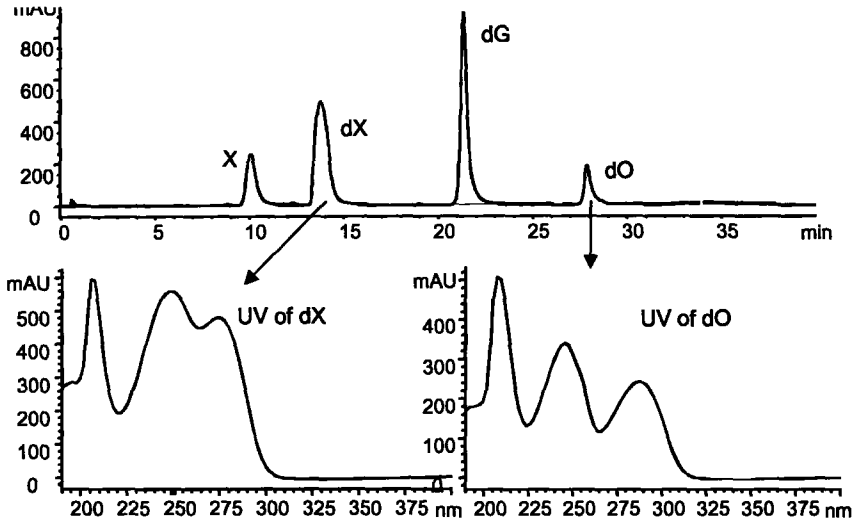

Figure 3. RT-HPLC profile of reaction products from the reaction of dG with nitrous acid. UV spectra of dX and dO were also included. X represents xanthine.

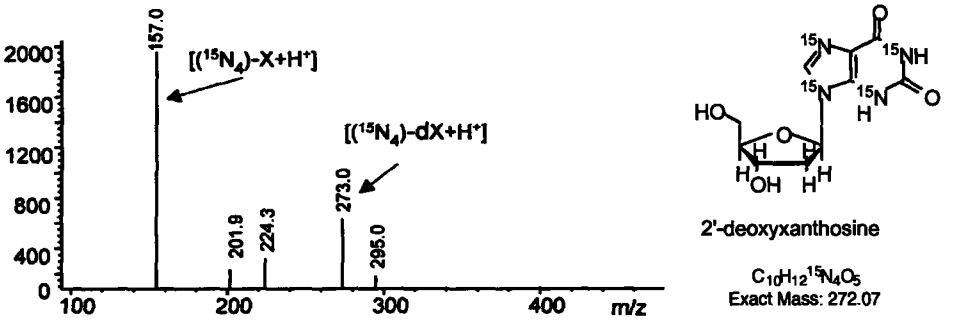

Figure 4. Electrospray ionization mass spectrum (positive ion mode) of $^{15}N_4$-dX. Quantification of dX was achieved using the molecular ion for the depurinated, $^{15}N_4$-labeled base at *m/z* 157 (*m/z* 153 for the unlabeled base).

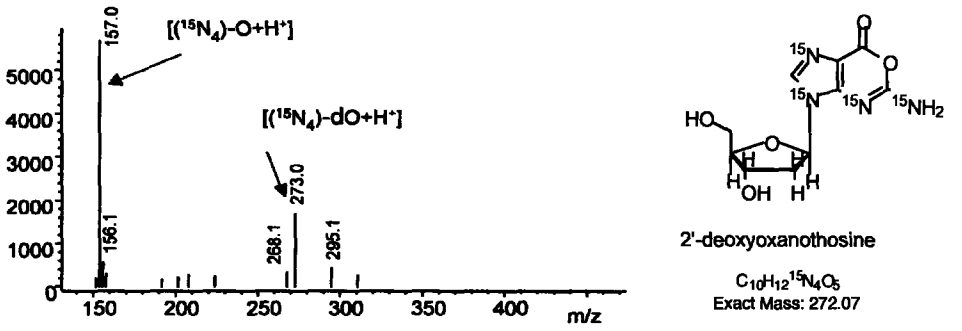

Figure 5. Electrospray ionization mass spectrum (positive ion mode) of $^{15}N_4$-dO. Quantification of dO was achieved using the molecular ion for the depurinated, $^{15}N_4$-labeled base at *m/z* 157 (*m/z* 153 for the unlabeled base).

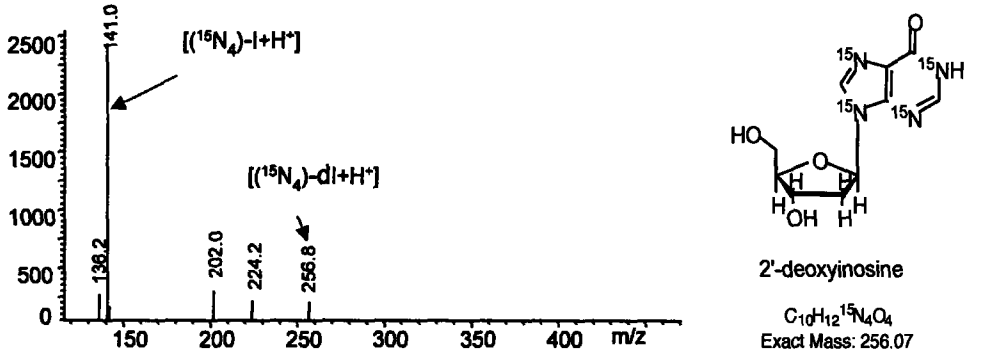

Figure 6. Electrospray ionization mass spectrum (positive ion mode) of $^{15}N_4$-dI. Quantification of dI was achieved using the molecular ion for the depurinated, $^{15}N_4$-labeled base at *m/z* 141 (*m/z* 137 for the unlabeled base).

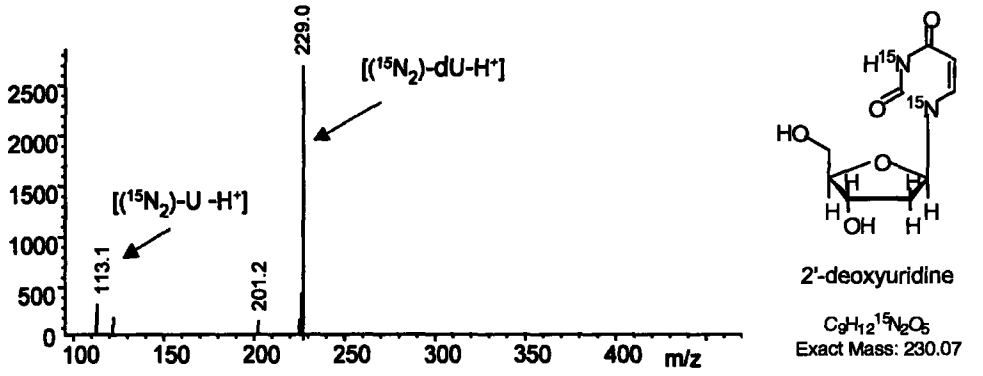

Figure 7. Electrospray ionization mass spectrum (negative ion mode) of $^{15}N_2$-dU. Quantification of dU was achieved using the molecular ion for the depurinated, $^{15}N_4$-dU at *m/z* 229 (*m/z* 227 for the unlabeled dU).

HPLC Separation of Normal and Deaminated Nucleobases. Measurement of DNA alteration products by LC-MS has usually been at the 2'-deoxynucleoside level since this usually gives easier resolution and better than direct measurement of nucleobases (Cadet et al., 2003). Separation of the analytes before mass analysis is normally adopted for two major reasons. The first is that DNA alteration, especially oxidation, may take place during the ionization, thus prior purification is necessary to avoid artifacts. The second reason is because the presence of highly abundant normal nucleosides often suppresses ionization of the less abundant molecules of interest. Hence, prior separation often leads to increased sensitivity. Figure 8 contains an example of the reversed-phase HPLC resolution of normal 2'-deoxynucleosides and deamination products using HPLC system 1. The retention time of each 2'-deoxynucleoside is as follow: dX, 10.6 min; dC, 18.7 min; dU, 22.4 min; dI, 27.8 min; dG, 29.6 min; dT, 33.2 min; dO, 37.6 min; dA, 41.3 min. To avoid the decrease in mass signal of $[M+H^+]^+$ due to the formation of other persudomolecular ions, the polar eluting solvent was chosen to include only H^+. Given the instability of dX at pH below 3 due to an increased propensity for depurination (Vongchampa et al., 2003), a mild acid, i.e. acetic acid, was added to buffer the pH around 4. However, the retention time of dX was found shifted, presumably by a solvent-induced change of the protonated state of dX. Therefore, the pH of the eluting solvent was precisely controlled to ensure the reproducibility of the chromatographic behavior of dX. Another drawback of only using acidified water as the eluting solvent is related to peak broadening, which can influence the separation efficiency. To solve these problems, a new reversed phase HPLC column from Phenomenex (Synergi, 250 x 4.6 mm, 4 μm particle size, 80 Å pore size) was applied in later studies. New conditions were optimized as follows to attain the same good baseline resolution of normal and deaminated nucleosides. At a flow rate of 0.4 mL/min, elution was performed by a

linear gradient of 8% acetonitrile in H_20 containing 0.01% of acetic acid (pH 4.2) for 40 min, then increased to 50% and held for 10 min, followed by a reversal of the gradient to 1% for 5 min, and an elution step at 1% acetonitrile over the final 10 min. The retention time of each 2'-deoxynucleoside under these chromatographic conditions is as follows: dC, 19.5 min, dU, 25.6 min, dI, 31.7 min, dG, 33.7 min, dX, 35.0 min, dT, 37.9 min, dO, 43.2 min, and dA, 46.9 min.

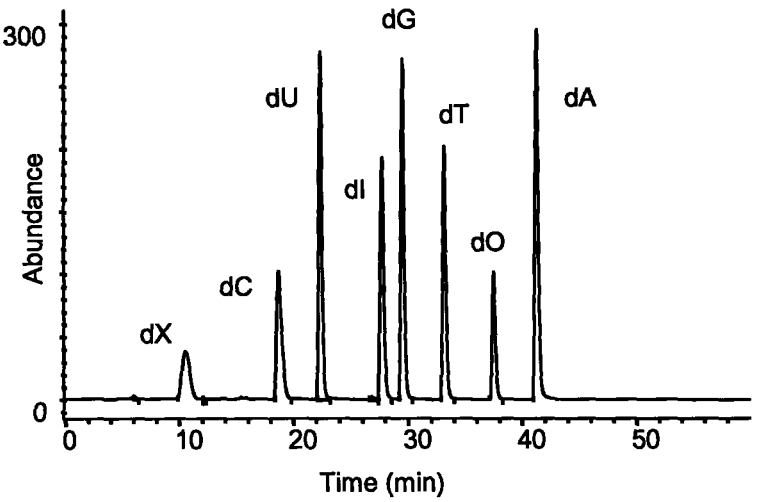

Figure 8. Example of the reversed-phase HPLC resolution of normal and deaminated 2'-deoxynucleosides.

Artifact Control. An additional problem encountered was the adventitious formation of dI by the action of a contaminant found in alkaline phosphatase stocks from several manufacturers. An example of this activity is shown in Figure 9, in which 12.5 μg of dA was incubated with 12.5 U of alkaline phosphatase (Sigma) under the same conditions used for DNA hydrolysis and dephosphorylation as described previously. Following filtration (Microcon YM-10) to remove the enzyme, the filtrate was subjected to LC-MS analysis. It is clear from Figure 9 that some

activity was causing deamination of dA to dI. To confirm the presence of contaminating adenosine deaminase, an identical incubation mixture was prepared that included coformycin, a specific inhibitor of this enzyme (Hong and Hosmane, 1997), at a concentration of 2.5 ng per unit of alkaline phosphatase. As shown in Figure 9, coformycin effectively inhibited the dA deamination activity without interfering with the alkaline phosphatase activity. All subsequent analyses of dI were performed in the presence of coformycin. Other deaminase activities for dG and dC were not detected in the enzymes that were used to digest DNA molecules.

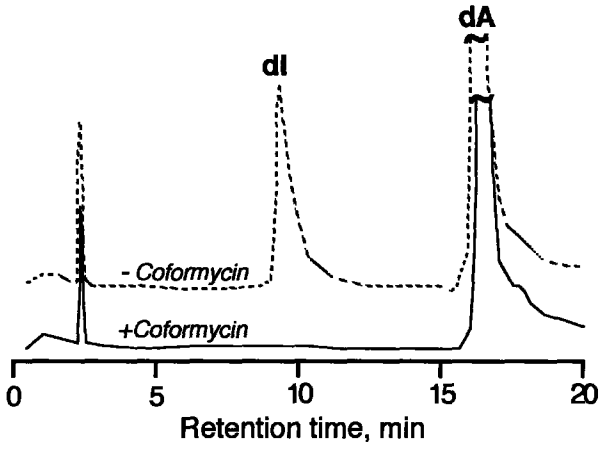

Figure 9. HPLC analysis of coformycin inhibition of dA deaminase activity present in alkaline phosphatase preparations. Dashed line: dA (12.5 μg) incubated with alkaline phosphatase (12.5 U); solid line: dA (12.5 μg) incubated with alkaline phosphatase (12.5 U) in the presence of coformycin (31 ng).

LC-MS Optimization and Calibration. The HPLC and mass spectrometric parameters for detection of dX, dO, dI and dU were individually optimized using standards. Optimization of the LC conditions was carried out by monitoring the ion currents representative of the $[M+H^+]^+$

persudomolecular ions for dX, dO and dI, and $[M-H^+]^-$ persudomolecular ion for dU. The best ionization responses were found using a 3 to 5% acetonitrile in dd-H_2O containing 0.1% of acetic acid. HPLC system 5 for the LC-MS analysis was developed accordingly.

The positive ion mode produced the strongest signals for dX, dO and dI, while the negative ion mode was optimal for dU. By varying the fragmentor potential, the following ions were found to produce optimal signals: dX and $^{15}N_4$-dX, protonated free base ion (BH^+) at *m/z* 153 and 157, respectively (75 V); dO and $^{15}N_4$-dO, BH^+ at *m/z* 153 and 157, respectively (50 V); dI and $^{15}N_4$-dI, BH^+ at *m/z* 137 and 141, respectively (75 V). For dU and $^{15}N_2$-dU in negative ion mode, a 75 V fragmentor potential produced optimal signals for the deprotonated molecular ion (M^-) at *m/z* 227 and 229, respectively. Calibration curves for the analyses of dX, dI, dO, and dU were then obtained. As shown in Figure 11, the curves were linear (r^2 is close to 1.00). The detection of the assay was determined to be 100 fmol for each deamination product, which equates to a sensitivity of 6 lesions per 10^7 nt in 50 μg of DNA. Experiments were also undertaken to evaluate the overall efficiency of the deamination product analyses. We determined the average percentage recovery of each product for the steps following nuclease and phosphatase digestion: dX, 51%; dI, 43%; dO, 40%; and dU, 28%.

Assay Specificity. The specificity of the analytical method for a particular deamination product was confirmed by monitoring the ion current resulting from the injection of plausibly interfering nucleosides. A mixture of four normal and four deaminated deoxynucleosides was made at concentration of 1 μM each and analyzed using the analytical method for each deamination product. Using dX as an example, as shown by the SIM (*m/z* 153) chromatogram in Figure 10, the channel was clear of interference from other 2'-deoxynucleosides except for dG and dO,

since dO has the same molecular weight as dX and a small percentage of dG also has the same molecular weight as dX due to isotopic natural abundance issues. However, the presence of dG and dO did not influence the specificity of the method for dX because of the 2'-deoxynucleosides were well resolved by HPLC. A similar chromatogram was obtained when evaluating the method specificity for dO.

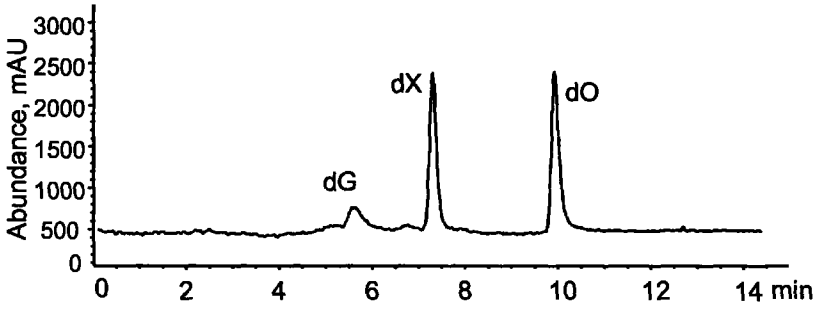

Figure 10. Mass chromatogram of a mixture of normal and deaminated 2'-deoxynucleosides analyzed by the LC-MS detection method for dX.

When the mixture was monitored using the detection method for dI and dU, the SIM channels (*m/z* 137 for dI and *m/z* 227 for dU) were also found clear of interference from the other 2'-deoxynucleosides except for dA and dC, respectively, again due to the isotopic natural abundance issues.

Method Validation. The analytical method for each deamination product was validated with respect to both intra-assay and inter-assay precision by analyzing calf thymus DNA samples reacted with nitrous acid (the reaction was performed by incubating 150 μg/ml calf thymus with 181 mM $NaNO_2$ in 3 M sodium acetate buffer, pH 3.8, for 1 hr). On the first day, the levels of

dX, dO, dI and dU measured in the samples were $8.2 \pm 0.8 \times 10^3$, $2.3 \pm 0.3 \times 10^3$, $10.2 \pm 1.1 \times 10^3$ and $15.5 \pm 1.3 \times 10^3$ (n = 3), respectively. On the second day, the values were found to be $8.8 \pm 0.7 \times 10^3$, $2.7 \pm 0.4 \times 10^3$, $11.1 \pm 1.2 \times 10^3$ and $13.5 \pm 1.4 \times 10^3$ (n = 3), respectively. Therefore, for the detection of each deamination product, the intra-assay precision was around 10%; the inter-assay variation was between 8 and 12%.

The accuracy of the method was evaluated by fortifying a DNA sample with a fixed amount of dX, dO, dI and dU (3 pmol). The incremental response for the co-eluting component was found to be 91 ± 3%, 96 ± 1%, 94 ± 2%, 92 ± 2% (n = 3) of added dX, dO, dI, and dU, respectively.

The accuracy of the analytical method was also validated by analyzing deoxyoligonucleotides containing a known amount of dI. A 30-mer deoxyoligonucleotide containing a single dI moiety (22.2 pmol) was subjected to digestion and LC-MS analysis. The amount of dI detected in the sample was 22.8 ± 1.9 pmol, which compares favorably with the calculated value and also indicates the effectiveness of the coformycin inhibition of adenosine deaminase.

A different assay using a combination of DNA glycosylase and plasmid nicking assay was also applied to further validate the LC-MS method for the detection of dU, dX and dI. A detailed description can be found in the following chapters (the validation of dU detection in Chapter 2, and the validation of dX and dI detection in Chapter 6)

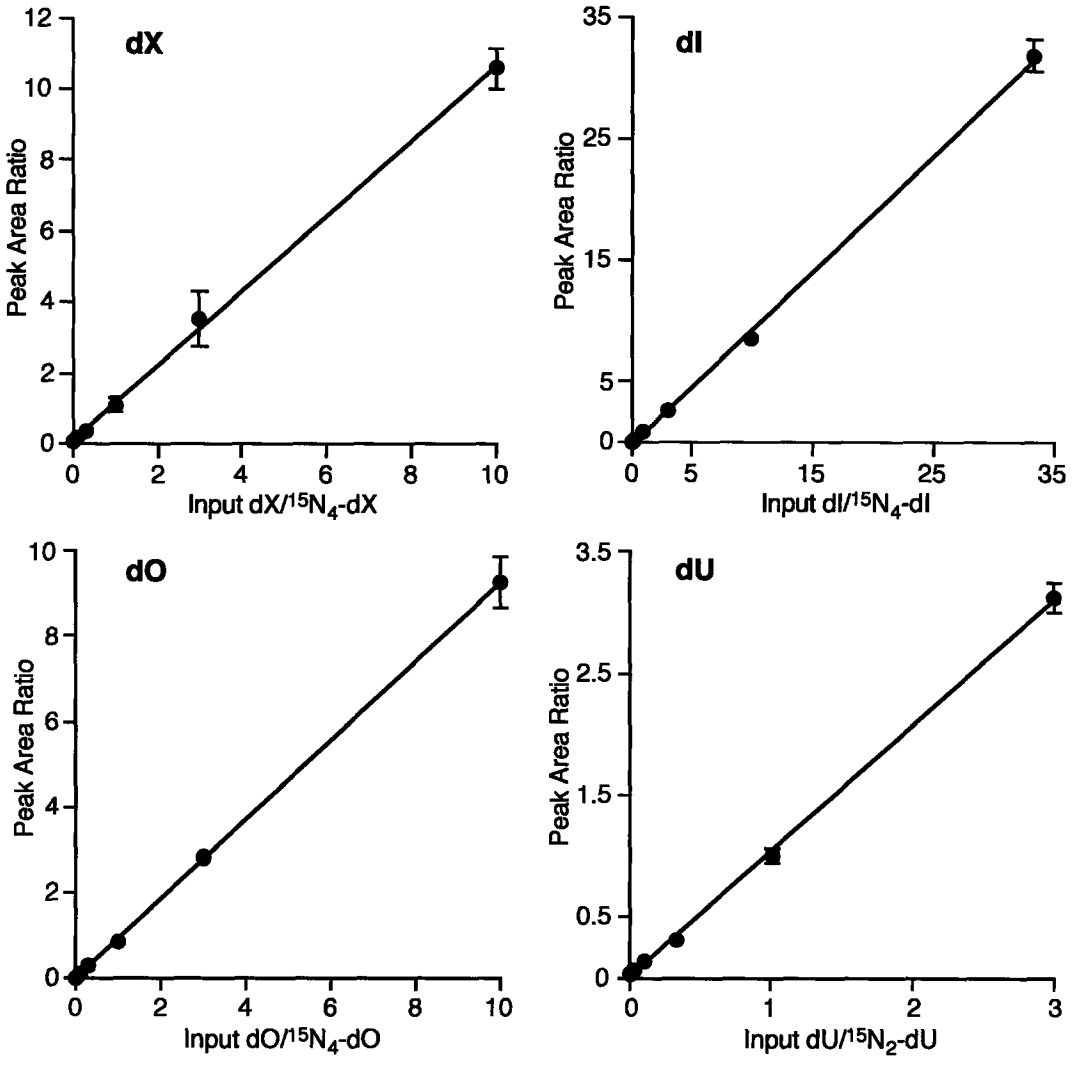

Figure 11. Calibration curves for LC-MS analysis of dX, dI, dO and dU. Samples were prepared by mixing varying amounts of unlabeled standard (0-10 ng) with 300 pg of ^{15}N-labeled standard. Following addition of 50 μg of plasmid DNA, the samples were processed for LC-MS analysis as described in Experimental Procedures. Data points represent mean ± SD for three experiments; several error bars are smaller than the symbol size.

2.5 Discussion

A novel and sensitive LC-MS method (Scheme 2) has been developed to quantify a spectrum of nucleobase products: 2'-deoxyxanthosine, 2'-deoxyoxanosine, 2'-dexyuridine and 2'-deoxyinosine.

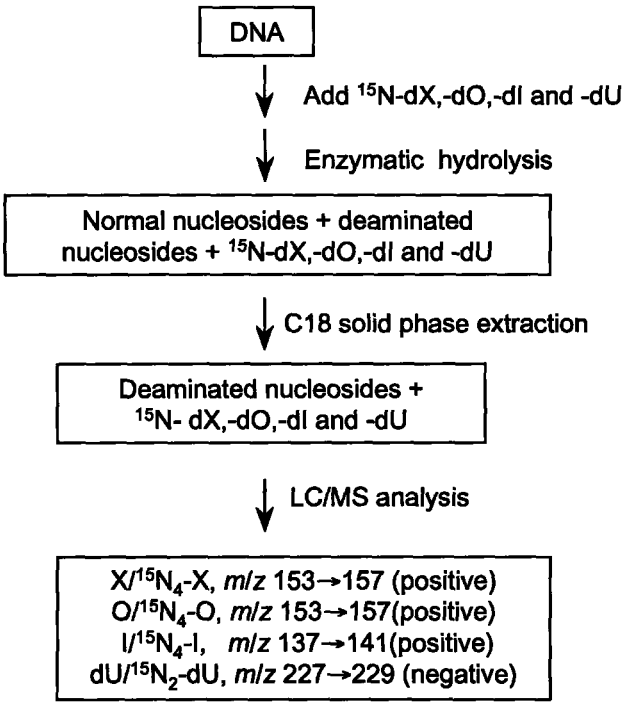

Scheme 2. LC-ESI/MS analysis of nucleobase deamination products in DNA

An ideal analytical method aimed at measuring altered DNA bases in complicated biological systems should first have a high sensitivity to enable the measurement of levels of DNA lesions as low as about one modification per 10^6 normal nucleotides. Second, the specificity of the method should be high in order to minimize contamination by alternate compounds capable of interference. These issues have been addressed in the development of this method.

Sensitivity. Three major strategies have been adopted to ensure the sensitivity of the analytical method. The first was the optimization of the enzymatic digestion conditions to allow complete and non-destructive release of the deamination products. The digestions were performed at neutral pH instead of at the commonly recommended acidic or alkaline conditions because of an increased susceptability of dX to depurination at acidic pH (Vongchampa et al., 2003) and the decomposition of dO at pH 9 (Dong et al., unpublished observations). The second was HPLC separation of deamination products from normal 2'-deoxynucleosides prior to MS quantification. Removal of intact nucleosides reduced the risk of ionization suppression, a process that leads to a decrease in sensitivity. The third was the application of SIM mode for quantitative analysis by the single quadrupole MS detector. In contrast to the scanning mode, the SIM mode allows the mass spectrometer to avoid making measurements of baseline noise between peaks or measurements of ions that are not relevant to the analysis, thus improving sensitivity. MS parameters in SIM mode were then optimized individually to achieve the best ionization for each analyte.

Specificity. The above-mentioned HPLC separation and the use of SIM mode also helped boost the specificity of the analytical method. Yet, the major contribution to specificity can be attributed to the addition of isotopically-labeled internal standards, which allows characterization of compounds that otherwise resolve poorly by chromatographic means. An additional benefit of conducting isotope dilution mass spectrometry is that these stable isotope internal standards can be used to correct for losses that occur during sample preparation and for variations in the mass spectrometric response.

Artifact Control. Sample preparation is considered to be the most important step in the quantification of DNA adducts by mass spectrometry and, in particular, the avoidance of artifacts is crucial to minimizing negative influences on assay sensitivity. Strategies for limiting artifacts vary and greatly depend on the type of samples to be analyzed. One emphasis, as mentioned earlier, is the ability to deactivate contaminating deaminase enzymes, such as those found in commercial stocks of DNA processing enzymes. Coformycin, a specific inhibitor of adenosine deaminase, was included during DNA enzymatic hydrolysis to prevent the artifactual generation of dI. Deaminase activities for dG and dC were not detected in enzyme stocks during method development with isolated DNA. However, in a later study, the presence of cellular dC deaminase activity was detected and found to compromise the results. Experimental designs for controlling the generation of artifacts that arise in cellular DNA samples during exposure to $NO^{\bullet}$ will be discussed in Chapter 4.

Future Improvement. The current analytical method, though satisfactory for most studies, needs further improvement to fulfill the goal of monitoring the formation of nucleobase deamination products in various biological and pathophysiological processes that are constrained by a limited amount of tissue available for analysis. A logical extension would be the use of tandem mass spectrometry since this instrument offers more specific and sensitive quantification than a single quadrupole detector does. Increased specificity comes from a characteristic fragmentation of the target molecule. Typically, the first quadrupole filters the major ion, usually the pseudomolecular ion of the molecule, which is formed during initial ionization. Thereafter, in the collision cell (which is usually a quadrupole), fragmentation of all subsequent ions occurs in the presence of a low-pressure inert gas (usually N_2). Furthermore, the third

quadrupole discriminates the daughter ions, which are then quantified using an electron multiplier detector. An increase in sensitivity can be achieved using a so-called "multiple reaction monitoring" (MRM) mode, resulting in a significant decrease in the background signal. Ravanat et al. have evaluated the sensitivity of the two detection modes, SIM and MRM, for the quantification of 8-oxo-dG (Ravanat et al., 1998). Sensitivity in the latter mode increased 25-fold to reach 20 fmol. Our preliminary findings suggest that a ~10-fold increase in sensitivity can be achieved by using LC-MS/MS for the quantification of nucleobase deamination products (see the Appendix of this Chapter).

Enrichment of deamination products *via* C18 solid phase separation is an important step of our current analytical method. Despite its significant contribution to the specificity and sensitivity of the method, this procedure is quite tedious and does limit any application to more systematic studies involving a substantial number of samples. To potentially address such limitations, a promising new technology, known as multidimensional chromatography, makes use of a two-dimensional on-line sample clean-up procedure by way of column-switching during HPLC. Typically, in the column-switch approach, the first column, normal referred to as the trap column, is used for separation, desalting, or other sample clean-up purposes (Scheme 3). The sample is loaded onto the trap column while the analytical column is being conditioned with the starting mobile phase. The effluent from the trap column is directed to the waste until shortly before the analyte of interest elutes. The retained analytes in the trap column are then back flushed onto the analytical column until all of the desired compounds are carried onto the analytical column. Successful examples using this technology in area of bioanalysis include quantification of etheno-DNA adducts using the on-line immunoaffinity clean-up chromatography (Doerge et al., 2000; Roberts et al., 2001).

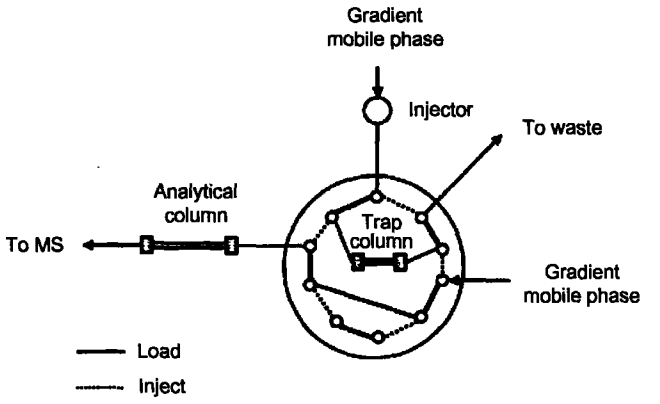

Scheme 3. A general scheme of a column-switching setup for on-line sample clean-up and separation.

In conclusion, our work has established a highly sensitive and reliable LC-MS method to quantify four common nucleobase deamination products: dX, dO, dI and dU. It provides a powerful tool for the systematic study of nucleobase deamination products and their significance in diseases such as chronic inflammation and related cancers. Because LC-MS (including tandem mass spectrometry) represents the current method of choice for measuring modified DNA bases, additional improvements will most assuredly meet the needs of future studies.

2.6 Appendix:

Analysis of Nucleobase Deamination Products with Nano-liquid Chromatography Coupled to Nano-electrospray Tandem Mass Spectrometry

Nano-HPLC Conditions. The nano-LC separation was performed on a 150 mm × 75 μm capillary column (360 OD, C18 BDS, 3 μm particles). Nanoliter flow-rates were established with an HPLC system (Agilent, Model 1100) and a pre-column splitter (Upchurch Scientific, Oak Harbor, WA). The post-column flow rate was determined and controlled at 200 nL/min. The capillary column was coupled directly to the tandem mass spectrometer with an 8 μm fused-silica tip (New Objective, Cambridge, MA). Samples were injected onto the capillary column using a Rheodyne injector (Rheodyne, Rohnert Park, CA) with a 0.5 µL internal loop and separated using a gradient of permanganate-treated H_2O containing 0.1% acetic acid (A) and acetonitrile containing 0.1% acetic acid (B), starting at 1% B, then increase to 10% in 50 min, followed by a change to 30% B and holding at 30% B for 10 min. Subsequently, the capillary column was balanced at 1% for 60 min before the next run.

Mass Spectrometric Conditions. LC-ESI-MS/MS was performed using an API 3000 LC-MS/MS system (Applied Biosystems, Foster City, CA, USA). All LC-MS/MS measurements were carried out using electrospray in the positive ion mode (+ES). Instrument parameters were optimized as follows. A voltage of 3.8 V was applied to the tip to produce the spray. The curtain gas was adjusted to a value of 10 bars. The cone voltage, corresponding to the declustering potential (DP) was fixed at 50 V. The focusing potential (FP) was at a setting of

125 eV. The entrance potential (EP) was 6 eV. Nitrogen gas was used for the collision gas. The gas cell pressure was 10-bar and the collision energy was set to 20 eV. The collision cell exit potential was fixed at 15.0 eV. The MS/MS measurement was operated in MRM (multiple-reaction monitoring) mode with low mass resolution at both Q1 and Q3. The dwell time for MRM experiments was 0.25 s. The mass spectrometer was programmed to admit the protonated molecules $[M+H]^+$ at m/z 273, 257, and 231 for U-^{15}N-dX/dO, dI, and dU; at m/z 269, 253, and 229 for dX/dO, dI, and dU respectively via the first quadrupole filter (Q1). Collision induced fragmentation at Q2 yielded the product ions $[B+H]^+$ at m/z 157, 141, and 115 for U-^{15}N-X/O, I, and U; at m/z 153, 137, and 111 for X/O, I, and U, respectively and were detected at Q3. Data collection, peak integration and calculations were performed using Analyst Software 1.1.

Results with capillary LC-MS/MS. As shown in Figure 12, the capillary HPLC system produced baseline resolution of a mixture of dX, dI, dU (250 fmol) and dO (62.5 fmol). The detection limit was determined to be 10 fmol for dX and dI, 20 fmol for dO, and 50 fmol for dU, which represents a 10-, 5- and 2-fold increase in sensitivity, respectively, over the other LC-MS method. For the purposes of the proposed studies of dX and dI, this amounts to a reduction in the quantity of DNA required for the assay from 50 to 5 μg. The multiple reaction monitoring mode (MRM) also provides increased specificity by quantifying two mass spectrometric signals.

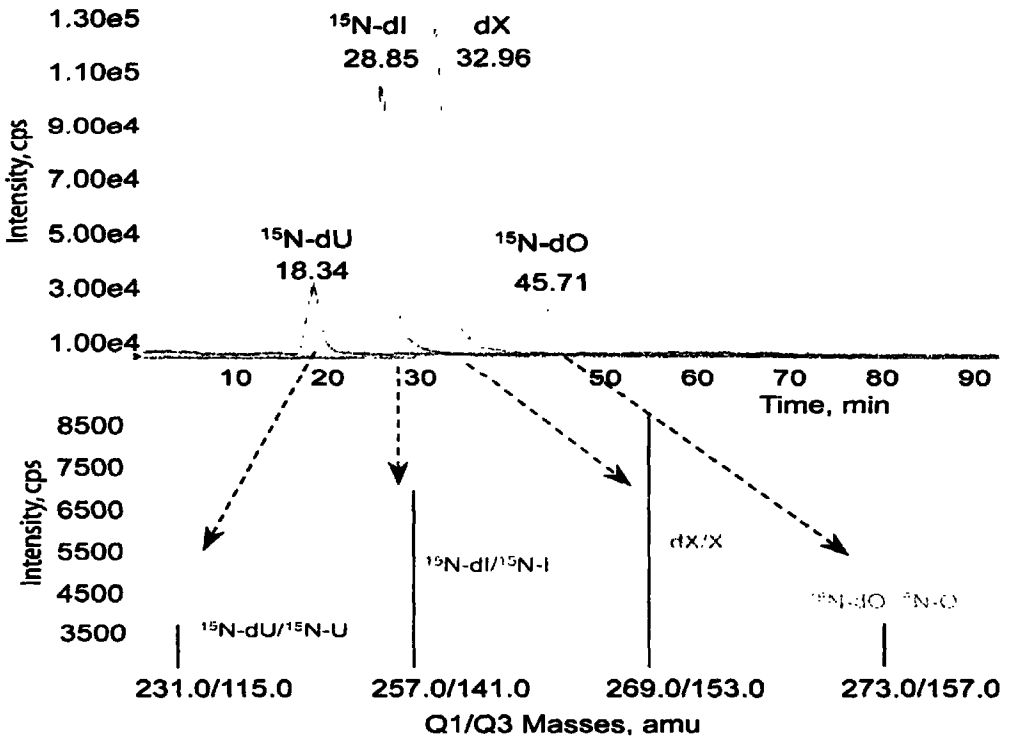

Figure 12. Capillary LC-ESI/MS/MS analysis of dX and ^{15}N-labeled dU, dI and dO. *Top panel*: Elution profile in MRM mode. *Bottom panel*: ratios of parent molecular ion and the loss of deoxyribose in MRM mode.

2.7 References

Bass, B. L.: RNA editing by adenosine deaminases that act on RNA. Annu Rev Biochem **71:** 817-46, 2002.

Blount, B. C., and Ames, B. N.: Analysis of uracil in DNA by gas chromatography-mass spectrometry. Anal Biochem **219** (2): 195-200, 1994.

Cadet, J., Douki, T., Frelon, S., Sauvaigo, S., Pouget, J. P., and Ravanat, J. L.: Assessment of oxidative base damage to isolated and cellular DNA by HPLC-MS/MS measurement. Free Radic Biol Med **33** (4): 441-9, 2002.

Cadet, J., Douki, T., Gasparutto, D., and Ravanat, J. L.: Oxidative damage to DNA: formation, measurement and biochemical features. Mutat Res **531** (1-2): 5-23, 2003.

Caulfield, J. L., Wishnok, J. S., and Tannenbaum, S. R.: Nitric oxide-induced deamination of cytosine and guanine in deoxynucleosides and oligonucleotides. J Biol Chem **273** (21): 12689-95, 1998.

Chan, T. S., Long, C., and Green, H.: A human-mouse somatic hybrid line selected for human deoxycytidine deaminase. Somatic Cell Genet **1** (1): 81-90, 1975.

Doerge, D. R., Churchwell, M. I., Fang, J. L., and Beland, F. A.: Quantification of etheno-DNA adducts using liquid chromatography, on-line sample processing, and electrospray tandem mass spectrometry. Chem Res Toxicol **13** (12): 1259-64, 2000.

Dubelman, S., and Shapiro, R.: A method for the isolation of cross-linked nucleosides from DNA: application to cross-links induced by nitrous acid. Nucleic Acids Res **4** (6): 1815-27, 1977.

Duthie, S. J., and Hawdon, A.: DNA instability (strand breakage, uracil misincorporation, and defective repair) is increased by folic acid depletion in human lymphocytes in vitro. Faseb J **12** (14): 1491-7, 1998.

Duthie, S. J., and McMillan, P.: Uracil misincorporation in human DNA detected using single cell gel electrophoresis. Carcinogenesis **18** (9): 1709-14, 1997.

Frederico, L. A., Kunkel, T. A., and Shaw, B. R.: A sensitive genetic assay for the detection of cytosine deamination: determination of rate constants and the activation energy. Biochemistry **29** (10): 2532-7., 1990a.

Frederico, L. A., Kunkel, T. A., and Shaw, B. R.: A sensitive genetic assay for the detection of cytosine deamination: determination of rate constants and the activation energy. Biochemistry **29** (10): 2532-7, 1990b.

Frelon, S., Douki, T., Ravanat, J. L., Pouget, J. P., Tornabene, C., and Cadet, J.: High-performance liquid chromatography--tandem mass spectrometry measurement of radiation-induced base damage to isolated and cellular DNA. Chem Res Toxicol **13** (10): 1002-10, 2000.

Green, D. A., and Deutsch, W. A.: Direct determination of uracil in [32P,uracil-3H]poly(dA.dT) and bisulfite-treated phage PM2 DNA. Anal Biochem **142** (2): 497-503, 1984.

Hodgen, B., Rayat, S., and Glaser, R.: Nitrosative adenine deamination: facile pyrimidine ring-opening in the dediazoniation of adeninediazonium ion. Org Lett **5** (22): 4077-80, 2003.

Hong, M. Y., and Hosmane, R. S.: Irreversible, tight-binding inhibition of adenosine deaminase by coformycins: Inhibitor structural features that contribute to the mode of enzyme inhibition. Nucleos. Nucleot. **16** (7-9): 1053-1057, 1997.

Jiang, H., Jiang, J., Hu, P., and Hu, Y.: Measurement of endogenous uracil and dihydrouracil in plasma and urine of normal subjects by liquid chromatography-tandem mass spectrometry. J Chromatogr B Analyt Technol Biomed Life Sci **769** (1): 169-76, 2002.

Karran, P., and Lindahl, T.: Hypoxanthine in deoxyribonucleic acid: generation by heat-induced hydrolysis of adenine residues and release in free form by a deoxyribonucleic acid glycosylase from calf thymus. Biochemistry **19** (26): 6005-11, 1980.

Kirchner, J. J., Sigurdsson, S. T., and Hopkins, P. B.: Interstrand cross-linking of duplex DNA by nitrous acid: Covalent structure of the dG-to-dG cross-link at the sequence 5'-CG. J. Am. Chem. Soc. **114** (11): 4021-4027, 1992.

Koc, H., and Swenberg, J. A.: Applications of mass spectrometry for quantitation of DNA adducts. J Chromatogr B Analyt Technol Biomed Life Sci **778** (1-2): 323-43, 2002.

Lewis, R. S., and Deen, W. M.: Kinetics of the reaction of nitric oxide with oxygen in aqueous solutions. Chem Res Toxicol **7** (4): 568-74, 1994.

Lindahl, T., and Nyberg, B.: Heat-induced deamination of cytosine residues in deoxyribonucleic acid. Biochemistry **13** (16): 3405-10., 1974.

Lucas, L. T., Gatehouse, D., Jones, G. D. D., and Shuker, D. E. G.: Characterization of DNA damage at purine residues in oligonucleotides and calf thymus DNA induced by the mutagen 1-nitrosoindole-3-acetonitrile. Chem. Res. Toxicol. **14:** 158-164, 2001.

Lucas, L. T., Gatehouse, D., and Shuker, D. E.: Efficient nitroso group transfer from N-nitrosoindoles to nucleotides and 2'-deoxyguanosine at physiological pH. A new pathway for N-nitrosocompounds to exert genotoxicity. J Biol Chem **274** (26): 18319-26, 1999.

Mashiyama, S. T., Courtemanche, C., Elson-Schwab, I., Crott, J., Lee, B. L., Ong, C. N., Fenech, M., and Ames, B. N.: Uracil in DNA, determined by an improved assay, is increased when deoxynucleosides are added to folate-deficient cultured human lymphocytes. Anal Biochem **330** (1): 58-69, 2004.

Nair, J., Gal, A., Tamir, S., Tannenbaum, S. R., Wogan, G. N., and Bartsch, H.: Etheno adducts in spleen DNA of SJL mice stimulated to overproduce nitric oxide. Carcinogenesis **19** (12): 2081-4, 1998.

Nguyen, T., Brunson, D., Crespi, C. L., Penman, B. W., Wishnok, J. S., and Tannenbaum, S. R.: DNA damage and mutation in human cells exposed to nitric oxide in vitro. Proc Natl Acad Sci U S A **89** (7): 3030-4, 1992.

Olive, P. L., Banath, J. P., and Durand, R. E.: Heterogeneity in radiation-induced DNA damage and repair in tumor and normal cells measured using the "comet" assay. Radiat Res **122** (1): 86-94, 1990.

Phillips, D. H., Farmer, P. B., Beland, F. A., Nath, R. G., Poirier, M. C., Reddy, M. V., and Turteltaub, K. W.: Methods of DNA adduct determination and their application to testing compounds for genotoxicity. Environ Mol Mutagen **35** (3): 222-33, 2000.

Podmore, I. D., Cooper, D., Evans, M. D., Wood, M., and Lunec, J.: Simultaneous measurement of 8-oxo-2'-deoxyguanosine and 8-oxo-2'-deoxyadenosine by HPLC-MS/MS. Biochem Biophys Res Commun **277** (3): 764-70, 2000.

Pouget, J. P., Douki, T., Richard, M. J., and Cadet, J.: DNA damage induced in cells by gamma and UVA radiation as measured by HPLC/GC-MS and HPLC-EC and Comet assay. Chem Res Toxicol **13** (7): 541-9, 2000.

Pouget, J. P., Ravanat, J. L., Douki, T., Richard, M. J., and Cadet, J.: Measurement of DNA base damage in cells exposed to low doses of gamma-radiation: comparison between the HPLC-EC and comet assays. Int J Radiat Biol **75** (1): 51-8, 1999.

Ravanat, J. L., Duretz, B., Guiller, A., Douki, T., and Cadet, J.: Isotope dilution high-performance liquid chromatography-electrospray tandem mass spectrometry assay for the measurement of 8-oxo-7,8-dihydro-2'-deoxyguanosine in biological samples. J Chromatogr B Biomed Sci Appl **715** (2): 349-56, 1998.

Roberts, D. W., Churchwell, M. I., Beland, F. A., Fang, J. L., and Doerge, D. R.: Quantitative analysis of etheno-2'-deoxycytidine DNA adducts using on-line immunoaffinity chromatography coupled with LC/ES-MS/MS detection. Anal Chem **73** (2): 303-9, 2001.

Schein, A. H.: Uracil in formic acid hydrolysates of deoxyribonucleic acid. Biochem J **98** (1): 311-6, 1966.

Serrano, J., Palmeira, C. M., Wallace, K. B., and Kuehl, D. W.: Determination of 8-hydroxydeoxyguanosine in biological tissue by liquid chromatography/electrospray ionization-mass spectrometry/mass spectrometry. Rapid Commun Mass Spectrom **10** (14): 1789-91, 1996.

Shapiro, R., DiFate, V., and Welcher, M.: Deamination of cytosine derivatives by bisulfite. Mechanism of the reaction. J Am Chem Soc **96** (3): 206-12, 1974.

Shapiro, R., and Klein, R. S.: The deamination of cytidine and cytosine by acidic buffer solutions. Mutagenic implications. Biochemistry **5** (7): 2358-62., 1966.

Shapiro, R., and Pohl, S. H.: The reaction of ribonucleosides with nitrous acid. Side products and kinetics. Biochemistry **7** (1): 448-55, 1968.

Shapiro, R., and Yamaguchi, H.: Nucleic acid reactivity and conformation. I. Deamination of cytosine by nitrous acid. Biochim Biophys Acta **281** (4): 501-6, 1972.

Shen, J.-C., Rideout III, W. M., and Jones, P. A.: The rate of hydroyltic deamination of 5-methylcytosine in double-stranded DNA. Nucleic Acids Res. **22** (6): 972-976, 1994a.

Shen, J. C., Rideout, W. M., 3rd, and Jones, P. A.: The rate of hydrolytic deamination of 5-methylcytosine in double-stranded DNA. Nucleic Acids Res **22** (6): 972-6, 1994b.

Stimson, M. M. R., Mary Agnita: Ultraviolet absorption spectra of nitrogenous heterocycles. VII. The effect of hydroxy substitution on the ultraviolet absorption of the series: hypoxanthine, xanthine and uric acid. J. Am. Chem. Soc. **65**: 153-155, 1943.

Suzuki, T., Kanaori, K., Tajima, K., and Makino, K.: Mechanism and intermediate for formation of 2'-deoxyoxanosine. Nucleic Acids Symp. Ser. (37): 313-314, 1997a.

Suzuki, T., Matsumura, Y., Ide, H., Kanaori, K., Tajima, K., and Makino, K.: Deglycosylation susceptibility and base-pairing stability of 2'-deoxyoxanosine in oligodeoxynucleotide. Biochemistry **36** (26): 8013-8019, 1997b.

Suzuki, T., Nakamura, T., Yamada, M., Ide, H., Kanaori, K., Tajima, K., Morii, T., and Makino, K.: Isolation and characterization of diazoate intermediate upon nitrous acid and nitric oxide treatment of 2'-deoxycytidine. Biochemistry **38** (22): 7151-8, 1999.

Suzuki, Y. R., Yamaoka, M., Nishi, H. I., and makino, K.: Isolation and characterization of a novel product, 2'-deoxyoxanosine. J. Am. Chem. Soc. **118** (10): 2515-2516, 1996.

Swenberg, J. A., Petzold, G. L., and Harbach, P. R.: In vitro DNA damage/alkaline elution assay for predicting carcinogenic potential. Biochem Biophys Res Commun **72** (2): 732-8, 1976.

Vongchampa, V., Dong, M., Gingipalli, L., and Dedon, P.: Stability of 2'-deoxyxanthosine in DNA. Nucleic Acids Res **31** (3): 1045-51, 2003.

Weimann, A., Belling, D., and Poulsen, H. E.: Measurement of 8-oxo-2'-deoxyguanosine and 8-oxo-2'-deoxyadenosine in DNA and human urine by high performance liquid chromatography-electrospray tandem mass spectrometry. Free Radic Biol Med **30** (7): 757-64, 2001.

Williams, M. G., Palandra, J., and Shobe, E. M.: Rapid determination of rat plasma uridine levels by HPLC-ESI-MS utilizing the Captiva plates for sample preparation. Biomed Chromatogr **17** (4): 215-8, 2003.

Wink, D. A., Kasprzak, K. S., Maragos, C. M., Elespuru, R. K., Misra, M., Dunams, T. M., Cebula, T. A., Koch, W. H., Andrews, A. W., Allen, J. S., and et al.: DNA deaminating ability and genotoxicity of nitric oxide and its progenitors. Science **254** (5034): 1001-3, 1991.

Zhang, X., and Mathews, C. K.: Effect of DNA cytosine methylation upon deamination-induced mutagenesis in a natural target sequence in duplex DNA. J. Biol. Chem. **269** (10): 7066-7069, 1994.

Chapter 3

Absence of 2'-Deoxyoxanosine and Presence of Abasic Sites in DNA Exposed to Nitric Oxide at Controlled Physiological Concentrations

[The work in this chapter has been published in "Dong, M., Wang, C., Deen, W. M. and Dedon, P. C. (2003). "Absence of 2'-deoxyoxanosine and presence of abasic sites in DNA exposed to nitric oxide at controlled physiological concentrations." Chem Res Toxicol **16**(9): 1044-55". A reprint of the paper is included in Appendix II]

3.1 Abstract

Extensive study *in vitro* suggests that oxidative and nitrosative reactions dominate the complicated chemistry of NO•-mediated genotoxicity. However, neither the spectrum of DNA lesions nor their consequences *in vivo* have been rigorously defined. We have approached this problem with a major effort, including the development of a novel LC-MS assay described in Chapter 2, to define the spectrum of nitrosative DNA lesions produced by NO•-derived reactive nitrogen species under biological conditions. The goals of the current *in vitro* study were two-fold: to validate the new analytical method and to investigate the spectrum of nitrosative DNA damage derived from exposure to NO• at controlled physiological concentrations. Plasmid pUC19 DNA was exposed to steady-state concentrations of 1.2 μM NO• and 186 μM O_2 (calculated steady-state concentrations of 40 fM N_2O_3 and 3 pM $NO_2^{\bullet}$) in a recently developed reactor that avoids the anomalous gas-phase chemistry of NO• and approximates the conditions at sites of inflammation in tissues. The resulting spectrum of nitrosatively-induced abasic sites and nucleobase deamination products was defined using plasmid nicking assay and a novel LC-MS assay, respectively. With a detection limit of 100 fmol and sensitivity of 6 lesions per 10^7 nt in 50 μg DNA, the LC-MS analysis revealed that 2'-deoxyxanthosine (dX), 2'-deoxyinosine (dI) and 2'-deoxyuridine (dU) were formed at nearly identical rates ($k = 1.2 \times 10^5\ M^{-1}s^{-1}$) to the extent of ~80 lesions per 10^6 nt after 12 hr exposure to NO• in the reactor. While reactions with HNO_2 resulted in the formation of high levels of 2'-deoxyoxanosine (dO), one of two products arising from deamination of dG, dO was not detected in 500 μg of DNA exposed to NO• in the reactor for up to 48 hr (<6 lesions per 10^8 nt). This result leads to the prediction that dO will not be

present at significant levels in inflamed tissues. Another important observation was the NO•-induced production of abasic sites, which likely arise by nitrosative depurination reactions, to the extent of ~10 per 10^6 nt after 12 hr of exposure to NO• in the reactor. In conjunction with other studies of nitrosatively-induced dG-dG cross-links, these results lead to the prediction of the following spectrum of nitrosative DNA lesions in inflamed tissues: ~2% dG-dG cross-links, 4-6% abasic sites and 25-35% each of dX, dI and dU.

3.2 Introduction

Research over the past decade has identified nitric oxide (NO$^{\bullet}$) as an important endogenous regulatory molecule in the cardiovascular, nervous and immune systems (Moncada et al. 1991; Nathan and Xie 1994; Schmidt and Walter 1994). However, NO$^{\bullet}$ and its derivatives display cytotoxic and mutagenic properties at sufficiently high concentrations, such as those produced by activated macrophages in inflammatory conditions, which suggests a causative role of NO$^{\bullet}$ in the pathophysiology of diseases such as cancer (Collier and Vallance 1991; Ohshima and Bartsch 1994; deRojas-Walker et al. 1995; Lewis et al. 1995; Tamir and Tannenbaum 1996). Though NO$^{\bullet}$ is a radical species, its genotoxicity likely arises from derivatives such as N_2O_3 and peroxynitrite ($ONOO^-$), which are formed in reactions with molecular oxygen and superoxide, respectively (Tamir et al. 1996). N_2O_3 is a powerful nitrosating agent that, in addition to reactions with sulfhydryl groups of proteins (Stamler et al. 1992) and with secondary amines to form *N*-nitrosamines (Tannenbaum et al. 1994), will react with the primary and heterocyclic amines in DNA bases to create mutagenic deamination products, abasic sites and DNA cross-links (Shapiro and Pohl 1968; Shapiro and Yamaguchi 1972; Dubelman and Shapiro 1977; Wink et al. 1991; Kirchner et al. 1992; Nguyen et al. 1992; Suzuki et al. 1997), as shown in Scheme 1.

An important biological source of N_2O_3 is the NO$^{\bullet}$ generated by macrophages activated as part of the inflammatory process. In macrophage cultures activated with lipopolysaccharide and INF-γ *in vitro*, NO$^{\bullet}$ is generated at a rate of ~6 pmol s^{-1} per 10^6 cells (Lewis et al. 1995) and leads to the formation of xanthine at levels five-fold higher than controls (deRojas-Walker et al. 1995). However, this study provided no information about the other base deamination products.

Attempts to mimic this biological exposure of DNA to NO• and the derivative N_2O_3 have employed several NO• delivery systems. For example, Nguyen *et al.* exposed DNA and TK6 cells to ~20 mM NO• by bolus delivery through a syringe and found that dX and dI were formed to the extent of 3 and 10 lesions per 10^3 nt, respectively, for isolated DNA, with 3-fold lower levels of each in TK6 cells (Nguyen et al. 1992). Yields of dI an dX in DNA were found to be 15- to 100-times higher, respectively, than those observed with free adenine and guanine (Nguyen et al. 1992). Similarly, Wink *et al.* exposed DNA to 1 M NO• by bubbling the gas into solution and found 5 dU per 10^3 nt (Wink et al. 1991). Caulfield *et al.* used a delivery system in which Silastic tubing allowed controlled diffusion of NO• into solution at a rate of 10-20 μM/min and found that xanthine was formed at twice the rate of uracil and single-stranded DNA oligodeoxynucleotides was nearly 10-fold more reactive than double-stranded DNA (Caulfield et al. 1998).

These studies present several problems that prevent extrapolation to the biological setting. First, in all of the delivery systems, NO• was present at significantly higher concentrations than occur at sites of inflammation *in vivo*, which are thought not to exceed steady-state concentrations of ~1 μM (Miwa et al. 1987; Stuehr and Marletta 1987; Lewis et al. 1995). Second, none of the studies addressed the complete spectrum of deamination products produced by exposure to NO•. Finally, the presence of a headspace containing air in each of these delivery systems alters the chemistry of NO• by biasing the formation of N_2O_3 and allowing formation of N_2O_4 (Mirvish 1975; Challis et al. 1981).

To define the spectrum of deamination products under biologically-relevant conditions of NO• exposure, we have developed a sensitive LC-MS approach to quantifying the dX, dO, dI,

and dU in DNA exposed to NO• in a recently developed delivery system designed to mimic pathological release of NO• *in vivo* to cell cultures (Wang and Deen 2003).

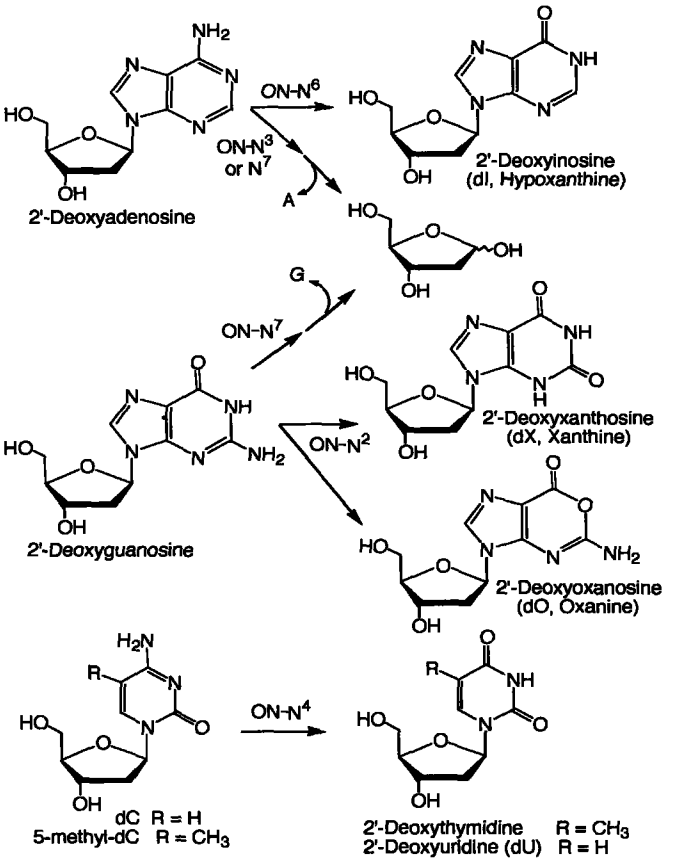

Scheme 1: Products of N-nitrosative nucleobase deamination

3.3 Materials and Methods

Materials. All chemicals and reagents were of highest purity available and were used without further purification unless noted otherwise. Calf thymus DNA, dG, dA, dU, dI, morpholine (Mor) and N-nitroso-morpholine (NMor) were purchased from Sigma Chemical Co. (St. Louis, MO). Nuclease P1 and acid phosphatase were obtained from Roche Diagnostic Corporation (Indianapolis, IN) and phosphodiesterase I from USB (Cleveland, Ohio). Alkaline phosphatases were obtained from a variety of sources, including Sigma, Roche, USB and New England Biolabs (Beverly, MA). Coformycin was obtained from Calibochem (San Diego, CA). Plasmid pUC19 was obtained from DNA Technologies, Inc. (Gaithersburg, MD). Uniformly ^{15}N-labeled 5'-triphosphate-2'-deoxyguanosine, 5'-triphosphate-2'-deoxyadenosine, and 5'-triphosphate-2'-deoxycytidine were obtained from Silantes (Munich, Germany). Acetonitrile and HPLC-grade water were purchased from Mallinckrodt Baker (Phillipsburg, NJ). Gas mixtures (10% NO/90% N_2 and 50% O_2/50% N_2) were purchased from BOC Gases (Edison, NJ). Water purified through a Milli-Q system (Millipore Corporation, Bedford, MA) was used for all other applications.

Instrumental Analyses. All HPLC analyses were performed on an Agilent Model 1100, equipped with a 1040A diode array detector. Mass spectra were recorded with an Agilent Model 1100 electrospray mass spectrometer coupled to an Agilent Model 1100 HPLC with diode array detector. UV spectra were obtained using a Beckman DU640 UV-visible spectrophotometer. Two different HPLC conditions were employed in these studies. System 1 consisted of a Varian C18 reversed phase column (250 x 4.6 mm, 5 μm particle size, 100 Å pore size, Varian

Analytical Supplies, Harbor, CA) with elution performed at a flow rate of 0.4 mL/min with a linear gradient of 1 to 10% acetonitrile in H_20 containing 0.03% of acetic acid for 50 min, followed by a reversal of the gradient to 1% for 5 min, and eluting at 1% acetonitrile over the last 5 min. System 2 consisted of a Vydac C 18 reversed phase column (250 x 2.1 mm, 5 μm particle size, 100 Å pore size, Grace Vydac, Hesperia, CA) with elution performed at a flow rate of 0.4 mL/min with a linear gradient of 1 to 5% acetonitrile in H_20 containing 0.1% acetic acid for 10 min, followed by eluting at 1% acetonitrile for 5 min.

Reaction of DNA and Morpholine with NO• and HNO_2. A novel delivery system, described in detail elsewhere (Wang and Deen 2003), was used to introduce NO• into the reaction buffer and to replenish O_2, allowing the concentrations of both to be maintained at constant, physiological levels. Briefly, two loops of gas-permeable polydimethylsiloxane tubing (Silastic, i.d. 1.47 mm, o.d. 1.96 mm) were immersed in a 120 mL stirred, liquid-filled, Teflon reactor. A 10% NO• gas mixture was passed through one loop and a 50% O_2 mixture through the other. The tubing lengths and gas flow rates were 7 cm and 150 sccm for NO• and 4 cm and 200 sccm for O_2 respectively. The performance of the system was tested by continuously monitoring the liquid concentrations using a NO• electrode (World Precision Instruments, ISO-NO Mark II system) and a Clark-type O_2 electrode (Orion, Model 810A Plus). Because the kinetics of morpholine nitrosation by N_2O_3 is relatively well known (see below), the rate of NMor formation was used as a measure of the N_2O_3 concentration. That is, rate constants for nucleobase deamination were calculated by comparing rates of deamination with rates of morpholine nitrosation measured in separate experiments. In the morpholine experiments, NO• and O_2 were delivered into 2 mM morpholine in 50 mM phosphate buffer (pH 7.4), and the concentration of

NMor was monitored continuously by UV absorbance at 250 nm (e_{250} = 5500 $M^{-1}cm^{-1}$), using a flow loop and a 1 cm flow cell. In the DNA experiments, NO• and O_2 were delivered into 20 μg/mL plasmid pUC19 (2686 bp) in the same buffer (but without morpholine). All experiments were at ambient temperature (23 ± 1 °C).

NO•-treatment of DNA was achieved using 120 mL solutions of plasmid pUC19 (20 μg/mL in 50 mM Chelex-treated potassium phosphate (K-PO_4) buffer, pH 7.4; plasmid stock solutions were dialyzed exhaustively against Chelex-treated K-PO_4 buffer, pH A control DNA solution exposed to pure Ar gas was prepared in a duplicate chamber of identical construction. At various times points after starting the gas flow, 2.5 mL aliquots of the reaction mixture were withdrawn from the chamber and replaced with an identical volume of fresh buffer. The DNA in each sample was recovered by ethanol precipitation and resuspension in water. All the experiments were conducted at ambient temperature.

In reactions with morpholine, NO• was delivered into 2 mM morpholine in K-PO_4 buffer (Chelex-treated, 50 mM, pH 7.4) at ambient temperature and the formation of nitrosation product, NMor, was quantified by UV absorbance at 250 nm (e_{250} = 5500 $M^{-1}cm^{-1}$) *via* a flow loop and a 1 cm flow cell.

Reactions with HNO_2 were performed by dissolving $NaNO_2$ (181 mM final concentration) in a solution containing calf thymus DNA (150 μg/mL) and 3 M sodium acetate buffer, pH 3.8. At various times during an incubation at 37 °C, 1 mL aliquots were removed and the reaction stopped by neutralization with 200 μL of 5 N NaOH. The solution was desalted by three 500 μL water washings using a Microcon YM-100 filtration system and the purified DNA was subjected to LC-MS analysis as described next.

DNA Samples Preparation and LC-MS Analysis. Samples of DNA (50 μg) were dissolved in 13 μL of sodium acetate buffer (30 mM, pH 5.8) and 10 μL of zinc chloride (10 mM) followed by addition of isotope-labeled internal standards (300 pg). The DNA was digested to deoxynucleoside monophosphates by addition of nuclease P1 (4 U, 2 μL, Roche) and incubation at 37 °C for 3 hr. Following addition of 30 μL of sodium acetate buffer (30 mM, pH 7.4), phosphate groups were removed with alkaline phosphatase (1 μL, 12.5 U, Sigma) and phosphodiesterase I (4 μL, 0.7 U, USB) by incubation at 37 °C for 6 hr. The enzymes were subsequently removed by passing the reaction mixture over a Microcon YM-30 column and deaminated 2'-deoxynucleosides were isolated by collection of HPLC (system 1) fractions bracketing empirically determined elution times for each product (see Figure 8 in Chapter 2): Fractions containing each product were pooled and the solvent removed under vacuum. Following resuspension of the HPLC fractions in 40 μL of 1% acetonitrile in water, the 2'-deoxynucleoside deamination products were quantified by the LC-MS method described in Chapter 2.

Quantification of Base Lesions and Abasic Sites in Plasmid DNA by Topoisomer Analysis. Abasic sites were quantified in plasmid DNA as described elsewhere (*e.g.*, refs. (Povirk and Goldberg 1985; Dedon et al. 1992; Tretyakova et al. 2000). Briefly, aliquots of plasmid solution containing ~3 μg of DNA, obtained from samples removed for LC-MS analysis, were divided and one portion treated with putrescine dihydrochloride (100 mM, pH 7) for 1 hr at 37 °C to cleave all abasic sites (Lindahl and Andersson 1972). Following resolution of the resulting plasmid topoisomers (nicked form II and supercoiled form I) on 1% agarose gels, the quantity of

abasic sites at each NO• exposure time was calculated as the difference in the quantity of nicked plasmid DNA in samples treated with putrescine and those not treated.

Uracil was quantified in a similar manner by treating the NO•-exposed plasmid DNA with uracil DNA glycosylase (1 ng, in Scharer and Jiricny, 2001) followed by putrescine to cleave the resulting abasic sites to strand breaks, as described above. The quantity of dU was then calculated from the net proportion of nicked (form II) plasmid DNA following resolution of the plasmid topoisomers on 1% agarose gels.

Reaction Scheme and Kinetic Model

Reactions. The principal nitrosating agent in oxygenated NO• solutions at physiological pH is N_2O_3 (Lewis et al. 1995), which is formed *via* reactions 1 and 2:

$$2NO + O_2 \xrightarrow{k_1} 2NO_2 \quad (1)$$

$$NO + NO_2 \xleftrightarrow{k_2, k_{-2}} N_2O_3 \quad (2)$$

Most of the N_2O_3 is hydrolyzed to nitrite, which can occur either directly or with the participation of various anions, including phosphate salts (Lewis et al. 1995). The two hydrolysis pathways under our experimental conditions were:

$$N_2O_3 + H_2O \xrightarrow{k_3} 2NO_2^- + 2H^+ \quad (3)$$

$$N_2O_3 + P_i + H_2O \xrightarrow{k_4} P_i + 2NO_2^- + 2H^+ \quad (4)$$

Under our conditions (50 mM phosphate at pH 7.4), reaction 4 is 20 times as fast as reaction 3. The additional reactions depend on which organic substrates are present. In morpholine solutions (no DNA present), N_2O_3 could react with unprotonated morpholine (Mor°) to form NMor:

$$N_2O_3 + Mor^\circ \xrightarrow{k_5} NMor + NO_2^- + H^+ \qquad (5)$$

In DNA solutions (no morpholine present), the three deamination reactions identified in our experiments were:

$$N_2O_3 + dG \xrightarrow{k_6} dX + NO_2^- + H^+ \qquad (6)$$

$$N_2O_3 + dA \xrightarrow{k_7} dI + NO_2^- + H^+ \qquad (7)$$

$$N_2O_3 + dC \xrightarrow{k_8} dU + NO_2^- + H^+ \qquad (8)$$

The rate constants for reactions 1-5, reported previously, are listed in Table 1. Those for dG, dA, and dC in plasmid DNA were calculated from the relative rates of nitrosation and deamination, as described below.

Table 1: Published reaction rate constants

Rate constant	Value	Units	Reference
k_1	2.1×10^6	$M^{-2}s^{-1}$	(Lewis and Deen 1994)
k_2	1.1×10^9	$M^{-1}s^{-1}$	(Graetzel et al. 1970)
k_{-2}	8.4×10^4	s^{-1}	(Graetzel et al. 1970)
k_3	1.6×10^3	s^{-1}	(Treinin and Hayon 1970)
k_4	6.4×10^5	$M^{-1}s^{-1}$	(Lewis et al. 1995)
k_5	6.4×10^7	$M^{-1}s^{-1}$	(Lewis et al. 1995)

The kinetic analysis is complicated by the fact that the delivery system creates two liquid regions with very different concentrations of N_2O_3. In addition to a well-stirred bulk liquid with a low concentration of N_2O_3, there is a very thin (~1 μm) boundary layer next to the NO• delivery tubing where the N_2O_3 concentration is much higher. It will be shown that, despite its small volume, the contribution of the boundary layer to the overall rates of nitrosation and deamination is comparable to that of the bulk liquid. High concentrations of NO_2• (and therefore N_2O_3) in the boundary layer appear to arise from reaction 1 occurring not just in the liquid, but within the wall of the Silastic tubing. A reaction-diffusion model that adds membrane oxidation of NO• to the known liquid-phase chemistry provides a quantitative explanation of the measured behavior of the delivery system, including the unexpectedly high rates of nitrite formation (Wang and Deen 2003). In the analysis that follows, the concentrations in the two regions are discussed first, and then the overall kinetics are considered.

Bulk concentrations. In the bulk liquid, the quasi-steady-state approximation in kinetics is applicable to both $NO_2^{\bullet}$ and N_2O_3. This is true for experiments with either organic substrate, so that:

$$2k_1[NO]^2[O_2] - k_2[NO][NO_2] + k_{-2}[N_2O_3]_M = 0 \quad (9)$$

$$2k_1[NO]^2[O_2] - k_2[NO][NO_2] + k_{-2}[N_2O_3]_D = 0 \quad (10)$$

$$k_2[NO][NO_2] - (k_{-2} + k_3 + k_4[P_i] + k_5[Mor^o])[N_2O_3]_M = 0 \quad (11)$$

$$k_2[NO][NO_2] - (k_{-2} + k_3 + k_4[P_i] + k_6[dG] + k_7[dA] + k_8[dC])[N_2O_3]_D = 0 \quad (12)$$

where $[N_2O_3]_M$ and $[N_2O_3]_D$ represent the bulk N_2O_3 concentrations in morpholine and DNA solutions, respectively. Solving equations 9-12 yields:

$$[N_2O_3]_M = \frac{2k_1[NO]^2[O_2]}{k_3 + k_4[P_i] + k_5[Mor^o]} \quad (13)$$

$$[N_2O_3]_D = \frac{2k_1[NO]^2[O_2]}{k_3 + k_4[P_i] + k_6[dG] + k_7[dA] + k_8[dC]} \quad (14)$$

As will be shown, the reactions of N_2O_3 with dG, dA, and dC are too slow (compared to hydrolysis) to influence the N_2O_3 concentration. Thus, equation 14 was simplified to:

$$[N_2O_3]_D = \frac{2k_1[NO]^2[O_2]}{k_3 + k_4[P_i]} \quad (15)$$

Because the NO• and O_2 concentrations were fixed by the delivery conditions, which were the same in the morpholine and DNA experiments, the numerators of equations 13 and 15 are identical. Consequently, the ratio of those equations gives:

$$\frac{[N_2O_3]_M}{[N_2O_3]_D} = \frac{k_3 + k_4[P_i]}{k_3 + k_4[P_i] + k_5[Mor^\circ]} \equiv \alpha_1 \tag{16}$$

This indicates that the bulk N_2O_3 concentration in the morpholine experiments was lower than in the DNA experiments, because of the competition of morpholine nitrosation with N_2O_3 hydrolysis. Although morpholine nitrosation affected the N_2O_3 level, the yield of NMor was low enough that [Mor°] was almost constant (independent of time). Therefore, the ratio of the N_2O_3 concentrations in the two types of experiments (a_1) was a constant.

Boundary layer concentrations. Of the several boundary layers in the delivery system, the one that most impacts the present experiments is a region next to the NO• tubing in which there are large and spatially varying concentrations of $NO_2^\bullet$ and N_2O_3. The variations in the $NO_2^\bullet$ concentration in that region are described by:

$$[NO_2] = [NO_2]_0 e^{-x/\lambda} \tag{17}$$

where $[NO_2]_0$ is the aqueous $NO_2^\bullet$ concentration at the tubing surface, x is distance from the surface, and λ is the characteristic thickness of the $NO_2^\bullet/N_2O_3$ layer (the distance for a 1/e decay in either concentration). It was shown previously that $[NO_2]_0$ is proportional to λ (equation A6 in Wang and Deen 2003), which is given by:

$$\lambda = \left(\frac{D_{NO_2}}{b[NO]_0}\right)^{1/2} \tag{18}$$

where D_{NO_2} is the diffusivity of $NO_2^{\bullet}$ and $[NO^{\bullet}]_0$ is the aqueous $NO^{\bullet}$ concentration at the tubing surface. The constant b in equation 18 is determined from the rate constants for N_2O_3 formation and consumption, and its value differs in morpholine (b_M) and DNA (b_D) solutions:

$$b_M = \frac{k_2(k_3 + k_4[P_i] + k_5[Mor^\circ])}{k_{-2} + k_3 + k_4[P_i] + k_5[Mor^\circ]} \tag{19}$$

$$b_D = \frac{k_2(k_3 + k_4[P_i])}{k_{-2} + k_3 + k_4[P_i]}. \tag{20}$$

Although $[NO^{\bullet}]_0$ was the same in all experiments (see below), the differing values of b created differences in both l and $[NO_2^{\bullet}]_0$ in the morpholine (l_M and $[NO_2]_{0M}$) and DNA solutions (l_D and $[NO_2]_{0D}$). From equations 18-20, one obtains:

$$\frac{[NO_2]_{0M}}{[NO_2]_{0D}} = \frac{\lambda_M}{\lambda_D} = \left(\frac{b_D}{b_M}\right)^{1/2} = \left(\frac{\alpha_1}{\alpha_2}\right)^{1/2} \tag{21}$$

with:

$$\alpha_2 \equiv \frac{k_{-2} + k_3 + k_4[P_i]}{k_{-2} + k_3 + k_4[P_i] + k_5[Mor^\circ]} \tag{22}$$

Although the quasi-steady-state approximation is not valid for $NO_2^{\bullet}$ in this boundary layer, it remains accurate for N_2O_3. The resulting expressions for the N_2O_3 concentrations are:

$$[N_2O_3]_{BM} = \frac{k_2}{k_{-2} + k_3 + k_4[P_i] + k_5[Mor^{\circ}]}[NO]_0[NO_2]_{0M} e^{-x/\lambda_M} \tag{23}$$

$$[N_2O_3]_{BD} = \frac{k_2}{k_{-2} + k_3 + k_4[P_i]}[NO]_0[NO_2]_{0D} e^{-x/\lambda_D} \tag{24}$$

where $[N_2O_3]_{BM}$ and $[N_2O_3]_{BD}$ are the boundary layer values in the morpholine and DNA experiments, respectively. As in equation 15, it is assumed in equation 24 that $k_6[dG] + k_7[dA] + k_8[dC] \ll k_{-2} + k_3 + k_4[P_i]$.

Although the concentration of $NO^{\bullet}$ next to the tubing differs from that in the bulk liquid (*i.e.*, $[NO^{\bullet}]_0 > [NO^{\bullet}]$), the $NO^{\bullet}$ concentration is nearly constant within the $NO_2^{\bullet}/N_2O_3$ boundary layer. The length scale for variations in the $NO^{\bullet}$ concentration under our experimental conditions is 67 μm (Wang and Deen 2003), whereas l_M and l_D were calculated to be 0.55 and 0.60 μm, respectively. Accordingly, equations 23 and 24 assume that the $NO^{\bullet}$ concentration in the $NO_2^{\bullet}/N_2O_3$ layer is independent of x. It can be shown that reactions in the boundary layer have a negligible effect on the aqueous $NO^{\bullet}$ concentration, and that $[NO^{\bullet}]_0$ will be identical in the absence and presence of morpholine or DNA. It is found that $[NO^{\bullet}]_0 = 16.6$ μM for 10% $NO^{\bullet}$ with a tubing length of 7 cm (Wang and Deen 2003).

Overall kinetics. In the stirred batch reactor used in our experiments, the rate of accumulation of NMor in the bulk liquid equals its rate of formation per unit volume. Adding the contributions of the two regions, the overall rate is given by

$$\frac{d[\mathrm{NMor}]}{dt} = k_5[\mathrm{Mor}^\circ]\left\{[\mathrm{N_2O_3}]_M + (A/V)\int_0^\infty [\mathrm{N_2O_3}]_{BM}dx\right\} \tag{25}$$

where A is the surface area of the NO• tubing and V is the total liquid volume (indistinguishable from the bulk volume). Using equation 23 in equation 25 and integrating, we obtain:

$$\frac{d[\mathrm{NMor}]}{dt} = k_5[\mathrm{Mor}^\circ]\left\{[\mathrm{N_2O_3}]_M + [\overline{\mathrm{N_2O_3}}]_M\right\} \tag{26}$$

$$[\overline{\mathrm{N_2O_3}}]_M = \frac{k_2}{k_{-2} + k_3 + k_4[\mathrm{P_i}] + k_5[\mathrm{Mor}^\circ]}[\mathrm{NO}]_0[\mathrm{NO_2}]_{0M}\frac{A\lambda_M}{V} \tag{27}$$

In equation 26, the contribution of the boundary layer to NMor formation is expressed as an apparent increment in the bulk N_2O_3 concentration; that increment, $[\overline{N_2O_3}]_M$, was evaluated using equation 27.

Taking dX formation from dG as an example, there are two contributions also to each rate of deamination:

$$\frac{d[\mathrm{dX}]}{dt} = k_6[\mathrm{dG}]\left\{[\mathrm{N_2O_3}]_D + (A/V)\int_0^\infty f(x)[\mathrm{N_2O_3}]_{BD}dx\right\} \tag{28}$$

where $f(x)$ is the ratio of the plasmid concentration in the boundary layer to that in the bulk solution. The reason for the $f(x)$ term is that the finite size of the plasmid will cause some steric exclusion of it from the boundary layer. If the plasmid is approximated as a rod of length l, then $f(x)$ will increase linearly from 0 to 1 over the interval $0 \le x \le l/2$, and be unity thereafter (White and Deen 2000). Incorporating that function into equation 28 and integrating, we obtain

$$\frac{d[\mathrm{dX}]}{dt} = k_6[\mathrm{dG}]\left\{[\mathrm{N_2O_3}]_D + \beta[\overline{\mathrm{N_2O_3}}]_D\right\} \tag{29}$$

where $[\overline{\mathrm{N_2O_3}}]_D$ is the apparent increment in the bulk N_2O_3 concentration for a point-size molecule and b represents the steric effect. With l @ 0.5 μm (estimated from electron microscopy) and $l_D = 0.60$ μm, those terms are evaluated as

$$\beta = \frac{2\lambda_D}{l}\left(1 - e^{-\frac{l}{2\lambda_D}}\right) \cong 0.82 \tag{30}$$

$$[\overline{\mathrm{N_2O_3}}]_D = \frac{k_2}{k_{-2} + k_3 + k_4[\mathrm{P_i}]}[\mathrm{NO}]_0[\mathrm{NO_2}]_{0D}\frac{A\lambda_D}{V}. \tag{31}$$

The expressions for the rates of dI and dU formation are analogous to equation 29.

From equations 21, 27 and 31, one finds that $[\overline{\mathrm{N_2O_3}}]_M/[\overline{\mathrm{N_2O_3}}]_D = a_1$, a result analogous to equation 16. Further combining equations 16, 26, and 29, and solving for k_6, we obtain

$$k_6 = \frac{k_5[\mathrm{Mor}^\circ]}{[\mathrm{dG}]} \frac{d[\mathrm{dX}]/dt}{d[\mathrm{NMor}]/\mathrm{dt}} \alpha_1 \left(\frac{1 + \frac{[\overline{N_2O_3}]_M}{[N_2O_3]_M}}{1 + \beta \frac{[\overline{N_2O_3}]_M}{[N_2O_3]_M}} \right) \tag{32}$$

As will be shown, [dG] can be approximated as constant in our experiments. Therefore, k_6 can be determined from the slopes of the [dX] and [NMor] data plotted *versus* time. The rate constants for dI and dU formation are related to k_6 by:

$$k_7 = k_6 \frac{[\mathrm{dG}]\, d[\mathrm{dI}]/\mathrm{dt}}{[\mathrm{dA}]\, d[\mathrm{dX}]/\mathrm{dt}} \tag{33}$$

$$k_8 = k_6 \frac{[\mathrm{dG}]\, d[\mathrm{dU}]/\mathrm{dt}}{[\mathrm{dC}]\, d[\mathrm{dX}]/\mathrm{dt}} \tag{34}$$

where [dA] and [dC] are constant, like [dG].

3.4 Results

Characterization of the NO• delivery system. Prior to the DNA experiments, the NO• and O_2 concentrations were measured to confirm that the delivery system was performing as expected. The results of two such tests are shown in Figure 1. The O_2 concentration remained constant at 186 μM throughout each experiment, whereas the NO• concentration reached a value of 1.2 μM about 15 min after NO• gas flow was initiated, and was constant thereafter. The solid curves in Figure 1 show the concentrations predicted using the mass transfer coefficients reported previously (Wang and Deen 2003). The agreement between those curves and the measured concentrations indicates that the final concentrations of both gases, and the duration of the initial NO• transient, were all predictable. The concentration of nitrite increased linearly with time (data not shown), with a formation rate of 1.45 μM/min. It is worth noting that the steady state level of NO• achieved here is similar to that generated by activated macrophages in a culture plate (~1 μM, in Chen and Deen 2002). Therefore, the experimental conditions used here are likely to be relevant to the pathophysiology of inflammation involving macrophages.

Given the measured (or calculated) NO• and O_2 concentrations, the steady state N_2O_3 concentration in the bulk liquid in the morpholine and DNA experiments can be estimated from equations 13 and 15, respectively. The calculated N_2O_3 concentrations were quite small, 3.1×10^{-14} M for the morpholine solution and 4.0×10^{-14} M for the DNA solution. These low levels are mainly due to the rapid hydrolysis of N_2O_3 to form nitrite. As mentioned earlier, the bulk N_2O_3 concentration was lower in the morpholine experiments because there was enough morpholine present to noticeably augment the consumption of N_2O_3; a similar lowering of the

N_2O_3 level by morpholine is expected in the $NO_2^{\bullet}/N_2O_3$ boundary layer. The low bulk concentrations of N_2O_3 notwithstanding, in the morpholine experiments NMor accumulation reached micromolar levels, as shown in Figure 1. As will be discussed shortly, our calculations indicate that N-nitrosation in the bulk solution and in the $NO_2^{\bullet}/N_2O_3$ boundary layer both contributed significantly to the observed rate of NMor formation.

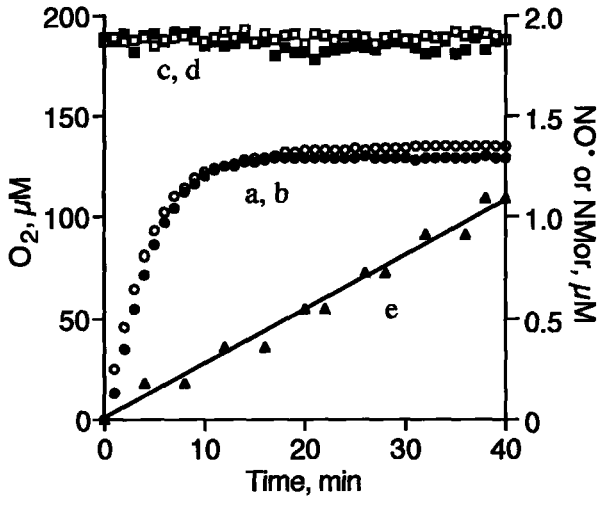

Figure 1. Time course for concentrations of NO• (a, b) and O_2 (c, d) in the reactor, with the N-nitrosation of morpholine (Nmor) kinetics (e) determined under the same conditions. The two sets of data (open and closed symbols) for NO• and O_2 represent single determinations for two separate experiments. The slope of the NMor line was used to calculate rate constant k5 in Equation 17.

LC-MS Analysis of Base Deamination Products Produced by NO• Exposure. The LC-MS method was now applied to the quantification of deamination products in DNA exposed to nitric oxide. Using the NO• reactor, plasmid pUC19 DNA (120 mL at 50 μg/mL in K-PO_4 buffer, pH

7.4) was exposed to $NO^{\bullet}$ and O_2 at steady state levels of 1 and 200 μM, respectively. At various times, 1 mL aliquots were removed and subjected to enzymatic digestion and LC-MS analysis as described earlier. The results of the analyses are shown in Figure 2. Here, it is apparent that there was a time-dependent increase in the quantities of all deamination products except dO.

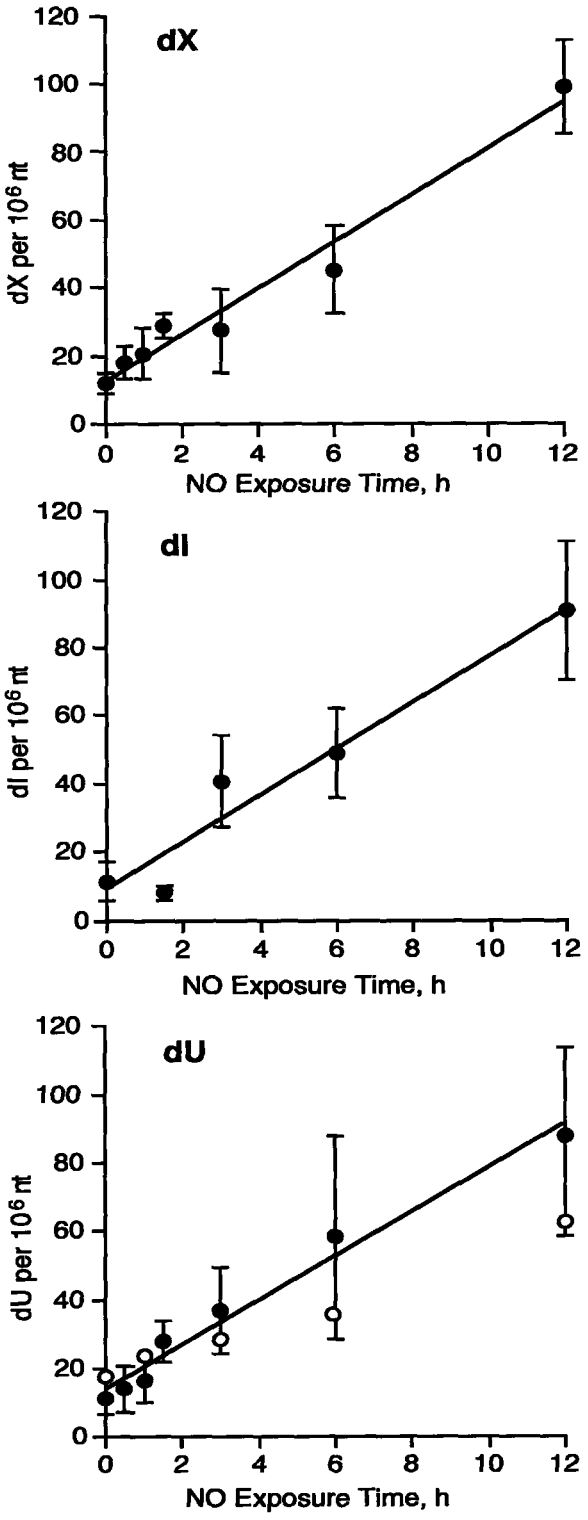

Figure 2. Time course for the formation of dX, dI and dU in plasmid DNA by exposure to 1.2 μM NO and 186 μM O_2. Data points represent mean ± SD for four determinations. The data were subjected to linear regression analysis, with the slope of each line used to calculate rate constants k_6 (dX), k_7 (dI), k_8 (dU) according to equations 17-20. Open circles in the panel for dU represent quantification of dU with uracil DNA glycosylase as described in Materials and Methods.

The inability to detect dO extended to the longest exposure time (24 hr) with ten-fold higher amounts of DNA subjected to analysis (500 μg; data not shown). This suggested either that dO was produced below the limit of detection of the assay (6 lesions per 10^8 nt with 500 μg of DNA) or that technical problems prevented the detection of dO. To rule out the latter, an experiment was performed in which calf thymus DNA was treated with nitrous acid, which is known to produce high levels of dO (Suzuki et al. 1997). As shown in Figure 3, there is a time-dependent formation of dO by HNO_2 in the DNA to the extent of nearly 1 lesion in 100 nt. The non-linearity of the time course is likely due to a reduction in the concentration of substrate dG.

The quantity of dU in NO$^{\bullet}$-treated plasmid DNA was confirmed using a plasmid-based nicking assay. Samples of plasmid DNA exposed to NO$^{\bullet}$ in the reactor were treated with uracil DNA glycosylase (Scharer and Jiricny 2001) followed by treatment with putrescine to cleave the resulting abasic sites to strand breaks (*e.g.*, refs. (Povirk and Goldberg 1985; Dedon et al. 1992; Tretyakova et al. 2000)) that were subsequently quantified following agarose gel resolution of nicked and supercoiled plasmid. As shown in Figure 2, the quantity of dU determined by the plasmid nicking study is within 30% of that determined by LC-MS, which attests to the precision of the LC-MS assay. One possible reason for the systematically lower levels of dU revealed by the plasmid nicking assay in comparison to the LC-MS method is the efficiency of uracil DNA glycosylase in recognizing its substrate *in vitro*.

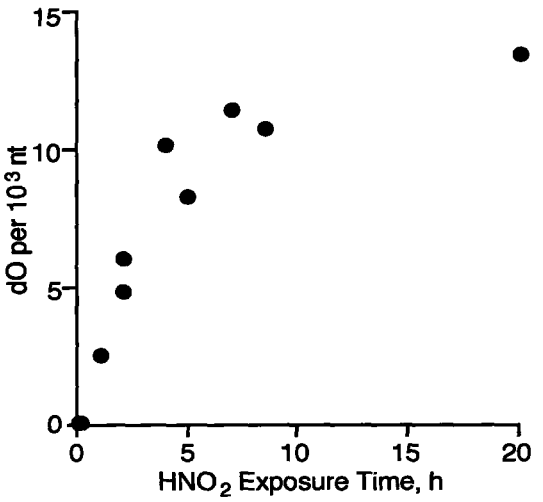

Figure 3. Time course for the production of dO in DNA treated with HNO_2. Data points represent individual determinations for **two experiments.**

Quantitation of Abasic Sites produced by Exposure of DNA to NO˙. Given the precedent for depurination of DNA by nitrosating agents (Lucas et al. 2001), we quantified abasic sites formed in the plasmid DNA exposed to NO˙ in the reactor, as described above. Aliquots of plasmid solution containing 3 μg of DNA, obtained from samples removed for LC-MS analysis, were divided and one portion treated with putrescine, as described above. Following resolution of the plasmid topoisomers on agarose gels, the quantity of abasic sites at each NO˙ exposure time was calculated as the difference in the quantity of nicked plasmid DNA in samples treated with putrescine and those not treated. The results are shown in Figure 4, in which it is apparent that there is a steady increase in the number of abasic sites as a function of NO˙ exposure time.

Rate Constants of N_2O_3 Reaction with Plasmid DNA Bases. To determine the rates of nucleobase deamination, the rate of N-nitrosation of morpholine was determined in the reactor (Figure 1) and the rate constant for N_2O_3 reaction with dG was then derived from experimental data using equation 21. The predetermined N_2O_3 concentrations in morpholine and DNA solutions can be used to calculate the $[N_2O_3]_M/[N_2O_3]_P$ ratio as 0.71. The slopes of NMor and dX were determined from their concentration-time plots (Figures 1 and 2), which were 0.0266 and 6.91 $x10^{-6}$ μM/min. Assume that [Mor^o] and [dG] were essentially 147 μM (the uncharged form) and 15 μM (dG represents 25.3% of the 2686 bp pUC19 sequence), respectively. Using the reported rate constant k_5 (6.4 x 10^7 $M^{-1}s^{-1}$; Table 1), k_6 was calculated to be 1.2 (± 0.2) x 10^5 $M^{-1}s^{-1}$ (mean ± S.D. for four determinations). Likewise, the slopes of dI and dU formation obtained from linear regression of data in Figure 2 yielded virtually identical values of 1.2 (± 0.3) x 10^5 and 1.2 (± 0.4) x 10^5 $M^{-1}s^{-1}$ for rate constants k_7 and k_8 using equations 23 and 24, respectively. The deamination rate constants between N_2O_3 with plasmid DNA bases are comparable to those with single-stranded oligonucleotides, but are three orders-of-magnitude lower than that with morpholine. Using the determined values for k_6, k_7 and k_8, the three terms, k_6[dG], k_7[dA] and k_8[dC], were all calculated to be 1.8 s^{-1}, which is much smaller than k_3 (1.6 x 10^3 s^{-1}). This validated the assumption that the k_6[dG] + k_7[dA] + k_8[dC] term in equation 14 was negligible.

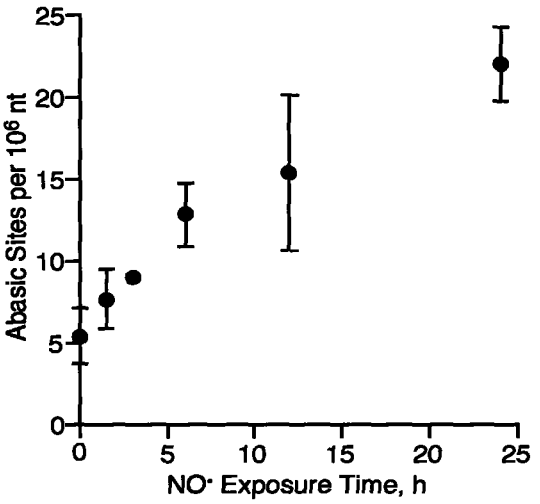

Figure 4. Time course for the formation of abasic sites by exposure of plasmid pUC19 to 1.2 μM NO· and 186 μM O_2. Values represent mean ± error about the mean for two experiments.

3.5 Discussion

Nitric oxide is a physiologically important molecule with genotoxic properties that may be involved in the pathophysiology of chronic inflammation (Tamir et al. 1996; Wink and Mitchell 1998). While the genotoxicity of reactive nitrogen species derived from NO• have been extensively studied, neither the biologically relevant chemistry nor the consequences of that chemistry *in vivo* have been rigorously defined. We thus developed and applied novel delivery and analytical methods to a comprehensive characterization of the spectrum of DNA lesions, with the exception of the G-G cross-link (Kirchner et al. 1992), produced by nitrosative NO• derivatives under conditions that approach biological relevance.

The Spectrum of Nitrosative DNA Lesions Produced by NO• Exposure. Among the spectrum of nitrosative DNA lesions produced by exposure to NO•, we approached the quantification of abasic sites by standard plasmid nicking assay. However, we were obliged to develop an LC-MS method sensitive enough to quantify nucleobase deamination products arising by nitrosative mechanisms at biologically relevant NO• concentrations (μM) in the presence of O_2. Most published studies of nucleobase deamination have employed GC-MS techniques (*e.g.*, refs. (Nguyen et al. 1992; Caulfield et al. 1998)). However, the acidic conditions used for depurination of DNA for GC-MS analysis cause decomposition of dO (Dong et al., unpublished observations). To avoid this problem, NO•-exposed DNA was enzymatically digested to nucleosides under conditions (37 °C, pH 7.4) that did not result in significant depurination of dX ($t_{1/2} > 2$ yr, in Vongchampa et al. 2003). The background levels of the

deamination products in the plasmid DNA, while relatively high at ~1 per 10^5 nt (Table 2), do not appear to be an artifact of the analytical method given the precision established for the quantification of dI in a defined oligonucleotide and for dU by comparison to an independent analytical method. It is thus likely that these background levels are those expected to occur *in vivo* or are the result of DNA purification and storage.

These analytical techniques were then applied to DNA exposed to controlled concentrations of NO$^\bullet$ and O_2 in a novel NO$^\bullet$ reactor. A summary of the results of these studies is shown in Table 2. NO$^\bullet$ and O_2 were delivered at steady-state concentrations of 1.2 μM and 186 μM, respectively, with the former approaching the 1 μM upper limit of NO$^\bullet$ concentration estimated to arise in tissues subjected to macrophage-mediated inflammation. These conditions resulted in a time-dependent increase in three nucleobase deamination products (dX, dI and dU) at nearly identical rates, which stands in contrast to the nearly two-fold higher rate of formation of dX than dU observed by Caulfield *et al.* (Caulfield et al. 1998). The basis for this small difference may lie in the NO$^\bullet$ delivery system used by Caulfield *et al.*, in which headspace air may have altered the spectrum of NO$^\bullet$ derivatives and thus the nitrosative chemistry in the reaction mixture. A comparison of NO$^\bullet$ the delivery systems will be made shortly.

The studies produced two unexpected results. The first was the observation of a time-dependent formation of abasic sites to the extent of 4-7% of the total number of DNA lesions (with the exception of dG-dG cross-links; Table 2). Shuker and coworkers have demonstrated that nitrosation of DNA by 1-nitrosoindole-3-acetonitrile causes the formation of abasic sites, presumably as a result transient nitrosation of the N^7 position of dG and the N^7 and N^3 positions of dA (Scheme 1; refs. (Lucas et al. 1999; Lucas et al. 2001)). We propose that a similar mechanism accounts for the formation of abasic sites as a result of nitrosation by N_2O_3 generated

in the reactor. It is unclear what role the abasic sites may play in NO•-induced mutagenesis, given the observation in repair-deficient *E. coli* exposed to nitrous acid that the G:C→T:A mutations expected for apurinic sites represented only 0.2% of total mutations (Schouten and Weiss 1999). The bulk of the mutations consisted of G:C→A:T and A:T→G:C transitions (Schouten and Weiss 1999). However, Engelward and coworkers have demonstrated that *E. coli* cells lacking AP endonuclease activity were highly sensitive to NO• exposure (Spek et al. 2001; Spek et al. 2002), which suggests that, along with base excision repair of nucleobase deamination products, the directly-formed abasic sites may contribute to NO•-induced toxicity in cells.

Table 2: Spectrum of DNA Lesions Produced by Exposure to 1.2 μM NO• and 186 μM O_2

	Lesions per 10^6 nt				
Time, hr	**AP[a]**	**dX**	**dI**	**dU**	**dO**
0	5.4 ± 1.6	12 ± 2.9	11 ± 5.7	11 ± 5.0	<0.06
3	9.0 ± 0.10	27 ± 12	41 ± 13	37 ± 12	<0.06
6	13 ± 1.9	45 ± 13	49 ± 13	58 ± 30	<0.06
12	15 ± 4.7	99 ± 14	91 ± 20	88 ± 26	<0.06
24	22 ± 2.3	131 ± 16	143 ± 38	109 ± 26	<0.06

[a] AP: abasic sites; values for all lesions represent mean ± SD for four determinations.

The observation of NO•-induced abasic sites expands the spectrum of lesions associated with the nitrosative intermediates derived from NO• under biologically relevant conditions. With consideration given to the formation of dG-dG cross-links in NO•-exposed DNA, we are now in a position to propose a testable quantitative spectrum of nitrosative DNA lesions in cells and tissues exposed to NO•. Recent studies by Caulfield *et al.* (submitted for publication) revealed that the dG-dG cross-link represented 6% of the amount of xanthine in oligodeoxynucleotides exposed to NO• delivered at 15 μM/min *via* Silastic tubing. We thus propose that the spectrum of nitrosative DNA lesions in cells and tissues exposed to physiological concentrations of NO• and O_2 will be comprised of ~2% dG-dG cross-links, 4-6% abasic sites, and 25-35% each of dX, dI and dU. We are presently testing this model in TK6 cells exposed to NO• in the reactor employed in the present studies and in the SJL mouse model for inflammation (Gal et al. 1997; Nair et al. 1998). Interestingly, there appears to little oxidative chemistry in the NO• reactor as judged by the lack of nicking induced in exposed plasmid DNA by treatment with Fpg and EndoIII glycosylases (data shown in Chapter 6), enzymes that recognize DNA damage produced by peroxynitrite.

The second novel observation is the absence of detectable dO in DNA exposed to biological concentrations of NO• and O_2. We were unable to detect this lesion in 500 μg of DNA, an amount ten-fold higher than that used for analysis of dX, dI and dU, which suggests that dO, if it arises at all, is present at less than 6 lesions per 10^8 nt (Table 2). The apparent absence of dO is not the result of analytical artifact given the detection of this lesion in DNA samples treated with nitrous acid (Figure 3). Shuker and coworkers also observed a significant disparity between dX and dO in DNA treated with the nitrosating agent, 1-nitrosoindole-3-acetonitrile, with dO formed at levels 10^3-fold lower than depurination and deamination products (Lucas et al. 2001).

However, our inability to detect dO stands in contrast to the observations of Suzuki *et al.* in reactions of deoxynucleosides and DNA with nitrous acid and NO• (Suzuki et al. 1996; Suzuki et al. 1997; Suzuki et al. 1999; Suzuki et al. 2000), in which dO and dX were formed in a ratio of 1:3-5. The basis for the differences observed with dO likely lie in the model systems employed for the DNA reactions. For example, while nitrous acid does indeed cause nitrosative deamination of DNA bases, the mechanisms and intermediates involved are substantially different than those associated with NO•/O_2 due to the low pH required (pH < 4; HNO_2 pK_a = 3.3), the presence of a different spectrum of nitrosating species (*e.g.*, NO^+, $H_2NO_2^+$, NO_X, N_2O_4; refs. (Turney and Wright 1959; Goldstein and Czapski 1996)), and the effects of acidic pH on nucleobase structure and reactivity. These differences almost certainly affect the reaction pathways and the spectrum of products.

Suzuki *et al.* also observed the formation of dO in DNA solutions exposed to NO• and O_2 (Suzuki et al. 1997). In contrast to the NO• delivery system employed in the present studies, Suzuki *et al.* performed reactions by bubbling NO• gas into an aerated, buffered solution of DNA exposed to air (Suzuki et al. 1997), which, as discussed shortly, significantly alters the chemistry of NO• due to alternative (and possibly physiologically irrelevant) gas-phase NO_x chemistry (Mirvish 1975; Challis et al. 1981). They also observed that the relative quantities of dX and dO vary as a function of the ratio of NO• to O_2, with formation of dO favored by an excess of NO• (Suzuki *et al.*, unpublished observations).

Given these differences, we hypothesize that dO will not be produced in significant quantities, relative to the other DNA lesions, in cells exposed to NO• and at sites of inflammation in tissues. This model is supported by our inability to detect dO in preliminary studies in TK6

cells exposed to NO• and O_2 in the reactor under conditions identical to those employed here with isolated DNA (Dong *et al.*, manuscript in preparation).

Comparison to Published Studies. This NO• delivery system represents a major improvement over previous systems in terms of biological relevance. Previous attempts to expose DNA to NO• and the derivative nitrosating species have employed several NO• delivery systems. For example, Nguyen *et al.* exposed DNA and TK6 cells to ~20 mM NO• by bolus delivery through a syringe and found that dX and dI were formed to the extent of three and ten lesions per 10^3 nt, respectively, for isolated DNA, with three-fold lower levels of each in TK6 cells (Nguyen et al. 1992). Yields of dI an dX in DNA were found to be 15- to 100-times higher, respectively, than those observed with free dA and dG *(Nguyen* et al. *1992).* Similarly, Wink *et al.* exposed DNA to 1 M NO• by bubbling the gas into solution and found five dU per 10^3 nt (Wink et al. 1991).

The previous studies that most closely approximated biological conditions were those performed by Caulfield *et al.* in which NO•-induced deamination of dC and dG in 2'-deoxynucleosides and oligonucleotides was studied using two different reactors. In the first reactor, they introduced O_2 into a deoxygenated solution containing NO•, morpholine, and dG, and measured the concentrations of NMor and dX formed as products. Through a kinetic competition analysis, the rate of dG conversion to dX was determined. In the second reactor, they used a Silastic membrane delivery system to introduce NO• into solutions containing dG and other nucleosides or nucleotides. Using the predetermined dG kinetics as a reference, the rate constants for dG and dC in different nucleic acids were determined. In general, relatively high 2'-deoxynucleoside and NO• concentrations were used in that study (stated as 10-20 nmol/mL/min); the latter was not determined but would not have been constant, due to the

depletion of O_2 during the experiments. The deamination rate constants found for plasmid DNA in the present studies (1.2×10^5 $M^{-1}s^{-1}$) are comparable to the values reported by Caulfield *et al.* for single-stranded oligonucleotides (9.8×10^4 $M^{-1}s^{-1}$ for dG and 5.6×10^4 $M^{-1}s^{-1}$ for dC), but they are about one order of magnitude higher than those determined by Caulfield *et al.* in double-stranded oligonucleotides (1.0×10^4 $M^{-1}s^{-1}$ for dG and 5.6×10^3 $M^{-1}s^{-1}$ for dC, in Caulfield et al. 1998). One possible explanation for the similarity of our results to those of Caulfield *et al.* in single-stranded DNA is that the plasmid DNA used in the present studies contains single-stranded regions as a result of negative supercoiling.

The previous studies present several problems that prevent extrapolation to the biological setting. First, in all of the delivery systems, NO• was present at significantly higher concentrations than occur at sites of inflammation *in vivo*, which are thought not to exceed steady-state concentrations of ~1 μM (Miwa et al. 1987; Stuehr and Marletta 1987; Lewis et al. 1995). Second, none of the studies addressed the complete spectrum of deamination products produced by exposure to NO•. Finally, the presence of a headspace containing air in each of these delivery systems alters the chemistry of NO• by biasing the formation of N_2O_3 and allowing formation of N_2O_4 (Mirvish 1975; Challis et al. 1981). These conditions were avoided with the novel NO• reactor used in the present studies.

Characterization of the NO• Reactor. The physiological relevance of the observed DNA lesion spectrum presented in the preceding discussion rests entirely on the NO• delivery system. The development of this system was motivated by the well-respected complexity of the reactions of NO• and O_2 in aqueous solutions (*e.g.*, Goldstein and Czapski 1996), as illustrated earlier by

the different results obtained with different NO• delivery mechanisms and rates. There are substantial differences in the relative concentrations and kinetics of the nitrosating intermediates depending on the concentrations of NO• and O_2, such that the only approach that provides biologically meaningful results is one in which the NO• and O_2 are delivered at controlled concentrations and rates that reflect the physiology of inflammation in tissues. The reactor employed in the present studies (Wang and Deen 2003) provides more constant and predictable levels of NO• and O_2 than could be achieved previously in long exposures (up to 24 hr). As shown in Figure 1, the dimensions of the Silastic tubing selected for the present studies produced a steady-state NO• concentration of 1.2 μM within 15 minutes of initiating gas flow. This level is comparable to the NO• production of 10^6 activated macrophages *in vitro* (Lewis et al. 1995; Chen and Deen 2002) and lies at the upper limit for estimates of NO• concentration at sites of inflammation (Miwa et al. 1987; Stuehr and Marletta 1987; Lewis et al. 1995). At this point, 1.2 μM is also the lowest level of NO• reliably achieved to date for *in vitro* studies. Molecular oxygen achieved a more rapid approach to a steady-state concentration of 186 μM that is analogous to the O_2 concentration in arterial blood in the extra-cellular space (Tortora et al. 2002). During the course of the NO• delivery, the pH remained at 7.4 while the nitrite level rose steadily at a rate of 1.4 μM/min to ~2 mM at 24 hr (data not shown). The steady-state levels of N_2O_3 and NO_2• under these conditions were calculated to be 40 fM and 3.3 pM, respectively. Although the delivery conditions were fixed in the present experiments, it is worth noting that the NO• and O_2 concentrations can each be varied in a predictable way, by changing the gas mixtures and Silastic tubing lengths (Wang and Deen 2003).

The NO• delivery system was designed mainly to carry out long-term cell culture studies, and has the disadvantage in kinetic measurements that a rather complicated analysis is needed to

interpret the results. The source of the complication is that, despite vigorous stirring, the interplay between NO• oxidation kinetics and diffusion creates two liquid regions with very different concentrations of NO_x compounds. In addition to the well-stirred bulk liquid, there is an extremely thin (~1 μm) boundary layer next to the NO• delivery tubing, in which the NO_2• and N_2O_3 concentrations greatly exceed those in the bulk liquid (Figure 5). The main experimental evidence for this boundary layer is that the rate of nitrite formation in the delivery system greatly exceeds (by an order of magnitude) that expected from the measured concentrations of NO• and O_2 in the bulk liquid. Those data, and a model that quantitatively explains the observed mass transfer characteristics of the device, are detailed elsewhere (Wang and Deen 2003). One of the present findings is that the N_2O_3 concentration in the boundary layer is high enough to contribute appreciably to the overall rates of morpholine nitrosation or DNA deamination, despite the seemingly negligible volume of the boundary layer. As described in the Results section, the rate of NMor formation in the boundary layer was 71% of that in the bulk solution. Put another way, some 40% of the total NMor formation was calculated to occur in the ultra-thin boundary layer. The contribution of the boundary layer to deamination was slightly smaller, because of steric exclusion of the plasmid DNA from part of that layer, as discussed shortly.

The issues that arise in using the NO• delivery device to study NO_2• or N_2O_3 chemistry in various applications are illustrated in Figure 5. As shown by the dots, morpholine is small enough (relative to 1 μm) that its concentration in the boundary layer will not differ from that in the bulk liquid, assuming that morpholine is present in large excess, as in the present experiments, so that it is not depleted by reaction. Molecules of plasmid DNA (2686 bp) with plectonemic supercoiling, however, are just large enough to experience some exclusion from the boundary layer. We estimated that the average concentration of pUC19 in the boundary layer

was 18% less than in the bulk solution, which had a modest (8%) effect on the calculated rate constants for deamination. In contrast to small molecules and plasmid DNA, mammalian cells have dimensions that are large enough (~10 μm) to almost fully exclude them from the $NO_2^{\bullet}/N_2O_3$ boundary layer. Accordingly, cells in this device will be exposed only to the bulk NO_x concentrations. Because bulk concentrations are more accessible experimentally (*e.g.*, using $NO^{\bullet}$ and O_2 electrodes), the chemical conditions there are less uncertain than they are in the $NO_2^{\bullet}/N_2O_3$ boundary layer.

We also found a kinetic discrepancy in the measured NMor formation rate, which was about 4- to 5-fold lower than expected from the rate constants in Table 1. As already noted, the present data and kinetic analysis indicate that the rate of NMor formation was enhanced by some 70% in the boundary layer. However, at the same $NO^{\bullet}$ and O_2 concentrations (but without morpholine), the boundary layer was found to give a 9-fold increase in the overall rate of nitrite formation (Wang and Deen 2003). Because the nitrite and NMor formation rates are both proportional to the N_2O_3 concentration, the boundary layer should augment them by similar amounts. The ~20% reduction in the N_2O_3 concentration caused by morpholine is too small to explain the difference. One possible explanation is that the phosphate effect on N_2O_3 hydrolysis (*i.e.*, the k_4 value) might have been underestimated. If the actual value of k_4 was larger than that in Table 1, then NMor formation would be reduced, but nitrite formation in a morpholine-free solution (which is controlled by the rate of reaction 1) would be unaffected. Another possibility is that the value of k_5 may have been overestimated. The discrepancy between the predicted and observed rates of NMor formation suggests a proportional uncertainty in the concentrations of N_2O_3, and a consequent 4- to 5-fold uncertainty in the absolute values of the deamination rate constants. However, because each deamination rate was compared with the same standard (rate of NMor

formation), there is little uncertainty in the relative rate constants for deamination of dG, dA, and dC.

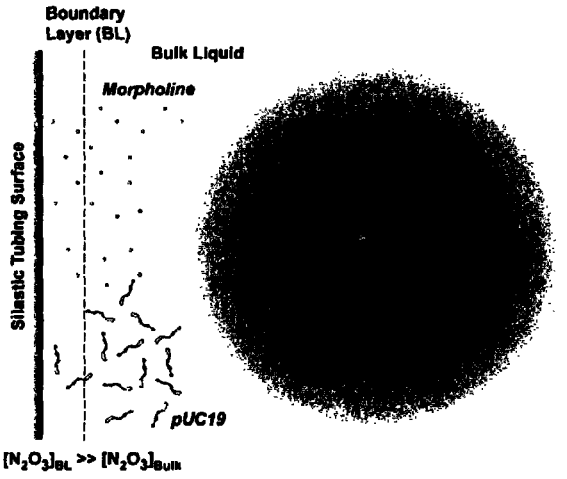

Figure 5. Heterogeneity of liquid concentrations in the NO• reactor. In a boundary layer (BL) of thickness ~1 μm next to the NO• delivery tubing, the concentration of N_2O_3 greatly exceeds that in the bulk liquid. Morpholine molecules (not to scale) have free access to the boundary layer, while plasmid molecules are partially excluded and cells are almost fully excluded.

3.6 References

Caulfield, J. L., Wishnok, J. S. and Tannenbaum, S. R. (1998). "Nitric oxide-induced deamination of cytosine and guanine in deoxynucleosides and oligonucleotides." J Biol Chem **273**(21): 12689-95.

Challis, B. C., Shuker, D. E. G., Fine, D. H., Goff, E. U. and Hoffman, G. A. (1981). Amine nitration and nitrosation by gaseous nitrogen dioxide,. N-nitroso Compounds: Occurrence and Biological Effects. H. Bartsch, I. K. O'Neill, M. Castegnaro and M. Okada. Lyon, IARC. **41:** 11-20.

Chen, B. and Deen, W. M. (2002). "Effect of liquid depth on the synthesis and oxidation of nitric oxide in macrophage cultures." Chem Res Toxicol **15**(4): 490-6.

Collier, J. and Vallance, P. (1991). "Physiological importance of nitric oxide." BMJ **302**(6788): 1289-90.

Dedon, P. C., Jiang, Z.-W. and Goldberg, I. H. (1992). "Neocarzinostatin-mediated DNA damage in a model AGT•ACT site: Mechanistic studies of thiol-sensitive partitioning of C4' DNA damage products." Biochemistry **31**: 1917-1927.

deRojas-Walker, T., Tamir, S., Ji, H., Wishnok, J. S. and Tannenbaum, S. R. (1995). "Nitric oxide induces oxidative damage in addition to deamination in macrophage DNA." Chem Res Toxicol **8**(3): 473-7.

Dubelman, S. and Shapiro, R. (1977). "A method for the isolation of cross-linked nucleosides from DNA: application to cross-links induced by nitrous acid." Nucleic Acids Res **4**(6): 1815-27.

Gal, A., Tamir, S., Kennedy, L. J., Tannenbaum, S. R. and Wogan, G. N. (1997). "Nitrotyrosine formation, apoptosis, and oxidative damage: relationships to nitric oxide production in SJL mice bearing the RcsX tumor." Cancer Res **57**(10): 1823-8.

Goldstein, S. and Czapski, G. (1996). "Mechanism of the nitrosation of thiols and amines by oxygenated NO˙ solutions: The nature of the nitrosating intermediates." J. Am. Chem. Soc. **118**: 3419-3425.

Graetzel, M., Taniguchi, S. and Henglein, A. (1970). "Pulse radiolytic investigation of NO oxidation and equilibrium N_2O_3 = NO+NO_2 in aqueous solution." Ber. Bunsenges. **74**: 488-492.

Kirchner, J. J., Sigurdsson, S. T. and Hopkins, P. B. (1992). "Interstrand cross-linking of duplex DNA by nitrous acid: Covalent structure of the dG-to-dG cross-link at the sequence 5'-CG." J. Am. Chem. Soc. **114**(11): 4021-4027.

Lewis, R. S. and Deen, W. M. (1994). "Kinetics of the reaction of nitric oxide with oxygen in aqueous solutions." Chem. Res. Toxicol. **7**: 568-574.

Lewis, R. S., Tamir, S., Tannenbaum, S. R. and Deen, W. M. (1995). "Kinetic analysis of the fate of nitric oxide synthesized by macrophages in vitro." J Biol Chem **270**(49): 29350-5.

Lewis, R. S., Tannenbaum, S. R. and Deen, W. M. (1995). "Kinetics of N-nitrosation in oxygenated nitric oxide solutions at physiological pH: role of nitrous anhydride and effects of phosphate and chloride." J. Am. Chem. Soc. **117**: 3933-3939.

Lindahl, T. and Andersson, A. (1972). "Rate of chain breakage at apurinic sites in double-stranded deoxyribonucleic acid." Biochemistry **11**: 3618-3623.

Lucas, L. T., Gatehouse, D., Jones, G. D. and Shuker, D. E. (2001). "Characterization of DNA damage at purine residues in oligonucleotides and calf thymus DNA induced by the mutagen 1-nitrosoindole-3-acetonitrile." Chem Res Toxicol **14**(2): 158-64.

Lucas, L. T., Gatehouse, D., Jones, G. D. D. and Shuker, D. E. G. (2001). "Characterization of DNA damage at purine residues in oligonucleotides and calf thymus DNA induced by the mutagen 1-nitrosoindole-3-acetonitrile." Chem. Res. Toxicol. **14**: 158-164.

Lucas, L. T., Gatehouse, D. and Shuker, D. E. (1999). "Efficient nitroso group transfer from N-nitrosoindoles to nucleotides and 2'-deoxyguanosine at physiological pH. A new pathway for N-nitrosocompounds to exert genotoxicity." J Biol Chem **274**(26): 18319-26.

Mirvish, S. S. (1975). "Formation of N-nitroso compounds: chemistry, kinetics, and in vivo occurrence." Toxicol Appl Pharmacol **31**(3): 325-51.

Miwa, M., Stuehr, D. J., Marletta, M. A., Wishnok, J. S. and Tannenbaum, S. R. (1987). "Nitrosation of amines by stimulated macrophages." Carcinogenesis **8**(7): 955-8.

Moncada, S., Palmer, R. M. and Higgs, E. A. (1991). "Nitric oxide: physiology, pathophysiology, and pharmacology." Pharmacol Rev **43**(2): 109-42.

Nair, J., Gal, A., Tamir, S., Tannenbaum, S. R., Wogan, G. N. and Bartsch, H. (1998). "Etheno adducts in spleen DNA of SJL mice stimulated to overproduce nitric oxide." Carcinogenesis **19**(12): 2081-4.

Nathan, C. and Xie, Q. W. (1994). "Regulation of biosynthesis of nitric oxide." J Biol Chem **269**(19): 13725-8.

Nguyen, T., Brunson, D., Crespi, C. L., Penman, B. W., Wishnok, J. S. and Tannenbaum, S. R. (1992). "DNA damage and mutation in human cells exposed to nitric oxide in vitro." Proc Natl Acad Sci U S A **89**(7): 3030-4.

Ohshima, H. and Bartsch, H. (1994). "Chronic infections and inflammatory processes as cancer risk factors: possible role of nitric oxide in carcinogenesis." Mutat Res **305**(2): 253-64.

Povirk, L. F. and Goldberg, I. H. (1985). "Endonuclease-resistant apyrimidinic sites formed by neocarzinostatin at cytosine residues in DNA: evidence for a possible role in mutagenesis." Proc Natl Acad Sci U S A **82**(10): 3182-6.

Scharer, O. D. and Jiricny, J. (2001). "Recent progress in the biology, chemistry and structural biology of DNA glycosylases." Bioessays **23**(3): 270-81.

Schmidt, H. H. and Walter, U. (1994). "NO at work." Cell **78**(6): 919-25.

Schouten, K. A. and Weiss, B. (1999). "Endonuclease V protects Escherichia coli against specific mutations caused by nitrous acid." Mutat Res **435**(3): 245-54.

Shapiro, R. and Pohl, S. H. (1968). "The reaction of ribonucleosides with nitrous acid. Side products and kinetics." Biochemistry **7**(1): 448-55.

Shapiro, R. and Yamaguchi, H. (1972). "Nucleic acid reactivity and conformation. I. Deamination of cytosine by nitrous acid." Biochim Biophys Acta **281**(4): 501-6.

Spek, E. J., Vuong, L. N., Matsuguchi, T., Marinus, M. G. and Engelward, B. P. (2002). "Nitric oxide-induced homologous recombination in *Escherichia coli* is promoted by DNA glycosylases." J Bacteriol **184**(13): 3501-7.

Spek, E. J., Wright, T. L., Stitt, M. S., Taghizadeh, N. R., Tannenbaum, S. R., Marinus, M. G. and Engelward, B. P. (2001). "Recombinational repair is critical for survival of *Escherichia coli* exposed to nitric oxide." J Bacteriol **183**(1): 131-8.

Stamler, J. S., Jaraki, O., Osborne, J., Simon, D. I., Keaney, J., Vita, J., Singel, D., Valeri, C. R. and Loscalzo, J. (1992). "Nitric oxide circulates in mammalian plasma primarily as an S-nitroso adduct of serum albumin." Proc. Natl. Acad. Sci. USA **89**(August): 7674-7677.

Stuehr, D. J. and Marletta, M. A. (1987). "Synthesis of nitrite and nitrate in murine macrophage cell lines." Cancer Res **47**(21): 5590-4.

Suzuki, T., Ide, H., Yamada, M., Endo, N., Kanaori, K., Tajima, K., Morii, T. and Makino, K. (2000). "Formation of 2'-deoxyoxanosine from 2'-deoxyguanosine and nitrous acid: mechanism and intermediates." Nucleic Acids Res. **28**(2): 544-551.

Suzuki, T., Kanaori, K., Tajima, K. and Makino, K. (1997). "Mechanism and intermediate for formation of 2'-deoxyoxanosine." Nucleic Acids Symp. Ser.(37): 313-314.

Suzuki, T., Yamada, M., Ishida, T., Morii, T. and Makino, K. (1999). "Reactivity of 2'-deoxyoxanosine, a novel DNA lesion." Nucleic Acids Symp Ser(42): 7-8.

Suzuki, T., Yamaoka, R., Nishi, M., Ide, H. and Makino, K. (1996). "Isolation and characterization of a novel product, 2'-deoxyoxanosine, from 2'-deoxyguanosine, oligodeoxynucleotide, and calf thymus DNA treated with nitrous acid and nitric oxide." J. Am. Chem. Soc. **118**: 2515-2516.

Tamir, S., Burney, S. and Tannenbaum, S. R. (1996). "DNA damage by nitric oxide." Chem Res Toxicol **9**(5): 821-7.

Tamir, S. and Tannenbaum, S. R. (1996). "The role of nitric oxide (NO.) in the carcinogenic process." Biochim Biophys Acta **1288**(2): F31-6.

Tannenbaum, S. R., Tamir, S., deRojas-Walker, T. and Wishnok, J. S., Eds. (1994). DNA damage and cytoxicity by nitric oxide. Nitrosamines and related N-nitroso compounds: Chemistry and biochemistry. Washington, D.C., American Chemical Society.

Tortora, G. J., Grabowski, S. R. and Prezbinodowski, K. S. (2002). Principles of Anatomy and Physiology.

Treinin, A. and Hayon, E. (1970). "Absorption spectra and reaction kinetics of NO_2, N_2O_3 and N_2O_4 in aqueous solution." J. Am. Chem. Soc. **92**: 5821-5828.

Tretyakova, N. Y., Burney, S., Pamir, B., Wishnok, J. S., Dedon, P. C., Wogan, G. N. and Tannenbaum, S. R. (2000). "Peroxynitrite-induced DNA damage in the supF gene: correlation with the mutational spectrum." Mutat Res **447**(2): 287-303.

Turney, T. A. and Wright, G. A. (1959). "Nitrous acid and nitrosation." Chem. Rev. **59**(3): 497-513.

Vongchampa, V., Dong, M., Gingipalli, L. and Dedon, P. (2003). "Stability of 2'-deoxyxanthosine in DNA." Nucleic Acids Res **31**(3): 1045-51.

Wang, C. and Deen, W. M. (2003). "Nitric oxide delivery system for cell culture studies." Ann. Biomed. Eng. **31**: 65-79.

White, J. A. and Deen, W. M. (2000). "Equilibrium partitioning of flexible macromolecules in fibrous membranes and gels." Macromolecules **33**(22): 8504-8511.

Wink, D. A., Kasprzak, K. S., Maragos, C. M., Elespuru, R. K., Misra, M., Dunams, T. M., Cebula, T. A., Koch, W. H., Andrews, A. W., Allen, J. S. and et al. (1991). "DNA deaminating ability and genotoxicity of nitric oxide and its progenitors." Science **254**(5034): 1001-3.

Wink, D. A., Kasprzak, K. S., Maragos, C. M., Elespuru, R. K., Misra, M., Dunams, T. M., Cebula, T. A., Koch, W. H., Andrews, A. W., Allen, J. S. and Keefer, L. K. (1991). "DNA deaminating ability and genotoxicity of nitric oxide and its progenitors." Science **254**(November 15): 1001-1003.

Wink, D. A. and Mitchell, J. B. (1998). "Chemical biology of nitric oxide: Insights into regulatory, cytotoxic, and cytoprotective mechanisms of nitric oxide." Free Radic Biol Med **25**(4-5): 434-56.

Chapter 4

Formation of Nucleobase Deamination Products in Human Lymphoblastoid Cells Exposed to Nitric Oxide at Controlled Physiological Concentrations

4.1 Abstract

Our previous *in vitro* investigation demonstrated that nucleobase deamination products can act as useful biomarkers for nitrosative chemistry caused by NO• at controlled physiological concentrations (Dong et al., 2003). We then sought to extend the *in vitro* observations to cultured human cells. The goals of these cell studies were as follows: First, we wanted to compare the results with the spectrum of nitrosative DNA lesions derived from the *in vitro* study. Second, we also wanted to correlate nucleobase deamination with other biological end points, including cell viability, apoptosis, etc. Third, and perhaps most important, we wanted to establish analytical parameters for subsequent probing of tissue samples from mouse models of inflammation.

TK6 human lymphoblastoid cells were first exposed to a relatively high steady-state level of NO• using the delivery system described in Chapter 3. Following a 12 hr exposure to 1.75 μM NO• and 186 μM oxygen, dO was not detected while the other deamination products were formed at comparable levels above baseline as follows: dX, a 3.5-fold increase from the baseline level; dI, a 3.8-fold increase; and dU, a 4.1-fold increase. In comparison, these levels were much lower than those reported in our *in vitro* studies. Furthermore, regarding cell viability and apoptosis, we found that a 12 hr NO• exposure compromised the growth of TK6 cells. Compared with the control group, 32.7 ± 3.5% of TK6 cells were either dead or undergoing apoptosis immediately after NO• exposure, while, 86.3 ± 4.7% of the cells were dead or undergoing apoptosis after a single doubling-time.

As a rational extension, formation of nucleobase deamination products was also examined at a low steady-state level of NO•. A 12 hr exposure to 0.65 μM NO• and 190 μM O_2, a total dose equal to three times the threshold value of 150 μM•min (Wang et al., 2003), caused observable increases above the baseline levels for each lesion as follows: dX, 1.7-fold; dI, 1.8-fold; and dU, 2.0-fold. Again, dO was not detected. Simultaneous analysis of cell viability revealed a ~15 ± 3.6% reduction in TK6 cells immediately after exposure to the same dose of NO•. This observation, together with the results mentioned above, lead to the conclusion that there may not be a causative relationship between nucleobase deamination and cell death arising from NO•.

GSH is the most abundant thiol in eucaryotic cells and represents a very important cell defense system against oxidative stress. We found that incubation of TK6 cells with 125 μM L-buthionine SR-sulfoximine (BSO), a specific inhibitor of GSH synthesis, for 24 hr virtually depleted all intracellular GSH, but resulted in no cell death. GSH depletion in TK6 cells prior to NO• treatment did not increase sensitivity to NO•-induced cell killing or increase the baseline level of any nucleobase deamination products. After a 12 hr exposure to steady-state levels of 0.65 μM NO• and 186 μM O_2, there was an ~2-fold increases for all nucleobase deamination products in GSH-depleted TK6 cells. This observation was smaller than expected, considering the effects of GSH on steady-state concentrations of N_2O_3 as eluded to in several *in vitro* kinetics studies, suggesting that there are other cellular factors that may significantly influence nucleobase deamination.

4.2 Introduction

A growing body of epidemiological evidence demonstrates a close association between chronic inflammation and an increased risk of cancer (Jaiswal et al., 2001; Lala and Chakraborty, 2001; Ohshima, 2003; Ohshima et al., 2003). Nitric oxide (NO$^{\bullet}$), as an identified inflammatory mediator, has been implicated in this process. NO$^{\bullet}$ participates at various stages of the multiple-step malignant transformation of somatic cells. Among various NO$^{\bullet}$-mediated noxious effects, DNA damage and cytotoxicity are of particular importance. Together with the infidelity of certain polymerases (Bebenek et al., 2001), DNA damage is a major factor leading to the inactivation of tumor suppressor genes and the activation of oncogenes (Dedon and Tannenbaum, 2004; Tamir et al., 1996), two mechanisms underpinning a multi-faceted path to carcinogenesis. Cytotoxicity, including cell injury and cell death, may induce compensatory cell proliferation which has been shown to increase cancer risk (Rosin et al., 1994) (Albina et al., 1996; Zamora et al., 2001).

The adverse effects of NO$^{\bullet}$ are normally studied by using NO$^{\bullet}$ from one of the three sources: various NO$^{\bullet}$ donor compounds, NO$^{\bullet}$ gas, or NO$^{\bullet}$ produced by either macrophages or endothelial cells after activation. Donor compounds, though easy to use, generally do not provide a steady rate of NO$^{\bullet}$ release, and their parent compounds and/or their decomposition products may contribute to the observed cellular response (Keefer et al., 1996; Tabor and Tabor, 1985). Similar drawbacks exist when using a co-culture system. The observed cellular effects in the target cells are not purely caused by NO$^{\bullet}$, but by a combination of reactive nitrogen and oxygen species formed in the generator cells (deRojas-Walker et al., 1995; Zhuang et al., 2002). The direct use of NO$^{\bullet}$ gas for cell exposure has been made possible by supplying NO$^{\bullet}$ continuously

through gas permeable polydemethylsiloxane tubing (Luperchio et al., 1996b; Tamir et al., 1993). In its day, the membrane delivery system was considered a pioneering method for controlled delivery of NO•. However, because oxygen reacts with NO• and is also consumed by the cells, it becomes progressively depleted from the medium, leading to two serious consequences: variation of the exposure conditions over time and confounding cellular effects induced by hypoxia. These imperfections have been addressed by a novel NO• delivery system (described in Chapter 3) that provides a constant level of both NO• and O_2 (Wang and Deen, 2003).

NO•-mediated cyto- and genotoxycity have been investigated using both types of membrane delivery systems. Burney et al. used the original system (NO• only) to investigate several DNA damage parameters in Chinese hamster ovary (CHO-AA8) and human lymphoblastoid (TK6) cells, over a range of NO• doses. Results indicated that NO•-induced toxicity is an extremely complex process involving multiple pathways: inhibition of DNA synthesis, cell cycle arrest, apoptosis, and necrosis (Burney et al., 1997). The same system was also applied by Li et al. to investigate the influences of NO• on other biological indices in two human lymphoblastoid cell lines, TK6 and WTK-1, which express wild-type and mutant p53, respectively (Li et al., 2002b). They observed that the status of p53 strongly affected the mutagenic and apoptotic response to NO•. Furthering these observations, Wang et al. made use of a newly developed membrane delivery system (with both NO• and O_2). They chose the NH32 cell line as a more appropriate counterpart to the TK6 cell line because, unlike WTK-1 cells which express a mutant p53 protein (Xia et al., 1995), NH32 cells were derived from TK6 cells by knocking out the p53 gene. Under controlled conditions, they discovered that various toxic effects, including cell viability, apoptosis, mitochondrial membrane depolarization, and mutation frequency became observable

only when NO• concentrations and dose were greater than threshold values of approximately 0.5 μM and 150 μM•min, respectively (Wang et al., 2003).

In contrast to the extensive studies of NO•-mediated cytotoxicity, there have been fewer investigations that directly monitor cellular DNA damage that arises when using membrane delivery systems. In studies by Burney et al. (Burney et al., 1997), the occurrence of DNA strand breaks increased with the increasing dose of NO•. A similar observation was reported by Li et al. (Li et al., 2002b). Given the diversity of DNA damage products resulting from NO• that have been identified *in vitro* (Caulfield et al., 1998; Dong et al., 2003), a sound molecular basis for the observed biological effects remains speculative until a quantitative analysis of various products has been accomplished. To approach this goal, we initiated a study to define DNA lesion spectra produced by NO• in cultured cells with a special focus on nucleobase deamination products and the resulting cytotoxicity and mutagenicity.

Determining a DNA lesion spectrum from within a cell is far more challenging than simply from naked DNA. The first important detail was to obtain DNA free of artifacts created by the isolation process itself. This point has been well documented by analysis of 8-oxo-dG. Many studies have indicated the oxidative generation of 8-oxo-dG during DNA isolation (Cadet et al., 2003; Douki et al., 1996). This problem can be addressed by working at reduced temperature and by adding an antioxidant such as desferrioxamine (Atamna et al., 2000) or TEMPO (2,2,6,6-tetramethylperidinoxyl)(Nakamura et al., 2000). In contrast, the risk of adventitious generation of deamination products during DNA isolation has been largely ignored. During method development, we discovered an artificial generation of dI from dA by the action of contaminating dA deaminases found in many commercially available DNA digestive enzymes.

Thereafter, we added coformycin, a specific inhibitor of dA deaminase, to our preparations (Dong et al., 2003).

Of course, the cellular environment may also complicate any analysis by acting as a determinant of the NO• chemistry. The role of various cytosolic and nuclear factors in NO•-induced nitrosative chemistry must therefore be determined. One such factor is glutathione (GSH), a small molecule known to protect cells from the toxic effects of free radicals and reactive oxygen species (Poulsen et al., 1998), and which has been shown to mediate the cytotoxicity caused by NO• (Luperchio et al., 1996b). Furthermore, several studies *in vitro* showed that GSH reacts with NO• to form an S-nitrosothiol, which reduces the effective cellular level of NO• and may serve as an NO• sink (Keshive et al., 1996a; Singh et al., 1996). In our present study, we chose to monitor the specific effects of glutathione by reducing intracellular glutathione levels in cells by treatment with buthionine sulfoximine (Anderson, 1985; Luperchio et al., 1996b).

4.3 Materials and Methods

Materials. All chemicals and reagents were of highest purity available and were used without further purification unless noted otherwise. Pure Ar gas, mixtures of 1% and 10% NO$^{\bullet}$ in Ar gas, and a mixture of 50% O_2 and 5% CO_2 in N_2 gas were purchased from BOC Gases (Edison, NJ). TK6 cell line was kindly provided by Dr. W. G. Thilly (Massachusetts of Institute of Technology). NH32 cell line was a generous gift from Dr. C. Harris (National Cancer Institute). RPMI-1640 medium, donor calf serum, glutamine, and penicillin/streptomycin were purchased from BioWhittaker (Walkersville, MD). An ApoAlert annexin V-FITC kit was obtained from Clontech (Palo Alto, CA). Trypan blue (4% in saline), spermidine, spermine, Nonidet P40, 8-hydroxyquinoline, 2'-deoxycytidine, hypoxanthine, aminopterin, thymidine, 2-(N-morphoino) ethanesulphonic acid (NEM), glutathione (GSH), glutathione disulfide (GSSG), nicotinamide adenine dinucleotide phosphate, reduced form (NADPH), glutathione reductase, 5,5'-dithiobis-2-nitrobenzoic acid (DTNB), meta-Phosphoric acid (MPA), 2'-Vinylpyridine, L-buthionine SR-sulfoximine (BSO), and alkaline phosphatases were obtained from Sigma Aldrich (St. Louis, MO). Coformycin and tetrahydrouridine were purchased from Calibochem (San Diego, CA). Nuclease P1, proteinase K, and DNase-free RNase A were purchased from Roche Diagnostic Corporation (Indianapolis, IN). Phosphodiesterase I was obtained from USB (Cleveland, Ohio). Uniformly ^{15}N, ^{13}C-labeled 5'-triphosphate-2'-deoxyguanosine, 5'-triphosphate-2'-deoxyadenosine, and 5'-triphosphate-2'-deoxycytidine were purchased from Silantes (Munich, Germany). Acetonitrile and HPLC-grade water were purchased from Mallinckrodt Baker (Phillipsburg, NJ). Water purified through a Milli-Q system (Millipore Corporation, Bedford,

MA) was used for all other applications. Silastic tubing (1.47 mm i.d., 1.96 mm o.d.) was purchased from Dow Corning (Midland, MI).

Instrumental Analyses. All HPLC analyses were performed on an Agilent Model 1100, equipped with a 1040A diode array detector. Mass spectra were recorded with an Agilent Model 1100 electrospray mass spectrometer coupled to an Agilent Model 1100 HPLC with diode array detector. UV spectra were obtained using a Beckman DU640 UV-visible spectrophotometer.

Preparation of Uniformly ^{13}C, ^{15}N-labeled dA, dG, and dC. Each U-^{13}C, ^{15}N-5'-triphosphate-2'-deoxyuncleotide, including dA, dG and dC, was first dephosphorylated by incubation with alkaline phosphatase (0.5 units/μg of nucleotides) at 37°C for 1 hr in the presence of coformycin (50 μg/mL of reaction solution). The resulting reaction mixture was first passed through a Microcon YM-30 column (Millipore Corporation, Bedford, MA) to remove the enzyme, and then applied to a HPLC system, which contains a HAISIL HL C18 reversed phase semi-preparation column (250 x 10 mm, 5 μm particle size, 100 Å pore size) eluted with acetonitrile/H_2O (v/v=5/95) at a flow rate of 4.0 mL/min, for the purification of U-^{13}C, ^{15}N-2'-deoxynucleosides. The "raw" fraction containing each U-^{13}C, ^{15}N-2'-deoxynucleoside was then subjected to a second-run HPLC purification using a HAISIL HL C18 reversed phase column (250 x 4.6 mm, 5 μm particle size, 100 Å pore size, Higgins Analytic Inc, Mountain View, CA) with isocratic conditions of acetonitrile/H_2O (5/95 v/v) at a flow rate of 0.4 mL/min. Individual fraction containing each pure product was dried under Speed Vacuum evaporation and stored at −80°C for the future use.

Cell Culture. TK6 and NH32 cells were maintained in exponentially growing suspension cultures at 37°C in a humidified atmosphere of 95% air / 5% CO_2 in RPMI-1640 medium supplemented with 10% (v/v) heat-inactivated donor calf serum, 100 units/mL penicillin, 100 μg/mL streptomycin, and 2 mM L-glutamine. Stock cells were subcultured and routinely passaged to maintain an optimal growth density (0.6-1.0 × 10^6/mL) in 150-mm dishes during experiments. Cells were treated with CHAT (10 μM 2'-deoxycytidine, 200 μM hypoxanthine, 0.1 μM aminopterin, and 17.5 μM thymidine) to remove mutant cells before each experiment as described previously (Liber and Thilly, 1982).

Glutathione Depletion by BSO. BSO was dissolved in autoclaved water and filter sterilized before addition to the PRMI 1640 medium containing TK6 cells. The toxicity of BSO and its efficiency in depleting GSH were determined by adding BSO at a range of concentrations (0-5 mM) to a suspension of 0.5 ×10^6 cells/mL and incubated at 37°C for 24 hr.

NO• Exposure of Cells. Cells at a density of 5 × 10^5 cells/mL in 115 mL of fresh RPMI 1640 medium containing 10% heat-inactivated calf serum were exposed to NO• at 37°C in the membrane delivery system described before (Dong et al., 2003). 1% and 10% NO• gas were used to achieve the desired steady-state NO• concentrations: 0.65 μM and 1.75 μM respectively. A 50% O_2 gas mixture (with 5% CO_2) was flowed through a second tubing loop to maintain the liquid O_2 level near air saturation. The length of tubing for NO• and O_2 is 7 cm and 4 cm respectively. The control cells were treated with Ar gas using the same length of tubing as in the NO• experiments. Immediately after exposure to NO• or Ar, samples were taken for the analysis

of cell survival, apoptosis and the formation of nucleobase deamination products. The remaining cells from the 10% NO• exposure groups were collected by centrifugation. The cell pellets were resuspended in fresh culture medium, plated at a density of 5×10^5 cells/mL, and continue grew at 37°C for 24 hr, then cell survival, apoptosis, and the formation of nucleobase deamination products were again determined. Each experiment was done in triplicate.

Analysis of Cell Survival. NO•-induced cell lethality determined by trypan blue exclusion was reported to produce approximately the same survival values as by the plating efficiency assay (Li et al., 2002b). Therefore, in this study cell survival was determined by staining cells with 0.4% trypan blue solution followed by enumeration of those excluding the stain under a phase-contrast microscope. The relative survival was calculated as the ratio of the live cell number in NO• experiments to that in Ar controls (expressed as a percentage).

Apoptosis Analysis. Quantitative estimation of apoptosis was accomplished by flow cytometry following annexin V-FITC and PI (propidium iodide) staining. Positive staining for annexin V was used as a marker of early apoptosis. Aliquots of cell suspensions containing 0.5 to 1 x 10^6 cells were placed into 1.5-mL Eppendorf tubes, washed once with 500 μL annexin binding buffer, and resuspended in 200 μL of binding buffer. The cells were stained for 15 min at room temperature in the dark with annexin V-FITC at a final concentration of 0.5 μg/mL and PI at a final concentration of 2.5 μg/mL. The volume was adjusted to 600 μL using ice-cold binding buffer for the flow cytometry analysis by using a Becton Dickinson FACScan (excitation light 488 nm) equipped with CellQuest software (MIT center for Cancer Research). Annexin V-FITC fluorescence was recorded in FL-1 channel and PI fluorescence in FL-2. Twenty thousand cells

were examined for each sample. Cells stained positive with annexin V only were designated as apoptotic, those with PI only as necrotic, those with both PI and annexin V as necrotic or late apoptotic, those unstained by either as alive and not undergoing measurable apoptosis. Cells treated with Ar gas served as controls, and the measured apoptotic fraction was subtracted from that in $NO^{\bullet}$-induced cells.

Glutathione Measurement. Reduced and oxidized glutathione were extracted from TK6 cells by a modified method of Griffith and Anderso (Anderson, 1985; Griffith, 1980). Briefly, 10^7 cells were resuspended in 1 mL ice-cold MES buffer (50 mM MES, pH6-7, 1 mM EDTA) containing 0.5% MPA (w/v) and lysed by three cycles of freeze thaw. Acid insoluble material was pelleted out and the supernatant was extracted and neutralized by adding $1/10^{th}$ of triethanolamine (final pH 7.5) before the analysis of soluble glutathione (GSH+GSSG). GSH level was determined according to the method primarily developed by Tieze (Tietze, 1969) with further adaptation to microplate reader. Briefly, 150 μL freshly prepared assay cocktail containing 3 mM NADPH, 6 mM DTNB, and 50 units/mL glutathione reductase in MES buffer was added to each assay well of a 96-well plate. Samples and standards were done in triplicate by adding 50 μL standard (0-200 pmol GSH per well) or sample to each well. The change in absorbance at 405 nm was recorded every 2 min over a period of 20 min by a PowerWave X microplate reader (Bio-Tek Instruments; Winoski, VT). GSH concentration in each sample well was calculated by a kinetic method. The GSH content in TK6 cell is presented in μg GSH per 10^7 cells.

Isolation of Genomic DNA from TK6 and NH32 Cells. Cell pellet (1-2 x 10^7 cells) was resuspended in 0.4 mL of buffer A (300 mM sucrose, 60 mM KCl, 15 mM NaCl, 60 mM Tris-HCl, pH 8.0, 0.5 mM spermidine, 0.15 mM spermine, 2 mM EDTA, 50 μg/mL coformycin, and 500 μg/mL tetrahydrouridine). Cells were then lysed by addition of 1% Nonidet P40 and incubate on ice for 5 min. The released nuclei were washed once in buffer A (4500 g for 10 min at 4 °C) and resuspended in 0.2 mL of buffer B (150 mM NaCl and 5 mM EDTA, pH 7.8, 50 μg/mL coformycin, and 500 μg/mL tetrahydrouridine) followed by addition of the same volume of buffer C (20 mM Tri-HCl, pH 8.0, 20 mM NaCl, 20 mM EDTA, and 1% sodium dodecyl sulfate) immediately before digestion with proteinase K (450 μg/mL; 37°C, 2 hr, an additional 250 μg/mL was added for additional 1 hr). DNase-free RNase A was then added (150 μg/mL; 37°C, 1 hr). DNA was purified by successive extraction with buffer-equilibrated phenol (0.1 M Tris-HCl, pH 8.0, 0.1% 8-hydroxyquinoline [w/v]), phenol: chloroform (1:1), and chloroform. DNA was recovered by precipitation in 200 mM NaCl and 2 vol. of absolute ethanol (-20°C; add slowly to facilitate DNA recovery). The floating DNA filament was recovered with a micropipette tip (or by centrifugation at 5000×g for 30 min) followed by two washes with 70% ethanol, air-drying at ambient temperature and resuspension in 10 mM Tris-EDTA (pH 8.0) buffer. The DNA concentration was then determined (UV spectroscopy) and the DNA sample was stored at -80°C.

Quantification of DNA Nucleobase Deamination by LC-MS Analysis. DNA samples from either NO˙ or Ar treatment were subjected to quantification of the nucleobase deamination products by the LC-MS method established previously (Dong et al., 2003). Briefly, 50 μg of DNA molecule was hydrolyzed by the combination of three enzymes (Nuclease P1,

phosphodiesterase I, and alkaline phosphatase) at the presence of appropriate amount of isotope-labeled internal standards and an adenosine deaminase inhibitor, coformycin. The resulting nucleoside mixture was separated by HPLC. Fraction containing each nucleobase deamination product was collected for the subsequent LC-MS quantification.

Estimation of the Artificial Generation of Nucleobase Deamination Products. The potential of the artificial generation of nucleobase deamination products was estimated at different stages of sample preparation, including DNA isolation, digestion, and HPLC pre-purification (Scheme 1 and 2). As marked in the diagram below, the DNA isolation procedure was further divided into two steps: the process of breaking cellular and nucleic membranes to release nuclei and the process of digesting the chromatin proteins to release DNA molecules. At each stage, appropriate amount of U-^{13}C,^{15}N-2'-dA, dG, and dC (19.95 μg, 21.45 μg and 17.94 μg respectively, calculated based on generating as much as 300 fmol of each corresponding nucleobase deamination product, 3-fold of detection limit), along with appropriate amount of U-^{15}N-dX, dI and dU (3 pmol of each), coformycin (5 μg/mL), and tetrahydrouridine (50 μg/mL) were added at the very beginning of the process. The potentially formed nucleobase deamination products were collected at the end of each process for the HPLC separation, followed by further LC-MS analysis. The LC-MS conditions were as same as those established before except for the change in the SIM number for each monitored lesion. The SIM numbers monitored here were for both U-^{13}C, ^{15}N-labeled nucleobase deamination products, which can only be generated by the deamination of the corresponding U-^{13}C, ^{15}N-labeled normal nucleosides, and U-^{15}N-labeled internal standards of corresponding nucleobase deamination products, specifically, m/z 162 for

U-^{13}C, ^{15}N-dX, dO, m/z 157 for U-^{15}N-dX in positive mode; m/z 146 for U-^{13}C, ^{15}N-dI, m/z 141 for U-^{15}N-dI in positive mode; m/z 233 for U-^{13}C, ^{15}N-U, m/z 229 for U-^{15}N-U in negative mode.

Scheme 1. Isolation of Genomic DNA in TK6 Cells

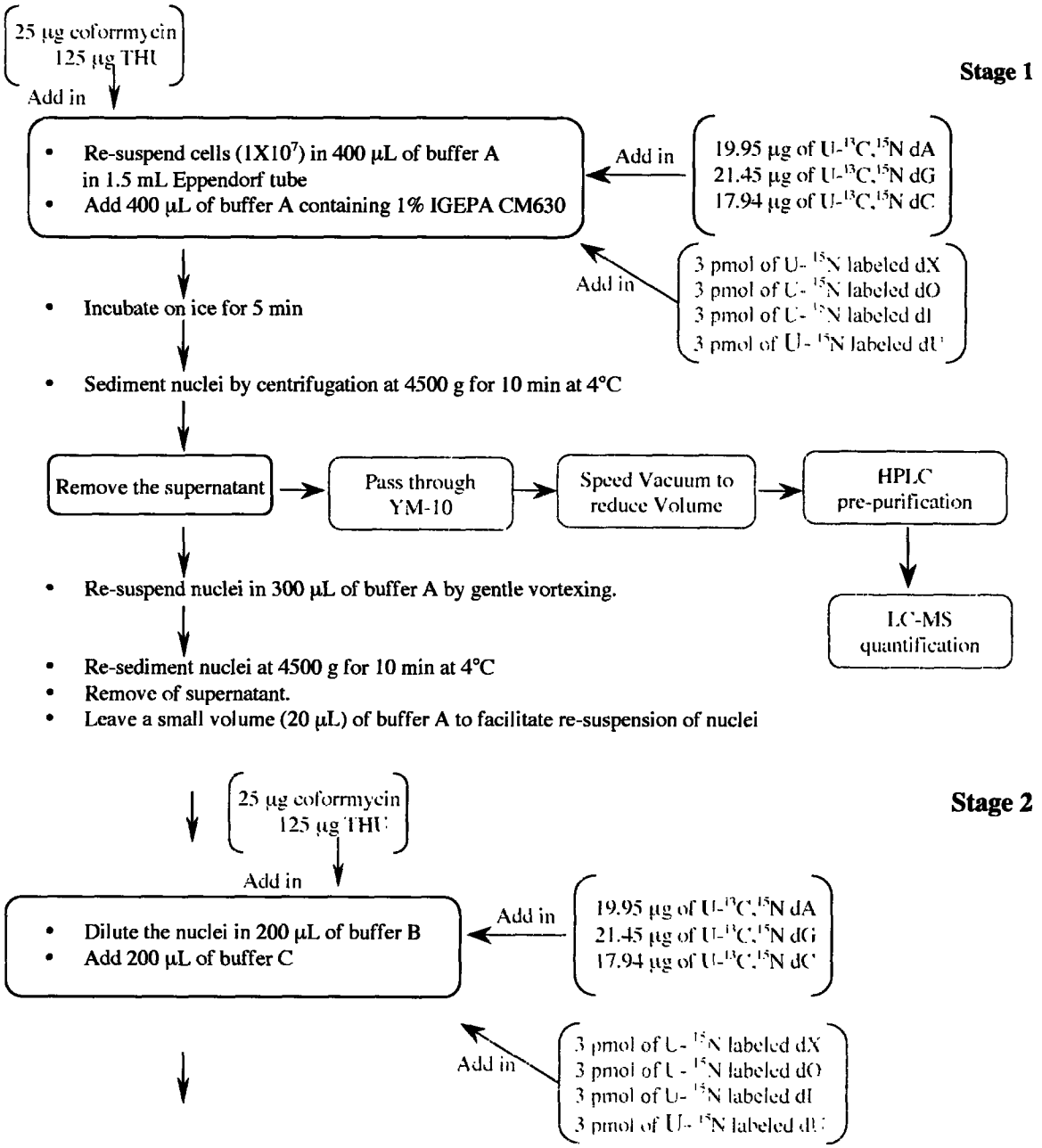

- Incubate at 37°C for 3 hr, shake occasionally

- Add 2.4 μL of RNase A (25 mg/ml) stock to a final concentration of 150 μg/mL
- Incubate at 37°C for 1 hr

- Purify DNA by extraction with 400 μL of phenol,
  400 μL of phenol: chloroform,
  and 400 μL of chloroform successively

- Precipitate DNA in 200 mM NaCl and 2 vol. of pre-cooled absolute ethanol.
- Add 16 μL of 5 M NaCl into 400 μL extracted solution, and then add 1 mL of pre-cooled absolute ethanol. Ethanol should be added slowly to facilitate DNA recovery, Rock the tube very gently.

- Recover DNA by spooling the floating DNA filament with a micropipette tip.
- If DNA is in small pieces or not clearly visible, recover DNA by centrifugation (5000 g for 30 min at 4°C).

- Remove supernatant → Pass through YM-10 → Speed Vacuum to reduce Volume → HPLC pre-purification → LC-MS quantification

- Wash DNA once with 10 mL of 70% ethanol

- Air-dry DNA pellet at room temperature.
- Dissolve DNA in 0.5 mL of dd H_2O.
- The quantity of DNA can be estimated based upon the number of cells that were initially used for DNA purification. About 6 μg of DNA should be purified from 1 X 10^6 cells
- Carefully measure DNA concentration by UV/VS spectrophotometry at 260 nm.

Scheme 2. Enzymatic Hydrolysis of Genomic DNA to Single Nucleosides

Stage 3

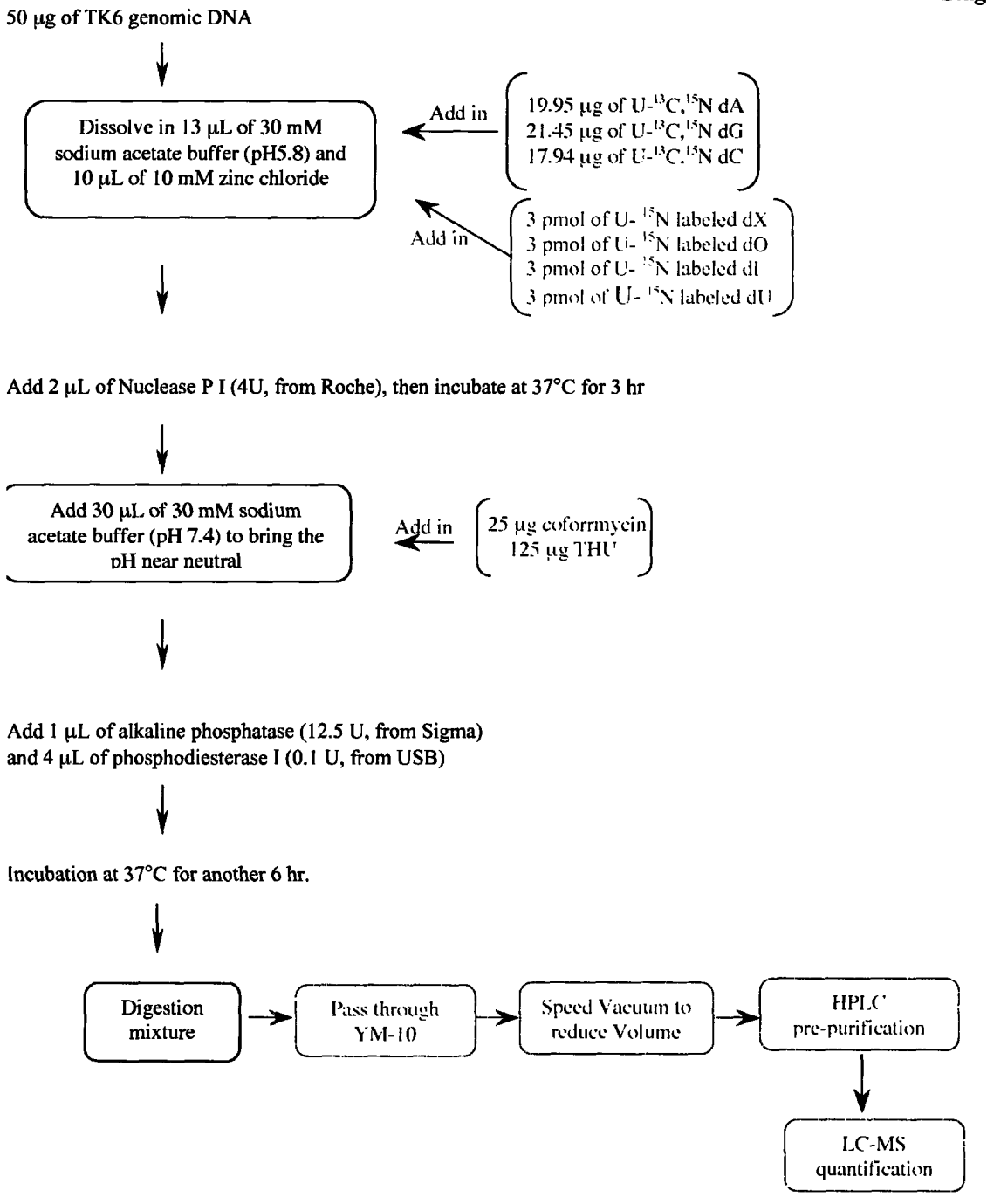

Stage 4 was the step of HPLC pre-purification. Double-labeled normal deoxynucleosides were subjected to HPLC separation in the present of U-^{15}N-dX, dO, dI and dU. Fractions at the eluting time bracketing each nucleobase deamination product were collected for the subsequent LC-MS quantification.

4.4 Results

Effect of NO• Exposure on Cell Viability. Figure 1 shows the relative cell viability obtained by trypan blue exclusion assay following various NO• exposures. The delivery system used for the current cell experiment was reported to have little or no effect on cell proliferation (Wang et al., 2003). We also found that in the control cells that were treated by Ar gas, the growth rate was similar to that for untreated plate cultures, though a slight decrease in the S-phase cell population was observed (unpublished results). After exposure, the control cells, both TK6 and NH32, continued to grow exponentially, with a similar doubling time of about 20 hr, further suggesting that any difference observed during NO• delivery could be attributed to NO•.

The relative cell viability was found inversely related to total NO• dose that was varied by using different NO• gas compositions and delivery times. As shown in Figure 1a, 1% NO•gas had no significant impact on TK6 cell viability until the total dose of NO• increased to 320 μM•min, which equals to ~ 8 hr NO• exposure. Further increasing the NO• dose to 450 μM•min resulted in ~15% reduction in cell viability. Figure 1b shows a similar trend when exposing to 10% NO•. A substantial loss of cell viability was observed at high NO• doses, culminating in a dramatic 87% reduction at 1260 μM•min.

For NH32 cells, cell viability also decreased with increasing dose of NO• exposure, but the reduction was less than that for identically treated TK6 cells. For example, as shown in Figure 1c, the relative cell survival of NH32 cells did not reduce significantly until 450 μM•min. Compare to TK6 cells, NH32 cells showed relatively higher cell survival to commensurate amount of 10% NO• exposure (Figure 1b and 1d).

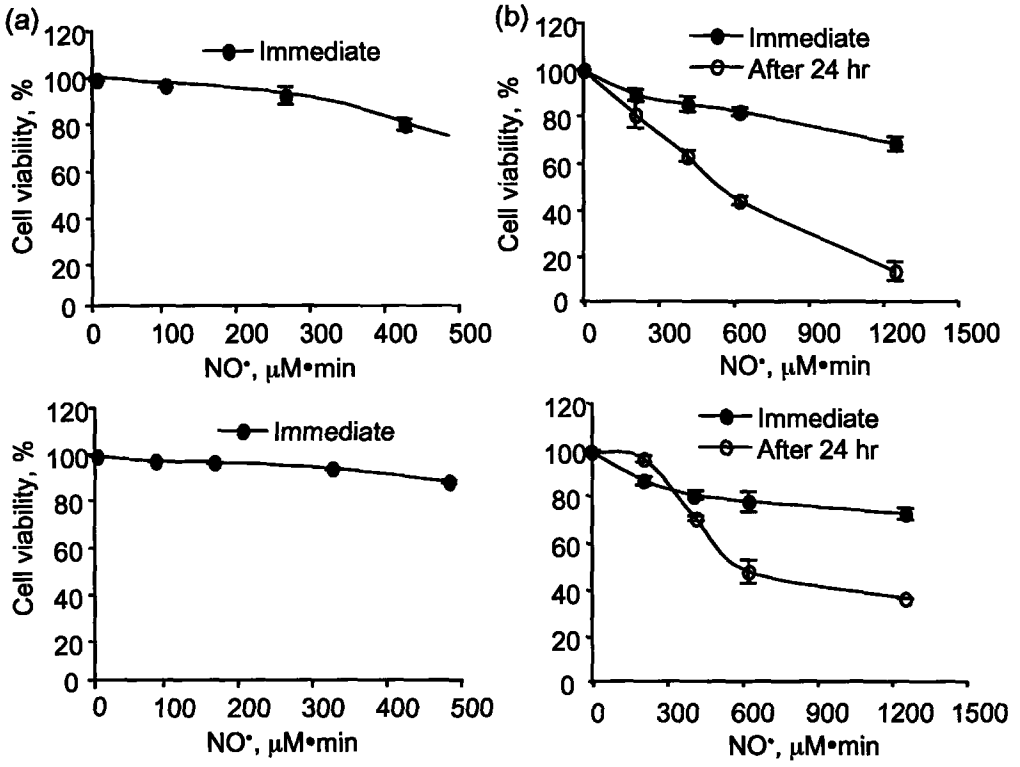

Figure 1. Cell viability determined by trypan blue exclusion assay at various doses of NO•. (a) TK6 cells with 1% NO• exposure rate; (b) TK6 cells with 10% NO• exposure rate; (c) NH32 cells with 1% NO• exposure rate; and (d) NH32 cells with 10% NO• exposure rate. In each panel, the abscissa is the dose of NO• calculated by multiplying the steady state concentration of NO• (1.75 μM for 10% NO• gas, 0.65μM for 1% NO•) with delivery time. The ordinate is the relative cell viability calculated as the ratio of cell number in NO• experiments to that in Ar controls (expressed as a percentage). The relative cell viability was also determined after a 24 hr recovery period following exposure in the 10% NO• experiments. These data represent the mean ± SD of eight measurements from two independent experiments.

Effect of NO• Exposure on Cell Apoptosis. Annexin V staining followed by flow cytometry was applied to quantify the apoptosis in TK6 and NH32 cells caused by NO• exposure. At an early stage of apoptosis, phosphatidylserine (PS) translocates from the inner to the outer leaflet of the cell membrane. FITC-conjugated annexin V protein can capture the PS, thereby labeling the cells and allowing their detection by flow cytometry. Some typical Annexin V and PI staining histograms of TK6 cells treated with different doses of NO• are shown in Figure 2. The percentages of cells with annexin V-positive staining, representing early apoptosis and late apoptosis or necrosis, for TK6 and NH32 cell lines, are shown in Figure 3.

For TK6 cells subjected to a 1% NO• exposure rate, as shown in Figure 3a, significant positive staining was observed only when the total dose of NO• was increased to 320 μM•min. For TK6 cells subjected to a 10% NO• exposure rate, a clear dose-dependent increase in apoptosis was observed as shown in Figure 3b. A maximum of 14.9% ± 3.0 of cells were stained with annexin V immediately following a dose of 1260 μM•min. The number of stained cells increased to 57.9% ± 1.7 after a 24 hr recovery period.

In the case of NH32 cells, for a 1% NO• exposure rate, as shown in Figure 3c, there was no significant increase in the number of stained cells for any dose of NO• tested. However, for the 10% NO• exposure rate, as shown in Figure 3d, there was a dose-dependent increase in positively stained cells, but to a lesser extent than shown for TK6 cells in Figure 3b. For instance, at a dose of 1260 μM•min, the fraction of stained NH32 cells was 11.0% ± 0.2, which is in contrast to 14.9% ± 3.0 for TK6 cells under identical conditions (compare Figure 3d with Figure 3b).

(a)

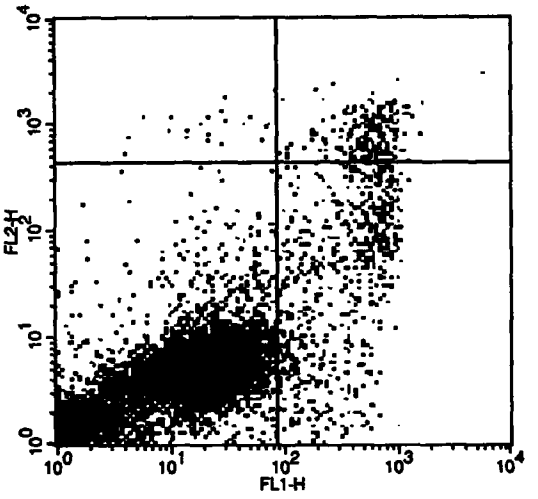

(b)

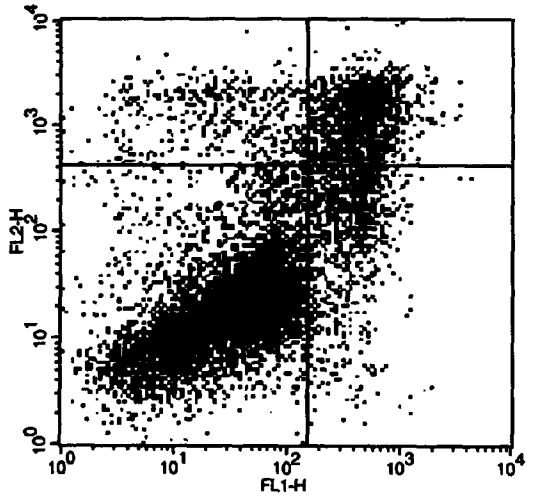

Figure 2. Annexin V and PI staining histograms of TK6 cells exposed to Ar (a) and NO• (b) for 12 hr respectively. In each histogram, cells stained positive with annexin V only (lower right panel) were designated as apoptotic, those with PI only as necrotic (upper left panel), those with both PI and annexin V as necrotic or late apoptotic (upper right panel), those unstained by either as alive and not undergoing measurable apoptosis.

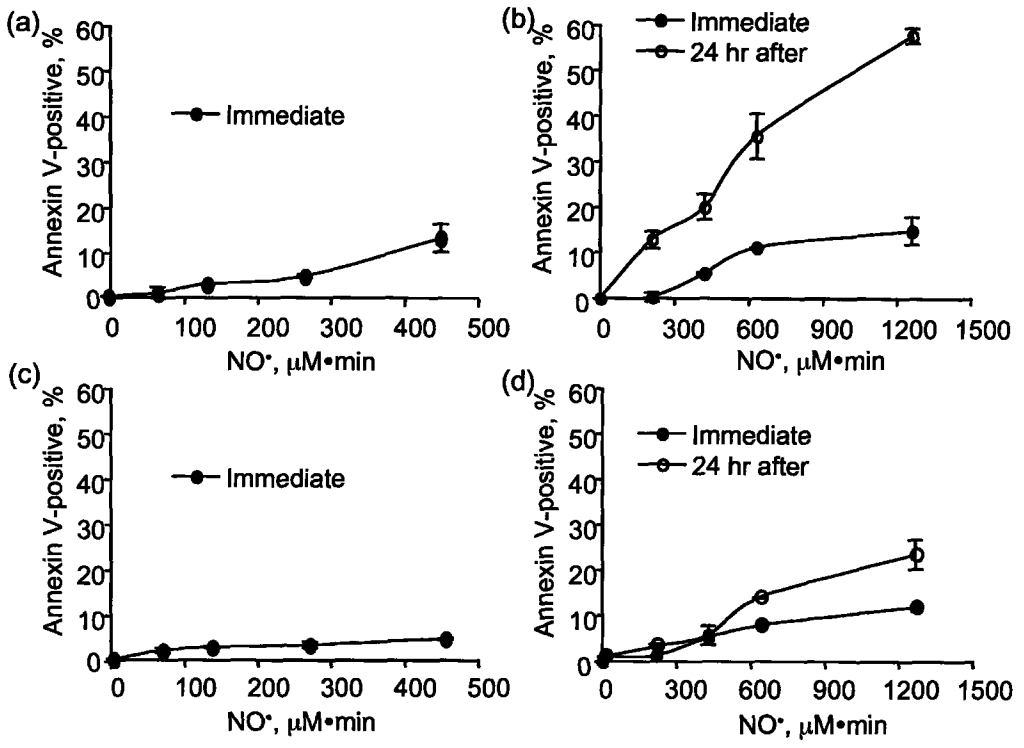

Figure 3. Percentages of annexin V-stained cells at various doses of NO•: (a) TK6 cells with 1% NO• exposure rate; (b) TK6 cells with 10% NO• exposure rate; (c) NH32 cells with 1% NO• exposure rate; and (d) NH32 cells with 10% NO• exposure rate. In each panel, the abscissa is dose of NO•. The total fractions of annexin V-stained cells were also determined after a 24 hr recovery period following NO• exposure in the 10% NO• experiments (b and d). These data represent the mean ± SD of three independent experiments.

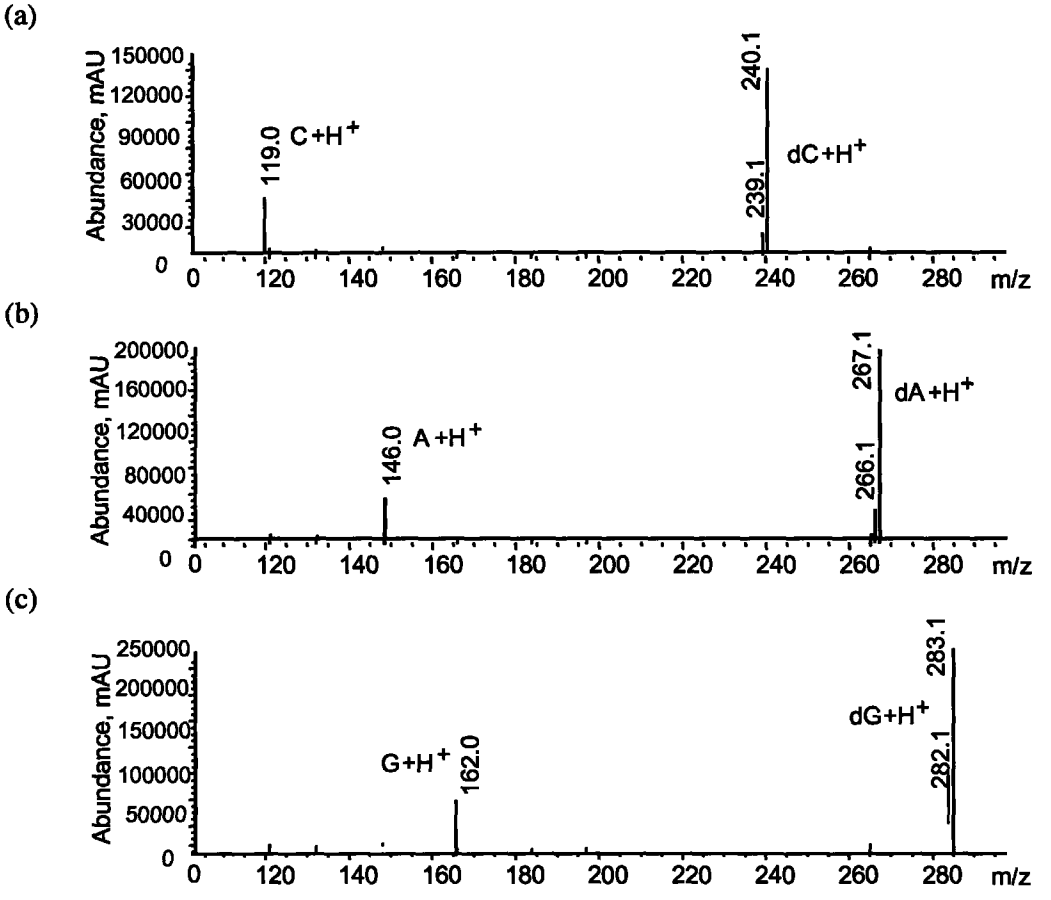

Figure 4. Electrospray ionization mass (positive ion mode) chromatograms for $^{13}C_8{}^{15}N_2$-labeled dC (a) and $^{13}C_{11}{}^{15}N_4$-labeled dA, dG (b and c). The exact mass of each double labeled deoxyribose nucleoside and its depurinated base are as follow, 239.1 for $^{13}C_8{}^{15}N_2$-dC and 118.0 for $^{13}C_3{}^{15}N_2$-C; 266.1 for $^{13}C_{11}{}^{15}N_4$-dA and 145.0 for $^{13}C_5{}^{15}N_4$-A; 282.1 for $^{13}C_{11}{}^{15}N_4$-dG and 161.0 for $^{13}C_5{}^{15}N_4$-G.

Uniformly ^{13}C, ^{15}N-labeled dA, dG, and dC. Figure 4 shows total ion chromatograms for uniformly ^{13}C, ^{15}N-labeled dA, dG and dC prepared by dephosphorylation of their corresponding 5'-triphosphate deoxyribose nucleotide precursors, which include the molecular ions and their depurinated nucleobase products. Products were further characterized by the UV spectroscopy relative to published data (Dizdaroglu, 1985; Peng et al., 1976; Trumbore et al., 1989).

Artifact Control. An important problem with any quantitative analysis is the generation of artifacts and it becomes even more challenging when measuring DNA damage products in cellular DNA. To this end, we carefully estimated the artifactual products of DNA deamination that might arise during extraction and subsequent processing. Preliminary measurements indicated suspiciously high baseline levels of dU and dI in DNA from the TK6 cells. Increases in dU and dI in plasmid pUC19 DNA after incubation with the whole cell extracts from TK6 cells confirmed our hunch that one or more cellular factors could be contributing to the level of artifacts (Figure 5). Endogenous endonuclease activities were shown to cause minimal nicking of plasmid pUC19 after incubation with cell extract for 1 hr at 37°C (Figure 6). However, this increase in dU and dI in pUC19 DNA could be inactivated after boiling the cell extract for 10 min, suggesting an enzymatic contribution (Figure 7). After surveying the literature, we hypothesized that adenosine and cytidine deaminases could be involved. Previous studies, for example, had documented a contaminating cytidine deaminase activity in commercial stocks of acidic phosphatase from Roche Diagnostic Corporation (Indianapolis, IN) (Dong et al., 2003). Therefore, we tested the ability of specific deaminase inhibitors, coformycin and tetrahydrouridine (THU), to reduce the generation of artifacts. The efficiency of coformycin in inhibiting dA deaminase activity had been demonstrated previously (Dong et al., 2003). We

designed an experiment to test the efficiency of THU in inhibiting dC deaminase activity (Figure 7). 10 μg of dC was incubated with 10 units of acidic phosphatase at 37°C for 3 hr. Following filtration (Microcon YM-10) to remove the enzyme, one tenth of the filtrate was subjected to LC-MS analysis. It is clear from Figure 7 that there is an activity in the incubation mixture that causes deamination of dC to form dU (dashed line). Suspecting that this activity represented a contaminating cytidine deaminase, an identical incubation mixture was prepared that included THU at a concentration of 25 ng per unit of acidic phosphatase (Cooper and Greer, 1973). Clearly, addition of the inhibitor was able to stabilize the nucleoside dC (solid line). Thereafter, THU was added together with coformycin during subsequent steps of DNA isolation to prevent the adventitious generation of dU by inactivation of cellular dC deaminases. As shown in Figure 8, the measured levels of dU and dI were reduced after including both inhibitors during DNA isolation. This reduction was further confirmed by the undetectable formation of uniformly [^{15}N, ^{13}C]-labeled dX, dO, dI and dU when the same doubly labeled dG, dA and dC were included during DNA isolation (see Material and Methods) (Figure 9).

After controlling the artifacts generated during DNA isolation, we attempted to limit any further sources of artifactual deamination during the remaining steps of sample preparation: enzymatic DNA hydrolysis and HPLC pre-purification. Figure 9 shows results obtained by monitoring potential formation of double-labeled nucleobase deamination products at each stage of sample preparation. Undetectable signals suggest a sufficient suppression of artifact formation.

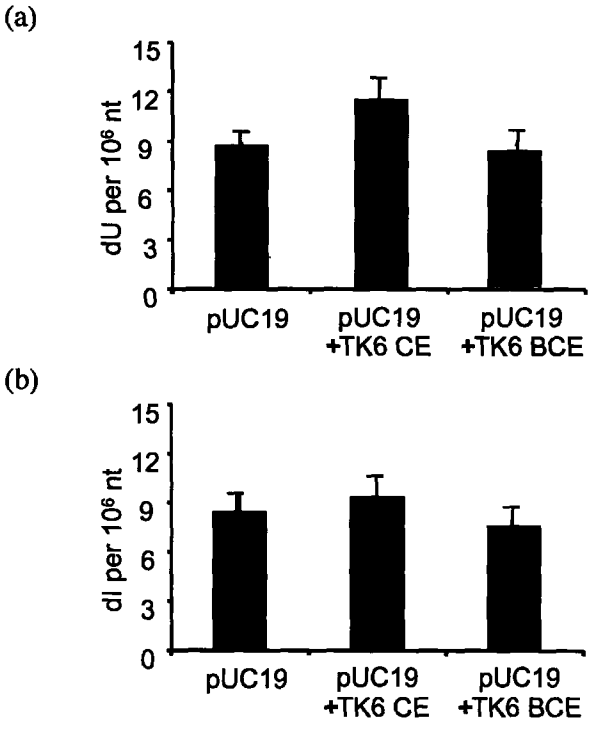

Figure 5. Levels of dU (a) and dI (b) in plasmid pUC19 DNA after incubation with cell extracts of TK6 cells. CE, cell extract; BCE, boiled cell extract. These data represent the mean ± SD of three independent experiments

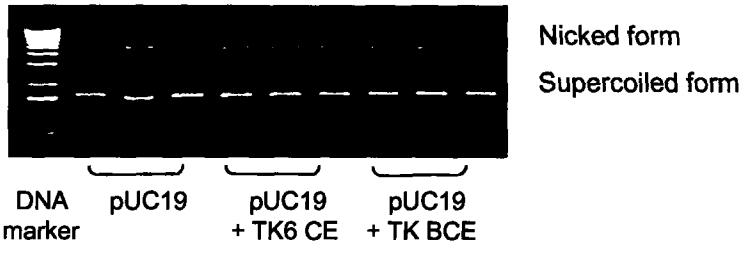

Figure 6. Endonuclease activities in TK6 cell extracts. CE, cell extract; BCE, boiled cell extract.

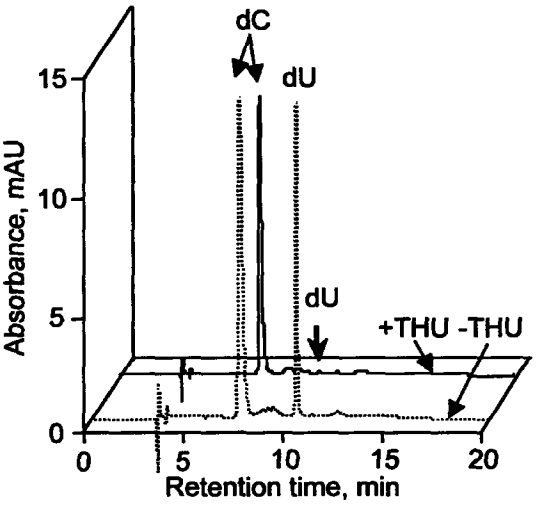

Figure 7. LC-MS analysis of tetrahydrouridine (THU) inhibition of dC deaminase activity present in acidic phosphatase preparations. Dashed line: dC (1 μg) incubated with alkaline phosphatase (1.5 units); solid line: dC (1 μg) incubated with acidic phosphatase (1 unit) in the presence of THU (3 ng).

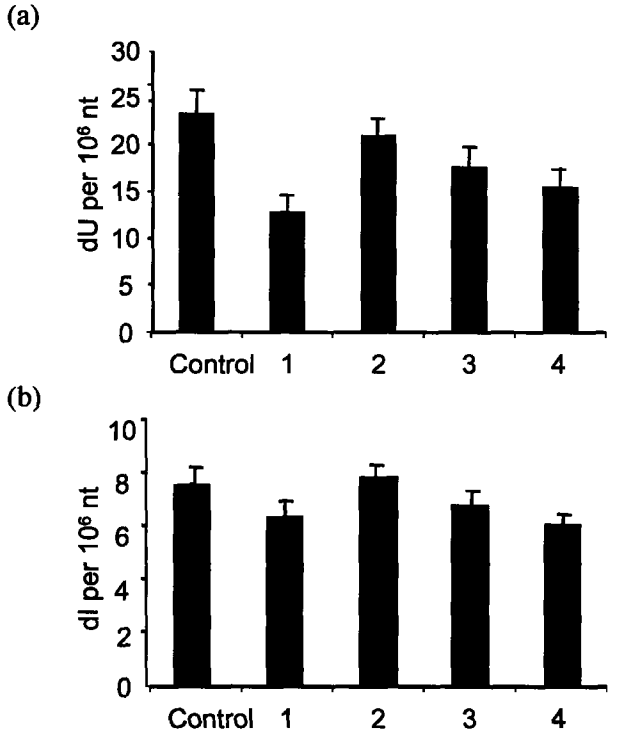

Figure 8. Levels of dU and dI in genomic DNA extracted from TK6 cells. In the control group DNA was isolated without adding inhibitors. In group 1 DNA was isolated by directly adding both inhibitors (coformycin and THU at 5 μg/mL and 50 μg/mL) during processing. In groups 2, 3 and 4 inhibitors were added to the culture medium 5, 10 and 30 min, respectively, prior to collection of cells and DNA isolation. These data represent the mean ± SD of three independent experiments.

Figure 9. SIM electrospray ionization mass spectrometry chromatogram for monitoring the formation of $^{13}C_{10}{}^{15}N_4$-dX, dO and dI and $^{13}C_8{}^{15}N_2$-dU from the corresponding double-labeled deoxyribose nucleoside dG, dA and dU. Quantification of $^{13}C_{10}{}^{15}N_4$-dX, dO and dI was achieved using the following molecular ions: depurinated $^{13}C_{10}{}^{15}N_4$-labeled bases at m/z 162, 162, and 146 (a, b, and c, respectively); and $^{15}N_4$-labeled bases at m/z 157, 157, 141 as internal standards. Quantification of $^{13}C_8{}^{15}N_2$-dU was achieved using the molecular ion at m/z 237 (d). An ion at m/z 229 for $^{15}N_2$-dU serves as an internal standard

.

(a)

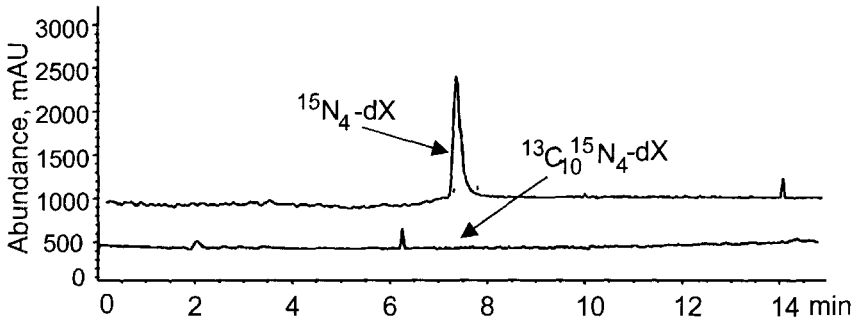
Abundance, mAU
3000
2500
2000
1500
1000
500
0
$^{15}N_4$-dX
$^{13}C_{10}{}^{15}N_4$-dX
0
2
4
6
8
10
12
14 min

(b)

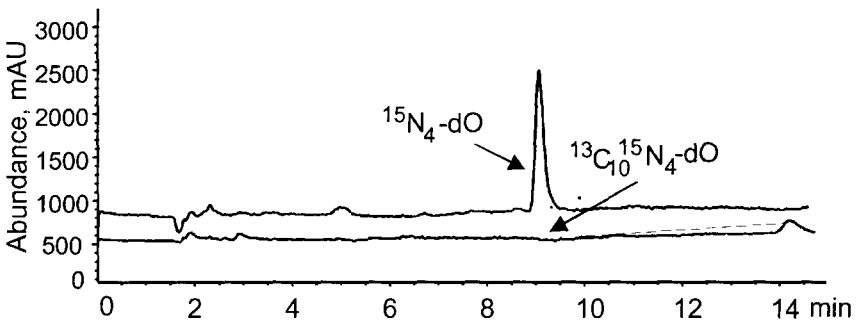
Abundance, mAU
3000
2500
2000
1500
1000
500
0
$^{15}N_4$-dO
$^{13}C_{10}{}^{15}N_4$-dO
0
2
4
6
8
10
12
14 min

(c)

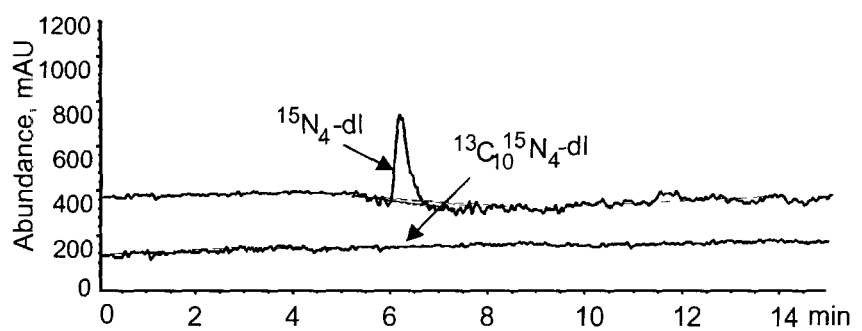
Abundance, mAU
1200
1000
800
600
400
200
0
$^{15}N_4$-dI
$^{13}C_{10}{}^{15}N_4$-dI
0
2
4
6
8
10
12
14 min

(d)

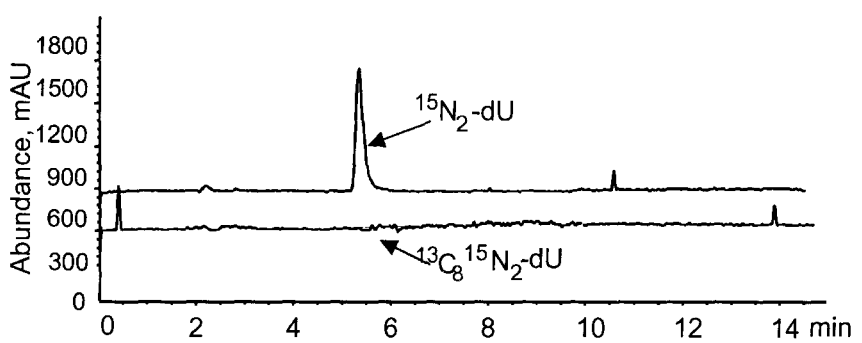
Abundance, mAU
1800
1500
1200
900
600
300
0
$^{15}N_2$-dU
$^{13}C_8{}^{15}N_2$-dU
0
2
4
6
8
10
12
14 min

Formation of Deamination Lesions in TK6 cells Following NO• Exposure. The LC-MS method was applied to the quantification of deamination products in genomic DNA isolated from TK6 and NH32 cells following NO• exposure (Figures 11-14). Cells were initially exposed to a relatively high steady state level of NO• (Figures 10 and 11). TK6 cells displayed a dose-dependent increase in dX, dI and dU, while dO was not detected at any dose of NO• (Figure 10). Following a 12 hr exposure to steady state levels of 1.75 μM NO• (total NO• dose of 1260 μM•min), dX, dI and dU were formed at comparable fold of increases above background as follows: dX at 7 ± 1.2 per 106 nt, a 3.5-fold increase from baseline (Figure 10a); dI at 25 ± 2.1 per 106 nt, a 3.8-fold increase (Figure 10b); and dU at 40 ± 3.8 106 per nt, a 4.1-fold increase (Figure 10c). Nucleobase deamination products were also quantified after one round of cell division (24 hr recovery period) and the levels showed only moderate repair, with dI and dU being repaired more efficiently than dX (Figure 10a, b, and c).

Along with increased formation of nucleobase deamination products, we also observed significant increases in cytotoxicity at the high doses of NO•. For example, in TK6 cells, a dose of 1260 μM•min dramatically compromised cell viability. Compared with the control group, about 32.7% ± 3.5 of TK6 cells were either dead or undergoing apoptosis immediately after NO• exposure, while about 86.3% ± 4.7 were dead or undergoing apoptosis after a 24 hr recovery period, which may be one of the possible reasons that account for the lack of significant repair.

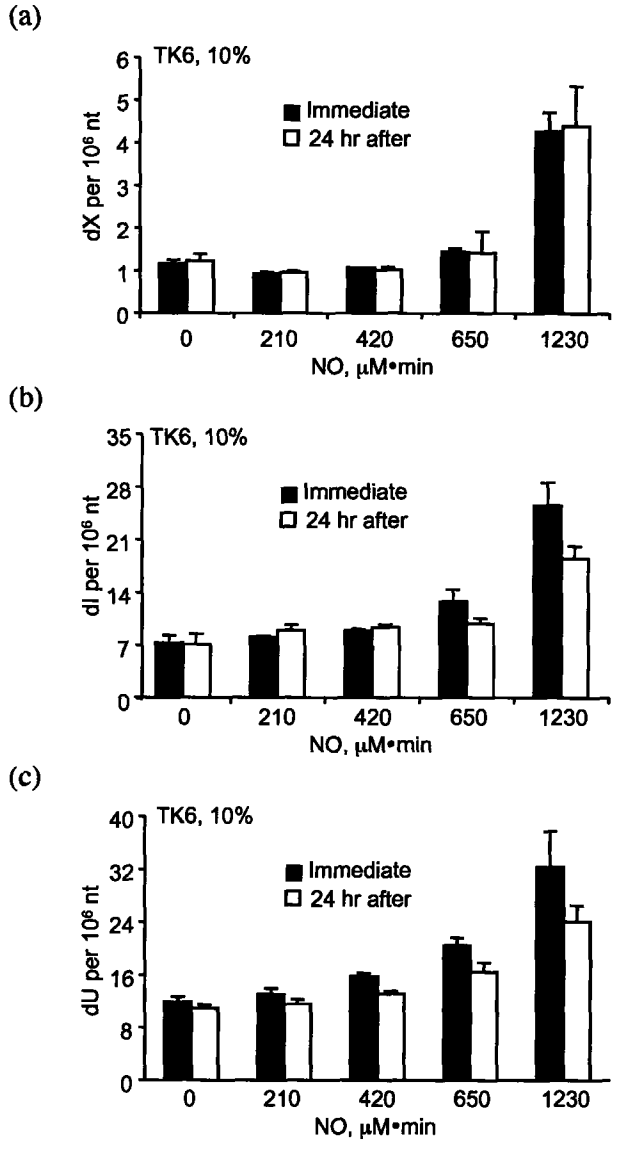

Figure 10. Nucleobase deamination products in cellular DNA from TK6 cells immediately after various doses of NO˙ exposure and after a 24 hr recovery period. (a) Amount of dX, (b) Amount of dI and (c) Amount of dU. These data represent the mean ± SD of three independent experiments.

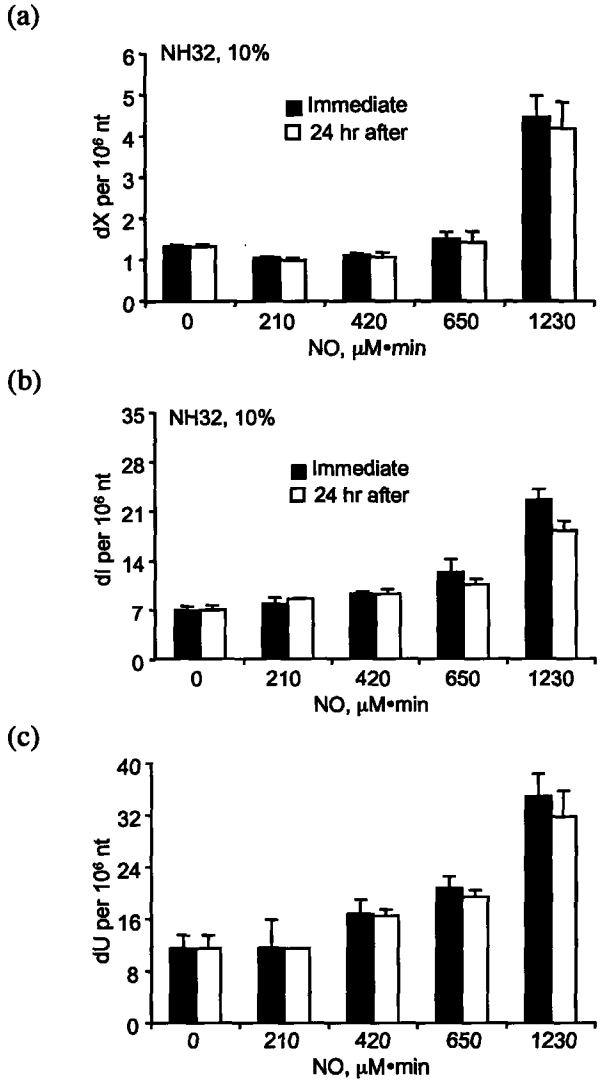

Figure 11. Nucleobase deamination products in cellular DNA of NH32 cells immediately after various doses of NO˙ exposure and after 24 hr recovery period. (a) Amount of dX, (b) Amount of dI and (c) Amount of dU. These data represent the mean ± SD of three independent experiments.

Formation of nucleobase deamination products in TK6 cells was also determined at a low steady-state concentration of NO•. Extensive studies by the research groups of Professors Deen and Wogan concluded that the toxic effect of NO• on TK6 cells becomes measurable only when the dose exceeds approximately 150 μM•min, which was achieved by delivering NO• at a steady-state level of 0.65 μM for 4 hr. We likewise found significant increases in dX, dI and dU in TK6 cells only when doses exceeded this threshold (Figure 12). For example, a 12 hr exposure to steady-state levels of 0.65 μM NO• and 186 μM O_2, equaling three times the reported threshold dose, caused observable increases in dX, dI and dU as follows: dX at 3.3 ± 1.7 per 10^6 nt, a 1.7-fold increase from baseline; dI at 10.5 ± 1.9 per 10^6 nt, a 1.8-fold increase; and dU at 23.1 ± 4.0 per 10^6 nt, a 2.0-fold increase. As before, dO was not detected. A simultaneous analysis of cell viability revealed a ~15% ± 3.6 reduction in TK6 cells immediately after exposure to the same dose of NO•. This observation, together with the findings mentioned above, suggested that a causative relationship may not exist between nucleobase deamination and cell death arising from NO• exposure.

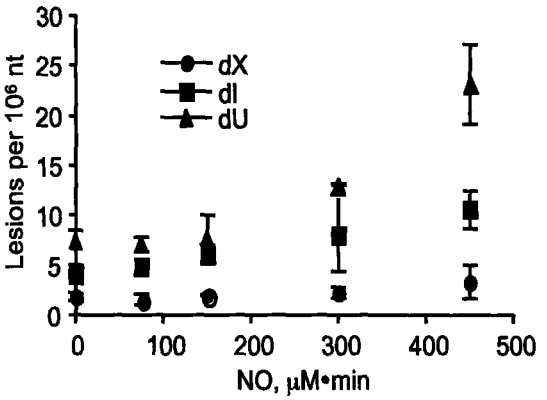

Figure 12. Formation of dX, dI and dU in cellular DNA of TK6cells immediately after NO˙ exposure. These data represent the mean ± SD of four measurements from two independent experiments.

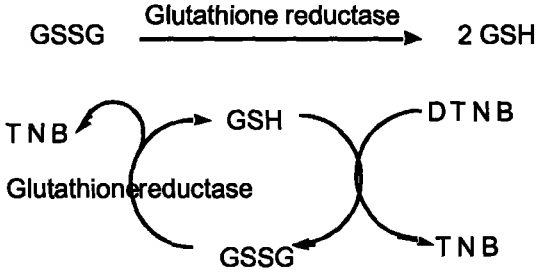

Scheme 1. The recycling of GSH

Glutathione Detection and Depletion. The relatively slow formation of nucleobase deamination products in whole cells compared to naked DNA suggests that certain cellular factors may modulate the relevant chemistries. One potential factor is glutathione (GSH). Initially, methods were developed to both deplete and monitor cellular GSH in TK6 cells, followed by an assay to measure deamination products. We adopted a glutathione assay previously developed by Griffith and Anderson (Anderson, 1985; Griffith, 1980). It is a carefully optimized enzymatic recycling method, using glutathione reductase for the quantification of GSH as listed in scheme 1. The sulfhydryl group of GSH reacts with DTNB (5,5'-dithiobis-2-nitrobenzoic acid, Elmman's reagent) and produces a yellow 5-thio-2-nitrobenzoic acid (TNB). The mixed disufide, GSTNB, that is concomitantly produced, is reduced by glutathione reductase to recycle the GSH and produce more TNB. The rate of TNB production is directly proportional to this cycling reaction, which is in turn directly proportional to the concentration of GSH in the sample. Measurement of the absorbance of TNB at 405 or 414 nm provides an accurate estimation of GSH. Because glutathione reductase is used in the assay, both GSH and GSSG are measured and therefore the assay reflects total glutathione levels. However, with only one additional step, which involves the derivatization of GSH with 2-viylpyridine, the assay can be adapted to quantify GSSG exclusively.

GSH concentrations can be determined by either the end point method or the kinetic method. The end point method is usually adequate, but if the levels of cysteine or other thiols are significant compared to GSH, the kinetic method is preferred, prompting us to use the latter in our experiments. An average spectroscopic absorbance for each standard and sample were plotted as a function of time and used to determine the "i-slope" as shown in Figure 13. Subsequently, the "i-slope" for each standard was plotted as a function of total GSH

concentration as shown in Figure 14. The slope of this curve is called the "f-slope". Total GSH for each sample was then calculated from their respective slopes using the slope *versus* GSH standard curve.

Levels of total GSH were kinetically measured in TK6 and NH32 cells as follows: 32.68 ± 0.68 and 27.38 ± 0.76 μg per10^7 cells, respectively. These results were comparable to those obtained independently using an alternate commercial method (Trevigen) which yielded 34.21 ± 1.61 and 28.21 ± 0.57 μg per10^7 cells for TK6 and NH32, respectively, suggesting that our GSH detection assay was accurate.

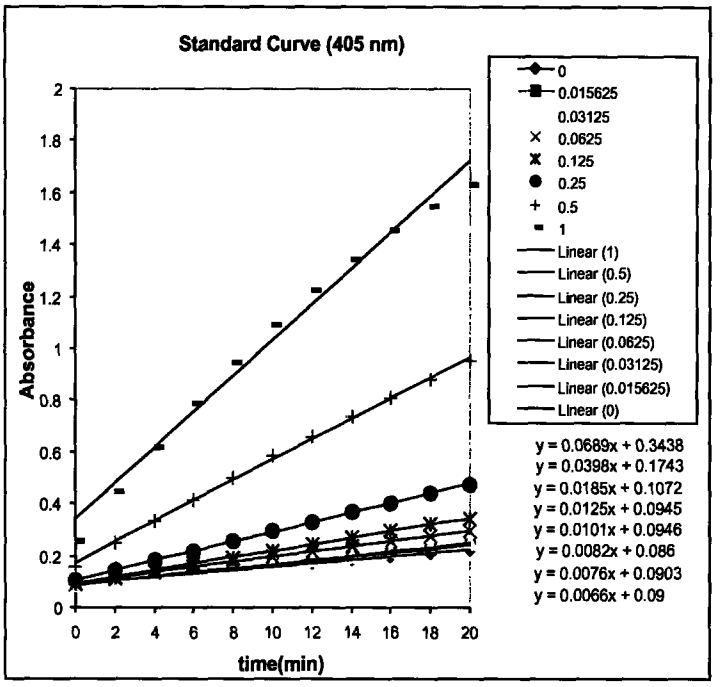

Figure 13. Plot of Absorbance *vs.* Time for each standard

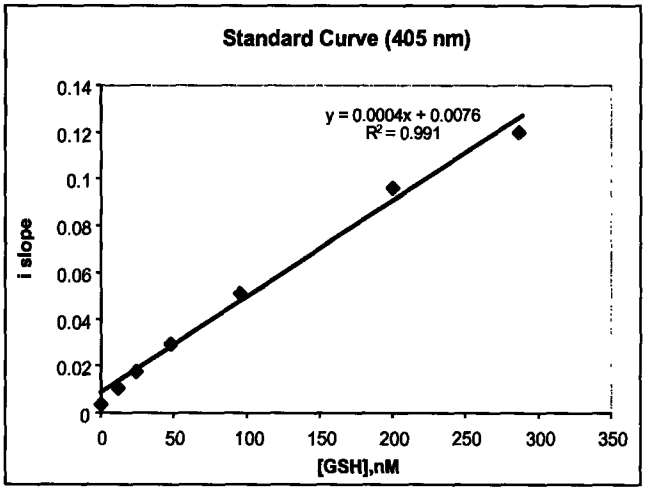

Figure 14. Plot of Slope *vs.* total GSH concentration

GSH Depletion in TK6 Cells. To gauge the significance of GSH on nitrosative chemistry, this cellular factor was depleted in TK6 cells prior to NO• exposure. Depletion was accomplished by treatment with L-buthionine-(S,R)-sulfoxamine (BSO), a glutathione synthesis inhibitor. The effectiveness of this method was examined over a broad range of BSO concentrations from 5μM to 5 mM. As shown in Figure 15, 25 μM BSO depleted ≥ 95% GSH and 125 μM BSO depleted ≥99% GSH in TK6 cells. We chose the latter concentration of BSO for our experiments to be consistent with a previous study (Luperchio et al., 1996a). Another advantage to using BSO is its low toxicity to mammalian cells. We found that 5 mM of BSO did not indicate a noticeable effect on cell viability after a 24 hr incubation with TK6 cells (Figure 16). The ability of GSH levels to recover during a lengthy NO• exposure was also monitored, but no significant upturn was observed.

Formation of Deamination Lesions in TK6 Cells Following NO• Exposure. The LC-MS method was used to quantify deamination products generated in genomic DNA isolated from TK6 cells following NO• exposure (Figure 17). An increase in dX, dI and dU was observed in both normal and GSH-depleted TK6 cells only when the NO• dose was greater than the threshold value, 150 μM•min. The formation of dX, dI and dU was faster in GSH-depleted TK6 cells: ~2- to 2.5-fold increase in dX, dI and dU in GSH-depleted TK6 cells compared with normal cells (at 450 μM•min of NO•). Again, the lesion dO was not detected, which is consistent with previously published results (Dong et al., 2003).

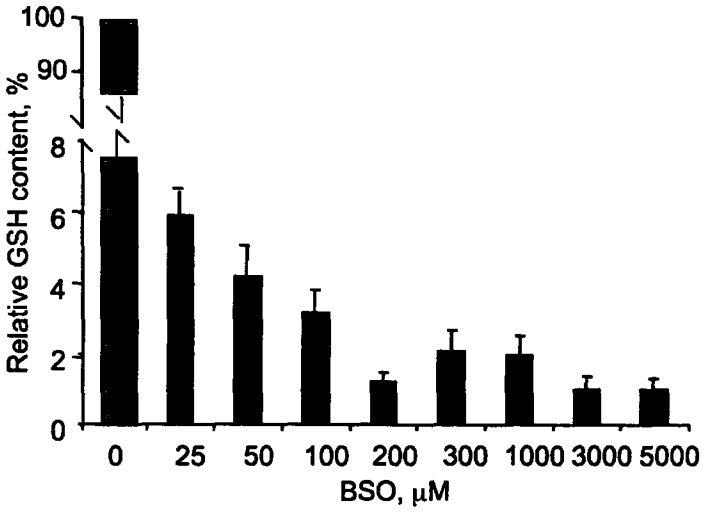

Figure 15. GSH depletion in TK6 cells by different concentrations of BSO after 24 hr. The abscissa is the concentration of BSO. The ordinate is the ratio of GSH in BSO-treated relative to untreated controls. These data represent the mean ± SD of eight measurements from two independent experiments.

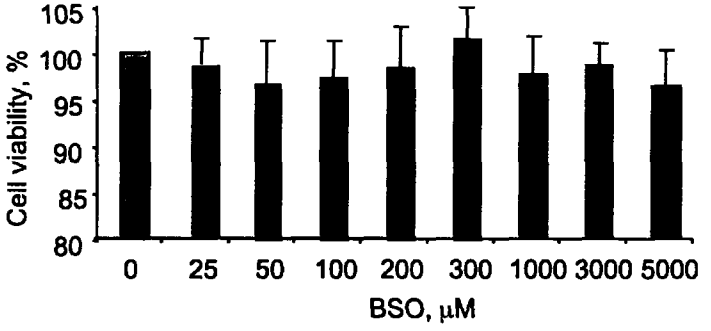

Figure 16. Cell viability of TK6 after a 24 hr recovery period with different concentrations of BSO. Viability was calculated as the ratio of cells excluding trypan blue in BSO-treated relative to untreated controls. These data represent the mean ± SD of three independent experiments.

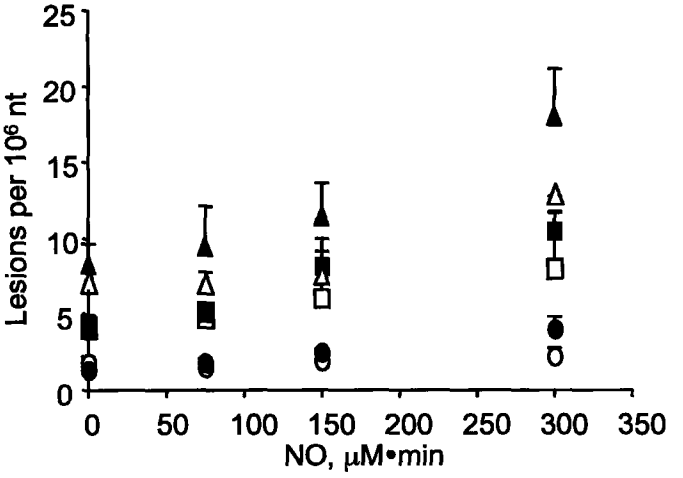

Figure 17. Formation of dX (circles), dI (squares), and dU (triangles) in DNA from TK6 cells immediately after increasing doses of NO$^{\bullet}$; either with (black) or without (white) pretreatment of 125 μM BSO for 24 hr. These data represent the mean ± SD of two experiments, each done in triplicate.

4.5 Discussion

It has long been known that chronic inflammation contributes to the development of cancer (Macarthur et al., 2004; Ohshima and Bartsch, 1994; Schwartsburd, 2003). Current knowledge suggests that NO$^{\bullet}$ is implicated in the process of carcinogenesis (Felley-Bosco, 1998; Maeda and Akaike, 1998; Wink et al., 1998). Although it is well established that NO$^{\bullet}$ creates reactive nitrogen species (RNS) that form DNA lesions *in vitro* (Bartsch, 1999; Burney et al., 1999; Szabo and Ohshima, 1997; Tamir et al., 1996), few studies have investigated the quantitative formation of DNA damage in cultured cells produced by RNS. Moreover, the impact of various DNA damage products on other biological end-points, including cytotoxicity and mutagenicity, is poorly understood. To this end, we exploited the chemistry of RNS to develop DNA biomarkers, with a special focus on nucleobase deamination products, which result from cellular exposure to inflammatory mediators. These biomarkers will serve to establish a better understanding of molecular changes that lead to cellular responses on the path to cancer.

Cytotoxicity of Nitric Oxide. NO$^{\bullet}$-mediated cytotoxicity in TK6 cells has been studied previously (Li et al., 2002a; Li et al., 2002b; Nguyen et al., 1992; Zhuang et al., 2000). The present investigation, as a parallel study of the published work done by Wang et al. (Wang et al., 2003), was performed using an exposure system that allowed the NO$^{\bullet}$ concentration and total dose in each experiment to be precisely controlled. In addition, two steady-state concentrations of NO$^{\bullet}$ were chosen: 1.75 μM and 0.65 μM, both of which are within the range of biologically relevant concentrations (0.1-10 μM) (Beckman et al., 1990; Brookes et al., 2000). Consistent with previous observations (Li et al., 2002b; Wang et al., 2003), we also found that NO$^{\bullet}$-induced

cytotoxicity in TK6 and NH32 cells was both dose and concentration dependent. Significant cell death was observed under conditions considered not biologically relevant and therefore not appropriate for our analysis of DNA damage products. Systematic investigations by Wang, et al. discovered that a threshold dose of NO• was required to cause measurable toxicity in the forms of cell viability and apoptosis (Wang et al., 2003). Their observations were confirmed in a later study by Li et al. (unpublished results) in which toxic effects became observable only when the NO• concentration and dose were greater than threshold values of ~0.5 μM and ~ 150 μM•min, respectively. Therefore, we chose to analyze the formation of nucleobase deamination products at NO• doses near these threshold values to see if any correlation existed.

We anticipated that the absence of p53 protein might make cells less sensitive to NO• in terms of lethality and apoptosis, since p53 protein has been shown to regulate multiple pathways. As with other damaging agents (Coelho et al., 2002; Leger and Drobetsky, 2002; Schwartz et al., 2003), NH32 cells exposed to NO• showed a reduced level of apoptosis and grew faster than TK6 cells.

In contrast to the previous reports (Luperchio et al., 1996a), GSH depletion did not increase the sensitivity of TK6 to NO•-induced cytotoxicity. This discrepancy may partly derive from the different NO• delivery systems used for each study. In a recent collaboration, the biological role of GSH in NO•-mediated cytotoxicity was re-evaluated using both cultured cells and an animal model (Li et al., submitted). Our findings suggest that the role of GSH in NO•-mediated toxicity is dependant on cell and tissue types, on NO• dose, and on the mode of exposure. NO• treatment alone effectively depleted GSH in human lymphoblastoid cells, but this was not critical for induced toxicity. Murine macrophages maintain homeostasis of GSH when exposed to endogenously produced NO•. In RcsX lymphoma-bearing mice, homeostasis of the

reduction/oxidation state is maintained by an increase in *de novo* synthesis of GSH, which also appears to protect against the toxic effects of NO$^{\bullet}$.

Artifact Control. When measuring DNA adducts by mass spectrometry, sample preparation is considered one of the most important steps. One challenge is to obtain DNA free of damage artifacts created during the isolation process. Unlike most altered DNA bases, special care is required for proper isolation and analysis of deamination products in order to prevent activation of endogenous deaminases (Franco et al., 1998; Harris et al., 2002; Petersen-Mahrt et al., 2002; Roberts, 2003). Enzymatic deamination can occur under a variety of molecular contexts, including at the level of nucleobases, nucleosides, and nucleotides (Petersen et al., 2002; Rehemtulla et al., 2004; Sherwood, 1991; Snyder et al., 2000).

Our hypothesis that cellular deaminases might be contributing to an artificial formation of dU and dI initially arose from an observation that both dU and dI have comparably higher baseline levels than does dX. This was further supported by detecting increased levels of dU and dI in plasmid pUC19 after incubation with TK6 cell extract. The activity of cytidine deaminase (CDA) has been reported in several mammalian cell lines (Ishii et al., 1984), but CDA only functions on liberated nucleosides or nucleotides (Sugiura et al., 1986). Alternatively, an activation-induced cytidine deaminase (AID) was recently discovered that appears to be required for the final stages of antibody maturation by introducing a wide variety of base substitutions in the immunoglobulin genes and by creating region-specific double-strand breaks (Petersen-Mahrt et al., 2002). The AID protein, which shuttles between the nucleus and cytoplasm (Ito et al., 2004), was originally thought only to deaminate cytidine within the context of single-stranded DNA (Bransteitter et al., 2003; Pham et al., 2003). However, Shen and Storb recently found that

AID can affect both strands of DNA when targeting supercoiled plasmid (Shen and Storb, 2004), which could account for our observation in the plasmid incubation experiment mentioned above. AID is a B-cell-specific protein and its expression has been confirmed in human B-cells and in non-Hodgkin's lymphomas (Greeve et al., 2003; Muto et al., 2000).

Tetrahudrouridine (THU) has a long history of being used as a means of enhancing the therapeutic antitumor efficacy of cytosine arabinoside, 5-chloro-2'-deoxycytidine, and other cytidine analogs through the inhibition of CDA (Greer et al., 1995; Hanze, 1967; Laliberte et al., 1992). THU is also an effective inhibitor of AID (Chaudhuri et al., 2004; Muramatsu et al., 1999). We therefore included it during DNA isolation to suppress both type of dC deaminases.

Like CDA, adenosine deaminase (ADA) is expressed intracellularly, but in some tissues, it is also associated with cell surface glycoproteins to regulate adenosine receptor signaling, a process which has been implicated in various cellular functions (Gonzalez-Gronow et al., 2004). Moreover, unlike the cytidine specific AID protein, a corresponding activation-induced adenosine deaminase has not been identified. Some adenosine deaminases, called (ADARs), act on RNA for the purpose of RNA-editing. Among the known ADARs, ADAR1 was found to recognize Z-DNA when surrounded by B-DNA (Kim et al., 2000). Although the biological function of such binding remains unclear, it suggests that ADARs in general may act on DNA.

In addition, we observed an increase in levels of dI in plasmid DNA after incubation with TK6 cell extract, although smaller when compared to levels of dU. We chose to add a specific inhibitor, coformycin, during DNA isolation based on our previous success in preventing dA deaminase activities in TK6 cell extracts (Chapter 2, artifact control). Inclusion of coformycin brought dI back to the original baseline level observed with no added cell extract (Figure 7). The overall effectiveness of artifact control during all stages of sample preparation was further

confirmed by an undetectable signal of uniformly [^{15}N, ^{13}C]-labeled dX, dO, dI and dU that would normally arise from the corresponding parent molecule under less stringent conditions.

Nucleobase Deamination in Human Lymphoblastoid Cells Caused by Nitric Oxide. Using proper artifact control, we observed formation of dX, dI and dU in the genomic DNA of TK6 cells exposed to physiologically relevant doses of NO$^{\bullet}$. Several studies have observed the formation of nucleobase deamination products in cellular DNA after NO$^{\bullet}$ exposure (deRojas-Walker et al., 1995; Nguyen et al., 1992; Spencer et al., 1995), but few have detected damage under physiologically relevant conditions. And none have sought to monitor a broad spectrum of nucleobase deamination products.

Our observed dose-dependent increase in deamination products is consistent with pioneering work done by the Tannenbaum group. Despite some discrepancies, they saw significant increases in xanthine and hypoxanthine in DNA from TK6 cells after NO$^{\bullet}$ exposure (Nguyen et al., 1992). For example, they observed higher baseline levels of xanthine and hypothanine (~5 and ~2 per 10^5 nt, respectively) compared with our measurements (~2 and ~5 per 10^6 nt, respectively). Different detection methods may account for these differences. Moreover, their relatively high baseline level of dI may have resulted from generation during DNA isolation, as discussed above. We speculate that their high baseline level of dX may have arisen from depurination by acid hydrolysis. Although there is no information regarding deamination of dG under acidic conditions, some evidence shows that ~5% of dC is deaminated to form dU under conditions of formic acid hydrolysis (Schein, 1966). Nguyen et al. also neglected to include an isotopically-labeled internal standard for dI; therefore, their methods were not similarly rigorous. Subsequent work by the Tannenbaum group demonstrated an ~ six fold increase in the number

of xanthine lesions (5 ± 0.9 per 10^6 nt) in activated macrophages when compare with control cells (deRojas-Walker et al., 1995). Unfortunately, other nucleobase deamination products were not addressed.

Formation of xanthine and hypoxanthine in cultured cells was also observed by the Halliwell group, although using gas-phase cigarette smoke instead of direct NO• gas (Spencer et al., 1995). Although the baseline level of dI detected in their epithelia cells was similar to that found in TK6 cells by Nguyen et al. (Nguyen et al., 1992), the level of dX was about 10-fold higher (Spencer et al., 1995). Differences in cell-type may have partially accounted for this disparity. Differing detection methods could have also played a role. For example, both groups used GC-MS, but the Halliwell group did not perform a rigorous quantification by including an isotopically-labeled internal standard (Spencer et al., 1995).

Many quantitative studies of uracil in cultured cells have been undertaken by the Ames group. Although their focus was not specifically on formation of uracil derived from exposure to NO•, their findings provide a good reference to evaluate our analytical method. Recently, they introduced an improved GC-MS assay for the detection of uracil in cellular DNA (Mashiyama et al., 2004). Through a careful use of controls, the baseline level of uracil in DNA from human mononuclear cells was reduced ~ 5-fold to 4.5 per 10^6 nt (Mashiyama et al., 2004). This was about 2-fold less than our measurements in the TK6 cells (10.5 ± 1.5 per 10^6 nt). However, TK6 cells may possess higher endogenous levels of dU due to their B-cell origin (Liber and Thilly, 1982). For example, a recent study by the Wabl group challenged a longstanding hypothesis that mutations in B-cells are actively targeted to the Ig loci (Wang et al., 2004). Instead, AID and other trans-acting hypermutation factors may function as general mutators (Wang et al., 2004) potentially leading to a high dU content throughout the entire B-cell genome.

Nucleobase Deamination vs. Cell Viability and Apoptosis. In order to understand the biological impact of nucleobase deamination products formed by exposure to NO•, we simultaneously monitored both cell viability and apoptosis. Overall, our findings did not support a causal relationship between nucleobase deamination and cell viability. Cell viability is sensitive to many different kinds of damage, including membrane damage, energy depletion, enzyme release due to organelle damage, and potentially DNA damage. Some evidence holds that NO•-mediated cell viability can be independent of DNA damage (Burney et al., 1997; Szabo, 2003). An example is the inhibition of critical metabolic enzymes such as glyceraldehyde-3-phosphate dehydrogenase leading to cell necrosis (Borutaite and Brown, 2003).

However, our data cannot be extrapolated to argue that NO•-induced apoptosis is also independent of nucleobase deamination. Apoptosis can be mediated by membrane death receptors or by a distinct mitochondrial damage pathway (Ashkenazi and Dixit, 1998; Shi, 2001; Vousden, 2000). As a genotoxic DNA damaging agent, NO• has been demonstrated to activate both pathways leading to cell death via apoptosis (Li et al., 2004). Although direct evidence linking DNA damage products formed by NO• to apoptosis is lacking, multiple lines of evidence suggest that those damage products can be further processed during replication to form double strand breaks (DSBs) (Spek et al., 2002; Spek et al., 2001). Double strand breaks, in turn, are commonly believed to trigger apoptosis (Kaina, 2003).

Another important consideration is the relationship between nucleobase deamination and mutagenicity. It is of interest to see that there is a positive correlation between the level of nucleobase deamination and the mutation frequencies (MF) of certain gene(s). Under the identical experimental conditions, Wang et al., found that the mutation rate in the thymidine

kinase (*tk1*) gene locus increased 3-4-fold to ~ 4 per 10^6 for TK6 cells treated with 1% NO• for 24 hr (Wang et al., 2003). Similar results were observed by Li et al in both *hprt* and *tk1* genes in TK6 cells using a different NO• delivery system (Li et al., 2002b). Previous studies have demonstrated that NO•-mediated deamination of nucleobases leads to a variety of mutations, including mostly G:C to A:T transitions (Routledge et al., 1994; Wink et al., 1991), and some A:T to G:C transitions (Kelman et al., 1997; Routledge et al., 1993). The former could arise from deamination of either guanine or cytosine, while the latter could arise from deamination of adenine.

Overall, the present study investigated the noxious effects of NO• on both direct DNA damage and cytotoxicity expressed by cell viability and apoptosis. It is not clear which effect is more important regarding the process of carcinogenesis. However, despite the close association between DNA damage and carcinogenesis, cytotoxicity itself is a factor that can contribute to cell transformation if compensatory growth of surrounding cells is induced (Davies and Hagen, 1997; Kan and Finkel, 2003).

Effect of GSH on the Nitrosative Chemistry by Nitric Oxide in Cells. The situation with the nucleobase deamination in DNA merits special consideration in light of the expectation that GSH depletion would lead to an increase in the formation of dX, dI and dU in cells exposed to NO•. This expectation arises from *in vitro* kinetic studies of the effects of GSH on the steady-state concentration of N_2O_3 (Dong et al., 2003; Keshive et al., 1996b; Lewis and Deen, 1994; Wink et al., 1994). GSH has long been shown to compete for N_2O_3, the nitrosating species for nucleobase deamination, in forming GSNO. The reaction is second order with respect to NO•

and first order in O_2 (Wink et al., 1994). The kinetics of GSNO formation in aqueous solution can be represented by the following reaction scheme:

$$2NO + O_2 \xrightarrow{k1} 2NO_2 \quad (1)$$

$$NO + NO_2 \xrightarrow{k2/k-2} N_2O_3 \quad (2)$$

The majority of N_2O_3 undergoes rapid hydrolysis to form nitrite (Equation 3) and can be catalyzed by different salts in the buffer (Equation 4 - 6).

$$N_2O_3 + H_2O \xrightarrow{k3} 2NO^- + 2H^+ \quad (3)$$

$$N_2O_3 + Pi \xrightarrow{k4} 2NO_2^- + 2H^+ \quad (4)$$

$$N_2O_3 + Cl^- \xrightarrow{k5} 2NO_2^- + 2H^+ \quad (5)$$

$$N_2O_3 + HCO_3^- \xrightarrow{k6} 2NO_2^- + 2H^+ \quad (6)$$

In the presence of GSH, N_2O_3 reacts with GSH to form GSNO,

$$N_2O_3 + GSH \longrightarrow GSNO + 2NO_2^- + 2H^+ \quad (7)$$

In bulk reaction buffer, the quasi-steady state N_2O_3 concentration can be described by the following equation (Dong et al., 2003):

$$C_{N_2O_3} = \frac{2k_1 C_{NO}{}^2 C_{O_2}}{k_3 + \sum_{i=4,5,6,7} k_i C_i}$$

where k_1 is the second-order rate constant for the reaction of $NO^\bullet$ with O_2 ($2.1 \times 10^6\ M^{-2}s^{-1}$), C_{NO} and C_{O2} are the steady state $NO^\bullet$ and O_2 concentrations, respectively, and k_3 through k_7 are

the second-order rate constants for the reaction of N_2O_3 with water (1.6×10^3 $M^{-2}s^{-1}$), inorganic phosphate (6.4×10^4 $M^{-2}s^{-1}$), chloride (1.5×10^4 $M^{-2}s^{-1}$), bicarbonate (1.5×10^5 $M^{-2}s^{-1}$) and GSH (6.6×10^7 $M^{-2}s^{-1}$), respectively, all of which have been defined *in vitro* (Caulfield et al., 1996; Keshive et al., 1996b; Lewis and Deen, 1994; Lewis et al., 1995). This model can be used to estimate the effects of varying the GSH concentration by a factor of 100, as occurred in the present studies. The values assumed in these calculations are the 1.75 μM steady-state NO• concentration used here, intracellular estimates for O_2, chloride, bicarbonate and inorganic phosphate of 210 μM, 1.07 mM, 10 mM and 40 mM, respectively (Guyton and Hall, 2000) and GSH ranging from 0.1 to 10 mM, as determined in the present studies. Using these values, there is an inverse variation in N_2O_3 concentration from 1 to 80 fM as a function of GSH concentration. Again, on the basis of our *in vitro* studies (Dong et al., 2003), this 60-fold variation in N_2O_3 concentration should result in a 60-fold change in the rate of nucleobase deamination in DNA. The fact that we observed a significantly smaller effect of GSH concentration on nucleobase deamination in the present studies suggests that there are other cellular factors, like the partition of N_2O_3 at each cellular compartment, the rate of DNA damage repair, the contribution from other cellular defense system, such as thiodoxin reductase system, must be accounted for in the model. This is consistent with our present observation of the relatively slow formation of nucleobase deamination products in human TK6 cells compared to isolated DNA (pUC19 plasmid DNA) following exposure to comparable levels of NO•.

There are several possible explanations for the observed lack of effect of GSH depletion on DNA deamination. One offered by Wink and coworkers (Espey et al., 2001) suggests that, due to the lipophilic nature of N_2O_3 and several other reactive nitrogen species, the functional effects of nitrosation may be limited to hydrophobic compartments in cells, such as lipid bilayers of the

cytosolic, mitochondrial and nuclear membrane systems as well as the endoplasmic reticulum and Golgi apparatus (Espey et al., 2001). In a similar manner, compartmentalization of GSH, rather than the uniform distribution assumed in our model, may bias its reactions with N_2O_3 and other reactive nitrogen species in cells. There are several reports of a heterogeneous distribution of GSH, with higher concentrations in both mitochondria and nuclei compared to cytosol (Devesa et al., 1993; Philbert et al., 1991; Voehringer et al., 1997). However, a higher GSH concentration in nuclei runs counter to the observed lack of effect of GSH concentration on DNA deamination chemistry.

Another possibility involves DNA repair. Our measurements of nucleobase deamination products represent steady-state levels that balance formation and repair, so it is possible that an increased rate of dX, dI and dU formation may have occurred in the presence of a reduced level of GSH, which could have been matched by an increase in repair activity. $NO^{\bullet}$ has indeed been shown to inactivate several DNA repair enzyme (Bau et al., 2001; Jaiswal et al., 2000; Jaiswal et al., 2001; Laval and Wink, 1994; Liu et al., 2002; Wink and Laval, 1994), which is consistent with our current observation that dX, dI and dU are not repaired efficiently in TK6 cells after exposure to relatively high doses $NO^{\bullet}$. On the other hand, Grishko et al. observed efficient repair of dI and dU in normal human fibroblasts (Grishko et al., 1999). Furthermore, Gallardo-Madueno et al. found that depletion of GSH in *E. coli* led to an increase in the expression of *Fpg* DNA glycosylase (Gallardo-Madueno et al., 1998). While this enzyme does not recognize dX, dI or dU *in vitro* (Dong et al., unpublished data), the observation suggests that the interruption of one cellular defense system may trigger compensatory activation of others, such as DNA repair.

A third possible explanation for the lack of effect of GSH depletion on DNA deamination lies in the fact that GSH is not the only cellular factor that may react with N_2O_3 and other

nitrosating species. Mounting evidence suggests that protein thiols or free cysteine residues may be strong competitors for S-nitrosation (Galli et al., 2002; Scharfstein et al., 1994; Scorza et al., 1997). Recently, Bryan et al. argued against the biological significance of S-nitrosation based on the need to invoke second- or third-order kinetics compared to first-order reactions such as heme-nitrosylation (Bryan et al., 2004). Also, their results showed that *N*- nitrosation is as ubiquitous as S-nitrosation and highlight a novel mechanism of protein functional modulation (Bryan et al., 2004). Any or all of these factors could contribute to the observed minor effect of GSH depletion on the quantity of N_2O_3-induced DNA damage detected in our experimental system.

Conclusion. To develop DNA biomarkers of cellular exposure to inflammatory mediators, we quantified nucleobase deamination products in human lymphoblastoid cells exposed to NO$^{\bullet}$ at controlled rates and doses encompassing those estimated to occur in inflamed tissues. Dose-response relationships for the formation of nucleobase deamination products were established, and DNA damage was further evaluated in the context of cell viability and apoptosis. Significant increases in deamination products in TK6 genomic DNA only occurred after cells have been exposed to NO$^{\bullet}$ at doses above the threshold value (150 μM•min). There exist a correlation between the formation of nucleobase deamination and the cell viability by NO$^{\bullet}$, but the relationship is not causative. The nonlinear formation of nucleobase deamination products in viable TK6 cells following NO$^{\bullet}$ exposure suggests the presence of DNA repair activities toward base deamination products. GSH, as an important cellular defense system, plays a role in determining the nitrosative chemistry of NO$^{\bullet}$, however, its importance is lower than expected.

4.6 References

Albina, J. E., Martin, B. A., Henry, W. L., Jr., Louis, C. A., and Reichner, J. S.: B cell lymphoma-2 transfected P815 cells resist reactive nitrogen intermediate-mediated macrophage-dependent cytotoxicity. J Immunol **157** (1): 279-83, 1996.

Anderson, M. E.: Determination of glutathione and glutathione disulfide in biological samples. *In* Methods Enzymol, vol. 113, pp. 548-55, 1985.

Ashkenazi, A., and Dixit, V. M.: Death receptors: signaling and modulation. Science **281** (5381): 1305-8, 1998.

Atamna, H., Cheung, I., and Ames, B. N.: A method for detecting abasic sites in living cells: age-dependent changes in base excision repair. Proc Natl Acad Sci U S A **97** (2): 686-91, 2000.

Bartsch, H.: Keynote address: exocyclic adducts as new risk markers for DNA damage in man. IARC Sci Publ (150): 1-16, 1999.

Bau, D. T., Gurr, J. R., and Jan, K. Y.: Nitric oxide is involved in arsenite inhibition of pyrimidine dimer excision. Carcinogenesis **22** (5): 709-16, 2001.

Bebenek, K., Matsuda, T., Masutani, C., Hanaoka, F., and Kunkel, T. A.: Proofreading of DNA polymerase eta-dependent replication errors. J Biol Chem **276** (4): 2317-20, 2001.

Beckman, J. S., Beckman, T. W., Chen, J., Marshall, P. A., and Freeman, B. A.: Apparent hydroxyl radical production by peroxynitrite: implications for endothelial injury from nitric oxide and superoxide. Proc Natl Acad Sci U S A **87** (4): 1620-4, 1990.

Borutaite, V., and Brown, G. C.: Nitric oxide induces apoptosis via hydrogen peroxide, but necrosis via energy and thiol depletion. Free Radic Biol Med **35** (11): 1457-68, 2003.

Bransteitter, R., Pham, P., Scharff, M. D., and Goodman, M. F.: Activation-induced cytidine deaminase deaminates deoxycytidine on single-stranded DNA but requires the action of RNase. Proc Natl Acad Sci U S A **100** (7): 4102-7, 2003.

Brookes, P. S., Salinas, E. P., Darley-Usmar, K., Eiserich, J. P., Freeman, B. A., Darley-Usmar, V. M., and Anderson, P. G.: Concentration-dependent effects of nitric oxide on mitochondrial permeability transition and cytochrome c release. J Biol Chem **275** (27): 20474-9, 2000.

Bryan, N. S., Rassaf, T., Maloney, R. E., Rodriguez, C. M., Saijo, F., Rodriguez, J. R., and Feelisch, M.: Cellular targets and mechanisms of nitros(yl)ation: an insight into their nature and kinetics in vivo. Proc Natl Acad Sci U S A **101** (12): 4308-13, 2004.

Burney, S., Caulfield, J. L., Niles, J. C., Wishnok, J. S., and Tannenbaum, S. R.: The chemistry of DNA damage from nitric oxide and peroxynitrite. Mutat Res **424** (1-2): 37-49, 1999.

Burney, S., Tamir, S., Gal, A., and Tannenbaum, S. R.: A mechanistic analysis of nitric oxide-induced cellular toxicity. Nitric Oxide **1** (2): 130-44, 1997.

Cadet, J., Douki, T., Gasparutto, D., and Ravanat, J. L.: Oxidative damage to DNA: formation, measurement and biochemical features. Mutat Res **531** (1-2): 5-23, 2003.

Caulfield, J. L., Singh, S. P., Wishnok, J. S., Deen, W. M., and Tannenbaum, S. R.: Bicarbonate inhibits N-nitrosation in oxygenated nitric oxide solutions. J Biol Chem **271** (42): 25859-63, 1996.

Caulfield, J. L., Wishnok, J. S., and Tannenbaum, S. R.: Nitric oxide-induced deamination of cytosine and guanine in deoxynucleosides and oligonucleotides. J Biol Chem **273** (21): 12689-95, 1998.

Chaudhuri, J., Khuong, C., and Alt, F. W.: Replication protein A interacts with AID to promote deamination of somatic hypermutation targets. Nature **430** (7003): 992-8, 2004.

Coelho, D., Fischer, B., Holl, V., Jung, G. M., Dufour, P., Bergerat, J. P., Denis, J. M., Gueulette, J., and Bischoff, P.: Involvement of TP53 in apoptosis induced in human lymphoblastoid cells by fast neutrons. Radiat Res **157** (4): 446-52, 2002.

Cooper, G. M., and Greer, S.: The effect of inhibition of cytidine deaminase by tetrahydrouridine on the utilization of deoxycytidine and 5-bromodeoxycytidine for deoxyribonucleic acid synthesis. Mol Pharmacol **9** (6): 698-703, 1973.

Davies, M. G., and Hagen, P. O.: Systemic inflammatory response syndrome. Br J Surg **84** (7): 920-35, 1997.

Dedon, P. C., and Tannenbaum, S. R.: Reactive nitrogen species in the chemical biology of inflammation. Arch Biochem Biophys **423** (1): 12-22, 2004.

deRojas-Walker, T., Tamir, S., Ji, H., Wishnok, J. S., and Tannenbaum, S. R.: Nitric oxide induces oxidative damage in addition to deamination in macrophage DNA. Chem Res Toxicol **8** (3): 473-7, 1995.

Devesa, A., O'Connor, J. E., Garcia, C., Puertes, I. R., and Vina, J. R.: Glutathione metabolism in primary astrocyte cultures: flow cytometric evidence of heterogeneous distribution of GSH content. Brain Res **618** (2): 181-9, 1993.

Dizdaroglu, M.: Formation of an 8-hydroxyguanine moiety in deoxyribonucleic acid on gamma-irradiation in aqueous solution. Biochemistry **24** (16): 4476-81, 1985.

Dong, M., Wang, C., Deen, W. M., and Dedon, P. C.: Absence of 2'-deoxyoxanosine and presence of abasic sites in DNA exposed to nitric oxide at controlled physiological concentrations. Chem Res Toxicol **16** (9): 1044-55, 2003.

Douki, T., Delatour, T., Bianchini, F., and Cadet, J.: Observation and prevention of an artefactual formation of oxidized DNA bases and nucleosides in the GC-EIMS method. Carcinogenesis **17** (2): 347-53, 1996.

Espey, M. G., Miranda, K. M., Thomas, D. D., and Wink, D. A.: Distinction between nitrosating mechanisms within human cells and aqueous solution. J Biol Chem **276** (32): 30085-91, 2001.

Felley-Bosco, E.: Role of nitric oxide in genotoxicity: implication for carcinogenesis. Cancer Metastasis Rev **17** (1): 25-37, 1998.

Franco, R., Valenzuela, A., Lluis, C., and Blanco, J.: Enzymatic and extraenzymatic role of ecto-adenosine deaminase in lymphocytes. Immunol Rev **161**: 27-42, 1998.

Gallardo-Madueno, R., Leal, J. F., Dorado, G., Holmgren, A., Lopez-Barea, J., and Pueyo, C.: In vivo transcription of nrdAB operon and of grxA and fpg genes is triggered in Escherichia coli lacking both thioredoxin and glutaredoxin 1 or thioredoxin and glutathione, respectively. J Biol Chem **273** (29): 18382-8, 1998.

Galli, F., Rossi, R., Di Simplicio, P., Floridi, A., and Canestrari, F.: Protein thiols and glutathione influence the nitric oxide-dependent regulation of the red blood cell metabolism. Nitric Oxide **6** (2): 186-99, 2002.

Gonzalez-Gronow, M., Hershfield, M. S., Arredondo-Vega, F. X., and Pizzo, S. V.: Cell surface adenosine deaminase binds and stimulates plasminogen activation on 1-LN human prostate cancer cells. J Biol Chem **279** (20): 20993-8, 2004.

Greer, S., Schwade, J., and Marion, H. S.: Five-chlorodeoxycytidine and biomodulators of its metabolism result in fifty to eighty percent cures of advanced EMT-6 tumors when used with fractionated radiation. Int J Radiat Oncol Biol Phys **32** (4): 1059-69, 1995.

Greeve, J., Philipsen, A., Krause, K., Klapper, W., Heidorn, K., Castle, B. E., Janda, J., Marcu, K. B., and Parwaresch, R.: Expression of activation-induced cytidine deaminase in human B-cell non-Hodgkin lymphomas. Blood **101** (9): 3574-80, 2003.

Griffith, O. W.: Determination of glutathione and glutathione disulfide using glutathione reductase and 2-vinylpyridine. *In* Anal Biochem, vol. 106, pp. 207-12, 1980.

Grishko, V. I., Druzhyna, N., LeDoux, S. P., and Wilson, G. L.: Nitric oxide-induced damage to mtDNA and its subsequent repair. Nucleic Acids Res **27** (22): 4510-6, 1999.

Guyton, A. C., and Hall, J.: Textbook of Medical Physiology, Saunders, Philadelhia, 2000.

Hanze, A. R.: Nucleic acids. IV. The catalytic reduction of pyrimidine nucleosides (human liver deaminase inhibitors). J Am Chem Soc **89** (25): 6720-5, 1967.

Harris, R. S., Petersen-Mahrt, S. K., and Neuberger, M. S.: RNA editing enzyme APOBEC1 and some of its homologs can act as DNA mutators. Mol Cell **10** (5): 1247-53, 2002.

Ishii, K., Sakamoto, H., Furuyama, J., and Hanaoka, M.: Cytidine deaminase levels in cultured mammalian cell lines measured by the growth tests and enzyme assays. Cell Struct Funct **9** (2): 117-23, 1984.

Ito, S., Nagaoka, H., Shinkura, R., Begum, N., Muramatsu, M., Nakata, M., and Honjo, T.: Activation-induced cytidine deaminase shuttles between nucleus and cytoplasm like apolipoprotein B mRNA editing catalytic polypeptide 1. Proc Natl Acad Sci U S A **101** (7): 1975-80, 2004.

Jaiswal, M., LaRusso, N. F., Burgart, L. J., and Gores, G. J.: Inflammatory cytokines induce DNA damage and inhibit DNA repair in cholangiocarcinoma cells by a nitric oxide-dependent mechanism. Cancer Res **60** (1): 184-90, 2000.

Jaiswal, M., LaRusso, N. F., and Gores, G. J.: Nitric oxide in gastrointestinal epithelial cell carcinogenesis: linking inflammation to oncogenesis. Am J Physiol Gastrointest Liver Physiol **281** (3): G626-34, 2001.

Kaina, B.: DNA damage-triggered apoptosis: critical role of DNA repair, double-strand breaks, cell proliferation and signaling. Biochem Pharmacol **66** (8): 1547-54, 2003.

Kan, H., and Finkel, M. S.: Inflammatory mediators and reversible myocardial dysfunction. J Cell Physiol **195** (1): 1-11, 2003.

Keefer, L. K., Nims, R. W., Davies, K. M., and Wink, D. A.: "NONOates" (1-substituted diazen-1-ium-1,2-diolates) as nitric oxide donors: convenient nitric oxide dosage forms. Methods Enzymol **268:** 281-93, 1996.

Kelman, D. J., Christodoulou, D., Wink, D. A., Keefer, L. K., Srinivasan, A., and Dipple, A.: Relative mutagenicities of gaseous nitrogen oxides in the supF gene of pSP189. Carcinogenesis **18** (5): 1045-8, 1997.

Keshive, M., Singh, S., Wishnok, J. S., Tannenbaum, S. R., and Deen, W. M.: Kinetics of S-nitrosation of thiols in nitric oxide solutions. *In* Chem Res Toxicol, vol. 9, pp. 988-93, 1996a.

Keshive, M., Singh, S., Wishnok, J. S., Tannenbaum, S. R., and Deen, W. M.: Kinetics of S-nitrosation of thiols in nitric oxide solutions. Chem Res Toxicol **9** (6): 988-93, 1996b.

Kim, Y. G., Lowenhaupt, K., Maas, S., Herbert, A., Schwartz, T., and Rich, A.: The zab domain of the human RNA editing enzyme ADAR1 recognizes Z-DNA when surrounded by B-DNA. J Biol Chem **275** (35): 26828-33, 2000.

Lala, P. K., and Chakraborty, C.: Role of nitric oxide in carcinogenesis and tumour progression. Lancet Oncol **2** (3): 149-56, 2001.

Laliberte, J., Marquez, V. E., and Momparler, R. L.: Potent inhibitors for the deamination of cytosine arabinoside and 5-aza-2'-deoxycytidine by human cytidine deaminase. Cancer Chemother Pharmacol **30** (1): 7-11, 1992.

Laval, F., and Wink, D. A.: Inhibition by nitric oxide of the repair protein, O6-methylguanine-DNA-methyltransferase. Carcinogenesis **15** (3): 443-7, 1994.

Leger, C., and Drobetsky, E. A.: Modulation of the DNA damage response in UV-exposed human lymphoblastoid cells through genetic-versus functional-inactivation of the p53 tumor suppressor. Carcinogenesis **23** (10): 1631-9, 2002.

Lewis, R. S., and Deen, W. M.: Kinetics of the reaction of nitric oxide with oxygen in aqueous solutions. Chem Res Toxicol **7** (4): 568-74, 1994.

Lewis, R. S., Tamir, S., Tannenbaum, S. R., and Deen, W. M.: Kinetic analysis of the fate of nitric oxide synthesized by macrophages in vitro. *In* J Biol Chem, vol. 270, pp. 29350-5, 1995.

Li, C. Q., Robles, A. I., Hanigan, C. L., Hofseth, L. J., Trudel, L. J., Harris, C. C., and Wogan, G. N.: Apoptotic signaling pathways induced by nitric oxide in human lymphoblastoid cells expressing wild-type or mutant p53. Cancer Res **64** (9): 3022-9, 2004.

Li, C. Q., Trudel, L. J., and Wogan, G. N.: Genotoxicity, mitochondrial damage, and apoptosis in human lymphoblastoid cells exposed to peroxynitrite generated from SIN-1. Chem Res Toxicol **15** (4): 527-35, 2002a.

Li, C. Q., Trudel, L. J., and Wogan, G. N.: Nitric oxide-induced genotoxicity, mitochondrial damage, and apoptosis in human lymphoblastoid cells expressing wild-type and mutant p53. Proc Natl Acad Sci U S A **99** (16): 10364-9, 2002b.

Liber, H. L., and Thilly, W. G.: Mutation assay at the thymidine kinase locus in diploid human lymphoblasts. Mutat Res **94** (2): 467-85, 1982.

Liu, L., Xu-Welliver, M., Kanugula, S., and Pegg, A. E.: Inactivation and degradation of O(6)-alkylguanine-DNA alkyltransferase after reaction with nitric oxide. Cancer Res **62** (11): 3037-43, 2002.

Luperchio, S., Tamir, S., and Tannenbaum, S. R.: No-induced oxidative stress and glutathione metabolism in rodent and human cells. *In* Free Radic Biol Med, vol. 21, pp. 513-9, 1996a.

Luperchio, S., Tamir, S., and Tannenbaum, S. R.: No-induced oxidative stress and glutathione metabolism in rodent and human cells. Free Radic Biol Med **21** (4): 513-9, 1996b.

Macarthur, M., Hold, G. L., and El-Omar, E. M.: Inflammation and Cancer II. Role of chronic inflammation and cytokine gene polymorphisms in the pathogenesis of gastrointestinal malignancy. Am J Physiol Gastrointest Liver Physiol **286** (4): G515-20, 2004.

Maeda, H., and Akaike, T.: Nitric oxide and oxygen radicals in infection, inflammation, and cancer. Biochemistry (Mosc) **63** (7): 854-65, 1998.

Mashiyama, S. T., Courtemanche, C., Elson-Schwab, I., Crott, J., Lee, B. L., Ong, C. N., Fenech, M., and Ames, B. N.: Uracil in DNA, determined by an improved assay, is increased when deoxynucleosides are added to folate-deficient cultured human lymphocytes. Anal Biochem **330** (1): 58-69, 2004.

Muramatsu, M., Sankaranand, V. S., Anant, S., Sugai, M., Kinoshita, K., Davidson, N. O., and Honjo, T.: Specific expression of activation-induced cytidine deaminase (AID), a novel member of the RNA-editing deaminase family in germinal center B cells. J Biol Chem **274** (26): 18470-6, 1999.

Muto, T., Muramatsu, M., Taniwaki, M., Kinoshita, K., and Honjo, T.: Isolation, tissue distribution, and chromosomal localization of the human activation-induced cytidine deaminase (AID) gene. Genomics **68** (1): 85-8, 2000.

Nakamura, J., La, D. K., and Swenberg, J. A.: 5'-nicked apurinic/apyrimidinic sites are resistant to beta-elimination by beta-polymerase and are persistent in human cultured cells after oxidative stress. J Biol Chem **275** (8): 5323-8, 2000.

Nguyen, T., Brunson, D., Crespi, C. L., Penman, B. W., Wishnok, J. S., and Tannenbaum, S. R.: DNA damage and mutation in human cells exposed to nitric oxide in vitro. Proc Natl Acad Sci U S A **89** (7): 3030-4, 1992.

Ohshima, H.: Genetic and epigenetic damage induced by reactive nitrogen species: implications in carcinogenesis. Toxicol Lett **140-141:** 99-104, 2003.

Ohshima, H., and Bartsch, H.: Chronic infections and inflammatory processes as cancer risk factors: possible role of nitric oxide in carcinogenesis. Mutat Res **305** (2): 253-64, 1994.

Ohshima, H., Tatemichi, M., and Sawa, T.: Chemical basis of inflammation-induced carcinogenesis. Arch Biochem Biophys **417** (1): 3-11, 2003.

Peng, S., Padva, A., and LeBreton, P. R.: Ultraviolet photoelectron studies of biological purines: the valence electronic structure of adenine. Proc Natl Acad Sci U S A **73** (9): 2966-8, 1976.

Petersen, C., Moller, L. B., and Valentin-Hansen, P.: The cryptic adenine deaminase gene of Escherichia coli. Silencing by the nucleoid-associated DNA-binding protein, H-NS, and activation by insertion elements. J Biol Chem **277** (35): 31373-80, 2002.

Petersen-Mahrt, S. K., Harris, R. S., and Neuberger, M. S.: AID mutates E. coli suggesting a DNA deamination mechanism for antibody diversification. Nature **418** (6893): 99-103, 2002.

Pham, P., Bransteitter, R., Petruska, J., and Goodman, M. F.: Processive AID-catalysed cytosine deamination on single-stranded DNA simulates somatic hypermutation. Nature **424** (6944): 103-7, 2003.

Philbert, M. A., Beiswanger, C. M., Waters, D. K., Reuhl, K. R., and Lowndes, H. E.: Cellular and regional distribution of reduced glutathione in the nervous system of the rat: histochemical localization by mercury orange and o-phthaldialdehyde-induced histofluorescence. Toxicol Appl Pharmacol **107** (2): 215-27, 1991.

Poulsen, H. E., Loft, S., Prieme, H., Vistisen, K., Lykkesfeldt, J., Nyyssonen, K., and Salonen, J. T.: Oxidative DNA damage in vivo: relationship to age, plasma antioxidants, drug metabolism, glutathione-S-transferase activity and urinary creatinine excretion. Free Radic Res **29** (6): 565-71, 1998.

Rehemtulla, A., Hamstra, D. A., Kievit, E., Davis, M. A., Ng, E. Y., Dornfeld, K., and Lawrence, T. S.: Extracellular expression of cytosine deaminase results in increased 5-FU production for enhanced enzyme/prodrug therapy. Anticancer Res **24** (3a): 1393-9, 2004.

Roberts, E. L.: Guanosine deaminase in human serum and tissue extracts--a reappraisal of the products. Br J Biomed Sci **60** (4): 197-203, 2003.

Rosin, M. P., Saad el Din Zaki, S., Ward, A. J., and Anwar, W. A.: Involvement of inflammatory reactions and elevated cell proliferation in the development of bladder cancer in schistosomiasis patients. Mutat Res **305** (2): 283-92, 1994.

Routledge, M. N., Wink, D. A., Keefer, L. K., and Dipple, A.: Mutations induced by saturated aqueous nitric oxide in the pSP189 supF gene in human Ad293 and E. coli MBM7070 cells. Carcinogenesis **14** (7): 1251-4, 1993.

Routledge, M. N., Wink, D. A., Keefer, L. K., and Dipple, A.: DNA sequence changes induced by two nitric oxide donor drugs in the supF assay. *In* Chem Res Toxicol, vol. 7, pp. 628-32, 1994.

Scharfstein, J. S., Keaney, J. F., Jr., Slivka, A., Welch, G. N., Vita, J. A., Stamler, J. S., and Loscalzo, J.: In vivo transfer of nitric oxide between a plasma protein-bound reservoir and low molecular weight thiols. J Clin Invest **94** (4): 1432-9, 1994.

Schein, A. H.: Uracil in formic acid hydrolysates of deoxyribonucleic acid. Biochem J **98** (1): 311-6, 1966.

Schwartsburd, P. M.: Chronic inflammation as inductor of pro-cancer microenvironment: pathogenesis of dysregulated feedback control. Cancer Metastasis Rev **22** (1): 95-102, 2003.

Schwartz, J. L., Jordan, R., Evans, H. H., Lenarczyk, M., and Liber, H.: The TP53 dependence of radiation-induced chromosome instability in human lymphoblastoid cells. Radiat Res **159** (6): 730-6, 2003.

Scorza, G., Pietraforte, D., and Minetti, M.: Role of ascorbate and protein thiols in the release of nitric oxide from S-nitroso-albumin and S-nitroso-glutathione in human plasma. Free Radic Biol Med **22** (4): 633-42, 1997.

Shen, H. M., and Storb, U.: Activation-induced cytidine deaminase (AID) can target both DNA strands when the DNA is supercoiled. Proc Natl Acad Sci U S A **101** (35): 12997-3002, 2004.

Sherwood, R. A.: The measurement of nucleoside deaminases by high performance liquid chromatography and their use in clinical chemistry. Biomed Chromatogr **5** (6): 235-9, 1991.

Shi, Y.: A structural view of mitochondria-mediated apoptosis. Nat Struct Biol **8** (5): 394-401, 2001.

Singh, S. P., Wishnok, J. S., Keshive, M., Deen, W. M., and Tannenbaum, S. R.: The chemistry of the S-nitrosoglutathione/glutathione system. *In* Proc Natl Acad Sci U S A, vol. 93, pp. 14428-33, 1996.

Snyder, F. F., Yuan, R. G., Bin, J. C., Carter, K. L., and McKay, D. J.: Human guanine deaminase: cloning, expression and characterisation. Adv Exp Med Biol **486:** 111-4, 2000.

Spek, E. J., Vuong, L. N., Matsuguchi, T., Marinus, M. G., and Engelward, B. P.: Nitric oxide-induced homologous recombination in Escherichia coli is promoted by DNA glycosylases. J Bacteriol **184** (13): 3501-7, 2002.

Spek, E. J., Wright, T. L., Stitt, M. S., Taghizadeh, N. R., Tannenbaum, S. R., Marinus, M. G., and Engelward, B. P.: Recombinational repair is critical for survival of Escherichia coli exposed to nitric oxide. J Bacteriol **183** (1): 131-8, 2001.

Spencer, J. P., Jenner, A., Chimel, K., Aruoma, O. I., Cross, C. E., Wu, R., and Halliwell, B.: DNA damage in human respiratory tract epithelial cells: damage by gas phase cigarette

smoke apparently involves attack by reactive nitrogen species in addition to oxygen radicals. FEBS Lett **375** (3): 179-82, 1995.

Sugiura, Y., Fujioka, S., and Yoshida, S.: Biosynthesis of pyrimidine nucleotides in human leukemic cells. Jpn J Cancer Res **77** (7): 664-73, 1986.

Szabo, C.: Multiple pathways of peroxynitrite cytotoxicity. Toxicol Lett **140-141:** 105-12, 2003.

Szabo, C., and Ohshima, H.: DNA damage induced by peroxynitrite: subsequent biological effects. Nitric Oxide **1** (5): 373-85, 1997.

Tabor, C. W., and Tabor, H.: Polyamines in microorganisms. Microbiol Rev **49** (1): 81-99, 1985.

Tamir, S., Burney, S., and Tannenbaum, S. R.: DNA damage by nitric oxide. Chem Res Toxicol **9** (5): 821-7, 1996.

Tamir, S., Lewis, R. S., de Rojas Walker, T., Deen, W. M., Wishnok, J. S., and Tannenbaum, S. R.: The influence of delivery rate on the chemistry and biological effects of nitric oxide. Chem Res Toxicol **6** (6): 895-9, 1993.

Tietze, F.: Enzymic method for quantitative determination of nanogram amounts of total and oxidized glutathione: applications to mammalian blood and other tissues. *In* Anal Biochem, vol. 27, pp. 502-22, 1969.

Trumbore, C. N., Hyde, C. T., Hudson, R. D., Jurman, L. A., Gehring, A. G., and Masselink, J. K.: Ultraviolet difference spectral studies in the gamma radiolysis of DNA and model compounds. I. Aqueous solutions of DNA bases. Int J Radiat Biol **56** (6): 923-41, 1989.

Voehringer, D. W., Story, M. D., O'Neil, R. G., and Meyn, R. E.: Modulating Ca2+ in radiation-induced apoptosis suppresses DNA fragmentation but does not enhance clonogenic survival. Int J Radiat Biol **71** (3): 237-43, 1997.

Vousden, K. H.: p53: death star. Cell **103** (5): 691-4, 2000.

Wang, C., and Deen, W. M.: Nitric oxide delivery system for cell culture studies. Ann Biomed Eng **31** (1): 65-79, 2003.

Wang, C., Trudel, L. J., Wogan, G. N., and Deen, W. M.: Thresholds of nitric oxide-mediated toxicity in human lymphoblastoid cells. Chem Res Toxicol **16** (8): 1004-13, 2003.

Wang, C. L., Harper, R. A., and Wabl, M.: Genome-wide somatic hypermutation. Proc Natl Acad Sci U S A **101** (19): 7352-6, 2004.

Wink, D. A., Kasprzak, K. S., Maragos, C. M., Elespuru, R. K., Misra, M., Dunams, T. M., Cebula, T. A., Koch, W. H., Andrews, A. W., Allen, J. S., and et al.: DNA deaminating ability and genotoxicity of nitric oxide and its progenitors. Science **254** (5034): 1001-3, 1991.

Wink, D. A., and Laval, J.: The Fpg protein, a DNA repair enzyme, is inhibited by the biomediator nitric oxide in vitro and in vivo. Carcinogenesis **15** (10): 2125-9, 1994.

Wink, D. A., Nims, R. W., Darbyshire, J. F., Christodoulou, D., Hanbauer, I., Cox, G. W., Laval, F., Laval, J., Cook, J. A., Krishna, M. C., and et al.: Reaction kinetics for nitrosation of cysteine and glutathione in aerobic nitric oxide solutions at neutral pH. Insights into the fate and physiological effects of intermediates generated in the NO/O2 reaction. Chem Res Toxicol **7** (4): 519-25, 1994.

Wink, D. A., Vodovotz, Y., Laval, J., Laval, F., Dewhirst, M. W., and Mitchell, J. B.: The multifaceted roles of nitric oxide in cancer. Carcinogenesis **19** (5): 711-21, 1998.

Xia, F., Wang, X., Wang, Y. H., Tsang, N. M., Yandell, D. W., Kelsey, K. T., and Liber, H. L.: Altered p53 status correlates with differences in sensitivity to radiation-induced mutation and apoptosis in two closely related human lymphoblast lines. Cancer Res **55** (1): 12-5, 1995.

Zamora, R., Alarcon, L., Vodovotz, Y., Betten, B., Kim, P. K., Gibson, K. F., and Billiar, T. R.: Nitric oxide suppresses the expression of Bcl-2 binding protein BNIP3 in hepatocytes. J Biol Chem **276** (50): 46887-95, 2001.

Zhuang, J. C., Lin, D., Lin, C., Jethwaney, D., and Wogan, G. N.: Genotoxicity associated with NO production in macrophages and co-cultured target cells. *In* Free Radic Biol Med, vol. 33, pp. 94-102, 2002.

Zhuang, J. C., Wright, T. L., deRojas-Walker, T., Tannenbaum, S. R., and Wogan, G. N.: Nitric oxide-induced mutations in the HPRT gene of human lymphoblastoid TK6 cells and in Salmonella typhimurium. Environ Mol Mutagen **35** (1): 39-47, 2000.

Chapter 5

Formation of Nucleobase Deamination Products in Spleen and Liver of SJL Mice Bearing the RcsX Tumor

5.1 Abstract

To test the hypothesis that genotoxic damage contributes to inflammation-associated cancer risk, a number of animal models have been developed, including the SJL mouse model in conjunction with RcsX tumor, which provides an established animal model for evaluating the production and genotoxicity of nitric oxide (NO•). SJL mice spontaneously develop B cell lymphoma and an apparently unrelated spontaneous myositis by ~ 1 year of age. With the implantation of RcsX tumor cells, SJL mice develop an RcsX lymphoma and exhibit elevated NO• production as reflected in urinary nitrate excretion. Inducible NO• synthase (iNOS) has been detected in the spleen, lymph nodes and resident macrophages of RcsX tumor-bearing mice. SJL/RcsX mice have been used as a model for *in vivo* toxicology studies of NO•, among which increases in etheno adducts of dA and dC in the spleen DNA of the challenged mice have been reported. Current study, as an integral part of a broad investigation aimed at establishing biomarker(s) of inflammation, is to test whether there is a correlation between nucleobase deamination and NO• production in this mouse model of inflammation.

Two groups of male SJL mice were housed in an ALAC accredited facility and one group of mice was injected intraperitoneally with 10^7 RcsX tumor cells in 200 μL PBS. The other group was treated with 200 μL PBS only, as the control. Animals were sacrificed 12 days after injection of the tumor cells. Livers and spleens were harvested, weighed and snap frozen in liquid nitrogen. Using rigorous artifact control, genomic DNA from mouse spleen and liver was isolated for quantification of nucleobase deamination and oxidation products. The treated mice showed a time-dependent increase in urinary nitrate excretion, beginning 4 days after injection of RcsX cells and culminating in a ~35-fold increases on day12 of the experiment. Despite the

dramatic increase in the nitrate excretion, which suggests a strong induction of NO• synthesis, there was only a moderate increases (~30%) in dX, dI and dU in both spleen and liver of the SJL/RcsX mice relative to the controls. For example, in the spleen DNA, dX was elevated to 3.7 ± 0.3 lesions per 10^6 nt compared to 2.8 ± 0.2 in the control; dI at 10.3 ± 1.3 lesions per 10^6 nt *vs.* 7.0 ± 0.5; dU at 37.5 ± 1.2 lesions per 10^6 nt *vs.* 27.5 ± 2.1. Neither the control nor the inflamed mice showed a detectable level of dO. Our observations were consistent with the results of nucleobase oxidation products in the same samples quantified by the research of Prof. Steven Tannenbaum, which followed a similar trend, with small increases (<30%) in spiroiminodihydantoin (Sp) and guanidinohydantoin (Gh), an undetectable nitroimidazole (NI) and oxazolone (Ox) (< 1 lesion per 10^7 bases), and even a decrease in 8-oxo-dG relative to the controls (Yu et al., personal communication). Taken together, these results suggest that direct reaction of RNS with DNA in the SJL/RcsX mice only produce moderate increase in DNA damage. The modest increases in the DNA damage products tested here reflected a net result of damage formation and repair. Further studies, including DNA repair kinetics and additional DNA damage products, such as the etheno adducts presumably derived from lipid peroxidation and, are needed to finally establish biomarkers of the inflammatory process in the SJL/RcsX model.

5.2 Introduction

Epidemiological studies demonstrate an association between chronic inflammation and increased cancer risk (Balkwill and Mantovani, 2001; Ohshima et al., 1994; Ohshima and Bartsch, 1994; Shacter and Weitzman, 2002). Examples include inflammatory bowel diseases (IBD) and colon cancer (Shacter and Weitzman, 2002) and *Helicobacter pylori* infection and gastric cancer (Asaka et al., 1997; Ebert et al., 2000). The strongest evidence for a mechanistic link between inflammation and cancer involves the generation of reactive oxygen and nitrogen species by macrophages and neutrophils that respond to cytokines and other signaling processes arising at sites of inflammation. These chemical mediators of inflammation can also damage surrounding host tissues causing oxidation, nitration, halogenation and deamination of biomolecules of all types, including lipids, proteins, carbohydrates, and nucleic acids, with the formation of toxic and mutagenic products.

To test the hypothesis that DNA damage contributes to inflammation-associated cancer risk, it is important to have appropriate animal models that feature the development of neoplasia with a high incidence and a short latent period, as well as the ability to modulate levels of inflammation *in vivo*. A number of animal models fulfill these criteria, an example of which is the established SJL/RcsX mouse model of increased $NO^{\bullet}$ production.

SJL/ RcsX Mouse Model. The SJL mouse strain, originally derived from Swiss Webster mice (Murphy, 1969), displays multiple immunological defects. It is highly susceptible to numerous experimentally induced autoimmune diseases and has been widely used as a model for experimental autoimmune encephalitis (EAE) and myositis (Arnon, 1981; Rosenberg and

Kotzin, 1989). The molecular basis for the immunodeficiencies in SJL mice includes the depletion of T-cell receptors, the lack of natural killer cells, and the insufficiency of suppressor T cells. (Behlke et al., 1985; Fitzgerald and Ponzio, 1979).

At ~1 year of age, SJL mice also display a very high incidence of B-cell lymphomas (historically described as reticulum cell sarcomas, RCS) resembling Hodgkin's disease (Murphy, 1969). In dissecting the underlying mechanisms, various tumor lines capable of inducing spontaneous lymphomas have been developed. A common feature of all these so-called RCS tumor cells is the presentation of a mouse mammary tumor virus (MMTV) surface superantigen that can stimulate a subset of T cells, the Vβ-16$^+$ T cells (Tsiagbe et al., 1993a; Tsiagbe et al., 1993b). When stimulated, the Vβ-16$^+$ T cells secret a mixture of cytokines, mainly IL-5 and γ-interferon, which are required for the growth of the tumor cells (Katz et al., 1981; Lasky and Thorbecke, 1988; Tsiagbe et al., 1992).

The interest in using SJL mice as an *in vivo* model for the study of NO$^\bullet$ toxicology arose from the observation that macrophages comprised more than 80% of the infiltrating cell population in experimental autoimmune myositis (Rosenberg and Kotzin, 1989). Tamir et al. later demonstrated a correlation between elevated NO$^\bullet$ production and increased severity of myositis in SJL mice (Tamir et al., 1995). However, the spontaneous myositis model was inappropriate for the analysis of NO$^\bullet$-mediated macromolecular damage due to the exceedingly long delay in the development of the symptom (Tamir et al., 1995). The model was also suffered from a nonuniform onset of clinical myositis among individual mice.

The observation that the host immune system was stimulated during the development of spontaneous lymphoma in the myositis model (Tsiagbe et al., 1992) inspired attempts to

establish a lymphoma model with increased NO• production. Gal et al. transplanted an aggressive lymphoma (RcsX) into SJL mice and observed the rapid growth of tumors as well as significantly elevated urinary nitrate excretion, the final metabolite of NO• *in vivo* (Gal et al., 1996). Carefully designed studies demonstrated that NO• production was generated by activated macrophages in spleen, lymph nodes and liver (Gal et al., 1997). Thus, the SJL/RcsX mouse model allowed physiological overproduction of NO• over a reasonable period (~ two weeks) at levels sufficient to investigate the damage to cellular macromolecles. The mechanisms underlying the induction of NO• production by macrophages in this model was later suggested to follow the "reverse immune surveillance" mechanism (Ponzio and Thorbecke, 2000; Thorbecke and Ponzio, 2000), which is, in brief, that endogenous superantigen expressed on the surface of the RcsX cells stimulates a subset of T helper-2 (Th2) cells, the $V\beta\text{-}16^{+}$ T cells, to produce tumor growth-promoting cytokines and IFN-γ that can activate macrophages. Activated macrophages in turn initiate the inflammation response along with the increased NO• production (Figure 1).

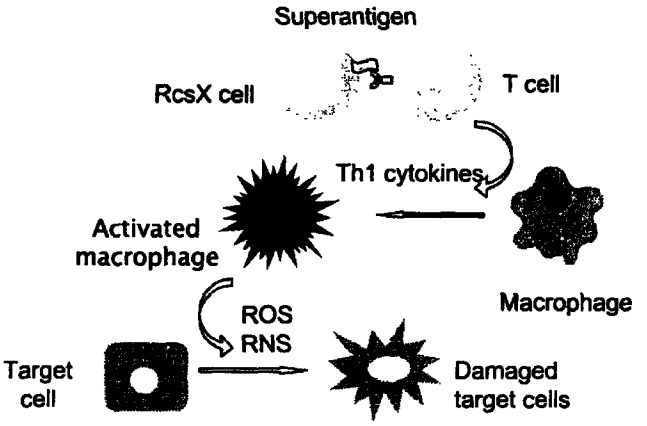

Figure 1. Macrophage-mediated cytotoxicity by RcsX cells. RcsX cells were derived from a reticulum cell sarcoma, the cells of which bear superantigen. The superantigens activate syngeneic $CD4^+$ $Vb16^+$ T cells to produce B cell growth factors that stimulate the proliferation of B cells and Th1 cytokines that activate macrophages. Activated macrophages then initiate the inflammation response.

As a model of NO• overproduction that occurs in inflammation, the SJL/RcsX mouse system has only been used in a few *in vivo* studies on the toxicology of NO•. Severe tissue damage manifested by pathological changes and cell apoptosis was found in close proximity to the sites of NO• production (Gal et al., 1997). A significant elevation in the mutant frequency (MF) of *lacZ* gene in the spleens, but not the kidneys, of tumor-bearing mice was observed. Furthermore, the increases in MF as well as NO• production were both abrogated by administration of N-methylarginine, a potent inhibitor of iNOS, to the SJL/RcsX mice, suggesting a contribution of NO• to mutagenicity (Gal and Wogan, 1996). The extent of DNA damage was also assessed. Despite a lack of increase in 8-oxo-dG, promutagenic etheno adducts 1,N6-

ethenodeoxyadenosine (ε-dA) and 3,N4-ethenodeoxycytidine (ε-dC) were both found elevated in the splenic DNA of the SJL/RcsX mice (Gal et al., 1997; Nair et al., 1998).

In order to provide a better understanding of the roles of nitrosative and oxidative DNA damage in the mutagenicity of SJL/RcsX mice, we, in collaboration with the research group of Prof. Steven Tannenbaum, quantified a battery of DNA damage products, including the nucleobase deamination lesions deoxyxanthosine (dX), deoxyoxanosine (dO), deoxyinosine (dI), and deoxyuridine (dU), and nucleobase oxidative lesions 8-oxo-dG, spiroiminodihydantoin (Sp), guanidinohydantoin (Gh), nitroimidazole (NI), and oxazolone (Ox). Additional purpose of this study is to determine whether one or more of these lesions could be used as biomarker(s) of the inflammatory process.

5.3 Materials and Methods

Materials. All chemicals and reagents were of highest purity available and were used without further purification unless noted otherwise. N^G-methyl L-arginine acetate (NMA), sodium pyruvate, and insulin (bovine) were purchased from Bhem Biochem Research (Salt Lake City, UT). Nuclease P1 and a kit for DNA isolation from cells and tissues were obtained from Roche Diagnostic Corporation (Indianapolis, IN). Phosphodiesterase I was purchased from USB (Cleveland, Ohio). Alkaline phosphatase and ammonium acetate were obtained from Sigma Chemicals (St. Louis, MO). Iscove's modified Dulbecco's medium, fetal calf serum, glutamine, and penicillin/streptomycin were purchased from BioWhittaker (Walkersville, MD). Coformycin and tetrahydrouridine were purchased from Calibochem (San Diego, CA). Acetonitrile and HPLC-grade water were purchased from Mallinckrodt Baker (Phillipsburg, NJ). Water purified through a Milli-Q system (Millipore Corporation, Bedford, MA) was used for all applications.

Instrumental Analyses. All HPLC analyses were performed on an Agilent Model 1100, equipped with a 1040A diode array detector. Mass spectra were recorded with an Agilent Model 1100 electrospray mass spectrometer coupled to an Agilent Model 1100 HPLC with diode array detector. UV spectra were obtained using a Beckman DU640 UV-visible spectrophotometer.

RcsX Cell Line (Performed by Ms. Laura Trudel). The RcsX cell line was kindly supplied by Dr. N. Ponzio (University of New Jersey Medical Center, Newark NJ). Cells are passaged through mice and harvested from lymph nodes 14 days after inoculation. Cells were manually

dissociated from the lymph nodes by teasing the tissues, followed by washing in PBS and freezing in aliquots of 5x 10^7 cells in 10% DMSO/FBS.

Animal Experiments (Performed by Ms. Laura Trudel). Of a group of 18 male SJL mice (5-6 weeks old, Jackson Labs, Bar Harbor, ME), 8 were each injected intraperitoneally with 10^7 cells of the ResX line in PBS. 10 kept as the controls by injecting with PBS. 4 treated and 6 control mice were killed 12 days after injection. Spleens, livers, and kidneys were removed, weighed and snap frozen in liquid nitrogen for DNA damage analysis. The rest of mice were used for other purposes.

DNA Isolation from Tissues. DNA from the liver and spleen of SJL mice was isolated using a Roche DNA isolation kit for cells and tissues (Roche Molecular Biochemicals, Indianapolis, IN) following the manufacturer's instructions with additional modifications and proper measures of artifact controls. Briefly, 400 mg samples of frozen tissue were homogenized in 10 mL of cellular lysis buffer containing a combination of deaminase inhibitors and antioxidant (5 μg/mL coformycin, 50 μg/mL tetrahydrouridine, and 0.1 mM desferrioxamine) for 20-30 s using a Brinkman Polytron homogenizer on a medium setting. The homogenate was digested with proteinase K (6.1 μL, 100 mg/mL) at 65°C for 1 hr. DNase-free RNase A was then added (400 μL, 25 mg/mL) for additional 30 min incubation at 37°C. Proteins were removed by adding 4.2 mL of protein precipitation solution followed by a 5 min incubation on ice and centrifugation at 26,900xg for 20 min at RT. The supernatant was carefully transferred to a fresh tube and DNA was recovered by precipitation in 200 mM NaCl and 2.5 volumes of absolute ethanol (-20°C; add slowly to facilitate DNA recovery). The floating DNA filament was recovered with a

micropipette tip (or by centrifugation at 5000 x g for 30 min) followed by two washes with 70% ethanol, air-drying at ambient temperature and resuspension in 10 mM Tris, 1 mM EDTA (pH 8.0). The DNA concentration was defined by UV spectroscopy and the sample was stored at –80 °C.

Quantification of DNA Nucleobase Deamination by LC-MS Analysis. Nucleobase deamination products in DNA samples from mouse spleen and liver were quantified by the LC-MS method established previously with minor modifications (Dong et al., 2003). Briefly, 50 μg of DNA was hydrolyzed by a combination of Nuclease P1, phosphodiesterase I and alkaline phosphatase in the presence of appropriate amounts of isotope-labeled internal standards and an adenosine deaminase inhibitor, coformycin. Tetrahydrouridine, a specific cytidine deaminase inhibitor, was not included, since careful screen of all enzyme stocks that were used to digest DNA did not find the action of a contaminant that led to the adventitious formation of dU. The resulting nucleoside mixture was separated by HPLC using a Phenomenex reversed phase column (Synergi, 250 x 4.6 mm, 4 μm particle size, 80 Å pore size), which resulted in better resolution of dX and dG compared with the previously used column. Fractions containing each nucleobase deamination product were collected for subsequent LC-MS quantification.

5.4 Results

DNA Isolation from Mouse Tissues. To obtain DNA free from damage artifacts created by the isolation process, we established a standard method for DNA isolation from mouse tissues for all DNA adduct analyses. The procedure includes sample homogenization followed by cellular lysis in the presence of a strong anionic detergent and Proteinase K. RNA is eliminated by RNase treatment and proteins are removed by selective precipitation and centrifugation. The purified DNA is subsequently recovered by isopropanol precipitation. A cocktail inhibition regimen (5 μg/mL coformycin, 50 μg/mL tetrahydrouridine, and 0.1 mM desferrioxamine) was added in each step to prevent the artifactual generation of oxidation and deamination products. Table 1 summarizes the recovery of DNA from SJL spleen and liver. The yield of the DNA is about 0.6 to 1% of the wet tissue weight. Reasonable purity of the isolated DNA was indicated by the OD_{260} to OD_{280} ratio.

Table 1. DNA recovery from SJL mouse tissues

Tissue (number of mice)		Wet Weight (mg)	Tissue weight used for DNA isolation (mg)	DNA recovered (mg)	OD_{260}/OD_{280}	Recover rate (%)
Spleen	Control / (6)	627.7	369.2	2.631	1.68	0.713
	RcsX #1 / (1)	811.4	364.4	4.136	1.67	1.141
	RcsX #2 / (1)	524.0	399.0	3.990	1.68	1.030
	RcsX #3 / (1)	824.5	381.2	3.263	1.61	0.820
Liver	Control / (6)	1905.3	367.3	3.318	1.71	0.90
	RcsX #1 / (1)	1410.2	326.2	2.362	1.63	0.724
	RcsX #2 / (1)	1239.9	390.5	2.485	1.65	0.641
	RcsX #3 / (1)	989.1	351.5	2.655	1.70	0.755

Note: the weight of the spleen is the weight for the whole organ. The weight of the liver is that of a slice. Six spleens from the control mice were pooled for the DNA isolation. Spleens from RcsX-treated mice were analyzed individually

Formation of Nucleobase Deamination Products in the SJL/RcsX Mice. Four nucleobase deamination products were quantified in the spleen and liver of SJL mice 12 days after injection of RcsX tumor cells. NO$^{\bullet}$ production was found to increase ~35-fold in the RcsX mice. However, except for dO, which was undetectable in both the control and the RcsX mice, there was only moderate increases (~30%) in dX, dI and dU in the spleen and liver of the RcsX mice compared to the controls, which follows that, in spleen, dX increased to 3.7 ± 0.3 lesions per 10^6 nt compared to 2.8 ± 0.2 in the control; dI at 10.3 ± 1.3 lesions per 10^6 nt *vs.* 7.0 ± 0.5; dU at 37.5 ± 1.2 lesions per 10^6 nt *vs.* 27.5 ± 2.1 (Figure 2).

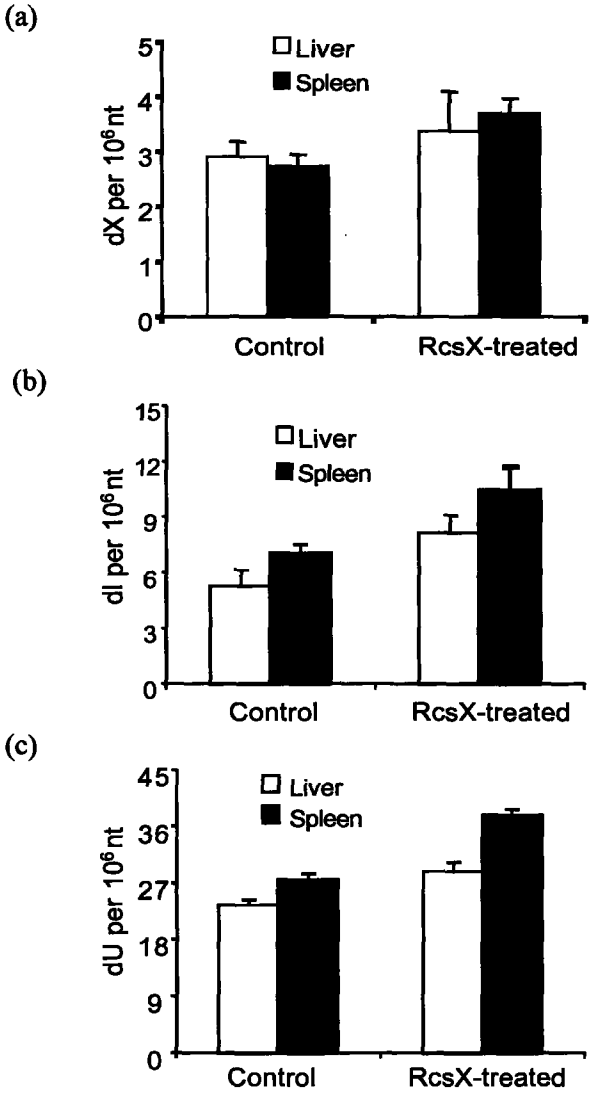

Figure 2. Formation of nucleobase deamination products in spleen and liver DNA of SJL mice bearing the RcsX tumor. Following isolation and processing of DNA from the tissues, dX (a), dI (b), and dU (c) were quantified by LC-MS. DNA of the control group was pooled from six mice, and data represent the mean ± SD of three measurements of the same pooled sample. Data for the SJL/RcsX mice represent the mean value (± S.D.) of duplicated measurements of each three different mice.

5.5 Discussion

Chronic inflammation has long been recognized as a risk factor for the development of a variety of human cancers (Balkwill and Mantovani, 2001; Ohshima et al., 1994; Ohshima and Bartsch, 1994; Shacter and Weitzman, 2002). The strongest evidence for a mechanistic link between inflammation and cancer involves the generation of reactive species by professional leukocytes that respond to cytokines and other signaling processes arising at sites of inflammation (Dedon and Tannenbaum, 2004; Ohshima et al., 2003). In particular, as part of the inflammatory process, activated macrophages produce increased quantity of $NO^{\bullet}$ and by reaction with oxygen and superoxide to produce nitrous anhydride (N_2O_3) and peroxynitrite ($ONOO^-$) respectively. These two derived RNS have been shown to cause a wide variety of DNA lesions, among which are nitrosative base deamination and DNA cross-links caused by N_2O_3 and oxidation and nitration lesions produced by $ONOO^-$. An unresolved question, however, is the relative quantities of different damage products arising in cells at sites of inflammation. To this end, we have initiated a series of studies to define the predominant DNA damage produced by RNS with a focus here on defining the spectrum of base damage products in the SJL/RcsX mouse model of inflammation.

The SJL/RcsX mice have been developed as a model of a lymphoma-induced inflammatory response with production of a large quantities of $NO^{\bullet}$ (Gal et al., 1997; Gal et al., 1996; Gal and Wogan, 1996; Tamir et al., 1995). This model provides an opportunity to study a primarily macrophage-driven inflammatory reaction associated with increases in nitrotyrosine and apoptosis apparent in the cells surrounding activated macrophages (Gal et al., 1997). Significant increase in MF of the *lacZ* gene in the spleen of the SJL/RcsX mice were observed (Gal and

Wogan, 1996). DNA damage products were also determined, but only limited to 8-oxo-dG, etheno adducts of dA and dC (Nair et al., 1998). Therefore, we extended the previous studies by including a more complete set of DNA damage products that include nucleobase deamiantion products, oxidation products, M_1G and etheno dA. Quantification of these lesions provides an opportunity to explore novel biomarkers of inflammation.

Spleen from the SJL/RcsX mice was chosen for the study of DNA damage caused by NO• because it is one of the target organs that have been shown increased NO• production (Gal et al., 1997; Gal et al., 1996; Gal and Wogan, 1996; Tamir et al., 1995). Cells in those organs, including spleen, lymph note, and liver, are exposed to higher concentrations of NO• and its derivative RNS than cells in other tissues because of the limited distance of NO•diffusion determined by its half-life under biological conditions.

It is of interesting to see that, in contrast to the previously reported ~6-fold increases in ε-dA and ε-dC in the splenic DNA of the SJL/RcsX mice (Nair et al., 1998), only modest increases (~30%) in dX, dI and dU were observed in the current study. Similar moderate increases were also observed by the research group of Prof. Tannenbaum when quantifying nucleobase oxidation products in the same set of samples, which were small increases (<30%) in Sp and Gh, undetectable NI and Ox (< 1 lesion per 10^7 bases), and a decrease in 8-oxo-dG relative to the control (Yu et al., unpublished observations). Etheno dA was found to increase ~3-fold, but no change in M_1G was observed (Zhou et al., unpublished observations). These discrepancies can be better explained in terms of damage formation and repair in the context of the time course of disease progress.

An estimation of NO• production by activated macrophages in the spleen of SJL/RcsX mice will help to elucidate the formation of DNA damage. The urinary nitrate secretion that was

measured as an index of NO• production was found to increase ~35-fold to 0.70 μmol/gr/day by 12 days after RcsX tumor injection (gr here represents per gram of the body weight) (Gal et al., 1996). For the sake of simplicity, assuming that all urinary nitrate was from NO• produced in the RcsX spleen, then, the rate of NO• production by activated macrophages can be estimated as much as 3.5 pmol/s/10^6 cells. The estimation is based on the following facts. First, the average body weight of a male SJL mouse is ~25 g and the average spleen weight of a male SJL/RcsX mouse is ~1 g (communicate by Ms. Laura Trudel). Second, the rate of nitrate formation approximately equals to the rate of NO• production according to the NO• kinetics described in Chapter 3. Therefore, the rate of NO• production in the SJL/RcsX spleen could be estimated as much as 17.5 μmol/gr/day (gr here represents per gram of the spleen weight). Since activated macrophages that expressed iNOS only consisted < 5% of the RcsX spleen cell population (Gal et al., 1996), the localized NO• production by activated macrophages could be as high as 350 μmol/gr/day. Normally, one gram wet-weight of tissue contains approximately 1 x 10^9 cells (Advanced Biotechnology Inc, http://www.abionline.com/products/cellbio/default.htm). The rate of NO• production by activated macrophages in the RcsX spleen is therefore estimated to be 3.5 pmol/s/10^6 cells, which is ~3-5 folds higher than those reported by deRojas-Walker et al (deRojas-Walker et al., 1995) and Zhuang et al (Zhuang et al., 1998) in their studies of activated macrophage *in vitro*. However, considering the fact that spleen is not the only inflamed organ, the actual rate of NO• production by activated macrophages in the RcsX spleen could be close to the *in vitro* value. The estimation here, though not strictly rigorous, suggests that with such high level of NO•, significant increases in the nucleobase deamiantion products should occur according to *in vitro* results (deRojas-Walker et al., 1995). This prediction is also based on the *in vitro* kinetic analysis of the steady-state concentration of N_2O_3 (Dong et al., 2003). In bulk

reaction buffer, the quasi-steady state N_2O_3 concentration can be described by the following equation:

$$C_{N2O3} = \frac{2k_1 C_{NO}^2 C_{O2}}{k_3 + \sum_{i=4,5,6,7} k_i C_i}$$

where k_1 is the second-order rate constant for the reaction of NO• with O_2 (2.1×10^6 $M^{-2}s^{-1}$), C_{NO} and C_{O2} are the steady state NO• and O_2 concentrations, respectively, and k_3 through k_7 are the second-order rate constants for the reaction of N_2O_3 with water (1.6×10^3 $M^{-2}s^{-1}$), inorganic phosphate (6.4×10^4 $M^{-2}s^{-1}$), chloride (1.5×10^4 $M^{-2}s^{-1}$), bicarbonate (1.5×10^5 $M^{-2}s^{-1}$) and GSH (6.6×10^7 $M^{-2}s^{-1}$), respectively, all of which have been defined *in vitro* (Caulfield et al., 1996; Keshive et al., 1996; Lewis and Deen, 1994; Lewis et al., 1995). This model can be used to estimate the effects of various reaction species on the effective concentration of N_2O_3. With ~35-fold increases in NO• (Gal et al., 1996) and ~2-fold increases in GSH (Wright et al., unpublished results) in spleen of the SJL/RcsX mice, and assuming that the intracellular estimations for O_2, chloride, bicarbonate and inorganic phosphate are of 210 μM, 1.07 mM, 10 mM and 40 mM, respectively (Guyton and Hall, 2000) and keep constant, there would be an expected ~600-fold increases in the N_2O_3 concentration, thus, commensurate increases in the deamiantion products. However, we only observed a moderate increases (~30%), much lower than predicted. The lower than expected level of nitrosative DNA damage suggests the unappreciated complexity of nitrosative chemistry *in vivo*.

One possible factor that may contribute to this complexity is DNA repair. DNA damage determined here reflects a steady-state level resulting from both damage formation and damage repair. It is possible that substantial increases in dX, dI and dU occurred in the spleen of

SJL/RcsX mice, but significant repair of those lesions might take place simultaneously. Although NO• has indeed been shown to inactivate several DNA repair enzymes (Jaiswal et al., 2000; Liu et al., 2002; Wink et al., 1994), there is no evidence indicating that the RcsX spleen cells were DNA repair compromised. Further, Grishko et al. observed efficient repair of dI and dU in normal human fibroblasts (Grishko et al., 1999), suggesting that DNA repair cannot be ignored in interpreting the level of DNA damage ever measured.

Another possible explanation is that the moderate increases in the deamination products may merely reflect a lesion-dilution effect when using the whole organ for the DNA lesion analysis, but only a small fraction of cells analyzed have actually been affected by NO•. As discussed previously, localized production by a small subpopulation of cells suggest that gradients of NO• concentration would likely exist within tissues and the exposure that an individual target cell can experience would depend on its proximity to the generator cells. The formation of DNA damage cannot be expected to be uniformly distributed in the whole organ, which suggests that using the whole RcsX spleen to estimate the formation of DNA damage products as an index of the inflammatory progress may not be an appropriate move.

Chemistry of NO• leading to nucleobase deamination is different from what causes the formation of etheno DNA adducts. The former is governed by N_2O_3, while the latter is by reactive species derived from $ONOO^-$-mediated lipid peroxidation. In the SJL/RcsX spleen, one type of NO• chemistry may be predominant, causing the preferential formation of a certain type of DNA damage product(s). Generation of $ONOO^-$ in the SJL/RcsX model has been assumed by the presence of nitrotyrosine, a biomarker of $ONOO^-$ under physiological conditions (Gal et al., 1997). $ONOO^-$ has been reported to induce peroxidation of membrane lipids, leading to the formation of malondialdehyde (Radi et al., 1991) and *trans*-4-hydroxy-2-nonenal (HNE)

(Stepien et al., 2000) that are proposed to lead the formation of M_1G and etheno DNA adducts, respectively. M_1G was not detected in DNA isolated from the RcsX spleen possibly because of the detection limit of the analytical procedure (Chaudhary et al., 1994a; Chaudhary et al., 1994b) or due to a completely different formation pathway, which, in stead of via MDA, but base propenals as an alternative (communicated by Mr. Xinfeng Zhou). Etheno adducts of dA and dC were found to increase (Nair et al., 1998; Zhou et al., unpublished results), a results that was supported by a recent observation from the research groups of Profs. Marnett and Tannenbaum. They showed that in SJL/RcsX mice, $ONOO^-$ primed the cyclooxygenase function of prostglandin synthase *in vivo*, which in turn contributed to lipid peroxidation and subsequent formation of DNA etheno adducts (Marnett et al., 2000).

Given the hypothesis that DNA damage products in the SJL/RcsX mice arise as a result of $NO^{\bullet}$ overproduction, the amount of the damage should be closely associated with the progress of inflammation. A 6-fold increase in the ε-dA and ε-dC was detected in the RcsX spleen 14-day after tumor injection (Nair et al., 1998). We therefore speculated that the increase would not be that large in the 12-day spleen. Preliminary measurements performed by Mr. Xinfeng Zhou confirmed our speculation, showing a ~3-fold increase. We can further speculate that the levels of nucleobase deamination products will be higher in the 14-day RcsX spleen compared to those in the 12-day spleen. Gal et al. reported that intraperitoneal injection of RcsX cells into SJL mice led to rapid growth of the tumor cells and the B cells in the lymph nodes, spleen, and liver, resulting in morbidity 15 days later (Gal et al., 1996). This implies a sever deterioration in the condition of the SJL/RcsX mice 14 day after tumor injection. Careful pathological analyses of the inflammatory progress in the SJL/RcsX mice will help to define an appropriate time frame for the quantification of these DNA damage products.

It is also of interest to see that the formation rates of deamination products observed in the current study was larger than the age-dependent formation rates observed in the Aag mice studies (Appendix I). The ~30% increases in deamination products accumulated in 12 days in the SJL/RcsX mice was approximately equivalent to those accumulated in 6 months in the normal C57BL/6 mice (Appendix I), suggesting that NO$^{\bullet}$ accelerates the endogenous DNA damage. The integrity of DNA is one of the major features in the process of aging (Zahn and Blattner, 1987). Accumulation of DNA damage can lead to decreased mRN expression and protein production with a direct effect on cellular function (Nawrocki et al., 1992). Ames and co-work found the increased DNA damage rate in the short-living organisms with high metabolic rate, such as mice and rats (Ames, 1989; Ames et al., 1993). Several factors have been identified to contribute to the increase in DNA damage. In normal cells, cellular oxidation is a major contributor to endogenous DNA damage. The ubiquitous presence of ROS ensures that 8-oxo-dG exists in the DNA of all living organisms (Ames et al., 1993). In addition to that, abasic sites produced by spontaneous or enzymatic release of bases from DNA (Lindahl and Nyberg, 1972; Loeb and Preston, 1986) and exocyclic DNA adducts formed from products of lipid peroxidation (Ohshima et al., 1990) are also present in substantial amount. Another cause of the age-dependent increases in the DNA damage products is the reduced DNA repair capacity in senescent cells (Lovell et al., 2000; Robison et al., 1987). The premature aging expressed in Werner syndrome (WS) has been shown to be attributable to the lack of a DNA helicase that may function in DNA mismatch repair (Bennett et al., 1997). Functions of some cellular defense systems, including superoxide dismutase, glutathione peroxidase, and catalase, have been found to decline with age (Cand and Verdetti, 1989). Furthermore, changes in membrane fluidity and lipid peoxidation, in addition to the increased internal mitochondrial peroxidade formation, can

all contribute to the increase in DNA damage (Yu et al., 1992). NO· and its reactive species can participate in most of the above events (reviewed in Krabbe et al., 2004), suggesting that it is possible that inflammatory mediators constitute a link between life style factors, infections and physiological changes in the process of ageing on the one hand and risk factors for age-associated diseases on the other.

Finally, in the current studies, liver was designed as a control organ for the DNA damage analysis. However, we did not observe significant differences in terms of the formation of nucleobase deamination products between the RcsX liver and spleen. Therefore, we argue that liver may not be a suitable control. In the RcsX liver, iNOS expression was also observed in macrophages comprising metastatic islands (Gal et al., 1996). With the tumor progression, it is expected that more macrophages will be present in liver and these cells would result in the enhancement of inflammation. Kidney has been suggested to be a better control organ, since the rate of apoptosis and extent of nitrotyrosine staining were found to be unaffected in the kidneys of tumor-bearing animals, and the mutant frequency did not increase in the RcsX kidneys (Gal et al., 1997).

Collectively, these results together suggest that direct reaction of RNS with DNA in the SJL/RcsX model produces moderate increases in DNA damage products. The small increases may either due to the insignificant lesion formation, or to the substantial contribution of lesion repair. Either of these two possibilities suggests the direction for further study. In the former case, other DNA biomarkers such as the etheno adducts presumably derived from lipid peroxidation are worthy of further exploration; in the latter case, DNA repair kinetics needs to be

considered to provide a better understanding of DNA damage under pathological conditions associated with inflammation.

5.6 References

Ames, B. N.: Endogenous oxidative DNA damage, aging, and cancer. Free Radic Res Commun **7** (3-6): 121-8, 1989.

Ames, B. N., Shigenaga, M. K., and Hagen, T. M.: Oxidants, antioxidants, and the degenerative diseases of aging. Proc Natl Acad Sci U S A **90** (17): 7915-22, 1993.

Arnon, R.: Experimental allergic encephalomyelitis--susceptibility and suppression. Immunol Rev **55:** 5-30, 1981.

Asaka, M., Takeda, H., Sugiyama, T., and Kato, M.: What role does Helicobacter pylori play in gastric cancer? Gastroenterology **113** (6 Suppl): S56-60, 1997.

Balkwill, F., and Mantovani, A.: Inflammation and cancer: back to Virchow? Lancet **357** (9255): 539-45, 2001.

Behlke, M. A., Spinella, D. G., Chou, H. S., Sha, W., Hartl, D. L., and Loh, D. Y.: T-cell receptor beta-chain expression: dependence on relatively few variable region genes. Science **229** (4713): 566-70, 1985.

Bennett, S. E., Umar, A., Oshima, J., Monnat, R. J., Jr., and Kunkel, T. A.: Mismatch repair in extracts of Werner syndrome cell lines. Cancer Res **57** (14): 2956-60, 1997.

Cand, F., and Verdetti, J.: Superoxide dismutase, glutathione peroxidase, catalase, and lipid peroxidation in the major organs of the aging rats. Free Radic Biol Med **7** (1): 59-63, 1989.

Caulfield, J. L., Singh, S. P., Wishnok, J. S., Deen, W. M., and Tannenbaum, S. R.: Bicarbonate inhibits N-nitrosation in oxygenated nitric oxide solutions. J Biol Chem **271** (42): 25859-63, 1996.

Chaudhary, A. K., Nokubo, M., Marnett, L. J., and Blair, I. A.: Analysis of the malondialdehyde-2'-deoxyguanosine adduct in rat liver DNA by gas chromatography/electron capture negative chemical ionization mass spectrometry. Biol Mass Spectrom **23** (8): 457-64, 1994a.

Chaudhary, A. K., Nokubo, M., Reddy, G. R., Yeola, S. N., Morrow, J. D., Blair, I. A., and Marnett, L. J.: Detection of endogenous malondialdehyde-deoxyguanosine adducts in human liver. Science **265** (5178): 1580-2, 1994b.

Dedon, P. C., and Tannenbaum, S. R.: Reactive nitrogen species in the chemical biology of inflammation. Arch Biochem Biophys **423** (1): 12-22, 2004.

deRojas-Walker, T., Tamir, S., Ji, H., Wishnok, J. S., and Tannenbaum, S. R.: Nitric oxide induces oxidative damage in addition to deamination in macrophage DNA. Chem Res Toxicol **8** (3): 473-7, 1995.

Dong, M., Wang, C., Deen, W. M., and Dedon, P. C.: Absence of 2'-deoxyoxanosine and presence of abasic sites in DNA exposed to nitric oxide at controlled physiological concentrations. Chem Res Toxicol **16** (9): 1044-55, 2003.

Ebert, M. P., Yu, J., Sung, J. J., and Malfertheiner, P.: Molecular alterations in gastric cancer: the role of Helicobacter pylori. Eur J Gastroenterol Hepatol **12** (7): 795-8, 2000.

Fitzgerald, K. L., and Ponzio, N. M.: Natural killer cell activity in reticulum cell sarcomas (RCS) of SJL/J mice. Cell Immunol **43** (1): 185-91, 1979.

Gal, A., Tamir, S., Kennedy, L. J., Tannenbaum, S. R., and Wogan, G. N.: Nitrotyrosine formation, apoptosis, and oxidative damage: relationships to nitric oxide production in SJL mice bearing the RcsX tumor. Cancer Res **57** (10): 1823-8, 1997.

Gal, A., Tamir, S., Tannenbaum, S. R., and Wogan, G. N.: Nitric oxide production in SJL mice bearing the RcsX lymphoma: a model for in vivo toxicological evaluation of NO. Proc Natl Acad Sci U S A **93** (21): 11499-503, 1996.

Gal, A., and Wogan, G. N.: Mutagenesis associated with nitric oxide production in transgenic SJL mice. Proc Natl Acad Sci U S A **93** (26): 15102-7, 1996.

Grishko, V. I., Druzhyna, N., LeDoux, S. P., and Wilson, G. L.: Nitric oxide-induced damage to mtDNA and its subsequent repair. Nucleic Acids Res **27** (22): 4510-6, 1999.

Guyton, A. C., and Hall, J.: Textbook of Medical Physiology, Saunders, Philadelhia, 2000.

Jaiswal, M., LaRusso, N. F., Burgart, L. J., and Gores, G. J.: Inflammatory cytokines induce DNA damage and inhibit DNA repair in cholangiocarcinoma cells by a nitric oxide-dependent mechanism. Cancer Res **60** (1): 184-90, 2000.

Katz, I. R., Chapman-Alexander, J., Jacobson, E. B., Lerman, S. P., and Thorbecke, G. J.: Growth of SJL/J-derived transplantable reticulum cell sarcoma as related to its ability to induce T-cell proliferation in the host. III. Studies on thymectomized and congenitally athymic SJL mice. Cell Immunol **65** (1): 84-92, 1981.

Keshive, M., Singh, S., Wishnok, J. S., Tannenbaum, S. R., and Deen, W. M.: Kinetics of S-nitrosation of thiols in nitric oxide solutions. Chem Res Toxicol **9** (6): 988-93, 1996.

Krabbe, K. S., Pedersen, M., and Bruunsgaard, H.: Inflammatory mediators in the elderly. Exp Gerontol **39** (5): 687-99, 2004.

Lasky, J. L., and Thorbecke, G. J.: Growth requirements of SJL lymphomas in vitro: effect of BCGF II. Adv Exp Med Biol **237**: 145-53, 1988.

Lewis, R. S., and Deen, W. M.: Kinetics of the reaction of nitric oxide with oxygen in aqueous solutions. Chem Res Toxicol **7** (4): 568-74, 1994.

Lewis, R. S., Tamir, S., Tannenbaum, S. R., and Deen, W. M.: Kinetic analysis of the fate of nitric oxide synthesized by macrophages in vitro. J Biol Chem **270** (49): 29350-5, 1995.

Lindahl, T., and Nyberg, B.: Rate of depurination of native deoxyribonucleic acid. Biochemistry **11** (19): 3610-8, 1972.

Liu, L., Xu-Welliver, M., Kanugula, S., and Pegg, A. E.: Inactivation and degradation of O(6)-alkylguanine-DNA alkyltransferase after reaction with nitric oxide. Cancer Res **62** (11): 3037-43, 2002.

Loeb, L. A., and Preston, B. D.: Mutagenesis by apurinic/apyrimidinic sites. Annu Rev Genet **20**: 201-30, 1986.

Lovell, M. A., Xie, C., and Markesbery, W. R.: Decreased base excision repair and increased helicase activity in Alzheimer's disease brain. Brain Res **855** (1): 116-23, 2000.

Marnett, L. J., Wright, T. L., Crews, B. C., Tannenbaum, S. R., and Morrow, J. D.: Regulation of prostaglandin biosynthesis by nitric oxide is revealed by targeted deletion of inducible nitric-oxide synthase. J Biol Chem **275** (18): 13427-30, 2000.

Murphy, E. D.: Transplantation behavior of Hodgkin's-like reticulum cell neoplasms of strain SJL-J mice and results of tumor reinoculation. J Natl Cancer Inst **42** (5): 797-807, 1969.

Nair, J., Gal, A., Tamir, S., Tannenbaum, S. R., Wogan, G. N., and Bartsch, H.: Etheno adducts in spleen DNA of SJL mice stimulated to overproduce nitric oxide. Carcinogenesis **19** (12): 2081-4, 1998.

Nawrocki, J., Elcioglu, M., Ghoraba, H., and Gabel, V. P.: [The role of vitrectomy in the treatment of retinal detachment with macular holes]. Klin Oczna **94** (2-3): 66-8, 1992.

Ohshima, H., Bandaletova, T. Y., Brouet, I., Bartsch, H., Kirby, G., Ogunbiyi, F., Vatanasapt, V., and Pipitgool, V.: Increased nitrosamine and nitrate biosynthesis mediated by nitric oxide synthase induced in hamsters infected with liver fluke (Opisthorchis viverrini). Carcinogenesis **15** (2): 271-5, 1994.

Ohshima, H., and Bartsch, H.: Chronic infections and inflammatory processes as cancer risk factors: possible role of nitric oxide in carcinogenesis. Mutat Res **305** (2): 253-64, 1994.

Ohshima, H., Friesen, M., Brouet, I., and Bartsch, H.: Nitrotyrosine as a new marker for endogenous nitrosation and nitration of proteins. Food Chem Toxicol **28** (9): 647-52, 1990.

Ohshima, H., Tatemichi, M., and Sawa, T.: Chemical basis of inflammation-induced carcinogenesis. Arch Biochem Biophys **417** (1): 3-11, 2003.

Ponzio, N. M., and Thorbecke, G. J.: Requirement for reverse immune surveillance for the growth of germinal center-derived murine lymphomas. Semin Cancer Biol **10** (5): 331-40, 2000.

Radi, R., Beckman, J. S., Bush, K. M., and Freeman, B. A.: Peroxynitrite-induced membrane lipid peroxidation: the cytotoxic potential of superoxide and nitric oxide. Arch Biochem Biophys **288** (2): 481-7, 1991.

Robison, S. H., Munzer, J. S., Tandan, R., and Bradley, W. G.: Alzheimer's disease cells exhibit defective repair of alkylating agent-induced DNA damage. Ann Neurol **21** (3): 250-8, 1987.

Rosenberg, N. L., and Kotzin, B. L.: Aberrant expression of class II MHC antigens by skeletal muscle endothelial cells in experimental autoimmune myositis. J Immunol **142** (12): 4289-94, 1989.

Shacter, E., and Weitzman, S. A.: Chronic inflammation and cancer. Oncology (Huntingt) **16** (2): 217-26, 229; discussion 230-2, 2002.

Stepien, K., Wilczok, A., Zajdel, A., Dzierzega-Lecznar, A., and Wilczok, T.: Peroxynitrite mediated linoleic acid oxidation and tyrosine nitration in the presence of synthetic neuromelanins. Acta Biochim Pol **47** (4): 931-40, 2000.

Tamir, S., deRojas-Walker, T., Gal, A., Weller, A. H., Li, X., Fox, J. G., Wogan, G. N., and Tannenbaum, S. R.: Nitric oxide production in relation to spontaneous B-cell lymphoma and myositis in SJL mice. Cancer Res **55** (19): 4391-7, 1995.

Thorbecke, G. J., and Ponzio, N. M.: Reverse immune surveillance: an adaptive mechanism used by tumor cells to facilitate their survival and growth. Semin Cancer Biol **10** (5): 327-30, 2000.

Tsiagbe, V. K., Asakawa, J., Miranda, A., Sutherland, R. M., Paterson, Y., and Thorbecke, G. J.: Syngeneic response to SJL follicular center B cell lymphoma (reticular cell sarcoma) cells is primarily in V beta 16+ CD4+ T cells. J Immunol **150** (12): 5519-28, 1993a.

Tsiagbe, V. K., Nicknam, M. H., Fattah, D., and Thorbecke, G. J.: IL-5 responsive subsets among normal and lymphomatous murine B cells. Ann N Y Acad Sci **651**: 270-3, 1992.

Tsiagbe, V. K., Yoshimoto, T., Asakawa, J., Cho, S. Y., Meruelo, D., and Thorbecke, G. J.: Linkage of superantigen-like stimulation of syngeneic T cells in a mouse model of follicular center B cell lymphoma to transcription of endogenous mammary tumor virus. Embo J **12** (6): 2313-20, 1993b.

Wink, D. A., Nims, R. W., Darbyshire, J. F., Christodoulou, D., Hanbauer, I., Cox, G. W., Laval, F., Laval, J., Cook, J. A., Krishna, M. C., and et al.: Reaction kinetics for nitrosation of cysteine and glutathione in aerobic nitric oxide solutions at neutral pH. Insights into the fate and physiological effects of intermediates generated in the NO/O2 reaction. Chem Res Toxicol **7** (4): 519-25, 1994.

Yu, B. P., Suescun, E. A., and Yang, S. Y.: Effect of age-related lipid peroxidation on membrane fluidity and phospholipase A2: modulation by dietary restriction. Mech Ageing Dev **65** (1): 17-33, 1992.

Zahn, K., and Blattner, F. R.: Direct evidence for DNA bending at the lambda replication origin. Science **236** (4800): 416-22, 1987.

Zhuang, J. C., Lin, C., Lin, D., and Wogan, G. N.: Mutagenesis associated with nitric oxide production in macrophages. Proc Natl Acad Sci U S A **95** (14): 8286-91, 1998.

Chapter 6

Development of Enzymatic Probes to Analyze DNA Damage Caused by Reactive Nitrogen Species

6.1 Abstract

Chronic inflammation has long been recognized as a risk factor for the development of a variety of human cancers. One possible connection between inflammation and cancer involves unregulated production of the ubiquitous and physiologically important nitric oxide ($NO^{\bullet}$) that leads to high levels of derivative reactive nitrogen species (RNS) that may be involved in pathological processes, including carcinogenesis. In particular, macrophages activated as part of the inflammatory process produce large quantities of $NO^{\bullet}$ that lead to the formation of nitrosoperoxynitrite ($ONOOCO_2^-$), a strongly oxidizing species that selectively oxidizes guanine bases in DNA, and nitrous anhydride (N_2O_3), a powerful nitrosating agent capable of causing nucleobase deamination in DNA. Given the presence of both $ONOOCO_2^-$ and N_2O_3 at sites of inflammation, it is possible that both oxidative and nitrosative DNA damage occur and either give rise to mutations directly or cause mutations as a result of increased cell turnover rates. To define the role of these different types of DNA damage in inflammation-mediated cancer, we have set out to develop analytical methods for oxidative and nitrosative DNA lesions. Here we sought to develop enzymatic probes for oxidative and nitrosative DNA lesions as a complement to the LC-MS methods developed in other chapters of this thesis. These probes would not only allow differential quantification of the two types of DNA damage, but would also allow the lesions to be mapped in any DNA sequence by coupling their activity with the technique of ligation-mediated PCR.

The development of enzymatic probes here focused on two groups of DNA glycosylase repair enzymes from *Escherichia coli,* one with activity against oxidative DNA damage (formamidopyrimidine DNA glycosylase, Fpg; endonuclease III, EndoIII) and the other with

activity against nucleobase deamination products (uracil DNA glycosylase, UDG; endonuclease V, EndoV; alkyladenine DNA glycosylase, AlkA). The experiments began by treating supercoiled plasmid pUC19 DNA with $ONOO^-$ by bolus addition or with N_2O_3 in the Silastic tubing-based $NO^{\bullet}/O_2$ delivery system described in Chapter 3 of this thesis. The level of damage was optimized to avoid exceeding one damage event per plasmid molecule, as judged by glycosylase activity and complementary analytical methods. The damaged DNA was then treated with varying amounts of each group of glycosylases and the quantity of base damage was calculated by plasmid topoisomer analysis. Results of the plasmid topoisomer studies were further validated by LC-MS analysis. Collectively, the results indicate that a combination of *E.coli* AlkA, Endo V and UDG react selectively with DNA containing only nitrosative damage, while *E. coli* Fpg and EndoIII react selectively with DNA containing oxidative base lesions caused by nitrosoperoxycarbonate. These results suggest that these enzyme combinations can be used as probes of DNA damage to define the location and quantity of the oxidative and nitrosative lesions associated with inflammation in humans.

6.2 Introduction

Chronic inflammation has long been recognized as a risk factor for the development of a variety of human cancers (Cassell, 1998; Ohshima and Bartsch, 1994). Numerous inflammatory mediators have been implicated in the link between chronic inflammation and carcinogenesis; current information strongly suggests that nitric oxide ($NO^{\bullet}$) is one such mediator (Felley-Bosco, 1998). Unregulated production of this ubiquitous and physiologically important molecule leads to high levels of derivative reactive nitrogen species (RNS) that may be involved in pathological processes, including carcinogenesis. In particular, macrophages activated as part of the inflammatory process produce large quantities of both $NO^{\bullet}$ ands peroxide that, in the presence of carbon dioxide, react to form nitrosoperoxycarbonate ($ONOOCO_2^-$), a strongly oxidizing species that selectively oxidizes guanine bases in DNA (Burney et al., 1999a; Dedon and Tannenbaum, 2004; Tamir et al., 1996). $NO^{\bullet}$ can also react with molecular oxygen (O_2) to form nitrous anhydride (N_2O_3), a powerful nitrosating agent capable of causing nucleobase deamination in DNA (Burney et al., 1999a; Dedon and Tannenbaum, 2004; Tamir et al., 1996). The DNA damage produced by these two genotoxins has been widely studies *in vitro* (Burney et al., 1999b; Tamir and Tannenbaum, 1996; Tretyakova et al., 1999). In addition to G-G cross-links, $NO^{\bullet}$-derived N_2O_3 causes nitrosative deamination of G to produce xanthine and oxanine; of C to produce uracil; and of A to yield hypoxanthine (Burney et al., 1999b; Caulfield et al., 2003; Suzuki et al., 1996; Tamir et al., 1996). $ONOOCO_2^-$ produces oxidative base lesions including 8-oxo-2'-deoxyguanosine (8-oxo-dG), cyanuric acid, oxazolone, nitroimidazole and oxaluric acid (Burney et al., 1999a; Dedon and Tannenbaum, 2004; Tamir et al., 1996).

In light of the deficiency in the knowledge of a broad quantitative lesion spectrum potentially present at sites of inflammation, we first developed sensitive LC-MS methods to define the predominant DNA damage produced by RNS (Dedon and Tannenbaum, 2004; Dong et al., 2003). The genome-wide DNA lesion levels, however, provide little information about the location of DNA lesions in critical genes, information that can be correlated with the locations and frequencies of mutations associated with cancer. To this end, we sought to develop enzymatic probes that could be used to differentially map these two types of DNA damage in human genes using ligation-mediated polymerase chain reaction (LMPCR). This technique is one the most successful methods for localizing DNA lesions in any DNA sequence and it involves conversion of base lesions to strand breaks that are mapped by PCR following ligation of a common linker sequence containing a PCR primer site (Pfeifer et al., 1998; Pfeifer et al., 1993; Wu et al., 1999; Xu et al., 1998). To goal of the work in this chapter was to develop DNA glycosylases as probes of oxidative and nitrosative DNA damage in DNA exposed to $ONOOCO_2^-$ and N_2O_3.

DNA glycosylases, first reported by Lindahl (1974), catalyze the scission of the glycosidic bond releasing damaged or mispaired bases as the first step of the base excision repair pathway (Dianov and Lindahl, 1994; Lindahl, 1974). Removal of damaged bases by a DNA glycosylase is generally associated with a specific type of damage. The specificity of DNA glycosylases, however, may also cross over to different types of DNA damage. Two groups of DNA repair enzymes from *Escherichia coli* were carefully chosen for this study. One includes formanidopyrimidine-DNA glycosylase (Fpg) and endonuclease III (Endo III) that have reported activities with oxidative DNA damage (reviewed in Izumi et al., 2003). Fpg was first shown to recognize the purines with an opened imidazole ring (Izumi et al., 2003). Subsequently, the

excision of 4,6-diamino-5-formamidopyrimidine (FapyAde) from γ-irradiated polydeoxynucleotides of adenine has been demonstrated (Breimer, 1984). Fpg also excises 8-oxodG and pyrimidine-derived lesions such as 5-hydroxycytosine and 5-hydroxyuracil from small duplex oligodeoxynucleotides with a single lesion embedded at a specific position (Tchou et al., 1991; Wallace, 1998). Besides the DNA glycosylase activity, Fpg possesses an AP-lyase activity on AP-sites by a β-δ-elimination mechanism and an activity excising 5'-terminal deoxyribose phosphate (dRpase) (Bailly et al., 1989a; Bailly et al., 1989b; Gilboa et al., 2002; Graves et al., 1992; O'Connor and Laval, 1989). Endo III is also endowed with both N-glycosylase and AP lyase activities (Cunningham et al., 1989). Endo III exhibits broad substrate specificity for cytosine- and thymine-derived lesions in DNA (reviewed in Gros et al., 2002). The substrates are thymine glycol, 5-hydroxycytosine and 5-hydroxyuracil, uracil glycol, 5,6-dihydroxycytosine etc. (Wallace, 1998).

The other group is comprised of endonuclease V (EndoV), alkyladenine DNA glycosylase (AlkA), and uracil DNA glycosylase (UDG), all of which have been reported to recognize various deamination products (Kow, 2002). EndoV was first identified as a promiscuous activity that recognized DNA heavily damaged by osmium tetroxide (Demple and Linn, 1982). It has been shown to be a major enzyme that recognizes hypoxanthine (Yao et al., 1994; Yao and Kow, 1995). In addition to hypoxanthine, the enzyme also recognizes a wide spectrum of DNA lesions and structures, including xanthine, base mismatches, AP sites, hairpins, unpaired loops, and pseudo-Y and flap structures (He et al., 2000; Yao et al., 1994; Yao and Kow, 1994; Yao and Kow, 1995). AlkA from *E. coli* is induced in response to DNA alkylation (Evensen and Seeberg, 1982; Nakabeppu et al., 1984a; Nakabeppu et al., 1984b; Samson and Cairns, 1977). AlkA has a very broad substrate range, catalyzing the excision of N-3 and N-7 alkyl purines as well as O^2-

alkyl pyrimidines (Bjelland et al., 1994; Bjelland et al., 1993). In addition to these common alkyl adducts, AlkA has also been shown to excise the cyclic etheno adducts of dA and εdC (Saparbaev et al., 1995; Saparbaev and Laval, 1994). Hypoxanthine was shown to be also released by AlkA (Saparbaev and Laval, 1994). Recent studies have demonstrated that AlkA can also recognize both xanthine and oxanine (Masaoka et al., 1999; Terato et al., 2002). UDG is a ubiquitous enzyme and highly expressed in almost all cells (Pearl, 2000). In addition to uracil, UDG also recognizes other modified bases, including 5-fluorouracil, 5-OH-Ura, and 5,6-dihydroxyuracil (Zastawny et al., 1995). UDG and AlkA leave abasic sites in DNA that are in turn processed by endonucleases cleaving the phosphodiester backbone hydrolytically at these sites (Dianov and Lindahl, 1994).

DNA repair enzymes have long been used as probes of DNA damage (Epe et al., 1996; Kuipers and Lafleur, 1998; Moe et al., 2003). In most instances, the enzymes are used to recognize and remove specific types of substrate DNA lesions, which results in the formation of single-strand breaks or abasic sites that could be converted to single-strand breaks. The resulting strand breaks can be very sensitively quantified by a variety of techniques such as alkaline elution (Epe and Hegler, 1994), alkaline unwinding (Hartwig et al., 1996), single-cell gel electrophoresis (comet assay) (Collins et al., 1993; Hininger et al., 2004; Pouget et al., 2000; Sauvaigo et al., 2002), nick translation (Czene and Harms-Ringdahl, 1995), and the plasmid relaxation assay (Kennedy et al., 1997). When several repair enzymes are used in parallel, DNA damage profiles are obtained. These profiles can serve as fingerprints of the ultimate DNA damaging species, thus providing evidence to identify the species responsible for the damage. Additional advantage of using glycosylases as probes of DNA damage is that DNA glycosylases

are active in the presence of EDTA and function independent of any complex that may form *in vivo*.

In this study, supercoiled plasmid pUC19 DNA was first treated with $ONOO^-$ by bolus addition or with N_2O_3 in the Silastic tubing-based $NO^{\bullet}/O_2$ delivery system described in Chapter 3 of this thesis. DNA damage profiles induced by $ONOO^-$ and $NO^{\bullet}$ were obtained after treatment with each group of enzymes and validated by LC-MS analysis. Our results indicate that a combination of *E.coli* AlkA, Endo V and UDG react selectively with DNA exposed to $NO^{\bullet}$, while *E. coli* Fpg reacts selectively with DNA treated with nitrosoperoxycarbonate.

6.3 Materials and Methods

Materials. All chemicals and reagents were of highest purity available and were used without further purification unless noted otherwise. Agarose was purchased from Sigma Chemical Co. (St. Louis, MO). Plasmid pUC19 was obtained from DNA Technologies Inc. (Gaithersburg, MD). Fpg, Endo III, and Endo V were purchased from Trevigen (Gaithersburg, MD). UDG was purchased from USB Corporation (Cleveland, Ohio). AlkA was obtained from two different sources: BD-PharMingen (San Diego, CA) and a generous gift from Dr. Thomas Ellenberger, Harvard Medical School.

Synthesis of Peroxynitrite. Peroxynitrite was synthesized by ozonolysis of sodium azide as described by Pryor et al. (Pryor et al., 1995). Briefly, ozone generated in a Welsbach ozonator (5% ozone in oxygen; 100 mL/min) was bubbled into 100 ml of 0.1 M sodium azide (pH adjusted to 12 with 1 N NaOH) chilled in an ice bath chilled to 0-4°C. Ozonation was generally terminated after 45 min and $ONOO^-$ concentration was determined spectrophotometrically in 0.1 N NaOH (ε_{302}=1670 M^{-1} cm^{-1}). $ONOO^-$ was further characterized for its ability to cause the nitration of L-tyrosine using a method first described by Beckman et al (Beckman et al., 1992) and latter modified by Pryor et al. (Pryor et al., 1995).

Treatment of pUC19 Plasmid DNA with Peroxynitrite. The plasmid DNA stock solution (1 mg/mL in Chelex-treated 150 mM potassium phosphate, 25 mM sodium bicarbonate, pH 7.4) was dialyzed three-times against the same buffer at 4 °C. A stock solution of $ONOO^-$ was diluted with 0.1 N NaOH and added at ambient temperature under vigorous stirring to this DNA

solution. The final $ONOO^-$ concentrations ranged from 0.1 to 100 μM. In all cases, the pH of the reaction mixtures did not increase above 7.4. After treatment, samples were routinely left at ambient temperature for 30 min before damage analysis. For the 100 μM $ONOO^-$ concentration, LC-MS analysis was also performed to check the formation of nucleobase deamination products. In the control group, an aliquot of $ONOO^-$ solution was added to phosphate buffer and incubated for 3 min at ambient temperature to ensure complete decomposition before adding into the DNA solution ($ONOO^-$ half-life under these conditions is ~ 1 s (Beckman et al., 1994)).

Exposure of pUC19 Plasmid DNA to N_2O_3. pUC19 DNA was exposed to $NO^\bullet$ delivered by a novel system as described previously (Dong et al., 2003). Briefly, 120 mL of plasmid DNA (20 μg/mL in Chelex-treated 150 mM potassium phosphate, 25 mM sodium bicarbonate, pH 7.4) was added into the chamber of the $NO^\bullet$ delivery system and into a duplicate chamber in which Argon gas was infused (instead of $NO^\bullet$) as a control. At different time points, 3 mL of reaction mixture was withdrawn from the chamber through a connected syringe. An equal volume of fresh buffer was immediately added and DNA was recovered by ethanol precipitation.

Enzyme Reactions with Damaged Plasmid DNA. After $ONOO^-$ or N_2O_3 treatment, a portion (200 ng) of the DNA was treated with putrescine (100 mM, pH 7.0, 1 hr, 37°C) to cleave abasic sites. Another portion (200 ng) was kept on ice as a control to measure direct strand breaks. The remainder of the DNA was used in the glycosylase-hased damage recognition assays as follows. To 18 μL of $ONOO^-$-treated DNA (400 ng) was added 2 μL of one of the corresponding concentrated reaction buffers: (A) 10 mM Tris-HCl (pH 7.5), 1 mM EDTA and 100 mM NaCl; (B) 10 mM Tris-HCl (pH 7.5), 2 mM $CaCl_2$ and 1 mM EDTA; (C) 10 mM Tris-HCl (pH 7.5), 2

mM $MgCl_2$; (D) 20 mM Tris-HCl (pH 8.0), 1 mM EDTA and 1 mM dithiothreitol; (E) 50 mM HEPES-KOH (pH 7.5), 1 mM EDTA and 5 mM 2-mercaptoethanol. The enzyme reaction was initiated by addition of 1 μL of one of the following enzymes: Fpg (1.5 Units), Endo III (3 Units), Endo V (3 Units), UDG (5 Units), and AlkA (300 ng), followed by incubation for 1 hr at 37 °C. The DNA was used directly in subsequent analyses.

Quantification of DNA Damage by a Plasmid Nicking Assay.

The enzyme-treated DNA was redissolved in H_2O and subjected to plasmid nicking assay as follows. The quantity of DNA in each band was determined by fluorescence imaging (Uiltra-Lum, Clarmont, CA). The average number of single strand breaks (SSBs) per plasmid was determined using the intensity values in equation (1):

$$\text{SSB/Plasmid} = -\ln[1.4 \bullet SC/(1.4 \bullet SC + OC)] \quad (1)$$

where SC and OC represent the intensities of the supercoiled (type I) and open circular (type II) forms of plasmid DNA, respectively (Figure1). A correction factor of 1.4 for SC DNA is used because the incorporation of ethidium bromide into SC DNA is lower than that into OC DNA (Hegler et al., 1993; Shubsda et al., 1997). At high concentrations of $ONOO^-$, a band of to linear plasmid was evident and in all cases, this signal was added to the OC value.

Quantification of DNA Nucleobase Deamination by LC-MS Analysis. Nucleobase deamination products in pUC19 plasmid DNA exposed to $ONOO^-$ or N_2O_3 were quantitatively determined by the LC-MS method published previously (Dong et al., 2003). Briefly, 50 μg of DNA was hydrolyzed to deoxynucleosides by a combination of three enzymes (nuclease P1,

phosphodiesterase I, and alkaline phosphatase) in the presence of an appropriate amount of isotope-labeled internal standard and an adenosine deaminase inhibitor, coformycin. The resulting deoxynucleoside mixture was resolved by HPLC and the fractions containing 2'-deoxyxanthosine (dX), 2'-deoxyinosine (dI) and 2'-deoxyuridine (dU) were collected for LC-MS quantification.

6.4. Results

Enzyme Recognition of Lesions in $ONOOCO_2^-$ modified Plasmid DNA. To assess the utility of DNA repair enzymes as probes of $ONOOCO_2^-$-induced DNA damage, exposed plasmid DNA was treated with each of the enzymes and the formation of enzyme-induced strand breaks was quantified by a plasmid-nicking assay. This assay is a widely used technique that has the demonstrated ability to reveal cleavage of DNA by a variety of reagents (Breimer and Lindahl, 1985; Epe et al., 1996; Kuipers and Lafleur, 1998). One single-strand break in supercoiled DNA results in conversion to an open circular form that migrates more slowly than the supercoiled form in an agarose matrix as shown in Figure 1.

Figure 1. Example of glycosylase recognition of plasmid DNA damaged by $ONOO^-$ in the plasmid nicking assay. $ONOO^-$-treated plasmid DNA was reacted with Fpg to convert base lesions and abasic sites to strand breaks. $ONOO^-$ concentrations are in half-log steps, ranging from 0.1 to 100 μM. First lane contains the control. SC represents the supercoiled form of plasmid DNA. OC represents the open circular form.

One important facet of these studies was the identification of optimal reaction conditions for the various enzymes. To define optimal Fpg concentrations, pUC19 plasmid DNA was treated with 10 μM $ONOO^-$ to generate oxidative damage and the extent of Fpg cleavage was quantified

using the plasmid-nicking assay. As shown in Figure 2, the reaction of Fpg was saturated at 1 Unit / 400 ng DNA. Based on this result, we chose 1.5 Units / 400 ng DNA as the amount of Fpg used for the analysis to guarantee the complete removal of its substrate base modifications. Similar verifications were performed with the other repair endonucleases and DNA glycosylases: Endo III, 3 units; Endo V, 3 units; AlkA, 300 ng; and UDG, 5 units.

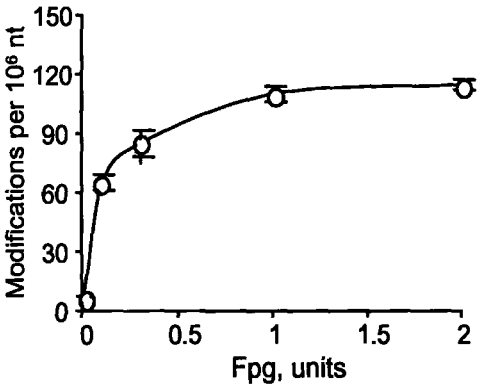

Figure 2. Optimization of Fpg concentration in reactions of $ONOOCO_2^-$-treated (10 _M) plasmid DNA. Data represent mean ± SD for three independent experiments.

Having optimized the enzyme concentrations, we proceeded to examine the recognition of $ONOOCO_2^-$-induced DNA damage by Fpg and the other enzymes. As shown in Figure 3, there is dose-dependent increase in direct strand breaks and, to a larger extent, Fpg-sensitive modifications, with the latter reaching a plateau. A similarly shaped curve has been reported previously (Tretyakova et al., 2000a). For both $ONOO^-$ and $NO^{\bullet}$ exposure, the formation of strand breaks was studied over a broad range of DNA damage frequencies. However, meaningful interpretation can only be achieved for damage occurring under single-hit conditions,

which corresponds to ~60 strand breaks in 10^6 nucleotides of pUC19 (2686 bp) according to a Poisson distribution (Dedon et al., 1993). The range beyond "single-hit conditions" requires adjustment of the damage frequency to avoid underestimation of the number of strand breaks, since additional nicks in an already nicked plasmid cannot be detected by topoisomer analysis.

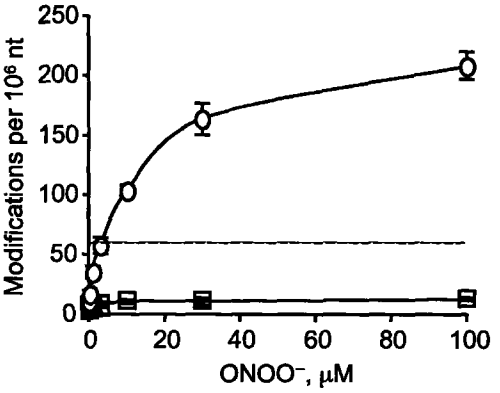

Figure 3. Direct strand breaks (□) and modifications sensitive to Fpg protein (○) induced by $ONOOCO_2^-$ in pUC19 DNA. Concentrations of $ONOO^-$ ranged from 0.1 μM to 100 μM (half-log steps). Data represent mean ± S.D. for 4-9 measurements. Data points lying above 60 strand breaks per 10^6 nt (dotted line) fall outside "single-hit" conditions (see the text for details).

Fpg protein recognizes a significant amount of modification in $ONOO^-$-treated pUC19 plasmid DNA, but other DNA repair enzymes do not, as shown in Figure 4. Under the assay conditions used, AlkA, Endo V and UDG detected almost the same degree of modification, while Endo III treatment revealed slightly more. There is an observed increase in modification after treatment with repair enzymes tested here. The increase was probably due to the presence of abasic sites that are sensitive to putrescine cleavage. It has been shown that $ONOO^-$ causes

the formation of 8-nitro-2'-deoxyguanosine (8-nitro-dG) that can quickly depurinate to form an abasic site (Tretyakova et al., 2000a; Yermilov et al., 1995). The small number of strand breaks caused by AlkA, Endo V, and UDG do not represent nucleobase deamination products, given the lack of detectable increase in dX, dI, and dU by the LC-MS quantification as shown in Figure 5. This suggests that nucleobase deamination is not predominant in the damage profile of pUC19 by $ONOO^-$. The slight increase in Endo III-sensitive sites with increasing $ONOO^-$ dose indicates the possible presence of a small percentage of pyrimidine oxidative products in the $ONOO^-$-treated pUC19 plasmid DNA.

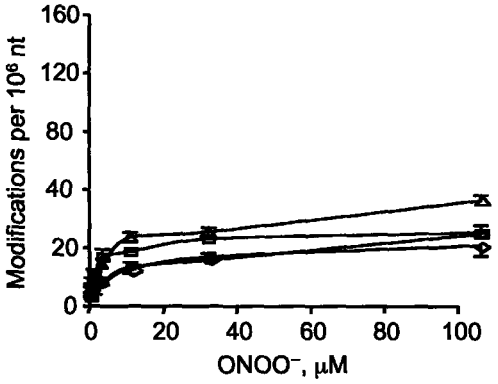

Figure 4. The quantity of $ONOOCO_2^-$-induced DNA damage sensitive to Endo III (Δ), Endo V (O), AlkA (), and UDG (◊) proteins. The concentrations of $ONOO^-$ ranged from 0.1 μM to 100 μM (half-log steps). Data represent mean ± S.D. for 4-9 measurements.

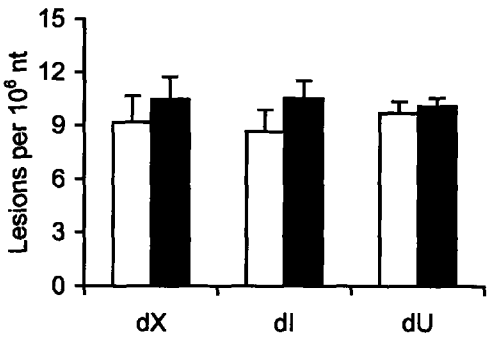

Figure 5. Levels of dX, dI and dU in pUC19 treated with 10 μM $ONOO^-$ as detected by LC-MS. Empty bar represents the controls; solid bar represents $ONOO^-$-treated pUC19 19. Data represent mean ± SD for three independent experiments.

DNA Damage Profile by NO•. NO• has been shown to cause the formation of nucleobase deamination products through nitrosative chemistry in the presence of oxygen (Dong et al., 2003). The *in vitro* spectrum of nitrosative DNA lesions by NO• that we have proposed includes approximately equal amounts of dX, dI and dU, about 6-fold fewer abasic sites, about 10-fold fewer dG-dG cross-links and no detectable dO (Dong et al., 2003). In these studies, uracil DNA glycosylase was used to verify the precision of the LC-MS assay for the detection of dU. A high correlation was found between the LC-MS method and the plasmid nicking assay in determining the quantity of dU. The purpose of the current study was to find a DNA repair enzyme that could effectively remove dX and dI from DNA molecules following NO• exposure.

AlkA has been shown to excise hypoxanthine from DNA (Saparbaev and Laval, 1994). Studies by our group and other groups have demonstrated that it also removes xanthine from DNA (Terato et al., 2002; Wuenschell et al., 2003). To confirm that AlkA can effectively

remove both dI and dX from NO• treated pUC19 plasmid DNA, we compared the detection of AlkA-sensitive modifications by the plasmid-nicking assay with the quantity of dX and dI as determined by LC-MS.

Figure 6 shows a strong correlation between the quantity of dX and dI detected by the LC-MS method and the number of the AlkA-sensitive modifications quantified by the plasmid-nicking assay.

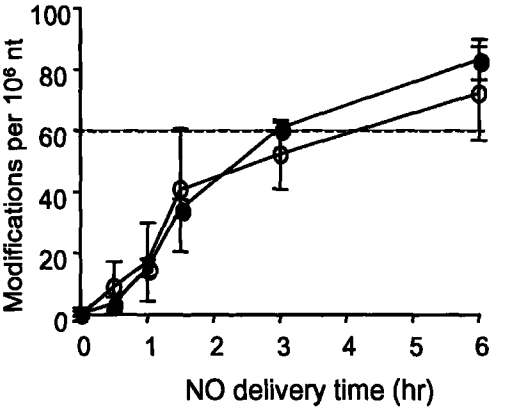

Figure 6. Comparison of N_2O_3-induced DNA lesions detected by AlkA-treatment coupled with the nicking assay (closed circles) and the quantity of dX and dI measured by the LC-MS analysis. Data represent mean ± SD for three independent experiments (± SD). Data points lying above 60 strand breaks per 10^6 nt (dotted line) fall outside "single-hit" conditions (see the text for details).

Fpg and Endo III proteins were both used to assay the NO• - treated pUC19 plasmid. No significant increase was observed in either Fpg-sensitive or Endo III-sensitive modifications (Figure 7). The time-dependent increase in DNA modifications shown in the figure overlaps

with the putrescine-sensitive sites, which is consistent with the AP endonuclease activity of both Fpg and Endo III.

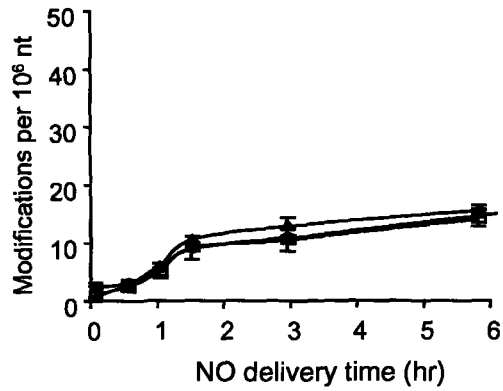

Figure 7. Quantification of N_2O_3-induced pUC19 DNA lesions sensitive to Fpg (O) and Endo III (Δ) proteins and putrescine treatment (). Data represent mean ± SD for three independent experiments.

6.5 Discussion

The goal of this set of studies was to identify groups of DNA repair enzymes capable of distinguishing oxidative from nitrosative DNA damage thought to arise at sites of inflammation. Two groups of DNA repair enzymes from *Escherichia coli* were found to differentiate base damage products caused by $ONOO^-$ and N_2O_3 using a validated plasmid-nicking assay. AlkA, Endo V and UDG react preferentially with DNA exposed to N_2O_3 arising in solutions of $NO^\bullet$ and O_2, while Fpg and EndoIII react selectively with DNA treated with $ONOO^-$ in the presence of bicarbonate.

The selection of these enzymes was based on the knowledge of the $NO^\bullet$ chemistry toward DNA. Direct DNA modification by $NO^\bullet$ is dominated by three processes, oxidation, nitration and deamination (Burney et al., 1999a; Dedon and Tannenbaum, 2004; Tamir and Tannenbaum, 1996).

Fpg Protein Selectively Reacts with $ONOO^-$-Damaged DNA. Two criteria govern whether a DNA repair enzyme is acceptable as a probe to distinguish between nitrosative and oxidative DNA damage for the current study: specificity and efficiency. The substrate specificity emphasized here is, however, not restricted exclusively to the recognition of an individual DNA lesion, but rather a group of structurally related damage products derived from the same category of DNA damage chemistry.

With regard to recognition of damage by Fpg and EndoIII, the oxidative and nitrative chemistry associated with reactive nitrogen species is mediated primarily by $ONOO^-$ and its CO_2 adduct, $ONOOCO_2^-$ (Wink et al., 1996). While $ONOOCO_2^-$ has greatly reduced activity toward

deoxyribose than $ONOO^-$, both oxidants react almost exclusively with dG in DNA to form 8-nitrodG, 8-oxo-dG, nitroimidazole, oxazolone along with a number of products of the secondary oxidation of 8-oxo-dG, including guanidinohydatoin, oxaluric acid, spiroiminodihydantoin and cyanuric acid (Dedon and Tannenbaum, 2004). Other oxidative products, such as 5-hyroxymethyl uridine and 8-oxodA, were also detected, but they are only present in very small quantities (deRojas-Walker et al., 1995).

It has been established that Fpg recognizes a wide array of oxidized purines (reviewed in Izumi et al., 2003). For instance, 8-oxo-dG and formamidopyrimidines are well-established substrates of Fpg protein, but recent studies indicated that Fpg protein also recognizes 8-nitro-dG, oxaluric acid, and to some extent oxazolone, guanidinohydantoin and spiroiminodihydantoin, lesions derived from oxidation of dG by $ONOO^-$ (Duarte et al., 2001; Leipold et al., 2000; Tretyakova et al., 2000b). Thus it was not surprising that Fpg did not recognize DNA damage caused by the nitrosative chemistry of $NO^{\bullet}$. We did not observe a significant increase in dX, dI and dU, in the plasmid DNA following $ONOO^-$ exposure. This observation is consistent with the lack of excision by either AlkA or Endo V enzyme toward $ONOO^-$ treated plasmid. However, it is inconsistent with the previous studies by the Halliwell group, in which both xanthine and hypoxanthine were detected when calf thymus DNA and epidermal skin cells were exposed to $ONOO^-$ (Spencer et al., 1995; Spencer et al., 1996). The most likely reason accounting for this discrepancy is the difference in analytical methods used for the quantification of the nucleobase deamination products. The Halliwell group applied a GC/MS method, which was rather novel in its day, but could be more rigorous if isotope-dilution mass spectrometry technology was adopted. Their analytical method included acidic hydrolysis which has been proven to accelerate the deamination of cytosine (Schein, 1966). We speculate

that under the acidic hydrolysis conditions used, the deamination of dA and dG would also be accelerated, thus expediting the formation of dI and dX. We observed additional limitations of the acidic hydrolysis required by most GC-MS analysis methods, which includes the destruction of both dI and dO, and the incomplete depyrimidination of dU. The inconsistency may also be attributed to the different methods for $ONOO^-$ preparation. We applied an alkaline ozonolysis method first reported by the Pryor group (Pryor et al., 1995), which produces $ONOO^-$ that is free of hydrogen peroxide and other contaminants. In their experiment, $ONOO^-$ was synthesized in a quenched flow reaction system by mixing H_2O_2 with $NaNO_2$ under acidic conditions. Although H_2O_2 was carefully removed by MnO_2, the risk of $NaNO_2$ contamination still existed. Under acidic conditions, $NaNO_2$ is converted to nitrous acid, an agent known to cause nucleobase deamination. Later studies from the same group reported the detection of deamination products in intact human respiratory tract epithelial cells exposed to $NaNO_2$. To investigate whether the $ONOO^-$ prepared by the ozonolysis method also induces nucleobase deamination, we treated dG with different concentrations of $ONOO^-$ in 50 mM phosphate buffer containing 25 mM bicarbonate with varying pH from 6.0 to 8.0 in half-pH unit increments. The formation of dX and dI was monitored by the LC-MS method reported previously (Dong et al., 2003). Neither dX nor dI was detected when $ONOO^-$ concentration reached 10 mM and the pH of the reaction buffer decreased to 6.0, suggesting that the $ONOO^-$ used in our experiment did not cause significant nucleobase deamination.

In addition to the specificity of Fpg to the oxidative DNA damage by $ONOO^-$ demonstrated here, the efficiency of Fpg in removing the oxidative products derived from $ONOO^-$ exposure has been investigated by different groups. It has been estimated that more than 90% of the nucleobase oxidation products caused by $ONOO^-$ can be removed by Fpg (Tretyakova et al.,

2000b). This estimation was supported by several succeeding studies. Leipold et al. showed that spiroiminodihydantoin (Sp) and guanidinohydantoin (Gh), resulting from the oxidation of 8-oxoG, are efficiently removed by Fpg (Leipold et al., 2000). The activity of Fpg toward other lesions, including N-[2,5-dioxo-3-(2-deoxy-b-D-ribofuranosyl)-4-imidazolidinylidene]-N'-nitro-guanidine (NO_2-DGh), and 3-(2-deoxy-b-D-erythro-pentofuranosyl) tetrahydro-2,4,6-trioxo-1,3,5-Triazine-1(2H)-carboximidamide (CAC), has not been reported yet. These latter lesions represent a minor portion of the spectrum of $ONOO^-$-induced oxidation of dG, such that they can be ignored in our studies of Fpg-sensitive lesions (Dedon and Tannenbaum, 2004). We thus conclude that the Fpg-sensitive lesions represent nucleobase oxidation produced by $ONOO^-$. Therefore, the broad substrate spectrum of Fpg toward oxidative products from $ONOO^-$, and its specificity to almost exclusively $ONOO^-$-induced DNA damage make it the best candidate to detect DNA damage from $ONOO^-$ chemistry that is potentially present in tissues afflicted with chronic inflammation.

AlkA Protein Selectively Reacts with NO•-damaged DNA. The arguments applied to $ONOOCO_2^-$-induced DNA damage recognition by Fpg and Endo III can be applied to nitrosative DNA damage. A plethora of experimental evidence suggests that N_2O_3 is the major nitrosative species in aqueous NO• reactions. Recent studies have shown that physiologically relevant levels of NO• exposure cause the formation of three major nitrosative deamination products: dI, dX, and dU. These arise from the deamination of dA, dG and dC respectively, at nearly identical rate. 2'-deoxyoxanosine (dO), one of the products arising from dG deamination, was not detected, leading to the prediction that it will not be present at a significant level in inflamed tissues. Apurinic/apyrimidinic sites, likely formed by nitrosation of the N7 positions of guanine

and adenine, were found to occur in NO• treated DNA. By supplementing our results with previous studies of nitrosatively induced dG-dG cross-links (Caulfield et al., 2003), the following spectrum of nitrosative DNA damage is proposed: ~2% dG-dG cross-link, 4-6% abasic sites, and 25%-35% each of dX, dI, and dU.

A substantial amount of experimental evidence indicates their potential importance in NO•-mediated mutagenesis (Zhuang et al., 1998; Zhuang et al., 2000). Living organisms have developed rapid base excision repair mechanisms to eliminate them. Hypoxanthine is generally excised from DNA by a family of methylpurine DNA glycosylases (Saparbaev and Laval, 1994), among which AlkA is the *E. coli* homologue. However, the biochemical properties of xanthine in DNA have only been explored recently. Existing as an enolate at physiological pH, xanthine is an unusual nucleobase. Under acidic conditions, xanthine is known to be susceptible to depurination, however, in contrast to conventional wisdom, we have demonstrated that xanthine is rather stable in double stranded DNA at neutral pH (Vongchampa et al., 2003). *In vitro* evidence indicates that xanthine in DNA is repaired by *E. coli* endonuclease V (Endo V) (He et al., 2000). Recent studies by our group (manuscript in preparation) and others show that xanthine is a substrate for several enzymes of the BER pathway, among which the strongest activity was noted for the *E. coli* AlkA protein, followed by human *N*-methylpurine DNA glycosylase (Mpg) and Fpg (Wuenschell et al., 2003).

In light of the fact that AlkA has activity toward both xanthine and hypoxanthine, we embarked on our effort to evaluate the efficiency of AlkA in removing those two nucleobase deamination products from DNA following NO• exposure. The excision of hypoxanthine from DNA by AlkA has been studied and compared to other alkylpurine DNA glycosylase homologues from yeast, rats, and humans. Although the *in vitro* kinetic constants show that

AlkA is less efficient than its partners of human or rat origin (Saparbaev and Laval, 1994), it indeed confers protection of *E.coli* from nitrous acid induced mutations (Sidorkina et al., 1997). Information regarding the excision of xanthine is relatively lacking, largely due to its instability (Lindahl, 1993). Only recently have systematic kinetic studies on this excision process been initiated. (Terato et al., 2002; Wuenschell et al., 2003). Research in our group demonstrated that AlkA is almost as efficient as *E. coli* Endo V in processing xanthine in double-stranded DNA oligonucleotides *in vitro* (Vongchampa, unpublished results). The kinetic constant is comparable with those recently reported by the Ide group and the Termini group (Terato et al., 2002; Wuenschell et al., 2003). Here we provide further evidence of the AlkA efficiency by comparing the amount of dX and dI in the $NO^{\bullet}$ - exposed plasmid pUC19 DNA measured by two distinct assays: LC-MS detection and the plasmid-nicking assay. We found a strong correlation between the results, which demonstrated the effectiveness of AlkA in removing dX and dI in DNA derived from $NO^{\bullet}$ exposure.

Although primarily described as an enzyme excising alkylated bases (Lindahl et al., 1988; Thomas et al., 1982), AlkA has been shown to have a broad substrate specificity. In addition to hypoxanthine, formyluracil, ethano-, and ethenobases have all been reported to be repaired by AlkA (Bjelland et al., 1994; Habraken et al., 1991; Saparbaev et al., 1995). However, we did not observe a significant increase in the excision of $ONOO^{-}$ -treated plasmid DNA by AlkA, which further confirms that the $ONOO^{-}$ chemistry is shifted more toward dG, and also suggests that AlkA itself is a good candidate to detect the nitrosative deamination products, mainly dX and dI, likely existing in tissues at the sites of inflammation.

Application of the Enzymatic Probes. DNA glycosylases have been used as valuable tools in the detection of DNA damage. They are useful for the detection of global DNA damage and repair (Cadet and Weinfeld, 1993; Dizdaroglu, 1993), DNA damage at the nucleotide level (Pfeifer et al., 1993; Xu et al., 1998), gene-specific repair (Grishko et al., 1999), detection of mutation (Hsu et al., 1994; Lu and Hsu, 1992). The use of these enzymes has also provided insight into biological processes including the coupling of transcription and DNA repair (Hanawalt, 1994).

DNA repair enzymes have also been used to detect DNA damage caused by reactive species derived from NO$^{\bullet}$. Epe et al. characterized DNA damage by $ONOO^-$ was with Fpg, EndoIII. Consistent with our observation, they also found that a high number of base modifications were sensitive to Fpg protein, while the numbers of modifications that are sensitive to EndoIII were relatively low.

In contrast to the well-established use of Fpg and EndoIII to detect oxidative DNA damage, there have been relatively few studies of using repair enzymes to detect nucleobase deamination products. One possible reason is that only till recently have EndoV and AlkA been demonstrated to recognize xanthine and hypoxanthine (He et al., 2000; Terato et al., 2002; Wuenschell et al., 2003; Yao and Kow, 1995), two major nucleobase deamiantion products caused by NO$^{\bullet}$ exposure (Burney et al., 1999a; Dong et al., 2003; Tamir et al., 1996). We broadened these observations by successfully demonstrating a real application of AlkA and EndoV, the detection of xanthine and hypoxanthine in plasmid DNA exposed to NO$^{\bullet}$ at controlled physiological concentrations.

The enzymatic probes developed here will ultimately be used to reveal the distribution of DNA damage caused by NO$^{\bullet}$ exposure along DNA sequences. These enzymes have been used

in our laboratory to cleave DNA at sites of base damage in preparation for mapping of DNA lesions in the *HPRT* gene at single nucleotide resolution by LMPCR. The mapping results from the $ONOO^-$-treated *HPRT* gene showed the damage pattern is by no means randomly distributed and that the lesions are concentrated on deoxyguanosine (Cloutier, unpublished results). Damage spectra produced by $NO^\bullet$ via N_2O_3 will also be analyzed in the *HPRT* gene, with the goal of comparing the damage and mutational spectra (Zhuang et al., 2002) associated with these two mediators, $ONOO^-$ and N_2O_3, of inflammation.

In conclusion, enzymatic probes were developed to distinguish nitrosative DNA damage from oxidative DNA damage produced by reactive nitrogen species found at sites of inflammation. A combination of *E. coli* AlkA, Endo V and UDG react selectively with DNA exposed to N2O3 derived from the reaction of $NO^\bullet$ with O_2, while *E. coli* Fpg reacts selectively with DNA treated with $ONOOCO_2^-$. These two sets of enzymes can be applied to map DNA damage in a specific genes from tissues impaired by chronic inflammation, thus generating valuable information to elucidate which DNA chemistry predominates, the nitrosative DNA damage or the oxidative DNA damage.

6.6 References

Bailly, V., Derydt, M., and Verly, W. G.: Delta-elimination in the repair of AP (apurinic/apyrimidinic) sites in DNA. Biochem J **261** (3): 707-13, 1989a.

Bailly, V., Verly, W. G., O'Connor, T., and Laval, J.: Mechanism of DNA strand nicking at apurinic/apyrimidinic sites by Escherichia coli [formamidopyrimidine]DNA glycosylase. Biochem J **262** (2): 581-9, 1989b.

Beckman, J. S., Chen, J., Crow, J. P., and Ye, Y. Z.: Reactions of nitric oxide, superoxide and peroxynitrite with superoxide dismutase in neurodegeneration. Prog Brain Res **103**: 371-80, 1994.

Beckman, J. S., Ischiropoulos, H., Zhu, L., van der Woerd, M., Smith, C., Chen, J., Harrison, J., Martin, J. C., and Tsai, M.: Kinetics of superoxide dismutase- and iron-catalyzed nitration of phenolics by peroxynitrite. Arch Biochem Biophys **298** (2): 438-45, 1992.

Bjelland, S., Birkeland, N. K., Benneche, T., Volden, G., and Seeberg, E.: DNA glycosylase activities for thymine residues oxidized in the methyl group are functions of the AlkA enzyme in Escherichia coli. J Biol Chem **269** (48): 30489-95, 1994.

Bjelland, S., Bjoras, M., and Seeberg, E.: Excision of 3-methylguanine from alkylated DNA by 3-methyladenine DNA glycosylase I of Escherichia coli. Nucleic Acids Res **21** (9): 2045-9, 1993.

Breimer, L. H.: Enzymatic excision from gamma-irradiated polydeoxyribonucleotides of adenine residues whose imidazole rings have been ruptured. Nucleic Acids Res **12** (16): 6359-67, 1984.

Breimer, L. H., and Lindahl, T.: Thymine lesions produced by ionizing radiation in double-stranded DNA. Biochemistry **24** (15): 4018-22, 1985.

Burney, S., Caulfield, J. L., Niles, J. C., Wishnok, J. S., and Tannenbaum, S. R.: The chemistry of DNA damage from nitric oxide and peroxynitrite. Mutat Res **424** (1-2): 37-49, 1999a.

Burney, S., Niles, J. C., Dedon, P. C., and Tannenbaum, S. R.: DNA damage in deoxynucleosides and oligonucleotides treated with peroxynitrite. Chem Res Toxicol **12** (6): 513-20, 1999b.

Cadet, J., and Weinfeld, M.: Detecting DNA damage. Anal Chem **65** (15): 675A-682A, 1993.

Cassell, G. H.: Infectious causes of chronic inflammatory diseases and cancer. Emerg Infect Dis **4** (3): 475-87, 1998.

Caulfield, J. L., Wishnok, J. S., and Tannenbaum, S. R.: Nitric oxide-induced interstrand cross-links in DNA. Chem Res Toxicol **16** (5): 571-4, 2003.

Collins, A. R., Duthie, S. J., and Dobson, V. L.: Direct enzymic detection of endogenous oxidative base damage in human lymphocyte DNA. Carcinogenesis **14** (9): 1733-5, 1993.

Cunningham, R. P., Asahara, H., Bank, J. F., Scholes, C. P., Salerno, J. C., Surerus, K., Munck, E., McCracken, J., Peisach, J., and Emptage, M. H.: Endonuclease III is an iron-sulfur protein. Biochemistry **28** (10): 4450-5, 1989.

Czene, S., and Harms-Ringdahl, M.: Detection of single-strand breaks and formamidopyrimidine-DNA glycosylase-sensitive sites in DNA of cultured human fibroblasts. Mutat Res **336** (3): 235-42, 1995.

Dedon, P. C., Salzberg, A. A., and Xu, J.: Exclusive production of bistranded DNA damage by calicheamicin. Biochemistry **32** (14): 3617-22, 1993.

Dedon, P. C., and Tannenbaum, S. R.: Reactive nitrogen species in the chemical biology of inflammation. Arch Biochem Biophys **423** (1): 12-22, 2004.

Demple, B., and Linn, S.: 5,6-Saturated thymine lesions in DNA: production by ultraviolet light or hydrogen peroxide. Nucleic Acids Res **10** (12): 3781-9, 1982.

deRojas-Walker, T., Tamir, S., Ji, H., Wishnok, J. S., and Tannenbaum, S. R.: Nitric oxide induces oxidative damage in addition to deamination in macrophage DNA. Chem Res Toxicol **8** (3): 473-7, 1995.

Dianov, G., and Lindahl, T.: Reconstitution of the DNA base excision-repair pathway. Curr Biol **4** (12): 1069-76, 1994.

Dizdaroglu, M.: Quantitative determination of oxidative base damage in DNA by stable isotope-dilution mass spectrometry. FEBS Lett **315** (1): 1-6, 1993.

Dong, M., Wang, C., Deen, W. M., and Dedon, P. C.: Absence of 2'-deoxyoxanosine and presence of abasic sites in DNA exposed to nitric oxide at controlled physiological concentrations. Chem Res Toxicol **16** (9): 1044-55, 2003.

Duarte, V., Gasparutto, D., Jaquinod, M., Ravanat, J., and Cadet, J.: Repair and mutagenic potential of oxaluric acid, a major product of singlet oxygen-mediated oxidation of 8-oxo-7,8-dihydroguanine. Chem Res Toxicol **14** (1): 46-53, 2001.

Epe, B., Ballmaier, D., Roussyn, I., Briviba, K., and Sies, H.: DNA damage by peroxynitrite characterized with DNA repair enzymes. Nucleic Acids Res **24** (21): 4105-10, 1996.

Epe, B., and Hegler, J.: Oxidative DNA damage: endonuclease fingerprinting. Methods Enzymol **234**: 122-31, 1994.

Evensen, G., and Seeberg, E.: Adaptation to alkylation resistance involves the induction of a DNA glycosylase. Nature **296** (5859): 773-5, 1982.

Felley-Bosco, E.: Role of nitric oxide in genotoxicity: implication for carcinogenesis. Cancer Metastasis Rev **17** (1): 25-37, 1998.

Gilboa, R., Zharkov, D. O., Golan, G., Fernandes, A. S., Gerchman, S. E., Matz, E., Kycia, J. H., Grollman, A. P., and Shoham, G.: Structure of formamidopyrimidine-DNA glycosylase covalently complexed to DNA. J Biol Chem **277** (22): 19811-6, 2002.

Graves, R. A., Tontonoz, P., Platt, K. A., Ross, S. R., and Spiegelman, B. M.: Identification of a fat cell enhancer: analysis of requirements for adipose tissue-specific gene expression. J Cell Biochem **49** (3): 219-24, 1992.

Grishko, V. I., Druzhyna, N., LeDoux, S. P., and Wilson, G. L.: Nitric oxide-induced damage to mtDNA and its subsequent repair. Nucleic Acids Res **27** (22): 4510-6, 1999.

Gros, L., Saparbaev, M. K., and Laval, J.: Enzymology of the repair of free radicals-induced DNA damage. Oncogene **21** (58): 8905-25, 2002.

Habraken, Y., Carter, C. A., Sekiguchi, M., and Ludlum, D. B.: Release of N2,3-ethanoguanine from haloethylnitrosourea-treated DNA by Escherichia coli 3-methyladenine DNA glycosylase II. Carcinogenesis **12** (10): 1971-3, 1991.

Hanawalt, P. C.: Transcription-coupled repair and human disease. Science **266** (5193): 1957-8, 1994.

Hartwig, A., Dally, H., and Schlepegrell, R.: Sensitive analysis of oxidative DNA damage in mammalian cells: use of the bacterial Fpg protein in combination with alkaline unwinding. Toxicol Lett **88** (1-3): 85-90, 1996.

He, B., Qing, H., and Kow, Y. W.: Deoxyxanthosine in DNA is repaired by Escherichia coli endonuclease V. Mutat Res **459** (2): 109-14, 2000.

Hegler, J., Bittner, D., Boiteux, S., and Epe, B.: Quantification of oxidative DNA modifications in mitochondria. Carcinogenesis **14** (11): 2309-12, 1993.

Hininger, I., Chollat-Namy, A., Sauvaigo, S., Osman, M., Faure, H., Cadet, J., Favier, A., and Roussel, A. M.: Assessment of DNA damage by comet assay on frozen total blood: method and evaluation in smokers and non-smokers. Mutat Res **558** (1-2): 75-80, 2004.

Hsu, I. C., Yang, Q., Kahng, M. W., and Xu, J. F.: Detection of DNA point mutations with DNA mismatch repair enzymes. Carcinogenesis **15** (8): 1657-62, 1994.

Izumi, T., Wiederhold, L. R., Roy, G., Roy, R., Jaiswal, A., Bhakat, K. K., Mitra, S., and Hazra, T. K.: Mammalian DNA base excision repair proteins: their interactions and role in repair of oxidative DNA damage. Toxicology **193** (1-2): 43-65, 2003.

Kennedy, L. J., Moore, K., Jr., Caulfield, J. L., Tannenbaum, S. R., and Dedon, P. C.: Quantitation of 8-oxoguanine and strand breaks produced by four oxidizing agents. Chem Res Toxicol **10** (4): 386-92, 1997.

Kow, Y. W.: Repair of deaminated bases in DNA. Free Radic Biol Med **33** (7): 886-93, 2002.

Kuipers, G. K., and Lafleur, M. V.: Characterization of DNA damage induced by gamma-radiation-derived water radicals, using DNA repair enzymes. Int J Radiat Biol **74** (4): 511-9, 1998.

Leipold, M. D., Muller, J. G., Burrows, C. J., and David, S. S.: Removal of hydantoin products of 8-oxoguanine oxidation by the Escherichia coli DNA repair enzyme, FPG. Biochemistry **39** (48): 14984-92, 2000.

Lindahl, T.: An N-glycosidase from Escherichia coli that releases free uracil from DNA containing deaminated cytosine residues. Proc Natl Acad Sci U S A **71** (9): 3649-53, 1974.

Lindahl, T.: Instability and decay of the primary structure of DNA. Nature **362** (6422): 709-15, 1993.

Lindahl, T., Sedgwick, B., Sekiguchi, M., and Nakabeppu, Y.: Regulation and expression of the adaptive response to alkylating agents. Annu Rev Biochem **57**: 133-57, 1988.

Lu, A. L., and Hsu, I. C.: Detection of single DNA base mutations with mismatch repair enzymes. Genomics **14** (2): 249-55, 1992.

Masaoka, A., Terato, H., Kobayashi, M., Honsho, A., Ohyama, Y., and Ide, H.: Enzymatic repair of 5-formyluracil. I. Excision of 5-formyluracil site-specifically incorporated into oligonucleotide substrates by alka protein (Escherichia coli 3-methyladenine DNA glycosylase II). J Biol Chem **274** (35): 25136-43, 1999.

Moe, A., Ringvoll, J., Nordstrand, L. M., Eide, L., Bjoras, M., Seeberg, E., Rognes, T., and Klungland, A.: Incision at hypoxanthine residues in DNA by a mammalian homologue of the Escherichia coli antimutator enzyme endonuclease V. Nucleic Acids Res **31** (14): 3893-900, 2003.

Nakabeppu, Y., Kondo, H., and Sekiguchi, M.: Cloning and characterization of the alkA gene of Escherichia coli that encodes 3-methyladenine DNA glycosylase II. J Biol Chem **259** (22): 13723-9, 1984a.

Nakabeppu, Y., Miyata, T., Kondo, H., Iwanaga, S., and Sekiguchi, M.: Structure and expression of the alkA gene of Escherichia coli involved in adaptive response to alkylating agents. J Biol Chem **259** (22): 13730-6, 1984b.

O'Connor, T. R., and Laval, J.: Physical association of the 2,6-diamino-4-hydroxy-5N-formamidopyrimidine-DNA glycosylase of Escherichia coli and an activity nicking DNA at apurinic/apyrimidinic sites. Proc Natl Acad Sci U S A **86** (14): 5222-6, 1989.

Ohshima, H., and Bartsch, H.: Chronic infections and inflammatory processes as cancer risk factors: possible role of nitric oxide in carcinogenesis. Mutat Res **305** (2): 253-64, 1994.

Pearl, L. H.: Structure and function in the uracil-DNA glycosylase superfamily. Mutat Res **460** (3-4): 165-81, 2000.

Pfeifer, G. P., Denissenko, M. F., and Tang, M. S.: PCR-based approaches to adduct analysis. Toxicol Lett **102-103**: 447-51, 1998.

Pfeifer, G. P., Drouin, R., and Holmquist, G. P.: Detection of DNA adducts at the DNA sequence level by ligation-mediated PCR. Mutat Res **288** (1): 39-46, 1993.

Pouget, J. P., Douki, T., Richard, M. J., and Cadet, J.: DNA damage induced in cells by gamma and UVA radiation as measured by HPLC/GC-MS and HPLC-EC and Comet assay. Chem Res Toxicol **13** (7): 541-9, 2000.

Pryor, W. A., Cueto, R., Jin, X., Koppenol, W. H., Ngu-Schwemlein, M., Squadrito, G. L., Uppu, P. L., and Uppu, R. M.: A practical method for preparing peroxynitrite solutions of low ionic strength and free of hydrogen peroxide. Free Radic Biol Med **18** (1): 75-83, 1995.

Samson, L., and Cairns, J.: A new pathway for DNA repair in Escherichia coli. Nature **267** (5608): 281-3, 1977.

Saparbaev, M., Kleibl, K., and Laval, J.: Escherichia coli, Saccharomyces cerevisiae, rat and human 3-methyladenine DNA glycosylases repair 1,N6-ethenoadenine when present in DNA. Nucleic Acids Res **23** (18): 3750-5, 1995.

Saparbaev, M., and Laval, J.: Excision of hypoxanthine from DNA containing dIMP residues by the Escherichia coli, yeast, rat, and human alkylpurine DNA glycosylases. Proc Natl Acad Sci U S A **91** (13): 5873-7, 1994.

Sauvaigo, S., Petec-Calin, C., Caillat, S., Odin, F., and Cadet, J.: Comet assay coupled to repair enzymes for the detection of oxidative damage to DNA induced by low doses of gamma-radiation: use of YOYO-1, low-background slides, and optimized electrophoresis conditions. Anal Biochem **303** (1): 107-9, 2002.

Schein, A. H.: Uracil in formic acid hydrolysates of deoxyribonucleic acid. Biochem J **98** (1): 311-6, 1966.

Shubsda, M. F., Goodisman, J., and Dabrowiak, J. C.: Quantitation of ethidium-stained closed circular DNA in agarose gels. J Biochem Biophys Methods **34** (1): 73-9, 1997.

Sidorkina, O., Saparbaev, M., and Laval, J.: Effects of nitrous acid treatment on the survival and mutagenesis of Escherichia coli cells lacking base excision repair (hypoxanthine-DNA glycosylase-ALK A protein) and/or nucleotide excision repair. Mutagenesis **12** (1): 23-8, 1997.

Spencer, J. P., Jenner, A., Chimel, K., Aruoma, O. I., Cross, C. E., Wu, R., and Halliwell, B.: DNA damage in human respiratory tract epithelial cells: damage by gas phase cigarette smoke apparently involves attack by reactive nitrogen species in addition to oxygen radicals. FEBS Lett **375** (3): 179-82, 1995.

Spencer, J. P., Wong, J., Jenner, A., Aruoma, O. I., Cross, C. E., and Halliwell, B.: Base modification and strand breakage in isolated calf thymus DNA and in DNA from human

skin epidermal keratinocytes exposed to peroxynitrite or 3-morpholinosydnonimine. Chem Res Toxicol **9** (7): 1152-8, 1996.

Suzuki, T., Yamaoka, R., MNishi, M., Ide, H., and Makino, K.: Isolation and Characterization of a Novel Product, 2'-deoxyoxanosine, from 2'-Deoxyguanosine, Oligodeoxynucleotide, and Calf Thymus DNA Treated by Nitrous Acid and Nitric Oxide. J. Am. Chem. Soc. **118** (10): 2515-2516, 1996.

Tamir, S., Burney, S., and Tannenbaum, S. R.: DNA damage by nitric oxide. Chem Res Toxicol **9** (5): 821-7, 1996.

Tamir, S., and Tannenbaum, S. R.: The role of nitric oxide (NO.) in the carcinogenic process. Biochim Biophys Acta **1288** (2): F31-6, 1996.

Tchou, J., Kasai, H., Shibutani, S., Chung, M. H., Laval, J., Grollman, A. P., and Nishimura, S.: 8-oxoguanine (8-hydroxyguanine) DNA glycosylase and its substrate specificity. Proc Natl Acad Sci U S A **88** (11): 4690-4, 1991.

Terato, H., Masaoka, A., Asagoshi, K., Honsho, A., Ohyama, Y., Suzuki, T., Yamada, M., Makino, K., Yamamoto, K., and Ide, H.: Novel repair activities of AlkA (3-methyladenine DNA glycosylase II) and endonuclease VIII for xanthine and oxanine, guanine lesions induced by nitric oxide and nitrous acid. Nucleic Acids Res **30** (22): 4975-84, 2002.

Thomas, L., Yang, C. H., and Goldthwait, D. A.: Two DNA glycosylases in Escherichia coli which release primarily 3-methyladenine. Biochemistry **21** (6): 1162-9, 1982.

Tretyakova, N. Y., Burney, S., Pamir, B., Wishnok, J. S., Dedon, P. C., Wogan, G. N., and Tannenbaum, S. R.: Peroxynitrite-induced DNA damage in the supF gene: correlation with the mutational spectrum. Mutat Res **447** (2): 287-303, 2000a.

Tretyakova, N. Y., Niles, J. C., Burney, S., Wishnok, J. S., and Tannenbaum, S. R.: Peroxynitrite-induced reactions of synthetic oligonucleotides containing 8-oxoguanine. Chem Res Toxicol **12** (5): 459-66, 1999.

Tretyakova, N. Y., Wishnok, J. S., and Tannenbaum, S. R.: Peroxynitrite-induced secondary oxidative lesions at guanine nucleobases: chemical stability and recognition by the Fpg DNA repair enzyme. Chem Res Toxicol **13** (7): 658-64, 2000b.

Vongchampa, V., Dong, M., Gingipalli, L., and Dedon, P.: Stability of 2'-deoxyxanthosine in DNA. Nucleic Acids Res **31** (3): 1045-51, 2003.

Wallace, S. S.: Enzymatic processing of radiation-induced free radical damage in DNA. Radiat Res **150** (5 Suppl): S60-79, 1998.

Wink, D. A., Grisham, M. B., Mitchell, J. B., and Ford, P. C.: Direct and indirect effects of nitric oxide in chemical reactions relevant to biology. Methods Enzymol **268**: 12-31, 1996.

Wu, J., Xu, J., and Dedon, P. C.: Modulation of enediyne-induced DNA damage by chromatin structures in transcriptionally active genes. Biochemistry **38** (47): 15641-6, 1999.

Wuenschell, G. E., O'Connor, T. R., and Termini, J.: Stability, miscoding potential, and repair of 2'-deoxyxanthosine in DNA: implications for nitric oxide-induced mutagenesis. Biochemistry **42** (12): 3608-16, 2003.

Xu, J., Wu, J., and Dedon, P. C.: DNA damage produced by enediynes in the human phosphoglycerate kinase gene in vivo: esperamicin A1 as a nucleosome footprinting agent. Biochemistry **37** (7): 1890-7, 1998.

Yao, M., Hatahet, Z., Melamede, R. J., and Kow, Y. W.: Purification and characterization of a novel deoxyinosine-specific enzyme, deoxyinosine 3' endonuclease, from Escherichia coli. J Biol Chem **269** (23): 16260-8, 1994.

Yao, M., and Kow, Y. W.: Strand-specific cleavage of mismatch-containing DNA by deoxyinosine 3'-endonuclease from Escherichia coli. J Biol Chem **269** (50): 31390-6, 1994.

Yao, M., and Kow, Y. W.: Interaction of deoxyinosine 3'-endonuclease from Escherichia coli with DNA containing deoxyinosine. J Biol Chem **270** (48): 28609-16, 1995.

Yermilov, V., Rubio, J., and Ohshima, H.: Formation of 8-nitroguanine in DNA treated with peroxynitrite in vitro and its rapid removal from DNA by depurination. FEBS Lett **376** (3): 207-10, 1995.

Zastawny, T. H., Doetsch, P. W., and Dizdaroglu, M.: A novel activity of E. coli uracil DNA N-glycosylase excision of isodialuric acid (5,6-dihydroxyuracil), a major product of oxidative DNA damage, from DNA. FEBS Lett **364** (3): 255-8, 1995.

Zhuang, J. C., Lin, C., Lin, D., and Wogan, G. N.: Mutagenesis associated with nitric oxide production in macrophages. Proc Natl Acad Sci U S A **95** (14): 8286-91, 1998.

Zhuang, J. C., Lin, D., Lin, C., Jethwaney, D., and Wogan, G. N.: Genotoxicity associated with NO production in macrophages and co-cultured target cells. Free Radic Biol Med **33** (1): 94-102, 2002.

Zhuang, J. C., Wright, T. L., deRojas-Walker, T., Tannenbaum, S. R., and Wogan, G. N.: Nitric oxide-induced mutations in the HPRT gene of human lymphoblastoid TK6 cells and in Salmonella typhimurium. Environ Mol Mutagen **35** (1): 39-47, 2000.

Chapter 7

Effects of Peroxynitrite Dose and Dose-rate on DNA Damage in the *supF* Shuttle Vector

[The work in this chapter is in press in Chem Res Toxicol as "Kim, MY., Dong, M., Dedon, P. C. and Wogan, G. N. (2004). "Effects of Peroxynitrite Dose and Dose Rate on DNA Damage and Mutation in the *supF* Shuttle Vector.". A reprint of the paper is included in Appendix III]

7.1 Abstract

It has been well established that peroxynitrite ($ONOO^-$) causes DNA damage and that it is mutagenic in model cell systems. To define the connection between $ONOO^-$-induced DNA damage and mutagenicity, several groups have used the pSP189 shuttle vector to correlate the spectrum of lesions and mutations in the *E. coli SupF* gene. However, no effort was made to correlate the damage and mutation or to correlate the role of dose form and dose rate of $ONOO^-$ on the damage and mutation. We have therefore undertaken a collaboration with the research group of Professor Gerald Wogan, to define the effects of $ONOO^-$ dose and dose-rate on the DNA damage and mutations induced in the *supF* gene by three different dosage regimes: (1) by infusion of $ONOO^-$ solution into suspensions of pSP189 at rates approximating those estimated to occur in inflamed tissues; (2) by exposure to 3-morpholinosydnonimine (SIN-1), which generates $ONOO^-$ spontaneously during decomposition; and (3) by bolus doses of $ONOO^-$ solution. In all cases, plasmid DNA was exposed in the presence of 25 mM bicarbonate, since the biologically relevant reaction of CO_2 with $ONOO^-$ (to form nitrosoperoxycarbonate) has a major impact on mutagenic potency of $ONOO^-$ in this system. Nucleobase and deoxyribose damage were evaluated by a plasmid-nicking assay immediately after $ONOO^-$ and SIN-1 exposures. Mutation frequency (MF) and mutational spectra in the *supF* gene were determined after plasmid pSP189 replicated in host *E. coli* cells (performed by Dr. Min Young Kim). A strong correlation between DNA damage frequency and MF produced by $ONOO^-$ was observed. Bolus $ONOO^-$ addition caused the highest amount of DNA damage, in the form of Fpg sensitive base lesions, direct strand breaks and abasic sites. SIN-1 was found to cause deoxyribose oxidation almost exclusively, while bolus addition generated predominantly base damage. MF

increased in a dose-dependent manner following all treatments, but infused $ONOO^-$ and SIN-1 exposures were less mutagenic than bolus $ONOO^-$ exposure.

Dose form and dose rate of $ONOO^-$ was also found to alter the mutation spectra. Those induced by infused- or bolus- $ONOO^-$ and SIN-1 consisted predominantly of G:C to T:A transversions, but in different amount (58%, 66% and 51%, respectively). G:C to C:G mutations were much less frequent following infusion and SIN-1 (8% and 19%, respectively) than those induced by bolus exposure (26%). A:T to T:A mutations induced were detected only after $ONOO^-$ infusion and SIN-1 exposure (9% and 11%, respectively).

In conclusion, both dose and dose-rate at which a genetic target is exposed to $ONOO^-$ substantially influence the damage and mutational response, indicating that these parameters will need to be taken into account in assessing the potential effects of $ONOO^-$ *in vivo*. Furthermore, the results indicate that the chemistry of SIN-1-induced DNA damage differs substantially from native $ONOO^-$, which suggests the need for caution in interpreting the biological relevance of SIN-1 as a surrogate for $ONOO^-$.

7.2 Introduction

Peroxynitrite ($ONOO^-$) produced *in vivo* primarily by activated macrophagesis a potent one oxidant that reacts readily towards many biological molecules, including lipids (Darley-Usmar et al., 1995; de Groot et al., 1993), proteins (Radi, R., 1991, Soszynski, M.,1996), and nucleic acids (Burney et al., 1999) (Tretyakova et al., 1999). Presumably as a result of damage to cellular molecules, elevated $ONOO^-$ levels have been implicated in a number of pathological conditions in humans and experimental animals, such as atherosclerosis (Bunderson et al., 2002), ischemia-reperfusion injury (Jugdutt, 2002), renal allograft rejection (MacMillan-Crow et al., 1996), and cancer (Goldstein et al., 1998), (Nair et al., 1998). As part of the overall effort to elucidate the role of $ONOO^-$ in inflammation-induced carcinogenesis, the project here focuses on $ONOO^-$ genotoxicity.

A critical feature of the link between any genotoxin and cancer is the underlying chemistry, which in the case of $ONOO^-$ is particularly complicated. The $ONOO^-$ chemistry is first complicated by the reactive species derived from $ONOO^-$ in biological systems, which are summarized in Figure 1 (Merenyi et al., 1998; Pfeiffer et al., 2000). In DNA, oxidation can occur at both deoxyribose (Kennedy et al., 1997) and nucleobases (Burney et al., 1999; Douki and Cadet, 1996). It has recently been recognized that the proportions of various DNA products are strongly dependent on the presence of CO_2 and thus the formation of nitrosoperoxycarbonate (Burney et al., 1999; Tretyakova et al., 1999). The presence of CO_2 caused a major shift in $ONOO^-$-induced DNA damage from the deoxyribose to the base with little change in the total number of lesions (Burney et al., 1999).

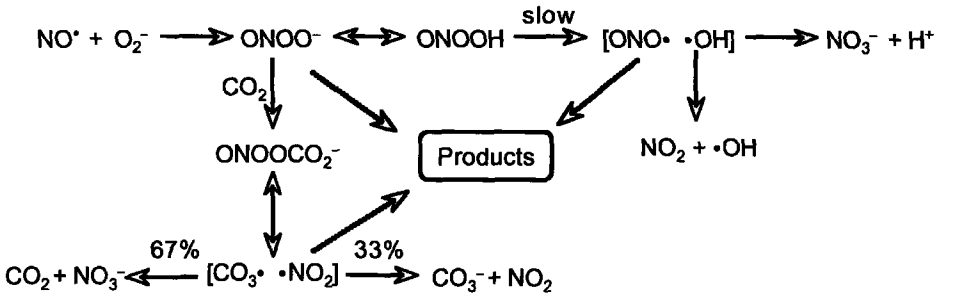

Figure 1. Peroxynitrite reaction pathway

The $ONOO^-$ chemistry is then complicated by the fact that the concentration and flux of $ONOO^-$ affect the product distribution and yield. Given the short half-life of $ONOO^-$ in a typical physiological environment ($t_{1/2}$, 0.02-1s) (Beckman et al., 1994; Radi et al., 2001), it is difficult to design experiments in which cells or biomolecules are exposed to low, relatively constant levels of $ONOO^-$ for sustained periods, thereby mimicking conditions in human cells subjected to inflammation. The most widely used method has been the addition of synthetic $ONOO^-$ to a rapidly stirred solution, either as a bolus (Kuhn et al., 1999; Pfeiffer and Mayer, 1998) or *via* a continuous infusion (Pfeiffer et al., 2000; Zhang et al., 2003). Another approach has been to generate $ONOO^-$ from a donor compound, 3-morpholinosydnonimine (SIN-1), which spontaneously decomposes to form $O_2^{\cdot-}$ and $NO^\bullet$ in neutral solutions, thus producing $ONOO^-$ (Reden, 1990; Singh et al., 1999), as shown in Figure 2.

The possibility that the concentration of $ONOO^-$ affects the product distribution and the yield was first raised in studies of the formation of 8-oxo-dG by $ONOO^-$. Several groups reported the absence of 8-oxo-dG when using high concentrations of $ONOO^-$ (Ohshima and Bartsch, 1994), while others were able to detect it at low concentrations of $ONOO^-$ with more sensitive

analytical methods (Kennedy et al., 1997). The conflict appeared to have been resolved after discovery that 8-oxo-dG is ~1000 times more reactive toward $ONOO^-$ than 2'-deoxyguanosine (dG) (Uppu and Pryor, 1996), which suggests that 8-oxo-dG is completed confounded at high $ONOO^-$ concentration. A battery of oxidative products derived from the reactions of dG and 8-oxo-dG with $ONOO^-$ have been characterized (Dedon and Tannenbaum, 2004) (Figures 3 and 4).

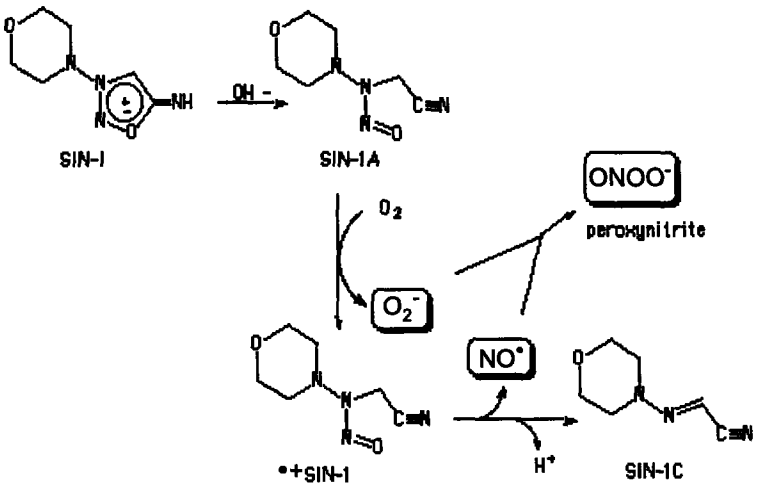

Figure 2. Degradation pathway of SIN-1, adapted from Reden, 1990)

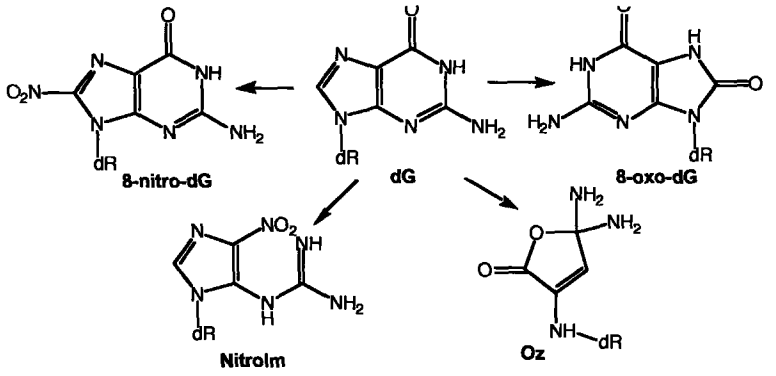

Figure 3. Oxidation products from the reaction of dG with $ONOO^-$ (primary oxidation products; adapted from Dedon and Tannenbaum, 2004)

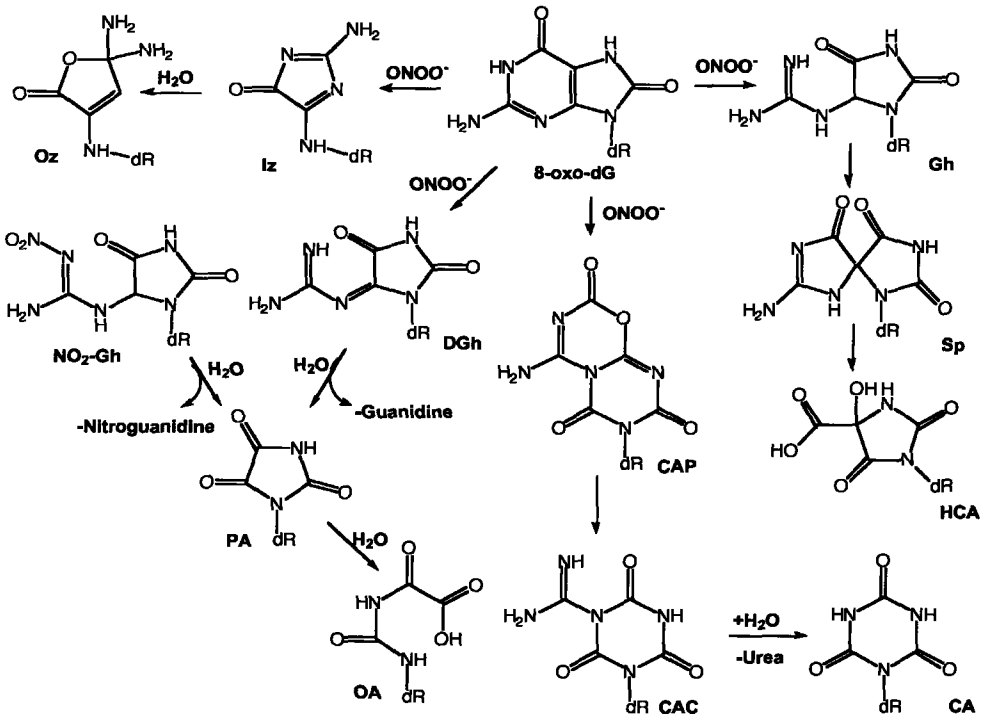

Figure 4. Oxidation products of dG reaction with $ONOO^-$ (secondary oxidation products; adapted from Dedon and Tannenbaum, 2004)

The influence of the $ONOO^-$ flux on the product distribution and yield has recently been examined by the research group of Professor Steven Tannenbaum (unpublished results). Several flux regimes were applied in these experiments, including (*i*) bolus addition and (*ii*) infusion of authentic $ONOO^-$, and (*iii*) SIN-1 mediated *in situ* $ONOO^-$ production, have been applied for the experiments. Under conditions of bolus addition, very high fluxes can be attained (~1600 μM/s for total $ONOO^-$ concentration of 800 μM). Lower fluxes (0.7-13 μM/s) are easily achieved during infusion. For SIN-1, the initial instantaneous $ONOO^-$ fluxes can be as low as 0.06 μM/s, based upon measured $NO^\bullet$ and $O_2^{\bullet-}$ production rates that have been reported (Doulias et al., 2001). The immediate products produced arising from bolus addition include [3-(2-deoxy-b-D-erythro-pentofuranosyl)-2,5-dioxo-4-imidazolidinylidene]-guanidine (DGh) (the major product), N-[2,5-dioxo-3-(2-deoxy-b-D-ribofuranosyl)-4-imidazolidinylidene]-N'-nitro-guanidine (NO_2-DGh) and 3-(2-deoxy-b-D-erythro-pentofuranosyl) tetrahydro-2,4,6-trioxo-1,3,5-triazine-1(2H)-carboximidamide (CAC). During infusion, the major product is spiroiminodihydantoin (Sp), followed by DGh, and lesser quantities of NO_2-DGh, CAC and a new product, NO_2-DGh or CAC. With SIN-1, the major product is Sp, with HCA as a minor product, and no formation of DGh, NO_2-DGh or CAC. Therefore, as the $ONOO^-$ flux is lowered, Sp formation increases largely at the expense of DGh.

While substantial numbers of investigations have been focused on the $ONOO^-$-induced nucleobase oxidation products, information regarding deoxyribose oxidation is minimal. Both deoxyribose and base damage resulting from exposure to $ONOO^-$ likely contribute to DNA mutation, so that defining the proportions of deoxyribose and base oxidation is important to elucidate the mechanism of $ONOO^-$-induced genotoxicity. To this end, our lab

has applied several novel analytical methods to define the relative quantity of deoxyribose damage that occurs as a result of $ONOO^-$, with the emphasis here on comparing damage and mutation in the pSP189 shuttle vector.

The *SupF* gene-containing pSP189 shuttle vector has proved to be a useful target gene for studying the range of mutations that can be induced by a variety of DNA damaging agents *in vitro* (Bigger et al., 1992; Parris and Seidman, 1992; Seidman et al., 1985). The particular advantages of the *supF* system are that few mutations are phenotypically silent and the treated DNA can be analyzed by other biological and analytical techniques (e.g., plasmid nicking assay, ^{32}P-postlabelling) in conjunction with the mutation studies (Bigger et al., 1992). The *supF* assay system has previously been used to study the mutation spectra caused by $ONOO^-$ (Jeong et al., 1998; Juedes and Wogan, 1996). However, a remaining unaddressed question is to correlate the damage and mutation or to correlate the role of dose form and dose rate of $ONOO^-$ on the damage and mutation. We have therefore undertaken a collaboration with the research group of Professor Gerald Wogan, to define the effects of $ONOO^-$ dose and dose-rate on the DNA damage and mutations induced in the *supF* gene using a plasmid-nicking assay to define the proportions of deoxyribose and base oxidation.

Plasmid-nicking assay is a sensitive method based on the fact that supercoiled plasmid DNA is converted by either a single-strand break (SSB) or the incision of a repair endonuclease into a relaxed (nicked) form that migrates separately from the supercoiled form in agarose gel electrophoresis. Quantification of both forms of DNA by fluorescence scanning after staining of the gel with ethidium bromide allows the calculation of the average number of SSBs per plasmid molecule or, if an incubation with a repair enzyme precedes the gel electrophoresis, the number of SSBs plus repair enzyme-sensitive sites.

In light of the possible influence of $ONOO^-$ flux on DNA damage chemistry, DNA damage and mutation frequencies induced by slow infusion of $ONOO^-$ and by SIN-1 were compared with those induced by bolus doses of $ONOO^-$ in the *supF* gene of pSP189 shuttle vector replicated in *E. coli* MBL50 cells. The present investigation provided useful information to elucidate how dose and dose-rate at which a genetic target is exposed to $ONOO^-$ will influence the damage and mutational response.

7.3 Materials and Methods

Materials. All chemicals and reagents were of highest purity available and were used without further purification unless noted otherwise. *E.coli* formamidopyrimidine-DNA glycosylase (Fpg) was purchased from Trevigen (Gaithersbury, MD) and was tested under cell-free conditions for its incision at 8-oxo-dG in an oligonucleotide to ensure that the correct substrate modifications are fully recognized and no incision at non-substrate modifications takes place. Agarose was purchased from Sigma Chemical Co. (St. Louis, MO). 3-Morpholinosydnonimine chloride (SIN-1) was purchased from Cayman chemical (Ann Arbor, MI).

Isolation of Plasmid pSP 189 from *E.coli* AB2463. The pSP189 shuttle vector containing an 8-bp 'signature sequence' was a gift from Dr. Michael M. Seidman (NIH, Bethesda, MD). The amber tyrosine suppressor tRNA gene (*supF*) in plasmid pSP189 carrying the ampicillin resistance gene was used as the target for mutation (Juedes and Wogan, 1996). Large-scale preparation of pSP189 plasmid was accomplished by inoculating 5 mL LB media and 50 μg/mL ampicillin (Sigma) with 0.1 mL of a frozen stock of transformed Ab2463 cells containing the complete population of plasmids. After incubation for 10 hr, the 5 mL culture was added to 1 liter LB media and placed in a 37 °C shaking incubator overnight. Plasmid DNA was isolated using the Qiagen Giga Plasmid/Cosmid Purification kit according to manufacturer's instructions. After washing the DNA pellet with 70% ethanol, the solvent was evaporated, and the DNA was redissolved in 150 mM potassium phosphate buffer containing 25 mM bicarbonate (pH7.4, treated with Chelex 100 resin). Plasmid DNA was exhaustively dialyzed against 150 mM potassium phosphate containing 1 mM DETA-PAC for 12 h at 4°C to remove trace metals and

then against 150 mM potassium phosphate/25 mM bicarbonate buffer for an additional 12 hr at 4°C. Following dialysis, the DNA concentration was determined by an UV/Vis spectrometer 260/280 nm. The pSP189 DNA was stored at –80°C.

Synthesis of $ONOO^-$. $ONOO^-$ was synthesized by ozonolysis of sodium azide as described by Pryor et al. (Pryor et al., 1995). Briefly, ozone generated in a Welsbach ozonator was bubbled into 100 mL of 0.1 M sodium azide chilled in an ice bath. Ozonation was generally terminated after 45 min and $ONOO^-$ concentration was determined spectrophotometrically in 0.1 N NaOH (ε_{302}=1670 M^{-1} cm^{-1}). Aliquots of the newly synthesized $ONOO^-$ were then stored as a stock solution in 0.1 N NaOH at –80 °C until use.

Treatment of pSP 189 Plasmid with Peroxynitrite. Bolus doses of $ONOO^-$ were introduced into plasmid solutions as previously described (Kennedy et al., 1997). Briefly, 20 μg of plasmid DNA dissolved in 90 μL 150 mM sodium phosphate, 25 mM $NaHCO_3$, pH 7.4, were placed into 1.5 mL Eppendorf tubes. For bolus $ONOO^-$ additions, aliquots (10 μL of 0-30 mM in half-log steps; diluted with 0.1 N NaOH) of $ONOO^-$ were placed on the inside of an Eppendorf tube cap and the plasmid solution was mixed by gently closing the cap and mixing by vortexing for 30 s; total reaction volume was 100 μL. After treatment, samples were incubated at ambient temperature for 30 min.

Infusion of $ONOO^-$ was performed using a syringe pump (Harvard Apparatus, model AH 55-4154), with constant mixing by vortexing. A total of 10 μL of $ONOO^-$ at concentrations ranging from 0-30 mM was infused at a constant rate (0.945 μL per min) into 90 μL of plasmid solution

with 25 mM $NaHCO_3$ to produce fluxes of $ONOO^-$ between 1.75×10^{-4} and 5.25 μM/s. The pH of the reaction mixtures (7.4) remained constant during and after the infusion procedure.

Treatment of Plasmid pSP189 with SIN-1. SIN-1 is stable at pH 5, but readily decomposes at pH 7.4 in oxygenated solution. One obstacle faced when comparing the studies of SIN-1 with authentic $ONOO^-$ is to find the concentration of SIN-1 that will release a predictable amount of $ONOO^-$ over defined incubation times. Doulias et al. have shown that decomposition of 1 mM SIN-1 in well-oxygenated cell culture medium produced $ONOO^-$ at a linear rate of 12 μM/min for at least 120 min, as assessed by the oxidation of dihydrorhodamine123 (DHR123), a sensitive and efficient two-electron oxidation probe for $ONOO^-$ (Doulias et al., 2001). In a similar manner, it has been shown that 1 mM SIN-1 decomposes to form $ONOO^-$ at a rate of ~10 μM/min in bacteria culture media (Brunelli et al., 1995; Motohashi and Saito, 2002). Control experiments revealed that 1, 2 and 4 mM SIN-1 decomposed to form $ONOO^-$ at approximate rates of 12, 21 and 31 μM $ONOO^-$ min^{-1}, respectively, as assessed by the oxidation of DHR123 (communication from Dr. Min Young Kim). We have therefore used these values as the rates of $ONOO^-$ production from SIN-1. In designing the SIN-1 experiment, we chose the incubation time of 100 min, the length of incubation at which, based on SIN-1 decomposition kinetics, SIN-1 will release a total amount of $ONOO^-$ that equals to the bolus and infusion SIN-1 was dissolved in 150 mM sodium phosphate buffer, pH 7.4, just before use and 10 μL aliquots were added to 90 μl plasmid solutions in 150 mM phosphate buffer containing 25 mM $NaHCO_3$. Final SIN-1 concentrations ranged from 0-3 mM in half-log steps. Reaction mixtures were incubated at 37 °C for 100 min in a shaking water bath. At the end of treatment, DNA samples were washed twice with cold TE buffer (pH 7.4) using Amicon Centricon-30 concentrators (Millipore,

Billerica, MA). The plasmid DNA was stored in TE buffer on ice for the succeeding DNA damage analysis.

Quantification of DNA Damage by A Plasmid-Nicking Assay. A plasmid-nicking assay was used to quantify the DNA deoxyribose and base damage. After $ONOO^-$ or SIN-1 treatments, a portion (200 ng) of the DNA was treated with putrescine (100 mM, pH 7.0, 1 h, 37°C) to cleave all type of abasic sites (*30*). Another portion (200 ng) was kept on ice as a control for the direct strand breaks. A third portion of the DNA sample was treated with *E.coli* formamidopyrimidine-DNA glycosylase (Fpg) (Trevigen, Gaithersbur, MD) to convert oxidized purines to strand breaks. Fpg treatment was performed in a volume of 10 μL containing 200 ng of $ONOO^-$-treated DNA, 1 μL of Fpg (~1.5 Units) and buffer containing 10 mM Tris-HCl (pH 7.5), 1 mM EDTA and 100 mM NaCl at 37 °C for 1 hr. Fpg was then removed by phenol/chloroform extraction. The recovered DNA was redissolved in H_2O and plasmid topoisomers were resolved by 1% agarose slab gel electrophresis in the presence of 0.1 μg/mL ethidium bromide. The quantity of DNA in each band was determined by fluorescence imaging (Ultra-Lum, Clarmont, CA).

7.3 Results

Formation of Direct Single Strand Breaks (SSBs). Using a plasmid-nicking assay, we first determined the relative quantities of nucleobase and deoxyribose damage caused by the different $ONOO^-$ exposure regimes. The quantities of direct strand breaks (SSBs), which are caused predominantly by deoxyribose oxidation, were found to increase with increasing concentrations of $ONOO^-$ (both bolus addition and infusion), and SIN-1 (incubation for 100 min) (Figure 4 and 5). Formation of SSBs was greater with SIN-1 exposure than either type of $ONOO^-$ addition, with infusion causing the lowest number of SSBs. For all three dosage regimes, the formation of strand breaks was studied over a broad range of DNA damage frequencies. However, meaningful interpretation can only be achieved for damage occurring under single-hit conditions, which corresponds to < 30-40 strand breaks in 10^6 nt of pSP189 according to a Poisson distribution (Dedon et al., 1993). The range beyond single-hit conditions requires adjustment of the damage frequency to avoid underestimation of the number of strand breaks, since additional nicks in an already nicked plasmid cannot be detected by topoisomer analysis.

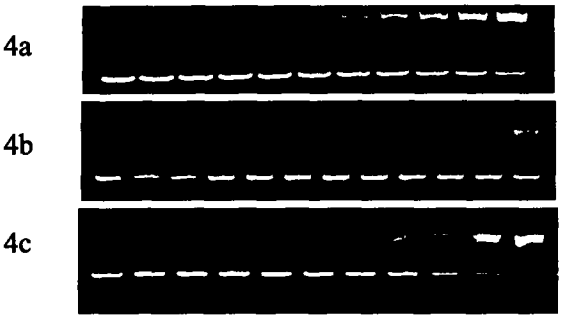

Figure 4. Plasmid topoisomer analysis of direct strand breaks in plasmid pSP189 caused by $ONOO^-$ and SIN-1 concentrations ranging from 0.1 μM to 3 mM (half-log steps; first lanes in 4a and 4b contain decomposed; second lanes in 4a and 4b and first lane in 4c contain untreated control). 4a: bolus $ONOO^-$ addition; 4b: infused $ONOO^-$ addition; 4c: SIN-1 (incubation for 100 min).

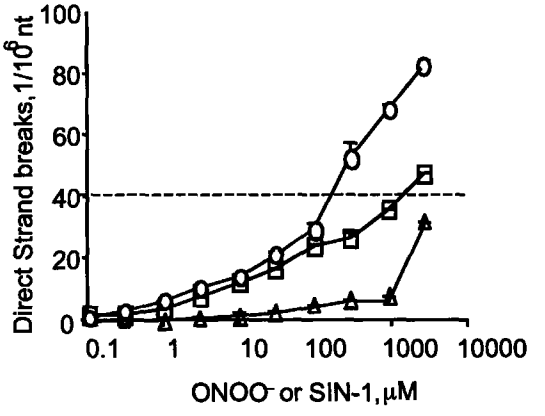

Figure 5. Direct strand breaks in pSP189 by $ONOO^-$ or SIN-1. The concentrations of bolus (□) and infused (△)$ONOO^-$ and SIN-1 (○; incubation for 100 min) ranged from 0.1 μM to 3 mM (half-log steps). Data represent mean ± S.D. for four measurements. Data points lying above the dot-line (40 strand breaks per 10^6 nt) fall outside single-hit conditions (see the text for details).

Effect of Putrescine Treatment on $ONOO^-$-treated Plasmid pSP189. Because oxidation of deoxyribose results in both strand breaks and abasic sites, we sought to quantify abasic site formation by converting the lesions to strand breaks with putrescine. This agent has been shown to cleave virtually all types of native and oxidized abasic sites in DNA (Dedon et al., 1993; Lindahl and Andersson, 1972; Lindahl and Nyberg, 1972; Yu et al., 1994). Interestingly, putrescine treatment only slightly increased the number of apparent strand breaks at low concentrations of both $ONOO^-$ deliveries and SIN-1 (incubation for 100 min), as seen by comparing Figures 5 and 6. For bolus addition, a small portion of these abasic sites may have arisen from depurination of 8-nitroguanine (8-nitro-G), which occurs with a half-life of ~4 h at 37 °C (Tretyakova et al., 2000). Such depurination likely does not account for abasic sites arising with infusion and SIN-1 treatments given the lower levels of base damage occurring with these treatments (vide infra) and the short time (1 hr) required for the putrescine reaction. The lack of significant putrescine effect for the three modes of $ONOO^-$ delivery also indicates that nucleobase modifications are not reactive toward putrescine and are stable during DNA processing.

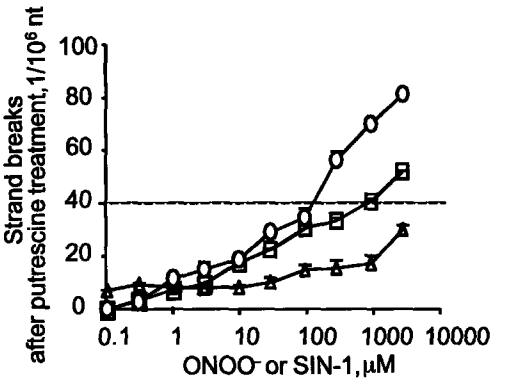

Figure 6. Strand breaks in $ONOO^-$ and SIN-1-treated plasmid pSP189. The concentrations of bolus (□) and infused (△)$ONOO^-$ and SIN-1 (○; incubation for 100 min) ranged from 0.1 μM to 3 mM (half-log steps). Data represent mean ± S.D. for four measurements. Data points lying above the dot-line (40 strand breaks per 10^6 nt) fall outside single-hit conditions (see the text for details).

Effect of Fpg Treatment on $ONOO^-$-treated Plasmid pSP189. With regard to nucleobase lesions, Fpg is a bi-functional DNA glycosylase that recognizes >90% of purine modifications caused by $ONOO^-$ (Tretyakova et al., 2000). The Fpg-sensitive sites can thus represent sites of both base oxidation and depurination. Along with direct strand breaks, the relaxed forms of plasmid pSP189 resolved on the agarose gel following Fpg-treatment represent the total quantity of DNA damage. The extent of total DNA damage was found to increase with $ONOO^-$/SIN-1 concentration (Figure 7). Clearly, the trend is that bolus addition method caused more total DNA damage than either infusion or SIN-1 (incubation for 100 min). At low concentrations, SIN-1 (incubation for 100 min) and $ONOO^-$ infusion produced similar amounts of total DNA damage, while at high concentrations (≥1 mM), infusion generated more damage.

Analysis of Nucleobase and Deoxyribose Oxidation Events. The goal of these studies was to quantify the effects of delivery method and delivery rate on the relative quantities of nucleobase and sugar damage produced by $ONOO^-$. To this end, we used the data presented in Figures 5, 6, and 7 to calculate nuceobase (Fpg-sensitive sites minus direct strand breaks) and deoxyriose oxidation events (putrescine-sensitive sites minus direct strand breaks). As shown in Figure 8, in the case of bolus $ONOO^-$ addition, both deoxyribose and nucleobase oxidation events were found to increase with increasing $ONOO^-$ dose, but the ratio was constant at ~2. For infusion at concentrations below 1 μM, there was no quantitative difference observed between deoxyribose and nucleobase oxidation, while above 1 μM, there was ~50% more nucleobase oxidation. However, in the case of SIN-1 (incubation for 100 min), deoxyribose oxidation events predominated over base oxidation events at all concentrations.

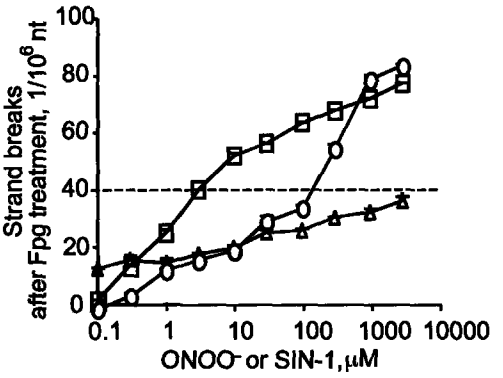

Figure 7. Strand breaks in pSP189 by $ONOO^-$ or SIN-1 after Fpg treatment. The concentrations of bolus (□) and infused (△)$ONOO^-$ and SIN-1 (○; incubation for 100 min) ranged from 0.1 μM to 3 mM (half-log steps). Data represent mean ± S.D. for four measurements. Data points lying above the dot-line (40 strand breaks per 10^6 nt) fall outside single-hit conditions (see the text for details).

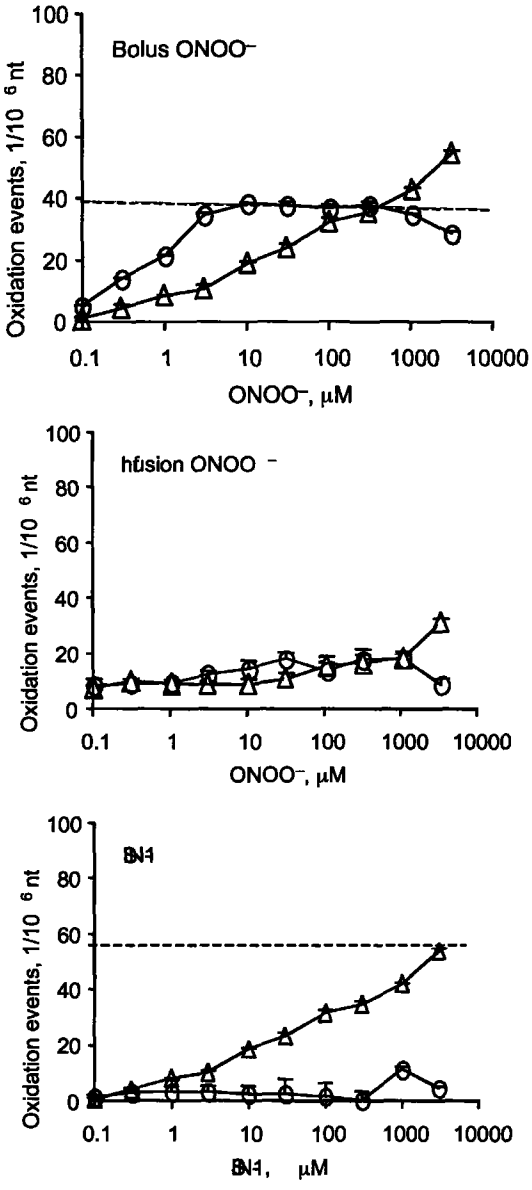

Figure 8. Deoxyribose (△) and base oxidation (○) events in pSP189 caused by different $ONOO^-$ exposure routes. 8a: bolus $ONOO^-$ addition; 8b: infused $ONOO^-$ addition; 8c: SIN-1 (incubation for 100 min). Data represent mean ± S.D. for four measurements. Data points lying above the dot-line (40 strand breaks per 10^6 nt) fall outside single-hit conditions (see the text for details).

7.5 Discussion

Effect of $ONOO^-$ Dose and Dose-rate on the Quantity of Total DNA Damage. A primary goal of this study was to determine the effects of dose and dose-rate of $ONOO^-$ exposure on the level of DNA damage, the frequency, and types and distribution of mutations, since these parameters may be of significance in the potential genotoxicity resulting from $ONOO^-$ formation *in vivo*.

We observed that the rate of $ONOO^-$ delivery influenced the yield of total DNA damage (Figure 7). Bolus $ONOO^-$ addition was shown to cause the most damage and infusion the least, with damage produced by SIN-1 felling between the other two (Figure 7). We believe that the difference is due to the chemistry underlying each exposure regimen. $ONOO^-$ reaction with DNA produces two major types of damage: direct strand breaks and abasic sites due to oxidation of deoxyribose, and the nitration and oxidation of guanine. While a comprehensive kinetic model to simulate the known features of $ONOO^-$ oxidation kinetics is beyond the scope of the current work, several explicit considerations are helpful to better understand the rates at which various types of DNA damage occur. $ONOO^-$ can react directly with target molecules. Those reaction rates are second-order overall, first-order in both $ONOO^-$ and the target. Additional reactions involve radicals that are generated during $ONOO^-$ decomposition. In the absence of CO_2, ONOOH decomposes via homolysis producing $^{\bullet}OH$ and $NO_2^{\bullet}$ radicals with up to 30-40% yield (Figure 1). Since radical formation is the rate-limiting step (Merenyi et al., 1998; Pfeiffer et al., 2000), this process will be first-order in $ONOO^-$ and zero-order in the targets. In the presence of physiological levels of CO_2, most $ONOO^-$ formed from $NO^{\bullet}$ and $O_2^{\bullet-}$ will react with CO_2 to give the $ONOOCO_2^-$ adduct. Homolytic decomposition of $ONOOCO_2^-$ yields (in part,

~33%) $NO_2^{\bullet}$ and $CO_3^{\bullet-}$ radicals, which cause one-electron oxidation or nitration of the substrate (Merenyi et al., 1998; Pfeiffer et al., 2000). In this case, the overall reaction rate depends on the $ONOO^-$ and CO_2 concentrations and is independent of the substrate concentration.

In this study, bolus addition and infusion of $ONOO^-$ and SIN-1 reactions were all performed in phosphate buffer containing the same concentration of bicarbonate (25 mM). Considering the fast reaction of $ONOO^-$ with CO_2, the major reactive species are therefore $NO_2^{\bullet}$ and $CO_3^{\bullet-}$, and the rates of DNA oxidation or nitration resulting from $NO_2^{\bullet}$ and $CO_3^{\bullet-}$ should be directly proportional to $ONOO^-$ concentration. We currently lack information on the steady-state $ONOO^-$ concentration for each type of addition, but the $ONOO^-$ flux can be used as a reasonable estimation of the local $ONOO^-$ concentration that a DNA molecule might encounter. Using 1 mM $ONOO^-$ as an example, under the condition of a bolus addition, the flux attained can be estimated as ~2000 μM/s, while for the infusion addition performed in this experiment, the flux was only ~2 μM/s. For SIN-1, the initial instantaneous $ONOO^-$ fluxes can be as low as 0.06 μM/s, based upon measured $NO^{\bullet}$ and $O_2^{\bullet-}$ production rates that have been reported (Doulias et al., 2001). Realizing that a quick formation rate does not necessarily lead to the accumulation of the product, we hypothesize that the ability of $ONOO^-$ to damage DNA through either nitration or oxidation is dependent on the *en mass* reaction at sufficient concentration (bolus) as opposed to an accrual of reactions over time with the infusion or *de novo* formation. Several observations from the studies of tyrosine nitration support this hypothesis. Espey et al. found that exposure of green fluorescent protein to bolus $ONOO^-$ resulted in a large increase of 3-nitrotyrosine formation, while the increase was not evident when the same amount of $ONOO^-$ was delivered by infusion addition was used (Espey et al., 2002). Zhang et al. reported a similar observation (Zhang et al., 2001). During bolus $ONOO^-$ addition, the levels of both nitration and oxidation of

tyrosine increased with increasing dose, while during slow infusion the level of nitration but not oxidation of tyrosine increased. The total number of tyrosine modifications was lower with infusion addition (Zhang et al., 2001).

Effect of Peroxynitrite Dose and Dose-rate on the Distribution of Deoxyribose and Nucleobase Oxidation Events. A further aim of this study was to define the proportions of deoxyribose and nucleobase oxidation by different exposure routes. As mentioned in the Introduction (Figures 2 and 3), different spectra of nucleobase oxidation products were observed for $ONOO^-$ delivery by the different methods, though the quantitative information regarding the formation of each product is not complete at present (Dedon and Tannenbaum, 2004). Bolus addition yields DGh, the major product, NO_2-DGh and CAC. Infusion forms Sp as the major product, followed by DGh, and lesser quantities of NO_2-DGh, CAC and HCA. SIN-1 only produces two products: Sp as a major, and HCA as a minor. The underlying mechanisms for production of these compounds proposed by the Tannenbaum group involved the initial formation of an electrophilic reactive intermediate, with the succeeding $ONOO^-$ and H_2O competition for this species (Dedon and Tannenbaum, 2004). Thus, during infusion additions, H_2O competes more effectively due to the sufficient decrease of steady-state concentration of $ONOO^-$, while, during SIN-1 exposure, H_2O exclusively traps this intermediate.

We observed differences in the yield of nucleobase oxidation products (Fpg-sensitive sites alone) with different $ONOO^-$ exposure routes, with bolus addition causing the highest level of nucleobase oxidation, and SIN-1 causing the least. In addition to possible reason that the flux of $ONOO^-$ may influence the kinetics of the formation of different oxidative products, the sensitivity of each product to Fpg treatment may also account for the difference. Leipold et al.

showed that Gh and Sp, resulting from the oxidation of 8-oxoG are efficiently removed by Fpg (Leipold et al., 2000). The activity of Fpg toward other lesions, including NO_2-DGh, CAC and HCA, has not been reported yet. These latter lesions represent a minor portion of the spectrum of $ONOO^-$-induced oxidation of dG, such that they can be ignored in our studies of Fpg-sensitive lesions (Dedon and Tannenbaum, 2004). We thus conclude that the Fpg-sensitive lesions represent nucleobase oxidation produced by $ONOO^-$.

There were several intriguing features in the studies to define the proportions of deoxyribose to nucleobase oxidation by different exposure routes, intriguing data were obtained. We found that SIN-1 exposure almost exclusively favored deoxyribose oxidation (Figure 8), though the ratio of deoxyribose to nucleobase oxidation increased with increasing concentrations of SIN-1 (Figure 8). We currently cannot explain the chemical basis for this result, except to speculate that the radical intermediate yielding $NO^\bullet$ and $O_2^{\bullet-}$ somehow participate in the DNA damage chemistry.

Effects of Peroxynitrite Dose and Dose-rate on DNA Damage and Mutation (in collaboration with Dr. Min Young Kim). Previous studies showed that bolus exposure of the pSP189 plasmid to 2.5 mM $ONOO^-$ increased the mutation frequency (MF) in plasmid replicated in *E. coli* MBL50 cells or in human cells (Juedes and Wogan, 1996; Pamir and Wogan, 2003). Linear and dose-dependent increases in MF were induced by exposure to $ONOO^-$ concentrations up to 4.5 mM, in both the presence and absence of $NaHCO_3/CO_2$, but the presence of bicarbonate substantially reduced the mutagenic response (Pamir and Wogan, 2003). Because single, large bolus doses were used in those experiments, Dr. Min Yong Kim investigated the MF associated with the different $ONOO^-$ delivery methods using the same DNA samples that we used for

damage analysis. The MF associated with all three exposures increased dose-dependently, but bolus exposure was most effective, indicating that $ONOO^-$ introduced slowly over time by either infusion or SIN-1 degradation was less capable of inducing mutation. Consistent with this interpretation, the transformation efficiency (an indication of total DNA damage) of plasmid molecule exposed to bolus addition of $ONOO^-$ was lower than that for infusion or to SIN-1 (data not shown). These results are also consistent with the DNA damage data discussed earlier.

To characterize the effects of dose and dose-rate of $ONOO^-$ exposure on mutation spectra, mutants (~100) induced by bolus, infusion and SIN-1 treatments, respectively, were sequenced and analyzed. Almost all hotspots were located at G:C sites and hot spots C108 and C168 were common to all exposures. G113, G115, G116 were common to both the bolus- and the infused-$ONOO^-$ exposures, whereas G129 was common to both the infused- $ONOO^-$ and SIN-1 exposures. Mutations tended to localize preferentially at certain sites following both the bolus and infused $ONOO^-$ exposures, whereas they were more randomly scattered along the *supF* gene following SIN-1 exposure. This result is consistent with sequence nonselective deoxyribose oxidation, and not guanine oxidation, as the major form of DNA damage produced by SIN-1 and it suggests that the chemistry of DNA damage induced by SIN-1 may differ from that induced by $ONOO^-$.

The predominant mutations found following all exposures were single base-pair substitutions, together with smaller numbers of multiple sequence changes, one base pair deletions and one base pair insertions. Multiple sequence changes are a ubiquitous component of shuttle vector mutagenesis. Since they have also been observed in cellular genes, the mechanisms responsible may be relevant to mutagenesis of cellular genes, including those involved in carcinogenesis (Strauss, 1998). Following bolus $ONOO^-$ exposure, most single base

substitutions occurred at G:C sites, and included G:C to T:A and G:C to C:G transversions as well as G:C to A:T transitions. In all exposure scenarios, G:C to T:A transversions were most frequent, along with lesser numbers of G:C to C:G transversions and G:C to A:T transitions, confirming that G:C pairs are the major targets damaged by $ONOO^-$ treatment, consistent with our previous findings (Juedes and Wogan, 1996; Pamir and Wogan, 2003).

It is of interest that G:C to T:A transversions comprise a significant fraction of mutations in oncogenes and tumor suppressor genes in human cancer, especially in lung cancer (Bennett et al., 1999; Hainaut and Pfeifer, 2001). G:C to T:A base substitutions can result from a variety of DNA lesions including thymine glycol, apurinic/apyrimidinic sites, 8-oxo-dG, 8-chloro-2′-deoxyguanosine (8-Cl-dG), or 8-bromo-2′-deoxyguanosine (8-Br-dG) formed in DNA in some systems (Juedes and Wogan, 1996; Masuda et al., 2001; Ohshima et al., 2003; Shibutani et al., 1991; Tretyakova et al., 2000; Wang et al., 1998), including those frequently found in tumor relevant genes (Bruner et al., 2000). It is well established that the two main types of chemistries attributed to $ONOO^-$ are oxidation and nitration (Beckman et al., 1990; Bonfoco et al., 1995; Ducrocq et al., 1999; Murphy et al., 1998; Squadrito and Pryor, 1998), resulting in the production of 8-oxo-dG or 8-nitro-G (Szabo, 2003). 8-Oxo-dG has been utilized as a biomarker for monitoring DNA damage with a number of oxidizing agents, and its formation in nucleic acid is known to cause mutations (Szabo, 2003). SIN-1 has also been shown to induce significant levels of 8-oxo-G in plasmid DNA and calf thymus DNA (Inoue and Kawanishi, 1995). 8-Nitro-dG undergoes spontaneous depurination leading to apurinic sites in DNA (Yermilov et al., 1995), leading to G:C to T:A transversions (Loeb and Preston, 1986). Our present results are therefore consistent with nitration and/or one-electron oxidations induced by $NO_2^{\bullet}$ and $CO_3^{\bullet-}$ radicals, as noted above, since all exposures were done in the presence of bicarbonate. In addition, 8-nitro-

dG nucleoside is capable of producing superoxide in the presence of certain oxidoreductases such as NADPH-cytochrome P450 reductase and NOS and might enhance oxidative DNA and tissue damage (Ohshima et al., 2003).

Interestingly, we found that G:C to C:G mutations were less frequent following infusion or SIN-1 than those induced by bolus exposure under our experimental conditions. G:C to C:G transversions have been observed in mutagenesis experiments with lipid peroxidation systems (Akasaka and Yamamoto, 1994), and their frequency is considerably higher under oxidative stress (Maehira et al., 1999; McBride et al., 1991; McBride et al., 1992; Oller and Thilly, 1992; Ono et al., 1995; Takimoto et al., 1999). Our results therefore suggest that infused- $ONOO^-$ and SIN-1 exposure may cause less oxidative damage compared with bolus- $ONOO^-$ exposure. Shin et al. (Shin et al., 2002) demonstrated that the initial formation of C:C or G:G mispairs provides the most plausible explanation for the elevated presence of the G:C to C:G mutations. Kino et al. (Kino and Sugiyama, 2001) reported that 8-oxo-G is not responsible for G:G to C:G transversions, because dGTP was not incorporated opposite 8-oxo-G in the DNA polymerase extension assay using a template containing 8-oxo-dG. These authors suggested that 8-oxo-G is further oxidized to 2, 5-diamino-4*H*-imidazol-4-one (Iz) and the specific formation Iz:G base pairs may cause G:C to C:G transversion mutations (Kino and Sugiyama, 2001), but the origin of G:C to C:G transverisons is still undefined.

Conclusion. In summary, reactive oxygen and nitrogen species generated by inflammatory cells have been proposed to induce DNA and tissue damage, chromosomal aberrations and mutations, which contribute to the multistage process of carcinogenesis (Ohshima et al., 2003). Increasing evidence now suggests that $ONOO^-$ is a major agent causing tissue damage in inflammatory

disorders, and oxidative damage to DNA is among events taking place during chronic inflammation *in vivo* (Cazevieille et al., 1993; Mulligan et al., 1991; White et al., 1994). An important source of $ONOO^-$ *in vivo* is the activated macrophage, which has been implicated in causing tissue damage during chronic inflammatory conditions by mechanisms that might involve $ONOO^-$ (Ischiropoulos et al., 1992). The genotoxic effects in the $NO^{\bullet}$-producing cells were previously characterized using mouse macrophage-like RAW264.7 cells as a co-culture system for the study of $NO^{\bullet}$-associated genotoxicity under physiologically relevant conditions (Zhuang et al., 2002). These studies demonstrated that $NO^{\bullet}$ overproduction might contribute to genotoxic risks associated with chronic inflammation. In work reported here, we found that both dose and dose-rate at which a genetic target is exposed to $ONOO^-$ substantially influence the amount and type of DNA damage, the mutagenic potency, and the types and distribution of mutations in the gene, indicating that these parameters will need to be taken into account in assessing the potential effects of $ONOO^-$ *in vivo*. Furthermore, the results indicate that the chemistry of SIN-1-induced DNA damage differs substantially from native $ONOO^-$, which suggests the need for caution in interpreting the biological relevance of SIN-1 as a surrogate for $ONOO^-$.

The systems used to introduce $ONOO^-$ in these experiments were designed to approximate conditions of exposure more physiologically relevant to chronic inflammation than bolus additions, since cells *in vivo* are likely to be exposed over longer periods of time rather than to high concentrations for short periods (Doulias et al., 2001). Hence, our findings provide important clues that dose and dose-rate $ONOO^-$ introduction may contribute to potential genotoxicity resulting from $ONOO^-$ formation *in vivo*. Further studies will be required to

elucidate precise mechanisms underlying these effects and their potential relevance to $ONOO^-$ induced cytotoxicity *in vivo*.

7.6 Reference

Akasaka, S., and Yamamoto, K.: Mutagenesis resulting from DNA damage by lipid peroxidation in the supF gene of Escherichia coli. *In* Mutat Res, vol. 315, pp. 105-12, 1994.

Beckman, J. S., Beckman, T. W., Chen, J., Marshall, P. A., and Freeman, B. A.: Apparent hydroxyl radical production by peroxynitrite: implications for endothelial injury from nitric oxide and superoxide. *In* Proc Natl Acad Sci U S A, vol. 87, pp. 1620-4, 1990.

Beckman, J. S., Chen, J., Ischiropoulos, H., and Crow, J. P.: Oxidative chemistry of peroxynitrite. *In* Methods Enzymol, vol. 233, pp. 229-40, 1994.

Bennett, W. P., Hussain, S. P., Vahakangas, K. H., Khan, M. A., Shields, P. G., and Harris, C. C.: Molecular epidemiology of human cancer risk: gene-environment interactions and p53 mutation spectrum in human lung cancer. *In* J Pathol, vol. 187, pp. 8-18, 1999.

Bigger, C. A., St John, J., Yagi, H., Jerina, D. M., and Dipple, A.: Mutagenic specificities of four stereoisomeric benzo[c]phenanthrene dihydrodiol epoxides. *In* Proc Natl Acad Sci U S A, vol. 89, pp. 368-72, 1992.

Bonfoco, E., Krainc, D., Ankarcrona, M., Nicotera, P., and Lipton, S. A.: Apoptosis and necrosis: two distinct events induced, respectively, by mild and intense insults with N-methyl-D-aspartate or nitric oxide/superoxide in cortical cell cultures. *In* Proc Natl Acad Sci U S A, vol. 92, pp. 7162-6, 1995.

Brunelli, L., Crow, J. P., and Beckman, J. S.: The comparative toxicity of nitric oxide and peroxynitrite to Escherichia coli. *In* Arch Biochem Biophys, vol. 316, pp. 327-34, 1995.

Bruner, S. D., Norman, D. P., and Verdine, G. L.: Structural basis for recognition and repair of the endogenous mutagen 8-oxoguanine in DNA. *In* Nature, vol. 403, pp. 859-66, 2000.

Bunderson, M., Coffin, J. D., and Beall, H. D.: Arsenic induces peroxynitrite generation and cyclooxygenase-2 protein expression in aortic endothelial cells: possible role in atherosclerosis. *In* Toxicol Appl Pharmacol, vol. 184, pp. 11-8, 2002.

Burney, S., Niles, J. C., Dedon, P. C., and Tannenbaum, S. R.: DNA damage in deoxynucleosides and oligonucleotides treated with peroxynitrite. *In* Chem Res Toxicol, vol. 12, pp. 513-20, 1999.

Cazevieille, C., Muller, A., Meynier, F., and Bonne, C.: Superoxide and nitric oxide cooperation in hypoxia/reoxygenation-induced neuron injury. *In* Free Radic Biol Med, vol. 14, pp. 389-95, 1993.

Darley-Usmar, V., Wiseman, H., and Halliwell, B.: Nitric oxide and oxygen radicals: a question of balance. *In* FEBS Lett, vol. 369, pp. 131-5, 1995.

de Groot, M. J., Coumans, W. A., Willemsen, P. H., and van der Vusse, G. J.: Substrate-induced changes in the lipid content of ischemic and reperfused myocardium. Its relation to hemodynamic recovery. *In* Circ Res, vol. 72, pp. 176-86, 1993.

Dedon, P. C., Salzberg, A. A., and Xu, J.: Exclusive production of bistranded DNA damage by calicheamicin. *In* Biochemistry, vol. 32, pp. 3617-22, 1993.

Dedon, P. C., and Tannenbaum, S. R.: Reactive nitrogen species in the chemical biology of inflammation. *In* Arch Biochem Biophys, vol. 423, pp. 12-22, 2004.

Douki, T., and Cadet, J.: Peroxynitrite mediated oxidation of purine bases of nucleosides and isolated DNA. *In* Free Radic Res, vol. 24, pp. 369-80, 1996.

Doulias, P. T., Barbouti, A., Galaris, D., and Ischiropoulos, H.: SIN-1-induced DNA damage in isolated human peripheral blood lymphocytes as assessed by single cell gel electrophoresis (comet assay). *In* Free Radic Biol Med, vol. 30, pp. 679-85, 2001.

Ducrocq, C., Blanchard, B., Pignatelli, B., and Ohshima, H.: Peroxynitrite: an endogenous oxidizing and nitrating agent. *In* Cell Mol Life Sci, vol. 55, pp. 1068-77, 1999.

Espey, M. G., Xavier, S., Thomas, D. D., Miranda, K. M., and Wink, D. A.: Direct real-time evaluation of nitration with green fluorescent protein in solution and within human cells reveals the impact of nitrogen dioxide vs. peroxynitrite mechanisms. *In* Proc Natl Acad Sci U S A, vol. 99, pp. 3481-6, 2002.

Goldstein, S. R., Yang, G. Y., Chen, X., Curtis, S. K., and Yang, C. S.: Studies of iron deposits, inducible nitric oxide synthase and nitrotyrosine in a rat model for esophageal adenocarcinoma. *In* Carcinogenesis, vol. 19, pp. 1445-9, 1998.

Hainaut, P., and Pfeifer, G. P.: Patterns of p53 G-->T transversions in lung cancers reflect the primary mutagenic signature of DNA-damage by tobacco smoke. *In* Carcinogenesis, vol. 22, pp. 367-74, 2001.

Inoue, S., and Kawanishi, S.: Oxidative DNA damage induced by simultaneous generation of nitric oxide and superoxide. *In* FEBS Lett, vol. 371, pp. 86-8, 1995.

Ischiropoulos, H., Zhu, L., and Beckman, J. S.: Peroxynitrite formation from macrophage-derived nitric oxide. *In* Arch Biochem Biophys, vol. 298, pp. 446-51, 1992.

Jeong, J. K., Juedes, M. J., and Wogan, G. N.: Mutations induced in the supF gene of pSP189 by hydroxyl radical and singlet oxygen: relevance to peroxynitrite mutagenesis. *In* Chem Res Toxicol, vol. 11, pp. 550-6, 1998.

Juedes, M. J., and Wogan, G. N.: Peroxynitrite-induced mutation spectra of pSP189 following replication in bacteria and in human cells. *In* Mutat Res, vol. 349, pp. 51-61, 1996.

Jugdutt, B. I.: Nitric oxide and cardioprotection during ischemia-reperfusion. *In* Heart Fail Rev, vol. 7, pp. 391-405, 2002.

Kennedy, L. J., Moore, K., Jr., Caulfield, J. L., Tannenbaum, S. R., and Dedon, P. C.: Quantitation of 8-oxoguanine and strand breaks produced by four oxidizing agents. *In* Chem Res Toxicol, vol. 10, pp. 386-92, 1997.

Kino, K., and Sugiyama, H.: Possible cause of G-C-->C-G transversion mutation by guanine oxidation product, imidazolone. *In* Chem Biol, vol. 8, pp. 369-78, 2001.

Kuhn, D. M., Aretha, C. W., and Geddes, T. J.: Peroxynitrite inactivation of tyrosine hydroxylase: mediation by sulfhydryl oxidation, not tyrosine nitration. *In* J Neurosci, vol. 19, pp. 10289-94, 1999.

Leipold, M. D., Muller, J. G., Burrows, C. J., and David, S. S.: Removal of hydantoin products of 8-oxoguanine oxidation by the Escherichia coli DNA repair enzyme, FPG. *In* Biochemistry, vol. 39, pp. 14984-92, 2000.

Lindahl, T., and Andersson, A.: Rate of chain breakage at apurinic sites in double-stranded deoxyribonucleic acid. *In* Biochemistry, vol. 11, pp. 3618-23, 1972.

Lindahl, T., and Nyberg, B.: Rate of depurination of native deoxyribonucleic acid. *In* Biochemistry, vol. 11, pp. 3610-8, 1972.

Loeb, L. A., and Preston, B. D.: Mutagenesis by apurinic/apyrimidinic sites. *In* Annu Rev Genet, vol. 20, pp. 201-30, 1986.

MacMillan-Crow, L. A., Crow, J. P., Kerby, J. D., Beckman, J. S., and Thompson, J. A.: Nitration and inactivation of manganese superoxide dismutase in chronic rejection of human renal allografts. *In* Proc Natl Acad Sci U S A, vol. 93, pp. 11853-8, 1996.

Maehira, F., Miyagi, I., Asato, T., Eguchi, Y., Takei, H., Nakatsuki, K., Fukuoka, M., and Zaha, F.: Alterations of protein kinase C, 8-hydroxydeoxyguanosine, and K-ras oncogene in rat lungs exposed to passive smoking. *In* Clin Chim Acta, vol. 289, pp. 133-44, 1999.

Masuda, M., Suzuki, T., Friesen, M. D., Ravanat, J. L., Cadet, J., Pignatelli, B., Nishino, H., and Ohshima, H.: Chlorination of guanosine and other nucleosides by hypochlorous acid and myeloperoxidase of activated human neutrophils. Catalysis by nicotine and trimethylamine. *In* J Biol Chem, vol. 276, pp. 40486-96, 2001.

McBride, T. J., Preston, B. D., and Loeb, L. A.: Mutagenic spectrum resulting from DNA damage by oxygen radicals. *In* Biochemistry, vol. 30, pp. 207-13, 1991.

McBride, T. J., Schneider, J. E., Floyd, R. A., and Loeb, L. A.: Mutations induced by methylene blue plus light in single-stranded M13mp2. *In* Proc Natl Acad Sci U S A, vol. 89, pp. 6866-70, 1992.

Merenyi, G., Lind, J., Goldstein, S., and Czapski, G.: Peroxynitrous acid homolyzes into *OH and *NO2 radicals. *In* Chem Res Toxicol, vol. 11, pp. 712-3, 1998.

Motohashi, N., and Saito, Y.: Induction of SOS response in Salmonella typhimurium TA4107/pSK1002 by peroxynitrite-generating agent, N-morpholino sydnonimine. *In* Mutat Res, vol. 502, pp. 11-8, 2002.

Mulligan, M. S., Hevel, J. M., Marletta, M. A., and Ward, P. A.: Tissue injury caused by deposition of immune complexes is L-arginine dependent. *In* Proc Natl Acad Sci U S A, vol. 88, pp. 6338-42, 1991.

Murphy, M. P., Packer, M. A., Scarlett, J. L., and Martin, S. W.: Peroxynitrite: a biologically significant oxidant. *In* Gen Pharmacol, vol. 31, pp. 179-86, 1998.

Nair, J., Gal, A., Tamir, S., Tannenbaum, S. R., Wogan, G. N., and Bartsch, H.: Etheno adducts in spleen DNA of SJL mice stimulated to overproduce nitric oxide. *In* Carcinogenesis, vol. 19, pp. 2081-4, 1998.

Ohshima, H., and Bartsch, H.: Chronic infections and inflammatory processes as cancer risk factors: possible role of nitric oxide in carcinogenesis. *In* Mutat Res, vol. 305, pp. 253-64, 1994.

Ohshima, H., Tatemichi, M., and Sawa, T.: Chemical basis of inflammation-induced carcinogenesis. *In* Arch Biochem Biophys, vol. 417, pp. 3-11, 2003.

Oller, A. R., and Thilly, W. G.: Mutational spectra in human B-cells. Spontaneous, oxygen and hydrogen peroxide-induced mutations at the hprt gene. *In* J Mol Biol, vol. 228, pp. 813-26, 1992.

Ono, T., Negishi, K., and Hayatsu, H.: Spectra of superoxide-induced mutations in the lacI gene of a wild-type and a mutM strain of Escherichia coli K-12. *In* Mutat Res, vol. 326, pp. 175-83, 1995.

Pamir, B., and Wogan, G. N.: Carbon dioxide modulation of peroxynitrite-induced mutagenesis of the supF gene in pSP189. *In* Chem Res Toxicol, vol. 16, pp. 487-92, 2003.

Parris, C. N., and Seidman, M. M.: A signature element distinguishes sibling and independent mutations in a shuttle vector plasmid. *In* Gene, vol. 117, pp. 1-5, 1992.

Pfeiffer, S., and Mayer, B.: Lack of tyrosine nitration by peroxynitrite generated at physiological pH. *In* J Biol Chem, vol. 273, pp. 27280-5, 1998.

Pfeiffer, S., Schmidt, K., and Mayer, B.: Dityrosine formation outcompetes tyrosine nitration at low steady-state concentrations of peroxynitrite. Implications for tyrosine modification by nitric oxide/superoxide in vivo. *In* J Biol Chem, vol. 275, pp. 6346-52, 2000.

Pryor, W. A., Cueto, R., Jin, X., Koppenol, W. H., Ngu-Schwemlein, M., Squadrito, G. L., Uppu, P. L., and Uppu, R. M.: A practical method for preparing peroxynitrite solutions of low ionic strength and free of hydrogen peroxide. *In* Free Radic Biol Med, vol. 18, pp. 75-83, 1995.

Radi, R., Peluffo, G., Alvarez, M. N., Naviliat, M., and Cayota, A.: Unraveling peroxynitrite formation in biological systems. *In* Free Radic Biol Med, vol. 30, pp. 463-88, 2001.

Reden, J.: Molsidomine. *In* Blood Vessels, vol. 27, pp. 282-94, 1990.

Seidman, M. M., Dixon, K., Razzaque, A., Zagursky, R. J., and Berman, M. L.: A shuttle vector plasmid for studying carcinogen-induced point mutations in mammalian cells. *In* Gene, vol. 38, pp. 233-7, 1985.

Shibutani, S., Takeshita, M., and Grollman, A. P.: Insertion of specific bases during DNA synthesis past the oxidation-damaged base 8-oxodG. *In* Nature, vol. 349, pp. 431-4, 1991.

Shin, C. Y., Ponomareva, O. N., Connolly, L., and Turker, M. S.: A mouse kidney cell line with a G:C --> C:G transversion mutator phenotype. *In* Mutat Res, vol. 503, pp. 69-76, 2002.

Singh, R. J., Hogg, N., Joseph, J., Konorev, E., and Kalyanaraman, B.: The peroxynitrite generator, SIN-1, becomes a nitric oxide donor in the presence of electron acceptors. *In* Arch Biochem Biophys, vol. 361, pp. 331-9, 1999.

Squadrito, G. L., and Pryor, W. A.: Oxidative chemistry of nitric oxide: the roles of superoxide, peroxynitrite, and carbon dioxide. *In* Free Radic Biol Med, vol. 25, pp. 392-403, 1998.

Strauss, B. S.: Hypermutability in carcinogenesis. *In* Genetics, vol. 148, pp. 1619-26, 1998.

Szabo, C.: Multiple pathways of peroxynitrite cytotoxicity. *In* Toxicol Lett, vol. 140-141, pp. 105-12, 2003.

Takimoto, K., Tano, K., Hashimoto, M., Hori, M., Akasaka, S., and Utsumi, H.: Delayed transfection of DNA after riboflavin mediated photosensitization increases G:C to C:G transversions of supF gene in Escherichia coli mutY strain. *In* Mutat Res, vol. 445, pp. 93-8, 1999.

Tretyakova, N. Y., Burney, S., Pamir, B., Wishnok, J. S., Dedon, P. C., Wogan, G. N., and Tannenbaum, S. R.: Peroxynitrite-induced DNA damage in the supF gene: correlation with the mutational spectrum. *In* Mutat Res, vol. 447, pp. 287-303, 2000.

Tretyakova, N. Y., Niles, J. C., Burney, S., Wishnok, J. S., and Tannenbaum, S. R.: Peroxynitrite-induced reactions of synthetic oligonucleotides containing 8-oxoguanine. *In* Chem Res Toxicol, vol. 12, pp. 459-66, 1999.

Uppu, R. M., and Pryor, W. A.: Carbon dioxide catalysis of the reaction of peroxynitrite with ethyl acetoacetate: an example of aliphatic nitration by peroxynitrite. *In* Biochem Biophys Res Commun, vol. 229, pp. 764-9, 1996.

Wang, D., Kreutzer, D. A., and Essigmann, J. M.: Mutagenicity and repair of oxidative DNA damage: insights from studies using defined lesions. *In* Mutat Res, vol. 400, pp. 99-115, 1998.

White, C. R., Brock, T. A., Chang, L. Y., Crapo, J., Briscoe, P., Ku, D., Bradley, W. A., Gianturco, S. H., Gore, J., and Freeman, B. A.: Superoxide and peroxynitrite in atherosclerosis. *In* Proc Natl Acad Sci U S A, vol. 91, pp. 1044-8, 1994.

Yermilov, V., Rubio, J., and Ohshima, H.: Formation of 8-nitroguanine in DNA treated with peroxynitrite in vitro and its rapid removal from DNA by depurination. *In* FEBS Lett, vol. 376, pp. 207-10, 1995.

Yu, L., Goldberg, I. H., and Dedon, P. C.: Enediyne-mediated DNA damage in nuclei is modulated at the level of the nucleosome. *In* J Biol Chem, vol. 269, pp. 4144-51, 1994.

Zhang, H., Joseph, J., Feix, J., Hogg, N., and Kalyanaraman, B.: Nitration and oxidation of a hydrophobic tyrosine probe by peroxynitrite in membranes: comparison with nitration and oxidation of tyrosine by peroxynitrite in aqueous solution. *In* Biochemistry, vol. 40, pp. 7675-86, 2001.

Zhang, H., Zhang, D. L., Li, R. F., and Guo, C. H.: [Role of expression inducible nitric oxide synthase-mRNA of leukocyte and nasal mucosa in allergic rhinitis]. *In* Zhonghua Er Bi Yan Hou Ke Za Zhi, vol. 38, pp. 32-4, 2003.

Zhuang, J. C., Lin, D., Lin, C., Jethwaney, D., and Wogan, G. N.: Genotoxicity associated with NO production in macrophages and co-cultured target cells. *In* Free Radic Biol Med, vol. 33, pp. 94-102, 2002.

Appendix I

Role of Purine Metabolism in the Cellular Burden of Mutagenic DNA Deamination Lesion.

Abstract

Endogenous processes and chemicals are increasingly recognized as important causes of DNA damage that leads to human diseases such as cancer. The most well studied examples include reactions of DNA bases with reactive oxygen and nitrogen species or with electrophiles generated from lipids, proteins and nucleic acids. We now present data consistent with a new paradigm in which perturbations of nucleobase metabolism may lead to incorporation of the purine precursors hypoxanthine (I) and xanthine (X) into DNA. As part of a systematic analysis of the genes affecting the levels of I and X in DNA, RNA and the nucleotide pool, this set of studies employed *E. coli* strains containing single or combinatorial deletions of the genes encoding deoxyribonucleotide triphosphate pyrophosphohydrolase *(rdgB)*, adenylosuccinate synthetase *(purA)*, endonuclease V *(nfi)*, adneylosuccinate lyase *(purB)*, GMP synthase *(guaA)*, and IMP dehydrogenase *(guaB)*. Purified genomic DNA from each strain was subjected to LC-MS analysis to quantify four nucleobase deamination products: deoxyxanthosine (dX), deoxyoxanosine (dO), deoxyinosine (dI), and deoxyuridine (dU). We observed that DNA from the *purA* mutant showed ~ two-fold increase in dI over the wild type strain (8 vs. 17 dI per 10^6 nt), but a 50- to 60-fold increase in dI in DNA was found in the double *rdgB* and *purA* mutant (500-600 dI per 10^6 nt). Increases in dX in DNA were observed in the *purA/rdgB/guaA* mutant over the wild type strain (2 vs. 10 dX per 10^6 nt), though the magnitude of the increase in dX is considerably smaller than changes observed in dI in spite of the parallel nature of the mutations. dO did not occur at detectable level in any tested strain (<6 lesions per 10^8 nt,), which is consistent with our previous studies *in vitro* and in cultured cells. These results reveal a genotoxic synergy that arises as a result of alterations in purine metabolism combined with

nucleotide pool repair enzymes, a synergy that may extend to pyrimidine metabolism and to other facets of DNA repair. Given the highly conserved nature of purine metabolism, the results will have implications for the genotoxic consequences of human genetic polymorphisms in purine metabolism in conjunction with ongoing inflammation and other sources of nitrosative stress. Furthermore, the results obtained in this study will assist in establishing a database for the creation of predictive models that link purine metabolism to the pathophysiology of cancer and aging.

Introduction

Deamination of nucleobases in DNA results in the formation of 2'-deoxyxanthosine, 2'-deoxyinosine, 2'-deoxyoxanosine and 2'-deoxyuridine (Figure 1). Several established mechanisms can lead to nucleobase deamination. In addition to exogenous agents such as bisulfite (Loeb and Kunkel, 1982), there are three major endogenous mechanisms for nucleobase deamination. The simplest is hydrolytic deamination that occurs in all aqueous environments. The propensity for hydrolytic deamination of DNA occurs in the order of 5-methyl-dC > dC > dA > dG (Frederico et al., 1990; Lindahl, 1974), with a half-life for dC in the range of 10^2-10^3 years for single-stranded DNA and 10^4-10^5 years in double-stranded DNA (Frederico et al., 1990; Shen et al., 1994; Zhang and Mathews, 1994). C^5-Methylation of dC increases the rate of deamination by 2- to 20-fold (Shen et al., 1994; Zhang and Mathews, 1994). The high deamination rate in dC and 5'-methyl-dC has been proposed to account for the fact that C→T mutations at CpG sites represent are the most common human mutation (Krokan et al., 2002).

A second major form of nucleobase deamination is associated with the chemistry of inflammation in humans. Macrophage-derived nitric oxide ($NO^{\bullet}$) is one of the major chemical mediators of inflammation. Though $NO^{\bullet}$ is a radical, its genotoxicity likely arises from derivatives such as N_2O_3 and peroxynitrite ($ONOO^-$), which are formed in reactions with O_2 and superoxide, respectively (Tamir et al., 1996). N_2O_3 is a strong nitrosating agent that, in addition to forming *N*-nitrosamines (Tannenbaum et al., 1994), will react with the 1° and heterocyclic amines in DNA bases to create mutagenic deamination products (Figure 1), abasic sites and DNA cross-links (Dubelman and Shapiro, 1977; Kirchner et al., 1992; Nguyen et al., 1992; Shapiro and Pohl, 1968; Shapiro and Yamaguchi, 1972; Suzuki et al., 1996; Wink et al., 1991).

The reactivity of DNA bases with N_2O_3 is reversed relative to hydrolysis (Caulfield et al., 1998). In addition to deamination of the exocyclic amines, nitrosation of the N^7-dG and N^7 or N^3 of dA destabilizes the glycosidic bond and leads to depurination (Lucas et al., 2001; Lucas et al., 1999).

A third form of nucleobase deamination, particular to 2'-deoxycytidine (dC), is associated with the activity of deaminases. An activation-induced cytidine deaminase (AID) was recently discovered that appears to be required for the final stages of antibody maturation by introducing a wide variety of base substitutions in the immunoglobulin genes and by creating region-specific double-strand breaks (Petersen-Mahrt et al., 2002). The AID protein, which shuttles between the nucleus and cytoplasm (Ito et al., 2004), was originally thought only to deaminate cytidine within the context of single-stranded DNA (Bransteitter et al., 2003; Pham et al., 2003), but recent studies by Shen, et al. indicated that AID can affect both strands of DNA in targeting supercoiled plasmids (Shen and Storb, 2004). AID is a B-cell-specific protein and its expression has been confirmed in human B-cells and in non-Hodgkin's lymphomas (Greeve et al., 2003; Muto et al., 2000).

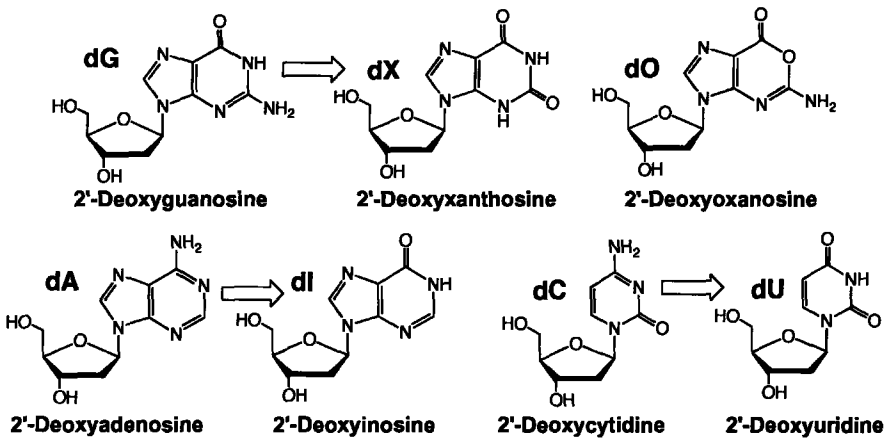

Figure 1. Nucleobase deamination products as 2'-deoxynucleosides.

We propose a fourth mechanism that represents a new paradigm in which perturbations of purine metabolism may lead to incorporation of the purine precursors I and X into DNA.

Figure 2: Purine biosynthesis in *E. coli*

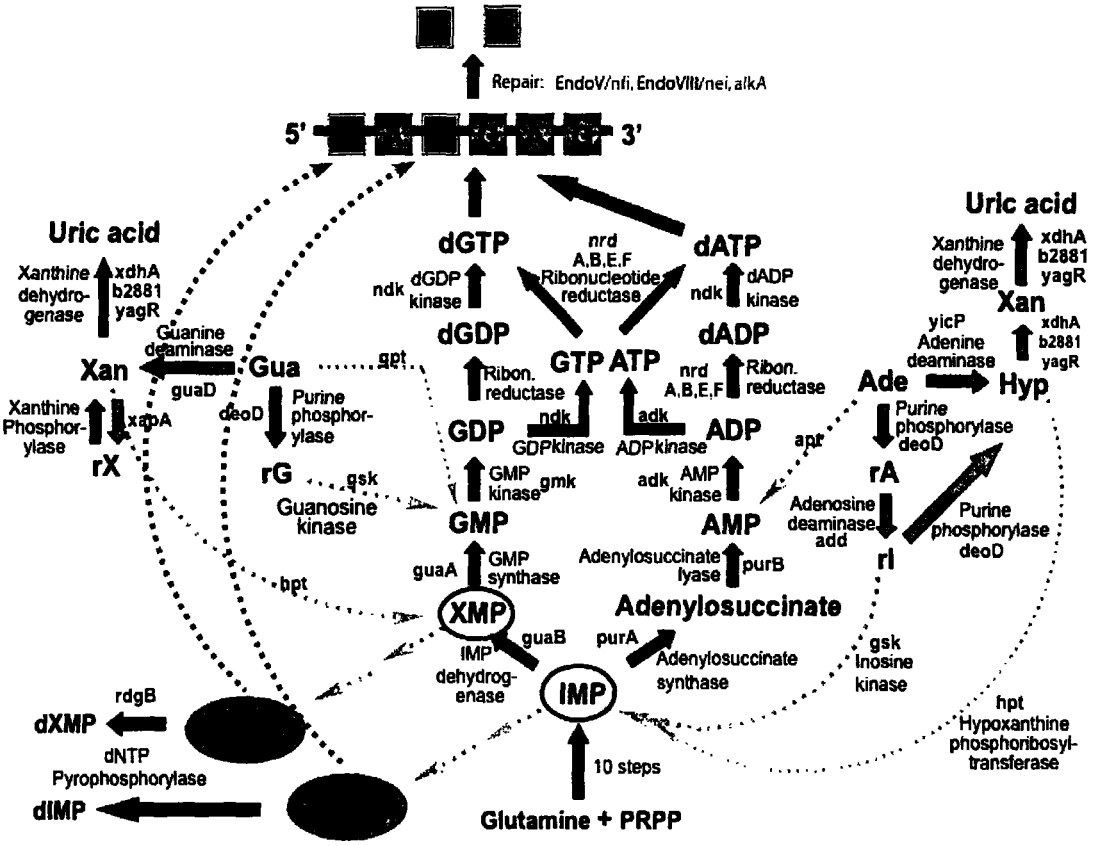

Purine Metabolism. The synthesis and utilization of purine bases and nucleotides is highly conserved in all living organisms with only minor differences between humans and *E. coli*, the model organism used in the proposed studies. As shown in Figure 2, X and I lie at the heart of all pathways of purine synthesis and catabolism.

The synthesis of purine ribo- and 2'-deoxyribonucleotides occurs by three mechanisms: *de novo* synthesis, salvage of purine bases by attachment to ribosephosphate; and salvage by phosphorylation of nucleosides. The *de novo* pathway is a 10-step reaction that starts with phosphoribosylpyrophosphate (PRPP) and ends in the formation of IMP, as shown in Figure 2. This precursor to AMP and GMP is normally present in cells at low μM concentrations (summarized in Curto et al., 1998). Conversion of IMP to AMP involves two steps: (1) displacement of the O^6 of IMP by the amino group of aspartate to form adenylosuccinate (mediated by adenylosuccinate synthase, the product of the *E. coli purA* gene); followed by (2) removal of fumarate to form AMP (mediated by adenylosuccinate lyase, the product of the *E. coli purB* gene). Phosphorylation steps lead to the formation of ADP and ATP, the latter present at mM concentrations in cells (Curto et al., 1998), while conversion to dADP involves the action of ribonucleotide reductase. The formation of GMP likewise derives from IMP but through the intermediacy of XMP. Oxidation of IMP by IMP dehydrogenase (*E. coli* GuaB protein) yields XMP that accepts an amino group from glutamine *via* GMP synthase (*E. coli* GuaA protein). Again, the appropriate di- and triphosphate and deoxyribonucleotide arise by analogous kinases and ribonucleotide reductase as with adenosine nucleotides.

The ribo- and deoxyribonucleotide pools are tightly controlled in all cells, with increases in pool concentration as the cell cycle enters S phase (*e.g.*, Nordenskjold et al., 1970). Imbalances in the dNTP pool have long been known to cause disease such as gout, immunodeficiency (Thompson et al., 2003; Ullman et al., 1978), and neurological disorders such as autism and the Lesch-Nyhan syndrome (Stanbury, 1983). The biochemical basis for these diseases lies in the absence or malfunction of key enzymes in the network of purine metabolism. A major consequence of defects in purine metabolism is disruption of the relative quantities of dNTP's in

the precursor pools in mammalian cells (Meuth, 1989). Mutations in purine biosynthesis have been observed to increase mutation rates in mammalian cell lines by up to 300-fold (reviewed in Meuth, 1989). One explanation for an increase in mutations associated with imbalanced dNTP pools involves DNA polymerase error rates that are dependent on the relative dNTP concentrations (Loeb and Kunkel, 1982). We propose another possible route by which defects in purine metabolism can lead to mutations: increased levels of dXTP and dITP.

Repair of dX and dI in DNA. The genetics and biochemistry of processes that ultimately prevent the accumulation of base deamination products in DNA are best understood in *E. coli*, the model organism used in the proposed studies. In addition to the mechanism of excluding dX and dI from DNA by removal of the cognate dNTP's from the DNA precursor pools (Chung et al., 2001; Chung et al., 2002; Lin et al., 2001), the cellular repair of dX and dI in *E. coli* is predominantly through the base excision repair (BER) pathway (reviewed in Kow, 2002). Originally described by Demple and Linn (Demple and Linn, 1982) and later as an endonuclease that incises DNA containing inosine (Yao et al., 1994), endonuclease V (EndoV) of *E. coli* is a Mg^{+2}-dependent enzyme that cuts the second phosphodiester bond located 3' to the damaged base (reviewed in Kow, 2002). In addition to dI, EndoV recognizes a variety of lesions including dU, base mismatches, AP sites, hairpins and flap structures and has recently been shown to be the major repair activity for dX in DNA (He et al., 2000). Recent studies have shown that dO, dX's partner as a guanine deamination product (Figure 1), is also recognized by EndoV (Hitchcock et al., 2004), but the biological relevance of this observation is questionable given our inability to detect dO in DNA exposed to biological nitrosating agents *in vitro* (Dong et al., 2003) or *in vivo* (results in Chapters 4 and 5). Biochemical studies have shown that AlkA protein (3-methyladenine glycosylase) reacts with dI (Mansfield et al., 2003; Saparbaev and Laval, 1994).

Recent studies indicated that AlkA is active on X in DNA (Terato et al., 2002; Wuenschell et al., 2003). Research in our group demonstrated that AlkA is almost as efficient as EndoV in processing X in double-stranded DNA oligonucleotides *in vitro* (Vongchampa, unpublished results).

To investigate the role of purine metabolism in the cellular burden of mutagenic DNA deamination lesions, in collaboration with Prof. Richard Cunningham, we perform a systematic analysis of the genes affecting the levels of X and I in DNA, RNA and the nucleotide pool in *E. coli*, a model organism with extremely well defined genetics. Current study, as a first step of the systematic analysis, focused on *E. coli* mutants defective in several aspects of purine metabolism and DNA repair (Table 1). dX and dI in DNA from those mutants were quantified by the LC-MS method established before (Dong et al., 2003).

Furthermore, in collaboration with Prof. Leona Samson, we also studied the role of the alkyladenine DNA glycosylase (Aag) in the removal of dI and dX from DNA. The basis for these studies is the known *in vitro* activity of purified Aag against dI and dX in DNA (Hollis et al., 2000; Masaoka et al., 1999; Terato et al., 2002; Wyatt et al., 1999), in addition to activity against etheno-adenine *in vitro* and *in vivo* (Ham et al., 2004). To assess the role of Aag in the level of dI *in vivo*, we quantified dI and dX in tissue samples from wild type control mice and $Aag^{-/-}$ mice.

Collectively, results of a set of studies reported here provide strong support for the model of genetic toxicology proposed by us, which is perturbations of purine metabolism may lead to incorporation of the purine precursors I and X into DNA. This new model has implications for genetic polymorphisms in purine metabolism in humans.

Materials and Method

Materials. All chemicals and reagents were of highest purity available and were used without further purification unless noted otherwise. Nuclease P1 and a kit for DNA isolation from cells and tissues were obtained from Roche Diagnostic Corporation (Indianapolis, IN). A kit for DNA isolation from bacteria was purchased from Qiagen (Valencia, CA). Phosphodiesterase I was purchased from USB (Cleveland, Ohio). Alkaline phosphatase and ammonium acetate were obtained from Sigma Chemicals (St. Louis, MO). Coformycin and tetrahydrouridine (THU) were purchased from Calibochem (San Diego, CA). Acetonitrile and HPLC-grade water were purchased from Mallinckrodt Baker (Phillipsburg, NJ). Water purified through a Milli-Q system (Millipore Corporation, Bedford, MA) was used for all applications.

Instrumental Analyses. All HPLC analyses were performed on an Agilent Model 1100, equipped with a 1040A diode array detector. Mass spectra were recorded with an Agilent Model 1100 electrospray mass spectrometer coupled to an Agilent Model 1100 HPLC with diode array detector. UV spectra were obtained using a Beckman DU640 UV-visible spectrophotometer.

DNA Isolation from *E. coli*. Log-phase cultures of the *E. coli* strains shown in Table 1 were pelleted by centrifugation and genomic DNA was isolated using a Qiagen kit with coformycin and THU added at various stages of the isolation process to control adventitious formation of dI and dU respectively. Cell pellets (~20 mg wet weight) were resuspended by vortexing in 3.5 mL of 50 mM Tris-EDTA, 0.5% Tween-20, 0.5% Triton X-100, pH 8, containing 0.7 mg RNase A, 35 μg coformycin and 350 μg THU, followed by addition of lysozyme (8 mg) and proteinase K

(450 μg). After incubation (37 °C, 1 hr), 1.2 mL of 3 M guanidine HCl, 20% Tween-20, 12 μg coformycin, 120 μg THU were added followed by incubation for 30 min at 50 °C. Following resolution on a Qiagen genomic-tip, the DNA was precipitated with isopropanol, washed with 70% ethanol and dried at ambient temperature. The yield and purity of DNA was determined by UV spectroscopy and the sample was stored at –80 °C.

DNA Isolation from Aag Mouse Liver. Liver tissue was isolated from wild type and $Aag^{-/-}$ mice (C5761/6J) ranging in age from 2 to 18 months and DNA was isolated from the tissues using a Roche DNA isolation kit for cells and tissues with additional measures to control adventitious formation of dI, dU and nucleobase oxidation products. Briefly, 400 mg samples of frozen tissue were homogenized in 10 mL of cellular lysis buffer containing a combination of deaminase inhibitors and antioxidant (5 μg/mL coformycin, 50 μg/mL THU, and 0.1 mM desferrioxamine) for 20-30 s using a Brinkman Polytron homogenizer on a medium setting. The homogenate was digested with proteinase K (6.1 μL, 100 mg/mL) at 65 °C for 1 hr. DNase-free RNase A was then added (400 μL, 25 mg/mL) for additional 30 min incubation at 37°C. Proteins were removed by adding 4.2 mL of protein precipitation solution followed by a 5 min incubation on ice and centrifugation at 26,900xg for 20 min at RT. The supernatant was carefully transferred to a fresh tube and DNA was recovered by precipitation in 200 mM NaCl and 2.5 volumes of absolute ethanol (-20 °C; add slowly to facilitate DNA recovery). The floating DNA filament was recovered with a micropipette tip (or by centrifugation at 5000 x g for 30 min) followed by two washes with 70% ethanol, air-drying at ambient temperature and resuspension in 10 mM Tris, 1 mM EDTA (pH 8.0). The DNA concentration was defined by UV spectroscopy and the sample was stored at –80 °C.

Quantification of DNA Nucleobase Deamination by LC-MS Analysis. Nucleobase deamination products in DNA samples from *E. coli* mutants and Aag mouse livers were quantified by the LC-MS method previously established, though with minor modifications (Dong et al., 2003). Briefly, 50μg of DNA was hydrolyzed by a combination of Nuclease P1, phosphodiesterase I and alkaline phosphatase in the presence of appropriate amounts of isotope-labeled internal standards and an adenosine deaminase inhibitor, coformycin. THU, a specific cytidine deaminase inhibitor, was not included, since careful screen of all the enzyme stocks did not find the action of a contaminant that leads to the adventitious formation of dU. The resulting nucleoside mixture was separated by HPLC using a Phenomenex reversed phase column (Synergi, 250 x 4.6 mm, 4 mm particle size, 80 Å pore size), which resulted in better resolution of dX and dG compared to the previously used. Fractions containing each nucleobase deamination product were collected for subsequent LC-MS quantification.

Table 1. *E. coli* mutants

	Strain number	Genotype
Strain KL16	KL 16	*wild type*
	NEB 20	*moa*
	NEB 38	*rdgB*
	NEB 53	*RdgB, nfi, Δ recA*
	NEB 83	*pur*
	NEB 88	*moa, purA, rdgB, nfi*
	NEB 114	*mob, rdgB, nfi*
	NEB 116	*nfi*
	NEB 831	*purA, moa*
	NEB 832	*purA, rdgB*
	NEB 833	PurA, nfi
Strain W3110	W3110	*wild type*
	WB01	*PurA-/PurA+*
	WB02	*purA, rdgB*
	WB03	*purB, rdgB*
	WB04	*purA, guaA, rdgB*
	WB05	*purA, guaB, rdgB*

Results

Formation of dX and dI in *E. coli* Mutants. The levels of dX and dI in the various *E. coli* mutants are shown Figures 3 and 4. With regard to the I pathways (studied in the KL16 strain, shown in Figure 3), there are increases in dI in DNA of 50-100% for the individual *rdgB*, *nfi* and *purA* mutants compare with the original KL16 strain (3a). The largest changes by far, however, occurred with loss of both *purA* and *rdgB*, which resulted in a 63-fold increase in dI in DNA (2a). No significant differences were observed in the levels of dX (3b) among those bacteria mutants.

Studies of the X pathways were performed in the *E. coli* W3110 strain with results qualitatively similar to dI (Figure 4). Increases in dX in DNA were observed in the *purA/rdgB/guaA* mutant, but the magnitude of the increases is considerably smaller than changes observed in dI in spite of the parallel nature of the mutations (Figure 4b). *Pur A and rdgB* double mutants in W3100 background also caused a substantial increase in dI in DNA (Figure 4a). dO was not detected in any strain derived from either KL16 or W3110.

Formation of dX and dI in Aag Knockout Mice. The levels of dX and dI in the Aag knockout mice are shown in Figure 5. The results revealed both an age dependence and Aag dependence of the dX and dI levels in the mouse DNA. Both dX and dI increased with the age of the mice in wild type and $Aag^{-/-}$ mice. It is also apparent in Figure 4 that the level of dI, but not dX, is dependent on the presence of Aag. About twice as much dI, dX were detected in $Aag^{-/-}$ mice compared with the same-aged wild type mice. There was no significant differences in dU levels

between the $Aag^{-/-}$ and the wild type mice, which is consistent with the lack of reported activity of Aag with dU. dO was again not detected in any tested mouse.

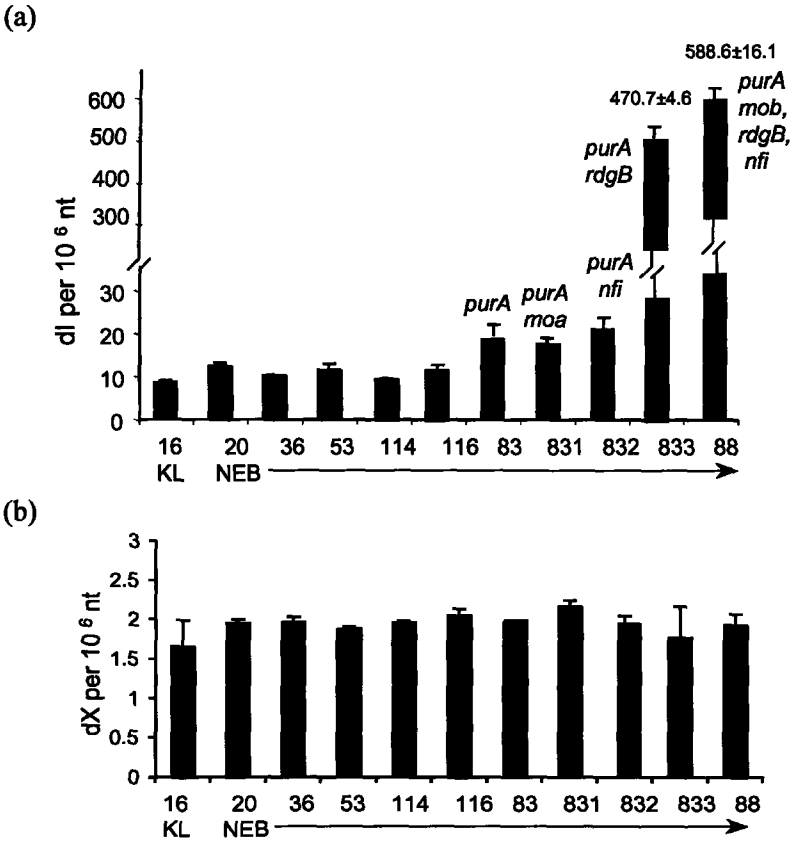

Figure 3. dI (a) and dX (b) levels in *E. coli* KL16 mutants (studies of the I pathways). Each value in the table represents triplicate analysis of a single culture of *E. coli.* See Table 1 for the genotype of each mutant

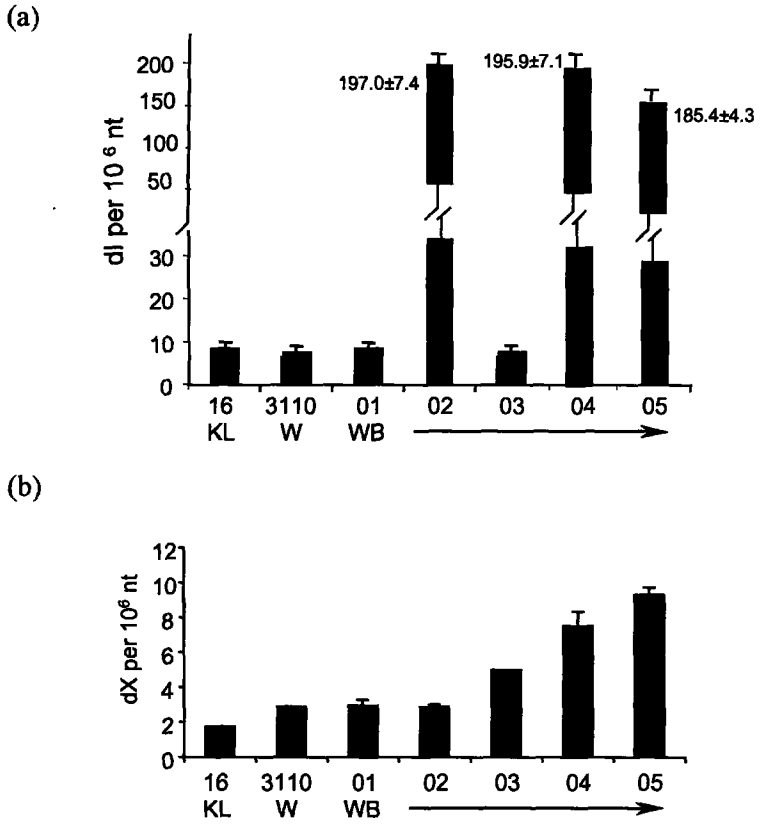

Figure 4. dI (a) and dX (b) levels in *E. coli* W3110 mutants (studies of the X pathway). Each value in the table represents triplicate analysis of a single culture of *E. coli*. See Table 1 for the genotype of each mutant

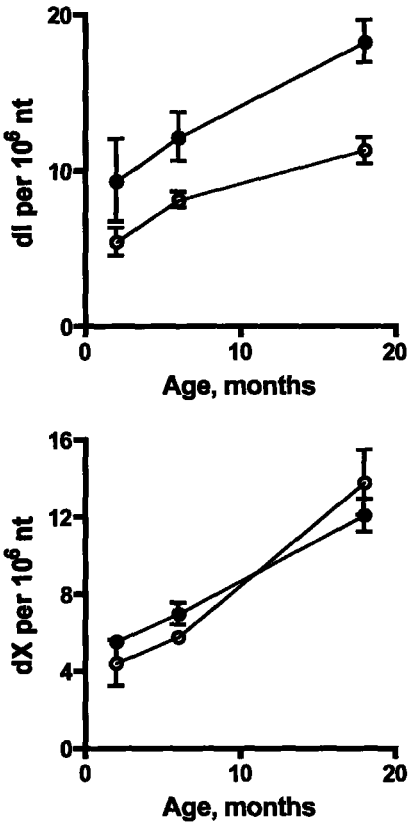

Figure 5. Age- and Aag-dependent changes in dI (upper) and dX (lower) in mouse liver DNA. Wild type, open circles; $Aag^{-/-}$, closed circles. n=2 for 2 month old mice, n=3 for 6 and 18 month animals.

Discussion

Deamination of nucleobases in DNA can occur by a variety of mechanisms, including simple hydrolysis (Frederico et al., 1990; Lindahl, 1974), nitrosative chemistry (Dubelman and Shapiro, 1977; Kirchner et al., 1992; Nguyen et al., 1992; Shapiro and Pohl, 1968; Shapiro and Yamaguchi, 1972; Suzuki et al., 1996; Wink et al., 1991) and deaminase enzyme activity (Harris et al., 2002; Ito et al., 2004; Muramatsu et al., 1999; Petersen-Mahrt et al., 2002). As an integrated part of a systematic investigation of the relationship between defects in purine metabolism and the quantities of X- and I-containing species in DNA, RNA and nucleotide pools, data obtained from this set of studies are consistent with a new paradigm in which perturbations of nucleobase metabolism leads to incorporation of the purine precursors X and I into DNA.

Escherichia coli, a model organism with extremely well defined genetics, was selected for the study. In construction of *E. coli* mutants, genes were chosen in part rationalized on the basis of known or suspected contributions to purine metabolism and DNA repair. As listed in Table 1, mutating the *purA* gene blocks a specific step in adenosine biosynthsis, thus creating cells that should accumulate IMP in purine biosynthesis (Burgis et al., 2003). Mutating the *rdgB* gene prevents the breakdown of dITP and dXIP (Burgis et al., 2003). Mutating *nif* prevents the excision of dX and dI from DNA (He et al., 2000; Kow, 2002). Those mutants can be clustered on the basis of pathways in which they participate (Table 1): the I pathway (studied in KL16 stains) and the X pathway (studied in W3110 strains). Our working model for a system to prevent the accumulation of non-canonical purines in DNA, including dX, dO and dI, can be summarized as follows. The dNTP forms of purine analogs can arise from (1) salvage of free

bases, (2) phosphorylation of naturally occurring IMP and XMP, or (3) deamination of the nucleotide forms of X and I. Whatever the source, RdgB protein will sanitize the precursor pools of dNTP and rNTP and prevent these species from being incorporated into DNA and RNA. If non-canonical bases do arise in DNA, then a repair event is initiated by incision next to the base by EndoV.

This model was first tested using the purine base analog, HAP, in collaboration with the research group of Prof. Cunningham. In the absence of RdgB protein, HAP supplied to *E. coli* as the free base causes increases in (1) GC to AT and AT to GC transition mutations, (2) recombination, (3) cell death, and (4) SOS-induction. These results suggest that HAP is converted into a dNTP and then incorporated into DNA where it is mutagenic and capable of causing double-strand breaks leading to SOS-induction, recombinational repair and cell death. When an *nfi* (EndoV) mutation is combined with loss of *rdgB*, the mutation rate increases even more, while SOS-induction, recombination and cell killing are suppressed. This suggests that HAP can be stably incorporated into DNA in the absence of DNA repair and results in very high levels of mutagenesis (Burgis et al., 2003).

Current study provided further evidence for this model. Results from the I pathways indicated that loss of individual *rdgB, nfi* and *purA* genes caused moderate increases (50-100%) in dI in DNA (Figure 3a). Loss of both *purA* and *rdgB,* however, resulted in a tremendous increase (~63-fold) in dI (Figure 3a), suggesting the synergy effects of these two enzymes in incorporation of dI in *E.coli* genomic DNA. As illustrated in Figure 6, the results are consistent with established metabolic pathways in *E. coli*, and can be rationalized as loss of *purA* leading to an increase in IMP formation that then results in increased level of dITP that, in the absence of *rdgB* protein, is incorporated by polymerase(s) into DNA.

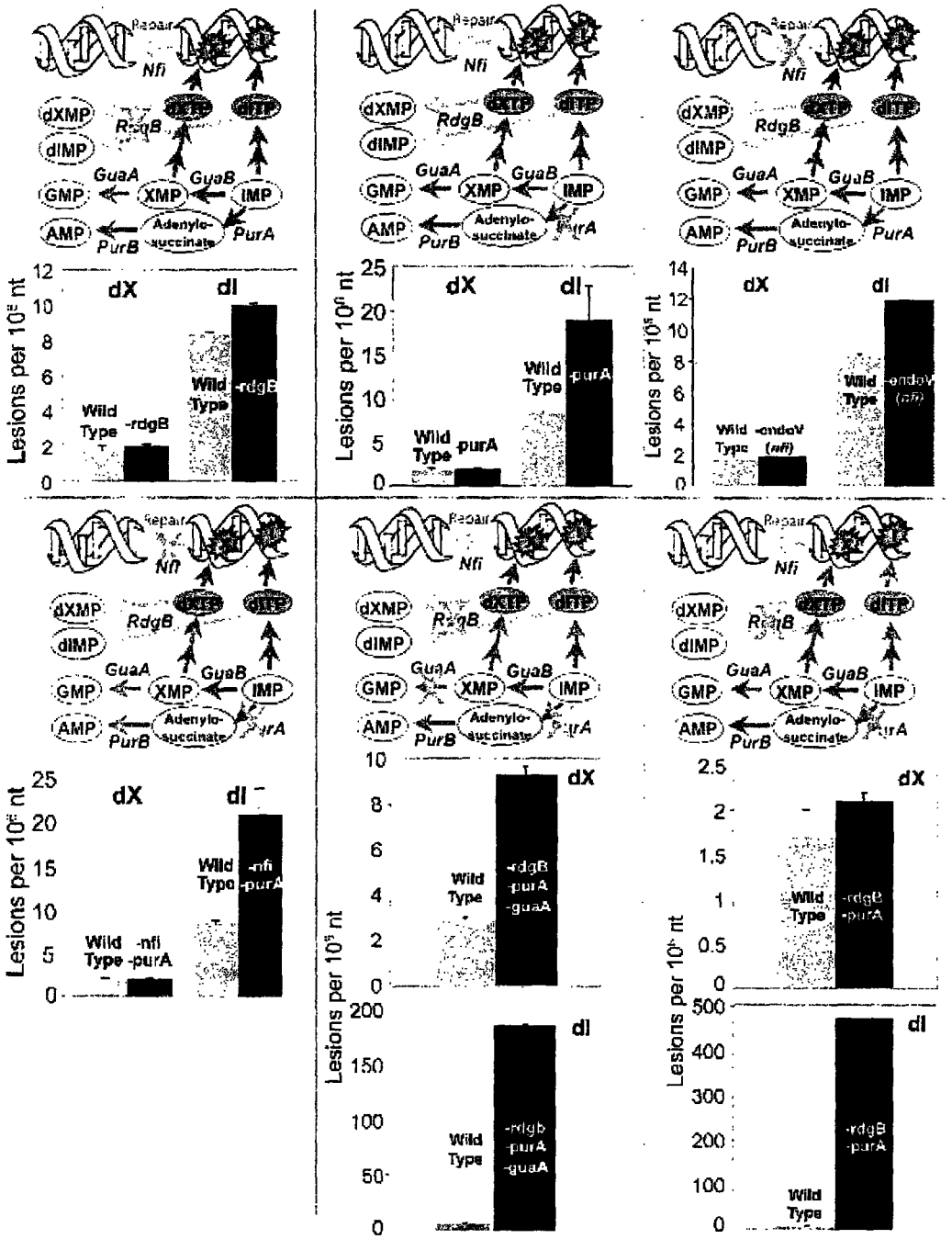

Figure 6: Illustrations of purine metabolic pathway defects and the DNA levels of dX and dI

Several observations related to DNA repair merit discussion. For example, loss of *nfi*, the gene encoding the EndoV DNA repair protein, resulted in relatively small increases in dI in the *purA/nfi* mutant (2.5-fold) (Figure 3a) and the *nfi* mutant (42% increase) (Figure 3a), however the *purA/rdgB* mutant maintains such a high level of dI (56-fold increase) in spite of the presence of EndoV. In light of the major role ascribed to EndoV for dI repair based on nitrous acid exposure studies of Weiss and coworkers (Guo and Weiss, 1998; Schouten and Weiss, 1999), this observation raised a controversy. One possible explanation is that EndoV is in relatively low abundance (or has slow turnover) under basal conditions and gene expression is induced by insults such as nitrous acid exposure. Other DNA repair enzymes like AlkA, with their activity against dI *in vitro* (Yao et al., 1994), may play a role in dI repair. The later speculation was confirmed by a parallel study of the role of Aag, the mouse counterpart of *E. coli* AlkA, in the removal of dI from DNA. As shown in Figure 5, both dX and dI showed an Aag-dependent increases in DNA of Aag knock out mice.

Studies of the X pathways were performed in the *E. coli* W3110 strains with results qualitatively similar to dI. Increases in dX in DNA were observed in the *purA/rdgB/guaA* mutant, which is consistent with the central role for the *guaA* gene product (GMP synthase) in the conversion of XMP to GMP (Figure 4). The magnitude of the increase in dX is considerably smaller than changes observed in dI in spite of the parallel nature of the mutations. One possible explanation is that the mutations result in similar levels of dITP and dXTP in the nucleotide pool but that the known selectivity of some DNA polymerases for dITP over dXTP (10- to 100-fold; refs. (Piccirilli et al., 1990; Suzuki et al., 1998; Valentine and Termini, 2001) leads to higher levels of dI in DNA. Alternatively, differences in DNA repair could account for the levels of

dX. Further study involves quantifying the roles of EndoV (*nfi*) and AlkA in dX levels in DNA will assist to elucidate the underlying mechanism.

It is worthy of mention that any disturbance in the highly interconnected purine metabolic pathways will likely to affect the steady-state concentrations of X and I in the nucleotide triphosphate pool. Therefore, it will be important to define the "flow" of X- and I-containing intermediates in the purine metabolic pathways as a function of these individual mutations. For example, a mutation in the *purA* gene should result in an increase in the IMP pool, but we only observed a slight increase in dI in DNA in *purA* mutants. It can be assumed that IMP is converted to dITP when present in excess. When an *rdgB* mutation is added to a *purA* mutation the amount of dI in DNA increases dramatically. This suggests that the dITP'ase is effectively removing dITP from the precursor pool for DNA replication. In these mutants, the presence of active IMP dehydrogenase (*guaB* gene product) could be relieving the accumulation of IMP by converting it to XMP.

In summary, current study revealed large increases in dX and dI in DNA in *E. coli* with mutations in key purine metabolic pathways, a phenomenon that expands the number of sources of nucleobase deamination in DNA. It is quite reasonable to assume that raising the baseline levels of dX and dI in DNA will exacerbate the toxicity associated with the nitrosative stress caused by chronic inflammation, such that further increases in dX and dI will exceed the capacity of a cell to repair the lesions and push the cell into apoptosis or a hypermutagenic state. It is also possible that increases in baseline dX and dI will increase the recombination rates present in B lymphocytes as a result of the physiological function of cytosine deaminase (AID protein) in promoting immunoglobulin diversity (Krokan et al., 2002; Reynaud et al., 2003). Given the

conservation of purine metabolic pathways, it is highly likely that analogous changes in X- and I-containing species will accompany genetic polymorphisms in purine metabolic pathways, the subject of future studies.

References

Bransteitter, R., Pham, P., Scharff, M. D., and Goodman, M. F.: Activation-induced cytidine deaminase deaminates deoxycytidine on single-stranded DNA but requires the action of RNase. *In* Proc Natl Acad Sci U S A, vol. 100, pp. 4102-7, 2003.

Burgis, N. E., Brucker, J. J., and Cunningham, R. P.: Repair system for noncanonical purines in Escherichia coli. *In* J Bacteriol, vol. 185, pp. 3101-10, 2003.

Caulfield, J. L., Wishnok, J. S., and Tannenbaum, S. R.: Nitric oxide-induced deamination of cytosine and guanine in deoxynucleosides and oligonucleotides. *In* J. Biol. Chem., vol. 273, pp. 12689-12695, 1998.

Chung, J. H., Back, J. H., Park, Y. I., and Han, Y. S.: Biochemical characterization of a novel hypoxanthine/xanthine dNTP pyrophosphatase from Methanococcus jannaschii. *In* Nucleic Acids Res, vol. 29, pp. 3099-107, 2001.

Chung, J. H., Park, H. Y., Lee, J. H., and Jang, Y.: Identification of the dITP- and XTP-hydrolyzing protein from Escherichia coli. *In* J Biochem Mol Biol, vol. 35, pp. 403-8, 2002.

Curto, R., Voit, E. O., Sorribas, A., and Cascante, M.: Mathematical models of purine metabolism in man. *In* Math Biosci, vol. 151, pp. 1-49, 1998.

Demple, B., and Linn, S.: On the recognition and cleavage mechanism of Escherichia coli endodeoxyribonuclease V, a possible DNA repair enzyme. *In* J Biol Chem, vol. 257, pp. 2848-55., 1982.

Dong, M., Wang, C., Deen, W. M., and Dedon, P. C.: Absence of 2'-deoxyoxanosine and presence of abasic sites in DNA exposed to nitric oxide at controlled physiological concentrations. *In* Chem Res Toxicol, vol. 16, pp. 1044-55, 2003.

Dubelman, S., and Shapiro, R.: A method for the isolation of cross-linked nucleosides from DNA: application to cross-links induced by nitrous acid. *In* Nucleic Acids Res, vol. 4, pp. 1815-27, 1977.

Frederico, L. A., Kunkel, T. A., and Shaw, B. R.: A sensitive genetic assay for the detection of cytosine deamination: determination of rate constants and the activation energy. *In* Biochemistry, vol. 29, pp. 2532-7, 1990.

Greeve, J., Philipsen, A., Krause, K., Klapper, W., Heidorn, K., Castle, B. E., Janda, J., Marcu, K. B., and Parwaresch, R.: Expression of activation-induced cytidine deaminase in human B-cell non-Hodgkin lymphomas. *In* Blood, vol. 101, pp. 3574-80, 2003.

Guo, G., and Weiss, B.: Endonuclease V (nfi) mutant of Escherichia coli K-12. *In* J Bacteriol, vol. 180, pp. 46-51, 1998.

Ham, A. J., Engelward, B. P., Koc, H., Sangaiah, R., Meira, L. B., Samson, L. D., and Swenberg, J. A.: New immunoaffinity-LC-MS/MS methodology reveals that Aag null mice are deficient in their ability to clear 1,N6-etheno-deoxyadenosine DNA lesions from lung and liver in vivo. *In* DNA Repair (Amst), vol. 3, pp. 257-65, 2004.

Harris, R. S., Sale, J. E., Petersen-Mahrt, S. K., and Neuberger, M. S.: AID is essential for immunoglobulin V gene conversion in a cultured B cell line. *In* Curr Biol, vol. 12, pp. 435-8, 2002.

He, B., Qing, H., and Kow, Y. W.: Deoxyxanthosine in DNA is repaired by Escherichia coli endonuclease V. *In* Mutat. Res., vol. 459, pp. 109-114, 2000.

Hitchcock, T. M., Gao, H., and Cao, W.: Cleavage of deoxyoxanosine-containing oligodeoxyribonucleotides by bacterial endonuclease V. *In* Nucleic Acids Res, vol. 32, pp. 4071-80, 2004.

Hollis, T., Lau, A., and Ellenberger, T.: Structural studies of human alkyladenine glycosylase and E. coli 3-methyladenine glycosylase. *In* Mutat Res, vol. 460, pp. 201-10, 2000.

Ito, S., Nagaoka, H., Shinkura, R., Begum, N., Muramatsu, M., Nakata, M., and Honjo, T.: Activation-induced cytidine deaminase shuttles between nucleus and cytoplasm like apolipoprotein B mRNA editing catalytic polypeptide 1. *In* Proc Natl Acad Sci U S A, vol. 101, pp. 1975-80, 2004.

Kirchner, J. J., Sigurdsson, S. T., and Hopkins, P. B.: Interstrand cross-linking of duplex DNA by nitrous acid: Covalent structure of the dG-to-dG cross-link at the sequence 5'-CG. *In* J. Am. Chem. Soc., vol. 114, pp. 4021-4027, 1992.

Kow, Y. W.: Repair of deaminated bases in DNA. *In* Free Radic Biol Med, vol. 33, pp. 886-93, 2002.

Krokan, H. E., Drablos, F., and Slupphaug, G.: Uracil in DNA--occurrence, consequences and repair. *In* Oncogene, vol. 21, pp. 8935-48, 2002.

Lin, S., McLennan, A. G., Ying, K., Wang, Z., Gu, S., Jin, H., Wu, C., Liu, W., Yuan, Y., Tang, R., Xie, Y., and Mao, Y.: Cloning, expression, and characterization of a human inosine triphosphate pyrophosphatase encoded by the itpa gene. *In* J Biol Chem, vol. 276, pp. 18695-701, 2001.

Lindahl, T.: An N-glycosidase from Escherichia coli that releases free uracil from DNA containing deaminated cytosine residues. *In* Proc Natl Acad Sci U S A, vol. 71, pp. 3649-53, 1974.

Loeb, L. A., and Kunkel, T. A.: Fidelity of DNA synthesis. *In* Annu Rev Biochem, vol. 51, pp. 429-57, 1982.

Lucas, L. T., Gatehouse, D., Jones, G. D. D., and Shuker, D. E. G.: Characterization of DNA damage at purine residues in oligonucleotides and calf thymus DNA induced by the mutagen 1-nitrosoindole-3-acetonitrile. *In* Chem. Res. Toxicol., vol. 14, pp. 158-164, 2001.

Lucas, L. T., Gatehouse, D., and Shuker, D. E.: Efficient nitroso group transfer from N-nitrosoindoles to nucleotides and 2'-deoxyguanosine at physiological pH. A new pathway for N-nitrosocompounds to exert genotoxicity. *In* J Biol Chem, vol. 274, pp. 18319-26, 1999.

Mansfield, C., Kerins, S. M., and McCarthy, T. V.: Characterisation of Archaeglobus fulgidus AlkA hypoxanthine DNA glycosylase activity. *In* FEBS Lett, vol. 540, pp. 171-5, 2003.

Masaoka, A., Terato, H., Kobayashi, M., Honsho, A., Ohyama, Y., and Ide, H.: Enzymatic repair of 5-formyluracil. I. Excision of 5-formyluracil site-specifically incorporated into oligonucleotide substrates by alka protein (Escherichia coli 3-methyladenine DNA glycosylase II). *In* J Biol Chem, vol. 274, pp. 25136-43, 1999.

Meuth, M.: The molecular basis of mutations induced by deoxyribonucleoside triphosphate pool imbalances in mammalian cells. *In* Exp Cell Res, vol. 181, pp. 305-16, 1989.

Muramatsu, M., Sankaranand, V. S., Anant, S., Sugai, M., Kinoshita, K., Davidson, N. O., and Honjo, T.: Specific expression of activation-induced cytidine deaminase (AID), a novel member of the RNA-editing deaminase family in germinal center B cells. *In* J Biol Chem, vol. 274, pp. 18470-6, 1999.

Muto, T., Muramatsu, M., Taniwaki, M., Kinoshita, K., and Honjo, T.: Isolation, tissue distribution, and chromosomal localization of the human activation-induced cytidine deaminase (AID) gene. *In* Genomics, vol. 68, pp. 85-8, 2000.

Nguyen, T., Brunson, D., Crespi, C. L., Penman, B. W., Wishnok, J. S., and Tannenbaum, S. R.: DNA damage and mutation in human cells exposed to nitric oxide *in vitro*. *In* Proc. Natl. Acad. Sci. USA, vol. 89, pp. 3030-3034, 1992.

Nordenskjold, B. A., Skoog, L., Brown, N. C., and Reichard, P.: Deoxyribonucleotide pools and deoxyribonucleic acid synthesis in cultured mouse embryo cells. *In* J Biol Chem, vol. 245, pp. 5360-8, 1970.

Petersen-Mahrt, S. K., Harris, R. S., and Neuberger, M. S.: AID mutates E. coli suggesting a DNA deamination mechanism for antibody diversification. *In* Nature, vol. 418, pp. 99-103, 2002.

Pham, P., Bransteitter, R., Petruska, J., and Goodman, M. F.: Processive AID-catalysed cytosine deamination on single-stranded DNA simulates somatic hypermutation. *In* Nature, vol. 424, pp. 103-7, 2003.

Piccirilli, J. A., Krauch, T., Moroney, S. E., and Benner, S. A.: Enzymatic incorporation of a new base pair into DNA and RNA extends the genetic alphabet. *In* Nature, vol. 343, pp. 33-7, 1990.

Reynaud, C. A., Aoufouchi, S., Faili, A., and Weill, J. C.: What role for AID: mutator, or assembler of the immunoglobulin mutasome? *In* Nat Immunol, vol. 4, pp. 631-8, 2003.

Saparbaev, M., and Laval, J.: Excision of hypoxanthine from DNA containing dIMP residues by the Escherichia coli, yeast, rat, and human alkylpurine DNA glycosylase. *In* Proc. Natl. Acad. Sci. USA, vol. 91, pp. 5873-5877, 1994.

Schouten, K. A., and Weiss, B.: Endonuclease V protects Escherichia coli against specific mutations caused by nitrous acid. *In* Mutat. Res., vol. 435, pp. 245-254, 1999.

Shapiro, R., and Pohl, S. H.: The reaction of ribonucleosides with nitrous acid. Side products and kinetics. *In* Biochemistry, vol. 7, pp. 448-55, 1968.

Shapiro, R., and Yamaguchi, H.: Nucleic acid reactivity and conformation. I. Deamination of cytosine by nitrous acid. *In* Biochim Biophys Acta, vol. 281, pp. 501-6, 1972.

Shen, H. M., and Storb, U.: Activation-induced cytidine deaminase (AID) can target both DNA strands when the DNA is supercoiled. *In* Proc Natl Acad Sci U S A, vol. 101, pp. 12997-3002, 2004.

Shen, J. C., Rideout, W. M., 3rd, and Jones, P. A.: The rate of hydrolytic deamination of 5-methylcytosine in double-stranded DNA. *In* Nucleic Acids Res, vol. 22, pp. 972-6, 1994.

Stanbury, J. B.: The Metabolic basis of inherited disease, pp. xvi, 2032 p., McGraw-Hill, New York, 1983.

Suzuki, T., Yamaoka, R., Nishi, M., Ide, H., and Makino, K.: Isolation and characterization of a novel product, 2'-deoxyoxanosine, from 2'-deoxyguanosine, oligodeoxynucleotide, and calf thymus DNA treated with nitrous acid and nitric oxide. *In* J. Am. Chem. Soc., vol. 118, pp. 2515-2516, 1996.

Suzuki, T., Yoshida, M., Yamada, M., Ide, H., Kobayashi, M., Kanaori, K., Tajima, K., and Makino, K.: Misincorporation of 2'-deoxyoxanosine 5'-triphosphate by DNA polymerases and its implication for mutagenesis. *In* Biochemistry, vol. 37, pp. 11592-8, 1998.

Tamir, S., Burney, S., and Tannenbaum, S. R.: DNA damage by nitric oxide. *In* Chem Res Toxicol, vol. 9, pp. 821-7, 1996.

Tannenbaum, S. R., Tamir, S., deRojas-Walker, T., and Wishnok, J. S.: DNA damage and cytoxicity by nitric oxide. *In* Nitrosamines and related N-nitroso compounds: Chemistry and biochemistry, ed. by C. J. Michejda, vol. 553, pp. 120-135, American Chemical Society, Washington, D.C., 1994.

Terato, H., Masaoka, A., Asagoshi, K., Honsho, A., Ohyama, Y., Suzuki, T., Yamada, M., Makino, K., Yamamoto, K., and Ide, H.: Novel repair activities of AlkA (3-methyladenine DNA glycosylase II) and endonuclease VIII for xanthine and oxanine, guanine lesions induced by nitric oxide and nitrous acid. *In* Nucleic Acids Res, vol. 30, pp. 4975-84, 2002.

Thompson, L. F., Vaughn, J. G., Laurent, A. B., Blackburn, M. R., and Van De Wiele, C. J.: Mechanisms of apoptosis in developing thymocytes as revealed by adenosine deaminase-deficient fetal thymic organ cultures. *In* Biochem Pharmacol, vol. 66, pp. 1595-9, 2003.

Ullman, B., Gudas, L. J., Cohen, A., and Martin, D. W., Jr.: Deoxyadenosine metabolism and cytotoxicity in cultured mouse T lymphoma cells: a model for immunodeficiency disease. *In* Cell, vol. 14, pp. 365-75, 1978.

Valentine, M. R., and Termini, J.: Kinetics of formation of hypoxanthine containing base pairs by HIV-RT: RNA template effects on the base substitution frequencies. *In* Nucleic Acids Res, vol. 29, pp. 1191-9, 2001.

Wink, D. A., Kasprzak, K. S., Maragos, C. M., Elespuru, R. K., Misra, M., Dunams, T. M., Cebula, T. A., Koch, W. H., Andrews, A. W., Allen, J. S., and Keefer, L. K.: DNA deaminating ability and genotoxicity of nitric oxide and its progenitors. *In* Science, vol. 254, pp. 1001-1003, 1991.

Wuenschell, G. E., O'Connor, T. R., and Termini, J.: Stability, miscoding potential, and repair of 2'-deoxyxanthosine in DNA: implications for nitric oxide-induced mutagenesis. *In* Biochemistry, vol. 42, pp. 3608-16, 2003.

Wyatt, M. D., Allan, J. M., Lau, A. Y., Ellenberger, T. E., and Samson, L. D.: 3-methyladenine DNA glycosylases: structure, function, and biological importance. *In* Bioessays, vol. 21, pp. 668-76, 1999.

Yao, M., Hatahet, Z., Melamede, R. J., and Kow, Y. W.: Purification and characterization of a novel deoxyinosine-specific endonuclease enzyme, deoxyinosine 3'-endonuclease, from Eschericia coli. *In* J. Biol. Chem., vol. 269, pp. 16260-16268, 1994.

Zhang, X., and Mathews, C. K.: Effect of DNA cytosine methylation upon deamination-induced mutagenesis in a natural target sequence in duplex DNA. *In* J Biol Chem, vol. 269, pp. 7066-9, 1994.

Appendix II

Dong, M., Wang, C., Deen, W. M. and Dedon, P. C. (2003). "Absence of 2'-deoxyoxanosine and presence of abasic sites in DNA exposed to nitric oxide at controlled physiological concentrations". Chem Res Toxicol **16**(9): 1044-55

Absence of 2′-Deoxyoxanosine and Presence of Abasic Sites in DNA Exposed to Nitric Oxide at Controlled Physiological Concentrations

Min Dong,† Chen Wang,‡ William M. Deen,†,‡ and Peter C. Dedon*,†

Biological Engineering Division, NE47-277, and Department of Chemical Engineering, Massachusetts Institute of Technology, 77 Massachusetts Avenue, Cambridge, Massachusetts 02139

Received March 8, 2003

Nitric oxide (NO•) is a physiologically important molecule at low concentrations, while high levels have been implicated in the pathophysiology of diseases associated with chronic inflammation, such as cancer. While an extensive study in vitro suggests that oxidative and nitrosative reactions dominate the complicated chemistry of NO•-mediated genotoxicity, neither the spectrum of DNA lesions nor their consequences in vivo have been rigorously defined. We have approached this problem with a major effort to define the spectrum of nitrosative DNA lesions produced by NO•-derived reactive nitrogen species under biological conditions. Plasmid pUC19 DNA was exposed to steady state concentrations of 1.3 μM NO• and 190 μM O_2 (calculated steady state concentrations of 40 fM N_2O_3 and 3 pM NO_2• in the bulk solution) in a recently developed reactor that avoids the undesired gas phase chemistry of NO• and approximates the conditions at sites of inflammation in tissues. The resulting spectrum of nitrosatively induced abasic sites and nucleobase deamination products was defined using plasmid topoisomer analysis and a novel LC/MS assay, respectively. With a limit of detection of 100 fmol and a sensitivity of 6 lesions per 10^7 nt in 50 μg of DNA, the LC/MS analysis revealed that 2′-deoxyxanthosine (dX), 2′-deoxyinosine (dI), and 2′-deoxyuridine (dU) were formed at nearly identical rates ($k = 1.2 \times 10^5$ M^{-1} s^{-1}) to the extent of ~80 lesions per 10^6 nt after 12 h exposure to NO• in the reactor. While reactions with HNO_2 resulted in the formation of high levels of 2′-deoxyoxanosine (dO), one of two products arising from deamination of dG, dO, was not detected in 500 μg of DNA exposed to NO• in the reactor for up to 24 h (<6 lesions per 10^8 nt). This result leads to the prediction that dO will not be present at significant levels in inflamed tissues. Another important observation was the NO•-induced production of abasic sites, which likely arise by nitrosative depurination reactions, to the extent of ~10 per 10^6 nt after 12 h of exposure to NO• in the reactor. In conjunction with other studies of nitrosatively induced dG−dG cross-links, these results lead to the prediction of the following spectrum of nitrosative DNA lesions in inflamed tissues: ~2% dG−dG cross links, 4−6% abasic sites, and 25−35% each of dX, dI, and dU.

Introduction

Research over the past decade has identified nitric oxide (NO•) as an important endogenous regulatory molecule in the cardiovascular, nervous, and immune systems (*1*−*3*). However, NO• and its derivatives display cytotoxic and mutagenic properties at sufficiently high concentrations, such as those produced by activated macrophages in inflammatory conditions, which suggest a causative role for NO• in the pathophysiology of diseases such as cancer (*4*−*8*). Although NO• is a radical species, its genotoxicity likely arises from derivatives such as N_2O_3 and peroxynitrite ($ONOO^-$), which are formed in reactions with molecular oxygen and superoxide, respectively (*9*). N_2O_3 is a powerful nitrosating agent that in addition to reactions with sulfhydryl groups of proteins (*10*) and with secondary amines to form *N*-nitrosamines (*11*), will react with the primary and heterocyclic amines in DNA bases to create mutagenic deamination products, abasic sites, and DNA cross-links (*12*−*18*), as shown in Scheme 1.

Nucleobase deamination by any mechanism results in the formation of X[1] (dX as a 2′-deoxynucleoside) from guanine, I (dI) from adenine, U (dU) from cytosine, and thymine (2′ deoxythymidine) from 5-methylcytosine, as shown in Scheme 1. Of particular interest is the observation of Suzuki et al. that deamination of guanine by nitrous acid in vitro partitions to form both X and O (dO; *18*). In addition to enzymatic deamination of deoxynucleosides (*19*, *20*) and bisulfite-induced deamination of dC (*21*), the two major mechanisms for deamination of nucleobases in DNA are hydrolysis and nitrosation. The propensity for hydrolytic deamination of bases in DNA occurs in the order 5 methylcytosine > cytosine >

* To whom correspondence should be addressed. Tel: 617-253-8017. Fax: 617-324 7554. E mail: pcdedon@mit.edu.
† Biological Engineering Division.
‡ Department of Chemical Engineering.

[1] Abbreviations: Bp, base pair; dA, 2′-deoxyadenosine; dC, 2′-deoxycytidine; dG, 2′-deoxyguanosine; dI, 2′-deoxyinosine; dO, 2′-deoxyoxanosine; dU, 2′-deoxyuridine; dX, 2′-deoxyxanthosine; DTPA, diethylenetriaminepentaacetic acid; I, hypoxanthine; Mor, morpholine; NMor, *N*-nitroso morpholine; nt, 2′-deoxynucleotides; O, oxanine; sccm, standard cubic centimeter per minute; U, uracil; X, xanthine.

10.1021/tx034046s CCC: $25.00
Published on Web 08/28/2003

Scheme 1. Products of Nucleobase N-Nitrosation

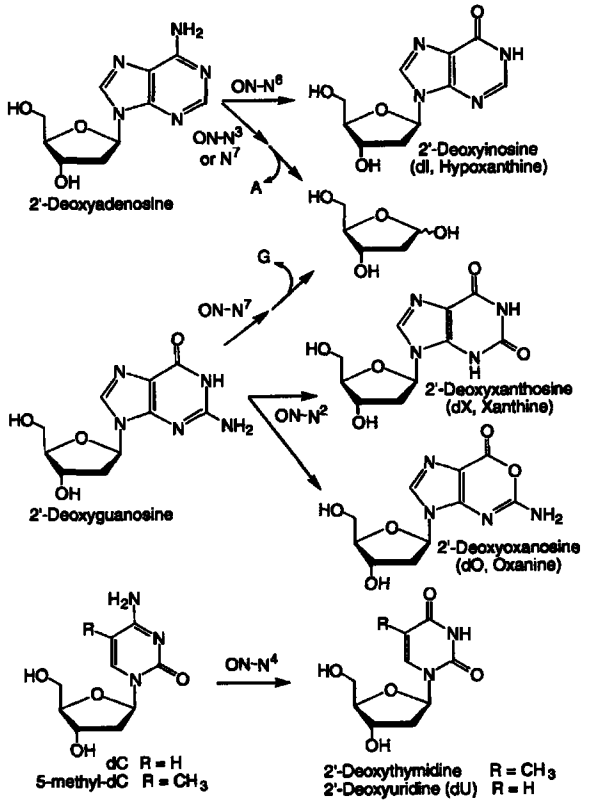

adenine > guanine (*22, 23*), with a half-life for cytosine in the range of 10^2–10^3 years for single-stranded DNA and 10^4–10^5 years in double-stranded DNA (*24–26*). C^5-Methylation of cytosine increases the rate of deamination by 2–20-fold (*25, 26*).

Nitrosative deamination of nucleobases has been shown to occur in acidified solutions of nitrite and in oxygenated solutions in the presence of NO• (*12–17, 27*). The reactive species in the latter case appears to be nitrous anhydride (N_2O_3; *28*), a potent nitrosating agent that causes deamination of aromatic amines by an aryl diazonium intermediate (reviewed in ref *29*). The reactivity of N_2O_3 with nucleobases is reversed relative to hydrolytic deamination (*30*). In addition to deamination of the exocyclic amines, nitrosation of the heterocyclic nitrogens of dA and dG leads to depurination, as shown in Scheme 1 (e.g., refs *31, 32*). The mechanistic basis for depurination may involve nitrosation of the N^7 of dG and N^7 or N^3 of dA, with the resulting destabilization of the glycosidic bond in the cationic bases (*31, 32*).

An important biological source of N_2O_3 is the NO• generated by macrophages activated as part of the inflammatory process. In macrophage cultures activated with lipopolysaccharide and INF-γ in vitro, NO• is generated at a rate of ~6 pmol s^{-1} per 10^6 cells (*5*) and leads to the formation of X at levels 5-fold higher than controls (*6*). However, this study provided no information about the other base deamination products. Attempts to mimic this biological exposure of DNA to NO• and the derivative N_2O_3 have employed several NO• delivery systems. For example, Nguyen et al. exposed DNA and TK6 cells to what was calculated to be a ~20 mM total dose of NO by bolus delivery of the gas through a syringe and they found that dX and dI were formed to the extent of 3 and 10 lesions per 10^3 nt, respectively, for isolated DNA, with 3-fold lower levels of each in cells (*12*). Yields of dI and dX in DNA were found to be 15–100 times higher, respectively, than those observed with free dA and dG (*12*). Similarly, Wink et al. found 5 dU per 10^3 nt in DNA exposed to NO• by bubbling the gas into solution until 1 mol/L had been absorbed (*33*). Caulfield et al. used a delivery system in which Silastic tubing allowed controlled diffusion of NO• into solution (with headspace) at a rate of 10–20 μM/min and found that X was formed at twice the rate of U and single-stranded DNA oligonucleotides were nearly 10-fold more reactive than double-stranded DNA (*30*).

These studies present several problems that prevent extrapolation to the biological setting. First, in all of the delivery systems, NO• was present at significantly higher concentrations than occur at sites of inflammation in vivo, which are thought not to exceed steady state concentrations of ~1 μM (*5, 34, 35*). Second, none of the studies addressed the complete spectrum of deamination products produced by exposure to nitric oxide. Finally, the presence of a headspace containing air in each of these delivery systems alters the chemistry of NO• by biasing the formation of N_2O_3 and allowing formation of N_2O_4 (*36, 37*).

To define the spectrum of deamination products under biologically relevant conditions of NO• exposure, we have developed sensitive analytical techniques to quantify dX, dO, dI, dU, and abasic sites in DNA exposed to NO• in a recently developed delivery system designed to mimic pathological release of NO• in vivo to cell cultures (*38*).

Experimental Procedures

Materials. All chemicals and reagents were of the highest purity available and were used without further purification unless noted otherwise. Calf thymus DNA, dG, dA, dU, dI, Mor, and NMor were purchased from Sigma Chemical Co. (St. Louis, MO). Nuclease P1 and acid phosphatase were obtained from Roche Diagnostic Corporation (Indianapolis, IN), and phosphodiesterase I was purchased from USB (Cleveland, OH). Alkaline phosphatases were obtained from a variety of sources, including Sigma, Roche, USB, and New England Biolabs (Beverly, MA). Coformycin was obtained from Calbiochem (San Diego, CA). Plasmid pUC19 was obtained from DNA Technologies Inc. (Gaithersburg, MD). Uniformly ^{15}N-labeled 5'-triphosphates of dG, dA, and dC were obtained from Silantes (Munich, Germany). Acetonitrile and HPLC grade water were purchased from Mallinckrodt Baker (Phillipsburg, NJ). Gas mixtures (10% NO•/90% N_2 and 50% O_2/50% N_2) were purchased from BOC Gases (Edison, NJ). Water purified through a Milli-Q system (Millipore Corporation, Bedford, MA) was used for all other applications.

Instrumental Analyses. All HPLC analyses were performed on a Hewlett-Packard model 1100, equipped with a 1040A diode array detector. Mass spectra were recorded with a Hewlett-Packard HP 5989B electrospray mass spectrometer coupled to a Hewlett-Packard model 1100 HPLC with a diode array detector. UV spectra were obtained using a Cary 100 Bio UV–visible spectrophotometer. Five different HPLC conditions were employed in these studies. System 1 consisted of a Phenomenex LUNA C18 reversed-phase column (250 mm × 3 mm, 5 μm particle size, 100 Å pore size, Phenomenex, Torrance, CA) with elution performed at a flow rate of 0.4 mL/min with 1% acetonitrile in 50 mM ammonium acetate (pH 7.4) for the first 5 min, followed by a linear gradient of 1–25% acetonitrile for 5 min; holding at 25% for 10 min; then a reversal of the gradient

to 1% for 5 min; and finally eluting at 1% acetonitrile over the last 5 min. System 2 consisted of a Haisil HL C18 reversed-phase column (250 mm × 4.6 mm, 5 μm particle size, 100 Å pore size, Higgins Analytic Inc, Mountain View, CA) with isocratic conditions of acetonitrile/H_2O (5/95 v/v) at a flow rate of 0.4 mL/min. System 3 consisted of a HAISIL HL C18 reversed-phase semipreparation column (250 mm × 10 mm, 5 μm particle size, 100 Å pore size) eluted with acetonitrile/H_2O (5/95 v/v) at a flow rate of 4.0 mL/min. System 4 consisted of a Varian C18 reversed phase column (250 mm × 4.6 mm, 5 μm particle size, 100 Å pore size, Varian Analytical Supplies, Harbor, CA) with elution performed at a flow rate of 0.4 mL/min with a linear gradient of 1−10% acetonitrile in H_2O containing 0.03% of acetic acid for 50 min, followed by a reversal of the gradient to 1% for 5 min, and eluting at 1% acetonitrile over the last 5 min. System 5 consisted of a Vydac C 18 reversed-phase column (250 mm × 2.1 mm, 5 μm particle size, 100 Å pore size, Grace Vydac, Hesperia, CA) with elutions performed at a flow rate of 0.4 mL/min with a linear gradient of 1−5% acetonitrile in H_2O containing 0.1% acetic acid for 10 min, followed by eluting at 1% acetonitrile for 5 min.

Synthesis of dX and dO. dX and dO were synthesized by a modification of the method of Suzuki et al. (*18*). Briefly, 10 mM dG was incubated with 100 mM $NaNO_2$ in 3.0 M sodium acetate buffer (pH 3.7) at 37 °C for 6 h. dX and dO were purified by HPLC using system 1, with retention times similar to literature values (*18*), followed by desalting with HPLC system 2 and drying under vacuum. Products were characterized by MS and UV spectroscopy relative to published data (*18*).

Synthesis of ^{15}N-Labeled dX, dO, dI, and dU. $^{15}N_5$ 5′ Triphosphate-2′-deoxyguanosine was dephosphorylated by incubation with alkaline phosphatase (0.5 U/μg nt) at 37 °C for 1 h, followed by purification of $^{15}N_5$-dG by sequential filtration on a Microcon YM-30 column (Millipore Corporation) and then by HPLC system 2. $^{15}N_4$-dX and -dO were prepared as described above for unlabeled dX and dO and quantified using the following extinction coefficients: $^{15}N_4$-dX, 7800 M^{-1} cm^{-1} at 260 nm; $^{15}N_4$ dO, 5100 M^{-1} cm^{-1} at 260 nm (*18*).

$^{15}N_4$ dI and $^{15}N_2$ dU were prepared by taking advantage of the presence of adenosine deaminase and dC deaminase, respectively, in commercial sources of alkaline phosphatase (Sigma) and acid phosphatase (Roche), respectively. $^{15}N_5$-5′-Triphosphate 2′ deoxyadenosine and dC were incubated with alkaline phosphatase and acid phosphatase (0.5 U/μg nt), respectively, at 37 °C for 3 h. The resulting $^{15}N_4$-dI and $^{15}N_2$-dU were purified using HPLC system 3 and characterized by HPLC coelution, MS, and UV spectroscopy relative to commercial standards. The products were quantified using the following extinction coefficients: $^{15}N_4$-dI, 12 800 M^{-1} cm^{-1} at 249 nm; $^{15}N_2$-dU, 10 100 M^{-1} cm^{-1} at 262 nm (*39*).

Reaction of DNA and Mor with NO• and HNO_2. A novel delivery system, described in detail elsewhere (*38*), was used to introduce NO• into the reaction buffer and to replenish O_2, allowing the concentrations of both to be maintained at constant, physiological levels. Briefly, two loops of gas permeable poly(dimethylsiloxane) tubing (Silastic, i.d. 1.47 mm, o.d. 1.96 mm; Dow Corning, Midland, MI) were immersed in a 120 mL stirred, liquid-filled, Teflon reactor. A 10:40 NO•:Ar gas mixture was passed through one loop and a 50:50 O_2:N_2 mixture through the other. The tubing lengths and gas flow rates were 7 cm and 150 sccm for NO• and 4 cm and 200 sccm for O_2. The performance of the system was tested by continuously monitoring the liquid concentrations using a NO• electrode (World Precision Instruments, ISO-NO Mark II system) and a Clark type O_2 electrode (Orion, model 810A Plus). Because the kinetics of Mor nitrosation by N_2O_3 are relatively well known (see below), the rate of NMor formation was used as a measure of the N_2O_3 concentration. That is, rate constants for nucleobase deamination were calculated by comparing rates of deamination with rates of Mor nitrosation measured in separate experiments.

NO• treatment of DNA was achieved using 120 mL solutions of plasmid pUC19 (20 μg/mL in 50 mM Chelex-treated potassium phosphate (K−PO_4) buffer, pH 7.4); plasmid stock solutions were dialyzed exhaustively against Chelex-treated K−PO_4 buffer, pH 7.4. A control DNA solution exposed to pure Ar was prepared in a duplicate chamber of identical construction. At various times points after starting the gas flow, 2.5 mL aliquots of the reaction mixture were withdrawn from the chamber and replaced with an identical volume of fresh buffer. The DNA in each sample was recovered by ethanol precipitation and resuspension in water. All of the experiments were conducted at ambient temperature.

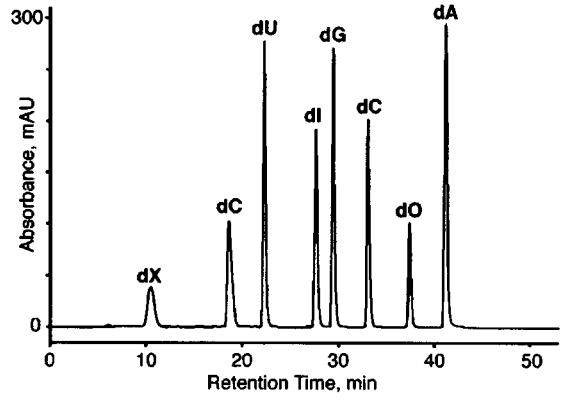

Figure 1. Example of the reversed-phase HPLC resolution of normal deoxynucleosides and deamination products.

In reactions with Mor, NO• was delivered into 2 mM Mor in K−PO_4 buffer (50 mM, pH 7.4) containing 0.1 mM DTPA at ambient temperature and the formation of the nitrosation product, NMor, was quantified by UV absorbance at 250 nm (ϵ_{250} = 5500 M^{-1} cm^{-1}) via a flow loop and a 1 cm flow cell.

Reactions with HNO_2 were performed by dissolving $NaNO_2$ (181 mM final concentration) in a solution containing calf thymus DNA (150 μg/mL) and 3 M sodium acetate buffer, pH 3.8. At various times during an incubation at 37 °C, 1 mL aliquots were removed and the reaction was stopped by neutralization with 200 μL of 5 N NaOH. The solution was desalted by three 500 μL water washings using a Microcon YM-100 filtration system, and the purified DNA was subjected to LC/MS analysis as described next.

Processing of DNA Samples for LC/MS Analysis. Samples of DNA (50 μg) were dissolved in 13 μL of sodium acetate buffer (30 mM, pH 5.8) and 10 μL of zinc chloride (10 mM) followed by addition of isotope-labeled internal standards (6 pmol). The DNA was digested to deoxynucleoside monophosphates by addition of nuclease P1 (4 U, 2 μL, Roche) and incubation at 37 °C for 3 h. Following addition of 30 μL of sodium acetate buffer (30 mM, pH 7.4), phosphate groups were removed with alkaline phosphatase (1 μL, 12.5 U, Sigma) and phosphodiesterase I (4 μL, 0.007 U, USB) by incubation at 37 °C for 6 h. The enzymes were subsequently removed by passing the reaction mixture over a Microcon YM-30 column, and deaminated deoxynucleosides were isolated by collection of HPLC (system 4) fractions bracketing empirically determined elution times for each product (see Figure 1): dX, 10.6 min; dC, 18.7 min; dU, 22.4 min; dI, 27.8 min; dG, 29.6 min; dT, 33.2 min; dO, 37.6 min; dA, 41.3 min. Fractions containing each product were pooled, and the solvent was removed under vacuum.

LC/MS Quantification of Deoxynucleoside Deamination Products. Following resuspension of the pooled HPLC fractions in 40 μL of 1% acetonitrile in water, the deoxynucleoside deamination products were quantified by LC/MS in selected ion monitoring mode. Samples (40 μL) were injected onto the HPLC column (system 5), and dX, dI, and dO were analyzed by atmospheric pressure ionization-electrospray (API-ES) ionization with detection in the positive ion mode; API-ES in the negative ion mode was used for dU. MS parameters were as follows: drying gas (N_2) flow, 12 L/min at 330 °C for dU and

350 °C for dX, dI, and dO; nebulizing gas pressure, 35 kPa; capillary potential, 3300 V; fragmentor potential, 50–125 V (optimized for each lesion); electron multiplier potential, 2500 V; quadruple temperature, 99 °C.

Quantification of Base Lesions and Abasic Sites in Plasmid DNA by Topoisomer Analysis. Abasic sites were quantified in plasmid DNA as described elsewhere (e.g., refs *40–42*). Briefly, aliquots of plasmid solution containing ~3 μg of DNA, obtained from samples removed for LC/MS analysis, were divided and one portion (200 ng) was treated with putrescine dihydrochloride (100 mM, pH 7) for 1 h at 37 °C to cleave all abasic sites (*43*). Following resolution of the resulting plasmid topoisomers (nicked form II and supercoiled form I) on 1% agarose gels, the quantity of abasic sites at each NO• exposure time was calculated as the difference in the quantity of nicked plasmid DNA in samples treated with putrescine and those not treated.

U was quantified in a similar manner by treating the NO•-exposed plasmid DNA (200 ng) with U DNA glycosylase (1 ng; *44*) followed by putrescine to cleave the resulting abasic sites to strand breaks, as described above. The quantity of dU was then calculated from the net proportion of nicked (form II) plasmid DNA following resolution of the plasmid topoisomers on 1% agarose gels.

Reaction Scheme and Kinetic Model. 1. Reactions. The principal nitrosating agent in oxygenated NO• solutions at physiological pH is N_2O_3 (*45*), which is formed via reactions 1 and 2:

$$2NO + O_2 \xrightarrow{k_1} 2NO_2 \quad (1)$$

$$NO + NO_2 \xrightarrow{k_2, k_{-2}} N_2O_3 \quad (2)$$

Most of the N_2O_3 is hydrolyzed to nitrite, which can occur either directly or with the participation of various anions, including phosphate salts (*45*). The two hydrolysis pathways under our experimental conditions were

$$N_2O_3 + H_2O \xrightarrow{k_3} 2NO_2^- + 2H^+ \quad (3)$$

$$N_2O_3 + P_i + H_2O \xrightarrow{k_4} P_i + 2NO_2^- + 2H^+ \quad (4)$$

Under our conditions (50 mM potassium phosphate buffer, pH 7.4), reaction 4 is 20 times as fast as reaction 3. The additional reactions depend on which organic substrates are present. In Mor solutions (no DNA present), N_2O_3 could react with unprotonated Mor (Mor°) to form NMor:

$$N_2O_3 + Mor° \xrightarrow{k_5} NMor + NO_2^- + H^+ \quad (5)$$

In DNA solutions (no Mor present), the three deamination reactions identified in our experiments were

$$N_2O_3 + dG \xrightarrow{k_6} dX + NO_2^- + H^+ \quad (6)$$

$$N_2O_3 + dA \xrightarrow{k_7} dI + NO_2^- + H^+ \quad (7)$$

$$N_2O_3 + dC \xrightarrow{k_8} dU + NO_2^- + H^+ \quad (8)$$

The rate constants for reactions 1–5, reported previously, are listed in Table 1. Those for dG, dA, and dC in plasmid DNA were calculated from the relative rates of nitrosation and deamination, as described below.

The kinetic analysis was complicated by the fact that the delivery system creates two liquid regions with very different concentrations of N_2O_3. In addition to a well-stirred bulk liquid with a low concentration of N_2O_3, there is a very thin (~1 μm) boundary layer next to the NO• delivery tubing, where the N_2O_3 concentration is much higher. It was found that despite its small volume, the contribution of the boundary layer to the overall rates of nitrosation and deamination was comparable to that of the bulk liquid. High concentrations of NO_2• (and therefore N_2O_3) in the boundary layer appear to arise from reaction 1 occurring not just in the liquid but within the wall of the Silastic tubing (*38*). A summary of the kinetic analysis follows; a more complete derivation of the model equations is provided in the Supporting Information.

Table 1. Published Reaction Rate Constants

rate constant	value	units	ref
k_1	2.1×10^6	$M^{-2}s^{-1}$	*28*
k_2	1.1×10^9	$M^{-1}s^{-1}$	*46*
k_{-2}	8.4×10^4	s^{-1}	*46*
k_3	1.6×10^3	s^{-1}	*47*
k_4	6.4×10^5	$M^{-1}s^{-1}$	*45*
k_5	6.4×10^7	$M^{-1}s^{-1}$	*45*

In the bulk liquid, the quasi-steady state approximation in kinetics was applied to both NO_2• and N_2O_3. The resulting bulk N_2O_3 concentrations in the Mor and DNA solutions were found to be

$$[N_2O_3]_M = \frac{2k_1[NO]^2[O_2]}{k_3 + k_4[P_i] + k_5[Mor°]} \quad (9)$$

$$\frac{[N_2O_3]_M}{[N_2O_3]_D} = \frac{k_3 + k_4[P_i]}{k_3 + k_4[P_i] + k_5[Mor°]} \equiv \alpha_1 \quad (10)$$

where $[N_2O_3]_M$ and $[N_2O_3]_D$ represent the bulk N_2O_3 concentrations in Mor and DNA solutions, respectively. Although Mor nitrosation affected the N_2O_3 level, the yield of NMor was low enough that [Mor°] was almost constant (independent of time). Therefore, the ratio of the N_2O_3 concentrations in the two types of experiments (α_1) was a constant.

The thickness of the NO_2•/N_2O_3 boundary layer (λ, the distance for a 1/e decay in either concentration) was evaluated using equation A6 in ref *38*. It was calculated to be slightly different in Mor (λ_M = 0.55 μm) and DNA (λ_D = 0.60 μm) solutions. The contributions of the boundary layer to NMor or deaminated base product formation were expressed as apparent increments in the bulk N_2O_3 concentrations, denoted as $\overline{[N_2O_3]_M}$ and $\overline{[N_2O_3]_D}$, respectively. The apparent concentration increments for the two types of solutions are related as

$$\frac{\overline{[N_2O_3]_M}}{\overline{[N_2O_3]_D}} = \alpha_1 \quad (11)$$

In the stirred batch reactor used in our experiments, the rates of accumulation of NMor and DNA products in the bulk liquid equaled their rates of formation per unit volume. Adding the contributions of the two regions, and using dX formation as an example, the overall rates are given by

$$\frac{d[NMor]}{dt} = k_5[Mor°]\{[N_2O_3]_M + \overline{[N_2O_3]_M}\} \quad (12)$$

$$\frac{d[dX]}{dt} = k_6[dG]\{[N_2O_3]_D + \beta\overline{[N_2O_3]_D}\} \quad (13)$$

In eq 13, β represents the effects of the partial exclusion of the plasmid from the boundary layer, due to the finite size of the plasmid. If the plasmid is approximated as a rod of length $l \approx$ 0.5 μm (estimated from electron microscopy; e.g., ref *48*), β is evaluated as

$$\beta = \frac{2\lambda_D}{l}(1 - e^{-l/2\lambda_D}) \cong 0.82 \quad (14)$$

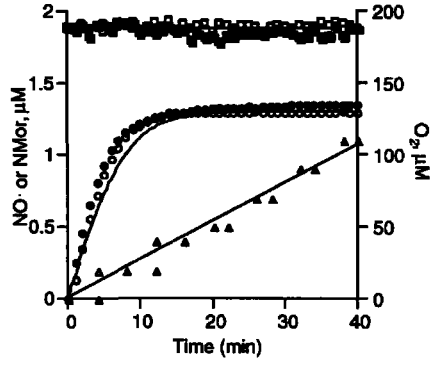

Figure 2. Time course for concentrations of NO· (a,b) and O_2 (c,d) in the reactor, with the NMor kinetics (e,f) determined under the same conditions. The two sets of symbols (open and closed) for each data set represent single determinations for two separate experiments. The curves for NO· and O_2 were fitted as described in the text; the NMor data were fit by linear regression.

Combining eqs 10–13 and solving for k_6, we obtain

$$k_6 = \frac{k_5[\text{Mor}^\circ]}{[\text{dG}]}\frac{\text{d}[\text{dX}]/\text{d}t}{\text{d}[\text{NMor}]/\text{d}t}\alpha_1\left(\frac{1+\frac{[\overline{N_2O_3}]_M}{[N_2O_3]_M}}{1+\beta\frac{[\overline{N_2O_3}]_M}{[N_2O_3]_M}}\right) \quad (15)$$

As will be shown, [dG] was approximately constant in our experiments (like [Mor°]). Therefore, k_6 could be determined from the slopes of the [dX] and [NMor] data plotted vs time. The rate constants for dI and dU formation, k_7 and k_8, respectively, were determined using relations analogous to eq 15.

Results

Characterization of the NO· Delivery System. Prior to the DNA experiments, the NO· and O_2 concentrations were measured to confirm that the delivery system was performing as expected. The results of two such tests are shown in Figure 2. The O_2 concentration remained constant at 190 μM throughout each experiment, whereas the NO· concentration reached a value of 1.3 μM about 15 min after NO· gas flow was initiated and was constant thereafter. The solid curves in Figure 2 show the concentrations predicted using the mass transfer coefficients reported previously (*38*). The agreement between those curves and the measured concentrations indicates that the final concentrations of both gases, and the duration of the initial NO· transient, were all predictable. The concentration of nitrite increased linearly with time (data not shown), with a formation rate of 1.45 μM/min. It is worth noting that the steady state level of NO· achieved here is similar to that generated by activated macrophages in culture (~1 μM; *49*, *50*). Therefore, the experimental conditions used here are likely to be relevant to the pathophysiology of inflammation involving macrophages.

Given the measured NO· and O_2 concentrations, the steady state N_2O_3 concentration in the bulk liquid in the Mor and DNA experiments can be estimated from eqs 13 and 15, respectively. The calculated N_2O_3 concentrations were quite small, with 3.1×10^{-14} M for the Mor solutions and 4.0×10^{-14} M for the DNA solutions. These

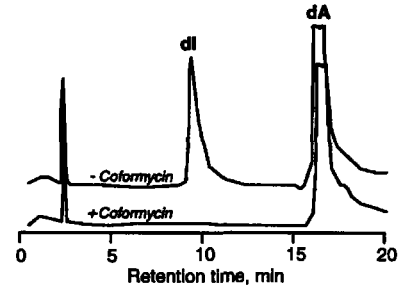

Figure 3. LC/MS analysis of coformycin inhibition of dA deaminase activity present in alkaline phosphatase preparations. Dashed line, dA (12.5 μg) incubated with alkaline phosphatase (12.5 U); solid line, dA (12.5 μg) incubated with alkaline phosphatase (12.5 U) in the presence of coformycin (31 ng).

low levels are mainly due to the rapid hydrolysis of N_2O_3 to form nitrite. As mentioned earlier, the bulk N_2O_3 concentration was lower in the Mor experiments because there was enough Mor present to noticeably augment the consumption of N_2O_3; a similar lowering of the N_2O_3 level by Mor is expected in the NO_2·/N_2O_3 boundary layer (vide infra). The low bulk concentrations of N_2O_3 notwithstanding, in the Mor experiments, NMor accumulation reached micromolar levels, as shown in Figure 2. As will be discussed, our calculations indicate that N-nitrosation in the bulk solution and in the NO_2·/N_2O_3 boundary layer both contributed significantly to the observed rate of NMor formation.

Development and Calibration of an LC/MS Method to Quantify Base Deamination Products. Mass spectrometric parameters for detection of dX, dO, dI, and dU were individually optimized using standards. Positive ion mode produced the strongest signals for dX, dO, and dI, while negative ion mode was optimal for dU. By varying the fragmentor potential, the following ions were found to produce optimal signals: dX and $^{15}N_4$-dX, protonated free base ion (BH^+) at *m/z* 153 and 157, respectively (75 V); dO and $^{15}N_4$-dO, BH^+ at *m/z* 153 and 157, respectively (50 V); dI and $^{15}N_4$ dI, BH^+ at *m/z* 137 and 141, respectively (75 V). For dU and $^{15}N_2$-dU in negative ion mode, a 50 V fragmentor potential produced optimal signals for the deprotonated molecular ion (M^-) at *m/z* 227 and 229, respectively. Total ion chromatograms for each deamination product are presented in Supporting Information.

One problem encountered in the LC/MS analysis of base deamination products was the adventitious formation of dI by the action of adenosine deaminase that was present as a contaminant in stocks of alkaline phosphatase from several manufacturers. An example of this activity is shown in Figure 3, in which 12.5 μg of dA was incubated with 12.5 U of alkaline phosphatase (Sigma in this case) under the same conditions used for plasmid DNA hydrolysis, as described in the Experimental Procedures. Following filtration (Microcon YM-10) to remove the enzyme, the filtrate was subjected to LC/MS analysis. It is clear from Figure 3 that there is an activity in the incubation mixture that causes deamination of dA to dI. On the suspicion that this activity represented adenosine deaminase, an identical incubation mixture was prepared that included coformycin, a specific inhibitor of adenosine deaminase (*51*), at a concentration of 2.5 ng per unit of alkaline phosphatase. As shown in Figure 3, the coformycin effectively inhibited the dA deamination activity

without interfering with the alkaline phosphatase. All subsequent analyses of dI were performed in the presence of coformycin. Other deaminase activities for dG and dC were not detected in enzymes selected for DNA processing (data not shown).

Calibration curves for the analyses of dX, dI, dO, and dU were obtained by adding known quantities of unlabeled deoxynucleosides (0–10 ng) to a fixed amount of N^{15}-labeled internal standard (300 pg) in K–PO_4 buffer (50 mM, pH 7.4). As shown in the Supporting Information, the curves were linear ($r^2 = 1.00$) and intercepted the *y*-axis at zero in all cases. The limit of the detection of the assay was determined to be 100 fmol for each deamination product, which equates to a sensitivity of 6 lesions per 10^7 nt in 50 μg of DNA.

Experiments were also undertaken to evaluate the overall efficiency of the deamination product analyses. First, we determined the average percentage recovery of each product for the steps following nuclease and phosphatase digestion: dX, 51%; dI, 43%; dO, 40%; and dU, 28%. With regard to the precision of the analytical method, 22.2 pmol of a 30-mer oligonucleotide containing a single dI moiety was subjected to digestion and LC/MS analysis. The amount of dI detected in the sample was 22.8 ± 1.9 pmol, which compares favorably with the calculated value and indicates the effectiveness of the coformycin inhibition of adenosine deaminase. A second assessment of analytical precision involved quantitation of dU by a combination of U DNA glycosylase and plasmid topoisomer analysis, as described shortly.

LC/MS Analysis of Base Deamination Products Produced by NO• Exposure. The LC/MS method was now applied to the quantification of deamination products in DNA exposed to nitric oxide. Using the NO• reactor, plasmid pUC19 DNA (120 mL at 50 μg/mL in K–PO_4 buffer, pH 7.4) was exposed to NO• and O_2 at steady state levels of 1.3 and 190 μM, respectively. At various times, 1 mL aliquots were removed and subjected to enzymatic digestion and LC/MS analysis as described earlier. The results of the analyses are shown in Figure 4. Here, it is apparent that there was a time-dependent increase in the quantities of all deamination products except dO.

The inability to detect dO extended to the longest exposure time (24 h) with 10-fold higher amounts of DNA subjected to analysis (500 μg; data not shown). This suggested either that dO was produced below the limit of detection of the assay (6 lesions per 10^8 nt with 500 μg of DNA) or that technical problems prevented the detection of dO. To rule out the latter, an experiment was performed in which calf thymus DNA was treated with nitrous acid, which is known to produce high levels of dO (*27*). As shown in Figure 5, there is a time-dependent formation of dO by HNO_2 in the DNA to the extent of nearly 1 lesion in 100 nt. The nonlinearity of the time course is likely due to a reduction in the concentration of substrate dG.

The quantity of dU in NO•-treated plasmid DNA was confirmed using a plasmid-based nicking assay. Samples of plasmid DNA exposed to NO• in the reactor were treated with U DNA glycosylase (*44*) followed by treatment with putrescine to cleave the resulting abasic sites to strand breaks (e.g., refs *40–42*) that were subsequently quantified following agarose gel resolution of nicked and supercoiled plasmid molecules. As shown in Figure 4, the quantity of dU determined by the plasmid nicking study

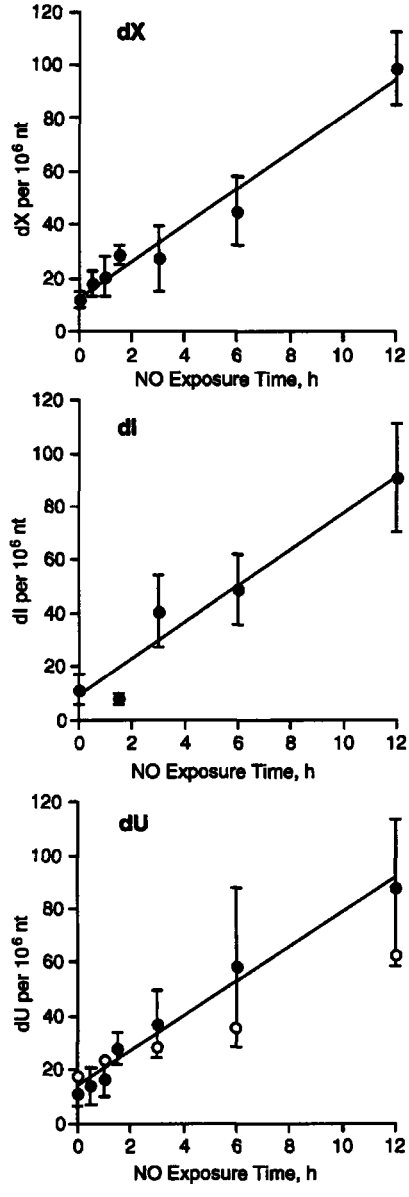

Figure 4. Time course for the formation of dX, dI, and dU in plasmid DNA by exposure to 1.3 μM NO and 190 μM O_2. Data points represent means ± SD for four determinations. The data were subjected to linear regression analysis, with the slope of each line used to calculate rate constants k_6 (dX), k_7 (dI), and k_8 (dU) according to eqs 32–34. Open circles in the panel for dU represent quantification of dU with U DNA glycosylase as described in the Experimental Procedures.

is within 30% of that determined by LC/MS, which attests to the precision of the LC/MS assay.

Quantitation of Abasic Sites Produced by Exposure of DNA to NO•. Given the precedent for depurination of DNA by nitrosating agents (*32*), we quantified abasic sites formed in the plasmid DNA exposed to NO• in the reactor, as described above. Aliquots of plasmid solution containing 3 μg of DNA, obtained from samples removed for LC/MS analysis, were divided, and one portion was treated with putrescine, as described above. Following resolution of the plasmid topoisomers on agarose gels, the quantity of abasic sites at each NO•

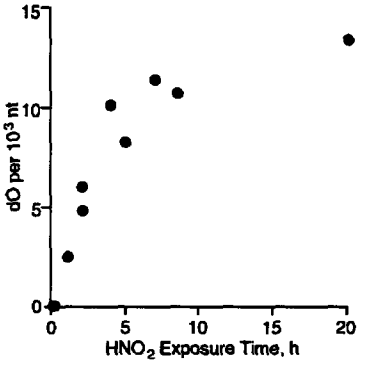

Figure 5. Time course for the production of dO in DNA treated with HNO_2. Data points represent individual determinations for two experiments.

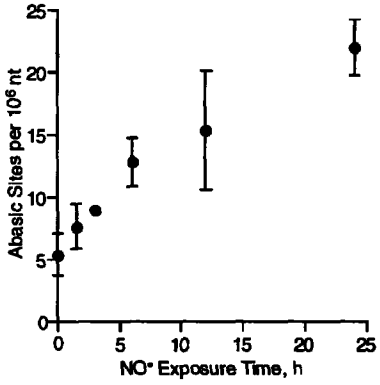

Figure 6. Time course for the formation of abasic sites by exposure of plasmid pUC19 to 1.3 μM NO• and 190 μM O_2. Values represent means ± error about the mean for two experiments.

exposure time was calculated as the difference in the quantity of nicked plasmid DNA in samples treated with putrescine and those not treated. The results are shown in Figure 6, in which it is apparent that there is a steady increase in the number of abasic sites as a function of NO• exposure time.

Rate Constants of N_2O_3 Reaction with Plasmid DNA Bases. The rate constant for the reaction of N_2O_3 with dG was estimated using eq 15, which requires several inputs. Equation 10 gives $\alpha_1 = 0.78$. The steric correction factor (β) was evaluated as in eq 14. The slopes of the NMor and dX concentration–time curves, as determined by linear regression of the data in Figures 2 and 4, were 2.99×10^{-2} and 6.83×10^{-6} μM/min, respectively. (Because it took ~15 min for NO• to reach a steady state, only the NMor data from 16 to 60 min were used to compute that slope.) Because of the low conversions, [Mor°] and [dG] were unchanged from their initial values of 147 and 15 μM, respectively. From eqs 9 and 12 and the NMor concentration data, $[\overline{N_2O_3}]_M/[N_2O_3]_M$ was calculated to be 0.71. Finally, using the value of k_5 in Table 1, k_6 was found to be 1.2 (± 0.1) × 10^5 M^{-1} s^{-1}. Likewise, the rates of dI and dU formation obtained from linear regression of data in Figure 4 were 6.92×10^{-6} and 6.57×10^{-6} μM/min, respectively, and the corresponding rate constants were $k_7 = 1.2$ (± 0.2) × 10^5 and $k_8 = 1.2$ (± 0.1) × 10^5 M^{-1} s^{-1}, which are identical to the rate constant for dX.

Table 2. Spectrum of DNA Lesions Produced by Exposure to 1.3 μM NO• and 190 μM O_2

time (h)	lesions per 10^6 nt				dO per 10^6 nt
	AP[a]	dX	dI	dU	
0	5.4 ± 1.6	12 ± 3	11 ± 6	11 ± 5	<0.06
3	9.0 ± 0.1	27 ± 12	41 ± 13	37 ± 12	<0.06
6	13 ± 2	45 ± 13	49 ± 13	58 ± 30	<0.06
12	15 ± 5	99 ± 14	91 ± 20	88 ± 26	<0.06
24	22 ± 2	131 ± 16	143 ± 38	109 ± 26	<0.06

[a] AP, abasic sites; values for all lesions represent means ± SD for four determinations.

In calculating deamination rate constants using eq 15, correcting for the different N_2O_3 concentrations in the Mor and DNA experiments turned out to be fairly important. That is, $\alpha_1 = 0.78$ indicates that the concentrations of N_2O_3 in the bulk liquid and in the NO_2•/N_2O_3 boundary layer were each 22% lower in the Mor experiments than in the DNA experiments. The steric effect, which is expressed by the large, bracketed term in eq 15 involving β and the N_2O_3 concentration ratio, was less influential. If there was no steric exclusion of the plasmid from the boundary layer (i.e., if $\beta = 1$), the bracketed term would be unity; using the inputs above, it was found to be 1.08. That is, steric exclusion of the plasmid increased the calculated rate constant for deamination by only 8%. The finding that $[\overline{N_2O_3}]_M/[N_2O_3]_M = 0.71$ indicates that the rates of N-nitrosation and deamination in both regions (bulk solution and boundary layer) were of comparable importance. In other words, the N_2O_3 concentration in the boundary layer is high enough to compensate for its small volume.

Discussion

Nitric oxide is a physiologically important molecule with genotoxic properties that may be involved in the pathophysiology of chronic inflammation (*9*, *52*). While the genotoxicity of reactive nitrogen species derived from NO• has been extensively studied, neither the biologically relevant chemistry nor the consequences of that chemistry in vivo have been rigorously defined. We thus developed and applied novel delivery and analytical methods to a comprehensive characterization of the spectrum of DNA lesions (with the exception of the G–G cross-link; *14*) produced by nitrosative NO• derivatives under conditions that approach biological relevance.

Spectrum of Nitrosative DNA Lesions Produced by NO• Exposure. Among the spectrum of nitrosative DNA lesions produced by exposure to NO•, we approached the quantification of abasic sites by standard plasmid topoisomer analysis. However, we were obliged to develop an LC/MS method sensitive enough to quantify nucleobase deamination products arising by nitrosative mechanisms at biologically relevant NO• concentrations (μM) in the presence of O_2. Most published studies of nucleobase deamination have employed GC/MS techniques (e.g., refs *12*, *30*). However, the acidic conditions used for depurination of DNA for GC/MS analysis cause decomposition of dO (Dong et al., unpublished observations). To avoid this problem, NO•-exposed DNA was enzymatically digested to nucleosides under conditions (37 °C, pH 7.4) that did not result in significant depurination of dX ($t_{1/2}$ > 2 years; *53*). The background levels of the deamination products in the plasmid DNA, while relatively high at ~1 per 10^5 nt (Table 2), do not appear to be an

artifact of the analytical method given the precision established for the quantification of dI in a defined oligonucleotide and for dU by comparison to an independent technique. It is thus likely that these background levels are those expected to occur in vivo or are the result of DNA purification and storage.

These analytical techniques were then applied to DNA exposed to controlled concentrations of NO• and O_2 in a novel NO• reactor. A summary of the results of these studies is shown in Table 2. NO• and O_2 were delivered at steady state concentrations of 1.3 and 190 μM, respectively. These conditions resulted in a time-dependent increase in three nucleobase deamination products (dX, dI, and dU) at nearly identical rates, which stands in contrast to the nearly 2-fold higher rate of formation of dX than dU observed by Caulfield et al. (*30*). The basis for this small difference may lie in the NO• delivery system used by Caulfield et al. (*30*), in which headspace air may have altered the spectrum of NO• derivatives and thus the nitrosative chemistry in the reaction mixture. A comparison of the NO• delivery systems will be later in the Discussion.

The studies produced two unexpected results. The first was the observation of a time-dependent formation of abasic sites to the extent of 4−7% of the total number of DNA lesions (with the exception of dG−dG cross-links; Table 2). Shuker and co-workers have demonstrated that nitrosation of DNA by 1-nitrosoindole-3-acetonitrile causes the formation of abasic sites, presumably as a result of transient nitrosation of the N^7 position of dG and the N^7 and N^3 positions of dA (Scheme 1; *31*, *32*). We propose that a similar mechanism accounts for the formation of abasic sites as a result of nitrosation by N_2O_3 generated in the reactor. The well-defined chemistry and low concentrations of the reactive nitrogen species produced in the reactor strengthen the argument for the biological relevance of the abasic sites, which account for ~5% of the total nitrosative DNA damage. It is unclear what role the abasic sites may play in NO•-induced mutagenesis, given the observation in repair deficient *Escherichia coli* exposed to nitrous acid that the G:C→T:A mutations expected for apurinic sites represented only 0.2% of total mutations (*54*). The bulk of the mutations consisted of G:C→A:T and A:T→G:C transitions (*54*). However, Engelward and co-workers have demonstrated that *E. coli* cells lacking AP endonuclease activity were highly sensitive to NO• exposure (*55*, *56*), which suggests that along with base excision repair of nucleobase deamination products, the directly formed abasic sites may contribute to NO•-induced toxicity in cells.

The observation of NO•-induced abasic sites expands the spectrum of lesions associated with the nitrosative intermediates derived from NO• under biologically relevant conditions. With consideration given to the formation of dG−dG cross-links in NO•-exposed DNA, we are now in a position to propose a testable quantitative spectrum of nitrosative DNA lesions in cells and tissues exposed to NO•. Recent studies by Caulfield et al. (submitted for publication) revealed that the dG−dG cross-link represented 6% of the amount of X in oligode oxynucleotides exposed to NO• delivered at 15 μM/min via Silastic tubing. Assuming that nitrosative chemistry is similar in vitro and in cells, we propose that the spectrum of nitrosative DNA lesions in cells and tissues exposed to physiological concentrations of NO• and O_2 will be comprised of ~2% dG−dG cross-links, ~4−6% abasic sites, and ~25−35% each of dX, dI, and dU. We are presently testing this model in TK6 cells exposed to NO• in the reactor employed in the present studies and in the SJL mouse model for inflammation (*57*, *58*). Interestingly, there appears to be little oxidative chemistry in the NO• reactor as judged by the lack of nicking induced in exposed plasmid DNA by treatment with Fpg and EndoIII glycosylases (data not shown), enzymes that recognize DNA damage produced by peroxynitrite (*43*).

The second novel observation is the absence of detectable dO in DNA exposed to biological concentrations of NO• and O_2. We were unable to detect this lesion in 500 μg of DNA, an amount 10-fold higher than that used for analysis of dX, dI, and dU, which suggests that dO, if it arises at all, is present at less than six lesions in 10^8 nt (Table 2). The apparent absence of dO is not the result of analytical artifact given the detection of this lesion in DNA samples treated with nitrous acid (Figure 5). Shuker and co-workers also observed a significant disparity between dX and dO in DNA treated with the nitrosating agent, 1-nitrosoindole-3-acetonitrile, with dO formed at levels 10^3-fold lower than depurination and deamination products (*32*). Our results with controlled exposure to NO• differ from the studies of nucleobase deamination with nitrous acid performed by Suzuki et al., in which it was observed that dO arose from dG in deoxynucleosides and DNA treated with nitrous acid at pH 3.7 and 37 °C with a yield 3−4-fold smaller than that of dX (*18*, *59*).

Insight into the basis for these differences in dO formation can be gained by consideration of the mechanisms of nucleobase deamination and the pH dependence of the spectrum of reactive nitrogen species. The work of Glaser and co-workers is relevant in this regard (*60*−*62*). On the basis of theoretical studies, the Glaser group has developed a model for guanine deamination that involves an intermediate, ring-opened, carbodiimide-substituted carbenium ion that can close to form either X or O (*60*−*62*). The absence of dO under biological conditions may result from pH sensitive intermediates in the ring closure reactions. However, it is also possible that the alternative nucleophilic displacement of the diazonium ion by water predominates at pH 7.4, thus reducing the ring opening reaction that would lead to dO (*60*−*62*).

Another possible explanation for the absence of dO is that the pH-dependent spectrum of reactive nitrogen species dictates the outcome of the deamination reactions (*63*, *64*). At neutral pH, N_2O_3 is the predominant reactive species while under the acidic conditions used with HNO_2 species such as $H_2NO_2^+$ and at pH ≤ 1, NO^+ contributes to the chemistry (*63*, *64*). Suzuki et al. have also observed the formation of dO in DNA solutions treated with NO• and O_2 (unpublished observations; *27*). In one set of studies, NO• was bubbled into a buffered solution of dG under aerobic conditions until the pH reached 2.9, which suggests the formation of nitrous acid derivatives. In other studies, buffered solutions of dG were exposed to NO• gas in the headspace of a sealed vessel, with small amounts of dO formed after 4 days. The presence of a headspace significantly alters the chemistry of NO• due to alternative (and possibly physiologically irrelevant) gas phase NO_x chemistry that includes formation of N_2O_4 (*36*, *37*).

Given these differences, we hypothesize that dO will not be produced in significant quantities, relative to the

other DNA lesions, in cells exposed to NO• at sites of inflammation in tissues. This model is supported by our inability to detect dO in preliminary studies in TK6 cells exposed to NO• and O_2 in the reactor under conditions identical to those employed here with isolated DNA (Dong et al., manuscript in preparation).

Comparison of NO• Delivery Systems. The NO• delivery system used in the present studies represents a major improvement over previous systems in terms of biological relevance (*12, 30, 33*). Previous attempts to expose DNA to NO• and the derivative nitrosating species have employed several NO• delivery systems. For example, Nguyen et al. exposed DNA and TK6 cells to high concentrations of NO by bolus delivery through a syringe and found that dX and dI were formed to the extent of 3 and 10 lesions per 10^3 nt, respectively, for isolated DNA, with 3-fold lower levels of each in cells (*12*). Yields of dI and dX in DNA were found to be 15−100 times higher, respectively, than those observed with free dA and dG (*12*). Similarly, Wink et al. exposed DNA to NO• by bubbling the gas into solution and found five dU per 10^3 nt (*33*).

The previous studies that most closely approximated biological conditions were those performed by Caulfield et al. in which NO•-induced deamination of dC and dG in deoxynucleosides and oligonucleotides was studied using two different reactors (*30*). In the first reactor, they introduced O_2 into a solution containing NO•, Mor, and dG and measured the concentrations of NMor and X formed as products. Through a kinetic competition analysis, the rate of dG conversion to dX was determined. In the second reactor, they used a Silastic membrane delivery system to introduce NO• into solutions containing dG and other nucleosides or nucleotides. Using the predetermined dG kinetics as a reference, the rate constants for dG and dC in different nucleic acids were determined. In general, relatively high deoxynucleoside and NO• concentrations were used in that study (stated as 10−20 nmol/mL/min); the latter was not determined but would not have been constant, due to the depletion of O_2 during the experiments. The deamination rate constants found for plasmid DNA in the present studies ($1.2 \times 10^5\ M^{-1}\ s^{-1}$) are comparable to the values reported by Caulfield et al. for single-stranded oligonucleotides ($9.8 \times 10^4\ M^{-1}\ s^{-1}$ for dG and $5.6 \times 10^4\ M^{-1}\ s^{-1}$ for dC), but they are about 1 order of magnitude higher than those determined in double stranded oligonucleotides ($1.0 \times 10^4\ M^{-1}\ s^{-1}$ for dG and $5.6 \times 10^3\ M^{-1}\ s^{-1}$ for dC; *30*). One possible explanation for the similarity of our results in double-stranded DNA to those of Caulfield et al. (*30*) in single stranded DNA is that the plasmid DNA used in the present studies contains single-stranded regions as a result of negative supercoiling. However, a rigorous comparison is difficult since the results of these and the other previous studies are confounded by extremely high NO• concentrations, the presence of headspace in the delivery systems that alters the spectrum of NO_x species present in solution (*36, 37*), and the narrow focus on one or two DNA lesions. These conditions were avoided in the present studies by the use of a novel NO• reactor.

Characterization of the NO• Reactor. The physiological relevance of the DNA lesion spectrum observed in the present studies rests entirely on the NO• delivery system. The development of this system was motivated

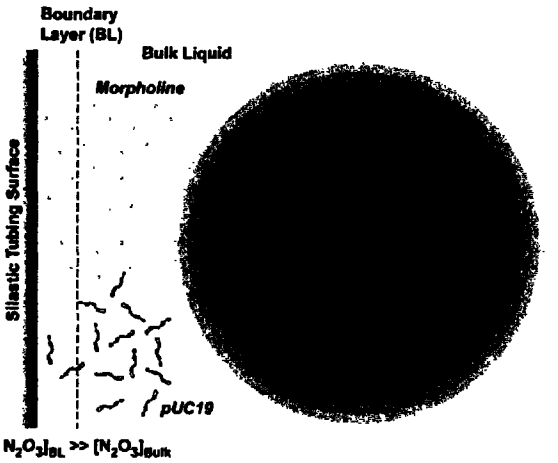

Figure 7. Heterogeneity of liquid concentrations in the reactor. In a boundary layer of thickness ~1 μm next to the NO• delivery tubing, the concentration of N_2O_3 greatly exceeds that in the bulk liquid. Mor molecules (not to scale) have free access to the boundary layer, while plasmid molecules are partially excluded and cells are almost fully excluded.

by the well-respected complexity of the reactions of NO• and O_2 in aqueous solutions (e.g., ref *64*), as illustrated earlier by the different results obtained with different NO• delivery mechanisms and rates. There are substantial differences in the relative concentrations and kinetics of the nitrosating intermediates depending on the concentrations of NO• and O_2, such that the only approach that provides biologically meaningful results is one in which the NO• and O_2 are maintained at concentrations that reflect the physiology of inflammation in tissues. The reactor employed in the present studies (*38*) provides more constant and predictable levels of NO• and O_2 than could be achieved previously in long exposures (up to 24 h). As shown in Figure 2, the dimensions of the Silastic tubing selected for the present studies produced a steady state NO• concentration of 1.3 μM within 15 min of initiating gas flow. This is comparable to NO• concentrations achieved by activated macrophages in vitro (*5, 50*) and is presumably representative of those at sites of inflammation. During the course of the NO• delivery, the pH remained at 7.4 while the nitrite level rose steadily at a rate of 1.4 μM/min to ~2 mM at 24 h (data not shown). The corresponding steady state levels of N_2O_3 and NO_2• in the bulk liquid were calculated to be 40 fM and 3.3 pM, respectively. Although the delivery conditions were fixed in the present experiments, it is worth noting that the NO• and O_2 concentrations can each be varied in a predictable way, by changing the gas mixtures and Silastic tubing lengths (*38*).

The NO• delivery system was designed mainly to carry out long-term cell culture studies and has the disadvantage in kinetic measurements that a rather complicated analysis is needed to interpret the results. The source of the complication is that despite vigorous stirring, the interplay between NO• oxidation kinetics and diffusion creates two liquid regions with very different concentrations of NO_x compounds. In addition to the well-stirred bulk liquid, there is an extremely thin (~1 μm) boundary layer next to the NO• delivery tubing, in which the NO_2• and N_2O_3 concentrations greatly exceed those in the bulk liquid (Figure 7). The main experimental evidence for this boundary layer is that the rate of nitrite formation in

the delivery system greatly exceeds (by an order of magnitude) that expected from the measured concentrations of $NO^{\bullet}$ and O_2 in the bulk liquid. Those data, and a model that quantitatively explains the observed mass transfer characteristics of the device, are detailed elsewhere (*38*). One of the present findings is that the N_2O_3 concentration in the boundary layer is high enough to contribute appreciably to the overall rates of Mor nitrosation or DNA deamination, despite the seemingly negligible volume of the boundary layer. This leads to a rate of NMor formation in the boundary layer that was 71% of that in the bulk solution. Put another way, some 40% of the total NMor formation was calculated to occur in the ultrathin boundary layer. The contribution of the boundary layer to nucleobase deamination was slightly smaller, because of steric exclusion of the plasmid DNA from part of that layer, as discussed shortly.

The issues that arise in using the $NO^{\bullet}$ delivery device to study $NO_2^{\bullet}$ or N_2O_3 chemistry in various applications are illustrated in Figure 7. As shown by the dots, Mor is small enough (relative to 1 μm) that its concentration in the boundary layer will not differ from that in the bulk liquid, assuming that Mor is present in large excess, as in the present experiments, so that it is not depleted by reaction. Molecules of plasmid DNA (2686 bp) with plectonemic supercoiling, however, are just large enough to experience some exclusion from the boundary layer. We estimated that the average concentration of pUC19 in the boundary layer was 18% less than in the bulk solution, which had a modest (8%) effect on the calculated rate constants for deamination. In contrast to small molecules and plasmid DNA, mammalian cells have dimensions that are large enough (~10 μm) to almost fully exclude them from the $NO_2^{\bullet}/N_2O_3$ boundary layer. Accordingly, cells in this device will be exposed only to the bulk NO_x concentrations. Because bulk concentrations are more accessible experimentally (e.g., using $NO^{\bullet}$ and O_2 electrodes), the chemical conditions are less uncertain than they are in the $NO_2^{\bullet}/N_2O_3$ boundary layer.

We also found a kinetic discrepancy in the measured NMor formation rate, which was about 4–5-fold lower than expected from the rate constants in Table 1. As already noted, the present data and kinetic analysis indicate that the rate of NMor formation was 70% larger than if the boundary layer was not present. However, at the same $NO^{\bullet}$ and O_2 concentrations (but without Mor), the boundary layer was found to give a 9-fold increase in the overall rate of nitrite formation (*38*). Because the nitrite and NMor formation rates are both proportional to the N_2O_3 concentration, the boundary layer should augment them by similar amounts. The ~20% reduction in the N_2O_3 concentration caused by Mor is too small to explain the difference. One possible explanation is that the phosphate effect on N_2O_3 hydrolysis (i.e., the k_4 value) might have been underestimated. If the actual value of k_4 was larger than that in Table 1, then NMor formation would be reduced, but nitrite formation in a Mor-free solution (which is controlled by the rate of reaction 1) would be unaffected. Another possibility is that the value of k_5 may have been overestimated. The discrepancy between the predicted and the observed rates of NMor formation suggests a proportional uncertainty in the concentrations of N_2O_3 and a consequent 4–5-fold uncertainty in the absolute values of the deamination rate constants. However, because each deamination rate was compared with the same standard (rate of NMor formation), there is little uncertainty in the relative rate constants for deamination of dG, dA, and dC.

In summary, we have used a novel nitric oxide delivery system to define the spectrum of nucleobase deamination products arising from exposure to biologically relevant concentrations of $NO^{\bullet}$ (1.3 μM) and O_2 (190 μM). The well-described chemistry of the $NO^{\bullet}$ delivery system described here is widely applicable to the study of the nitrosative reactions with other biological molecules, with the advantage of generating reactive nitrogen species at concentrations expected in vivo. The two important observations of these studies in DNA, the absence of detectable dO, and the presence of nitrosatively induced abasic sites lead to a testable model for nitrosative chemistry in cells and necessitate a reconsideration of the spectrum of nitrosative DNA lesions expected in cells at sites of inflammation in humans.

Acknowledgment. We thank Dr. Toshinori Suzuki for discussions of $NO^{\bullet}$ chemistry, for review of this manuscript, and for providing the results of unpublished studies; and Drs. John Wishnok and Koli Taghizadeh and Ms. Elaine Plummer for their assistance with mass spectrometry. This work was supported by a grant from the National Cancer Institute (CA26735). LC/MS analyses were performed in the Bioanalytical Facilities Core of the Center for Environmental Health Sciences at MIT, which is supported by a Center grant from the NIEHS (ES02109).

Supporting Information Available: Total ion chromatograms and LC/MS calibration curves for dX, dI, dO, and dU; reaction scheme and detailed derivation of a kinetic model. This material is available free of charge via the Internet at http://pubs.acs.org.

References

(1) Moncada, S., Palmer, R. M., and Higgs, E. A. (1991) Nitric oxide: Physiology, pathophysiology, and pharmacology. *Pharmacol. Rev.* **43**, 109–142.

(2) Nathan, C., and Xie, Q. W. (1994) Regulation of biosynthesis of nitric oxide. *J. Biol. Chem.* **269**, 13725–13728.

(3) Schmidt, H. H., and Walter, U. (1994) NO at work. *Cell* **78**, 919–925.

(4) Ohshima, H., and Bartsch, H. (1994) Chronic infections and inflammatory processes as cancer risk factors: Possible role of nitric oxide in carcinogenesis. *Mutat. Res.* **305**, 253–264.

(5) Lewis, R. S., Tamir, S., Tannenbaum, S. R., and Deen, W. M. (1995) Kinetic analysis of the fate of nitric oxide synthesized by macrophages in vitro. *J. Biol. Chem.* **270**, 29350–29355.

(6) deRojas-Walker, T., Tamir, S., Ji, H., Wishnok, J. S., and Tannenbaum, S. R. (1995) Nitric oxide induces oxidative damage in addition to deamination in macrophage DNA. *Chem. Res. Toxicol.* **8**, 473–477.

(7) Tamir, S., and Tannenbaum, S. R. (1996) The role of nitric oxide ($NO^{\bullet}$) in the carcinogenic process. *Biochim. Biophys. Acta* **1288**, F31–F36.

(8) Collier, J., and Vallance, P. (1991) Physiological importance of nitric oxide. *BMJ* **302**, 1289–1290.

(9) Tamir, S., Burney, S., and Tannenbaum, S. R. (1996) DNA damage by nitric oxide. *Chem. Res. Toxicol.* **9**, 821–827.

(10) Stamler, J. S., Jaraki, O., Osborne, J., Simon, D. I., Keaney, J., Vita, J., Singel, D., Valeri, C. R., and Loscalzo, J. (1992) Nitric oxide circulates in mammalian plasma primarily as an S-nitroso adduct of serum albumin. *Proc. Natl. Acad. Sci. U.S.A.* **89**, 7674–7677.

(11) Tannenbaum, S. R., Tamir, S., deRojas-Walker, T., and Wishnok, J. S. (1994) *DNA Damage and Cytoxicity by Nitric Oxide*, American Chemical Society, Washington, DC.

(12) Nguyen, T., Brunson, D., Crespi, C. L., Penman, B. W., Wishnok, J. S., and Tannenbaum, S. R. (1992) DNA damage and mutation in human cells exposed to nitric oxide in vitro. *Proc. Natl. Acad. Sci. U.S.A.* **89**, 3030−3034.
(13) Wink, D. A., Kasprzak, K. S., Maragos, C. M., Elespuru, R. K., Misra, M., Dunams, T. M., Cebula, T. A., Koch, W. H., Andrews, A. W., Allen, J. S., and et al. (1991) DNA deaminating ability and genotoxicity of nitric oxide and its progenitors. *Science* **254**, 1001−1003.
(14) Kirchner, J. J., Sigurdsson, S. T., and Hopkins, P. B. (1992) Interstrand cross-linking of duplex DNA by nitrous acid: Covalent structure of the dG-to-dG cross-link at the sequence 5′-CG. *J. Am. Chem. Soc.* **114**, 4021−4027.
(15) Dubelman, S., and Shapiro, R. (1977) A method for the isolation of cross linked nucleosides from DNA: Application to cross links induced by nitrous acid. *Nucleic Acids Res.* **4**, 1815−1827.
(16) Shapiro, R., and Pohl, S. H. (1968) The reaction of ribonucleosides with nitrous acid. Side products and kinetics. *Biochemistry* **7**, 448−455.
(17) Shapiro, R., and Yamaguchi, H. (1972) Nucleic acid reactivity and conformation. I. Deamination of cytosine by nitrous acid. *Biochim. Biophys. Acta* **281**, 501−506.
(18) Suzuki, T., Yamaoka, R., Nishi, M., Ide, H., and Makino, K. (1996) Isolation and characterization of a novel product, 2′-deoxyoxanosine, from 2′-deoxyguanosine, oligodeoxynucleotide, and calf thymus DNA treated with nitrous acid and nitric oxide. *J. Am. Chem. Soc.* **118**, 2515−2516.
(19) Bass, B. L. (2002) RNA editing by adenosine deaminases that act on RNA. *Annu. Rev. Biochem.* **71**, 817−846.
(20) Chan, T. S., Long, C., and Green, H. (1975) A human mouse somatic hybrid line selected for human deoxycytidine deaminase. *Somatic Cell Genet.* **1**, 81−90.
(21) Shapiro, R., DiFate, V., and Welcher, M. (1974) Deamination of cytosine derivatives by bisulfite. Mechanism of the reaction. *J. Am. Chem. Soc.* **96**, 206−212.
(22) Lindahl, T., and Nyberg, B. (1974) Heat-induced deamination of cytosine residues in deoxyribonucleic acid. *Biochemistry* **13**, 3405−3410.
(23) Shapiro, R., and Klein, R. S. (1966) The deamination of cytidine and cytosine by acidic buffer solutions. Mutagenic implications. *Biochemistry* **5**, 2358−2362.
(24) Frederico, L. A., Kunkel, T. A., and Shaw, B. R. (1990) A sensitive genetic assay for the detection of cytosine deamination: Determination of rate constants and the activation energy. *Biochemistry* **29**, 2532−2537.
(25) Zhang, X., and Mathews, C. K. (1994) Effect of DNA cytosine methylation upon deamination induced mutagenesis in a natural target sequence in duplex DNA. *J. Biol. Chem.* **269**, 7066−7069.
(26) Shen, J.-C., Rideout, W. M., III, and Jones, P. A. (1994) The rate of hydrolytic deamination of 5-methylcytosine in double-stranded DNA. *Nucleic Acids Res.* **22**, 972−976.
(27) Suzuki, T., Kanaori, K., Tajima, K., and Makino, K. (1997) Mechanism and intermediate for formation of 2′-deoxyoxanosine. *Nucleic Acids Symp. Ser.* 313−314.
(28) Lewis, R. S., and Deen, W. M. (1994) Kinetics of the reaction of nitric oxide with oxygen in aqueous solutions. *Chem. Res. Toxicol.* **7**, 568−574.
(29) Singer, B., and Grunberger, D. (1983) *Molecular Biology of Mutagens and Carcinogens*, Plenum, New York.
(30) Caulfield, J. L., Wishnok, J. S., and Tannenbaum, S. R. (1998) Nitric oxide-induced deamination of cytosine and guanine in deoxynucleosides and oligonucleotides. *J. Biol. Chem.* **273**, 12689−12695.
(31) Lucas, L. T., Gatehouse, D., and Shuker, D. E. (1999) Efficient nitroso group transfer from *n*-nitrosoindoles to nucleotides and 2′-deoxyguanosine at physiological pH. A new pathway for *n*-nitrosocompounds to exert genotoxicity. *J. Biol. Chem.* **274**, 18319−18326.
(32) Lucas, L. T., Gatehouse, D., Jones, G. D. D., and Shuker, D. E. G. (2001) Characterization of DNA damage at purine residues in oligonucleotides and calf thymus DNA induced by the mutagen 1-nitrosoindole-3-acetonitrile. *Chem. Res. Toxicol.* **14**, 158−164.
(33) Wink, D. A., Kasprzak, K. S., Maragos, C. M., Elespuru, R. K., Misra, M., Dunams, T. M., Cebula, T. A., Koch, W. H., Andrews, A. W., Allen, J. S., and Keefer, L. K. (1991) DNA deaminating ability and genotoxicity of nitric oxide and its progenitors. *Science* **254**, 1001−1003.
(34) Miwa, M., Stuehr, D. J., Marletta, M. A., Wishnok, J. S., and Tannenbaum, S. R. (1987) Nitrosation of amines by stimulated macrophages. *Carcinogenesis* **8**, 955−958.
(35) Stuehr, D. J., and Marletta, M. A. (1987) Synthesis of nitrite and nitrate in murine macrophage cell lines. *Cancer Res.* **47**, 5590−5594.
(36) Mirvish, S. S. (1975) Formation of *N*-nitroso compounds: Chemistry, kinetics, and in vivo occurrence. *Toxicol. Appl. Pharmacol.* **31**, 325−351.
(37) Challis, B. C., Shuker, D. E. G., Fine, D. H., Goff, E. U., and Hoffman, G. A. (1981) Amine nitration and nitrosation by gaseous nitrogen dioxide. In *N-Nitroso Compounds: Occurrence and Biological Effects* (Bartsch, H., O'Neill, I. K., Castegnaro, M., and Okada, M., Eds.) pp 11−20, IARC, Lyon.
(38) Wang, C., and Deen, W. M. (2003) Nitric oxide delivery system for cell culture studies. *Ann. Biomed. Eng.* **31**, 65−79.
(39) Stimson, M. M., and Reuter, M. A. (1943) Ultraviolet absorption spectra of nitrogenous heterocycles. VII. The effect of hydroxy substitution on the ultraviolet absorption of the series: Hypoxanthine, xanthine and uric acid. *J. Am. Chem. Soc.* **65**, 153−155.
(40) Tretyakova, N. Y., Burney, S., Pamir, B., Wishnok, J. S., Dedon, P. C., Wogan, G. N., and Tannenbaum, S. R. (2000) Peroxynitrite-induced DNA damage in the supF gene: Correlation with the mutational spectrum. *Mutat. Res.* **447**, 287−303.
(41) Dedon, P. C., Jiang, Z.-W., and Goldberg, I. H. (1992) Neocarzinostatin-mediated DNA damage in a model AGT•ACT site: Mechanistic studies of thiol sensitive partitioning of C4′ DNA damage products. *Biochemistry* **31**, 1917−1927.
(42) Povirk, L. F., and Goldberg, I. H. (1985) Endonuclease-resistant apyrimidinic sites formed by neocarzinostatin at cytosine residues in DNA: Evidence for a possible role in mutagenesis. *Proc. Natl. Acad. Sci. U.S.A.* **82**, 3182−3186.
(43) Lindahl, T., and Andersson, A. (1972) Rate of chain breakage at apurinic sites in double-stranded deoxyribonucleic acid. *Biochemistry* **11**, 3618−3623.
(44) Scharer, O. D., and Jiricny, J. (2001) Recent progress in the biology, chemistry and structural biology of DNA glycosylases. *Bioessays* **23**, 270−281.
(45) Lewis, R. S., Tannenbaum, S. R., and Deen, W. M. (1995) Kinetics of *n*-nitrosation in oxygenated nitric oxide solutions at physiological pH: Role of nitrous anhydride and effects of phosphate and chloride. *J. Am. Chem. Soc.* **117**, 3933−3939.
(46) Graetzel, M., Taniguchi, S., and Henglein, A. (1970) Pulse radiolytic investigation of NO oxidation and equilibrium N_2O_3 = NO + NO_2 in aqueous solution. *Ber. Bunsen-Ges.* **74**, 488−492.
(47) Treinin, A., and Hayon, E. (1970) Absorption spectra and reaction kinetics of NO_2, N_2O_3 and N_2O_4 in aqueous solution. *J. Am. Chem. Soc.* **92**, 5821−5828.
(48) Adrian, M., ten Heggeler Bordier, B., Wahli, W., Stasiak, A. Z., Stasiak, A., and Dubochet, J. (1990) Direct visualization of supercoiled DNA molecules in solution. *EMBO J.* **9**, 4551−4554.
(49) Lewis, R. S., Tamir, S., Tannenbaum, S. R., and Deen, W. M. (1995) Kinetic analysis of the fate of nitric oxide synthesized by macrophages in vitro. *J. Biol. Chem.* **270**, 29350−29355.
(50) Chen, B., and Deen, W. M. (2002) Effect of liquid depth on the synthesis and oxidation of nitric oxide in macrophage cultures. *Chem. Res. Toxicol.* **15**, 490−496.
(51) Hong, M. Y., and Hosmane, R. S. (1997) Irreversible, tight-binding inhibition of adenosine deaminase by coformycins: Inhibitor structural features that contribute to the mode of enzyme inhibition. *Nucleosides Nucleotides* **16**, 1053−1057.
(52) Wink, D. A., and Mitchell, J. B. (1998) Chemical biology of nitric oxide: Insights into regulatory, cytotoxic, and cytoprotective mechanisms of nitric oxide. *Free Radical Biol. Med.* **25**, 434−456.
(53) Vongchampa, V., Dong, M., Gingipalli, L., and Dedon, P. (2003) Stability of 2′-deoxyxanthosine in DNA. *Nucleic Acids Res.* **31**, 1045−1051.
(54) Schouten, K. A., and Weiss, B. (1999) Endonuclease V protects *Escherichia coli* against specific mutations caused by nitrous acid. *Mutat. Res.* **435**, 245−254.
(55) Spek, E. J., Wright, T. L., Stitt, M. S., Taghizadeh, N. R., Tannenbaum, S. R., Marinus, M. G., and Engelward, B. P. (2001) Recombinational repair is critical for survival of *Escherichia coli* exposed to nitric oxide. *J. Bacteriol.* **183**, 131−138.
(56) Spek, E. J., Vuong, L. N., Matsuguchi, T., Marinus, M. G., and Engelward, B. P. (2002) Nitric oxide induced homologous recombination in *Escherichia coli* is promoted by DNA glycosylases. *J. Bacteriol.* **184**, 3501−3507.
(57) Nair, J., Gal, A., Tamir, S., Tannenbaum, S. R., Wogan, G. N., and Bartsch, H. (1998) Etheno adducts in spleen DNA of SJL mice stimulated to overproduce nitric oxide. *Carcinogenesis* **19**, 2081−2084.
(58) Gal, A., Tamir, S., Kennedy, L. J., Tannenbaum, S. R., and Wogan, G. N. (1997) Nitrotyrosine formation, apoptosis, and oxidative damage: Relationships to nitric oxide production in SJL mice bearing the RcsX tumor. *Cancer Res.* **57**, 1823−1828.
(59) Suzuki, T., Ide, H., Yamada, M., Endo, N., Kanaori, K., Tajima, K., Morii, T., and Makino, K. (2000) Formation of 2′-deoxy-

oxanosine from 2′-deoxyguanosine and nitrous acid: Mechanism and intermediates. *Nucleic Acids Res.* **28**, 544−551.

(60) Glaser, R. (1996) Pyrimidine ring opening in the unimolecular dediazoniation of guanine diazonium ion. An ab initio theoretical study of the mechanism of nitrosative guanosine deamination. *J. Am. Chem. Soc.* **118**, 10942−10943.

(61) Glaser, R., Sundeep, R., Lewis, M., Son, M.-S., and Meyer, S. (1999) Theoretical studies of DNA base deamination. 2. Ab initio study of DNA base diazonium ions and of their linear, unimolecular dediazoniation paths. *J. Am. Chem. Soc.* **121**, 6108−6119.

(62) Glaser, R., and Lewis, M. (1999) Single- and double-proton-transfer in the aggregate between cytosine and guaninediazonium ion. *Org. Lett.* **2**, 273−276.

(63) Williams, D. L. H. (1988) *Nitrosation*, Cambridge University Press, Cambridge, New York.

(64) Goldstein, S., and Czapski, G. (1996) Mechanism of the nitrosation of thiols and amines by oxygenated $NO^{\bullet}$ solutions: The nature of the nitrosating intermediates. *J. Am. Chem. Soc.* **118**, 3419−3425.

TX034046S

Appendix III

Vongchampa, V., Dong, M., and Dedon, P. C. (2003). "Stability of 2'-deoxyxanthosine in DNA". Nucleic Acids Research **31**(3): 1045-51

Nucleic Acids Research, 2003, Vol. 31, No. 3 **1045–1051**
DOI: 10.1093/nar/gkg177

Stability of 2′-deoxyxanthosine in DNA

Viengsai Vongchampa, Min Dong, Lakshman Gingipalli and Peter Dedon*

Biological Engineering Division, 56-787, Massachusetts Institute of Technology, Cambridge, MA 02139, USA

Received September 6, 2002; Revised and Accepted November 25, 2002

ABSTRACT

The deamination of nucleobases in DNA occurs by a variety of mechanisms and results in the formation of hypoxanthine from adenine, uracil from cytosine, and xanthine and oxanine from guanine. 2′-Deoxyxanthosine (dX) has been assumed to be an unstable lesion in cells, yet no study has been performed under biological conditions. We now report that dX is a relatively stable lesion at pH 7, 37°C and 110 mM ionic strength, with a half-life ($t_{1/2}$) of 2.4 years in double-stranded DNA. The stability of dX as a 2′-deoxynucleoside ($t_{1/2}$ = 3.7 min at pH 2; 1104 h at pH 6) was increased substantially upon incorporation into a single-stranded oligodeoxynucleotide, in which the half-life of dX at different pH values was found to range from 7.7 h at pH 2 to 17 700 h at pH 7. Incorporation of dX into a double-stranded oligodeoxynucleotide resulted in a statistically insignificant increase in the half-life to 20 900 h at pH 7. Data for the pH dependence of the stability of dX in single-stranded DNA were used to determine the rate constants for the acid-catalyzed (2.6×10^{-5} s^{-1}) and pH-independent (1.4×10^{-8} s^{-1}) depurination reactions for dX as well as the dissociation constant for the N^7 position of dX (6.1×10^{-4} M). We conclude that dX is a relatively stable lesion that could play a role in deamination-induced mutagenesis.

INTRODUCTION

The deamination of nucleobases in DNA can occur by simple hydrolysis, by the action of deaminase enzymes (1–3) or by reactions with endogenous genotoxins, most notably nitric oxide (4–6). Among the products of nucleobase deamination, 2′-deoxyxanthosine (dX) has received the least attention in terms of DNA repair in part due to the assumption that it is unstable and undergoes rapid depurination (7,8). We now report the results of studies aimed at defining the stability of dX under biological conditions.

All mechanisms of nucleobase deamination result in the formation of xanthine (dX as a 2′-deoxynucleoside) from guanine, hypoxanthine (2′-deoxyinosine, dI) from adenine, uracil (2′-deoxyuridine, dU) from cytosine, and thymine (2′-deoxythymidine) from 5-methylcytosine (Fig. 1). Additionally, the reaction of nitrous acid with guanine *in vitro* has been shown to partition to form both xanthine and oxanine (2′-deoxyoxanosine, dO) (8), though the biological relevance of dO has not been demonstrated. The propensity for hydrolytic deamination occurs in the order 5-methylcytosine > cytosine > adenine > guanine (9,10). The half-life of uracil formation from cytosine lies in the range of 10^2–10^3 years with an increase to 10^4–10^5 years in double-stranded DNA (11–13), while C^5-methylation of cytosine increases the rate deamination by 2- to 20-fold (12,13).

Nitrosative deamination of nucleobases represents another physiologically important mechanism. Among the many sources of nitric oxide (NO), macrophages activated as part of the inflammatory process generate NO at a rate of ~6 pmol s^{-1} per 10^6 cells (14). The NO reacts rapidly with O_2 to produce nitrous anhydride (N_2O_3), a potent nitrosating agent that causes deamination of aromatic amines by formation of an aryl diazonium ion (reviewed in 15). The reactivity of N_2O_3 with nucleobases is reversed relative to hydrolytic deamination, with xanthine formation proposed to occur at twice the rate of uracil (6) and hypoxanthine (16). In human lymphoblastoid TK6 cells exposed to NO, the levels of both xanthine and hypoxanthine increased ~40-fold over untreated controls (16).

The deamination products of DNA bases have been implicated in the formation of mutations. Especially important is the high rate of G:C→A:T mutations at CpG sites containing 5′-methylcytosine (17), which may result from the deamination of 5-methylcytosine to thymine (18). The deamination of cytosine to uracil also produces G:C→A:T mutations possibly by base pairing of uracil with adenine (18,19). On the basis of *in vitro* studies (20,21), xanthine represents another possible source of G:C→A:T mutations. However, the assumption of rapid depurination of dX has led to the suggestion (6–8) that the G:C→A:T mutations arise by insertion of adenine opposite the resulting abasic site (22–24).

Recently, the Kow and Weiss groups (25,26) presented evidence that *Escherichia coli* endonuclease V efficiently repairs xanthine residues. We now couple this observation with the first direct determination of the stability of dX under biological conditions and we conclude that dX is a relatively stable lesion with a half-life of 2 years at 37°C and pH 7 in double-stranded DNA. These results support models in which dX plays a direct role in deamination-induced mutagenesis in cells.

*To whom correspondence should be addressed. Tel: +1 617 253 8017; Fax: +1 617 258 0225; Email: pcdedon@mit.edu
Present address:
Lakshman Gingipalli, ArQule Inc., 19 Presidential Way, Woburn, MA 01801-5140, USA

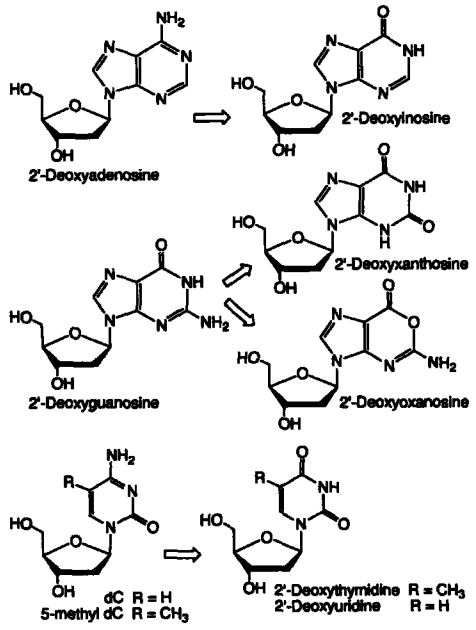

Figure 1. Nucleobase deamination products.

MATERIALS AND METHODS

Materials

All chemicals used in the synthesis of dX and its derivatives were obtained from Sigma-Aldrich (St Louis, MO). [γ-^{32}P]ATP was obtained from Perkin Elmer Life Sciences (Boston, MA). Enzymes for 5′-end-labeling were obtained from New England Biolabs (Beverly, MA). The dX-containing oligodeoxynucleotide and its complement (with dC opposite dX) were synthesized by DNAgency (Berwyn, PA) using dX phosphoramidite synthesized as described below.

Synthesis of dX

O^6-*p*-nitrophenylethyl-protected dX was synthesized from dG according to the procedure of Eritja *et al.* (20) with ^{1}H-NMR chemical shifts (D_2O) identical to published values (20); ESI-MS, *m/z* 567 (MH^+). The *p*-nitrophenylethyl-protecting group was removed using 1,8-diazabicyclo[5.4.0]undec-7-ene as described by Eritja *et al.* (20). The resulting dX was purified by HPLC with a Haisil HL reversed-phase semi-preparative column (5 µm, C18; 250 × 10 mm) and a 0–20% acetonitrile gradient (1% increase per minute) in 50 mM ammonium acetate, pH 7, at 3 ml/min. Under these conditions, dX had a retention time of 11.5 min compared with a retention time of 9.9 min for xanthine base. Purified dX: UV spectroscopy, 248 and 277 nm (λ_{max}); ESI-MS, *m/z* 269 (MH^+), 153 (MH^+-2′-deoxyribose).

Synthesis of an oligodeoxynucleotide containing dX

The O^6-*p*-nitrophenylethyl-protected dX was converted to the phosphoramidite by standard procedures (27). The product displayed the expected ^{31}P-NMR chemical shifts of 149.8 and 150.1 p.p.m. The phosphoramidite was incorporated into a 30mer oligodeoxynucleotide (DNAgency, Inc.) with the following sequence: GACCGATCCTCTAGAYCGACC-TGCAGGCAG, where Y is either dX or dG; the complementary strand paired the dX or dG with dC. The oligodeoxynucleotide was purified by denaturing 20% polyacrylamide gel electrophoresis (28). To establish the presence of dX, the purified oligodeoxynucleotide was subjected to digestion with nuclease P1 and the released nucleotides were characterized by reversed-phase HPLC (Agilent 1100; Phenomenex LUNA 5 µm, C18, 250 × 3 mm; coupled to an Agilent 5989B ESI-mass spectrometer). ESI-MS analysis (PE Sciex API365) of the intact oligodeoxynucleotide indicated a mass of 9204 (theoretical 9203) compared with a mass of 9203 for the same oligodeoxynucleotide with dG replacing dX (theoretical 9202).

HPLC analysis of the stability of dX

Aliquots of a solution of dX (200 µM) in 10 mM Tris, 1 mM EDTA, pH 7.4, were diluted 20-fold into preheated (37 or 50°C) potassium phosphate buffer (50 mM, varying pH) containing 10 µM 2′-deoxythymidine (internal standard). At various times, aliquots were removed and subjected to HPLC analysis for the disappearance of dX (and appearance of X), as described for the synthesis of dX except that an analytical (3 mm) HPLC column was employed. The first-order rate constants for depurination of dX were determined from the loss of parent dX as a function of time.

Electrophoretic analysis of the stability of dX in an oligodeoxynucleotide

Substrate oligodeoxynucleotides were prepared by 5′-^{32}P-end-labeling of the dX-containing strand by standard procedures (28). The labeled strand (1 µM) was annealed to its complement (3 µM) in 10 mM Tris, 1 mM EDTA, pH 7.4, by heating to 95°C for 3 min followed by slow cooling to ambient temperature. An aliquot of the duplex oligodeoxynucleotide solution (1 µl) was then added to potassium phosphate buffer (50 mM, pH 2–12, 100 µl) and the sample incubated at either 37 or 50°C. At various times, aliquots were removed from the solution, the pH was adjusted to 7.4 (with HCl or NaOH), and abasic sites arising from depurination of dX were cleaved by putrescine dihydrochloride (100 mM; 1 h, 37°C) (29,30). The reaction mixture was dried *in vacuo*, resuspended in 95% formamide/0.02% xylene cyanol/0.02% bromophenol blue, heated at 95°C for 30 s and immediately placed on ice. Each sample was then loaded onto a 20% polyacrylamide sequencing gel (7 M urea; 30 cm × 60 cm × 0.4 mm) run at 2000 V for 3 h. Bands corresponding to the parent oligodeoxynucleotide and the cleavage product derived from depurination of dX were quantified by phosphorimager analysis using ImageQuant software (Molecular Dynamics); the location of the cleavage product was verified by comigration with a ^{32}P-labeled oligodeoxynucleotide of the corresponding sequence and length. At pH 7.4, dX depurination in the oligodeoxynucleotide proved to be sufficiently slow (see Results) to permit the incubation with putrescine to cleave abasic sites. Control reactions revealed that putrescine did not affect the stability of the dX-containing oligodeoxynucleotide (data not shown). The first-order rate constants for depurination of dX in single- and double-stranded oligodeoxynucleotides were determined from the decrease in the signal intensity

of the parent oligodeoxynucleotide as a percentage of the total radioactivity present in the sequencing gel lane. The data were fit to equation 2 using Kaleidagraph version 3.52 (Synergy Software).

Melting temperature determination for duplex oligodeoxynucleotides

The melting temperatures for duplex oligodeoxynucleotides containing dX, dI and dG were determined using a Cary 100 Bio UV-visible spectrophotometer. Melting temperatures were determined in potassium phosphate buffer (50 mM, pH 7.0) using a duplex oligodeoxynucleotide concentration of 718 nM and the following parameters: 260 nm wavelength; 50–90°C temperature range; 5°C/min ramp; 1 data point per °C. Three separate experiments were performed for each oligodeoxynucleotide. Studies with the single-stranded oligodeoxynucleotides did not reveal a melting temperature (data not shown), which is consistent with a lack of significant secondary structure in the individual strands.

RESULTS

Characterization of dX and the dX-containing oligodeoxynucleotide

We performed the studies of the stability of dX as a nucleoside and in an oligodeoxynucleotide using direct synthesis of dX and its derivatives. The alternative approach of *in situ* generation of nucleobase deamination products in an oligodeoxynucleotide by treatment with nitrous acid (8) runs the risk of contamination with dO, which is formed along with dX during deamination of dG (31), and obviates the presence of dG in one strand of the oligodeoxynucleotide. Given the presumed instability of dX, we were careful to rigorously characterize dX and its derivatives and the dX-containing oligodeoxynucleotide to ensure proper structure and purity, with emphasis on the presence of abasic sites due to dX depurination. The protection strategy used for the synthesis of dX ensures that the phosphoramidite is incorporated into the oligodeoxynucleotide in the correct orientation and that the base does not undergo depurination during phosphoramidite synthesis (20). At each step of the synthesis of the 2′-deoxynucleoside and oligodeoxynucleotide, we verified product structure by NMR, ESI-MS and HPLC. Analysis of nuclease digestion products by LC/ESI-MS (positive ion mode) revealed a species that migrated with standard dX and yielded the expected ions at *m/z* 269 (MH^+) and 153 (MH^+-2′-deoxyribose). Finally, the position of the dX was confirmed by comparing the reaction of *Methanobacterium thermoautotrophicum* T/G mismatch DNA glycosylase (Trevigen, Inc.) (32) with duplex oligodeoxynucleotides containing either dX or dG opposite dT. The enzyme was able to cleave thymine of the T:G mismatch construct but not the T:X mismatch (data not shown).

Stability of dX

The kinetics of depurination of dX as a 2′-deoxyribonucleoside were determined by HPLC as loss of parent dX (and the appearance of X). Studies in oligodeoxynucleotides were performed by sequencing gel resolution of DNA fragments arising from depurination of dX in the ^{32}P-labeled oligodeoxynucleotide, as shown in Figure 2 for the example at pH 2. Examples of the kinetics of dX depurination are shown in the graphs in Figure 3 and the rate constants are summarized in Table 1.

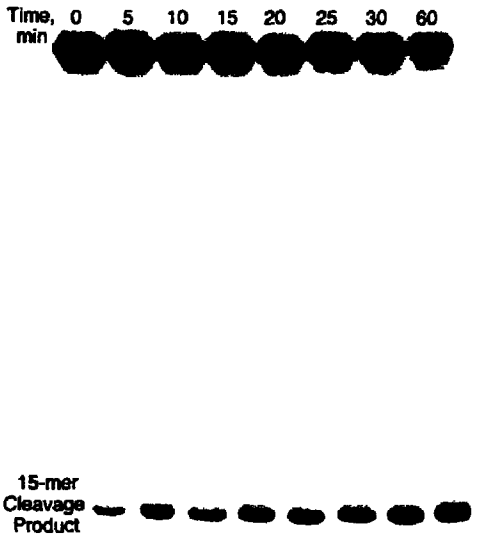

Figure 2. Example of the sequencing gel analysis of dX depurination in a single-stranded oligodeoxynucleotide. Following incubation at 37°C and pH 2, the pH was adjusted to 7 and abasic sites cleaved with putrescine. Depurination at dX is indicated by the formation of a 15mer fragment. The small amount of cleavage product in the $t = 0$ lane was present in all samples and represents a cumulative background of dX depurination that arises during oligodeoxynucleotide synthesis and sample processing.

As expected, the 2′-deoxyribonucleoside form of dX underwent depurination at a higher rate under acidic conditions, with a half-life at 37°C of 2×10^2 s at pH 2 ($k_{obs} = 3.2 \times 10^{-3}$ s^{-1}) and 4×10^6 s at pH 6 ($k_{obs} = 1.7 \times 10^{-7}$ s^{-1}). These rates are considerably faster than those determined for single- and double-stranded oligodeoxynucleotides under conditions of varying pH and temperature, as shown in Figure 3 and Table 1. There is a decrease in the rate of depurination as pH is elevated, reaching what amounts to a plateau at pH 7 and above, as depicted in Figure 4. At neutral and alkaline pH, there is variation in the experimental values due to the errors inherent in measuring small changes in the quantities of cleavage product. However, it is clear from Figure 4 that there is at least a three order-of-magnitude stabilization of dX as the pH is raised from 2 to 7.

The data for the pH dependence of dX depurination permitted estimation of the acid dissociation constant for the N^7 of dX and the rate constant for the acid-catalyzed hydrolysis of dX. By analogy to the generally established depurination of dG (33–38), depurination of dX appears to occur by two mechanisms depending on the pH, as shown in Scheme 1. At low pH (<6), there is a rapid protonation of N^7 followed by a rate-limiting cleavage of the N-glycosidic bond and rapid addition of water to the C1 position of the cationic abasic site. At pH $\geq$ 7, the depurination rate becomes independent of pH due to a slower, rate-limiting direct cleavage of the N-glycosidic bond followed by rapid protonation of the anionic base and addition of water to the

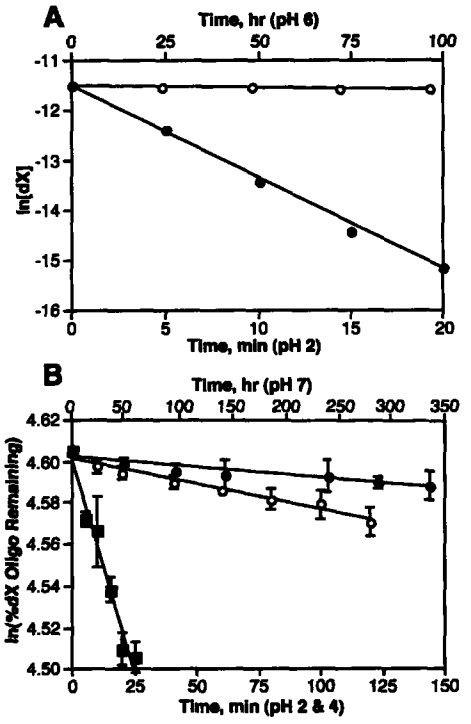

Figure 3. Kinetics of dX depurination at 37°C. (A) 2′-Deoxyribonucleoside at pH 2 (closed circles) and pH 6 (open circles); data points represent mean ± SD (error bars smaller than symbol size) for three experiments. (B) Single-stranded oligodeoxynucleotide at pH 2 (squares), pH 4 (open circles) and pH 7 (closed circles); values represent mean ± SD for three to four experiments.

cationic sugar residue. The following rate equation thus applies to these processes:

$$d[X] / dt = k_{dX} \cdot [dX] + k_{dXH} \cdot [dXH] \quad 1$$

where X is depurinated xanthine base, k_{dX} and k_{dXH} are the rate constants for the two depurination pathways depicted in Scheme 1, and dXH is N^7-protonated dX. It can be shown by appropriate substitution and integration of equation 1 that:

$$k_{obs} = (k_{dXH} \cdot K_a^{-1} \cdot [H^+] + k_{dX}) / (K_a^{-1} \cdot [H^+] + 1) \quad 2$$

where k_{obs} is the apparent rate constant for depurination of dX, K_a is the acid dissociation constant for the N^7 position of dX, and $[H^+]$ is the hydronium ion concentration. The value of the rate constant for pH-independent hydrolytic depurination of dX, k_{dX}, can be derived from the limiting rate constant at pH > 7 (1.35×10^{-8} s^{-1}; see Table 1). A reasonable initial value for k_{dXH} is the rate constant determined at pH 2 (2.5×10^{-5} s^{-1}). Due to the presence of the electron-withdrawing O^2 in dX, the proton dissociation constant for the N^7 position of dX is likely to be higher than that for dG (2.3) (39), so that the majority of dX will be protonated at pH 2 and the depurination rate constant thus a reasonable estimate of k_{dXH}. Using values of K_a in the range of 10^{-2}–10^{-3} M and k_{dXH} in the range of 1–5 × 10^{-5} s^{-1} as initial estimates, we fitted the depurination data from Table 1 (single-stranded oligodeoxynucleotide at 37°C) to equation 2 and a best fit was achieved for $K_a = 6.1 \times 10^{-4}$ M and $k_{dXH} = 2.6 \times 10^{-5}$ s^{-1}.

The data in Table 1 also demonstrate that, at both 37 and 50°C, there is little additional stabilization of dX afforded by conversion of single-stranded to double-stranded DNA (statistically insignificant 10–15% increase in the half-life of the dX-containing strand at pH 7). That the double-stranded oligodeoxynucleotide retains its secondary structure at 50°C was confirmed by T_m studies. Under conditions identical to those employed in the dX stability studies, the following melting temperatures were determined for the duplex oligodeoxynucleotides containing dG, dI or dX: dG, 78.16 ± 0.26°C; dI, 74.16 ± 1.10°C; and dX, 73.26 ± 0.53°C. The 5°C decrease in the duplex stability caused by the change from a G:C base pair to X:C is consistent with previous observations (8,20).

Control reactions indicated that the putrescine treatment employed to cleave abasic sites resulting from depurination of dX in oligodeoxynucleotides (29,40) did not affect the stability of dX (data not shown). The small quantity of cleavage product apparent in the $t = 0$ lane in Figure 2 (3%) was present in all samples at all pHs and represents a cumulative background of dX depurination that arises during oligodeoxynucleotide synthesis and sample processing. This background cleavage was subtracted from the time course data. Depurination rate determinations at pH ≥ 6 required reaction times of up to 2 weeks, which amounts to one half-life

Table 1. Observed rate constants (s^{-1}) for the depurination of dX as a 2′-deoxyribonucleoside and in single- and double-stranded oligodeoxynucleotides as a function of pH and temperature[a]

pH	37°C dX	Single	Double	50°C Single	Double
2	$3.2 (\pm 0.1) \times 10^{-3}$	$2.5 (\pm 0.2) \times 10^{-5}$[b]			
4		$3.8 (\pm 1.0) \times 10^{-6}$[b]			
6	$1.7 (\pm 0.1) \times 10^{-7}$	$3.7 (\pm 1.2) \times 10^{-8}$[b]			4.3×10^{-4}[c]
7		$1.1 (\pm 0.3) \times 10^{-8}$	$9.2 (\pm 3.4) \times 10^{-9}$	8×10^{-5}[c]	8.3×10^{-5}[c]
8		$1.8 (\pm 0.3) \times 10^{-8}$[b]			8.3×10^{-5}[c]
10		$1.3 (\pm 0.1) \times 10^{-8}$			
12		$1.3 (\pm 0.3) \times 10^{-8}$			

[a]Rate constants (s^{-1}) were derived from four independent experiments, with data representing mean (± SD). dX, 2′-deoxyxanthosine; single and double, single- and double-stranded oligodeoxynucleotide, respectively.
[b]Significantly different from pH 7, $P < 0.05$ for Student's t-test.
[c]Results from a single experiment.

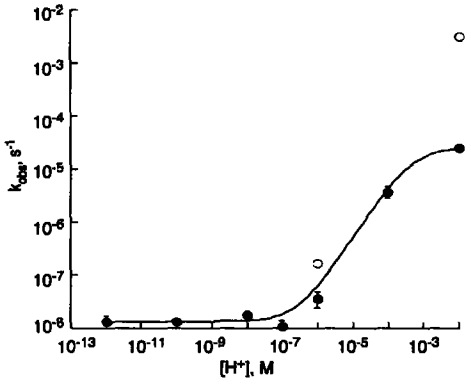

Figure 4. Plot of the dX depurination rate constants at 37°C versus [H+] in a single-strand oligodeoxynucleotide (closed circles) and as a 2′-deoxynucleoside (open circles). Error bars indicate standard deviation for three to five experiments; the error bars are smaller than symbol size in some cases. The curve was generated from equation 2, as described in the text, using the single-strand oligodeoxynucleotide data; $r = 0.998$; $\chi^2 = 1.6 \times 10^{-12}$.

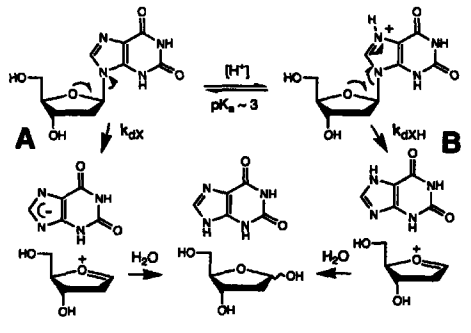

Scheme 1. Proposed mechanisms of dX depurination.

for the ^{32}P label on the oligodeoxynucleotide. In all cases, however, the quantity of cleavage product was determined relative to the total radioactivity present in the gel lane, so decay of the ^{32}P did not affect the rate determinations.

DISCUSSION

The present studies were undertaken to define the stability of dX under biological conditions of temperature and pH. The only other study of dX stability, that reported by Suzuki *et al.* (8), was performed at pH 4 and 70°C and, without knowledge of the temperature and pH dependence of dX depurination, it is not possible to extrapolate the data to biological conditions. The results of our studies reveal that dX is a relatively stable 2′-deoxynucleoside under biological conditions of temperature and pH. At pH 7, 37°C and 110 mM ionic strength, dX in single-stranded DNA has a half-life of ~2 years. The results also reveal novel insights into the chemistry of dX depurination.

The depurination rate constant for dX in a single-stranded oligodeoxynucleotide was found to be inversely proportional to [H+] at pH < 7 and independent of pH above 7 (Fig. 4). This behavior is entirely consistent with the observed pH dependence for depurination of dG and dA as 2′-deoxynucleosides and in DNA (33–38) and thus represents two depurination mechanisms: a specific acid-catalyzed (33) N-glycosidic bond cleavage of dX at pH < 7 and a pH-independent direct N-glycosidic bond cleavage at pH > 7 (Scheme 1). The studies revealed that the rate constant for the acid-catalyzed depurination of dX, $k_{dXH} = 2.6 \times 10^{-5}$ s^{-1}, is 2000-fold greater than the pH-independent hydrolysis of dX, $k_{dX} = 1.3 \times 10^{-8}$ s^{-1}. The latter value is ~100-fold greater than the analogous rate constant of $\sim 10^{-10}$ s^{-1} for depurination of dG and dA in DNA at 37°C and pH 7 determined by Lindahl and Nyberg (38).

It was also observed that the incorporation of dX into single- and double-stranded DNA stabilizes it toward depurination. We observed a ~5-fold stabilization of dX at pH 7 afforded by incorporation of the deoxynucleoside into single-strand oligodeoxynucleotide, which is considerably larger than the 1.1-fold effect observed by Suzuki *et al.* (8) at pH 4. The basis for this difference may lie in the different oligodeoxynucleotide substrates used for the two sets of studies. Suzuki *et al.* (8) used a 12mer oligodeoxynucleotide in which the dX residue was surrounded entirely by dT (d[T_5XT_6]), while we employed a 30mer oligodeoxynucleotide in which the dX was embedded in mixture of purines and pyrimidines (-AGAXCGA-). Given the strong (4–5-fold) sequence context effects for depurination of dG and dA (36), it is likely that the difference in dX depurination rates observed in our studies and those of Suzuki *et al.* (8) arise as a result of the different oligodeoxynucleotide sequences employed.

Regarding differences between single- and double-stranded DNA, there was a small (1.2–2-fold), but statistically insignificant, reduction in the rate of dX depurination in the double-stranded oligodeoxynucleotide compared with the single-stranded form. This is less than the 3–4-fold reduction in depurination of dG and dA in the analogous structural transition in DNA observed by Lindahl and Nyberg (38), though some caution must be exercised in the interpretation of our results given the relatively large error incurred in the determination of depurination rates at pH 7 (Table 1). Though speculative in the absence of NMR data, one possible explanation for the lack of a stabilizing effect in double-stranded DNA involves a dX-induced disruption of local DNA structure, such as aberrant or weak H-bonding. Such helical destabilization is supported by our observation of a 5°C decrease in the melting temperature of the duplex oligodeoxynucleotide stability containing dX. The source of the helical destabilization may be related to the relatively low pK_a for the N^3 of dX (~5.6 for the 2′-deoxynucleoside) (41), which would result in a fair degree of negative charge on the xanthine bases at pH 7. However, is likely that the N^3 pK_a is affected by H-bonding in the double-stranded structure, as observed in other studies (42,43).

The stability of dX may play a role in the mutagenicity of base deamination products. If dX were an unstable species, then depurination would occur prior to DNA replication and any resulting mutations, apart from those induced during repair synthesis, would result from the abasic site. However, we have demonstrated that dX is relatively stable in DNA with

a half-life of 2 years. At this rate, endogenously formed dX residues, if not repaired, can be expected to undergo depurination to the extent of 3 and 11% in 1 and 4 months, respectively. Given the relatively slow rate of cell division in tissues such as the human colon (three divisions per year) (44), the bulk of dX residues present in a cell will be present during cell replication and may thus contribute to mutagenesis. This hypothesis is supported by several studies. In repair-deficient *E.coli* exposed to nitrous acid, an agent that causes nucleobase deamination (25), the G:C→T:A mutations expected for a preponderance of apurinic sites at presumably unstable dX residues (22) represented only 0.2% of the mutations. The bulk of the mutations consisted of G:C→A:T and A:T→G:C transitions (25). While the G:C→A:T mutations could arise by deamination of dC or 5-methyl-dC, dX has been shown to cause G:C→A:T mutations *in vitro* (20). Consistent with these studies is the increase in nitrous acid-induced G:C→A:T mutations in *E.coli* lacking endonuclease V (25), an enzyme that has been shown by He *et al.* (26) to repair dX with high efficiency. It is thus likely that dX contributes to the burden of mutagenic lesions in a cell.

ACKNOWLEDGEMENTS

The authors wish to thank Xinfeng Zhou for helpful discussions about the depurination kinetics and to acknowledge financial support from grant CA26735-20 from the National Cancer Institute and grant ES02109-24 from the National Institute of Environmental Health Sciences.

REFERENCES

1. Anant,S. and Davidson,N.O. (2001) Molecular mechanisms of apolipoprotein B mRNA editing. *Curr. Opin. Lipidol.*, **12**, 159–165.
2. Jacobs,H. and Bross,L. (2001) Towards an understanding of somatic hypermutation. *Curr. Opin. Immunol.*, **13**, 208–218.
3. Maas,S. and Rich,A. (2000) Changing genetic information through RNA editing. *Bioessays*, **22**, 790–802.
4. Park,M. and Loeppky,R.N. (2000) *In vitro* DNA deamination by alpha-nitrosaminoaldehydes determined by GC/MS-SIM quantitation. *Chem. Res. Toxicol.*, **13**, 72–81.
5. Fix,D.F., Koehler,D.R. and Glickman,B.W. (1990) Uracil-DNA glycosylase activity affects the mutagenicity of ethyl methanesulfonate: evidence for an alternative pathway of alkylation mutagenesis. *Mutat. Res.*, **244**, 115–121.
6. Caulfield,J.L., Wishnok,J.S. and Tannenbaum,S.R. (1998) Nitric oxide-induced deamination of cytosine and guanine in deoxynucleosides and oligonucleotides. *J. Biol. Chem.*, **273**, 12689–12695.
7. Lindahl,T. (1993) Instability and decay of the primary structure of DNA. *Nature*, **362**, 709–714.
8. Suzuki,T., Matsumura,Y., Ide,H., Kanaori,K., Tajima,K. and Makino,K. (1997) Deglycosylation susceptibility and base-pairing stability of 2′-deoxyoxanosine in oligodeoxynucleotide. *Biochemistry*, **36**, 8013–8019.
9. Lindahl,T. and Nyberg,B. (1974) Heat-induced deamination of cytosine residues in deoxyribonucleic acid. *Biochemistry*, **13**, 3405–3410.
10. Shapiro,R. and Klein,R.S. (1966) The deamination of cytidine and cytosine by acidic buffer solutions. Mutagenic implications. *Biochemistry*, **5**, 2358–2362.
11. Frederico,L.A., Kunkel,T.A. and Shaw,B.R. (1990) A sensitive genetic assay for the detection of cytosine deamination: determination of rate constants and the activation energy. *Biochemistry*, **29**, 2532–2537.
12. Zhang,X. and Mathews,C.K. (1994) Effect of DNA cytosine methylation upon deamination-induced mutagenesis in a natural target sequence in duplex DNA. *J. Biol. Chem.*, **269**, 7066–7069.
13. Shen,J.-C., Rideout,W.M.,III and Jones,P.A. (1994) The rate of hydrolytic deamination of 5-methylcytosine in double-stranded DNA. *Nucleic Acids Res.*, **22**, 972–976.
14. Lewis,R.S., Tamir,S., Tannenbaum,S.R. and Deen,W.M. (1995) Kinetic analysis of the fate of nitric oxide synthesized by macrophages *in vitro*. *J. Biol. Chem.*, **270**, 29350–29355.
15. Singer,B. and Grunberger,D. (1983) *Molecular Biology of Mutagens and Carcinogens*. Plenum, New York.
16. Nguyen,T., Brunson,D., Crespi,C.L., Penman,B.W., Wishnok,J.S. and Tannenbaum,S.R. (1992) DNA damage and mutation in human cells exposed to nitric oxide *in vitro*. *Proc. Natl Acad. Sci. USA*, **89**, 3030–3034.
17. Duncan,B.K. and Weiss,B. (1978) In Hanawalt,P.C., Errol,C., Friedberg,E.C. and Fox,F. (eds), *DNA Repair Mechanisms*. Academic Press, New York, pp. 183–186.
18. Coulondre,C., Miller,J.H., Farabaugh,P.J. and Gilbert,W. (1978) Molecular basis of base substitution hotspots in *Escherichia coli*. *Nature*, **274**, 775–780.
19. Duncan,B.K. and Miller,J.H. (1980) Mutagenic deamination of cytosine residues in DNA. *Nature*, **287**, 560–561.
20. Eritja,R., Horowitz,D.M., Walker,P.A., Ziehler-Martin,J.P., Boosalis,M.S., Goodman,M.F., Itakura,K. and Kaplan,B.E. (1986) Synthesis and properties of oligonucleotides containing 2′-deoxynebularine and 2′-deoxyxanthosine. *Nucleic Acids Res.*, **14**, 8135–8153.
21. Kamiya,H., Miura,H., Suzuki,M., Murata,N., Ishikawa,H., Shimizu,M., Komatsu,Y., Murata,T., Sasaki,T., Inoue,H. *et al.* (1992) Mutations induced by DNA lesions in hot spots of the c-Ha-ras gene. *Nucleic Acids Symp. Ser.*, 179–180.
22. Loeb,L.A. and Preston,B.D. (1986) Mutagenesis by apurinic/apyrimidinic sites. *Annu. Rev. Genet.*, **20**, 201–230.
23. Boiteux,S. and Laval,J. (1982) Coding properties of poly(deoxycytidylic acid) templates containing uracil or apyrimidinic sites: *in vitro* modulation of mutagenesis by deoxyribonucleic acid repair enzymes. *Biochemistry*, **21**, 6746–6751.
24. Strauss,B., Rabkin,S., Sagher,D. and Moore,P. (1982) The role of DNA polymerase in base substitution mutagenesis on non-instructional templates. *Biochimie*, **64**, 829–838.
25. Schouten,K.A. and Weiss,B. (1999) Endonuclease V protects *Escherichia coli* against specific mutations caused by nitrous acid. *Mutat. Res.*, **435**, 245–254.
26. He,B., Qing,H. and Kow,Y.W. (2000) Deoxyxanthosine in DNA is repaired by *Escherichia coli* endonuclease V. *Mutat. Res.*, **459**, 109–114.
27. Beaucage,S.L., Bergstrom,D.E., Glick,G.D. and Jones,R.A. (2000) *Current Protocols in Nucleic Acid Chemistry*. John Wiley and Sons, New York.
28. Ausubel,F.M., Brent,R., Kingston,R.E., Moore,D.D., Seidman,J.G., Smith,J.A. and Struhl,K. (1989) *Current Protocols in Molecular Biology*. John Wiley and Sons, New York.
29. Lindahl,T. and Andersson,A. (1972) Rate of chain breakage at apurinic sites in double-stranded deoxyribonucleic acid. *Biochemistry*, **11**, 3618–3623.
30. Yu,L., Golik,J., Harrison,R. and Dedon,P. (1994) The deoxyfucose-anthranilate of esperamicin A1 confers intercalative DNA binding and causes a switch in the chemistry of bistranded DNA lesions. *J. Am. Chem. Soc.*, **116**, 9733–9738.
31. Suzuki,T., Kanaori,K., Tajima,K. and Makino,K. (1997) Mechanism and intermediate for formation of 2′-deoxyoxanosine. *Nucleic Acids Symp. Ser.*, 313–314.
32. Horst,J.P. and Fritz,H.J. (1996) Counteracting the mutagenic effect of hydrolytic deamination of DNA 5-methylcytosine residues at high temperature: DNA mismatch N-glycosylase Mig.Mth of the thermophilic archaeon *Methanobacterium thermoautotrophicum* THF. *EMBO J.*, **15**, 5459–5469.
33. Zoltewicz,J.A., Clark,D.F., Sharpless,T.W. and Grahe,G. (1970) Kinetics and mechanism of the acid-catalyzed hydrolysis of some purine nucleosides. *J. Am. Chem. Soc.*, **92**, 1741–1749.
34. Venner,H. (1966) Research on nucleic acids. XII. Stability of the N-glycoside bond of nucleotides. *Hoppe Seylers Z. Physiol. Chem.*, **344**, 189–196.
35. Shapiro,R. and Danzig,M. (1972) Acidic hydrolysis of deoxycytidine and deoxyuridine derivatives. The general mechanism of deoxyribonucleoside hydrolysis. *Biochemistry*, **11**, 23–29.
36. Suzuki,T., Ohsumi,S. and Makino,K. (1994) Mechanistic studies on depurination and apurinic site chain breakage in oligodeoxyribonucleotides. *Nucleic Acids Res.*, **22**, 4997–5003.

37. Bender,M.L. (1971) *Mechanisms of Homogeneous Catalysis from Protons to Proteins*. Wiley-Interscience, New York.
38. Lindahl,T. and Nyberg,B. (1972) Rate of depurination of native deoxyribonucleic acid. *Biochemistry*, **11**, 3610–3618.
39. Acharya,P., Trifonova,A., Thibaudeau,C., Foldesi,A. and Chattopadhyaya,J. (1999) The transmission of the electronic character of guanin-9-yl drives the sugar-phosphate backbone torsions in guanosine 3′,5′-bisphosphate. *Angew. Chem. Int. Ed. Engl.*, **38**, 3645–3650.
40. Dedon,P.C., Salzberg,A.A. and Xu,J. (1993) Exclusive production of bistranded DNA damage by calicheamicin. *Biochemistry*, **32**, 3617–3622.
41. Roy,K.B. and Miles,H.T. (1983) Tautomerism and ionization of xanthosine. *Nucl. Nucl.*, **2**, 231–242.
42. Sheppard,T.L., Ordoukhanian,P. and Joyce,G.F. (2000) A DNA enzyme with N-glycosylase activity. *Proc. Natl Acad. Sci. USA*, **97**, 7802–7807.
43. Legault,P. and Pardi,A. (1997) Unusual dynamics and pK_a shift at the active site of a lead-dependent ribozyme. *J. Am. Chem. Soc.*, **119**, 6621–6628.
44. Herrero-Jimenez,P., Tomita-Mitchell,A., Furth,E.E., Morgenthaler,S. and Thilly,W.G. (2000) Population risk and physiological rate parameters for colon cancer. The union of an explicit model for carcinogenesis with the public health records of the United States. *Mutat. Res.*, **447**, 73–116.

Appendix IV

Kim, M. Y., Dong, M., Dedon, P. C. and Wogan, G. N. (2005). "Effects of Peroxynitrite Dose and Dose Rate on DNA Damage and Mutation in the *supF* Shuttle Vector". Chem Res Toxicol (in press)

Effects of Peroxynitrite Dose and Dose Rate on DNA Damage and Mutation in the *supF* Shuttle Vector

Min Young Kim,[†] Min Dong,[†] Peter C. Dedon,[†] and Gerald N. Wogan*[,†,‡]

Biological Engineering Division and Chemistry Department, Massachusetts Institute of Technology, 77 Massachusetts Avenue, Cambridge, Massachusetts 02139

Received August 11, 2004

Peroxynitrite ($ONOO^-$) induces oxidative and nitrosative DNA damage, and previous studies by our group have shown that it is strongly mutagenic in the *supF* shuttle vector pSP189 replicated in *Escherichia coli* MBL50 cells. In those experiments, however, the pSP189 plasmid was exposed under unphysiological conditions to large single bolus doses of $ONOO^-$, which limits extrapolation of the data to in vivo pathological states in which $ONOO^-$ may play a role. We have thus sought to define the effects of $ONOO^-$ dose and dose rate on the DNA damage and mutations induced in the *supF* gene by three different dosage mechanisms: (i) by infusion of $ONOO^-$ solution into suspensions of pSP189 at rates approximating those estimated to occur in inflamed tissues; (ii) by exposure to 3-morpholinosydnonimine (SIN-1), which generates $ONOO^-$ spontaneously during decomposition; and (iii) by bolus doses of $ONOO^-$ solution. In all cases, plasmid DNA was exposed in the presence of 25 mM bicarbonate, since the reaction of CO_2 with $ONOO^-$ (to form nitrosoperoxycarbonate) has a major impact on mutagenic potency of $ONOO^-$ in this system. Nucleobase and deoxyribose damage were evaluated by a plasmid nicking assay immediately after $ONOO^-$ and SIN-1 exposures. Mutation frequency (MF) and mutational spectra in the *supF* gene were determined after plasmid pSP189 replicated in host *E. coli* cells. Bolus $ONOO^-$ addition caused the highest amount of DNA damage, including base and deoxyribose lesions, while infusion caused the least. SIN-1 was found to induce almost exclusively deoxyribose oxidation, while bolus addition generated a high percentage of base damage. MF increased in a dose-dependent manner following all treatments, but infused $ONOO^-$ and SIN-1 exposures were less mutagenic than bolus $ONOO^-$ exposure. MFs induced by infusion and by SIN-1 incubated for 100 min at the highest level (4 mM) were 63 and 43% less, respectively, than that induced by bolus. All mutational hot spots were located at G:C sites except for A121 and A177 induced by SIN-1 exposure. Hot spots at C108 and C168 were common to all exposures; G113, G115, and G116 were common to bolus and infused $ONOO^-$ exposures; and G129 was common to infused $ONOO^-$ and SIN-1 exposures. Almost all mutations were single base pair substitutions under all exposure conditions. Whereas those induced by infused or bolus $ONOO^-$ and SIN-1 consisted predominantly of G:C to T:A transversions (66, 65, and 51%, respectively), G:C to C:G mutations were much less frequent following infusion and SIN-1 (8 and 19%, respectively) than those induced by bolus exposure (29%). A:T to T:A mutations induced were detected only after $ONOO^-$ infusion and SIN-1 exposure (9 and 11%, respectively). In conclusion, both dose and dose rate at which a genetic target is exposed to $ONOO^-$ substantially influence the damage and mutational response, indicating that these parameters will need to be taken into account in assessing the potential effects of ONOO in vivo. Furthermore, the results indicate that the chemistry of SIN-1-induced DNA damage differs substantially from native $ONOO^-$, which suggests the need for caution in interpreting the biological relevance of SIN-1 as a surrogate for $ONOO^-$.

Introduction

Peroxynitrite ($ONOO^-$)[1] is one of the chemical mediators of inflammation in humans and arises in a variety of mammalian cells including endothelial cells, neurons, neutrophils, and macrophages and by the reaction of nitric oxide ($NO^•$) with superoxide anion ($O_2^{•-}$) at diffusion-limited rates (*1*–*5*). $ONOO^-$ potently oxidizes and nitrates all major classes of biological molecules including proteins, lipids, cellular thiols, and nucleic acids (*1*–*5*). Under physiological conditions, $ONOO^-$ is in equilibrium with its protonated form, peroxynitrous acid (ONOOH), which in turn decays with a 1 s half-life to generate nitrite or, by homolytic bond scission, nitrogen dioxide

* To whom correspondence should be addressed. Tel: 617-253-3188. Fax: 617-258-0499. E-mail: wogan@mit.edu.
† Biological Engineering Division.
‡ Chemistry Department.

[1] Abbreviations: $ONOO^-$, peroxynitrite; ONOOH, peroxynitrous acid; $^•NO_2$, nitrogen dioxide; $^•OH$, hydroxyl radical; $NO^•$, nitric oxide; $O_2^{•-}$, superoxide; $ONOOCO_2^-$, nitrosoperoxocarboxylate; $CO_3^{•-}$, carbonate radical anion; MF, mutation frequency; SIN-1, 3-morpholinosydnonimine; RNS, reactive nitrogen species; ROS, reactive oxygen species; DHR123, dihydrorhodamine123; Fpg, formamidopyrimidine-DNA glycosylase; SSBs, single strand breaks; 8-nitro-G, 8-nitroguanosine; 8-oxo-dG, 8-oxodeoxyguanosine; 8-Cl-dG, 8-chloro-2′-deoxyguanosine; 8-Br-dG, 8-bromo-2′-deoxyguanosine; 8-oxo-G, 8-oxoguanine; 8-nitro-dG, 8-nitrodeoxyguanosine; NOS, nitric oxide species; Iz, 2,5-diamino-4*H*-imidazol-4-one.

10.1021/tx049777m CCC: $30.25
Published on Web 00/00/0000 PAGE EST: 10.5

($^{\bullet}NO_2$) and hydroxyl radical ($^{\bullet}OH$) (*6*). In the presence of sodium bicarbonate ($NaHCO_3$)/carbon dioxide (CO_2) at physiological pH, the nitrosoperoxocarbonate ($ONOOCO_2^-$) adduct is formed, which decomposes to yield carbonate radical anion ($CO_3^{\bullet-}$), a potent oxidant, together with $^{\bullet}NO_2$ (*7*). $ONOO^-$ and $ONOOCO_2^-$ are highly reactive in vitro (*8–15*) and in biological matrices cause rapid oxidation of sulfhydryl groups and thioesters, as well as nitration and hydroxylation of aromatic compounds such as tyrosine and tryptophan (*8*). Cells exposed to $ONOO^-$ show oxidative DNA damage, DNA strand breakage, and activation of poly (ADP-ribosyl) polymerase, which can modify cell signaling, protein function, and apoptosis or necrosis (*9–15*). It is thus not surprising that $ONOO^-$ formation in vivo has been implicated in a variety of pathological disorders such as rheumatoid arthritis, inflammation, neurodegenerative diseases, coronary artery disease, cirrhosis, hepatitis infection, and gastrointestinal cancers (*1*, *2*).

Previously, we reported that $ONOO^-$ is strongly mutagenic in the *supF* shuttle vector pSP189 replicated in bacteria or human cells (*16*). The mutation frequency (MF) increased 21-fold in pSP189 replicated in *Escherichia coli* and 9-fold in plasmid replicated in human cells, with the majority of mutations occurring at G:C base pairs, predominantly involving G:C to T:A transversions (*16*). In view of the significant effects of CO_2 on $ONOO^-$ chemistry, we also characterized its effects on the mutagenesis of the *supF* gene in the shuttle vector pSP189 and showed that bicarbonate reduced the mutagenic response by 47–77% for $ONOO^-$ exposures ranging from 0 to 4 mM (*17*).

SIN-1 (3-morpholinosydnonimine) is a metabolite of nitrovasodilator molsidomine and slowly decomposes at physiological pH to release both $NO^{\bullet}$ and $O_2^{\bullet-}$ to produce $ONOO^-$ in situ (*18*). For this reason, it has been used as a reagent for investigating $ONOO^-$-mediated effects in chemical and biological systems (*18–20*). Others have demonstrated that SIN-1 produces a strong oxidant that degrades deoxyribose, oxidizes low-density lipoproteins, and kills cultured neurons and *E. coli* (*19–22*). Motohashi and Saito showed that $ONOO^-$ generated from SIN-1 penetrates through the cell membrane, damages DNA, and induces the SOS response in *Salmonella typhumurium* (*23*). Finally, we demonstrated that $ONOO^-$ generated from SIN-1 induced cytotoxicity, genotoxicity, apoptosis, and mitochondrial damage in human lymphoblastoid cells (*24*).

The pathobiochemistry resulting from overproduction of reactive nitrogen species (RNS) and reactive oxygen species (ROS) is thought to be associated with chronic inflammation and carcinogenesis (*25*). RNS and ROS produced by activated inflammatory cells during chronic inflammation can alter functionally important biological molecules, resulting in effects such as mutations in oncogenes and tumor suppressor genes or posttranslational modification of proteins associated with an increased risk for a variety of cancers (*25*). A critical feature of the link between any genotoxin and cancer is the underlying chemistry, which in the case of $ONOO^-$ is complicated by the possibility that concentration and flux of $ONOO^-$ affect the product distribution and yields. This is illustrated by recent observations of different nucleobase damage chemistry depending on the means of $ONOO^-$ delivery (*26*). In addition to bolus addition, infusion and a donor compound generating the precursors of $ONOO^-$ provide useful surrogate means for determining DNA damage and mutagenic responses to low levels of $ONOO^-$ administered continuously over substantial time periods. In light of the possible influence of $ONOO^-$ flux on DNA damage chemistry, we have compared the DNA damage and MFs and spectra induced by slow infusion of $ONOO^-$ and by SIN-1 with those induced by bolus doses of $ONOO^-$ in the *supF* gene of pSP189 replicated in *E. coli* MBL50 cells.

Experimental Procedures

Plasmid Amplification. The pSP189 shuttle vector containing an eight bp "signature sequence" was a gift from Dr. Michael M. Seidman (NIH, Bethesda, MD). The amber tyrosine suppressor tRNA gene (*supF*) in plasmid pSP189 carrying the ampicillin resistance gene was used as the target for mutation (*16*). As described previously (*17*), large-scale preparation of pSP189 plasmid was accomplished by inoculating 5 mL of LB media and 5 mg/mL ampicillin (Sigma) with 0.1 mL of a frozen stock of transformed Ab2463 cells containing the complete population of plasmids. After incubation for 10 h, the 5 mL culture was added to 1 L of LB media and placed in a 37 °C shaking incubator overnight. Plasmid DNA was purified with the Maxi DNA isolation and purification kit (Qiagen). The purity and concentration were verified using UV absorbance (model Du-65 spectrophotometer, Beckman) and electrophoresis of aliquots on 1% agarose gel with ethidium bromide. Plasmid DNA in TE buffer (pH 7.4) was stored at −20 °C until use.

Treatment of Plasmid with $ONOO^-$ and SIN-1. $ONOO^-$ was synthesized by ozonolysis of sodium azide as described by Pryor et al. (*27*). Briefly, ozone generated in a Welsbach ozonator was bubbled into 100 mL of 0.1 M sodium azide chilled in an ice bath. Ozonation was generally terminated after 45 min, and $ONOO^-$ concentration was determined spectrophotometrically in 0.1 N NaOH (ϵ_{302} = 1670 M^{-1} cm^{-1}). Aliquots of the newly synthesized $ONOO^-$ were then stored as a stock solution in 0.1 N NaOH at −80 °C until use.

Bolus doses of $ONOO^-$ were introduced into plasmid solutions as previously described (*17*). Briefly, 20 μg of plasmid DNA dissolved in 150 mM sodium phosphate, 25 mM $NaHCO_3$, pH 7.4, were placed into Eppendorf tubes; 25 mM $NaHCO_3$ was freshly prepared from 0.1 N $NaHCO_3$ stock solutions and added to plasmid solutions immediately prior to $ONOO^-$ exposure. For bolus $ONOO^-$ additions, aliquots (10 μL) of $ONOO^-$ diluted with 0.1 N NaOH were placed on the inside of an Eppendorf tube cap and the plasmid suspension was mixed by gently closing the cap and mixing by vortexing for 30 s; the total reaction volume was 100 μL. The mixture was incubated at ambient temperature for 90 s, and the reaction was terminated after 2 min by addition of 10 μL of β-mercaptoethanol. Infusion of $ONOO^-$ was performed by delivery from a syringe pump (model AH 55-4154, Harvard Apparatus), with constant mixing by vortexing. $ONOO^-$ (0–4 mM diluted in 0.1 N NaOH) was infused at a constant rate (0.945 μL per min) and time (9 min, 27 s) into 90 μL of plasmid suspension with 25 mM $NaHCO_3$ at fluxes of $ONOO^-$ between 0.175 and 0.7 μM/s. The pH of the reaction mixtures (7.4) remained constant during and after the infusion procedure.

SIN-1 (Biomol Research Laboratories, Plymouth Meeting, PA) is stable at pH 5 but readily decomposes at pH 7.4 in oxygenated solution. An obstacle in comparing the studies of SIN-1 with authentic $ONOO^-$ is to find the concentration of SIN-1 that will release a predictable amount of $ONOO^-$ over defined incubation times. Doulias et al. have shown that decomposition of 1 mM SIN-1 in well-oxygenated cell culture medium produced $ONOO^-$ at a linear rate of 12 μM/min for at least 120 min, as assessed by the oxidation of dihydrorhodamine123 (DHR123), a sensitive and efficient two-electron oxidation probe for $ONOO^-$ (*28*). In a similar manner, it has been shown that 1 mM SIN-1 decomposes to form $ONOO^-$ at a rate of ~10 μM/min in bacteria culture

media (22, 23). Control experiments revealed that 1, 2, and 4 mM SIN-1 decomposed to form $ONOO^-$ at rates of ~12, ~21, and ~31 μM $ONOO^-$ min^{-1}, respectively, as assessed by the oxidation of DHR123 (data not shown). We have therefore used these values as the rates of $ONOO^-$ production from SIN-1. We also chose 180 min as well as 30 and 100 min as incubation times since Cai et al. demonstrated that a maximal plasmid DNA damage level occurred within 180 min of exposure to SIN-1 at 37 °C (29). SIN-1 was dissolved in 150 mM sodium phosphate buffer, pH 7.4, just before use, and 10 μL aliquots were added to 90 μL plasmid solutions in buffer containing 25 mM $NaHCO_3$. Final SIN-1 concentrations ranged from 0 to 4 mM. Suspensions were incubated at 37 °C for 30, 100, or 180 min in a shaking water bath. At the end of treatment, DNA samples were washed twice with cold TE buffer (pH 7.4) using Amicon Centricon-30 concentrators (Millipore, Billerica, MA). The plasmid DNA was stored in TE buffer on ice until the DNA damage analysis, and the transformation into MBL50 cells was carried out within 1–2 h of treatment.

Quantification of DNA Damage by a Plasmid Nicking Assay. A plasmid nicking assay was used to quantify the DNA deoxyribose and base damage. After $ONOO^-$ or SIN-1 treatments, a portion (200 ng) of the DNA was treated with putrescine (100 mM, pH 7.0, 1 h, 37 °C) to cleave all types of abasic sites (30). Another portion (200 ng) was kept on ice as a control for the direct strand breaks. A third portion of the DNA sample was treated with *E. coli* formamidopyrimidine-DNA glycosylase (Fpg) (Trevigen, Gaithersburg, MD) to convert oxidized purines to strand breaks. Fpg treatment was performed in a volume of 10 μL containing 200 ng of $ONOO^-$-treated DNA, 1 μL of Fpg (~1.5 units), and buffer containing 10 mM Tris-HCl (pH 7.5), 1 mM EDTA, and 100 mM NaCl at 37 °C for 1 h. Fpg was then removed by phenol/chloroform extraction. The recovered DNA was redissolved in H_2O, and plasmid topoisomers were resolved by 1% agarose slab gel electrophresis in the presence of 0.1 μg/mL ethidium bromide. The quantity of DNA in each band was determined by fluorescence imaging (UltraLum, Clarmont, CA).

DNA Transformation into MBL50 Cells and Selection of the Mutated *supF* Gene. MBL50 cells were grown to a log phase density of $OD_{600} \approx 0.5$–0.6, washed twice with cold H_2O to remove salts, and placed in an ice cold 2 mm gap electroporation cuvette (VWR). Plasmid DNA (10 ng, 2 μL) was added, and the cuvette was pulsed (12.5 Kv/cm, 50 μF, 129 Ω) in an Electro Cell Manipulator 600, BTX. Cells were then added to 900 μL of cold SOC buffer and incubated at ambient temperature for 30 min, centrifuged at 3000*g* for 10 min, and resuspended in PBS, pH 7.0. Aliquots (225 μL) were plated on medium A with 50 μg/mL ampicillin, 20 μg/mL IPTG (Roche), and 10 μg/mL X-gal (Roche) and supplemented with 2 g/L L-arabinose (Sigma) to determine arabinose resistant cells. The remaining suspension was diluted appropriately and plated onto LB agar containing IPTG and X-gal for the determination of the total number of transformants. The plates were incubated at 37 °C for 24–96 h. The transformation efficiency was expressed as the number of colony forming units (cfu) produced by 1 μg of competent cells transformed with pSP189 DNA. Transformants were selected on L-arabinose-containing medium A in the presence of IPTG and X-gal, which allowed detection of bacteria-bearing plasmids with an active *supF* tRNA gene (blue colonies) or a mutated gene (white or light blue colonies). White or light blue colonies were regrown on the same medium to confirm the mutant phenotype. MF was defined as the ratio of total mutants to total transformants (17). Background MFs were determined in plasmids exposed to aliquots of 0.1 N NaOH and 150 mM sodium phosphate buffer, the solvents for $ONOO^-$ and SIN-1, respectively.

Analysis of Mutated *supF* Gene. Mutants were expanded by overnight incubation of 5 mL cultures of cells picked from individual light blue or white colonies, and plasmid DNA was isolated using Wizard plus plasmid miniprep kits (Promega). DNA sequencing was carried out by the Harvard University DNA Sequencing Facility (Cambridge, MA) using a 20-mer primer with the following sequence: 5′-GGCGACACGG-AAAT-GTTGAA-3′ (IDT, Coralville, IA). The signature sequence was identified using the Sequencer program (Gene Codes Corporation, version 4.1.4). Poisson distribution analysis was used to assess randomness of the distribution of mutations, with a hot spot defined as a site at which the number of observed mutations was at least five times higher than that predicted by the Poisson distribution (31).

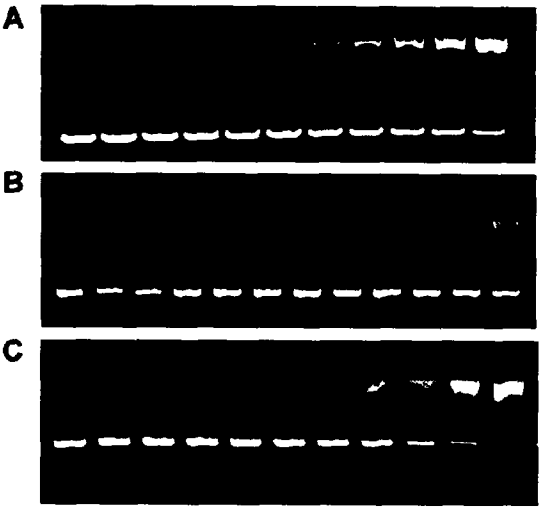

Figure 1. Example of plasmid topoisomer analysis of DNA damage in plasmid pSP189 caused by $ONOO^-$ and SIN-1 concentrations ranging from 0.1 to 3 mM (half-log steps; first lane contains untreated control). (A) Bolus $ONOO^-$ addition, (B) infused $ONOO^-$ addition, and (C) SIN-1 (incubation for 100 min).

Results

DNA Damage from $ONOO^-$ Exposure. Using a plasmid nicking assay, we first determined the relative quantities of nucleobase and deoxyribose damage caused by the different $ONOO^-$ exposure regimes. The quantities of direct single strand breaks (SSBs), which are caused predominantly by deoxyribose oxidation, were found to increase with increasing concentrations of $ONOO^-$ (both bolus addition and infusion) and SIN-1 (incubation for 100 min) (Figures 1 and 2A). In the cases of bolus $ONOO^-$ and SIN-1 (incubation for 100 min), the extent of SSBs was found to reach a plateau. In contrast, a nearly linear dose–response was observed with $ONOO^-$ infusion. Formation of SSBs was greater with SIN-1 exposure than either type of $ONOO^-$ addition, with infusion causing the lowest number of SSBs. For all oxidizing reactions, the formation of strand breaks was studied over a broad range of DNA damage frequencies. However, meaningful interpretation can only be achieved for damage occurring under single-hit conditions, which corresponds to <30–40 strand breaks in 10^6 nt of pSP189 according to a Poisson distribution (30). The range beyond single-hit conditions requires adjustment of the damage frequency to avoid underestimation of the number of strand breaks, since additional nicks in an already nicked plasmid cannot be detected by topoisomer analysis.

Because oxidation of deoxyribose results in both direct strand breaks and abasic sites, we sought to quantify the abasic site formation by converting the lesions to strand breaks with putrescine. This agent has been shown to

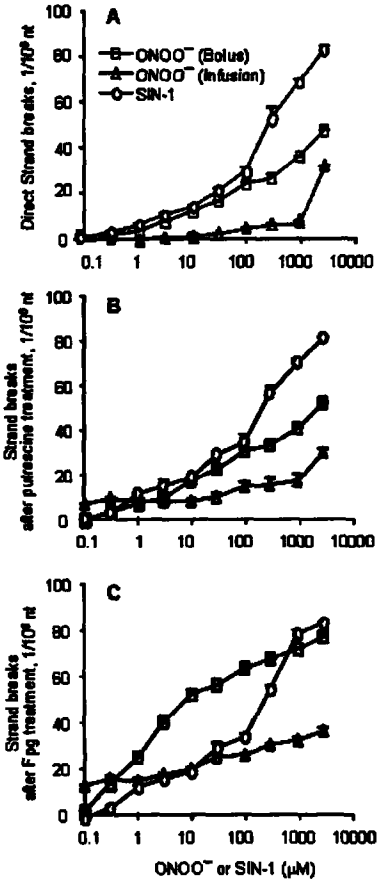

Figure 2. DNA damage in pSP189 by $ONOO^-$ or SIN-1. The concentrations of bolus (□) and infused (△) $ONOO^-$ and SIN-1 (○; incubation for 100 min) ranged from 0.1 to 3 mM (half-log steps). (A) Direct strand breaks in pSP189, (B) strand breaks in pSP189 after putrescine treatment, and (C) strand breaks in pSP189 after Fpg treatment. Data represent means ± SDs for four measurements. Data points lying above 40 strand breaks per 10^6 nt fall outside "single-hit" conditions (see the text for details).

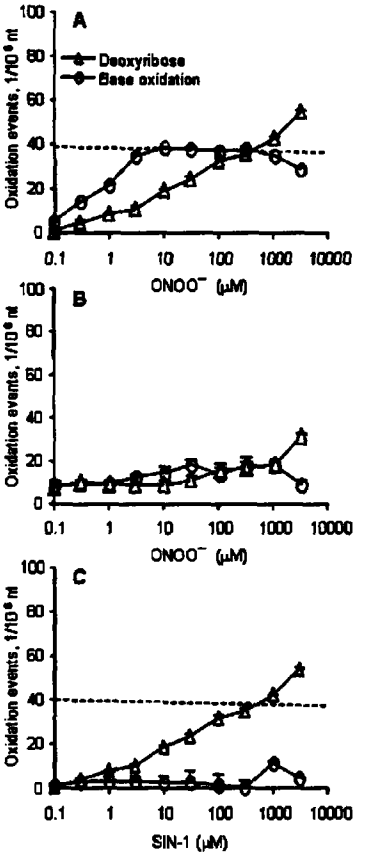

Figure 3. Deoxyribose (△) and base oxidation (○) events in pSP189 caused by different $ONOO^-$ exposure routes. (A) Bolus $ONOO^-$ addition, (B) infused $ONOO^-$ addition, and (C) SIN-1 (incubation for 100 min). Data represent means ± SDs for four measurements. Data points lying above the dotted line fall outside single-hit conditions (see the text for details).

cleave virtually all types of abasic sites in DNA, including native and oxidized abasic sites (*30, 32–34*). Interestingly, putrescine treatment only slightly increased the number of apparent strand breaks at low concentrations of both $ONOO^-$ deliveries and SIN-1 (incubation for 100 min) but increased to a plateau at high concentrations (Figure 2B). While for bolus addition, a small portion of these abasic sites may have arisen from depurination of 8-nitroguanosine (8-nitro-G), which occurs with a half-life of ~4 h at 37 °C (*35*), such depurination likely does not account for abasic sites arising with infusion and SIN-1 treatments give the lower levels of base damage occurring with these treatments (vide infra) and the short time (1 h) required for the putrescine reaction. The lack of significant putrescine effect also indicates that nucleobase modifications are not reactive toward putrescine and are stable during DNA processing.

With regard to nucleobase lesions, Fpg is a bifunctional DNA glycosylase that recognizes >90% of purine modifications caused by $ONOO^-$ (*35*). The Fpg sensitive sites can thus represent sites of both base oxidation and depurination. Along with direct strand breaks, the relaxed forms of plasmid pSP189 resolved on the agarose gel following Fpg treatment thus represent the total quantity of DNA damage. The extent of total DNA damage was found to increase with $ONOO^-$/SIN-1 concentration (Figure 2C). Clearly, the trend is that bolus addition caused more total DNA damage than either infusion or SIN-1 (incubation for 100 min). At low concentrations, SIN-1 (incubation for 100 min) and $ONOO^-$ infusion produced similar amounts of total DNA damage, while at high concentrations (≥ 1 mM), infusion generated more damage.

We further compared the ratio of deoxyribose oxidation events to nucleobase oxidation events (Figure 3). In the case of bolus $ONOO^-$ addition, both deoxyribose and nucleobase oxidation events were found to increase with increasing $ONOO^-$ dose, but the ratio was constant at ~2. For infusion at concentrations below 1 μM, there was no quantitative difference observed between deoxyribose and nucleobase oxidation, while above 1 μM, there was ~50% more nucleobase oxidation. However, in the case of SIN-1 (incubation for 100 min), deoxyribose oxidation events predominated over base oxidation events.

MF. The MF also increased following bolus and infused $ONOO^-$ treatments (Figure 4A). The MFs for pSP189 plasmid exposed to 1, 2, and 4 mM bolus doses of $ONOO^-$ were 2.1×10^{-6}, 5.7×10^{-6}, and 8.6×10^{-6}, respectively, whereas those exposed to infused $ONOO^-$ were 1.1×10^{-6}, 2.7×10^{-6}, and 3.2×10^{-6}. Bolus $ONOO^-$ exposure

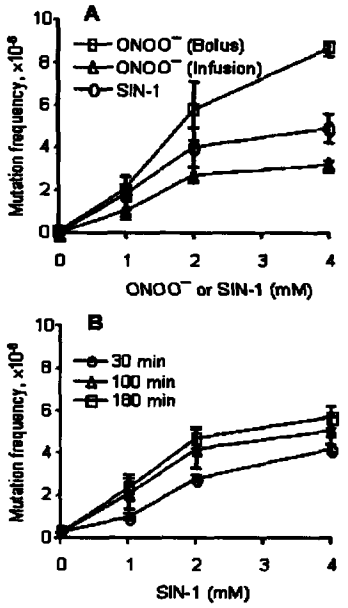

Figure 4. MF induced by (A) ONOO⁻ delivered by bolus or infusion and SIN-1 incubated for 100 min and (B) SIN-1 exposure for various times. Experiments were conducted in the presence of 25 mM $NaHCO_3$, and the damaged pSP189 was replicated in bacterial MBL50 cells. Data represent means ± SDs for three experiments. The MF of spontaneous mutation is subtracted from those induced by ONOO⁻ and SIN-1.

to 4 mM ONOO⁻ increased the MF 3.5-fold, to 12.1 × 10^{-6} from 3.5 × 10^{-6} in the untreated plasmid. Infusion of 4 mM ONOO⁻ caused an MF increase of 2.2-fold over the control value (2.6 × 10^{-6} vs 5.7 × 10^{-6}) (Figure 4A). At a dose of 4 mM, bolus delivery of ONOO⁻ increased the MF 2.7-fold over infusion value (3.2 × 10^{-6} vs 8.6 × 10^{-6}, Figure 4A). MF also increased in a dose- and time-dependent manner following SIN-1 treatment (Figure 4B). When plasmids were treated with 4 mM SIN-1 and incubated for 180 min, the MF (8.05 × 10^{-6}) was 3.2-fold higher than that of the control (2.52 × 10^{-6}) (Figure 4B). While all treatments were mutagenic, increases in MF induced by infused ONOO⁻ and SIN-1 (incubation for 100 min) at 4 mM were 63 and 43% less, respectively, than that induced by bolus exposure (Figure 4A), confirming that gradual ONOO⁻ exposure was less effective than bolus exposure in inducing mutations.

Types of Mutations Induced. On the basis of MF results, we selected mutants induced by 4 mM ONOO⁻ and 4 mM SIN-1 (exposure for 180 min) for characterization of mutation spectra. Damaged plasmid DNA was transformed into *E. coli* MBL50 cells that were then grown for 24–96 h to allow DNA replication and mutation fixation. Spectral characterization involved 26, 23, and 20 independent spontaneous mutants from untreated control plasmids from bolus, infusion, and SIN-1 experiments, respectively (Figure 7). The majority of spontaneous mutations observed were single base pair substitutions in each instance (96, 83, and 75%, respectively) (Figure 7). Other mutations included one base pair deletion (4%) in bolus and multiple sequence changes (17 and 15%) in infused ONOO⁻ and SIN-1 exposures.

Sequence analysis of 109 and 103 mutants derived from bolus and infusion exposures, respectively, revealed that single base pair substitutions were also the most frequent nucleotide sequence alterations induced by

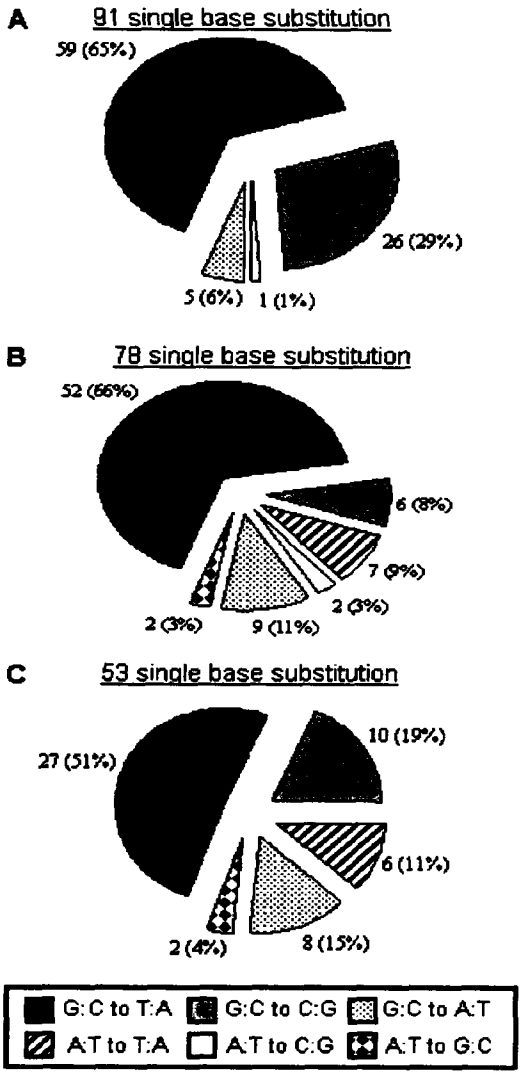

Figure 5. Types of single base substitutions induced by bolus (A) and infused (B) ONOO⁻ and SIN-1 (C) in the presence of 25 mM $NaHCO_3$. The damaged pSP189 was replicated in bacterial MBL50 cells.

ONOO⁻ (Table 1), comprising 83 and 76%, respectively. Other mutations included multiple sequence changes (10 and 16%, Figure 6), one base pair deletion (3 and 5%), and one base pair insertion (4 and 3%) in these treatment groups (Table 1). Following bolus exposure, 99% of the single base pair substitutions occurred at G:C base pairs; G:C to T:A was predominant (65%), followed by G:C to C:G transversions (29%), G:C to A:T transitions (6%), and A:T to C:G transversions (1%) (Figure 5). A similar distribution of base pair substitutions was also induced by infusion; G:C base pairs (83%) and G:C to T:A (66%) predominated (Figure 5). The proportions of G:C to A:T (11%), A:T to T:A (9%), and G:C to C:G (8%) base substitutions were also similar (Figure 5). In mutants induced by SIN-1, the mutation spectrum was substantially different. Single base pair substitutions comprised 48%, and multiple sequence changes comprised 28% (Figure 6), while the remaining 24% were one base pair deletions (17%) and one base pair insertions (7%) (Table 1). Whereas the single base pair substitution induced by

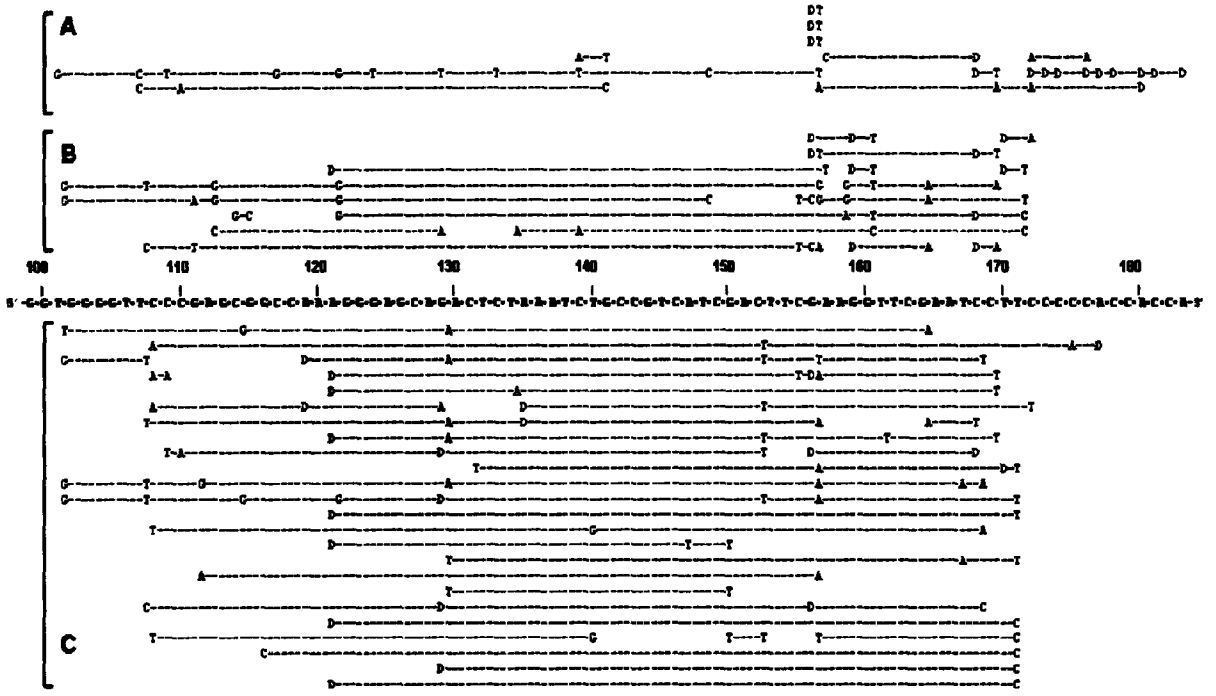

Figure 6. Distribution of multiple sequence changes in the mutated *supF* gene. The diagram shows the locations of base substitution mutations (unshaded columns), single base insertions (shaded columns), and single base pair deletions (denoted by "D") in the *supF* gene in pSP189 exposed to bolus (A) and infused (B) $ONOO^-$ and SIN-1 (C). Mutations linked by a dotted line were derived from a single clone of mutant *supF*.

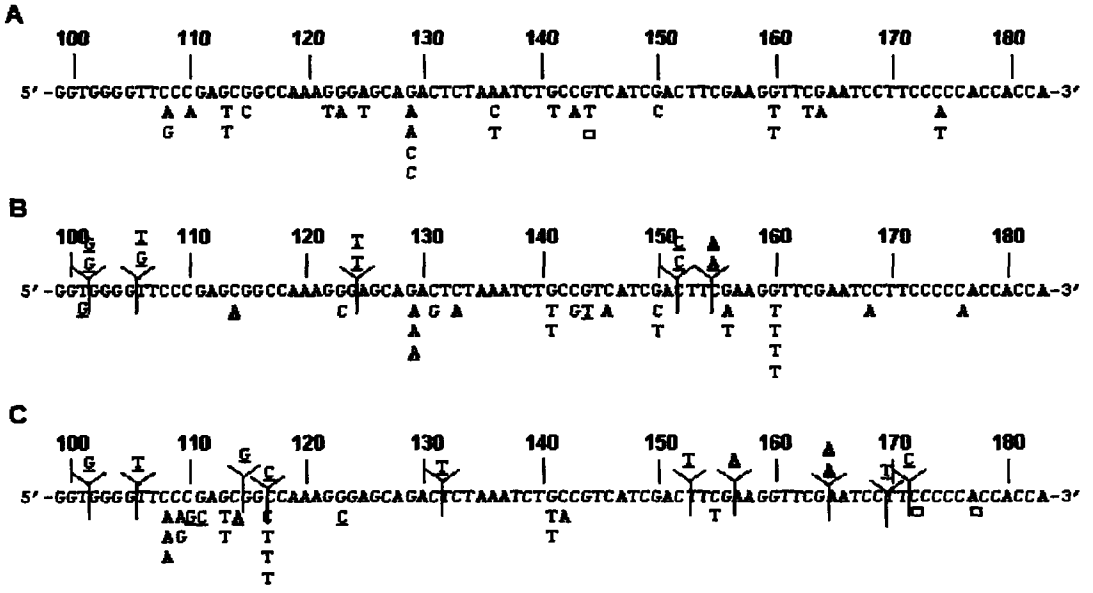

Figure 7. Mutation spectra in spontaneous mutants from unexposed controls in experiments evaluating bolus (A) and infused (B) $ONOO^-$ and SIN-1 (C). Open square symbols (□) indicate one base pair deletion. Underlined (_) symbols indicate components of multiple sequence changes within one plasmid.

infused or bolus $ONOO^-$ as well as SIN-1 consisted predominantly of G:C to T:A transversions (66, 65, and 51%, respectively), G:C to C:G transversions were much less frequent following infusion or SIN-1 (8 and 19%) than those induced by bolus exposure (29%) (Figure 6). A:T to T:A transversions (9 and 11%) were detected only in mutants induced by infused $ONOO^-$ and SIN-1 (Figure 5).

Mutation Spectra. Figures 7 and 8 show the distribution of the mutations detected in the *supF* gene. Subtle differences in mutational spectra present in mutants induced by the different exposure protocols were observed. The spectrum induced by bolus exposure to $ONOO^-$ included eight hot spots (C108, C110, G113, G115, G116, G141, C168, and C172), and that induced by infused $ONOO^-$ included six hot spots (C108, G113,

Table 1. Types of Mutations Induced by ONOO⁻ and SIN-1 in the *supF* Gene of pSP189 Replicated in *E. coli* MBL50 Cells

	number of mutations (% of total)		
	ONOO⁻		
mutation type	bolus	infusion	SIN-1
single base pair substitutions	91 (83)	78 (76)	53 (48)
one base pair deletions	3 (3)	5 (5)	18 (17)
one base pair insertions	4 (4)	3 (3)	8 (7)
multiple sequence changes	11 (10)	17 (16)	31 (28)
total mutants	109 (100)	103 (100)	110 (100)

G115, G116, G129, and C168). The eight hot spots induced by SIN-1 were located at positions C108, A121, G129, C139, G150, G156, C168, and A177. All hot spots induced by all treatments were located at G:C sites except for A121 and A177 following SIN-1 exposure. C108 and C168 were common to all exposures; G113, G115, and G116 were common to bolus and the infused ONOO⁻, while G129 was common to both the infused ONOO⁻ and SIN-1 exposures. Hot spots at sites C110, G141, and C172 were only found in the bolus ONOO⁻ exposure group, whereas hot spots A121, C139, G150, G156, and A177 occurred only after SIN-1 exposure (Figure 8).

Discussion

Our previous studies of ONOO⁻ mutagenesis using the *supF* shuttle vector revealed that the presence of $NaHCO_3$/CO_2 reduced the mutagenic potency of ONOO⁻ and resulted in predominantly G:C to C:G and G:C to T:A transversions (*17*). However, in this and other studies, ONOO⁻ concentrations were high and the oxidant was delivered as a bolus, which results in a short duration of action but locally high concentrations of ONOO⁻ (*16*, *35*–*43*). This approach may be problematic for two reasons. First, high ONOO⁻ concentrations cause numerous damage events in a single plasmid DNA molecule as indicated by large quantities of linearized pSP189 plasmid DNA induced by treatment with 1–5 mM ONOO⁻ (*16*). Destruction or degradation of a significant portion of the intact plasmid DNA could reduce the quantity of DNA capable of replication in *E. coli* for determination of mutations and thus bias the resulting spectrum. A second problem arises from recent observations that the DNA damage chemistry is dependent on ONOO⁻ concentration (*26*). For these reasons, we have assessed the mutagenesis of *supF* gene induced by ONOO⁻ following bolus or infusion exposure and SIN-1 exposure, all in the presence of 25 mM $NaHCO_3$. An additional aim of this study was to determine the effects of dose and dose rate of ONOO⁻ exposure on the levels of DNA damage, and the frequency, types, and distribution of mutations, since these parameters may be of significance in the potential genotoxicity resulting from ONOO⁻ formation in vivo.

We observed that the rate of ONOO⁻ delivery influenced the yield of total DNA damage (Figures 1 and 2).

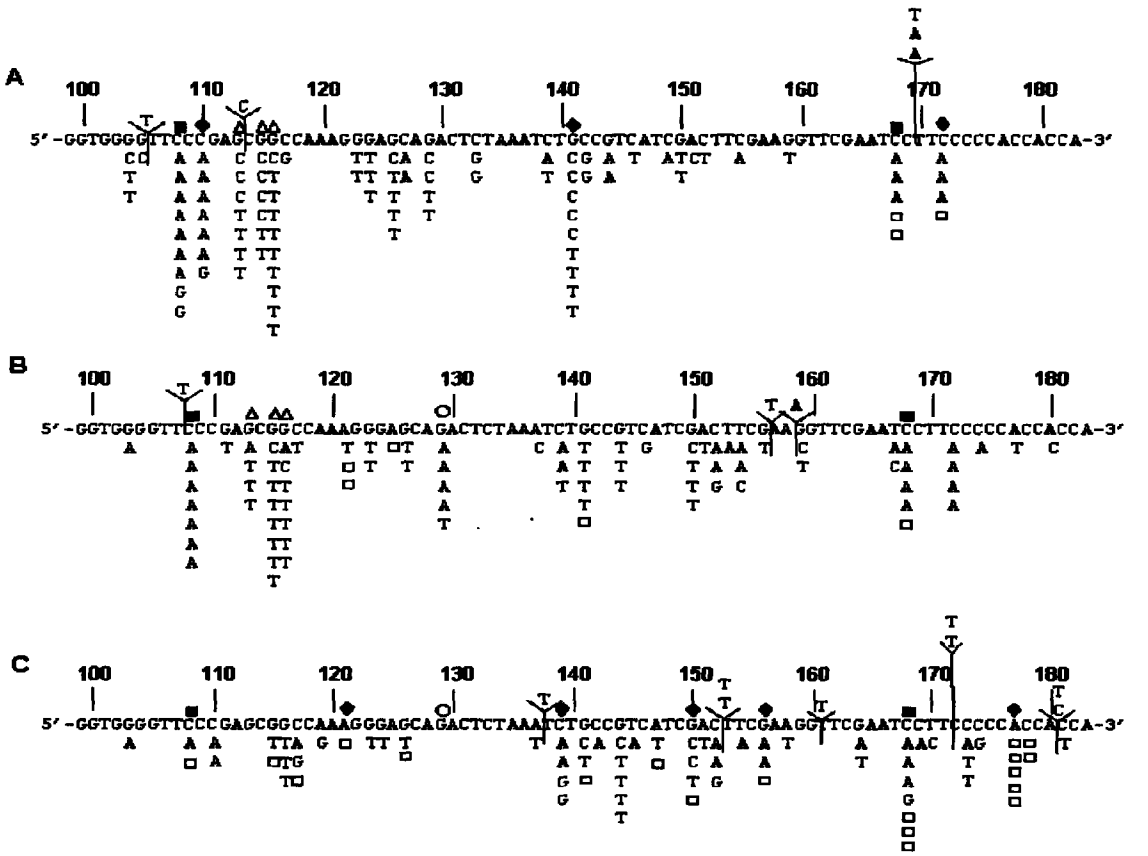

Figure 8. Distribution of mutations induced in the *supF* gene by bolus (A) and infused (B) ONOO⁻ and SIN-1 (C) in the presence of 25 mM $NaHCO_3$. The damaged pSP189 was replicated in bacterial MBL50 cells. Symbol key: ■, hot spot sites that were common to all exposures; △, hot spots common to both the bolus and the infused ONOO⁻; ○, hot spots common to both the infused ONOO⁻ and the SIN-1 exposures; ◆, present only in each exposure. Open square symbols in the columns of point mutations (□) indicate one base pair deletion. Multiple sequence changes illustrated in Figure 6 have been omitted.

Bolus $ONOO^-$ addition was shown to cause the most damage, while infusion produced the least. Damage caused by $ONOO^-$ formed de novo from SIN-1 fell in the middle (Figures 1 and 2). We believe that the difference is due to the chemistry underlying each exposure regimen. $ONOO^-$ reactions with DNA produce two major types of damage: direct strand breaks and abasic sites due to oxidation of deoxyribose moieties and nitration and oxidation of guanine. While a comprehensive kinetic model to simulate the known features of $ONOO^-$ oxidation kinetics is beyond the scope of the current work, several explicit considerations are helpful to better understand the rates at which various types of DNA damage occur. $ONOO^-$ or $ONOOH$ can react directly with target molecules. Those reaction rates are second-order overall, first-order in both $ONOO^-$ and the target. Additional reactions involve radicals that are generated during $ONOO^-$ decomposition. In the absence of CO_2, $ONOOH$ decomposes via homolysis producing $^{\bullet}OH$ and $^{\bullet}NO_2$ radicals with up to 30–40% yields (*44*). Because radical formation is the rate-limiting step, this process will be first-order in $ONOO^-$ and zero-order in the targets. In the presence of physiological levels of CO_2, most $ONOO^-$ formed from $NO^{\bullet}$ and $O_2^{\bullet-}$ will react with CO_2 to give the $ONOOCO_2^-$ adduct. The decomposition of that adduct yields (in part, ~33%) $NO_2^{\bullet}$ and $CO_3^{\bullet-}$ radicals, which cause one-electron oxidation or nitration of the substrate (*45*, *46*). In this case, the overall reaction rate depends on the $ONOO^-$ and CO_2 concentrations and is independent of the substrate concentration.

In this study, both bolus addition and infusion were performed in phosphate buffer containing the same concentration of bicarbonate (25 mM). Considering the fast reaction of $ONOO^-$ with CO_2, the major reactive species are therefore $^{\bullet}NO_2$ and $CO_3^{\bullet-}$, and the rates of DNA oxidation or nitration resulting from $^{\bullet}NO_2$ and $CO_3^{\bullet-}$ should be directly proportional to $ONOO^-$ concentration. We currently lack information on the steady state $ONOO^-$ concentration in each type of addition, but the $ONOO^-$ flux can be used as a reasonable estimation of the local $ONOO^-$ concentration that a DNA molecule might encounter. Using 1 mM $ONOO^-$ as an example, under the condition of bolus addition, the flux attained can be estimated as ~2000 $\mu M/s$, while for the infusion addition performed in this experiment, the flux was only ~2 $\mu M/s$. Knowing that quick formation rate does not necessarily lead to the accumulation of the product, we hypothesize that the ability of $ONOO^-$ to damage DNA through either nitration or oxidation is dependent on en mass reaction at sufficient concentration (bolus) as opposed to an accrual of reactions over time with the infusion or de novo formation. Several observations from the studies of tyrosine nitration support this hypothesis. Espey et al. found that exposure of a purified green fluorescent protein to bolus $ONOO^-$ resulted in profound increase of 3-nitrotyrosine formation, while the increase was not evident when infusion addition was used (*47*). Zhang et al. reported a similar observation (*48*). During bolus $ONOO^-$ addition, the levels of both nitration and oxidation of tyrosine increased with increasing dose, while during slow infusion the level of nitration but not oxidation of tyrosine increased. The total number of tyrosine modifications was lower with infusion addition (*48*).

Another major observation in the damage study came from our efforts to define the proportions of deoxyribose and nucleobase oxidation by different exposure routes. We found that SIN-1 exposure almost exclusively favored deoxyribose oxidation (Figure 3), although the ratio of deoxyribose to nucleobase oxidation increased with increasing concentrations of SIN-1 (Figure 3). One explanation, which is being rigorously tested in our group, is that the loss of bicarbonate in the reaction buffer during incubation shifted the $ONOO^-$ chemistry. We previously reported that in the presence of CO_2, which converts $ONOO^-$ to $ONOOCO_2^-$, the number of deoxyribose oxidation events was reduced 4-fold while Fpg sensitive base lesions increased by the same amount. The observation here is the opposite, in that the loss of CO_2 caused a shift in $ONOO^-$-induced DNA damage from the base to the sugar. Such a dramatic difference leads us to conclude that chemistry elicited by SIN-1 may be different from that resulting from authentic $ONOO^-$.

We previously showed that bolus exposure of the pSP189 plasmid to 2.5 mM $ONOO^-$ increased the MF in plasmid replicated in *E. coli* MBL50 cells or in human cells (*16*, *17*). Linear and dose-dependent increases in MF were induced by exposure to $ONOO^-$ concentrations up to 4.5 mM, in both the presence and the absence of $NaHCO_3/CO_2$, but the presence of bicarbonate substantially reduced the mutagenic response (*17*). Because single, large bolus doses were used in those experiments, here, we investigated responses to infused $ONOO^-$ and SIN-1 as well as bolus exposure, all in the presence of 25 mM bicarbonate. MF induced by all three exposures increased dose dependently, but bolus exposure was most effective, indicating that $ONOO^-$ introduced slowly over time by either infusion or SIN-1 degradation was less capable of inducing mutagenesis. Consistent with this interpretation, transformation efficiency (an indication of total DNA damage) of plasmids exposed to bolus additions of $ONOO^-$ was lower than those exposed by infusion or to SIN-1 (data not shown). These results are also consistent with the DNA damage data in Figure 2.

To characterize effects of dose and dose rate of $ONOO^-$ exposure on mutation spectra, 109, 103, and 110 mutants induced by bolus, infusion, and SIN-1 treatments, respectively, were sequenced and analyzed (Figure 8). Almost all hot spots were located at G:C sites, and hot spots C108 and C168 were common to all exposures. G113, G115, and G116 were common to both the bolus and the infused $ONOO^-$ exposures, whereas G129 was common to both the infused $ONOO^-$ and the SIN-1 exposures. Mutations tended to localize preferentially at certain sites following both the bolus and the infused $ONOO^-$ exposures, whereas they were more randomly scattered along the *supF* gene following SIN-1 exposure. This result is consistent with sequence nonselective deoxyribose oxidation, and not guanine oxidation, as the major form of DNA damage produced by SIN-1, and it suggests that the chemistry of DNA damage induced by SIN-1 may differ from that induced by $ONOO^-$.

The types of mutations detected are summarized in Table 1. The predominant mutations found following all exposures were single base pair substitutions, together with smaller numbers of multiple sequence changes, one base pair deletion, and one base pair insertion. Multiple sequence changes are an ubiquitous component of shuttle vector mutagenesis. Because they have also been observed in cellular genes, the mechanisms responsible may be relevant to mutagenesis of cellular genes, including those involved in carcinogenesis (*49*, *50*). One possible

mechanism contributing to the occurrence of these multiply mutated sequences is the formation of more than one base lesion or deoxyribose oxidation event in close proximity. Extrapolation of the $ONOO^-$ data presented in Figure 2 to 4 mM suggests that treatment of the pSP189 plasmid with this concentration of $ONOO^-$ exceeds the single-hit condition of a Poisson distribution and results in multiple lesions occurring in a single copy of the *supF* sequence. Because strand breaks are themselves mutagenic (*51*), the proximate lesions giving rise to multiply mutated sites could consist of various combinations of deoxyribose oxidation events and base lesions.

Following bolus $ONOO^-$ exposure, most single base substitutions occurred at G:C sites and included G:C to T:A and G:C to C:G transversions as well as G:C to A:T transitions (Figure 5). In all exposure scenarios, G:C to T:A transversions were most frequent, along with lesser numbers of G:C to C:G transversions and G:C to A:T transitions, confirming that G:C pairs are the major targets damaged by $ONOO^-$ treatment, consistent with our previous findings (*16*, *17*).

It is of interest that G:C to T:A transversions comprise a significant fraction of mutations in oncogenes and tumor suppressor genes in human cancer, especially in lung cancer (*52*, *53*). G:C to T:A base substitutions can result from a variety of DNA lesions including thymine glycol, apurinic/apyrimidinic sites, 8-oxodeoxyguanosine (8-oxo-dG), 8-chloro-2′-deoxyguanosine (8-Cl-dG), or 8-bromo-2′-deoxyguanosine (8-Br-dG) formed in DNA in some systems (*16*, *35*, *54*–*57*), including those frequently found in tumor relevant genes (*58*). It is well-established that the two main types of chemistries attributed to $ONOO^-$ are oxidations and nitrations (*1*–*5*), resulting in the production of 8-oxo-dG or 8-nitro-G (*59*). 8-Oxo-dG has been utilized as a biomarker for monitoring DNA damage with a number of oxidizing agents, and its formation in nucleic acid is known to cause mutations (*59*). SIN-1 has also been shown to induce significant levels of 8-oxoguanine (8-oxo-G) in plasmid DNA and calf thymus DNA (*60*). 8-Nitro-G undergoes spontaneous depurination leading to apurinic sites in DNA (*61*), leading to G:C to T:A transversions (*62*). Our present results are therefore consistent with nitration and/or one-electron oxidations induced by $NO_2^{\bullet}$ and $CO_3^{\bullet-}$ radicals, as noted above, since all exposures were done in the presence of bicarbonate. In addition, 8-nitrodeoxyguanosine (8-nitro-dG) nucleoside is capable of producing $O_2^{\bullet-}$ in the presence of certain oxidoreductases such as NADPH-cytochrome P450 reductase and nitric oxide species (NOS) and might enhance oxidative DNA and tissue damage (*57*).

Interestingly, we found that G:C to C:G mutations were less frequent following infusion or SIN-1 than those induced by bolus exposure under our experimental conditions (Figure 5). G:C to C:G transversions have been observed in mutagenesis experiments with lipid peroxidation systems (*63*), and their frequency is considerably higher under oxidative stress (*64*–*69*). Our results therefore suggest that infused $ONOO^-$ and SIN-1 exposure may cause less oxidative damage as compared with bolus $ONOO^-$ exposure. Shin et al. (*70*) demonstrated that the initial formation of C:C or G:G mispairs provides the most plausible explanation for the elevated presence of the G:C to C:G mutations. Kino et al. (*71*) reported that 8-oxo-G is not responsible for G:G to C:G transversions, because dGTP was not incorporated opposite 8-oxo-G in the DNA polymerase extension assay using a template containing 8-oxo-G. These authors suggested that 8-oxo-G is further oxidized to 2,5-diamino-4*H*-imidazol-4-one (Iz) and the specific formation Iz·G base pairs may cause G:C to C:G transversion mutations (*71*), but the origin of G:C to C:G transverisons is still undefined.

ROS and NOS generated by inflammatory cells have been proposed to induce DNA and tissue damage, chromosomal aberrations, and mutations, which contribute to the multistage process of carcinogenesis (*25*). Increasing evidence now suggests that $ONOO^-$ is a major agent causing tissue damage in inflammatory disorders, and oxidative damage to DNA is among events taking place during chronic inflammation in vivo (*72*–*74*). An important source of $ONOO^-$ in vivo is the activated macrophage, which has been implicated in causing tissue damage during chronic inflammatory conditions by mechanisms that might involve $ONOO^-$ (*75*). We previously characterized genotoxic effects in the $NO^{\bullet}$-producing cells using mouse macrophage-like RAW264.7 cells as a coculture system for the study of $NO^{\bullet}$-associated genotoxicity under physiologically relevant conditions and demonstrated that $NO^{\bullet}$ overproduction may contribute to genotoxic risks associated with chronic inflammation (*76*). In the work reported here, we found that both dose and dose rate at which the *supF* gene is exposed to $ONOO^-$ strongly influence the amount and type of DNA damage, the mutagenic potency, types, and distribution of mutations in the gene. The systems used to introduce $ONOO^-$ in these experiments were designed to approximate conditions of exposure more physiologically relevant to chronic inflammation than bolus additions, since cells in vivo are likely to be exposed over longer periods of time rather than to high concentrations for short periods (*28*). Hence, our findings provide important clues that dose and dose rate $ONOO^-$ introduction may contribute to potential genotoxicity resulting from $ONOO^-$ formation in vivo. Further studies will be required to elucidate precise mechanisms underlying these effects and their potential relevance to $ONOO^-$ induced cytotoxicity in vivo.

Acknowledgment. We are grateful to Laura J. Trudel for technical assistance and manuscript preparation. This work was supported by National Cancer Institute Grant 5 P01 CA26731 and NIEHS Center Grant ES02109.

References

(1) Murphy, M. P., Packer, M. A., and Scarlett, S. W. (1998) Peroxynitrite: A biologically significant oxidant. *Gen. Pharmacol. 31*, 179–286.

(2) Squadrito, G. L., and Pryor, W. L. (1998) Oxidative chemistry of nitric oxide: the roles of superoxide, peroxynitrite and carbon dioxide. *Free Radical Biol. Med. 25*, 392–403.

(3) Ducrocq, C., Blanchard, B., Pignatelli, B., and Ohshima, H. (1999) Peroxynitrite: An endogenous oxidizing and nitrating agent. *CMLS Cell Mol. Life Sci. 55*, 1068–1077.

(4) Beckman, J. S., Beckman, T. W., Chen, J., Marshall, P. A., and Freeman, B. A. (1990) Apparent hydroxyl radical production by peroxynitrite: Implications for endothelial injury from nitric oxide and superoxide. *Proc. Natl. Acad. Sci. U.S.A. 87*, 1620–1624.

(5) Bonfoco, E., Krainc, D., Ankarcrona, M., Nicotera, P., and Lipton, S. A. (1995) Apoptosis and necrosis: Two distinct events induced, respectively, by mild and intense insults with *N*-methyl-D-aspartate or nitric oxide superoxide in cortical cell cultures. *Proc. Natl. Acad. Sci. U.S.A. 92*, 7162–7166.

(6) Huie, R. E., and Padmaja, S. (1993) The reaction of NO with superoxide. *Free Radical Res. Commun. 18*, 195–199.

(7) Bonini, M. G., Radi, R., Ferrer-Sueta, G., Ferreira, A., and Augusto, O. (1999) Direct EPR detection of the carbonate radical anion produced from peroxynitrite and carbon dioxide. *J. Biol. Chem. 274*, 10802–10806.

(8) Pryor, W., and Squadrito, G. (1995) The chemistry of peroxynitrite: A product from the reaction of nitric oxide with superoxide. *Am. J. Physiol. 268*, L699–L722.

(9) Szabó, C., Zingarelli, B., O'Connor, M., and Salzman, A. L. (1996) DNA strand breakage, activation of poly (ADP-ribose) synthetase, and cellular energy depletion are involved in the cytotoxicity of macrophages and smooth muscle cells exposed to peroxynitrite. *Proc. Natl. Acad. Sci. U.S.A. 93*, 1753–1758.

(10) Cookson, M. R., Ince, P. G., and Shaw, P. J. (1998) Peroxynitrite and hydrogen peroxide induced cell death in the NSC34 neuroblastoma x spinal cord cell line: Role of poly (ADP-ribose) polymerase. *J. Neurochem. 70*, 501–508.

(11) Casaina, P., Peluffo, H., Pehar, M., Martinez-Palma, L., Ressia, A., Beckman, J. S., Estevez, A. G., and Barbeito, L. (2002) Peroxynitrite triggers a phenotypic transformation in spinal cord astrocytes that induces motor neuron apoptosis. *J. Neurosci. Res. 67*, 21–29.

(12) Bapat, S., Verkleij, A., and Post, J. A. (2001) Peroxynitrite activates mitogen activated protein kinase (MAPK) via a MEK-independent pathway: A role for protein kinase C. *FEBS Lett. 499*, 21–26.

(13) Oh-Hashi, K., Maruyama, W., and Isobe, K. (2001) Peroxynitrite induces GADD 34, 45, and 153 VIA p38 MAPK in human neuroblastoma SH-SY5Y cells. *Free Radical Biol. Med. 30*, 213–221.

(14) Go, Y. M., Patel, R. P., Maland, M. C., Park, H., Beckman, J. S., Darley-Usmar, V. M., and Jo, H. (2001) Evidence for peroxynitrite as a signaling molecule in flow-dependent activation of c-Jun NH (2)-terminal kinase. *Am. J. Physiol. 277*, H1647–H1653.

(15) Rose, P., Widder, S., Looft, J., Pickenhagen, W., Ong, C. N., and Whiteman, M. (2003) Inhibition of peroxynitrite-mediated cellular toxicity, tyrosine nitration, and α1-antiproteinase inactivation by 3-mercapto-2-methylpentan-1-ol, a novel compound isolated from *Allium cepa*. *Biochem. Biophys. Res. Commun. 302*, 397–402.

(16) Juedes, M. J., and Wogan, G. N. (1996) Peroxynitrite-induced mutation spectra of pSP189 following replication in bacteria and in human cells. *Mutat. Res. 349*, 51–56.

(17) Pamir, B., and Wogan, G. N. (2003) Bicarbonate modulation of peroxynitrite-induced mutagenesis of the *supF* gene in pSP189. *Chem. Res. Toxicol. 16*, 487–492.

(18) Singh, R. J., Hogg, N., Joseph, J., Konorev, E., and Kalyanaraman, B. (1999) The peroxynitrite generator, SIN-1, becomes a nitric oxide donor in the presence of electron acceptors. *Arch. Biochem. Biophys. 361*, 331–339.

(19) Darley-Usmar, V. M., Hogg, N., O'Leary, V. J., Wilson, M. T., and Moncada, S. (1992) The simultaneous generation of superoxide and nitric oxide can initiate lipid peroxidation in human low-density lipoprotein. *Free Radical Res. Commun. 17*, 9–20.

(20) Hogg, N., Darley-Usmar, V. M., Wilson, M. T., and Moncada, S. (1992) Production of hydroxyl radicals from the simultaneous generation of superoxide and nitric oxide. *Biochem. J. 281*, 419–424.

(21) Lipton, S. A., Choi, Y., Pan, Z., Lei, S. Z., Chen, H. V., Sucher, N. J., Loscalso, J., Singel, D. J., and Stamler, J. S. (1993) A redox-based mechanism for the neuroprotective and neurodestructive effects of nitric oxide and related nitroso-compounds. *Nature 364*, 626–632.

(22) Brunelli, L., Crow, J. P., and Beckman, J. S. (1995) The comparative toxicity of nitric oxide and peroxynitrite to *Escherichia coli*. *Arch. Biochem. Biophys. 316*, 327–334.

(23) Motohashi, N., and Saito, Y. (2002) Induction of SOS response in *salmonella typhimurium* TA4107/pSK1002 by peroxynitrite-generating agent, N-morpholino sydnonimine. *Mutat. Res. 502*, 11–18.

(24) Li, C. Q., Trudel, L., and Wogan, G. N. (2002) Genotoxicity, mitochondrial damage, and apoptosis in human lymphoblastoid cells exposed to peroxynitrite generated from SIN-1. *Chem. Res. Toxicol. 15*, 527–535.

(25) Ohshima, H., Tatemichi, M., and Sawa, T. (2003) Chemical basis of inflammation-induced carcinogenesis. *Arch. Biochem. Biophys. 417*, 3–11.

(26) Dedon, P. C., and Tannenbaum, S. R. (2004) Reactive nitrogen species in the chemical biology of inflammation. *Arch. Biochem. Biophys. 423*, 12–22.

(27) Pryor, W. A., Cueto, R., Jin, X., Koppenol, W. H., Ngu-Schwemlein, M., Squadrito, G. L., Uppu, P. L., and Uppu, R. M. (1995) A practical method for preparing peroxynitrite solutions of low ionic strength and free of hydrogen peroxide. *Free Radical Biol. Med. 18*, 75–83.

(28) Doulias, P., Barbouti, A., Galaris, D., and Ischiropoulos, H. (2001) SIN-1 induced DNA damage in isolated human peripheral blood lymphocytes as assessed by single cell gel electrophoresis (Comet assay). *Free Radical Biol. Med. 30*, 679–685.

(29) Cai, L., Klein, J. B., and Kang, Y. J. (2000) Metallothionein inhibits peroxynitrite-induced DNA and lipoprotein damage. *J. Biol. Chem. 275*, 38957–38960.

(30) Dedon, P. C., Salzberg, A. A., and Xu, J. (1993) Exclusive production of bistranded DNA damage by calicheamicin. *Biochemistry 32*, 3617–3622.

(31) Mendenhall, W., Wackerly, D. D., and Scheaffer, R. L. (1990) *Mathematical Statistics with Applications*, 4th ed., PWS-Kent Publishing, Boston.

(32) Lindahl, T., and Andersson, A. (1972) Rate of chain breakage at apurinic sites in double stranded deoxyribonucleic acid. *Biochemistry 11*, 3618–3623.

(33) Lindahl, T., and Nyberg, B. (1972) Rate of depurination of native deoxyribonucleic acid. *Biochemistry 11*, 3610–3608.

(34) Yu, L., Goldberg, I. H., and Dedon, P. C. (1994) Enediyne-mediated DNA damage in nuclei is modulated at the level of the nucleosome. *J. Biol. Chem. 269*, 4144–4151.

(35) Tretyakova, N. Y., Burney, S., Parmir, B., Wishnok, J. S., Dedon, P. C., Wogan, G. N., and Tannenbaum, S. R. (2000) Peroxynitrite-induced DNA damage in the *supF* gene: correlation with the mutational spectrum. *Mutat. Res. 447*, 287–303.

(36) Yermilov, V., Yoshie, Y., Rubio, J., and Ohshima, H. (1996) Effects of carbon dioxide/bicarbonate on induction of DNA single-strand breaks and formation of 8-nitroguanine, 8-oxo-guanine and base-propenal mediated by peroxynitrite. *FEBS Lett. 399*, 67–70.

(37) Epe, B., Ballmaier, D., Roussyn, I., Briviba, K., and Sies, H. (1996) DNA damage by peroxynitrite characterized with DNA repair enzymes. *Nucleic Acids Res. 24*, 4105–4110.

(38) Groves, J. T., and Marla, S. S. (1995) Peroxynitrite-induced DNA strand scission mediated by a manganese porphyrin. *J. Am. Chem. Soc. 117*, 9578–9579.

(39) Salgo, M. G., Stone, K., Squadrito, G. L., Battista, J. R., and Pryor, W. A. (1995) Peroxynitrite cause DNA nicks in plasmid pBR322. *Biochem. Biophys. Res. Commun. 210*, 1025–1030.

(40) Roussyn, I., Briviba, K., Masumoto, H., and Sies, H. (1996) Selenium-containing compounds protect DNA from single-strand breaks caused by peroxynitrite. *Arch. Biochem. Biophys. 330*, 216–218.

(41) Yoshie, Y., and Ohshima, H. (1997) Nitric oxide synergistically enhances DNA strand breakage induced by polyhydroxyaromatic compounds, but inhibits that induced by the Fenton reaction. *Arch. Biochem. Biophys. 342*, 13–21.

(42) Tamir, S., Burney, S., and Tannenbaum, S. R. (1996) DNA damage by nitric oxide. *Chem. Res. Toxicol. 9*, 821–827.

(43) Kim, S. Y., Lee, J. H., Yang, E. S., Kil, J. S., and Park, J. W. (2003) Human sensitive to apoptosis gene protein inhibits peroxynitrite-induced DNA damage. *Biochem. Biophys. Res. Commum. 301*, 671–674.

(44) Merenyi, G., Lind, J., Goldstein, S., and Czapski, G. (1998) Peroxynitrous acid homolyzes into $^{\bullet}OH$ and $^{\bullet}NO_2$ radicals. *Chem. Res. Toxicol. 11*, 712–713.

(45) Goldstein, S., Czapski, G., Lind, J., and Merényi, G. (2000) Tyrosine nitration by simultaneous generation of $^{\bullet}NO$ and O_2^- under physiological conditions. How the radicals do the job. *J. Biol. Chem. 275*, 3031–3036.

(46) Pfeiffer, S., Schmidt, K., and Mayer, B. (2000) Dityrosine formation outcompetes tyrosine nitration at low steady-state concentrations of peroxynitrite. Implications for tyrosine modification by nitric oxide/superoxide in vivo. *J. Biol. Chem. 275*, 6346–6352.

(47) Espey, M. G., Xavier, S., Thomas, D. D., Miranda, K. M., and Wink, D. A. (2002) Direct real-time evaluation of nitration with green fluorescent protein in solution and within human cells reveals the impact of nitrogen dioxide vs peroxynitrite mechanisms. *Proc. Natl. Acad. Sci. U.S.A. 99*, 3481–3486.

(48)) Zhang, H., Joseph, J., Feix, J., Hogg, N., and Kalyanaraman, B. (2001) Nitration and oxidation of a hydrophobic tyrosine probe by peroxynitrite in membranes: comparison with nitration and oxidation of tyrosine by peroxynitrite in aqueous solution. *Biochemistry 40*, 7675–7686.

(49) Strauss, B. S. (1998) Hypermutability in carcinogenesis. *Genetics 148*, 1619–1626.

(50) Harwood, J., Tachibana, A., and Meuth, M. (1991) Multiple dispersed spontaneous mutations: A novel pathway of mutation in a malignant human cell line. *Mol. Cell. Biol. 11*, 3163–3170.

(51) Seidman, M. M., Bredberg, A., Seetharam, S., and Kraemer, K. H. (1987) Multiple point mutations in a shuttle vector propagated in human cells: Evidence for an error-prone DNA polymerase activity. *Proc. Natl. Acad. Sci. U.S.A. 84*, 4944–4948.

(52) Bennett, W. P., Hussain, S. P., Vahakangas, K. H., Khan, M. A., Shields, P. G., and Harris, C. C. (1999) Molecular epidemiology of human cancer risk gene-environment interactions and p53 mutation spectrum in human lung cancer. *J. Pathol. 187*, 8–18.

(53) Hainaut, P., and Pfeifer, G. P. (2001) Patterns of p53 G→T transversions in lung cancers reflect the primary mutagenic signature of DNA-damage by tobacco smoke. *Carcinogenesis 22*, 367–374.

(54) Masuda, M., Suzuki, T., Friesen, M. D., Ravanat, J. L., Cadet, J., Pignatelli, B., Nishino, H., and Ohshima, H. (2001) Chlorination of guanosine and other nucleosides by hypochlorous acid and myeloperoxidase of activated human neutrophils. *J. Biol. Chem. 276*, 40486–40496.

(55) Wang, D., Kreutzer, D. A., and Essigmann, J. M. (1998) Mutagenicity and repair of oxidative DNA damage: Insights from studies using defined lesions. *Mutat. Res. 400*, 99–115.

(56) Shibutani, S., Takeshita, M., and Grollman, A. P. (1991) Insertion of specific bases during DNA synthesis past the oxidation-damaged base 8-oxodG. *Nature 349*, 431–434.

(57) Ohshima, H., Tatemich, M., and Sawa, T. (2003) Chemical basis of inflammation-induced carcinogenesis. *Arch. Biochem. Biophys. 417*, 3–11.

(58) Brunner, S. D., Norman, D. P., and Verdine, G. L. (2000) Structural basis for recognition and repair of the endogenous mutagen 8-oxoguanine in DNA. *Nature 403*, 859–866.

(59) Szabó, C. (2003) Mutiple pathways of peroxynitrite cytotoxicity. *Toxicol. Lett. 140–141*, 105–112.

(60) Inoue, D., and Kawanishi, S. (1995) Oxidative DNA damage induced by simultaneous generation of nitric oxide and superoxide. *FEBS Lett. 371*, 86–88.

(61) Yermilov, V., Rubio, J., and Ohishima, H. (1995) Formation of 8-nitroguanine in DNA treated with peroxynitrite in vitro and its rapid removal from DNA by depurination. *FEBS Lett. 376*, 207–210.

(62) Loeb, L. A., and Preston, B. D. (1986) Mutagenesis by apurinic/apyrimidinic sites. *Annu. Rev. Genet. 20*, 201–230.

(63) Akasaka, S., and Yamamoto, K. (1994) Mutagenesis resulting from DNA damage by lipid peroxidation in the *supF* gene of *Escherichia coli*. *Mutat. Res. 315*, 105–112.

(64) Mcbride, T. J., Schneider, J. E., Floyd, R. A., and Loeb, L. A. (1992) Mutations induced by methylene blue plus light in single-stranded M13mp2. *Proc. Natl. Acad, Sci. U.S.A. 89*, 6866–6870.

(65) Ono, T., Negishi, K., and Hayatsu, H. (1995) Spectra of superoxide-induced mutations in the *lacI* gene of a wild-type and a *mutM* strain of *Escherichia coli* K-12. *Mutat. Res. 326*, 175–183.

(66) Mcbride, T. J., Preston, B. D., and Loeb, L. A. (1991) Mutagenic spectrum resulting from DNA damage by oxygen radicals. *Biochemistry 30*, 207–213.

(67) Oller, A. R., and Thilly, W. G. (1992) Mutational spectra in human B-cells: Spontaneous, oxygen and hydrogen peroxide-induced mutations at *hprt* gene. *J. Mol. Biol. 228*, 813–826.

(68) Takimoto, K., Tano, K., Hashimoto, M., Hori, M., Akasaka, S., and Utsumi, H. (1999) Delayed transfection of DNA after riboflavin mediated photosensitization increases G:C to C:G transversions of *supF* gene in *Escherichia coli* mutY strain. *Mutat. Res. 445*, 93–98.

(69) Maehira, F., Miyagi, I., Asato, T., Eguchi, Y., Takei, H., Nakatsuki, K., Fukuoka, M., and Zaha, F. (1999) Alterations of protein kinase C, 8-hydroxydeoxyguanosine, and *K-ras* oncogene in rat lungs exposed to passive smoking. *Clin. Chim. Acta 289*, 133–144.

(70) Shin, C. Y., Ponomareva, O. N., Connolly, L., and Turker, M. S. (2002) A mouse kidney cell line with a G:C→C:G transversion mutator phenotype. *Mutat. Res. 503*, 69–76.

(71) Kino, K., and Sugiyama, H. (2001) Possible cause of G·C→C·G transversion mutation by guanine oxidation product, imidazolone. *Chem. Biol. 8*, 369–378.

(72) Mulligan, M. S., Hevel, J. M., Meynier, F., and Ward, P. A. (1991) Tissue injury caused by deposition of immune complexes is L-arginine dependent. *Proc. Natl. Acad. Sci. U.S.A. 88*, 6338–6342.

(73) Cazevielle, C., Muller, A., Meynier, F., and Bonnie, C. (1993) Superoxide and nitric oxide cooperation in hypoxia/reoxygenation-induced neuron injury. *Free Radical Biol. Med. 14*, 389–395.

(74) White, C. R., Brook, T. A., Chung, L. Y., Crapo, J., Briscoe, P., Ku, D., Bradley, W. A., Gianturco, S. H., Gore, J., Freeman, B. A., and Tarpey, M. M. (1994) Superoxide and peroxynitrite in atherosclerosis. *Proc. Natl. Acad. Sci. U.S.A. 91*, 1044–1048.

(75) Ischiropoulos, H., Zhu, L., and Beckman, J. S. (1992) Peroxynitrite formation from macrophage-derived nitric oxide. *Arch. Biochem. Biophys. 298*, 446–451.

(76) Zhuang, J. C., Lin, D., Lin, C., Jethwaney, D., and Wogan, G. N. (2002) Genotoxicity associated with NO production in macrophages and co-cultured target cells. *Free Radical Biol. Med. 33*, 94–102.

TX049777M